

# **Multimodal Imaging of Inflammation at the Neurovascular Interface in Cerebrovascular Disease**

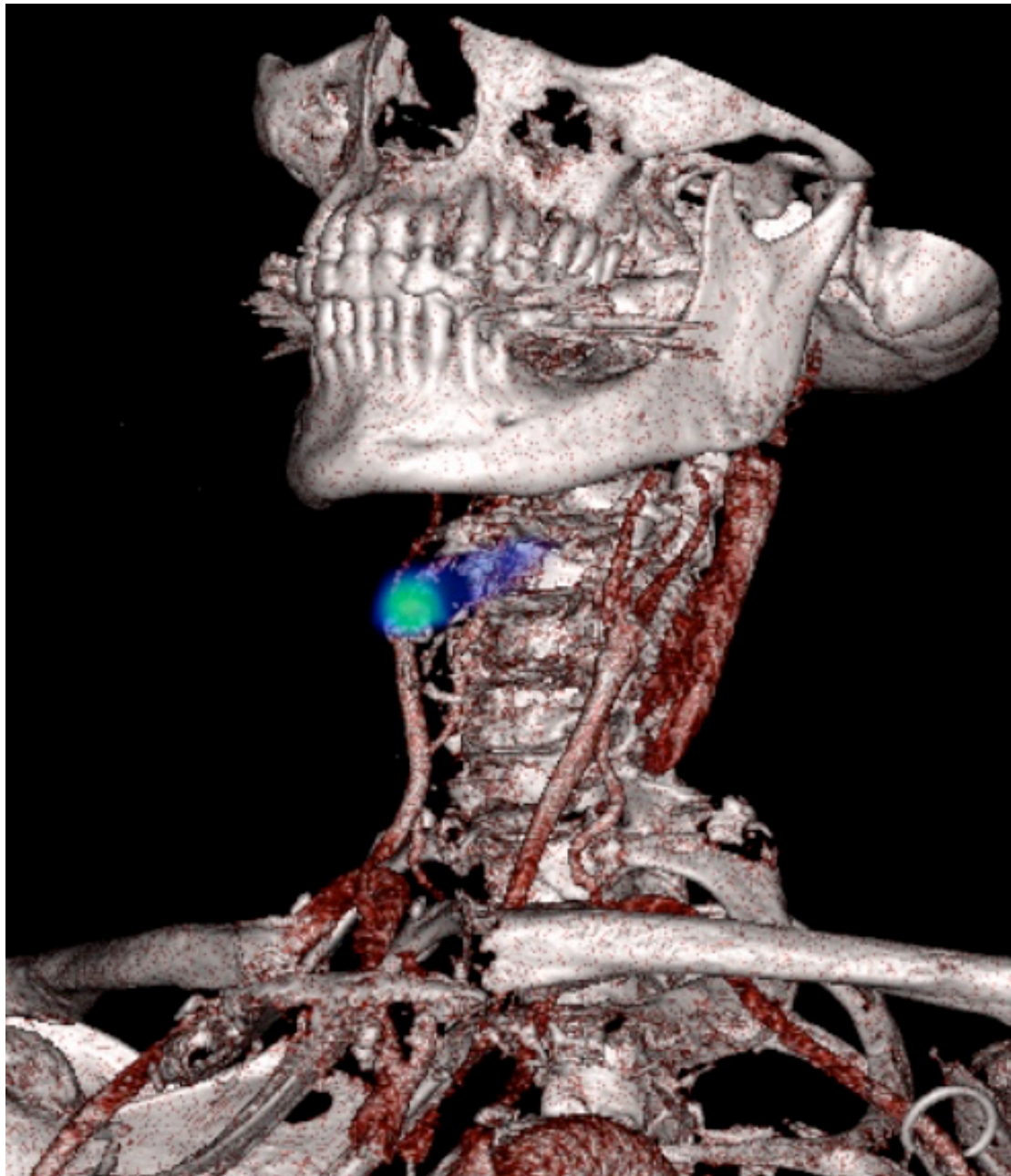
Dr Nicholas Evans

MA (Cantab.) MB BChir MRCP

Gonville & Caius College  
Department of Clinical Neurosciences  
University of Cambridge

This dissertation is submitted for the degree of Doctor of Philosophy

October 2017



**NaF-PET Image showing a symptomatic right internal carotid artery atheroma.  
Wellcome Image Award winner 2017  
(©Nicholas Evans/Wellcome Images)**

## Summary

A carotid atherosclerotic plaque represents a nidus of inflammation mere centimetres below the blood-brain barrier. This inflammation, along with associated regions of microcalcification, are histopathological features of atheroma at risk of rupture (so-called “vulnerable plaques”) that trigger thromboembolic stroke. While conventional clinical imaging simply measures the degree of vessel stenosis, it is a crude measure that reveals little of the metabolic processes affecting plaque vulnerability.

Our research demonstrates the utility of positron emission tomography (PET) using  $^{18}\text{F}$ -fluorodeoxyglucose (FDG) and  $^{18}\text{F}$ -sodium fluoride (NaF), measuring inflammation and microcalcification respectively, to identify culprit carotid atheroma *in vivo*, and establish how these processes influence plaque vulnerability.

Furthermore, for stroke care it is the downstream thromboembolic effects upon the brain that are key. While proinflammatory conditions may increase the risk of stroke, the relationship between atheroma inflammation and the peri-infarct inflammatory response following a stroke remains poorly defined. Our work demonstrates how inflammatory activity in symptomatic carotid atheroma, measured using PET, influences both chronic small vessel disease and the evolution of lesion volume in the post-stroke period.

Using metabolic imaging we can both identify vulnerable atheroma *in vivo* and demonstrate how these processes affect infarct evolution. We show that whilst inflammation is a generalised process, microcalcification is a focal process that may represent a point of maximum vulnerability. These results also reveal the complexity of the atheroma-brain interaction that may simultaneously trigger events while also influencing stroke evolution in the early recovery period. This has important implications for understanding pathophysiology of both atherosclerosis and stroke evolution, advancing drug-discovery, and potential clinical applications to minimise the impact from this devastating disease.



## **Declaration**

This dissertation is the result of my own work and includes nothing which is the outcome of work done in collaboration except as declared in the Preface and specified in the text.

It is not substantially the same as any that I have submitted, or, is being concurrently submitted for a degree or diploma or other qualification at the University of Cambridge or any other University or similar institution except as declared in the Preface and specified in the text. I further state that no substantial part of my dissertation has already been submitted, or, is being concurrently submitted for any such degree, diploma or other qualification at the University of Cambridge or any other University or similar institution except as declared in the Preface and specified in the text.

It does not exceed the prescribed word limit for the Clinical Medicine and Clinical Veterinary Medicine Degree Committee (60,000 words).

The work described in this thesis has been conducted primarily in the Department of Clinical Neurosciences at the University of Cambridge; and Ward R2, Neurovascular outpatient clinics, the PET/CT unit, and the Magnetic Resonance Imaging and Spectroscopy (MRIS) unit at Addenbrooke's Hospital, Cambridge University Hospitals NHS Foundation Trust.

I was personally involved in the drafting of the protocol for the Imaging Carotid Atherosclerosis in the Recovery and Understanding of Stroke Severity (ICARUSS) Study and led the application through Research and Development, ARSAC, and Research Ethics Committee approvals.

I have actively screened and recruited participants into the study, performed data collection and clinical examinations, and been present for the imaging sessions undertaken. I have personally analysed all the ICARUSS study imaging and clinical datasets, including statistical analysis.

The work was conducted with the support of the following individuals:

Professor Jonathan Gillard (Professor of Neuroradiology, University of Cambridge), and Drs Martin Graves and Andrew Patterson (both Clinical Scientists, Department of Radiology, University of Cambridge) assisted with MRI protocol development.

Dr John Buscombe (Clinical Lead and Consultant in the Department of Nuclear Medicine, Addenbrooke's Hospital) held the study ARSAC licence and reported the studies from a clinical governance perspective. He and Dr Sarah Heard (Nuclear Medicine Physicist, Addenbrooke's Hospital) assisted with PET/CT protocol development.

Mr Mohammed Chowdhury (Clinical Research Fellow, Division of Vascular Surgery, Department of Surgery, University of Cambridge) assisted with inter-rater testing for NaF-PET/CT as described in Chapter Three.

Dr Jason Tarkin (Clinical Research Fellow, Division of Cardiovascular Medicine, Department of Medicine, University of Cambridge) performed FDG-PET/CT analysis of participants in the VISION study, the results of which are used as a comparator for results presented in Chapter Four.

Miss Jessica Walsh (Research Associate, Department of Clinical Neurosciences, University of Cambridge) assisted with inter-rater testing for Fazekas scale scoring as described in Chapter Five.

Dr Simon Bond (Lead Statistician, Cambridge Clinical Trials Unit, Addenbrooke's Hospital) assisted with the initial statistical design and power calculations. Drs Loes Rutten-Jacobs and Ali Amin (both Research Associates, Department of Clinical Neurosciences, University of Cambridge) provided guidance for statistical analysis as described in Chapter Two.

This work has been supervised throughout by Drs Elizabeth Warburton and James Rudd (Primary Supervisor and Secondary Supervisor respectively).

## **Dedication**

At the end of the PhD it is hard to fully express what the last four years has meant to me. What started as an opportunity to explore research and take a side-step from clinical work turned into a life-changing experience that has fundamentally changed my approach to medicine. This change – both in myself and life around me – has provided new challenges and opportunities, and ultimately proven extremely rewarding. It would not have been possible without the large group of people with whom it has been a privilege to work.

The teams in PET/CT (Vic, Helen, Angie, Rob, Katie, Sue x2, Sarah Heard, John Buscombe) and MRIS (Ilse Joubert, Dario Prudencio, Wendy Phillips, Andrew Patterson, and Martin Graves) have been fantastic; knowledgeable, enthusiastic, and supportive of innumerable requests for scanning slots.

The support of the clinical team on R2 has been immense and I'm incredibly grateful. The enthusiasm that the research nurses (Diana Day, Elaine Amis, Jenny Mitchell, Jo Mcgee, Sarah Finlay, Nicki Church), SpRs (Lané van der Poel, James Bailey, Helen Hayhoe, Derek Hayden, Caoilfhionin O'Donoghue, Denish Chandrasena), and consultants (Eoin O'Brien, Niamh Hannon, Kayvan Khadjooi, Peter Martin) have shown for the project, and their genuine commitment to it, has been uplifting and key to its success.

R3 has been my home for the last few years and it has undergone a myriad of changes in both structure and personnel over this time. The sheer number of people makes it hard to give credit to each of them, but I particularly want to thank Loes Rutten-Jacobs for always being ready to provide guidance on statistics and life in general, Rhea Tan for her enthusiasm, Isuru Induruwa for chats over a range of drinks in a variety of countries, Brie Stark for always being ready to talk about rowing, and Hilary Gibson for both her support and her tolerance in printing things out for me for four years due to my failure to figure out how the printer worked. I also want to thank Hugh Markus for his professorial guidance and encouragement.

Staring at multicoloured blobs all day has done little for my eyesight but has formed a bond of solidarity with those in similar situations. It has been a pleasure working with Jason Tarkin and Mo Chowdhury, and I look forward to ongoing collaborations and friendship with them.

The study was dependent upon the goodwill and enthusiasm from the participants and their families. To have completed a rigorous scanning protocol in the early stages after stroke is a testament to their commitment and I am extremely grateful to them.

The support of The Dunhill Medical Trust has been key and it has been a pleasure working with them. Their mission to improve the health of an ageing population is vital, particularly given current population trends.

I have been incredibly fortunate to have two fantastic supervisors over the course of the PhD. James' understanding of the topic, attention to detail, and overall productivity is a model for aspiring clinical academics. Liz's knowledge of stroke, approach to research, and mentorship is nothing short of inspirational. Her enthusiasm in all things and commitment to patients is an exemplar of a true physician.

I want to thank my family for all their love and support, both during the PhD and always. Despite being 'real' doctors, both Dad and Jessica have taken an honorary doctor under their wings and tried to make him into something approaching a halfway competent scientist. Dad's support and sacrifices in getting to me to this point are a testament to him as a father, and Mum would be proud of him for finally getting both their children to graduate. Diolch yn fawr iawn.

Throughout this entire endeavour, Jessica has remained my biggest supporter, my most constructive critic, and my best friend. My admiration of her intelligence and grace continues to grow with each passing year and is exceeded only by my love for her. Thank you for everything.

Finally, I want to dedicate this work to the most significant change in my life. Thomas, thank you for brightening every day with a smile.

## Table of Contents

	<b>Page</b>
i. Summary	1
ii. Declaration	3
iii. Dedication	5
iv. Table of Contents	7
v. List of Figures	15
vi. List of Tables	18
vii. Glossary of Terms	23

### **Chapter One: Carotid Atherosclerosis: Clinical Context, Pathophysiology, and Imaging**

1.1 Carotid atherosclerosis: clinical context, pathophysiology, and imaging	28
1.1.1 Clinical aspects of large-vessel aetiology stroke	28
1.1.2 Anatomical criteria in the management of carotid stenosis	30
1.1.3 Vascular remodeling in the presence of atheroma	31
1.1.4 The cellular and molecular basis of atherogenesis	33
1.1.5 The ‘vulnerable plaque’ hypothesis	37
1.1.6 Microcalcification in atherosclerosis	43
1.1.7 Arterial macrocalcification	45
1.1.8 Atherothrombosis in carotid atherosclerosis	45
1.1.9 Morphological imaging using Magnetic Resonance Imaging	48
1.1.10 Pathophysiological imaging using Positron Emission Tomography	49
1.1.11 PET/CT applications in atherosclerosis drug development trials	54
1.1.12 Atherosclerosis and its effects on the brain	55
1.2 Objectives of the thesis	57

### **Chapter Two: Study Participants and General Methods**

2.1 The ICARUSS Study: approvals and support	58
2.2 Study eligibility and recruitment	58
2.3 Study investigations	63
2.4 PET/CT technical and methodological information	65

2.4.1	NaF-PET/CT scanning parameters	65
2.4.2	Carotid CT angiography	65
2.4.3	FDG-PET/CT scanning parameters	66
2.4.4	Radiation exposure	67
2.4.5	Image co-registration	68
2.4.6	Radiotracer uptake measurement	68
2.4.7	PET methodological considerations	72
	2.4.7.1 Partial volume correction	72
	2.4.7.2 SUV versus TBR	73
	2.4.7.3 Reproducibility	74
2.5	CT calcium scoring of the carotid artery	75
2.6	MRI technical and methodological information	77
	2.6.1 General MRI information	77
	2.6.2 MRI brain	78
	2.6.3 Carotid MRA	78
	2.6.4 Assessment of leukoaraiosis	79
	2.6.5 Measurement of brain lesion volume	80
2.7	Clinical assessments	82
2.8	Blood biomarkers	83
2.9	Statistical analysis	83

**Chapter Three: Sodium Fluoride PET for Identifying Culprit Carotid Atheroma and Investigating the Relationship between Microcalcification and Macrocalcification**

3.1	Introduction	86
	3.1.1 Aims of the chapter	86
	3.1.2 <i>In vivo</i> NaF-PET imaging	86
	3.1.2.1 NaF-PET imaging in asymptomatic plaques	87
	3.1.2.2 NaF imaging in symptomatic and vulnerable plaques	89
	3.1.3 <i>Ex vivo</i> NaF-PET histological validation	91
	3.1.4 Carotid artery macrocalcification and stroke risk	93
3.2	Methods	96
3.3	Results	97

3.3.1	Study population	97
3.3.2	NaF uptake in symptomatic and asymptomatic arteries	99
3.3.2.1	NaF SUVs in symptomatic and asymptomatic arteries	99
3.3.2.2	NaF TBRs in symptomatic and asymptomatic arteries	101
3.3.3	Relationship of NaF uptake to stroke severity	102
3.3.4	Relationship between NaF uptake and degree of luminal stenosis	104
3.3.5	Spatial distribution of NaF uptake	105
3.3.6	Comparison of SUV and TBR readings	107
3.3.7	Reproducibility	109
3.3.8	NaF uptake and risk factors	109
3.3.8.1	Univariable analysis of NaF uptake according to risk factors	109
3.3.8.2	Multivariable analysis of NaF uptake according to risk factors	109
3.3.9	Relationship with hsCRP	112
3.3.10	Carotid calcification scoring	113
3.3.10.1	Carotid artery calcium score	113
3.3.10.2	Carotid artery calcium volume	115
3.3.10.3	Carotid artery calcium mass	117
3.3.11	Spatial distribution of macrocalcification	119
3.3.12	Relationship between NaF uptake and macrocalcification	120
3.4	Discussion	124
3.4.1	NaF-PET to identify culprit atheroma	124
3.4.2	Spatial distribution of NaF uptake	126
3.4.3	Comparison of measures of NaF uptake	129
3.4.4	Carotid calcification and culprit arteries	131
3.4.5	Relationship between NaF uptake and macrocalcification	132
3.4.6	Relationship between NaF uptake, calcification, and vascular risk profile	136
3.4.6.1	Prior statin use	137
3.4.6.2	Age	139
3.4.6.3	Smoking	141
3.4.6.4	Sex	142
3.4.6.5	Lipid profile	144

3.4.6.6 Cardiovascular history	144
3.4.6.7 Antiplatelet therapy	146
3.4.6.8 Other risk factors	146
3.4.7 Strengths of this study	147
3.4.8 Limitations of this study	148
3.5 Summary of findings	149

## **Chapter Four: Dual Tracer FDG and NaF PET to Investigate the Relationship between Inflammation and Microcalcification**

4.1 Introduction	150
4.1.1 Aims of the chapter	150
4.1.2 FDG-PET imaging of atherosclerosis	151
4.1.3 Lessons from dual FDG and NaF PET studies	155
4.2 Methods	156
4.3 Results	156
4.3.1 Study population	156
4.3.2 FDG uptake in symptomatic versus asymptomatic arteries	158
4.3.3 Spatial patterns of inflammation, microcalcification, and macrocalcification	161
4.3.4 Relationship between FDG uptake and macrocalcification	166
4.3.5 Variation in the relationship between FDG and NaF uptake according to macrocalcification	168
4.3.6 FDG uptake in TIA versus stroke	169
4.3.7 Effect of cardiovascular risk factors on FDG uptake	170
4.3.8 Multivariable analysis of FDG uptake according to risk factors	170
4.3.9 hsCRP and the inflammation/microcalcification/macrocalcification complex	172
4.4 Discussion	174
4.4.1 FDG-PET can differentiate between symptomatic versus asymptomatic atheroma in individuals with stroke	174
4.4.2 Spatial distribution of inflammation relative to microcalcification	179
4.4.3 Physiological relationship between inflammation and macrocalcification	187

4.4.4	Physiological relationship inflammation and microcalcification, and modulation by macrocalcification	189
4.4.5	Risk factors affecting FDG uptake	191
4.4.6	hsCRP as a biomarker in specific plaque types	191
4.5	Summary of findings	192

## **Chapter Five: Carotid Atherosclerosis and Small Vessel Disease**

5.1	Introduction	193
5.1.1	Aims of this chapter	193
5.1.2	Introduction to small vessel disease	193
5.1.3	Relationship between carotid disease and small vessel disease	196
5.1.4	Pathophysiology of small vessel disease	199
5.1.5	Endothelial failure, inflammation, and blood-brain barrier dysfunction	200
5.2	Methods	202
5.3	Results	202
5.3.1	Study cohort	202
5.3.2	FDG uptake according to leukoaraiosis severity	204
5.3.3	Logistic regression of vascular features in relation to leukoaraiosis severity	206
5.3.4	NaF uptake according to leukoaraiosis severity	210
5.3.5	Macrocalcification and leukoaraiosis severity	212
5.3.6	hsCRP and leukoaraiosis severity	212
5.3.7	Fazekas score reproducibility	212
5.4	Discussion	212
5.4.1	Association between carotid plaque physiology and white matter disease	212
5.4.2	Risk factors associated with leukoaraiosis	214
5.4.3	Limitations	215
5.4.4	Implications and future work	216
5.5	Summary of findings	217

## **Chapter Six: Inflammation within Carotid Atheroma and the Evolution of Cerebral Infarction**

6.1 Introduction	218
6.1.1 Aims of this chapter	218
6.1.2 Inflammatory pathways contributing to infarct volumes	218
6.1.3 The microglial response in ischaemic stroke	219
6.1.4 Disruption of the blood-brain barrier in acute stroke	221
6.1.5 Infiltration of circulating inflammatory cells into the central nervous system	223
6.1.6 Inflammatory cytokines and their effect on infarct development	224
6.1.7 Thromboinflammation	224
6.1.8 Understanding the evolution of acute ischaemic stroke using PET	224
6.1.8.1 PET imaging of the developing acute infarct	225
6.1.8.2 PET imaging of post-infarct neuroinflammation	228
6.1.9 Pathophysiology of MRI lesions	230
6.2 Methods	230
6.3 Results	231
6.3.1 Study cohort	231
6.3.2 Baseline infarct volumes	232
6.3.3 Follow-up infarct volumes and evolution	233
6.3.4 Relationship between FDG uptake and baseline DWI volume	233
6.3.5 Relationship between FDG uptake and baseline FLAIR volume	234
6.3.6 Relationship between FDG uptake and baseline DWI and FLAIR mismatch	235
6.3.7 Relationship between FDG uptake and follow-up FLAIR volume	236
6.3.8 Relationship between FDG uptake and FLAIR lesion evolution	237
6.3.9 Role of thrombolysis in lesion evolution	240
6.3.10 Carotid endarterectomy in lesion evolution	241
6.3.11 Stroke event to baseline MRI interval and lesion characteristics	241
6.3.12 Regression analysis of carotid FDG uptake and FLAIR lesion evolution	241
6.3.13 hsCRP and infarct evolution	243
6.4 Discussion	243

6.4.1	Carotid inflammation and baseline infarct volume	243
6.4.2	Carotid inflammation, final lesion size, and lesion evolution	244
6.4.3	Limitations	248
6.4.4	Future work	249
6.5	Summary of findings	249

## **Chapter Seven: Clinical Outcomes**

7.1	Introduction	250
7.1.1	Aims of this chapter	250
7.1.2	Functional outcomes	250
7.1.3	Post-stroke cognition	252
7.2	Methods	254
7.3	Results	254
7.3.1	Modified Rankin scale outcomes	254
7.3.1.1	Baseline modified Rankin scale	254
7.3.1.2	Three-month modified Rankin scale	255
7.3.2	Barthel index	255
7.3.2.1	Baseline Barthel index	255
7.3.2.2	Three-month Barthel index	256
7.3.3	Cognitive function	256
7.3.3.1	Baseline MoCA	256
7.3.3.2	Follow-up MoCA	257
7.3.3.3	Multiple logistic regression analysis of cognitive results	259
7.3.4	Contribution of cerebrovascular disease	260
7.4	Discussion	261
7.4.1	Cognitive outcomes	261
7.4.2	Modified Rankin scale outcomes	263
7.4.3	Barthel index outcomes	263
7.5	Summary of findings	264

<b>Chapter Eight: From the Vulnerable Plaque to the Vulnerable Brain: General Discussion and Future Work</b>	
8.1 Summary of work	265
8.1.1 Inflammation, microcalcification, and the vulnerable plaque	265
8.1.2 Beyond the vulnerable plaque – the “vulnerable brain”	266
8.1.3 Beyond the biology – the “vulnerable patient”	268
8.2 Alternative approaches and future directions in PET imaging of atherosclerosis	268
8.3 Planned papers from this thesis	271
8.4 Ongoing and future work	272
8.4.1 Vascular imaging	272
8.4.2 Imaging the vulnerable brain	273
8.4.3 Considerations for future work	274
8.5 Conclusion	275
<b>Appendix A: Prizes, Papers, and Presentations during PhD</b>	277
<b>Appendix B: Degrees of Carotid Stenosis</b>	280
<b>Appendix C: NaF Univariable Analysis</b>	281
<b>Appendix D: FDG Univariable Analysis</b>	288
<b>Appendix E: Vascular Risk Factors Influencing FDG Uptake</b>	295
E.1 Smoking and FDG uptake	295
E.2 Diabetes and hyperglycaemia	298
E.3 Other risk factors	301
<b>Appendix F: hsCRP as a Biomarker in Specific Plaque Types</b>	303
<b>References</b>	312

## List of Figures

	<b>Page</b>
<b>Chapter One</b>	
1.1	Plaque morphology and recurrent events 29
1.2	Initiation of atherosclerosis 33
1.3	Macrophage accumulation in the atherosclerotic plaque 37
1.4	Recruitment of circulating monocytes 38
1.5	Recruitment of T lymphocytes 39
1.6	The natural history of atherosclerosis 42
1.7	Microcalcification in the fibrous cap 44
1.8	Radioligand targeting of plaque pathophysiology 52
<b>Chapter Two</b>	
2.1	Flow diagram of participant recruitment 61
2.2	Flow chart of study procedures 64
2.3	Schema of the relationship between SHS, MDS, and WV readings 70
2.4	Radiological representation of SHS, MDS, and WV readings 71
2.5	Semi-automated brain lesion marking 81
<b>Chapter Three</b>	
3.1	NaF histological validation 93
3.2	NaF uptake in symptomatic disease 98
3.3	NaF SUV <sub>max</sub> 99
3.4	NaF SUV <sub>mean</sub> 100
3.5	NaF TBR <sub>max</sub> 101
3.6	NaF TBR <sub>mean</sub> 102
3.7	Associations between NIHSS and symptomatic artery SUVs 103
3.8	NaF SUVs categorised by degree of luminal stenosis 104
3.9	NaF TBRs categorised by degree of luminal stenosis 105
3.10	Spatial distribution of NaF SUV <sub>max</sub> 106
3.11	Spatial distribution of NaF SUV <sub>mean</sub> 106

3.12	Spatial distribution of NaF $TBR_{max}$	107
3.13	Spatial distribution of NaF $TBR_{mean}$	107
3.14	Associations between corresponding NaF SUV and TBR measures	108
3.15	Associations between age and carotid artery calcium score	113
3.16	Spatial distribution of CACS	120
3.17	Associations between CACS and NaF SUVs in symptomatic arteries	122
3.18	Associations between CACS and NaF SUVs in asymptomatic arteries	123
3.19	Comparative spatial distributions of $SUV_{max}$ and $TBR_{max}$	126
3.20	Composite NaF SUV spatial distributions	127
3.21	Composite NaF TBR spatial distributions	128
3.22	NaF uptake in the carotid bifurcation according to the degree of macrocalcification	133
3.23	Spatial distribution of NaF SUVs and macrocalcification	135
3.24	Spatial distribution of NaF TBRs and macrocalcification	135

## Chapter Four

4.1	Increased FDG uptake in symptomatic carotid atherosclerosis	159
4.2	FDG SUVs by degree of luminal stenosis	160
4.3	FDG TBRs by degree of luminal stenosis	161
4.4	Spatial distribution of FDG $SUV_{max}$	162
4.5	Spatial distribution of FDG $SUV_{mean}$	162
4.6	Spatial distribution of FDG $TBR_{max}$	163
4.7	Spatial distribution of FDG $TBR_{mean}$	163
4.8	Composite FDG SUV spatial distributions	164
4.9	Composite FDG TBR spatial distributions	164
4.10	FDG uptake in the carotid bifurcation according to degree of macrocalcification	168
4.11	Comparative spatial distributions of FDG and NaF $SUV_{max}$	179
4.12	Comparative spatial distributions of FDG and NaF $SUV_{mean}$	180
4.13	Comparative spatial distributions of FDG and NaF $TBR_{max}$	180
4.14	Comparative spatial distributions of FDG and NaF $TBR_{mean}$	181
4.15	Blood flow at an arterial branch point	183
4.16	Blood flow across an atherosclerotic plaque	184

## **Chapter Five**

5.1	Carotid FDG uptake according to leukoaraiosis severity	204
-----	--	-----

## **Chapter Six**

6.1	Derivation of cohorts in the ischaemic lesion volume part of the study	231
6.2	FLAIR lesion evolution	238
6.3	Association between FDG uptake and change in FLAIR volume	239
6.4	Association between FDG uptake and change in FLAIR volume (adjusted)	240

## **Chapter Seven**

7.1	Modified Rankin scale for study participants at baseline and three months	254
-----	---	-----

## **Chapter Eight**

8.1	Direct thrombus imaging	273
-----	-------------------------	-----

## **Appendix E**

E.1	Pathophysiological mechanisms of smoking in vascular disease	297
-----	--	-----

## **Appendix F**

F.1	hsCRP, FDG uptake, and macrocalcification	305
F.2	hsCRP, FDG uptake, and macrocalcification (adjusted)	305

## List of Tables

	<b>Page</b>
<b>Chapter One</b>	
1.1 Radiotracers used in cerebrovascular PET studies	50
<b>Chapter Two</b>	
2.1 Inclusion and exclusion criteria for study population	59
2.2 Summary of participant clinical characteristics	62
2.3 MRI brain imaging parameters	78
2.4 Carotid MRA imaging parameters	79
<b>Chapter Three</b>	
3.1 Clinical characteristics of the NaF-PET/CT cohort	97
3.2 NaF SUV <sub>max</sub> readings for symptomatic and asymptomatic carotid arteries	99
3.3 NaF SUV <sub>mean</sub> readings for symptomatic and asymptomatic carotid arteries	100
3.4 NaF TBR <sub>max</sub> readings for symptomatic and asymptomatic carotid arteries	101
3.5 NaF TBR <sub>mean</sub> readings for symptomatic and asymptomatic carotid arteries	102
3.6 Regression modeling of clinical risk factors associated with NaF SUV	109
3.7 Regression modeling of clinical risk factors associated with NaF TBR	111
3.8 Univariable analysis for CACS and risk factors	114
3.9 Multiple regression analysis of risk factors associated with CACS	115
3.10 Univariable analysis of carotid artery calcium volume and vascular risk factors	116
3.11 Multiple regression analysis of risk factors associated with carotid artery calcium volume	117

3.12	Univariable analysis of carotid artery calcium mass and vascular risk factors	118
3.13	Multiple regression analysis of risk factors associated with carotid artery calcification mass	119
3.14	Correlations between CACS and NaF TBRs	123
3.15	Comparison of NaF uptake between bifurcation and non-bifurcation	128
3.16	Comparison of NaF uptake between bifurcation and non-bifurcation according to symptomatic and non-symptomatic carotid arteries	129
3.17	Summary of vascular risk factors found to be associated with NaF uptake in literature to date	137

## **Chapter Four**

4.1	Characteristics of the 26 participant cohort	157
4.2	Characteristics of the 27 participant cohort	157
4.3	Comparison of FDG SUV <sub>max</sub> and SUV <sub>mean</sub> measures between symptomatic and asymptomatic carotid arteries	158
4.4	Comparison of FDG TBR <sub>max</sub> and TBR <sub>mean</sub> measures between symptomatic and asymptomatic carotid arteries	159
4.5	Comparison of FDG and NaF uptake in bifurcation and non-bifurcation regions	165
4.6	Comparison of FDG and NaF uptake between bifurcation and non-bifurcation regions according to symptomatic and non-symptomatic carotid arteries	165
4.7	Correlations between FDG uptake and whole artery CACS in symptomatic and asymptomatic arteries	166
4.8	Correlations between FDG and NaF uptake in the carotid bifurcations according to the degree of macrocalcification	169
4.9	FDG uptake in TIA and stroke	170
4.10	Multiple linear regression for vascular risk factors and FDG TBRs	171
4.11	Correlations between FDG uptake measures and hsCRP by extent of arterial calcification	173
4.12	Correlations between NaF uptake measures and hsCRP by extent of arterial calcification	174

## **Chapter Five**

5.1	Clinical characteristics according to dichotomised severity of leukoaraiosis	203
5.2	Comparison of FDG uptake between Fazekas score dichotomisation for culprit and non-culprit carotid arteries	205
5.3	Multiple logistic regression for factors associated with severity of leukoaraiosis for the non-culprit artery	207
5.4	Multiple logistic regression for factors associated with severity of leukoaraiosis for the culprit artery	209
5.5	Comparison of NaF uptake between dichotomised leukoaraiosis severity cohorts for culprit and non-culprit carotid arteries	211

## **Chapter Six**

6.1	Clinical characteristics of each cohort	232
6.2	Correlations between FDG TBR measures and baseline DWI total lesion volume	233
6.3	Correlations between FDG TBR measures and baseline DWI primary lesion volume	234
6.4	Correlations between FDG TBR measures and baseline FLAIR total lesion size	234
6.5	Correlations between FDG TBR measures and baseline FLAIR primary lesion size	235
6.6	Correlations between FDG TBR measures and difference in volume between FLAIR and DWI total lesion volumes	235
6.7	Correlations between FDG TBR measures and difference in volume between FLAIR and DWI primary lesion volumes	236
6.8	Correlations between FDG TBR measures and follow-up FLAIR total lesion size	236
6.9	Correlations between FDG TBR measures and follow-up FLAIR primary lesion size.	237
6.10	Correlations between FDG TBR and FLAIR total volume change	238

6.11	Correlations between FDG TBR and FLAIR primary lesion volume change	239
6.12	Regression analysis of factors associated with FLAIR primary lesion volume evolution	242

## **Chapter Seven**

7.1	Associations between FDG TBRs and baseline BI	256
7.2	Associations between FDG TBRs and three-month BI	256
7.3	Associations between FDG uptake and baseline MoCA score	257
7.4	FDG uptake measures in individuals with cognitive impairment and normal cognition at baseline	257
7.5	Associations between FDG uptake and three-month MoCA score	258
7.6	FDG uptake measures in individuals with cognitive impairment and normal cognition at three months	258
7.7	Multiple logistic regression for factors associated with cognitive impairment on three-month MoCA	259

## **Appendix B**

B.1	Symptomatic side and degree of stenosis in each carotid artery for each participant (in the 26 participant cohort)	280
-----	--	-----

## **Appendix C**

C.1	Correlations between age and NaF uptake	281
C.2	NaF uptake by sex	281
C.3	Correlations between BMI and NaF uptake	282
C.4	NaF uptake by smoking status	282
C.5	NaF uptake by diabetes status	283
C.6	NaF uptake by hypertension status	283
C.7	NaF uptake by statin therapy	284
C.8	Correlations between NaF uptake and lipid profile	284
C.9	NaF uptake by antiplatelet therapy	285

C.10	NaF uptake by cardiovascular history	285
C.11	NaF uptake by arterial side	286
C.12	Correlations between stroke onset-to-scan interval and NaF uptake	286
C.13	NaF uptake by thrombolysis status	287

## **Appendix D**

D.1	Association between age and FDG uptake	288
D.2	FDG uptake by sex	288
D.3	Association between BMI and FDG uptake	289
D.4	FDG uptake by smoking status	289
D.5	FDG uptake by diabetes status	290
D.6	FDG uptake by smoking status	290
D.7	FDG uptake by statin medication	291
D.8	Correlations between FDG uptake and lipid profile	291
D.9	FDG uptake by antiplatelet medication	292
D.10	FDG uptake by cardiovascular history	292
D.11	FDG uptake by artery side	293
D.12	Association between stroke onset-to-scan interval and FDG uptake	293
D.13	FDG uptake by thrombolysis	294
D.14	Association between FDG uptake and NIHSS	294

## **Appendix F**

F.1	Revised correlations between FDG uptake and hsCRP in symptomatic arteries with high CACS	306
-----	--	-----

## Glossary of Terms

1.5T	1.5 Tesla
3T	Three Tesla
2D	Two-dimensional
3D	Three-dimensional
ACAS	Asymptomatic Carotid Atherosclerosis Study
AIC	Akaike information criteria
ApoE	Apolipoprotein E
ATP	Adenosine triphosphate
BBB	Blood-brain barrier
BI	Barthel index
BMI	Body mass index
BMP	Bone morphogenetic proteins
BSP	Bone sialoprotein
CACS	Carotid artery calcium score
CANTOS	Canakinumab Anti-inflammatory Thrombosis Outcomes Study
CAS	Carotid artery stenting
CBF	Cerebral blood flow
Cbfa1	Core binding factor alpha 1
CCA	Common carotid artery
CCR	C-C chemokine receptor
CD	Cluster of differentiation
CEA	Carotid endarterectomy
ceMRA	Contrast-enhanced magnetic resonance angiogram
CI	Confidence interval
CMRO <sub>2</sub>	Cerebral metabolic rate of oxygen consumption
CRP	C-reactive protein
CT	Computed tomography
CTA	Computed tomography angiogram
DAMP	Danger-associated molecular pattern molecule
DC	Dendritic cell
DCE	Dynamic contrast-enhanced

DOTATATE	[1,4,7,10-tetraazacyclododecane-N,N',N'',N'''-tetraacetic acid]- d-Phe1,Tyr3-octreotate
DTI	Direct thrombus imaging
DWI	Diffusion-weighted imaging
ECST	European Carotid Surgery Trial
eGFR	Estimated glomerular filtration rate
FDG	Fluorodeoxyglucose
FMZ	Flumazenil
eNOS	Endothelial nitric oxide synthase
FLAIR	Fluid-attenuated inversion recovery
FMISO	Fluoromisonidazole
GABA	Gamma aminobutyric acid
GLUT	Glucose transporter
GRE	Gradient echo
GTM	Geometric transfer matrix
HADS	Hospital anxiety and depression scale
HbA <sub>1c</sub>	Glycated haemoglobin A <sub>1c</sub>
HDL	High density lipoprotein
HIF	Hypoxia-inducible transcription factor
HK	Hexokinase
HR	Hazard ratio
hsCRP	High sensitivity C-reactive protein
HU	Hounsfield unit
ICA	Internal carotid artery
ICAM	Intercellular adhesion molecule
ICC	Intra-class correlation coefficient
IGF	Insulin-like growth factor
IFN	Interferon
IL	Interleukin
IMT	Intima-media thickness
IPH	Intraplaque haemorrhage
IQR	Interquartile range
IRCP	International Commission on Radiological Protection

IVUS	Intravascular ultrasound
LDL	Low density lipoprotein
LDL-C	Low-density lipoprotein-cholesterol
LPS	Lipopolysaccharide
MAPK	Mitogen-activated protein kinase
MCAO	Middle cerebral artery occlusion
MCP	Monocyte chemoattractant protein
MDS	Most diseased segment
MDS SUV	Most diseased segment standardised uptake value
MDS TBR	Most diseased segment tissue-to-background ratio
MES	Microembolic signal
MGP	Matrix G1a protein
MMP	Matrix metalloproteinase
MMSE	Mini-mental state examination
MoCA	Montreal cognitive assessment
MRA	Magnetic resonance angiogram
MRI	Magnetic resonance imaging
mRS	Modified Rankin scale
MWT	Mean wall thickness
NaF	Sodium fluoride
NASCET	North American Symptomatic Carotid Endarterectomy Trial
NF- $\kappa$ B	Nuclear factor kappa-light-chain-enhancer of activated B cells
NIHSS	National Institutes for Health Stroke Scale
NK	Natural killer
NKT	Natural killer T-cell
NLR	Nucleotide-binding oligomerisation domain-like receptors
NO	Nitric oxide
NOD	Nucleotide-binding oligomerisation domain
OCSP	Oxford Community Stroke Project
OCT	Optical coherence tomography
OEF	Oxygen extraction fraction
OR	Odds ratio
oxLDL	Oxidised low-density lipoprotein

OXVASC	Oxford Vascular Study
PAR	Protease-activated receptor
PiB	Pittsburgh compound B
PBR	Peripheral benzodiazepine receptor
PET	Positron emission tomography
PK11195	<i>N</i> -methyl- <i>N</i> -[1-methylpropyl]-1-[2-chlorophenyl]-isoquinoline-3-carboxamide
PVC	Partial volume correction
PVE	Partial volume error
RANK	Receptor activator of nuclear factor- $\kappa$ B
RANKL	Receptor activator of nuclear factor- $\kappa$ B ligand
ROI	Region of interest
ROS	Reactive oxygen species
SD	Standard deviation
SHS	Single hottest slice
SHS SUV	Single hottest slice standardised uptake value
SHS TBR	Single hottest slice tissue-to-background ratio
SIS	Stroke impact scale
SNL	Selective neuronal loss
SST	Somatostatin receptor type
SUV	Standardised uptake value
SVD	Small vessel disease
T-reg	Regulatory T-lymphocyte
TBR	Tissue-to-background ratio
TC	Total cholesterol
TCACS	Total carotid arterial calcification score
TCD	Transcranial Doppler
TE	Echo time
TF	Tissue factor
TGF	Transforming growth factor
TI	Inversion time
TIA	Transient ischaemic attack
TIMP	Tissue inhibitor of metalloproteinase

TLR	Toll-like receptor
TNF	Tumour necrosis factor
TOF	Time of flight
TR	Repetition time
TSPO	Translocator protein
UK-TIA	United Kingdom Transient Ischaemic Attack Aspirin Trial
VEGF	Vascular endothelial growth factor
VCAM	Vascular cell adhesion molecule
VSMC	Vascular smooth muscle cell
WMH	White matter hyperintensity
WV SUV	Whole vessel (median) standardised uptake value
WV TBR	Whole vessel (median) tissue-to-background ratio

## Chapter One:

### Carotid Atherosclerosis: Clinical Context, Pathophysiology, and Imaging

#### 1.1 Carotid atherosclerosis: clinical context, pathophysiology, and imaging

##### *1.1.1 Clinical aspects of large-vessel aetiology stroke*

Ischaemic stroke is a heterogeneous disease in both its presentation and aetiology. Large artery atherosclerosis – literally, “hardening of arteries” – is estimated to underlie between 15% to 25% of ischaemic strokes (Lanfranconi and Markus, 2013, Chung et al., 2014), and consequently the carotid arteries represent one of the most dangerous few centimetres in the human body. Atherosclerosis involves the development of lipid-rich atheroma (also termed “plaques”) in response to vascular risk factors, including age, male sex, ethnicity, hyperlipidaemia, hypertension, smoking, and diabetes mellitus (Arboix, 2015). Carotid atherosclerosis will typically occur on the background of systemic atherosclerosis, with concomitant disease within the coronary arteries estimated to occur in 28-58% of asymptomatic individuals (Baber et al., 2015, Sillesen et al., 2012, Bjerrum et al., 2013).

Unlike coronary artery disease where angina may precede an infarct, strokes may have few ischaemic warning symptoms. However, when such transient warning symptoms do occur in a cerebrovascular setting they are often a harbinger of imminent infarcts. The risk of stroke following a transient ischaemic attack (TIA) is highest in the immediate period; a systematic review by Rothwell et al. including the Oxford Vascular Study (OXVASC), Oxfordshire Community Stroke Project (OCSP), UK TIA Aspirin Trial (UK-TIA), and European Carotid Surgery Trial (ECST) showed a close temporal relationship between a TIA and first stroke, with 48% of harbinger TIAs occurring within the seven days preceding stroke (Rothwell and Warlow, 2005). Whilst this has underpinned the target for early surgical intervention, a number of studies have suggested that features of the atherosclerotic plaque other than the degree of stenosis influence recurrence in large artery atherosclerotic stroke. In a pooled analysis from retrospective registry data and a prospective Dublin study, the recurrence rate of ischaemic events in individuals with symptomatic carotid atherosclerosis was 11.5% within two weeks, rising to 18.8% by 90 days. While the

risk of recurrence was associated with age and location of ischaemia, the degree of stenosis and vascular risk factors were not significantly associated with recurrence on multivariable analysis (Johansson et al., 2016).

Prognostic modeling of the ECST data showed that simply using the degree of carotid stenosis overlooks other important considerations required for risk stratification, where Rothwell et al. considered plaque characteristics in deriving a risk stratification score for subsequent stroke events. Whilst a strong determinant for future events, the degree of carotid stenosis counted only for a maximum score of two, with a score of four being the cut-off for a high risk plaque. Plaque characteristics, including plaque surface irregularity, were independently associated with risk in this model and mean that factors other than the degree of stenosis heavily influence the incidence of recurrent cerebrovascular events (**Figure 1.1**) (Rothwell and Warlow, 1999).

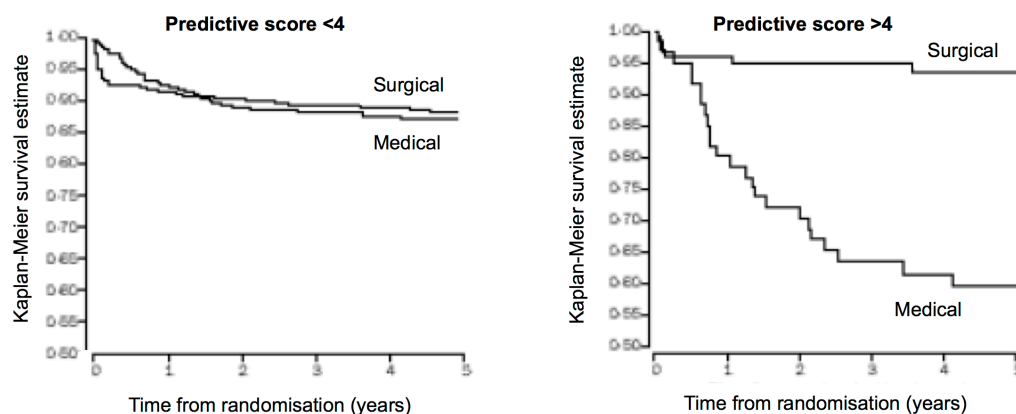


**Figure 1.1: Plaque morphology and recurrent events.** Effect on endarterectomy on risk of ipsilateral carotid territory major ischaemic stroke and operative major stroke or death in patients with 70-99% carotid stenosis, censoring non-stroke death, according to low risk (left) versus high-risk plaque features (right). Reproduced with permission from (Rothwell and Warlow, 1999).

The role of carotid atherosclerosis in stroke aetiology makes it an important risk factor for screening after a stroke. However, the relationship between the pathophysiological characteristics of the plaque and their effects on the pattern of stroke is poorly understood. Considerations other than the degree of stenosis are likely to play a role in the pathogenesis of an infarct. Subsequent sections will consider the

shortcomings of solely anatomical carotid artery criteria when considering the atherosclerotic process, and this and future chapters will discuss how the pathophysiology of the atheroma may influence stroke severity and recovery.

### *1.1.2 Anatomical criteria in the management of carotid stenosis*

Current clinical management of symptomatic carotid atherosclerosis (atherosclerosis that is the causative pathology for an ischaemic stroke or TIA) is determined by anatomical criteria. Symptomatic carotid atheroma may be removed surgically by a carotid endarterectomy (CEA). Two large studies have investigated how the degree of stenosis affects stroke recurrence and how this risk is modified by CEA. The North American Symptomatic Carotid Endarterectomy Trial (NASCET) demonstrated that CEA for symptomatic stenosis of 70-99% was strongly associated with a reduced rate of major or non-fatal stroke by 2 years compared with best medical therapy (North American Symptomatic Carotid Endarterectomy Trial Collaborators, 1991). CEA for moderate stenosis of 50-69% also resulted in a significant reduction in the risk of further cerebrovascular events compared to best medical therapy, though this risk reduction was less than for severe stenosis, and there was no benefit for surgery versus best medical therapy for stenosis of <50% (Barnett et al., 1998). The ECST, whilst using a different method to calculate stenosis, also found a significant risk reduction in future cerebrovascular events following CEA (European Carotid Surgery Trialists' Collaborative Group, 1998). In contrast, the Asymptomatic Carotid Atherosclerosis Study (ACAS) investigated asymptomatic carotid stenosis and discovered that CEA for stenosis of >60% offered a moderate but significant reduction in the aggregate risk over five years for ipsilateral stroke compared to aspirin (Executive Committee for the Asymptomatic Carotid Atherosclerosis Study, 1995). However, it is important to note that in each study the best medical therapy used in the control groups has now been superseded by improved pharmacological therapy.

The prevalence of asymptomatic carotid stenosis is hard to estimate and has not been studied in detail. A meta-analysis of 23,706 participants from four epidemiological studies estimated that the prevalence of asymptomatic moderate (50-69%) stenosis varied between 0.2% for men below 50 years and 7.5% for men aged over 80 years.

In women, the prevalence was 0% and 5% respectively. Severe asymptomatic carotid (70-99%) stenosis was 0.1% in men aged under 50 years and 3.1% in men aged 80 years and over. The prevalence in women was 0% and 0.9% in those aged under 50 and over 80 years respectively (de Weerd et al., 2010). The 11% 5-year risk of further stroke for those receiving best medical therapy in the ACAS trial means that the majority of the estimated prevalence of asymptomatic carotid stenosis will remain asymptomatic (Executive Committee for the Asymptomatic Carotid Atherosclerosis Study, 1995). Therefore, factors other than the degree of stenosis need to be considered for the pathogenesis of ischaemic stroke with carotid atheroma.

### *1.1.3 Vascular remodeling in the presence of atheroma*

Factors other than the degree of stenosis have been demonstrated to influence the stability of coronary plaques. Mann et al. showed that there was no relationship between the atheroma core volume and either the absolute size of the atheroma or the degree of stenosis of the symptomatic coronary arteries from post-mortem studies, where only 34.4% of plaques were predicted to be detectable on angiography (Mann and Davies, 1996). The presence of atheroma in angiographically normal coronary arteries suggests vascular remodeling to accommodate the plaque burden whilst maintaining a normal luminal diameter. Evidence to support this compensatory enlargement has been provided by intravascular ultrasound demonstrating increased total arterial area and internal elastic lamina area in the presence of atheroma and vascular risk factors, suggesting that the coronary arteries adapt to atheroma burden by outwards expansion rather than narrowing of the lumen (Nakamura et al., 1996, Hausmann et al., 1996). In a large study by Mintz et al. only 60 out of 884 symptomatic, but angiographically normal coronary arteries, were found to be normal using intravascular ultrasound (Mintz et al., 1995). Importantly, these results suggest that considering ischaemia entirely as a product of impaired flow misses an intrinsic pathophysiological process within the atheroma and it is this process that triggers rupture and thrombus formation that accounts for ischaemia in vessels with no significant observed stenosis.

Whether the same process of expansion occurs within the carotid artery remains a subject of debate. Magnetic resonance imaging (MRI) of symptomatic carotid stenosis

of 50-99% and asymptomatic stenosis of 70-99% has shown that expansive remodeling, the enlargement of the artery due to outward plaque growth, is significantly higher with symptomatic than asymptomatic disease (Yoshida et al., 2015). Furthermore, it is important to note that in this study the mean stenosis (using NASCET criteria) was significantly less in the symptomatic group (mean symptomatic stenosis was  $68.5\% \pm 21.3\%$ , mean asymptomatic stenosis was  $79.4\% \pm 8.85\%$ ,  $p=0.0011$ ), suggesting that a similar process to that occurring in the coronary arteries also occurs in the carotid arteries. Such results also suggest that the burden of atheroma in the carotid artery is not necessarily related to the degree of stenosis. However, in this study the authors did not comment upon the type and constituency of the atheroma (such as the degree of calcification) and whether this affected expansive remodeling or presence of symptoms.

Similar results to Yoshida et al. have also been seen using computed tomography angiograms (CTA). Symptomatic carotid arteries were found to have significantly higher expansive remodeling than asymptomatic carotid arteries, though there was no difference in either the degree of stenosis or maximum vessel thickness between symptomatic and asymptomatic groups (Hardie et al., 2007).

Expansive remodeling of the carotid artery has been linked with different patterns of atheroma. In a combined CTA and MRI study, stroke symptoms had a significantly higher prevalence in carotid arteries with positive (expansive) remodeling than negative (vessel shrinking) remodeling with the same degree of stenosis, whilst expansive remodeling was associated with higher signal intensities indicating lipid-rich cores or haemorrhage (Miura et al., 2011).

A further study using CTA to image symptomatic carotid arteries showed only a moderate correlation between plaque volume and the degree of luminal stenosis (Rozie et al., 2009). Therefore, the degree of luminal stenosis in the carotid artery and its use as an anatomical criterion for vascular surgery may overlook culprit atheroma. As the plaque burden may not be flow-limiting in its mechanism for causing a stroke it is necessary further consider how biological processes in the atheroma may trigger and affect cerebrovascular events.

#### 1.1.4 The cellular and molecular basis of atherogenesis

Atheroma formation is a gradual process whereby the formation of small fatty streaks (initiation) progresses via vertical and lateral growth resulting in coalescence (expansion). In turn, these coalescing areas begin to demonstrate intimal smooth muscle cell recruitment, collagen deposition, and formation of a fibrous cap (progression). Circulating monocytes are recruited during initiation and expansion phases, maturing into macrophages and endocytosing low density lipoprotein cholesterol (LDL-C), thereby transforming into “foam cells” that accumulate to form the necrotic core of fatty streaks and atheromatous plaques (Ross, 1999) (**Figure 1.2**).

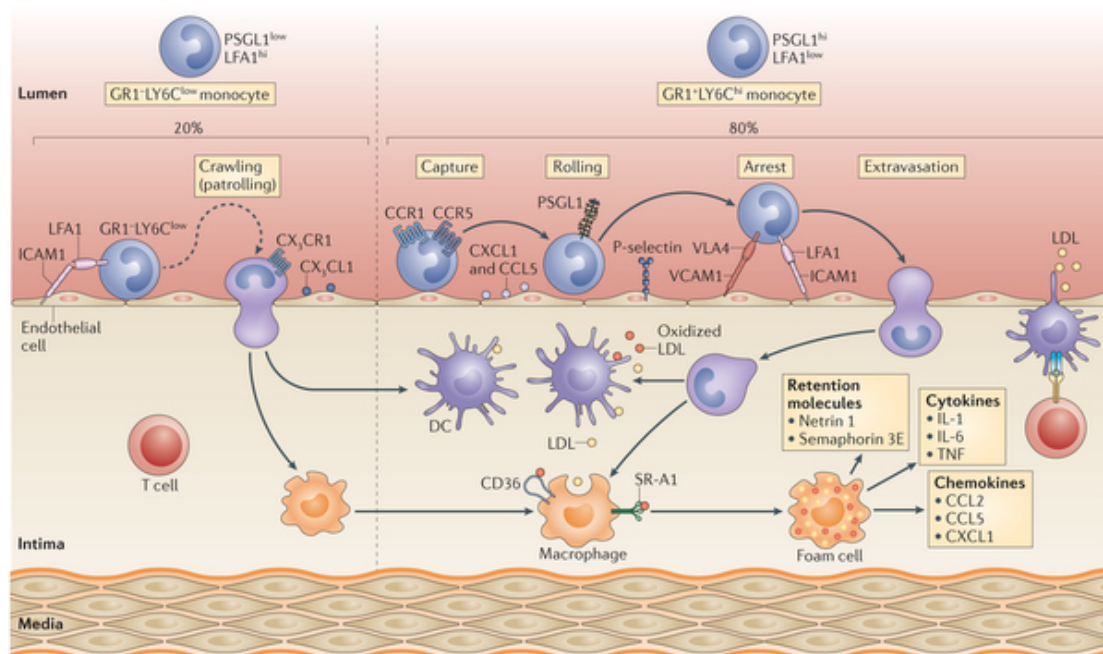


**Figure 1.2: Initiation of atherosclerosis.** Mechanisms regulating monocyte recruitment, accumulation, and maturation in plaques. Reproduced with permission from (Moore et al., 2013).

Key to the initiation of atherosclerosis is dysfunctional endothelial nitric oxide synthase (eNOS). In addition to its vasodilative effects, the anti-atherosclerotic effects of nitric oxide (NO) are numerous; inhibition of platelet aggregation and release of pro-atherogenic platelet-derived growth factors (Radomski et al., 1987, Alheid et al., 1987, Busse et al., 1987), downregulation of gene expression of chemoattractant proteins and adhesion proteins to reduce monocyte recruitment (Zeicher et al., 1995,

Tsao et al., 1997, Arndt et al., 1993, Kubes et al., 1991, Davenpeck et al., 1994, Gauthier et al., 1995, De Caterina et al., 1995, Tsao et al., 1996), and reduction in the proliferation of vascular smooth muscle cells (Garg and Hassid, 1989, Nakaki et al., 1990, Cayatte et al., 1994). Increased production of reactive oxygen species (ROS) in the presence of vascular risk factors leads to oxidative stress and the uncoupling of eNOS and inactivation of NO, thereby reducing the anti-atherosclerotic effects of NO and promoting leukocyte and platelet recruitment and activation (Forstermann, 2008, Li et al., 2014).

Reduced NO levels and endothelial dysfunction promotes the recruitment of monocytes into the atheroma through the upregulation of adhesion proteins located on the luminal side of vascular endothelium, notably vascular cell adhesion molecule-1 (VCAM-1) and intercellular adhesion molecule-1 (ICAM-1), that are cytokine-inducible members of the immunoglobulin gene superfamily that bind leukocytes (Springer, 1994). VCAM-1 is particularly associated with atheroma formation as its expression is largely restricted to atheroma and atheroma-prone lesions, in contrast to the widespread arterial distribution of ICAM-1, and has been shown to be upregulated over the developing plaque in hypercholesterolaemic animal models (Iiyama et al., 1999). This was supported by the work of Cybulsky et al. that demonstrated hypercholesterolaemic diets prompted upregulation of leukocyte adhesion molecules homologous to human VCAM-1 over early foam cell lesions in rabbit aortic endothelium (Cybulsky and Gimbrone, 1991). In mice models, atheroma formation was reduced in a VCAM-1 domain 4 knockout mouse model compared to wild type at the same lipid concentrations (Cybulsky et al., 2001).

VCAM-1 expression is regulated through the transcription factor NF- $\kappa$ B, which is found only in areas of atheroma (Brand et al., 1996). NF- $\kappa$ B increases in relation to LDL-C in endothelial cells (Khan et al., 1995) and decreases in the presence of NO (De Caterina et al., 1995) and anti-oxidants (Erl et al., 1997). NF- $\kappa$ B also contributes to atherogenesis by upregulating gene expression of genes promoting resistance to apoptosis (Wang et al., 1998).

Atheroma formation typically occurs at arterial branches and curvatures where the flow of blood is disturbed. Areas away from branches and curvatures, which do not normally show atherosclerosis, usually experience laminar blood flow resulting in shear stress. *In vitro* laminar flow modeling demonstrated that disturbed blood flow causes increased NF- $\kappa$ B and a consequent increase in endothelial cell entry into the cell cycle (Nagel et al., 1999, Gimbrone et al., 2000). Regions of hypoxia tend to co-localise with areas of abnormal shear stress patterns and this abnormal flow may form an effective mechanical barrier contributing to the hypoxia detectable within plaques and its correlation with the presence of plaque macrophages (Sluimer et al., 2008, Mayr et al., 2008).

As the core expands with increasing number of foam cells, the increasing distance from the vessel lumen means areas of the core become vulnerable to hypoxia. In mouse models, plaques with cores greater than 500  $\mu$ m thick were characterised by adenosine triphosphate (ATP) depletion, decreased glucose concentrations, and increased lactate concentrations with ATP depletion contributing to the death of macrophages and the formation of a necrotic core, predominantly deep within the core than close to the lumen (Leppanen et al., 2006). In the presence of significant hypoxia within the core, there is induction of hypoxia-inducible transcription factor 1 (HIF-1) in macrophages, that promotes the transcription of vascular endothelial growth factor (VEGF), and hexokinase-1 and -2 (HK-1 and -2) (Sluimer et al., 2008), which in turn promotes macrophage activity (Folco et al., 2011). VEGF, HK-1 and HK-2 are implicated in angiogenesis within the atheroma and increased levels are correlated with increased microvessel density (Sluimer et al., 2008).

VCAM-1 expression is upregulated by the presence of pro-inflammatory cytokines (such as IL-1 $\alpha$ , TNF- $\alpha$ , IL-4, and IFN- $\gamma$ ) and Gram negative bacteria lipopolysaccharide, all of which were associated with increased VCAM-1 expression in rabbit aorta within seven days of starting an atherogenic diet, preceding the accumulation of macrophages within the intima by three weeks (Li et al., 1993).

NF- $\kappa$ B upregulates monocyte chemoattractant protein-1 (MCP-1) chemoattractant chemokine that acts upon the C-C chemokine receptor-2 (CCR2) receptor on

macrophages in order to aid initiation of fatty streaks, the absence of which leads to decreased atheroma formation in mouse models (Boring et al., 1998). Once the macrophages have been recruited to the tissues then they take up LDL-C via scavenger receptors. Smith et al. demonstrated that in hypercholesterolaemic apolipoprotein E (ApoE) knock out mice, the absence of macrophage colony-stimulating factor (through a frame shift mutation in the encoding gene) resulted in an almost 3-fold increase in plasma cholesterol but a significant decrease in the atheroma formation, thereby showing LDL-C uptake by macrophages to be important in fatty streak and atheroma core formation (Smith et al., 1995). Furthermore, in human patients there was an attenuation of NF- $\kappa$ B signaling, neutrophil (but not macrophage) activation, and increased collagen deposition following statin therapy (Lenglet et al., 2014).

Other plaque features may have a similar propagating effect in plaque inflammation and development. The accumulation of cholesterol, and its morphological changes, within the plaque may contribute to both plaque inflammation and instability. Crystal build-up occurs as a consequence of the disruption of cholesterol homeostasis, resulting in the accumulation of free cholesterol rather than esterified LDL. Typically cholesterol ester hydrolase enzymes convert esterified cholesterol to free cholesterol whilst acyl-coenzyme A cholesterol acyltransferase 1 results in the opposite conversion (Janoudi et al., 2016). Inhibition of the latter has been shown to increase cholesterol crystal formation in macrophages (Kellner-Weibel et al., 1999). Endothelial cells have also been implicated in the uptake and metabolism of LDL resulting in the formation of cholesterol crystals, a consequence that in turn compromises endothelial function (Baumer et al., 2017). The crystallisation of cholesterol from liquid to solid form within the plaque also results in volume expansion and the perforation of the fibrous cap by sharp-tipped cholesterol crystals (Abela and Aziz, 2006, Abela et al., 2009, Liu et al., 2011, Janoudi et al., 2016). The combination of these processes result in a pro-atherogenic environment, and one that ultimately predisposes to plaque disruption. Statins have been found to decrease the peak volume expansion of cholesterol crystals in a dose-dependent fashion, blunt the crystal structure, and decrease cholesterol crystal density (Abela et al., 2011).

Ezetimibe has also been found to reduce cholesterol crystallisation and inflammation (Patel et al., 2011).

Ultimately, the vascular wall injury provoked by mechanical and chemical factors (sheer stress, hypertension, diabetes mellitus, hypercholesterolaemia, smoking) triggers cellular (particularly monocyte) recruitment. The ongoing accumulation of a lipid-rich and macrophage-rich core eventually outgrows its blood supply, becoming necrotic and triggering further cytokine release. This change signifies a transition from a previously stable atheroma to one vulnerable to rupture (**Figure 1.3**).

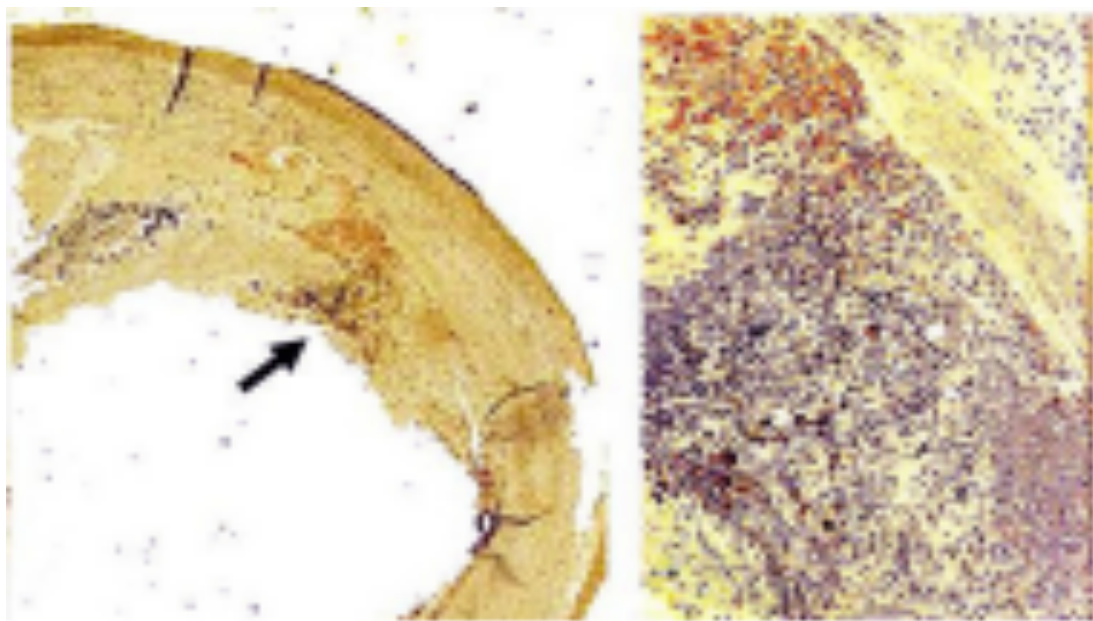


**Figure 1.3: Macrophage accumulation in the atherosclerotic plaque.** CD68 staining showing the presence of macrophages in an excised symptomatic carotid atheroma. Reproduced with permission from (Fifer et al., 2011).

#### *1.1.5 The 'vulnerable plaque' hypothesis*

The recognition that factors other than the degree of luminal stenosis determine the risk of clinical events has led to the creation of the 'vulnerable plaque' hypothesis. Whilst the necrotic core of the atheroma was previously viewed as little more than cellular debris, it is increasingly recognised that the atheroma core is metabolically active, acting as an inflammatory nidus to promote the production of cytokines by foam cells and consequently leading to atheroma destabilisation.

The inflammatory nidus represented by an atherosclerotic plaque contains a range of cellular infiltrates. Recruited monocytes differentiate into macrophages; expressing scavenger receptors (scavenger receptor A and CD36) that lead to the internalisation of cholesteryl esters. Internalisation of these modified lipoproteins results in the transformation of intimal macrophages into foam cells. These foam cells contribute to the core of the atheroma, release pro-inflammatory cytokines and matrix metalloproteinases (MMPs), and apoptose as the size of the core increases and they receive insufficient oxygen (**Figure 1.4**) (Libby, 2002).

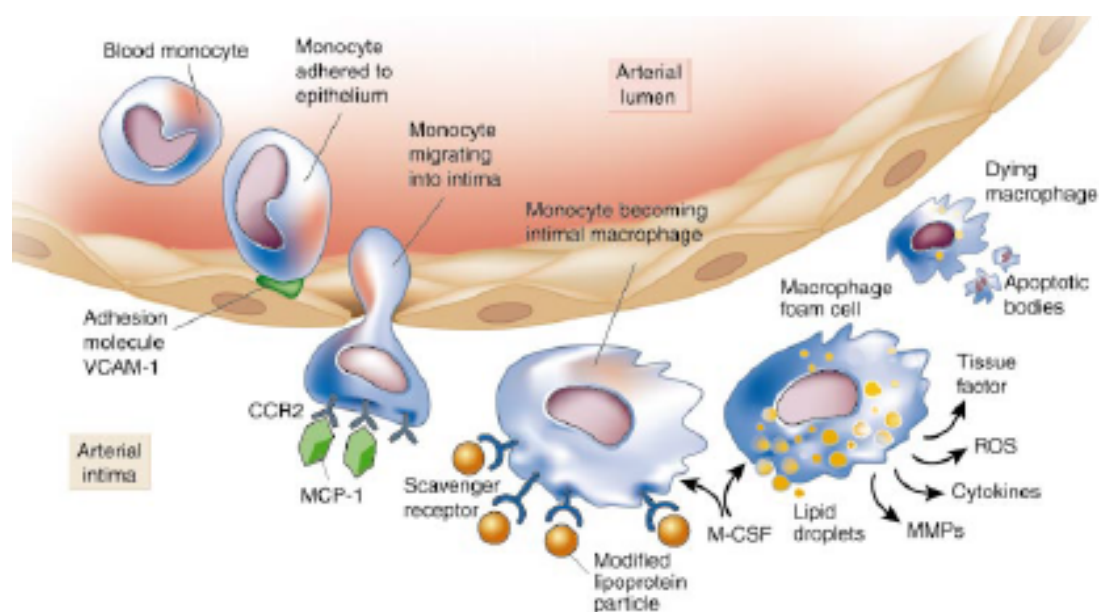


**Figure 1.4: Recruitment of circulating monocytes.** Recruitment of circulating monocytes and maturation into intimal macrophages and foam cells. Reproduced with permission from (Libby, 2002).

The development of the necrotic core may involve several pathophysiological components. Phagocytosis of oxidised LDL is toxic to tissue macrophages/foam cells and triggers apoptosis, though foam cell death in large quantities may overwhelm clearance mechanisms, resulting in cellular detritus that may provoke further inflammation (Mallat and Tedgui, 2000, Libby et al., 2014). Programmed cell death and necroptosis may also contribute to the pool of dead macrophages, and likely promotes a greater pro-inflammatory state than that seen with cellular apoptosis (Karunakaran et al., 2016, Vandenabeele et al., 2010). Finally, increasing

inflammation within the plaque may promote neo-angiogenesis, where fragile capillary-like vessels may result in intraplaque haemorrhage and the release of free cholesterol to further exacerbate intra-plaque inflammation and plaque vulnerability (Kolodgie et al., 2003, Moreno et al., 2004, Virmani et al., 2005, Michel et al., 2011).

Monocytes/macrophages are not the only inflammatory cell infiltrating the atheroma. Different subsets of T-lymphocytes are found within the atheroma and have a range of functions, both protective and destructive. Atheroprotective regulatory T-cells (Tregs) that produce anti-inflammatory cytokines have been shown to reduce in mouse models in response to high cholesterol diets, resulting in an increased atherosclerotic burden (Maganto-Garcia et al., 2011). In contrast, pro-inflammatory activated CD4 Th1 T-cells are found in higher numbers in hypercholesterolaemic mouse models (Wilhelm et al., 2009). T-lymphocytes then interact directly or via cytokine-mediated signals to upregulate foam cell activity (**Figure 1.5**).

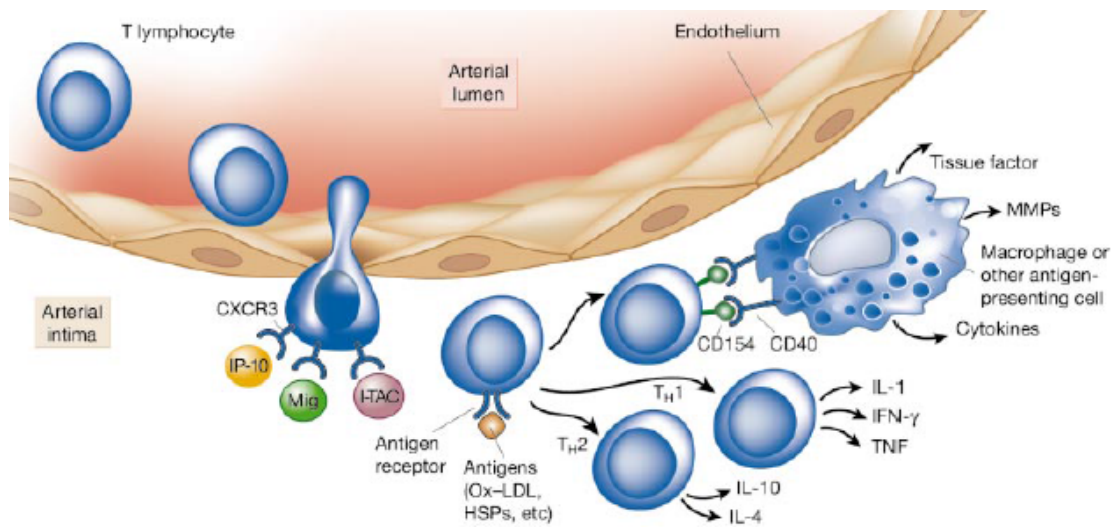


**Figure 1.5: Recruitment of T lymphocytes.** Recruitment of T lymphocytes and their release of cytokines and interaction with macrophages/foam cells. Reproduced with permission from (Libby, 2002).

The polarisation of CD4<sup>+</sup> effector cells within atheroma from an anti-inflammatory Th2 T-cells towards pro-inflammatory Th1 T-cells is accompanied by other lymphocytes. Dendritic cells (DCs) have both been shown to induce Th1 T-cell proliferation in response to oxidised LDL (Liu et al., 2015a). Though less is known about their role and mechanisms in atherosclerosis, natural killer (NK) cells and

natural killer T-cells (NKTs) have both been shown to be pro-atherogenic through release of IFN- $\gamma$  and stimulation of Th1 T-cell differentiation (Nakai et al., 2004, Selathurai et al., 2014).

Atherogenesis is completed by the formation of a fibrous cap composed of triple-helical collagen, where collagen formation is promoted by vascular smooth muscle cells (VSMCs) in a dynamic process in response to cytokine signaling (Libby, 2002, Libby, 2008). Atheromatous plaques have been found to be associated with increased levels of metalloproteinases MMP-1 and MMP-13 (Sukhova et al., 1999), MMP-8 (Herman et al., 2001) and MMP-1, MMP-2 and MMP-3 (Galis et al., 1994). In these studies, increased MMP levels were associated with increased collagenolysis and thinner fibrous caps. In particular, MMP-8 was shown to be produced from *in vitro* differentiated peripheral blood monocyte-derived macrophages stimulated with CD40 ligand (Herman et al., 2001). Increased production of MMPs may also be upregulated by CD40 positive T-cells that accumulate at atheroma or by the direct interaction between macrophages and smooth muscle cells, both of which express MMPs (Lee et al., 1995, Schonbeck et al., 1997). The increased levels of MMPs have been co-localised to plaque “shoulders,” the most vulnerable regions of the atheroma to rupture, and around the lipid core itself (Galis et al., 1994, Sukhova et al., 1999).

The destabilisation of the fibrous cap occurs as a result of several inflammatory-mediated processes. IFN- $\gamma$  induces apoptosis in vascular smooth muscle cells, the main producer of collagen in the cap (Rosner et al., 2006). Consequently, the presence of this pro-inflammatory cytokine reduces the collagen component of the cap, weakening it as a result. This effect is compounded by the direct effect of MMP interstitial collagenases (MMP-1, -8, and -13) causing initial proteolytic damage in the collagen that is then exacerbated by MMP gelatinases (MMP-2 and MMP-9) for further collagen catabolism (Galis et al., 1994, Sukhova et al., 1999, Herman et al., 2001). Higher inflammatory responses resulting in increased levels of these MMPs mean that tissue inhibitors of metalloproteinases (TIMPs) are overwhelmed in atherosclerotic plaques (Sukhova et al., 1999).

The extent to which the fibrous cap has to thin in order to become “vulnerable” remains a matter of debate. Until recently only small studies had been conducted that

demonstrated thin fibrous caps were more prevalent in ruptured plaques, though the difference in modalities and methodologies made it hard to compare and devise a critical cap thickness threshold for vulnerability (Carr et al., 1996, Devuyst et al., 2005). However, in the Oxford Plaque Study, either a minimum cap thickness  $<200$   $\mu\text{m}$  and/or an average plaque thickness of  $<500$   $\mu\text{m}$  were found to be associated with rupture (Redgrave et al., 2008). These features of a vulnerable plaque were also seen to have a strong association with other high-risk plaque characteristics, particularly a large lipid core, intraplaque haemorrhage, fibrous cap macrophage infiltration, and plaque macrophage infiltration.

By combining samples from the Oxford Plaque Study and the Athero-Express study, Howard et al. analysed a pooled sample of 1,640 symptomatic plaques. From this pooled data they showed that plaque thrombus, fibrous content, macrophage infiltration, high microvessel density and overall plaque instability were each significantly associated with predicted stroke risk (Howard et al., 2015). Of these, plaque inflammation and a large lipid core were more prevalent in those plaques removed within 30-days of the event compared to those removed after 30-days. Interestingly, in contrast to their previous study, fibrous cap thickness was not significantly associated with calculated stroke risk.

The role of inflammation in the vulnerable plaque has been a target of interest in a number of studies that aim to reduce cardiovascular events using anti-inflammatory strategies. In the Canakinumab Anti-inflammatory Thrombosis Outcomes Study (CANTOS) – a randomised double-blind trial of a monoclonal antibody targeting IL- $1\beta$  – recently reported a dose-dependent reduction in high-sensitivity C-reactive protein (hsCRP), though no reduction in lipid levels, and a reduction in the primary efficacy endpoint (a combination of non-fatal myocardial infarction, non-fatal stroke, or cardiovascular death) in the 150 mg dose subgroup (Ridker et al., 2017). This indicates a beneficial effect of anti-inflammatory therapy, independent of any lipid-lowering effect. However, it is important to note that there was an associated higher incidence of fatal infection than with placebo, a finding that is likely to limit adoption in routine clinical practice. Studies considering other specific anti-inflammatory treatments, such as methotrexate (Everett et al., 2013, Moreira et al., 2013), are

ongoing. Finally, other anti-inflammatory studies that have utilised PET imaging endpoints, such as the dal-PLAQUE study, are discussed later in this chapter.

The key event in the pathophysiology underlying stroke in large vessel disease is the rupture of the atherosclerotic plaque. This exposes procoagulant factors, particularly the expression of tissue factor, which initiate thrombogenesis. The role that inflammation plays in procoagulant factor expression is discussed in later chapters.

Whilst this section has considered the enzymatic (MMP-mediated) destabilisation of the plaque, other inter-dependent mechanisms may also contribute to plaque rupture through mechanical destabilisation. Microcalcium deposits – calcium deposits smaller than 50  $\mu\text{m}$  as detected by *ex vivo* CT (Maldonado et al., 2012) – frequently represent both a consequence and precipitant of inflammation, and may either contribute to plaque rupture or coalesce to form protective macrocalcification (**Figure 1.6**) (Chen and Dilsizian, 2013). The mechanisms of microcalcification and macrocalcification are explored in greater detail in subsequent sections.

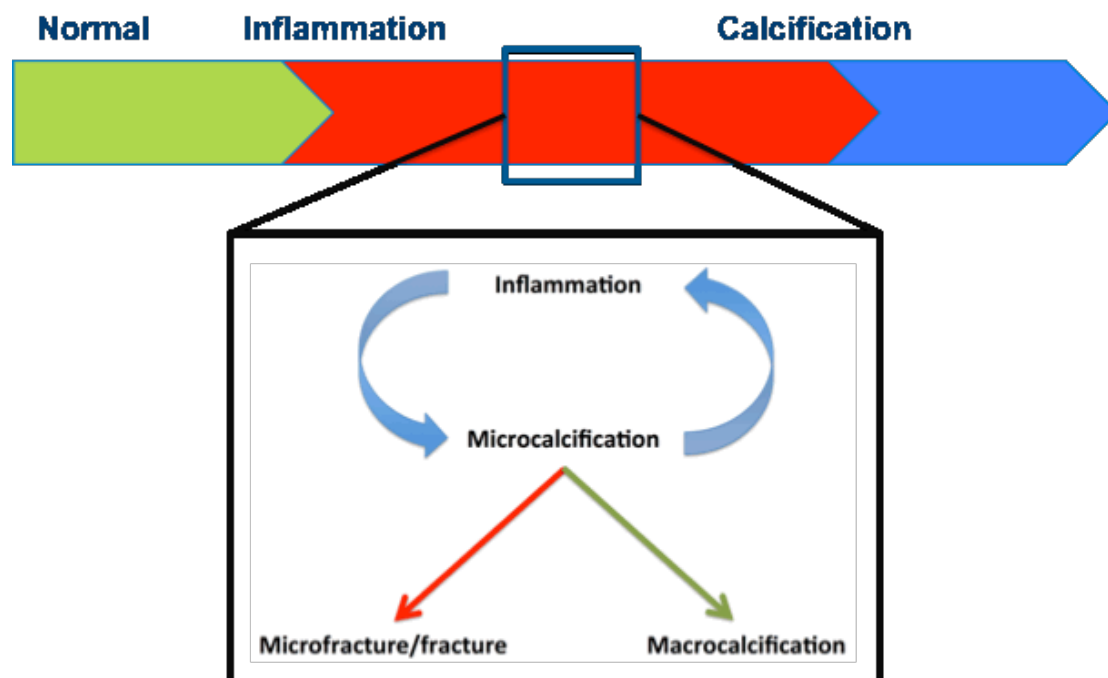


**Figure 1.6: The natural history of atherosclerosis.** Schema of the relationship of inflammation and microcalcification in the natural history of atherogenesis.

### *1.1.6 Microcalcification in atherosclerosis*

Vascular calcification may occur through active and passive mechanisms. ‘Passive’ calcification occurs secondary to debris from apoptotic and necrotic cells within the atheroma necrotic core, the release of matrix vesicles that serve as sites for calcium complex crystallisation, and reduced local expression of mineralisation inhibitors, while ‘active’ calcification is an active cellular calcification process that is similar to that seen in bone formation (Nakahara et al., 2017, Panizo et al., 2009). Atherosclerosis in peripheral arteries is frequently associated with both intimal and medial calcification, and the cellular mechanisms for calcification may differ between them: intimal calcification may be promoted by a range of cell types and inflammatory cytokines, with propagation by chondrocyte-like cells, while medial calcification is believed to be under the action of osteoblast-like cells (Otsuka et al., 2014, Nakahara et al., 2017).

Proinflammatory macrophages release matrix vesicles (small membranous structures 30-300 nm in diameter surrounded by a lipid bilayer) that are implicated in the initiation of the calcification process (New et al., 2013, New and Aikawa, 2013). These matrix vesicles are rich in calcium-binding proteins annexins and phosphatidylserine (Kapustin et al., 2011). The higher concentration of annexin, particularly annexin II and VI, is associated with greater uptake of calcium (Chen et al., 2008). The high concentrations of alkaline phosphatase in matrix vesicles also contributes to the calcification process by increasing the hydrolysis of organic phosphate substances, resulting in increased availability of free phosphate ions for apatite crystallisation, and through removal of inhibitors of mineralisation such as pyrophosphate (Chen et al., 2008, Anderson and Reynolds, 1973).

Apoptotic bodies, as well as matrix vesicles, may serve as acellular nucleation sites for hydroxyapatite (Doherty et al., 2003, Nakahara et al., 2017). Hydroxyapatite is believed to constitute the majority of calcium deposits within arteries (Luo et al., 1997), and the majority of ruptured plaques contain hydroxyapatite deposits (Jono et al., 2000, Doherty et al., 2003, Johnson et al., 2006) (**Figure 1.7**).

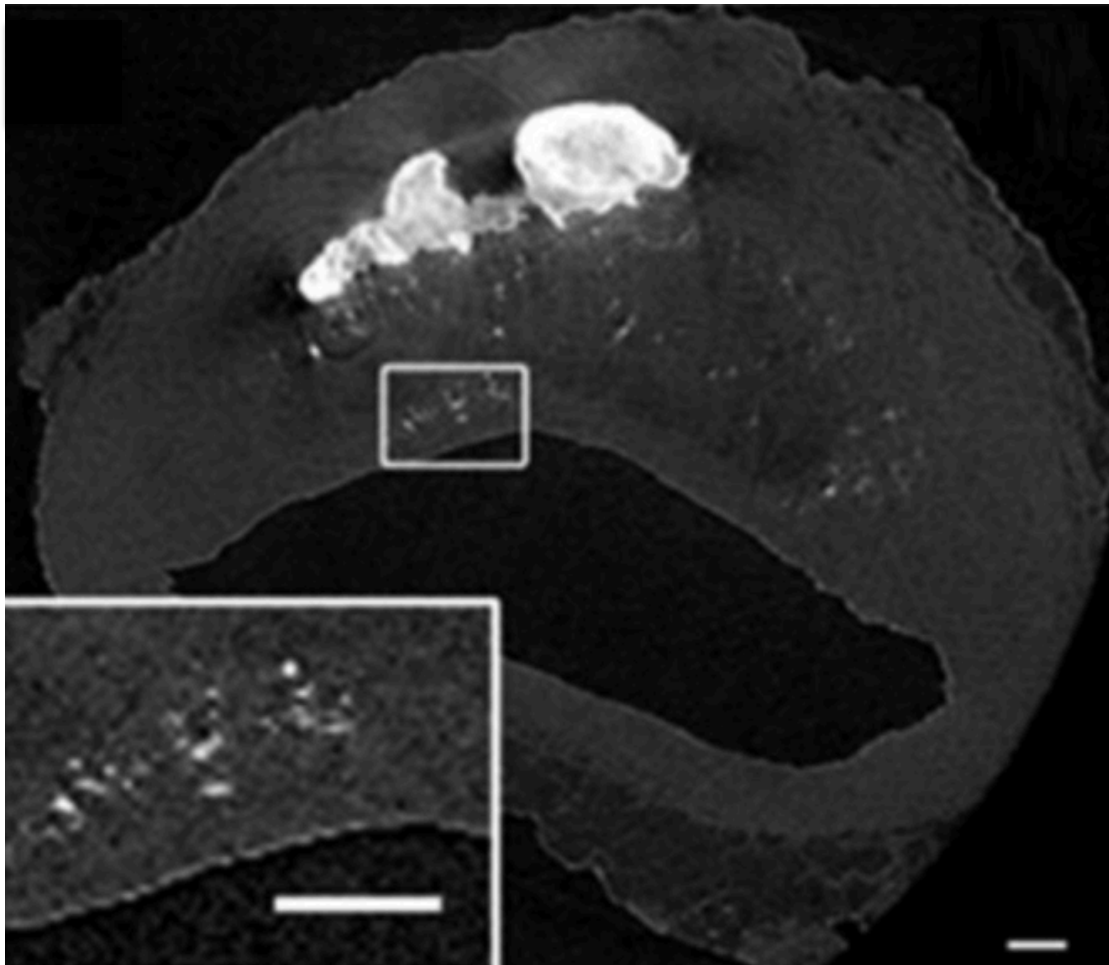


**Figure 1.7: Microcalcification in the fibrous cap.** High-resolution  $\mu$ CT images of human coronary atheroma at 2.1  $\mu$ m resolution with microcalcification deposits within the fibrous cap (inset). Scale bar: 100  $\mu$ m. Reproduced with permission from (Kelly-Arnold et al., 2013).

In bone, in order for mineralisation to progress the matrix vesicle requires collagen. Not only does collagen provide a scaffold for calcification propagation, it also appears important for promoting calcium uptake by the microvesicle (Wu et al., 1991, Kirsch and Wuthier, 1994). Arterial mineralisation by matrix vesicles requires type I collagen, which is upregulated in atherosclerotic plaques (Rekhter et al., 1993, Chen et al., 2008).

The inflammatory focus within the necrotic core promotes an osteogenic environment that affects cellular transdifferentiation. VSMCs are derived from the same pluripotent mesenchymal cell as osteoblasts and can undergo osteogenic

transformation. Receptor activator of nuclear factor- $\kappa$ B ligand (RANKL), a member of the tumour necrosis factor super-family (Lacey et al., 1998), and bone morphogenetic proteins (BMPs), may tip the balance of VSMC differentiation towards an osteoblastic phenotype (Panizo et al., 2009, Callegari et al., 2014, Hayashi et al., 2006, Mikhaylova et al., 2007, Hruska et al., 2005, Dhore et al., 2001). This differentiation into osteoblast-like cells results in an increase in the cellular expression of the transcription factor core binding factor alpha 1 (Cbfa1) that upregulates osteopontin and osteocalcin expression (Steitz et al., 2001, Engelse et al., 2001). These, and other osteogenic-associated proteins (bone sialoprotein (BSP), BMPs, and matrix Gla protein (MGP)), are secreted into the extracellular matrix and bind calcium salts with high affinity and have been found within atherosclerotic plaques (Tyson et al., 2003, Vattikuti and Towler, 2004, Engelse et al., 2001, Dhore et al., 2001).

#### *1.1.7 Arterial macrocalcification*

As illustrated in **Figure 1.6**, microcalcium deposits may aggregate to form spotty calcification and macrocalcification (Otsuka et al., 2014). Spotty calcification was observed to be associated with plaques in individuals with acute myocardial infarction while extensive calcification was more commonly associated with stable angina in one intravascular ultrasound (IVUS) study of the coronary arteries (Ehara et al., 2004), suggesting increasing macrocalcification confers plaque stability. Furthermore, plaques with more extensive macrocalcification appear to be more resistant to undergoing changes in size in response to systemic interventions (Nicholls et al., 2007).

The role of macrocalcification within carotid atherosclerosis has received less attention than that within coronary atherosclerosis, and the conflicting findings are explored further in chapter three.

#### *1.1.8 Atherothrombosis in carotid atherosclerosis*

As well as affecting plaque stability, the pathophysiological processes described above also have implications for the consequences of plaque rupture. Thrombus

formation has been shown to have complex interactions with the immune system in a process termed ‘thromboinflammation.’ At the site of arterial occlusion, inflammation contributes to a sequence of prothrombotic events. Damage at these sites triggers deposition of fibrin and activation of endothelial cells, platelets, and complement (Peerschke et al., 2010, del Zoppo et al., 1991, Hyman et al., 2009). There is accompanying upregulation of P-selectin on endothelial cells and platelets, and decreased NO production that will increase platelet aggregation and leukocyte adhesion (Yilmaz and Granger, 2010, Iadecola and Anrather, 2011).

Lymphocytes play an important role in the formation of microvascular thrombosis with evidence in mouse models that lymphocyte depletion reduces both thrombus formation and infarct size (Kraft et al., 2013). In the myeloid lineage, macrophages express procoagulant tissue factor (TF) antigen with high levels of this antigen being found in the intravascular “gruel” (the atheroma contents spilling into the systemic circulation following atheroma rupture) that correlated strongly with the atheroma macrophage content of ruptured coronary plaques (Leatham et al., 1995, Lo et al., 1995, Ott et al., 2001, Moreno et al., 1996).

Atorvastatin treatment in mouse models of venous thromboinflammation reduced the macrophage content and overall volume of thrombus (Kessinger et al., 2015). However, it is not possible to attribute the reduction in thrombus volume entirely to a statin-induced reduction of macrophages as statin therapy was also associated with a reduction of TF, reduced expression of NF- $\kappa$ B, and reduced platelet aggregation in the same study. The direct role of monocyte/macrophages upon thrombus formation was demonstrated through the inhibition of platelet-monocyte interaction in humans treated with rosuvastatin following myocardial infarction, with the rosuvastatin group having significantly lower levels of hsCRP and cardiac necrosis markers compared to controls after 24 hours (Sexton et al., 2015). Simvastatin has also been shown to reduce monocyte TF and was associated with a normalisation of thrombin-antithrombin complex and D-dimer compared to controls (Holschermann et al., 2000).

Rutten et al. observed that platelet reactivity was significantly associated with a high concentration of macrophages in excised symptomatic carotid atherosclerotic plaques (Rutten et al., 2014). No significant difference between TF levels in symptomatic and

asymptomatic carotid plaques was found by Migdalski et al., though the sample sizes were small and carotid samples were homogenised (Migdalski et al., 2005). Developing this further, Krupinski et al. supported the findings that there was no difference in TF expression between symptomatic and asymptomatic atheroma but found that there was a difference in expression of TF between active (macrophage-rich) plaques and non-active plaques whilst it was blood-borne TF concentration, rather than local atheroma TF expression, that correlated with recurrent cerebrovascular events at one year after CEA (Krupinski et al., 2008). One possible explanation for this may be that arterial regions neighbouring the carotid may also have actively inflamed atheroma that becomes unstable, though is overlooked as conventional clinical imaging looks in detail only at the anatomical stenosis of the carotid and imaging for atheroma in the arch of the aorta is rarely performed. <sup>18</sup>F-fluorodeoxyglucose-positron emission tomography (FDG-PET) has shown the strong association between uptake of FDG in neighbouring arterial territories (Rudd et al., 2009). Hence, an inflamed carotid atheroma may not occur in isolation but rather as part of a systemically inflamed arterial system. This would also provide an explanation for why recurrent strokes may occur despite CEA.

It has been suggested that the level of TF expression in the atheroma varies according to the morphology of the plaque. In contrast to the above, symptomatic calcified atheroma were found to have a lower expression of TF than symptomatic lipid-rich plaques by a factor of 2.5 (Basavaraj et al., 2012). Lipid-rich plaques encourage macrophage TF expression in response to oxidised low-density lipoprotein (oxLDL) levels and increased expression of TF promoting molecules, whilst calcified plaques also have a higher expression of inhibitors of TF (Sovershaev et al., 2010, Egorina et al., 2011, Owens and Mackman, 2012).

Finally, in the large Tromsø Study, increased carotid plaque area was associated with increased red cell distribution width, which in turn was independently associated with stroke risk (after adjustment for conventional atherosclerotic risk factors) and other thromboembolic events (Lappegard et al., 2015, Lappegard et al., 2016, Skjelbakken et al., 2014, Ellingsen et al., 2015, Zoller et al., 2014).

### 1.1.9 Morphological imaging using Magnetic Resonance Imaging

Conventional clinical carotid imaging modalities, Doppler ultrasonography and CTA, are limited in the amount of morphological information they can provide. MRI, using either contrast-enhancement or black-blood imaging, has proven to be an effective non-invasive imaging modality for assessing and quantifying plaque morphological features whilst also avoiding radiation exposure. Morphology including a thin fibrous cap, large lipid core volume and a greater mean wall thickness (MWT) are associated with a greater risk of stroke. These different plaque characteristics demonstrate different relaxation properties and signal intensities depending upon the weighting between T1 and T2 sequences. Exploiting the differences in relaxation times allows different morphological aspects to be imaged (Usman et al., 2015, Singh et al., 2015).

1.5T MRI has been shown to have good accuracy for in vivo measurement of maximum wall thickness when compared to excised *ex vivo* samples (Yuan et al., 1998). In a follow-up study, Yuan et al were able to demonstrate the difference in fibrous cap appearance on MRI was associated with symptomatic plaques, with the appearance of a thin cap or rupture being more likely to be associated with symptoms compared to thick fibrous caps (Yuan et al., 2002). Similar results were seen in a two-year longitudinal study by Sadat et al that showed there was a higher risk of subsequent cerebrovascular events seen in plaques with fibrous cap rupture, plaque haemorrhage, or higher structural stress (Sadat et al., 2010). Advances in field strength has shown 3T MRI to be superior to 1.5T MRI in imaging the vessel wall, with significantly increased wall signal-to-noise and contrast-to-noise ratios, whilst having good agreement of luminal size and MWT between the field strengths (Yarnykh et al., 2006). A similar improvement in signal-to-noise ratio using 3T was also shown by Young et al (Young et al., 2012).

T1-weighted sequences have been shown to have a strong agreement in detecting intraplaque hemorrhage (IPH) compared to histology (Bitar et al., 2008, Ota et al., 2010b, Narumi et al., 2014). Albuquerque et al demonstrate a strong association between T1-weighted hyperintensities and IPH on histology, as well as significantly higher hsCRP levels in those with T1-weighted hyperintensities (Albuquerque et al., 2007). In a large cohort of patients, van Dijk et al found the prevalence of IPH to be

significantly higher in symptomatic plaques than for asymptomatic plaques and that IPH was independently associated with disruption to the fibrous cap after adjustment for age, sex, diabetes mellitus, and the degree of stenosis (van Dijk et al., 2015).

Contrast-enhancement has been particularly effective in the assessment of fibrous cap thickness and lipid core volume, where the former is enhanced while there is no enhancement in the latter (Cai et al., 2005). Multicontrast-weighted MRI has been used in surveillance of asymptomatic plaques and demonstrated larger lipid cores, thicker MWT, thin/ruptured fibrous caps, and IPH to each have significantly increased hazard ratios for subsequent symptomatic events (Takaya et al., 2006). Finally, contrast-enhancement has also been shown to have superior accuracy relative to time of flight (TOF) imaging for estimating the degree of luminal stenosis (Platzek et al., 2014).

However, whilst MRI offers an effective method for imaging morphological features associated with plaque vulnerability, it remains highly user-dependent on accurate coil placement and reproducibility of technical sequences and image generation. Furthermore, evidence that non-stenotic lesions may be vulnerable to rupture means that simple anatomical quantification of morphology may overlook these underlying biological processes. Whilst measuring anatomical hallmarks of vulnerability, such imaging measures serve only to measure the outcome of the biological processes at work within the atheroma. These considerations, along with a call for imaging biological processes that cannot be seen on high-resolution MRI (such as hypoxia, microcalcification, and neovascularisation) and the ability to measure dynamic changes in plaque biological processes in response to therapy, has led to other imaging modalities being sought to identify the vulnerable plaque.

#### *1.1.10 Pathophysiological imaging using Positron Emission Tomography*

Positron emission tomography (PET) utilises positron-emitting radioligands that target different metabolic targets or processes (from inflammation, through hypoxia and apoptosis, to microcalcification) and accumulate at regions of interest (ROI) where these processes occur. In the ROIs, the positrons quickly encounter electrons in neighbouring tissue, leading to an annihilation reaction whereby gamma photons are

emitted that can be detected by scintillation detectors and used to quantify the biological processes of interest. PET does not provide structural information, and consequently requires co-registration with CT (PET/CT) or MRI (PET/MRI) to provide anatomical co-localisation for tracer uptake.

A range of radioligands have been used in PET imaging across different facets of cerebrovascular disease, including large artery atherosclerosis, acute infarction, neuroinflammation, and chronic small vessel disease (Evans et al., 2017) (**Table 1.1**). Specific radioligands can be used in PET imaging to target the metabolic processes involved in atherogenesis and plaque disruption. Broadly, the main pathophysiological processes associated with plaque vulnerability can be split into inflammation, microcalcification, and hypoxia. The work in this thesis will concentrate PET imaging of two related processes affecting plaque vulnerability – inflammation and microcalcification – using  $^{18}\text{F}$ -fluorodeoxyglucose (FDG) and  $^{18}\text{F}$ -sodium fluoride (NaF) that target these processes respectively (**Figure 1.8**).

Tracer name	Chemical name	Molecular target	Cellular/physiological target	Technical considerations
$^{18}\text{F}$ -FDG	Fluorodeoxyglucose	NA	Increased metabolic rate (inflammation)	High sensitivity but potential for suboptimal signal-to-noise ratios
$^{68}\text{Ga}$ -DOTATATE	[1,4,7,10-tetraazacyclododecane- $\text{N},\text{N}'$ , $\text{N}''$ , $\text{N}'''$ -tetraacetic acid]-d-Phe1,Tyr3-octreotate	Somatostatin receptor type 2 (SST2)	Macrophages	High specific binding activity
$^{18}\text{F}$ -NaF	Sodium fluoride	Hydroxyapatite	Microcalcification	Potential spillover from vertebrae or mandible
$^{18}\text{F}$ -FMISO	Fluoromisonidazole	Selective reduction in hypoxia	Hypoxia	Long tracer uptake time (120–180 min)
$^{11}\text{C}$ -PK11195	<i>N</i> -methyl- <i>N</i> -[1-methylpropyl]-1-[2-chlorophenyl]-isoquinoline-3-carboxamide	Translocator protein (TSPO)	Macrophages/microglia	Short half-life, suboptimal signal-to-noise ratio intracerebrally
$^{11}\text{C}$ -PBR28	Nacetyl-N-(2-	TSPO	Macrophages/microglia	Variable binding affinity and short

	[ <sup>11</sup> C]methoxybenzyl)-2-phenoxy-5-pyridinamine			half-life
<sup>18</sup> F-DPA-714	<sup>18</sup> F- <i>N,N</i> -diethyl-2-(2-(4-(2-fluoroethoxy)phenyl)-5,7-dimethylpyrazolo[1,5- $\alpha$ ]pyrimidin-3-yl)acetamide	TSPO	Macrophages/microglia	Superior signal-to-noise ratio but paucity of human data
<sup>11</sup> C-vinpocetine	(3 $\alpha$ ,16 $\alpha$ )-Eburnamenine-14-carboxylic acid ethyl ester	TSPO	Macrophages/microglia	Superior signal-to-noise ratio but paucity of human data and short half-life
<sup>18</sup> F-GE-180	Flutriciclamide (4 <i>S</i> )- <i>N,N</i> -Diethyl-9-[2- <sup>18</sup> F]-fluoroethyl]-5-methoxy-2,3,4,9-tetrahydro-1 <i>H</i> -carbazole-4-carboxamide	TSPO	Macrophages/microglia	Superior signal-to-noise ratio but paucity of human data
<sup>11</sup> C-FMZ	Flumazenil Ethyl 8-fluoro-5-methyl-6-oxo-5,6-dihydro-4 <i>H</i> -benzo[ <i>f</i> ]imidazo[1,5- <i>a</i> ][1,4]diazepine-3-carboxylate	GABA-A receptor	Neurons	Short half-life
<sup>11</sup> C-PiB	Pittsburgh compound B <i>N</i> -methyl-[ <sup>11</sup> C]-2-(4'-methylaminophenyl)-6-hydroxybenzothiasole	Analogue of thioflavin T	Amyloid	Short half-life
<sup>18</sup> F-FNDP	<i>N</i> -(3,3-diphenylpropyl)-6- <sup>18</sup> F-fluoronicotinamide	Epoxide hydrolase enzyme that inactivates vasoactive and anti-inflammatory epoxyeicosatrienoic acids	Neurons (levels are elevated in individuals with vascular cognitive impairment (Nelson et al., 2014))	High specificity (80–90% in animal models (Horti et al., 2016))
<sup>18</sup> F-NS14490	4-[5-(( <i>N</i> -2-[ <sup>18</sup> F]fluoroethyl)indolyl)-[1,3,4]oxadiazol-2-yl)-1,4-diazabicyclo[3.2.2]nonane	$\alpha$ 7 nicotinic acetylcholine receptor	Expressed on neurons, astrocytes, microglia and endothelial cells	Proof-of-principle applications in intracerebral and vascular imaging (Rotering et al., 2014)
<sup>18</sup> F-labeled isatins	Isatin sulfonamide compounds	Caspase 3 and 7	Apoptosis	In development (Medoc et al., 2016)

**Table 1.1:** Radiotracers used in cerebrovascular PET studies.

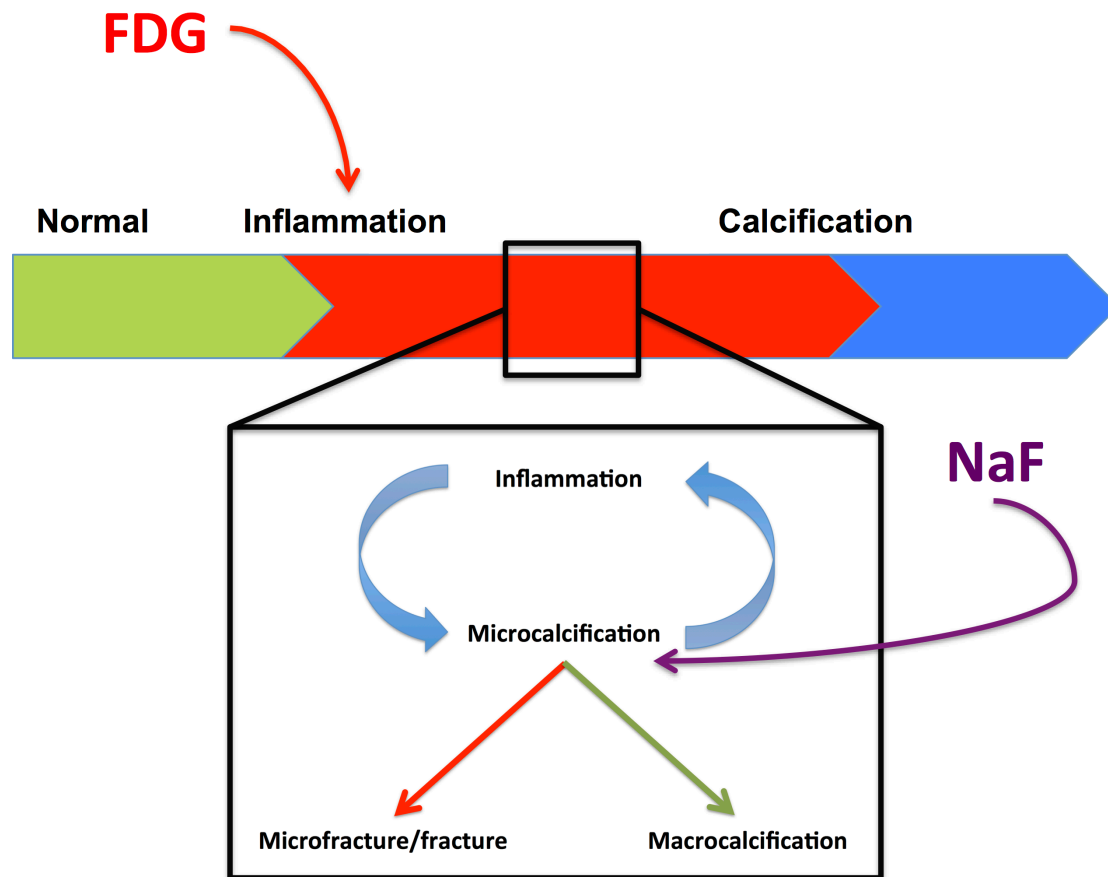


**Figure 1.8: Radioligand targeting of plaque pathophysiology.** The natural history of atherosclerosis and the targeting of inflammation and microcalcification using radioligands. FDG =  $^{18}\text{F}$ -fluorodeoxyglucose; NaF =  $^{18}\text{F}$ -sodium fluoride.

FDG has become the mainstay PET tracer in vascular imaging over the last 15 years after early studies by Rudd et al. identified its utility for identifying culprit atheroma *in vivo* (Rudd et al., 2002). The tracer has been validated in both pre-clinical and clinical settings. In rabbit models of atherosclerosis, FDG uptake was higher in atherosclerotic plaques compared to normal arterial wall, and that subsequent positron-sensitive probe counts correlated with the intima:media ratio (Lederman et al., 2001). Furthermore, FDG uptake was found to correlate with macrophage burden in aortic atherosclerotic plaques in rabbit models ( $r=0.93$ ,  $p<0.0001$ ), and FDG uptake was approximately 19-fold higher in pro-atherogenic rabbits compared to controls (Tawakol et al., 2005). Later rabbit models have confirmed these earlier findings; Davies et al. found that atherosclerotic plaques of rabbits fed a high-cholesterol diet had significantly higher levels of macrophage density than plaques in rabbits fed a high-cholesterol diet followed by a low-cholesterol diet and statin, and that there was

a high correlation between macrophage density and FDG uptake in the plaque on *ex vivo*  $\mu$  PET ( $r=0.95$ ,  $p<0.001$ ), though interestingly this relationship was not significant using *in vivo*  $\mu$ PET ( $r=0.16$ ,  $p=0.57$ ) (Davies et al., 2010). This latter result may be a result of partial volume error and/or spill-over from neighbouring structures.

In humans, an exploratory *ex vivo* analysis of carotid endarterectomy specimens incubated with tritiated deoxyglucose (an analogue of FDG) found uptake in macrophage-rich areas of the plaque, predominantly at the lipid core/fibrous cap border of the lesions, but little or no uptake in other areas of the plaque seen on autoradiography (Rudd et al., 2002). In the clinical setting, histological analysis of carotid endarterectomy specimens found a strong correlation between pre-operative carotid FDG uptake and the burden of CD68-positive macrophages in the plaque (Tawakol et al., 2006). It is worth noting that the same study found no correlation between FDG uptake and plaque area, plaque thickness, or area of smooth muscle cell staining, strengthening the argument that inflammatory activity and FDG uptake is not necessarily influenced by the size of plaque or degree of luminal stenosis.

Despite the utility of FDG-PET to detect physiological processes *in vivo*, the technique has several limitations worth noting at the outset. Firstly, despite its sensitivity, FDG has a low specificity for inflammation given its ubiquitous uptake in highly metabolically active tissues. This is demonstrated by extensive uptake seen in tissues such as the myocardium, which also generates substantial signal that ‘spills over’ into the neighbouring coronary arteries, making it extremely difficult to detect uptake in coronary artery atherosclerosis amongst the adverse signal-to-noise ratio. Furthermore, even when FDG uptake is related to the atherosclerotic plaque, it cannot provide information on other processes key to plaque destabilisation, such as microcalcification.

In our study, as well as considering the enzymatic destabilisation caused by inflammation, we also set out to study the contribution of microcalcification in the mechanical destabilisation of the plaque *in vivo*. NaF-PET has only recently been used in imaging vascular microcalcification, primarily within the coronary arteries (Joshi et al., 2014). Our study aims to investigate NaF as an alternative radioligand in

carotid atherosclerosis imaging that provides complementary information to FDG about plaque pathophysiology. How tracer uptake – and the different processes they represent – varies within the plaque is likely to provide us with a vital understanding of how plaque vulnerability may occur. Furthermore, NaF also has the advantage over FDG in that it is less commonly affected by spill-over from neighbouring structures due to its higher specificity.

The pharmacodynamics and historical context of the use of both NaF and FDG radiotracers, along with their use in vascular imaging to date, are discussed in more detail in Chapters Three and Four respectively. Previous work using NaF has also demonstrated the close relationship between microcalcification and macrocalcification in carotid atherosclerosis (Derlin et al., 2011c), and hence it is important to consider how carotid macrocalcification influences tracer (both NaF and FDG) uptake in our study. As demonstrated above, there is progression through the natural history of the atheroma (from inflammation to the development of microcalcification and then macrocalcification) and any consideration of plaque stability and its relation to clinical events should consider all three of these facets. Despite it being a common finding on carotid investigations, to date the role of macrocalcification in carotid atherosclerosis in clinical events remains poorly understood. Consequently, this thesis will consider each of these complementary processes and how they relate to each other and to plaque stability.

As well as the use of these radiotracers for helping elucidate pathophysiological processes in plaque destabilisation, PET/CT has started to be used for sensitive surrogate endpoints in clinical trials, further demonstrating its utility in assessing vascular disease.

#### *1.1.11 PET/CT applications in atherosclerosis drug development trials*

As well as its utility for understanding the pathophysiology of atherosclerosis, PET/CT has an important application for measuring the effects of drug treatment. FDG-PET has also offered key insights into mechanisms of atheroma stabilisation with statins, in particular their observed anti-inflammatory effects upon the atheroma

in addition to their effect on lipid profiles (Tahara et al., 2006, Tawakol et al., 2013, Wu et al., 2012).

The capacity to measure atherosclerotic metabolic processes non-invasively *in vivo* has been shown to provide a useful endpoint for drug discovery and efficacy trials. The dal-PLAQUE phase 2b randomised clinical trial of dalcetrapib (a modulator of cholesteryl ester transfer protein that raises high-density lipoprotein cholesterol) used FDG uptake as its primary endpoint, demonstrating that there were no safety concerns over the six months whilst on dalcetrapib. In this study, dalcetrapib failed to reduce carotid FDG uptake when compared to placebo, which was consistent with the later randomised placebo-controlled clinical outcome study (Fayad et al., 2011a, Schwartz et al., 2012). FDG-PET endpoints have also been used by Emami et al. who used it to compare the therapeutic effects of BMS-582949 (a p38 mitogen-activated protein kinase inhibitor) against placebo, but again no significant difference was seen between these two cohorts (Emami et al., 2015b). This study did reinforce the finding that statin treatment leads to a reduction in FDG uptake in the control group and this may contribute to the lack of significance between cohorts. Importantly, these studies serve as an important proof of principle for the use of PET endpoints in randomised clinical trials.

#### *1.1.12 Atherosclerosis and its effects on the brain*

As will be discussed in more detail in Chapter Four, inflammation within atherosclerosis is a systemic process, and the extent of this inflammation appears to be associated with the severity of cardiovascular disease, with aortic FDG uptake found to be higher in those with recent ST-elevation myocardial infarction than those with non-ST elevation myocardial infarction, and higher carotid uptake observed for those with acute coronary syndromes than those with chronic stable angina (Joshi et al., 2015, Rudd et al., 2009, Kim et al., 2015). While the heart represents an important end-organ for cardiologists, the brain as the equivalent for the stroke physician or neurologist has received less attention. Little comparable work has been undertaken considering the extent of inflammation within carotid atherosclerosis and how it affects neurological pathology and outcomes.

In this thesis I will consider the impact of inflammation and microcalcification on both chronic and acute cerebrovascular disease. Given the proximity of the carotid atheroma to the blood-brain barrier it is feasible that plaque inflammation may disrupt the integrity of the neurovascular interface, resulting in the development of leukoaraiosis and affecting the severity and evolution of acute infarcts. There are a number of mechanisms by which this may occur, and these will be explored in further detail in Chapters Five (chronic small vessel disease) and Six (acute ischaemic stroke).

Aside from its potential role in the development of ischaemic lesions and leukoaraiosis, inflammation has also been implicated in a range of clinical brain diseases, including depression, schizophrenia, and dementia (Howren et al., 2009, Valkanova et al., 2013, Singh and Chaudhuri, 2014, Frodl and Amico, 2014, Kuo et al., 2005, Ershler and Keller, 2000). Hence, it is conceivable that vascular inflammation in symptomatic atherosclerosis may also contribute to a decline in clinical function and/or cognition. Hence, as well as considering the neuroimaging repercussions, I will also consider the effect upon the individual in an exploratory analysis of the effect upon participant outcomes (Chapter Seven).

## 1.2 Objectives of the thesis

This thesis aims to address the following research questions:

- i. Can NaF-PET differentiate between culprit and non-culprit carotid atherosclerotic plaques non-invasively *in vivo*? (Chapter Three).
- ii. How does the spatial distribution of inflammation and microcalcification within carotid atherosclerotic plaques compare? (Chapter Four).
- iii. Is inflammation within carotid atheroma associated with the presence of chronic cerebral small vessel disease? (Chapter Five).
- iv. Does inflammation within carotid atheroma influence the size and evolution of the acute infarct? (Chapter Six).
- v. How do these processes relate to the clinical presentation, progression, and recovery following acute stroke? (Chapter Seven).

The primary hypothesis of the thesis is:

**NaF-PET will be able to differentiate between culprit and non-culprit carotid atherosclerotic plaques *in vivo*.**

The secondary hypotheses of the thesis are:

- 1. Increased inflammation within carotid atherosclerosis (as measured by FDG TBR) will be associated with larger infarcts at baseline.**
- 2. Increased inflammation within carotid atherosclerosis (as measured by FDG TBR) will be associated with expansion of the infarct (FLAIR lesion).**

## **Chapter Two: Study Participants and General Methods**

### **2.1 The ICARUSS Study approvals and support**

The Imaging Carotid Atherosclerosis in the Recovery and Understanding of Stroke Severity (ICARUSS) Study ran between June 2014 and November 2016. It was approved by the Nottingham 1 Research Ethics Committee (14/EM/0128). The review by the Research Ethics Committee included approval for ongoing participation in the study by participants who lost capacity following initial consent and baseline investigations (unless felt inappropriate by the research or clinical teams decided in conjunction with the participant's next-of-kin and primary care team). Approval was also granted by the Administration of Radioactive Substances Advisory Committee (999/9000/31328). The study was supported by the National Institute Health Research through inclusion in its Clinical Research Network Portfolio.

The study was funded by a Research Training Fellowship to NRE from The Dunhill Medical Trust (RTF44/0114). The funders did not have any input into study design, data collection, or interpretation of the results.

### **2.2 Study eligibility and recruitment**

Participants were recruited from individuals who had an ischaemic stroke as a result of carotid disease. In order to achieve this clinical model of large vessel disease stroke, recruitment to the study included a number of strict inclusion and exclusion criteria (**Table 2.1**).

INCLUSION	EXCLUSION
<ul style="list-style-type: none"> <li>• Able to give informed consent.</li> <li>• Aged 40 years or above.</li> <li>• Ischaemic stroke in the last seven days confirmed to be due to atheroma in the carotid/vertebral artery.</li> <li>• Evidence of at least 50% stenosis in the ipsilateral artery (either on Doppler, CTA or MRA).</li> </ul>	<ul style="list-style-type: none"> <li>• Haemorrhagic stroke.</li> <li>• Women of childbearing potential.</li> <li>• Atrial fibrillation.</li> <li>• Complete occlusion of vessel.</li> <li>• Other chronic neurological condition.</li> <li>• Limited life expectancy.</li> <li>• Contra-indication to MRI.</li> <li>• Unable to give informed consent.</li> <li>• eGFR &lt;30 ml/min/1.73m<sup>2</sup>.</li> <li>• Medical history or clinical examination finding deeming subject ineligible for inclusion.</li> <li>• Already participating in two other research studies.</li> </ul>

**Table 2.1:** Inclusion and exclusion criteria for study population.

Individuals experiencing a TIA were not recruited as the secondary aim of the study considers the evolution of the infarct and recovery. Hence, only individuals with clinical symptoms persisting for longer than 24-hours (or with evidence of acute infarction on diffusion-weighted imaging (DWI)), were approached for recruitment. Furthermore, we also wished to consider an individual's clinical recovery and, using the a clinical definition of TIA returning to baseline status within 24 hours, decided that longitudinal assessments in individuals already back at their functional baseline would not be applicable.

The sample size for the study was discussed with Dr Simon Bond (Senior Statistician, NIHR Research Development Service East of England, and Cambridge Clinical Trials Unit Lead for Statistics). Given the study was observational in nature, rather than a randomised control study, it was felt that a sample size calculation to detect significance between two groups was not necessary. Instead, a pragmatic recruitment target of 30 participants was adopted. This sample size was consistent with recruitment to previous studies at our centre and was felt to be sufficiently large to allow robust statistical analysis as described later in this chapter.

Participants were recruited either from the Acute Stroke Unit or Cerebrovascular Clinics at Cambridge University Hospitals NHS Foundation Trust. Individuals with ischaemic strokes underwent Doppler ultrasound or CTA for assessment of large vessel atherosclerosis as part of routine clinical care. These individuals were subsequently screened by clinical and research teams and any individual identified with  $\geq 50\%$  stenosis of the ipsilateral common or internal carotid artery (measured using the NASCET method (North American Symptomatic Carotid Endarterectomy Trial Collaborators, 1991)) was approached for further screening and discussion for inclusion in the study. A flow diagram of participant recruitment is shown in **Figure 2.1**.

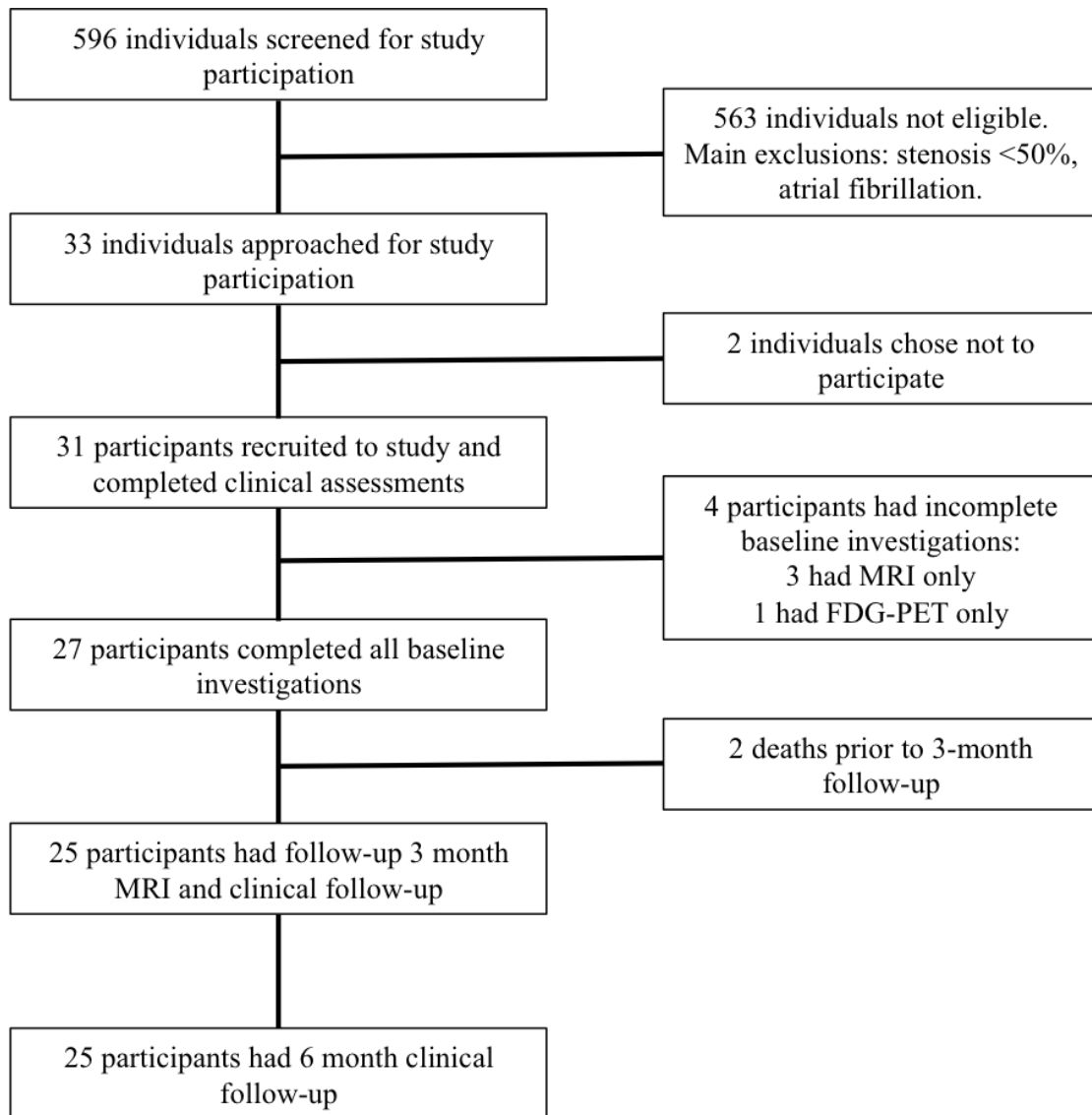


**Figure 2.1: Flow diagram of participant recruitment.**

Upon enrolment to the study, participants were allocated a four-digit randomly-generated participant number. All imaging, biochemical, and clinical/functional data was identified using this participant number.

Clinical information for the study participants is shown in **Table 2.2**.

Participant ID	Age	Sex	Smoker	Diabetes	Hypertension	Current statin	Current antiplatelet	Cardiovascular history	Thrombolysis	CEA prior to three months
3455	80	Male	Ex	No	Yes	No	No	No	No	Yes
2547	54	Female	Yes	No	Yes	No	No	No	No	No
1483	81	Female	No	No	Yes	Yes	Yes	Yes	No	No
3914	68	Male	Ex	Yes	Yes	Yes	Yes	Yes	No	No
5505	71	Male	No	No	No	No	No	No	No	Yes
7346	62	Male	Yes	No	No	No	No	No	No	Yes
4549	89	Male	Ex	No	Yes	Yes	Yes	No	No	No
7968	62	Male	No	Yes	Yes	No	No	No	No	No
2441	62	Female	Yes	No	No	No	No	Yes	No	No
9508	84	Female	No	No	Yes	No	No	Yes	Yes	Yes
5341	76	Male	No	No	Yes	Yes	Yes	Yes	No	No
3612	86	Female	No	Yes	No	No	No	No	No	No
6995	75	Male	Ex	No	Yes	No	No	No	No	No
1735	69	Male	Yes	Yes	Yes	Yes	Yes	Yes	No	No
3399	86	Male	No	Yes	Yes	Yes	Yes	Yes	No	No
2812	78	Male	Ex	No	Yes	No	No	No	No	No
7119	65	Male	Yes	No	Yes	No	No	No	No	No
9681	80	Male	No	No	Yes	Yes	No	No	No	Yes
6996	66	Male	Yes	No	No	No	No	No	Yes	No
9391	73	Male	Yes	No	Yes	Yes	Yes	Yes	No	No
3488	72	Male	Ex	Yes	No	No	No	No	Yes	Yes
3356	65	Male	Ex	No	No	No	No	No	Yes	Yes
5936	68	Male	No	No	No	No	No	No	Yes	Yes
8584	70	Female	Yes	No	Yes	Yes	Yes	Yes	No	No
1133	78	Female	Yes	No	Yes	Yes	No	No	No	Yes
7622	69	Female	Yes	No	No	No	No	No	No	No
8904	94	Female	Ex	No	Yes	No	Yes	Yes	No	No
5377	63	Male	Yes	No	Yes	No	No	No	No	No
4307	74	Male	Yes	Yes	Yes	Yes	Yes	No	No	No
4187	88	Female	No	No	No	No	No	No	No	No
5048	74	Male	Ex	No	Yes	Yes	Yes	Yes	Yes	No

**Table 2.2:** Summary of participant clinical characteristics.

Individuals were classified as having a history of hypertension if they had received either a previous diagnosis, were on treatment for hypertension, or were diagnosed with hypertension during the admission. The same approach was adopted for diabetes.

The degree of stenosis for each carotid artery is shown in Appendix B.

### **2.3 Study investigations**

Individuals participating in the study underwent the following investigations:

#### **Baseline**

Imaging: FDG-PET/CT, NaF-PET/CT, Carotid CTA, MRI brain, and carotid MRA (TOF and contrast-enhanced).

Clinical: Medical and drug history, modified Rankin scale (mRS), Barthel index (BI), National Institutes of Health Stroke Scale (NIHSS), Montreal cognitive assessment (MoCA).

Biomarker: hsCRP

#### **Three month follow-up**

Imaging: MRI brain and carotid MRA (TOF and contrast-enhanced).

Clinical: Medical and drug history, mRS, BI, NIHSS, MoCA, HADS, SIS.

#### **Six month follow-up**

Clinical: Medical and drug history, mRS, BI, NIHSS, MoCA, HADS, SIS.

An example schedule for study participation is shown in **Figure 2.2**.

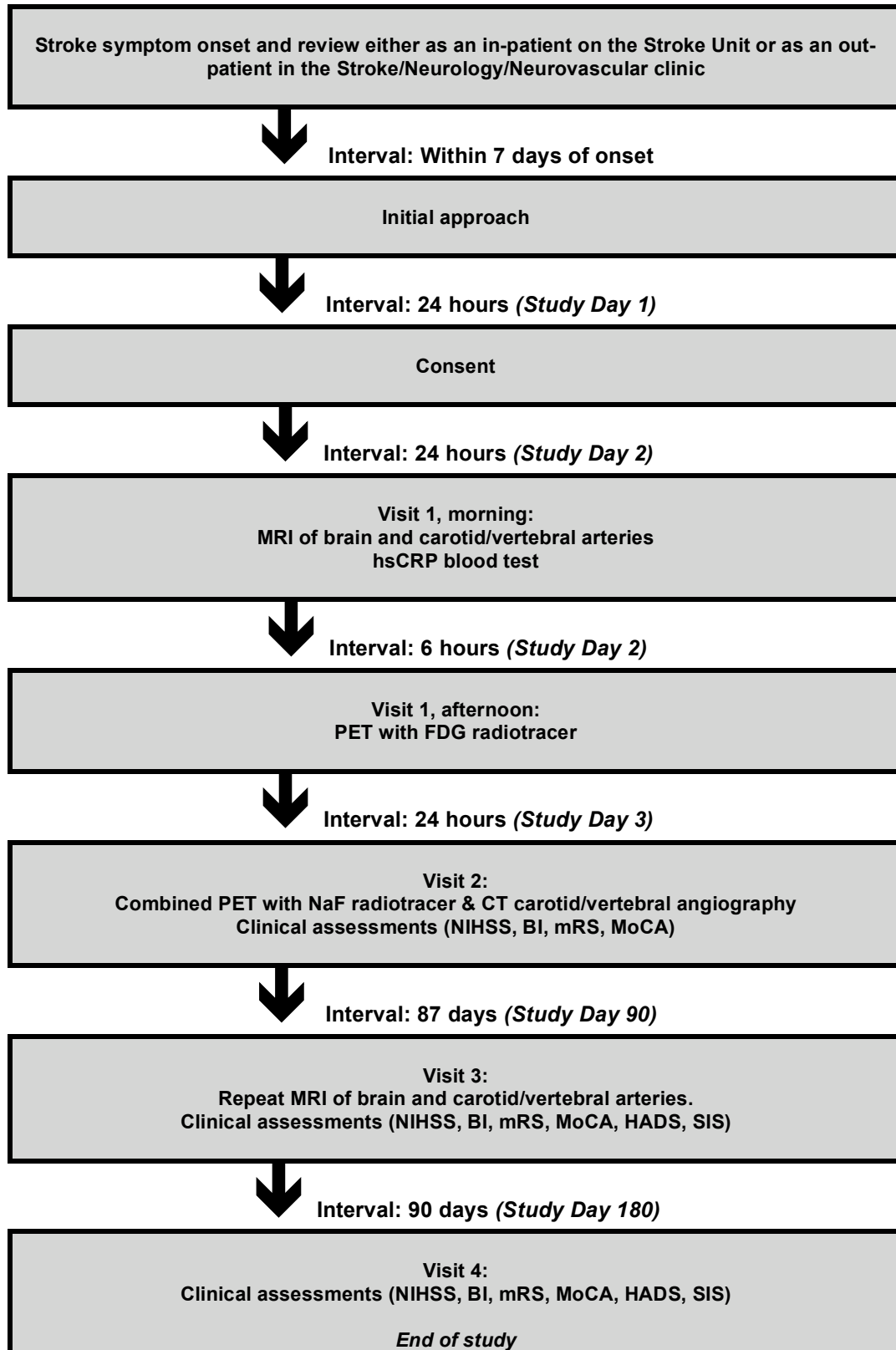


Figure 2.2: Flow chart of study procedures.

## **2.4 PET/CT technical and methodological information**

### *2.4.1 NaF-PET/CT scanning parameters*

NaF-PET/CT scans were performed using a GE Discovery 690 (GE Medical Systems Ltd, Hatfield, UK) with 64-slice computed tomography in the PET/CT Department of Addenbrooke's Hospital, Cambridge University Hospitals NHS Foundation Trust within 14 days of ischaemic stroke.

Unlike FDG-PET/CT, NaF-PET/CT scans do not require a pre-scan fast or to be below a blood glucose threshold. Participants were injected intravenously with a target of 125 MBq of NaF (sourced from Erigal Ltd, Keele, UK) followed by a 60 minute uptake time (dose and uptake time as per previous work (Dweck et al., 2012)). After this uptake period, participants were positioned supine on the scanning table, with the head and neck supported in a hard trauma collar and head holder.

After AP and lateral scouts (voltage 120 kV, tube current 10 mA), an unenhanced low-dose CT scan was performed to cover one bed position from the arch of the aorta to the external auditory meatus. CT acquisition parameters: tube voltage 120kV, tube current 40mA, rotation time 0.5 seconds, pitch 1.375, direct field of view 50cm, section thickness 3.75mm reconstructed to 3.27mm.

PET data was acquired in 3-dimensional (3D) mode over 15 minutes, covering the carotid arteries in one bed position, during which time the patient was encouraged to breathe gently. Acquisition parameters used were: matrix 256 x 256 x 47, filter 6.4mm, pixel size 2.73 x 2.73 x 3.27 mm, direct field of view 70 cm, with reconstruction using VUE Point FX<sup>TM</sup> time-of-flight reconstructions with corrections for attenuation, dead time, random coincidences, and scatter.

### *2.4.2 Carotid CT angiography*

A contrast-enhanced CTA of the carotid arteries was also performed immediately after the NaF-PET/CT scan on the same GE 690 PET/CT.

70ml Niopam 300 (Bracco UK Ltd, High Wycombe, UK) radiocontrast was injected at 5 ml/second, followed by a 50ml sodium chloride chaser. The scan was bolus-triggered once the signal in the aortic arch reached 100 HU with a 7 second monitoring delay. The CTA covered the arch of the aorta to the circle of Willis. Acquisition parameters: tube voltage 120kV, maximum tube current 200mA (with SmartPrep<sup>TM</sup> on), rotation time of 0.8 seconds, pitch 0.969:1, slice thickness 0.625mm reconstructed at 0.4mm.

#### *2.4.3 FDG-PET/CT scanning parameters*

FDG-PET/CT scans were performed using a GE Discovery 690 (GE Medical Systems Ltd, Hatfield, UK) with 64-slice computed tomography in the PET/CT Department of Addenbrooke's Hospital, Cambridge University Hospitals NHS Foundation Trust within 14 days of ischaemic stroke.

Dietary restriction has been shown to reduce myocardial FDG uptake, with SUVs of  $3.2 \pm 2.3$  and  $6.7 \pm 4.2$  in those with and without dietary restriction respectively ( $p < 0.001$ ) (Dweck et al., 2012). In this study we adopted a six-hour fast prior to injection as per previous studies (Rudd et al., 2009).

In participants without diabetes, blood glucose concentrations were confirmed as  $\leq 7.0$  mmol/L prior to tracer injection, as recommended by a position paper for cardiovascular imaging published by the European Association of Nuclear Medicine (Bucerius et al., 2015). Participants with diabetes mellitus were instructed to take their usual oral antidiabetic medications as normal, but insulin was omitted within the four hours prior to imaging, in line with the clinical protocols in our centre and previous methodology (Tarkin et al., 2017, Joshi et al., 2017). However, participants taking metformin will have been advised to omit their metformin for 48 hours following the CTA performed with the NaF-PET/CT, so metformin will not have been taken if the NaF-PET/CT preceded the FDG-PET/CT within this time window. NaF-PET/CT For participants with diabetes mellitus, if the blood glucose level was  $> 11$  mmol/L then tracer was not administered and imaging was rescheduled according to our standard clinical practice.

Participants were injected intravenously with a target of 250 MBq of  $^{18}\text{F}$ -FDG (sourced from Erigal Ltd, Keele, UK), followed by a 90 minute uptake time to reduce signal from the jugular vein, as per previous work (Tarkin et al., 2017, Joshi et al., 2017). A silence protocol (minimal vocalisation, only small sips of water permitted) was adopted during this uptake period to reduce physiological tracer uptake by neighbouring structures in close proximity to the carotid arteries. After this uptake period, participants were positioned supine on the scanning table, with the head and neck supported in a hard trauma collar and head holder.

After AP and lateral scouts (voltage 120kV, tube current 10mA), an unenhanced low-dose CT scan was performed to cover one bed position from the arch of the aorta to the external auditory meatus. CT acquisition parameters: tube voltage 120kV, tube current 40mA, rotation time 0.5 seconds, pitch 1.375, direct field of view 50cm, section thickness 3.75mm reconstructed to 3.27mm.

PET data was acquired in 3-dimensional (3D) mode over 15 minutes, covering the carotid arteries in one bed position, during which time the patient was encouraged to breathe gently. Acquisition parameters used were: matrix 256 x 256 x 47, filter 6.4mm, pixel size 2.73 x 2.73 x 3.27mm, direct field of view 70cm, with reconstruction using VUE Point FX<sup>TM</sup> time-of-flight reconstructions with corrections for attenuation, dead time, random coincidences, and scatter.

#### 2.4.4 Radiation exposure

Addition radiation exposure of the study is as follows:

125 MBq NaF	3 mSv
250 MBq FDG	5 mSv
CT for attenuation correction	$0.45 \times 2 = 0.9$ mSv
CT angiogram	3mSv
<b>Total</b>	<b>12 mSv</b>

For comparison, the dose to participants is equivalent to less than 5 years of exposure to natural background radiation in the UK. Using a risk estimate of detriment of 4.2%

/ Sv from the International Commission on Radiological Protection (ICRP) publication 103, the estimated risk of cancer (fatal or non-fatal) and of severe hereditary risks for the total research protocol dose is approximately 1 in 2000. This can be considered in the light of the natural incidence of fatal cancer, which is of the order of one in four.

#### *2.4.5 Image co-registration*

Hybrid PET/CT systems allow anatomical imaging to be performed directly after PET imaging, reducing patient movement that may result in mis-registration and avoids the need for registration against an anatomic dataset performed on a different scanner. Due to the short duration and static nature of the scan in this study it was not felt necessary to perform non-rigid co-registration that is required to accommodate patient movement over a long scan duration, as performed by Joshi et al. (Joshi et al., 2017). Consequently, rigid body co-registration was performed with optimisation performed using a combination of fiducial markers and internal anatomical landmarks, using updated methods described by Rudd et al. (Rudd et al., 2002).

For the FDG-PET/CT scan, attenuation-corrected FDG-PET images were co-registered against the low-dose CT scan. For the NaF-PET/CT, as participants underwent contrast-enhanced CTA immediately upon completion of the PET study, the attenuation-corrected NaF-PET images were co-registered against this contrast-enhanced CTA rather than the low-dose CT component of the PET/CT.

#### *2.4.6 Radiotracer uptake measurement*

For both NaF-PET/CT and FDG-PET/CT, co-registered images were resampled to 3 mm slice thickness and ROIs were drawn manually on fused PET/CT images along the common carotid and internal carotid artery to encompass the region approximately 1 cm proximal and 3 cm distal to the carotid bifurcation (i.e. 3 slices below and 10 slices above the carotid bifurcation, producing 14 slices in total including the carotid bifurcation), as per previously established methodology (Rudd et al., 2007, Joshi et al., 2017, Tarkin et al., 2017). ROIs were then transferred onto the co-registered PET to produce standardised uptake values (SUV).

SUV represents the ratio of radiotracer concentration in the target tissue to the injected radiotracer activity adjusted for weight. It is given by the equation:

$$\text{SUV} = \frac{\text{Tissue radiotracer concentration (MBq/kg)}}{\text{Injected radiotracer activity (MBq) / body weight (kg)}}$$

SUV may be further analysed as  $\text{SUV}_{\text{max}}$  and  $\text{SUV}_{\text{mean}}$ . The  $\text{SUV}_{\text{max}}$  is calculated using the highest tissue radiotracer concentration in the ROI whilst  $\text{SUV}_{\text{mean}}$  is calculated using the mean tissue radiotracer concentration throughout the ROI.

Whilst SUV may be used for all types of tissue and ROIs, the tissue-to-background ratio (TBR) was developed to correct for blood uptake of radiotracer (“blood pooling”). To calculate TBR readings ( $\text{TBR}_{\text{max}}$  and  $\text{TBR}_{\text{mean}}$ ), corresponding carotid SUVs were divided by venous  $\text{SUV}_{\text{mean}}$ . Venous  $\text{SUV}_{\text{mean}}$  was calculated by drawing mid-luminal ROIs in the jugular vein over five contiguous 3 mm slices without evidence of spill-over from neighbouring structures, and calculating the mean of the  $\text{SUV}_{\text{mean}}$  of these ROIs (Tawakol et al., 2006).

The  $\text{SUV}_{\text{max}}$ ,  $\text{SUV}_{\text{mean}}$ ,  $\text{TBR}_{\text{max}}$ , and  $\text{TBR}_{\text{mean}}$  for symptomatic and asymptomatic carotid arteries were compared for the single hottest slice (SHS), most diseased segment (MDS), and median whole vessel (WV). The SHS is defined as the single ROI with the highest tracer uptake for the artery. The MDS considers the most diseased 6 mm of the artery (based on tracer uptake) and represents the mean of ROIs of three contiguous axial slices where the central ROI is the SHS, along with the slice immediately proximal and immediately distal to SHS, as per previous methodology (Fayad et al., 2011a). Finally, the WV is the median of tracer uptake in all 14 axial slices of the artery (see **Figures 2.3** and **2.4**).

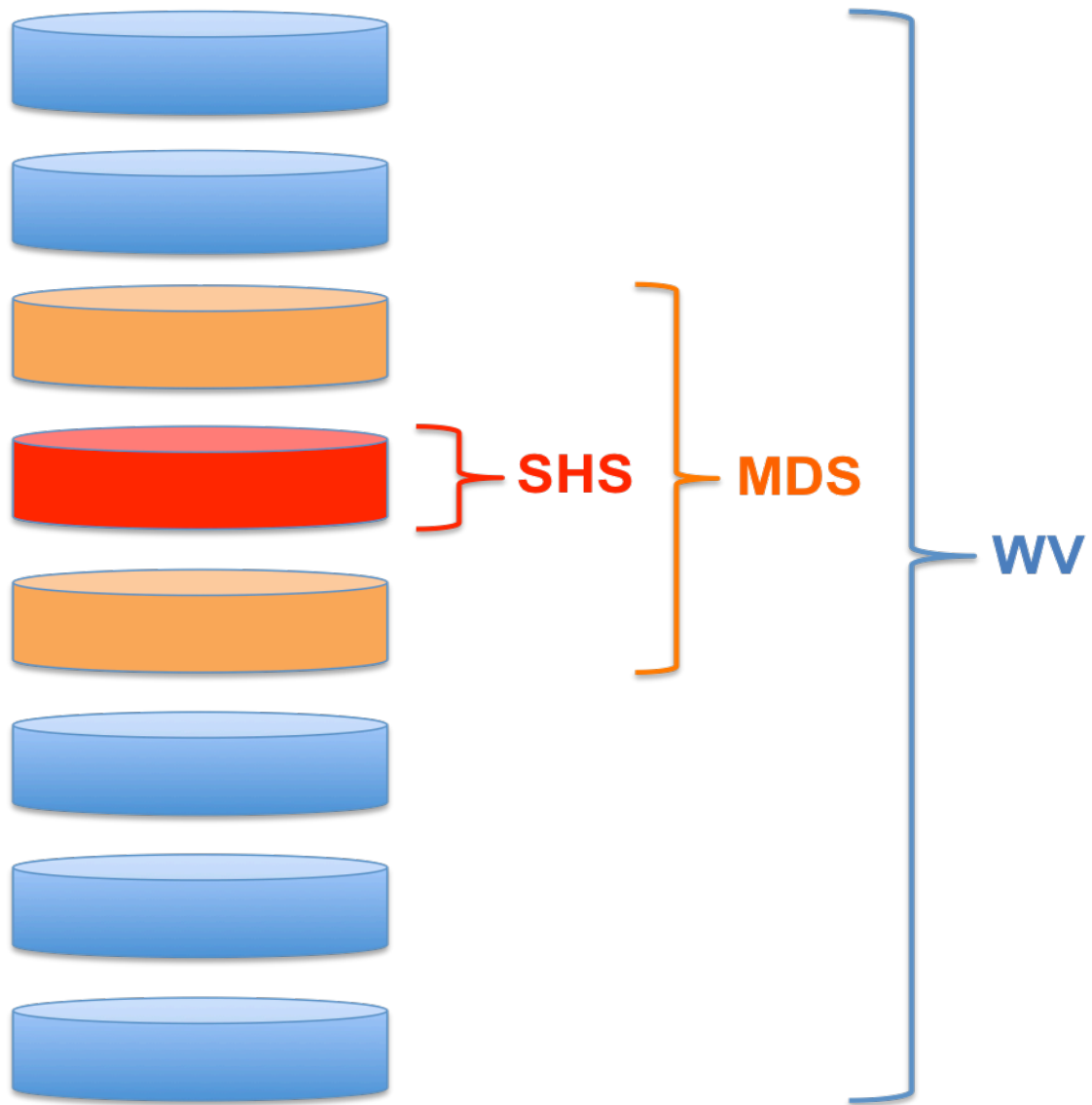


**Figure 2.3: Schema of the relationship between SHS, MDS, and WV readings.** The single hottest slice (SHS) is the axial slice with the highest radiotracer uptake; the most diseased segment (MDS) is the mean of the three contiguous axial slices surrounding the SHS; whole vessel (WV) is the median of all 14 axial slices along the carotid artery.

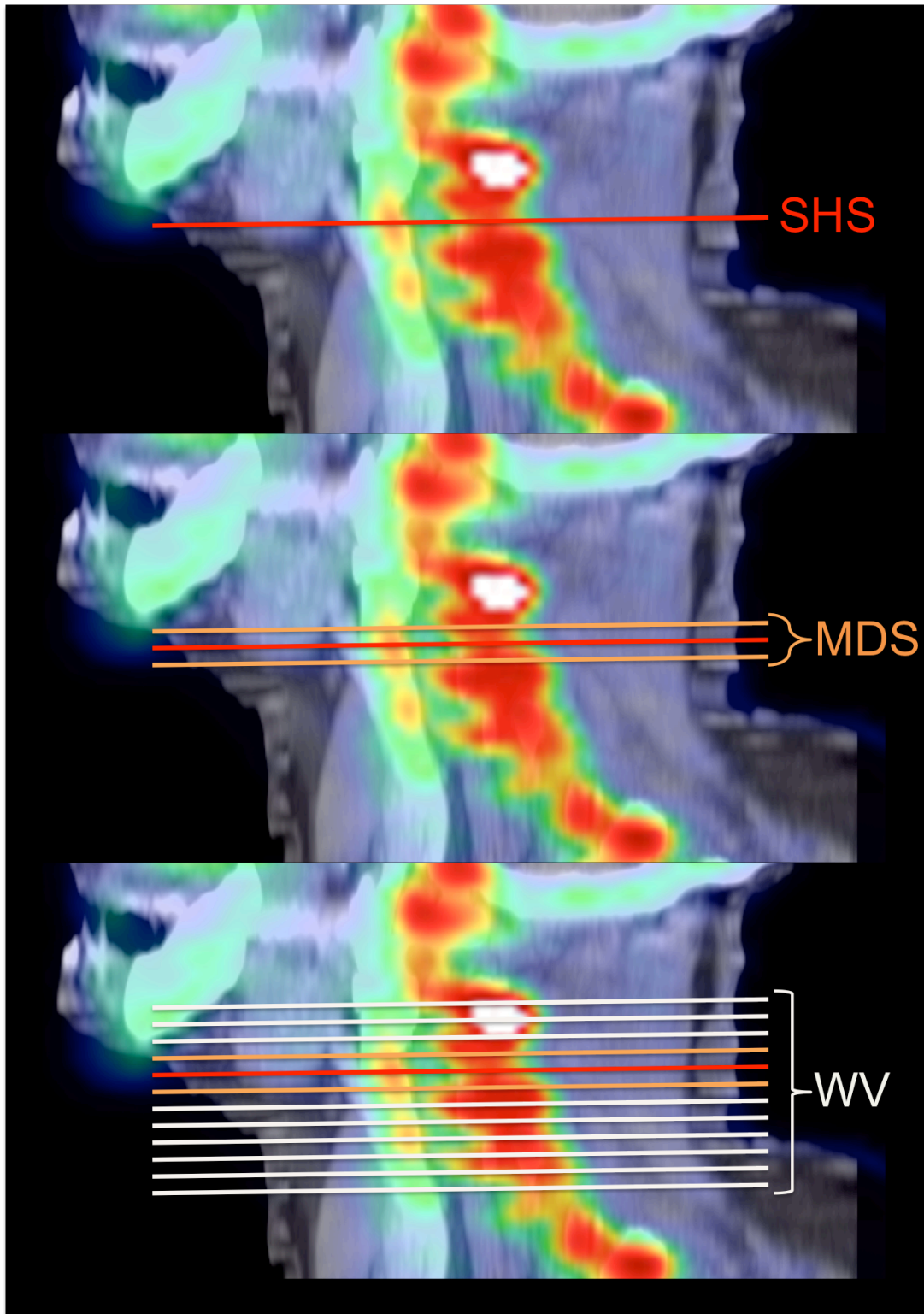


**Figure 2.4: Radiological representation of SHS, MDS, and WV readings.** SHS, MDS, and WV measures of tracer uptake shown relative to plaque uptake (using NaF-PET/CT in this example).

The primary reader (NRE) was blinded to the symptomatic artery. As described above, participants were allocated a randomly generated four digit participant identifier on study enrolment, so individual participants were not identifiable to the reader. Initial analysis of the first seven participants was conducted for interim analysis in June 2015. Remaining analysis was conducted after the study ended (including re-analysis of the original cohort).

PET imaging datasets were analysed using OsiriX (version 5.7.1, OsiriX Imaging Software, Geneva, Switzerland) using an iMac desktop computer (Apple Inc., Cupertino, California, United States of America).

#### *2.4.7 PET methodological considerations*

There are a number of methodological and technical considerations in PET/CT assessment of the plaque. At a single study level, these primarily include partial volume correction and methods of tracer uptake quantification. In contrast, the heterogeneity of different study protocols within the field also has implications for reproducibility and the ability to pool results in larger meta-analyses.

##### *2.4.7.1 Partial volume correction*

Measurement of tracer uptake within the atheroma is dependent upon the size of the atheroma and the resolution of the scanner. The partial-volume effect occurs when limited resolution results in difficulty differentiating the tracer activity of the ROI from the tracer activity of the surrounding tissues. This may lead to “spill-out,” where the tracer signal from the atheroma falls outside of the ROI, and “spill-in” where tracer signal from adjacent tissue falls within the ROI. The combination of these two effects results in partial volume error (PVE). Small atheromatous lesions falling below the spatial resolution of the scanner are particularly at risk of PVE. It is estimated that the dimensions of a homogenous ROI need to be two to three times the spatial resolution of the scanner in order to minimise PVE (Hoffman et al., 1979). Reduction of PVE through partial volume correction (PVC) can be performed using a geometric transfer matrix (GTM), whereby co-registration with a higher resolution modality allows restriction of the tracer signal to a corresponding voxel-based volume

of interest that can then undergo further voxel-based adjustment for PVE using an algorithm proposed by Rousset et al. (Rousset et al., 1998). This method has been applied to atheroma imaging (using co-registration with MRI) and was found to improve quantification of tracer activity and to be highly reproducible (Izquierdo-Garcia et al., 2009).

#### 2.4.7.2 SUV versus TBR

This study will measure both SUV and TBR values ( $SUV_{\text{mean}}$ ,  $SUV_{\text{max}}$ ,  $TBR_{\text{mean}}$ , and  $TBR_{\text{max}}$ ). This approach has been adopted for two reasons. Firstly, whilst TBR will accommodate factors that may increase blood pooling (such as impaired renal clearance), the majority of vascular imaging studies have used SUV. Hence, SUV will allow comparison to previous studies (given limitations by different scan methodologies). Secondly, there remains debate over the accuracy of TBR as often the SUV in blood pool activity is low and hence small changes in the value have a significant effect on the TBR (Chen and Dilsizian, 2015). ‘Spill-out’ effects, where the poor spatial resolution of PET results in vascular wall activity being mistakenly measured as part of SUV blood pool activity, may also lead to TBR being a more variable and less reproducible measure compared to SUV (Huet et al., 2015). Finally, measuring both SUV and TBR will allow both to be correlated with outcome measures to see if one is more tightly correlated.

Studies conducted to date have varied in their use of SUV or TBR, and the most appropriate quantification method remains a subject of debate (Huet et al., 2015). In a simulated atherosclerotic plaque model, marked bias was found in both measured  $SUV_{\text{max}}$  and  $SUV_{\text{mean}}$  compared to the modeled values, largely due to the spatial resolution of the reconstructed image typically being more than three times the thickness of the atherosclerotic plaque, resulting in a reduced ability to correct for PVE. Bias was more marked when fewer iterations were used during image reconstruction (Huet et al., 2015).

In a study of 32 patients undergoing endarterectomy, Niccoli et al. compared the ability of  $SUV_{\text{max}}$ ,  $SUV_{\text{mean}}$ ,  $TBR_{\text{max}}$ , and  $TBR_{\text{mean}}$  to differentiate *in vivo* plaques classified as either inflamed or non-inflamed following histological examination *ex*

*vivo*. Within the symptomatic arteries, the authors found that the differences for  $SUV_{max}$  and  $SUV_{mean}$  between inflamed and non-inflamed plaques were non-significant, whilst both  $TBR_{max}$  and  $TBR_{mean}$  were able to differentiate between plaques found to be inflamed or non-inflamed on histology (Niccoli Asabella et al., 2014).

TBR is not without its criticisms. Blood-pool SUV has been shown to decrease with increasing injection to scan intervals (Mean SUV within the jugular vein was 1.04 +/- 0.16 at 1 hour, 0.79 +/- 0.03 at 2 hours, 0.66 +/- 0.04 at 3 hours). Consequently, plaque TBR values differed significantly between cohorts scanned at two and three hours. In contrast, tissue  $SUV_{max}$  did not differ between these time points (Oh et al., 2010). Furthermore, impaired renal function will also contribute to increased blood-pool activity. Blood-pool SUV has been found to be inversely proportional to the estimated glomerular filtration rate, resulting in a lower TBR with lower renal clearance (Derlin et al., 2011a).

Whilst there has been an overall shift towards TBR in arterial PET imaging, the possible confounders described above must be considered when comparing results both within the same study and against other studies. Standardisation of scan methodologies and patient cohorts will help address this.

#### *2.4.7.3 Reproducibility*

Increasingly specific radioligands have resulted in improved signal-to-background ratios and reproducibility, with high intra-rater and inter-rater reproducibility reported for NaF and  $^{68}Ga$ -DOTATATE (Rominger et al., 2010, Dweck et al., 2012). However, a major consideration within the field of vascular PET imaging is the wider reproducibility of individual studies. Typically most vascular PET studies of symptomatic patients are small, with fewer than 50 participants. Whilst the multitude of FDG studies would seem prime for meta-analysis, the heterogeneous patient populations and variations in methodology pose barriers to such analyses. Variations in tracer doses, interval between symptoms and imaging, blood glucose thresholds, and measurement techniques (SUV versus TBR) are a few of the differences in studies that make direct comparison difficult. The effect of the symptom to scan

interval on the potential variability of the PET signal is difficult to quantify as radiation exposure is a barrier to longitudinal studies and should therefore be analysed in any multivariate analysis. Consequently, there is a move towards establishing a recognised common standard for arterial PET imaging. A recent position paper from the European Association of Nuclear Medicine has recommended such common standards for FDG-PET, particularly with regards to injected dose, circulation uptake time, prescan fasting glucose limits, and suggested quantification using TBR in most cases (Bucerius et al., 2015). Adopting a unified approach to scanning protocols and quantification will allow the high inter-rater reproducibility to be exploited, existing data to be pooled into larger meta-analyses, and standardisation of multicenter PET imaging studies.

To assess intra-rater reproducibility, the primary reader (NRE) repeated ROI measurements in 20% of the NaF-PET/CTs two months apart to assess agreement on the site of the carotid bifurcation and reproducibility of NaF uptake measurements.

A second experienced reader (Mr Mohammed Chowdhury (MMC), Academic Clinical Fellow, Department of Vascular Surgery, University of Cambridge) repeated ROIs in 20% of the NaF-PET/CTs to assess inter-rater agreement on the site of the carotid bifurcation and reproducibility of NaF uptake measurements.

Both intra-rater and inter-rater reproducibility was calculated on an axial slice basis, meaning that each of the 6 participants' 14 ROIs were compared, resulting in 84 readings in total being tested for reproducibility. Both intra-rater and inter-rater reproducibility was calculated using intra-class correlation coefficients (ICC), as per previous methodology (Dweck et al., 2012, Giannotti et al., 2017).

## **2.5 CT calcium scoring of the carotid artery**

A wide variety in methods to measure carotid calcification have been used in studies (dichotomous 'present'/'absent', semi-quantitative ordinal grading scales, extent of involvement of arterial circumference) while conventional coronary artery calcium scoring uses methods proposed by Agatston et al. (Agatston et al., 1990), an approach that has been validated within the carotid arteries in proof of principle work (Katano

and Yamada, 2007). The Agatston score for an area of coronary calcification is calculated by:

$$\text{Agatston score} = \text{weighted density} \times \text{area (mm}^2\text{)}$$

Where weighted density is scored according to the peak density in Hounsfield Units in the lesion:

<b>Peak density</b>	<b>Weighted density</b>
130–199 HU	1
200–299 HU	2
300–399 HU	3
≥400 HU	4

Conventionally, the coronary artery calcium score is given for the whole heart by summing the calcium scores of each coronary artery. More recently, it has been proposed that calcium scoring in the coronary arteries should be performed on a vessel-by-vessel or lesion-by-lesion basis. This allows consideration of the spatial distribution of calcifications, including distribution in low versus high-risk areas. In a comparative study, Qian et al. showed that maximum lesion-based Agatston scores were able to identify obstructive coronary artery disease whilst whole-heart Agatston scores could not (Qian et al., 2010).

The use of multidetector CT angiography to detect calcified coronary plaque has been shown to be highly sensitive and specific (94% for both respectively) (Achenbach et al., 2004). In the carotid artery, there is a strong association between calcium score and luminal stenosis, and calcium scoring is highly reproducible, with an intraclass correlation coefficient of 0.98 (95% confidence interval 0.97-0.99) reported (Nandalur et al., 2006).

Carotid Agatston scores were measured from the unenhanced CT carotid angiogram (performed during PET/CT) using the Calcium Scoring Plugin (version 1.0) in OsiriX (version 5.7.1, OsiriX Imaging Software, Geneva, Switzerland) using an iMac

desktop computer (Apple Inc., Cupertino, California, United States of America). The detection threshold for calcification was set at 130 HU.

Carotid calcification was measured using three approaches. The first approach measured the carotid artery calcification score (CACS) from the origin of the common carotid artery to the skull base, giving a total value for each artery that was considered for each artery individually. These were also combined in a second approach using an individual's symptomatic and asymptomatic carotid arteries to give a 'total carotid arterial calcification score' (TCACS) as a measure of an individual's overall cardiovascular risk profile.

The third approach measured carotid calcium scores on an axial slice-by-slice basis in the same 14 axial slice regions identified by the ROIs in the NaF-PET/CT analysis, thereby allowing co-registration of microcalcification and macrocalcification.

## **2.6 MRI technical and methodological information**

### *2.6.1 General MRI information*

Baseline and follow-up MRIs of the brain and carotid arteries took place in the Magnetic Resonance Imaging and Spectroscopy Unit (MRIS). MRI brain and carotid MRA sequences were chosen in consultation with Professor Jonathan Gillard (Professor of Neuroradiology, University of Cambridge) and MRI physicists (Dr Martin Graves, Clinical Scientist and Head of MR Physics, and Andrew Patterson, Clinical Scientist, both in the Department of Radiology, Cambridge University Hospitals NHS Foundation Trust).

MRI brain and carotid MRA was conducted primarily on a 3T MRI (or 1.5T if limited by safety factors such as MRI-compatible metal implants not able to be scanned on a 3T machine or physical factors such as body habitus). 3T imaging of the brain and carotid arteries was performed on a 3T GE MR750 whole body scanner with a 12-channel head, neck, and spine coil with a brachial plexus attachment. 1.5T imaging was performed on a 1.5T GE MR750 whole body scanner using the same coil.

Individuals were scanned on the same scanner at the same field strength for both the baseline and follow-up imaging.

### 2.6.2 MRI brain

Baseline and follow-up MRI brain included T1, T2, DWI, fluid-attenuated inversion recovery (FLAIR), and gradient echo (GRE) sequences. The imaging parameters for each sequence are the same as for standard clinical investigations and are listed in **Table 2.3**.

Sequence	Imaging mode	Plane	Flip angle (degrees)	Echo time (TE) (ms)	Number of echoes	Repetition time (TR) (ms)	Inversion time (TI) (ms)	Echo train length	Receiver bandwidth (Hz)	Field of view (cm)	Slice thickness (mm)
T1	2D	Oblique	111	20.0	1	2646.3	813	7	31.25	24	5
T2	2D	Oblique	111	85.0	1	4156.0	-	24	62.50	24	6
FLAIR	2D	Oblique	111	120.0	1	8000.0	2000	-	41.67	24	6
DWI	2D	Oblique	-	-	1	6000.0	-	-	-	24	5
GRE	2D	Oblique	20	15.0	1	500.0	-	-	19.23	24	6

**Table 2.3:** 3T MRI brain imaging parameters.

### 2.6.3 Carotid MRA

Carotid MRA was also performed at baseline and at three-month follow-up. Sequences included a time of flight (TOF) MRA and contrast-enhanced MRA (ceMRA), T1-based imaging of the fibrous cap using 3D CUBE sequences pre- and post-contrast, and direct thrombus imaging (DTI). Technical parameters of the sequences are included in **Table 2.4**.

Sequence	Imaging mode	Plane	Flip angle (degrees)	Echo time (TE) (ms)	Number of echoes	Repetition time (TR) (ms)	Inversion time (TI) (ms)	Echo train length	Receiver bandwidth (Hz)	Field of view (cm)	Slice thickness (mm)
TOF	2D	Axial	90	Min	1	Min	-	-	31.25	30	6
DTI	3D	Coronal	30	Min	-	-	300	-	25.0	16	1
3D CUBE	3D	Coronal		Min	1	580.0	-	28	50.0	16	1.4
ceMRA	3D	Oblique	25	Min	-	-	-	-	62.50	31	1.4
3D CUBE	3D	Coronal	-	Min	1	580.0	-	28	50.00	16	1.4

**Table 2.4:** 3T carotid MRA imaging parameters.

#### 2.6.4 Assessment of leukoaraiosis

The extent of leukoaraiosis was scored semi-quantitatively from the axial fluid attenuation inversion recovery (FLAIR) sequence using the scoring system proposed by Fazekas et al. (Fazekas et al., 1987), and later modified by Pantoni et al. (Pantoni et al., 2005). The Fazekas scale has been shown to have a good degree of both intra-rater and inter-rater reliability (Boutet et al., 2016, Kapeller et al., 2003).

The Fazekas score has been dichotomised previously (Takami et al., 2012), and in this study we dichotomised global (i.e. whole brain) periventricular and deep white matter hyperintensities according to no/mild or moderate/severe leukoaraiosis (using the visual scale described and illustrated by Pantoni et al. (Pantoni et al., 2005)) given that the majority of our vasculopathic cohort showed some small vessel disease.

MRI interpretation of study baseline MRI scans was performed by two experienced readers (NRE and Ms. Jessica Walsh, Research Associate, Department of Clinical Neurosciences, University of Cambridge), both of whom have completed internal training in marking of small vessel disease lesions. Intra-class correlation coefficients for inter-rater reliability were then calculated. Both readers were blinded to the clinical characteristics and PET/CT results at the time of interpretation.

Imaging datasets were analysed using OsiriX (version 5.7.1, OsiriX Imaging Software, Geneva, Switzerland) using an iMac desktop computer (Apple Inc., Cupertino, California, United States of America).

#### *2.6.5 Measurement of brain lesion volume*

In the genesis of FLAIR lesions, increasing vasogenic oedema following ischaemia results in T2 prolongation. In animal studies, changes after 2.5 hours of middle cerebral artery occlusion (MCAO) were more marked in T2-weighted sequences than DWI (Neumann-Haefelin et al., 2000). These changes peaked at approximately 48 hours after MCAO and were typically larger than the DWI lesion, this difference likely representing vasogenic oedema (Neumann-Haefelin et al., 2000).

Infarct volumes were measured from DWI and FLAIR sequences, with baseline infarcts defined as the FLAIR lesion corresponding to a DWI hyperintensity on the DWI sequence. Follow-up lesion volume was calculated by drawing around the same lesion(s) on the repeat imaging.

In the case of multiple regions of increased signal, the total lesion volume was calculated as the sum of all individual volumes. The same approach was employed when re-measuring lesion volumes on follow-up imaging, with comparison with original scan to ensure all hyperintensities at baseline were included on repeat imaging. In the event of cavitating infarcts, the infarct volume was measured including the cavitation. Lesion volumes were also calculated for the ‘primary lesion,’ defined as the largest contiguous region of increased signal but excluding smaller satellite lesions.

When comparing FLAIR lesion volumes at baseline and at follow-up, we considered only lesions where the baseline FLAIR primary lesion volume was greater than 1 ml. This is due to the technical limitations of measuring small volume lesions frequently limited to a single axial slice, and which may be affected by the positioning of the participant in the scanner. Jha et al. used a similar approach but used a cut-off of 5 ml (Jha et al., 2014). In a longitudinal MRI study by Beaulieu et al., 19 (90.5%) had initial DWI volumes greater than 1 ml (with the remaining two being 0.9 ml and 0.7

ml), which provided sufficient volume to assess interval lesion change (Beaulieu et al., 1999). We used a 1 ml cut-off for these reasons.

Lesion marking of DWI and FLAIR lesions using a semi-automated technique in cerebrovascular disease has been shown to have good levels of intra-rater and inter-rater reliability, and the reproducibility is increased with larger lesion volumes (Luby et al., 2006), consistent with the above consideration. The use of FLAIR lesion volume measurement in follow-up studies has been shown to be superior to the use of T2 lesion volume measurements in terms of inter-rater reproducibility (Neumann et al., 2009).

Lesion volumes were calculated using semi-automatic ROI marking using Jim Imaging Software (version 7.0, Xinapse Systems Ltd., Essex, United Kingdom) (**Figure 2.5**).

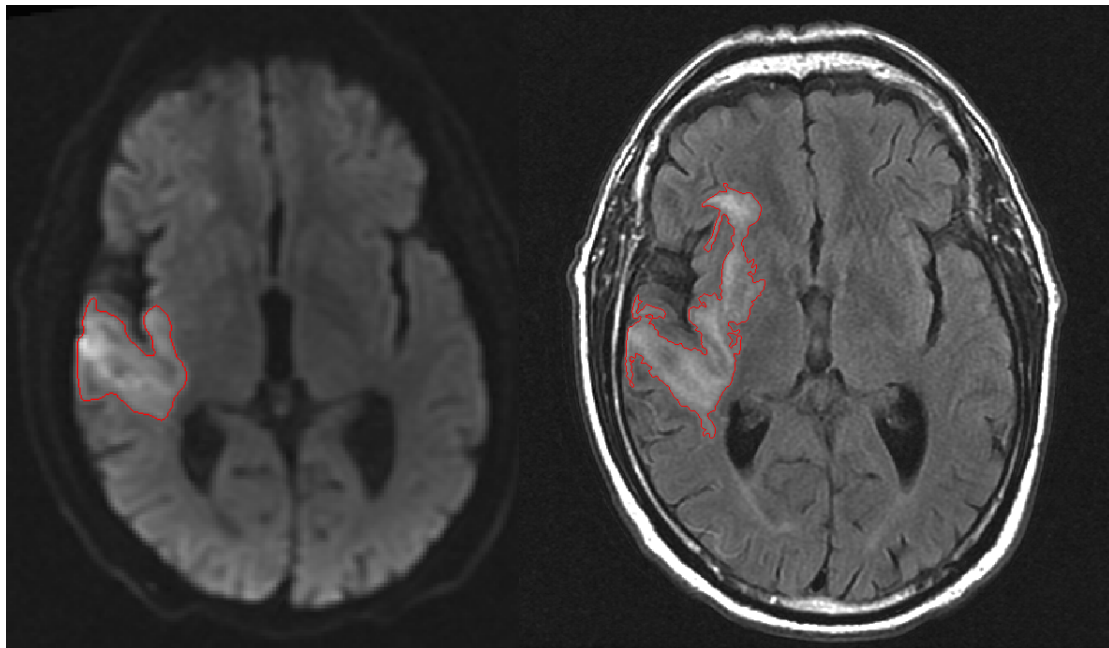


**Figure 2.5: Semi-automated brain lesion marking.** Axial DWI (left) and FLAIR (right) slices illustrating semi-automated lesion marking (red line) of baseline imaging for participant 3541.

Images were anonymised using randomly allocated numerical identifiers and image analysis was performed blinded to the participant's clinical characteristics, clinical outcomes, and PET readings.

## **2.7 Clinical assessments**

Physical, functional, and cognitive assessments following the stroke were conducted in addition to the radiological investigations. At baseline, functional assessment were performed with a patient interview including pre-morbid and current modified Rankin Scale (mRS), National Institutes for Health Research Stroke Scale (NIHSS), pre-morbid and current Barthel Index (BI) and Montreal Cognitive Assessment (MoCA) (Muir et al., 1996, Sulter et al., 1999, Pendlebury et al., 2010).

In order to assess recovery, clinical assessments were repeated (mRS, NIHSS, BI and MoCA), as well as the Hospital Anxiety and Depression Score (HADS) and Stroke Impact Scale (SIS) at three and six months (Allan et al., 2013, Duncan et al., 2003).

Montreal Cognitive Assessment (MoCA): This assessment was performed within seven days of the stroke, and at three and six months after the stroke. It is a 30-point test that is validated to assess several cognitive domains, including short-term memory recall, visuospatial, attention, concentration, working memory, orientation to time and place, and language. Three validated versions of the MoCA exist, and a different version was used at each study visit in order to reduce carry-over between tests.

Modified Rankin Scale (mRS): This assessment measures the functional status of the individual using a 0-6 scale (0 being no symptoms, 6 being dead, and the range in between representing degrees of functional impairment). This was assessed through clinical history and examination.

Barthel Index (BI): The Barthel Index is an ordinal scale measuring the ability to perform activities of daily living. It consists of ten domains, each scored according to a 10-point scale. Higher scores reflect greater independence in performing activities of daily living. This was assessed through clinical history.

National Institutes of Health Stroke Scale (NIHSS): The National Institutes of Health Stroke Scale measures the degree of functional stroke severity using a 42-point scale across eleven items. Higher scores reflect greater severity and functional impairment. This was assessed through clinical examination.

Hospital Anxiety and Depression Scale (HADS): The Hospital Anxiety and Depression Scale is an ordinal scale across 14 domains related to levels of anxiety and depression (7 each). Each domain is scored from 0-3 giving a maximum score of 21 for both anxiety and depression.

Stroke Impact Scale (SIS): This assessment is an ordinal scale measuring the individual's perception of the impact of stroke upon their health and life. It assesses 8 domains across 59 questions, each with a 5-point Likert scale. Each domain has a score ranging from 0-100. It was completed through patient interview.

Copyright permissions were granted for academic use for the BI, MoCA, HADS, and SIS.

## **2.8 Blood biomarkers**

4.9 mL of venous blood was drawn and stored in serum gel at the time of FDG-PET/CT and sent for analysis for hsCRP by Clinical Biochemistry, Cambridge University Hospitals NHS Foundation Trust. Samples were anonymised using the participant's randomly allocated four-digit participant number.

## **2.9 Statistical analysis**

Continuous data was tested for normality using Shapiro-Wilk testing. Parametric data was reported as mean $\pm$ SD and non-parametric data reported as median and IQR. Specifically for PET tracer uptake, the distribution of uptake along all the ROIs along a single artery was tested. The finding that tracer uptake was not normally distributed along the length of the artery resulted in us using the median value to represent the WV uptake measures. The spread of SHS, MDS, and WV uptake measures for

symptomatic arteries and asymptomatic arteries were tested for normality and appropriate tests used accordingly as discussed below.

When comparing unpaired groups, parametric readings were compared using t-testing and non-parametric readings were compared using Wilcoxon rank sum testing as appropriate. The cut-off for statistical significance was set at  $p=0.05$ .

Paired testing was performed comparing radiotracer (NaF and FDG) uptake in the symptomatic carotid artery against uptake in the corresponding asymptomatic carotid artery in the same participant, with parametric readings compared using paired t-testing or non-parametric readings compared using Wilcoxon signed-rank testing as appropriate.

Correlations were tested using two-tailed Spearman's rho correlation (for non-parametric or ordinal data) or Pearson's correlation coefficient (for parametric data).

Tracer uptake was adjusted for the degree of stenosis using stenosis categories ("1-29%", "30-49", "50-69%", "70-89%", "90-99%") considering both symptomatic and asymptomatic arteries. The trend was tested using Kruskal-Wallis one-way ANOVA testing (for non-parametric data).

Multivariable analysis was performed by adding all risk factors considered on univariable testing (regardless of significance) into a regression model, which was subsequently refined using likelihood-ratio testing using backwards elimination. This approach successively removes variables from the model in the order of least significance at each stage until the 'goodness of fit' is maximised for the model. The goodness of fit was measured using the Akaike information criteria (AIC) until the minimum value for the model was achieved (indicating the best fit). Resulting adjusted  $R^2$  and AIC values indicating the goodness of fit are reported. Multiple linear regression was performed if residuals fulfilled criteria in regression diagnostics. Log transformation of the dependent variable was performed when indicated from regression diagnostics. This statistical approach was discussed and regression diagnostics reviewed prior to analysis and resulting outputs discussed with an

epidemiological statistician with experience in cerebrovascular disease (Dr Ali Amin, Department of Clinical Neurosciences, University of Cambridge).

The initial statistical approach to the study was discussed with Dr Simon Bond (Senior Statistician, NIHR Research Development Service East of England, and Cambridge Clinical Trials Unit Lead for Statistics). Further statistical assistance and review was provided by two epidemiological statisticians with experience in cerebrovascular disease and risk factor analysis (Dr Ali Amin, Research Associate, Department of Clinical Neurosciences, University of Cambridge and Dr Loes Rutten-Jacobs, Research Associate, Department of Clinical Neurosciences, University of Cambridge).

Statistical analysis was performed using R (version 3.3.1, 2016, R Foundation for Statistical Computing, Vienna, Austria) and SPSS Statistics (version 23, 2015, International Business Machines Corporation, Armonk, New York, United States of America).

**Chapter Three:  
Sodium Fluoride PET for Identifying Culprit Carotid Atheroma and  
Investigating the Relationship between Microcalcification and  
Macrocalcification.**

### **3.1 Introduction**

#### *3.1.1 Aims of the chapter*

This chapter will consider the use of NaF-PET in vascular imaging and has the following specific questions:

1. Can NaF-PET discriminate between culprit and non-culprit carotid artery atherosclerotic plaques non-invasively *in vivo*?
2. Is there an association between NaF uptake and stroke severity?
3. Does the degree of luminal stenosis affect NaF uptake?
4. Does the extent of macrocalcification differ between symptomatic and asymptomatic carotid arteries?
5. What is the relationship between NaF uptake and macrocalcification in terms of the extent and distribution of the disease?
6. How do conventional vascular risk factors influence both microcalcification and macrocalcification?

The main hypothesis for this chapter is:

- i. NaF uptake (both SUV and TBR) will be higher in culprit atheroma than asymptomatic non-culprit atheroma.

#### *3.1.2 In vivo NaF-PET imaging*

As discussed in chapter one, microcalcification within the fibrous cap is implicated in mechanical destabilisation of the atheroma. However, despite its importance in plaque rupture, the ability to detect microcalcification *in vivo* remains limited. The small size of microcalcification – calcium deposition smaller than 50  $\mu\text{m}$  as detected by *ex vivo*  $\mu\text{CT}$  (Maldonado et al., 2012) – means that it falls below the spatial resolution for

detection by either CT or MRI *in vivo* clinical imaging, and does not produce an echogenic appearance on ultrasound. The solution to this problem may lie in imaging the underlying molecular processes rather than relying on structural imaging.

$^{18}\text{F}$ -NaF is a radioligand that has been used for bone imaging since 1962, finding clinical use in the PET evaluation of osseous metastatic disease over the subsequent decades (Blau et al., 1962). NaF identifies sites of active microcalcification, where radiolabelled fluoride is exchanged for the hydroxyl group in hydroxyapatite to form fluoroapatite (Hawkins et al., 1992).

### *3.1.2.1 NaF-PET imaging in asymptomatic plaques*

Vascular uptake of NaF was first investigated by Derlin et al. where incidental arterial uptake was detected in 57 (76%) of 75 asymptomatic individuals undergoing whole-body NaF-PET for assessment for bone metastases. This retrospective study found 254 sites of uptake across all arterial territories (common carotid arteries, thoracic and abdominal aorta, iliac arteries, and femoral arteries) in these individuals, but although NaF uptake was more likely to occur in lesions with extensive macrocalcification, there was no statistically significant association between NaF  $\text{SUV}_{\text{max}}$  and calcium score using an ordinal 0-4 scale. Furthermore, distinct areas of NaF uptake and macrocalcification occurring in isolation suggested NaF uptake reflected the active mineralisation process in microcalcification rather than simply the burden of macrocalcification (Derlin et al., 2010).

Further examples of a lack of co-localisation between regional macrocalcification and regional NaF uptake have been found in other asymptomatic cohorts, with an inverse relationship between NaF TBR and semi-quantitative plaque calcium density across all arterial territories reported by Fiz et al. (Fiz et al., 2015, Morbelli et al., 2014). Morbelli et al. demonstrated that the presence of cardiovascular risk factors (as measured by a Framingham risk score) correlated with NaF uptake (both  $\text{SUV}_{\text{max}}$  and  $\text{TBR}_{\text{max}}$ ) but not arterial macrocalcification (measured using Agatston scoring), through the study's measurement of uptake across the whole vessel may miss focal concomitant areas of macrocalcification and NaF uptake (Morbelli et al., 2014).

Further studies have found strong associations between carotid NaF uptake and calcification and the presence of cardiovascular risk factors in a neurologically asymptomatic oncologic population. In one study, Derlin et al. found 140 (26%) of 538 carotid artery segments had both NaF uptake and macrocalcification detectable by CT, and 46 (8.6%) had macrocalcification but no NaF uptake (Derlin et al., 2011c). In contrast to the results of the aforementioned studies, there were no areas of NaF uptake without visible macrocalcification. In this asymptomatic population, NaF  $SUV_{max}$  correlated strongly with the extent of calcification within the carotid plaque (measured as an ordinal scale according to proportion of arterial wall circumference calcified) ( $r=0.85$ ,  $p<0.0001$ ). As arterial macrocalcification reflects the vascular risk profile (Ulusoy et al., 2015), it is unsurprising that the same study found associations between NaF  $SUV_{max}$  and some cardiovascular risk factors; age, male sex, hypertension, and hypercholesterolaemia. However, there was no association with previous cardiovascular events, although associations of NaF uptake with a history of smoking or diabetes approached, but did not reach, significance ( $p=0.12$  and  $p=0.11$  respectively). Tracer accumulation weakly correlated inversely with BMI ( $r = -0.13$ ,  $p=0.04$ ). In contrast, the presence of plaque macrocalcification was significantly associated with age, male sex, hypertension, hypercholesterolaemia, diabetes, history of smoking, and prior cardiovascular events. Finally, individuals with multiple cardiovascular risk factors had a higher proportion of plaques with NaF uptake as a dichotomous measure, though there was no significant correlation between quantified NaF uptake and the number of cardiovascular risk factors.

In addition to this relationship between NaF uptake and macrocalcification, dual-tracer studies have elucidated the relationship between different metabolic processes within an asymptomatic cohort. Derlin et al. performed a dual-tracer PET/CT study using FDG-PET and NaF-PET in a further asymptomatic oncological patient cohort and found that of 215 arterial lesions identified by either tracer (across aorta, carotid, iliac, and femoral arteries), only in 14 (6.5%) was there concomitant FDG and NaF uptake. These results imply that macrophage-driven inflammation and microcalcification are two related but distinct processes. Furthermore, whilst 77.1% of NaF-positive plaques co-localised with macrocalcification, only 14.5% of FDG-positive plaques co-localised with macrocalcification (Derlin et al., 2011b). In

contrast to their previous study, in this study Derlin et al. found a moderate correlation between NaF SUV<sub>max</sub> and calcification score ( $r=0.36$ ,  $p<0.001$ ).

### *3.1.2.2 NaF imaging in symptomatic and vulnerable plaques*

While oncological cohorts have indicated the ability of NaF-PET to identify plaques in asymptomatic disease, there has been increasing attention to the use of the tracer to identify high vulnerability plaques. In 2012, Dweck et al. were the first to assess disease within the coronary arteries when they performed a prospective dual tracer (FDG and NaF) study in individuals with and without coronary artery disease (CAD, the presence of which was defined as a previous clinical diagnosis or having a coronary calcium score above zero) (Dweck et al., 2012). Unlike the ubiquitous myocardial uptake of FDG, NaF showed a better signal-to-noise ratio and its uptake was quantifiable in 96% of the coronary territories examined. This study had a small control group (thirteen participants) but was able to demonstrate NaF uptake to be higher in those with coronary artery disease than the control group (TBR<sub>max</sub>  $1.64\pm 0.49$  versus  $1.23\pm 0.24$  respectively;  $p=0.003$ ). As was observed in asymptomatic cohorts, the authors noted focal NaF uptake both overlying and distinct from areas of macrocalcification, as well as areas of macrocalcification with no tracer uptake. Of participants with the highest level of macrocalcification (coronary Agatston scores  $>1,000$ ), only 59% showed significant NaF uptake above that of controls. However, overall within plaques there was a strong correlation between coronary calcification score and NaF uptake ( $r=0.652$ ,  $p<0.001$ ). In individuals with multiple coronary plaques, culprit plaques had an average 50% increase in NaF uptake compared to inactive plaques ( $2.14\pm 0.42$  versus  $1.43\pm 0.32$  respectively;  $p<0.001$ ). Finally, NaF uptake reflected both disease severity (proportion with angina symptoms, need for prior revascularisation, and previous major adverse cardiac events) and cardiovascular risk burden (Framingham risk scores), where uptake was significantly higher.

The above study largely considered those with atherosclerosis, but not necessarily after acute events. Joshi et al. compared NaF uptake in individuals recruited prospectively with recent myocardial infarction (both ST-segment and non-ST-segment elevation) and stable angina. They showed increased tracer uptake is associated with symptomatic coronary plaques: in those with myocardial infarction,

the average  $TBR_{max}$  of the culprit plaque (1.66; SD 1.4-2.25) was higher than elsewhere in the coronary vasculature (1.24; SD 1.06-1.38) ( $p < 0.0001$ ). It is interesting to note that three individuals who had a myocardial infarction showed no NaF uptake, and of those two were younger with only mild irregularities on angiography, suggesting that these events may be triggered by thrombosis from plaque erosion rather than plaque rupture. Supporting this, those with NaF positive lesions (those with a TBR more than 25% than a proximal reference lesion) had higher concentrations of plasma troponin at baseline (median 3.35 [IQR 2.35-10.2] versus 2.45 [1.85-4.02] ng/L;  $p = 0.047$ ), implying a role for plaque erosion or subclinical rupture in the NaF negative lesions (Joshi et al., 2014). It is also worth noting that of NaF positive plaques, only 28% were obstructive on coronary angiography ( $>70\%$  luminal stenosis).

In the same study, increased NaF uptake was also seen in morphologically high-risk but unruptured plaques seen on intravascular ultrasound (greater positive remodeling, greater microcalcification, and larger necrotic core) and CT. This implies that NaF uptake reflects the microcalcification process rather than increased surface area following plaque rupture (Joshi et al., 2014). Similar results were seen in another study across 123 coronary atherosclerotic lesions assessed by CT (Kitagawa et al., 2017).

Recent studies of carotid atheroma in transient ischaemic attacks and minor strokes have found increased NaF uptake in culprit atheroma (Cocker et al., 2016, Vesey et al., 2017). Interestingly, Vesey et al. reported that although NaF uptake was higher in culprit versus asymptomatic atheroma, FDG did not differ significantly. Similar findings were reported in a smaller dual tracer study of symptomatic carotid atheroma (Quirce et al., 2013). This contrast with earlier FDG-PET/CT studies supports the concept that the different tracers are targeting two distinct but related processes. Furthermore, the finding that FDG-PET failed to discriminate between symptomatic and asymptomatic atheroma, in contrast to a number of earlier studies (Rudd et al., 2002, Tawakol et al., 2006), warrants further evaluation and is discussed in the next chapter.

In contrast to the pleiotropic effects of statins reducing FDG uptake, statins have not been reported to affect NaF uptake (Derlin et al., 2010, Dweck et al., 2012). However, whilst LDL levels do not differ between low NaF and high NaF uptake groups in one study, the HDL levels were higher in the low NaF uptake group (Dweck et al., 2012).

Technically, NaF-PET has been shown to have excellent reproducibility. Dweck et al. report reproducibility of  $TBR_{max}$  had an intra-class correlation coefficient of 0.99 (95% CI 0.98 to 1.00) across 20 scans by two trained observers (Dweck et al., 2012).

As with FDG-PET, it remains a subject of debate whether SUV or TBR is the more appropriate measure of NaF uptake in vascular PET imaging. Although not commented upon by the authors of the study, in a large retrospective NaF-PET study of 269 participants the mean  $SUV_{max}$  and mean  $TBR_{max}$  were very similar:  $1.9 \pm 0.5$  (range 0.8 to 4.2) and  $2.2 \pm 0.6$  (range 1.0 to 4.5) respectively (Derlin et al., 2011c).

### *3.1.3 Ex vivo NaF-PET histological validation*

Although incidental uptake of NaF was noted in atheroma in oncologic cohorts, the early emphasis on coronary disease meant histological validation was limited. This validation had to wait until imaging findings could be paired with histology available from CEA samples.

Joshi et al.'s study of symptomatic atheroma included nine individuals undergoing CEA for symptomatic carotid artery disease. *Ex vivo* NaF-PET/CT demonstrated tracer uptake localised to the site of macroscopic plaque rupture in all samples, and tracer uptake was associated with significantly higher increased calcification activity (percentage tissue non-specific alkaline phosphatase, percentage osteocalcin, concentration of CD68+ macrophage infiltration) and cell death (apoptosis with percentage cleaved-caspase-3, and presence of necrotic core) (Joshi et al., 2014).

It was only in 2015 that Irkle et al. provided definitive characterisation of selectivity, specificity, and pharmacodynamics of NaF uptake in vascular disease through a multi-technique, multimodal study. Using electron probe X-ray microdialysis the authors were able to measure NaF presence by identifying a spectroscopic peak for fluoride

that co-localised with calcification, exhibiting an approximately two-fold greater uptake for microcalcification than for macrocalcification. Autoradiography of histological specimens also demonstrated strong specific binding for NaF with negligible non-specific binding. Further examination of the pharmacodynamics of NaF revealed a positive linear relationship between the radioactivity and concentration of NaF in tissues, thereby validating quantification using PET, with a very high affinity (affinity constant,  $K_D$ , of 0.6 pM), rapid association (a half-time for association of  $14.3 \pm 1.9$  minutes), and slow dissociation (half-time for dissociation of  $254 \pm 43$  minutes). Subsequent *in vivo* work in humans showed that by 60 minutes post-injection, plasma activity was 4-8% of its peak activity and demonstrated excellent contrast between vascular wall and blood pool activity. Immunohistochemical analysis using markers for calcification, macrophages, endothelial markers of neovascularisation, and smooth muscle showed specific co-localisation of NaF only with vascular calcification, with no other binding seen with other cellular components of processes believed to trigger arterial calcification. Finally, preclinical and clinical PET/CTs showed binding of NaF to microcalcification but absent binding to large areas of macrocalcification, and only to the surface of macrocalcific deposits when there was binding. The constellation of these findings demonstrates the binding of NaF does not simply reflect the overall quantity of calcium but rather binds to areas of active microcalcification (**Figure 3.1**) (Irkle et al., 2015).

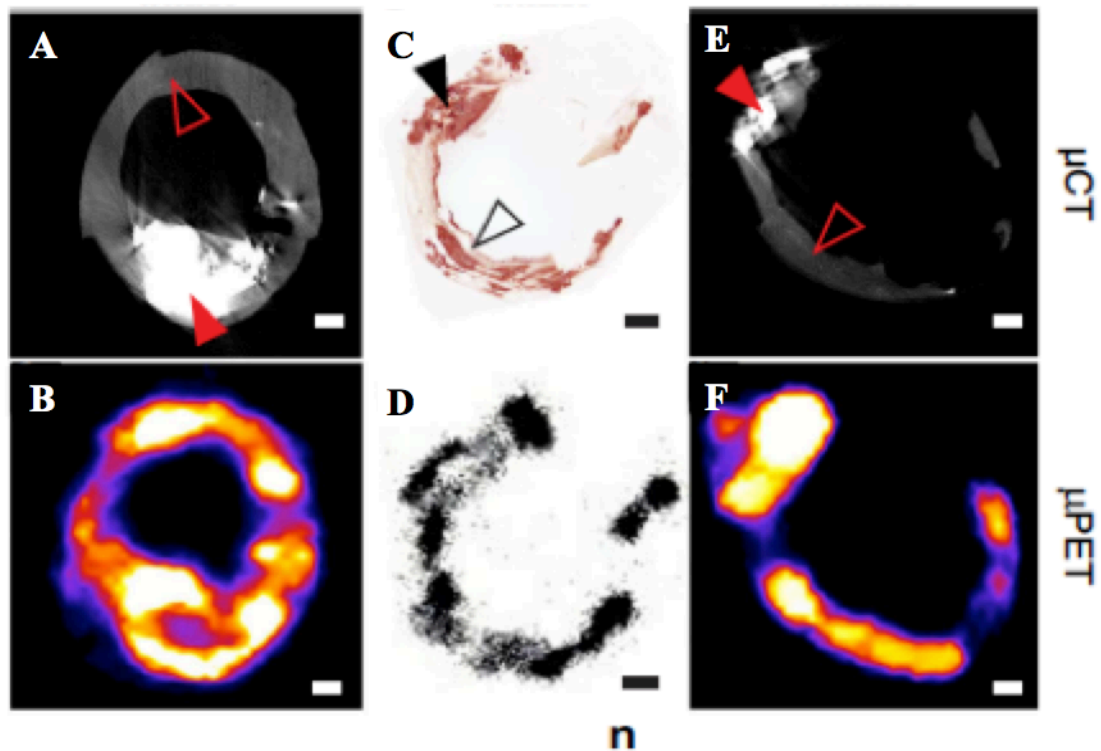


**Figure 3.1: NaF histological validation.** Carotid histology is incubated in NaF then sectioned. NaF is only able to bind to the surface level of macrocalcifications (closed arrowheads), while binding occurs to all microcalcification (open arrowheads) (A,B). NaF binding solely to the surface level of macrocalcifications can also be observed in a  $\mu$ PET/ $\mu$ CT scan, if the macrocalcification size is larger than  $\mu$ PET resolution (C, E). Microcalcifications that are detected with Alizarin Red histology (C) and autoradiography (D) cannot be detected using  $\mu$ CT (E), but may be detected on corresponding  $\mu$ PET (F). Reproduced with permission from (Irkle et al., 2015).

#### 3.1.4 Carotid artery macrocalcification and stroke risk

In contrast to microcalcification, arterial macrocalcification is easily detected by CT and is a common finding on imaging of the carotid arteries. However, the significance of how vascular calcification in atherosclerotic carotid arteries relates to stroke risk is unclear. In comparison, CT-derived coronary artery calcium (CAC) scoring is widely used by cardiologists for risk stratification in coronary artery disease. The CAC score is an independent predictor of cardiovascular events in individuals after adjustment for other risk factors and is part of the NICE chest pain assessment guidelines (Elkeles et al., 2008, National Institute for Health and Care Excellence, 2010). To date there

have been only a few small studies measuring calcium in carotid arteries in differing patient cohorts with conflicting results (Kwee, 2010, Nandalur et al., 2006, Eesa et al., 2010). Importantly, the role of arterial calcification in stroke recurrence in symptomatic individuals is unknown.

Carotid calcium burden is associated with cardiovascular risk factors and to the development of atherosclerotic disease (Al-Mutairy et al., 2009, Odink et al., 2010). The large longitudinal Rotterdam study found age and smoking status were the strongest predictors of arterial calcification in the coronary and carotid arteries, and arch of the aorta. Hypertension, hypercholesterolaemia, and diabetes were also independently associated with calcification, although not consistently in one sex or arterial region (Odink et al., 2010). Calcium scores in the coronary arteries, aortic arch, and carotid arteries are correlated; indicating that calcification in atherosclerosis is typically a systemic process (Odink et al., 2007). Furthermore, calcium volume is associated with the degree of carotid atherosclerosis within a general population, where all carotid stenoses of >40% stenosis had detectable calcification (McKinney et al., 2005) whilst individuals without calcification have a very low (1%) prevalence of subclinical atherosclerosis (Ho et al., 2012).

Despite these associations, studies investigating the association between carotid artery or aortic arch calcification and clinical events are few. In a 2010 meta-analysis, lower carotid calcium volume and weight (8 studies) and plaque calcification percentage (8 studies) were associated with a higher risk of clinical ischaemic events, although the pooled association (9 studies) between the degree of plaque calcification using a dichotomous scoring scale and clinical ischaemic symptoms crossed the equivalence line (Kwee, 2010). These pooled analyses should be interpreted with caution however, due to the paucity of studies, small samples, and the heterogeneity of methods (particularly the techniques used to measure calcification). The imaging modalities used varied, some studies used histology rather than imaging (Peeters et al., 2009), the time interval between symptoms and calcium assessment ranged between one week to six months, and different definitions of the asymptomatic control groups were used. Furthermore, only half of the studies explicitly excluded individuals with atrial fibrillation, raising concerns about confounding and questions over the source of thromboemboli. Finally, whilst one study assessing histology had 630 symptomatic

arteries (which was equivocal for the association between calcification and with clinical events) (Peeters et al., 2009), the median number of participants in the remaining studies was 30.5 (IQR 23.5). This meta-analysis highlights that there has been no accepted single technique for measuring calcification within the carotids and demonstrates the need for a consensus approach for recruitment, measurement, and analysis with the need for a larger-scale study.

More recent studies have used quantitative rather than dichotomised/semi-quantitative measures of calcification. Carotid calcium volume was associated with an increased risk of stroke after adjustment for the degree of vessel stenosis in individuals undergoing computed tomography (CT) (Nandalur et al., 2006). A large retrospective study embedded within the Rotterdam Study reviewed CT scans of 2,521 individuals, 96 of whom had a previous stroke. Carotid, aortic arch, and coronary artery calcium scores were independently associated with a history of stroke after adjustment for cardiovascular risk factors, though only carotid artery calcification remained significant after adjustment for calcification in other arterial beds. Consequently, the odds ratio of having had a stroke between the highest versus lowest quartile of carotid calcium scores was 3.3 (95% confidence interval 1.4-7.8) (Elias-Smale et al., 2010). Carotid calcification has also been shown to be associated with atheroma inflammation, itself a risk factor for recurrent cerebrovascular events (Joshi et al., 2016, Marnane et al., 2012).

van Dijk et al. assessed calcium volume using CT angiography in symptomatic carotid arteries and aorta in 708 TIA/strokes. Prevalence of calcification was high (50-73% depending on arterial territory and location of TIA/stroke). They found an increasing volume of aortic calcification was independently associated with a higher risk of non-lacunar versus lacunar events (odds ratio 1.11; 95% CI 1.02-1.21), though neither intracranial nor extracranial symptomatic carotid artery calcium volume were associated with an excess of either lacunar or non-lacunar stroke (van Dijk et al., 2014). Increasing semi-quantitative calcium volume (highest tertile versus lowest tertile) of coronary, aortic arch, or carotid arteries in this asymptomatic population was not associated with increased odds of stroke (but increasing scores in the coronary and carotid arteries were associated with significantly higher odds of subsequent cardiovascular events) (Elias-Smale et al., 2011). It is important to note

the number of strokes was low in this sub-study (2.5%) compared to the broader Rotterdam study (Bots et al., 1996). Furthermore, individuals with atrial fibrillation were not excluded and this may confound if cardio-embolic strokes were included. Finally, the rate of recurrence in symptomatic individuals remains unknown.

Other studies have suggested calcification may be protective. In 673 individuals with symptomatic carotid artery stenosis, extensive calcification assessed by CT was more common in asymptomatic contralateral stenosis after adjustment for age, sex, and the degree of luminal stenosis (Eesa et al., 2010). However, this study did not quantify the calcium score or consider density of calcification, but graded the extent of calcification according to a visual scale of “mild”, “moderate”, and “extensive.” Another study found symptomatic carotid artery atheroma have fewer clusters of calcium compared to asymptomatic controls, though this was only significant when examining the 3 cm proximal and distal to the bifurcation together, rather than either individually (Wintermark et al., 2008), supporting earlier work on calcification location by Culebras et al. (Culebras et al., 1989).

These conflicting results may arise when using different semi-quantitative scores as there may exist a bimodal distribution of vulnerability in calcified plaques. Katano et al. found rates of symptomatic plaques peaked at calcium scores of 200-400 and 600-800 (Katano et al., 2015) and this bimodal distribution may have a confounding effect where symptomatic plaques were measured qualitatively or semi-quantitatively.

Consequently, there remains uncertainty over the role of macrocalcification in symptomatic carotid atherosclerosis. Given the pathophysiological relationship between microcalcification and macrocalcification, for the purposes of this NaF-PET study it is also necessary to consider the role of macrocalcification.

### **3.2 Methods**

Methodology for this chapter is discussed in Chapter Two.

### 3.3 Results

#### 3.3.1 Study population

Of the 31 participants recruited to the ICARUSS study, 27 underwent NaF-PET/CT (of the 4 recruited who did not undergo scanning: 2 clinically deteriorated prior to scanning, 1 had expedited endarterectomy prior to NaF-PET/CT, and 1 was unable to complete the scan due to claustrophobia).

Of this 27, 26 had imaging suitable for analysis (1 participant had an uninterpretable asymptomatic carotid artery due to uncorrectable spill-over artifact and was excluded from analysis).

The participant characteristics of the analysed 26 participant cohort are shown in **Table 3.1**.

Mean age (years)	74.8 (SD 9.7)
Men	18 (69.2%)
Median BMI	26 (IQR 3.9)
Smoking history (current or ex-smokers)	17 (65.4%)
Diabetes mellitus	4 (15.4%)
Hypertension	17 (65.4%)
Current statin	9 (34.6%)
Current antiplatelet	8 (30.8%)
Cardiovascular history (previous ischaemic heart disease or myocardial infarction)	8 (30.8%)
Median NIHSS	4.5 (IQR 10.75)
Thrombolysed	6 (23.1%)
CEA (following imaging)	9 (34.6%)
Modal degree of symptomatic stenosis	70-89%
Mean symptom-scan time (days)	9.7 (SD 4.1)

**Table 3.1:** Clinical characteristics of the NaF-PET/CT cohort.

NaF uptake was visualised in symptomatic and asymptomatic carotid arteries as demonstrated in **Figure 3.2**.

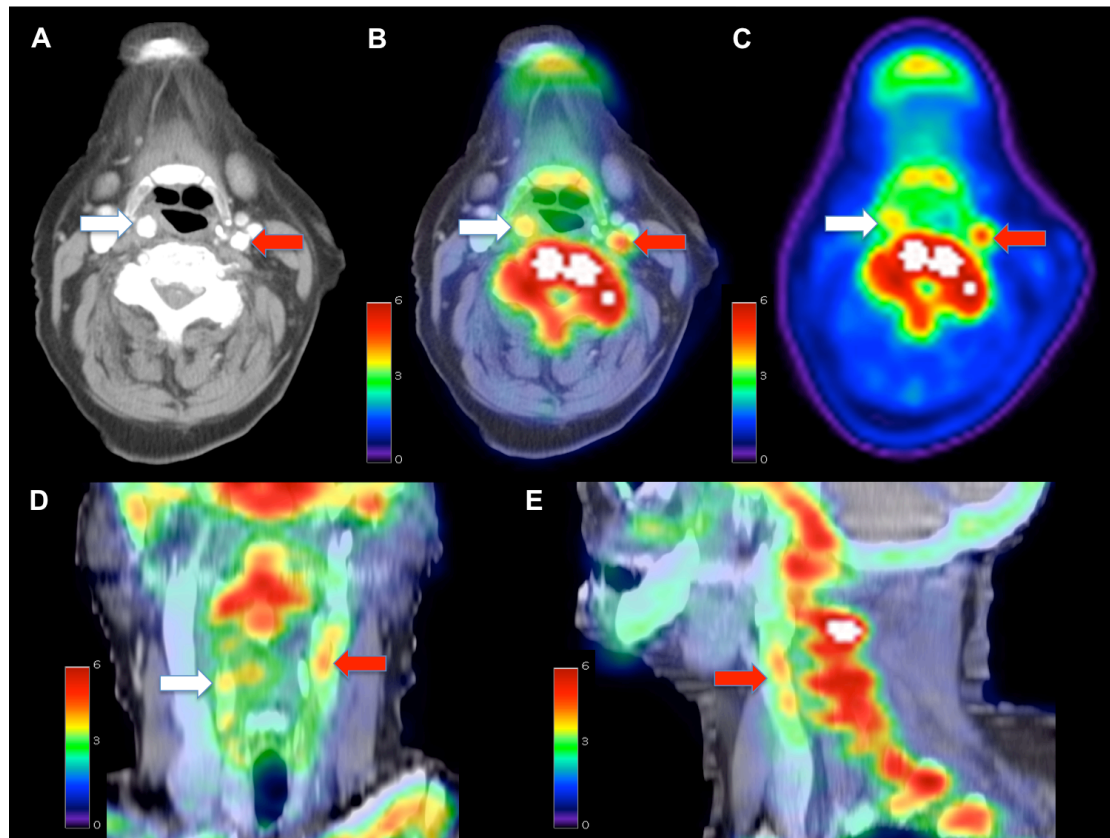


**Figure 3.2: NaF uptake in symptomatic disease.** (a) axial CT angiogram, (b) axial NaF-PET/CT, (c) axial PET, (d) coronal NaF-PET/CT, (e) sagittal NaF-PET/CT showing an asymptomatic right carotid artery (white arrow) and a symptomatic left carotid artery (red arrow).

### 3.3.2 NaF uptake in symptomatic and asymptomatic arteries

#### 3.3.2.1 NaF SUVs in symptomatic and asymptomatic arteries

Results for SUV<sub>max</sub> are shown in **Table 3.2** and **Figure 3.3**.

	Symptomatic carotid artery	Asymptomatic carotid artery	Significance
Median SHS SUV <sub>max</sub> (IQR)	2.16 (0.76)	1.88 (0.94)	p<0.001
Median MDS SUV <sub>max</sub> (IQR)	2.04 (0.66)	1.76 (0.83)	p<0.001
Median WV SUV <sub>max</sub> (IQR)	1.36 (0.36)	1.33 (0.40)	p=0.09

**Table 3.2:** NaF SUV<sub>max</sub> readings for symptomatic and asymptomatic carotid arteries.

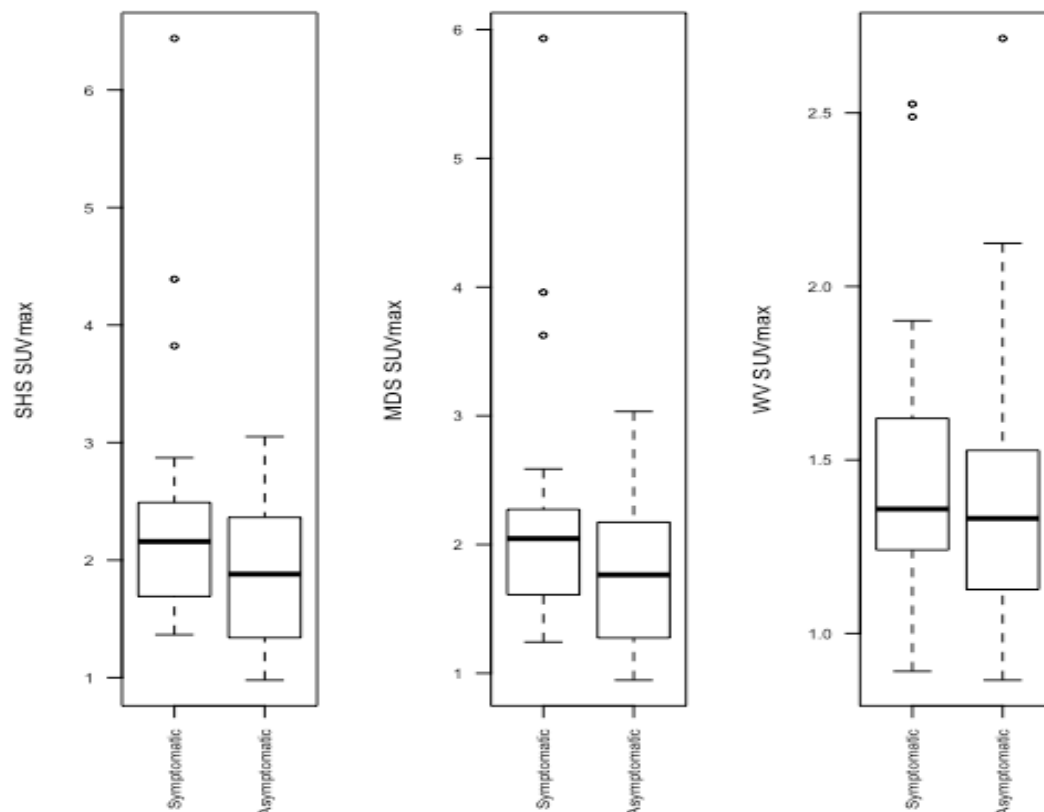


**Figure 3.3:** NaF SUV<sub>max</sub>. Boxplots showing SUV<sub>max</sub> between symptomatic and asymptomatic arteries for SHS (left), MDS (middle), and WV (right) SUV<sub>max</sub>.

Results for  $SUV_{mean}$  are shown in **Table 3.3** and **Figure 3.4**.

	Symptomatic carotid artery	Asymptomatic carotid artery	Significance
Median SHS $SUV_{mean}$ (IQR)	1.78 (0.55)	1.60 (0.63)	$p < 0.001$
Median MDS $SUV_{mean}$ (IQR)	1.65 (0.56)	1.47 (0.57)	$p < 0.001$
Median MWV $SUV_{mean}$ (IQR)	1.18 (0.26)	1.16 (0.43)	$p = 0.02$

**Table 3.3:** NaF  $SUV_{mean}$  readings for symptomatic and asymptomatic carotid arteries.

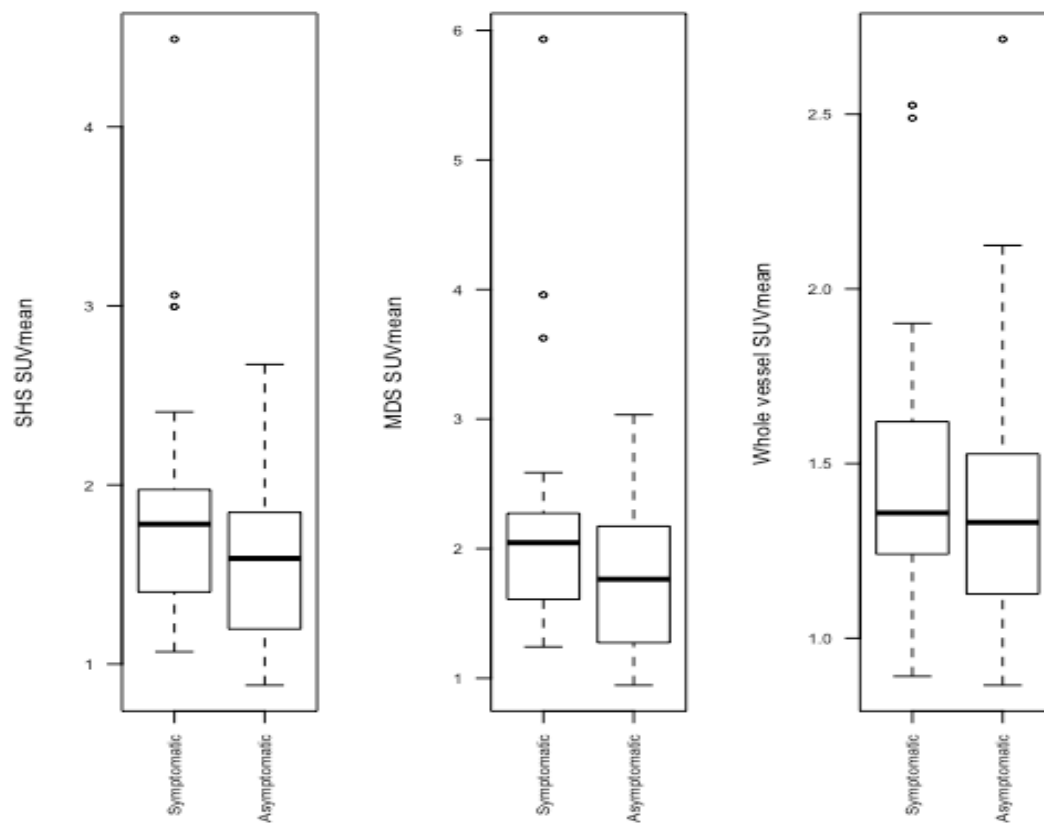


**Figure 3.4:** NaF  $SUV_{mean}$ . Boxplots showing  $SUV_{mean}$  between symptomatic and asymptomatic arteries for SHS (left), MDS (middle), and WV (right)  $SUV_{mean}$ .

### 3.3.2.2 NaF TBRs in symptomatic and asymptomatic arteries

Mean venous SUV was 0.78 (SD 0.19). Results for TBR<sub>max</sub> are shown in **Table 3.4** and **Figure 3.5**.

	Symptomatic carotid artery	Asymptomatic carotid artery	Significance
Median SHS TBR <sub>max</sub> (IQR)	2.84 (IQR 0.67)	2.52 (IQR 1.08)	p<0.001
Median MDS TBR <sub>max</sub> (IQR)	2.68 (IQR 0.63)	2.39 (IQR 1.02)	p<0.001
Median MWV TBR <sub>max</sub> (IQR)	1.85 (IQR 0.28)	1.79 (IQR 0.60)	p=0.10

**Table 3.4:** NaF TBR<sub>max</sub> readings for symptomatic and asymptomatic carotid arteries.

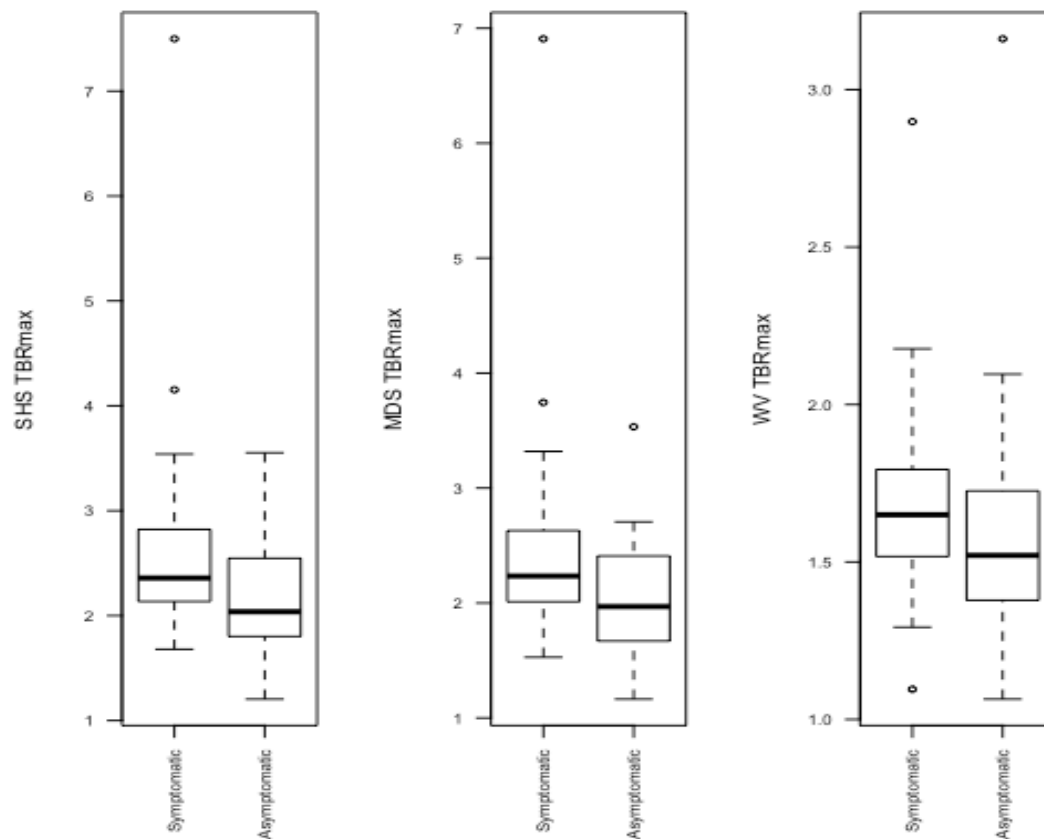


**Figure 3.5:** NaF TBR<sub>max</sub>. Boxplots showing TBR<sub>max</sub> between symptomatic and asymptomatic arteries for SHS (left), MDS (middle), and WV (right) TBR<sub>max</sub>.

Results for TBR<sub>mean</sub> are shown in **Table 3.5** and **Figure 3.6**.

	Symptomatic carotid artery	Asymptomatic carotid artery	Significance
Median SHS TBR <sub>mean</sub> (IQR)	2.21 (IQR 0.74)	2.09 (IQR 0.87)	p<0.001
Median MDS TBR <sub>mean</sub> (IQR)	2.13 (IQR 0.64)	1.98 (IQR 0.80)	p<0.001
Median MWV TBR <sub>mean</sub> (IQR)	1.57 (IQR 0.28)	1.55 (IQR 0.48)	p=0.02

**Table 3.5:** NaF TBR<sub>mean</sub> readings for symptomatic and asymptomatic carotid arteries.

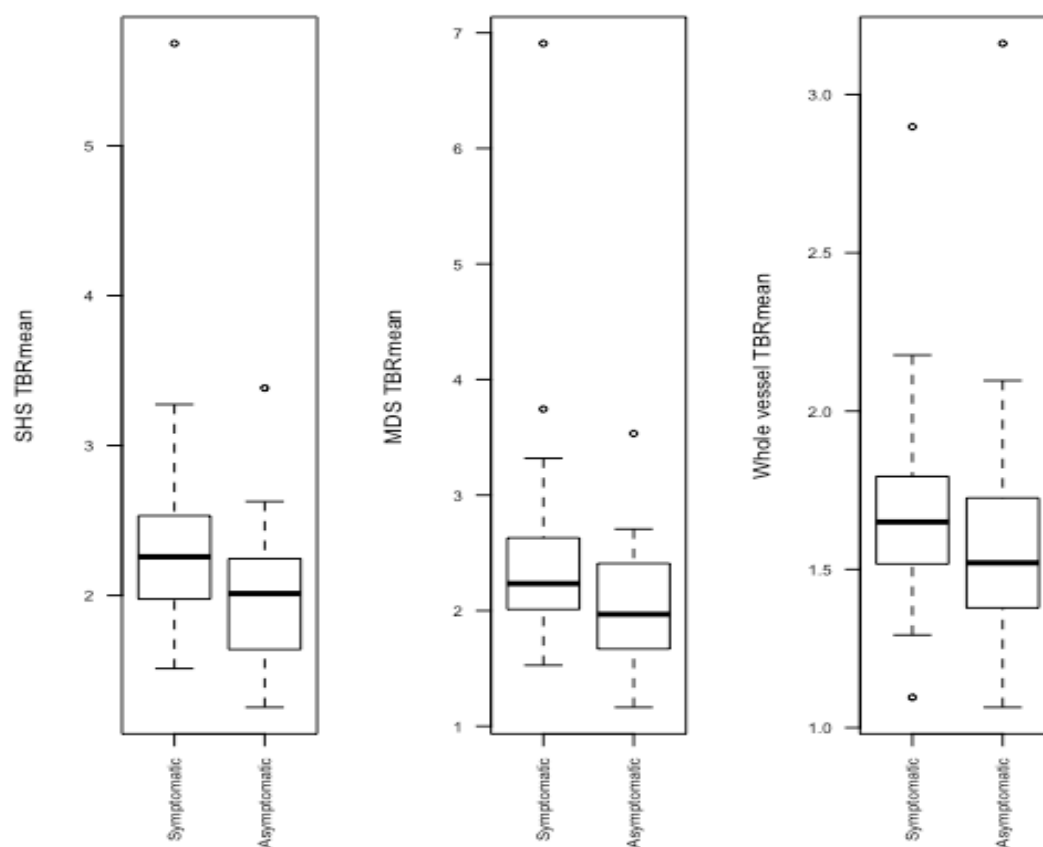


**Figure 3.6:** NaF TBR<sub>mean</sub>. Boxplots showing TBR<sub>mean</sub> between symptomatic and asymptomatic arteries for SHS (left), MDS (middle), and WV (right) TBR<sub>mean</sub>.

### 3.3.3 Relationship of NaF uptake to stroke severity

There was also no correlation between any measures of NaF uptake in the symptomatic artery and stroke severity as recorded by the NIHSS: SHS SUV<sub>max</sub> ( $r=-$

0.14,  $p=0.51$ ), MDS  $SUV_{max}$  ( $r=-0.15$ ,  $p=0.46$ ), WV  $SUV_{max}$  ( $r=-0.14$ ,  $p=0.50$ ), SHS  $SUV_{mean}$  ( $r=-0.22$ ,  $p=0.27$ ), MDS  $SUV_{mean}$  ( $r=-0.20$ ,  $p=0.33$ ), and WV  $SUV_{mean}$  ( $r=-0.17$ ,  $p=0.41$ ) (**Figure 3.7**). A similar pattern of a lack of correlation was also observed with TBR values: SHS  $TBR_{max}$  ( $r=-0.11$ ,  $p=0.58$ ), MDS  $TBR_{max}$  ( $r=-0.07$ ,  $p=0.72$ ), WV  $TBR_{max}$  ( $r=0.05$ ,  $p=0.82$ ), SHS  $TBR_{mean}$  ( $r=-0.14$ ,  $p=0.49$ ), MDS  $TBR_{mean}$  ( $r=-0.17$ ,  $p=0.40$ ), WV  $TBR_{mean}$  ( $r=-0.03$ ,  $p=0.90$ ).

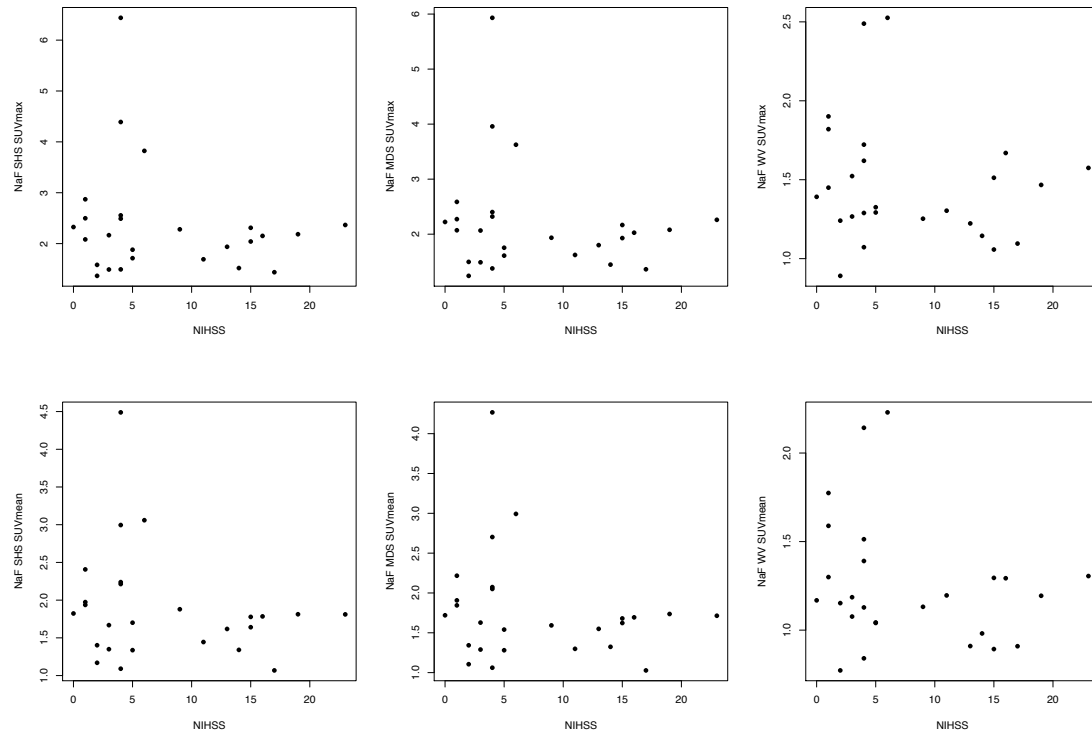


**Figure 3.7: Associations between NIHSS and symptomatic artery SUVs.**

### 3.3.4 Relationship between NaF uptake and degree of luminal stenosis

There was no significant relationship between the degree of luminal stenosis and SHS  $SUV_{max}$  ( $p=0.32$ ), MDS  $SUV_{max}$  ( $p=0.25$ ), SHS  $SUV_{mean}$  ( $p=0.25$ ), or MDS  $SUV_{mean}$  ( $p=0.19$ ) (**Figure 3.8**).

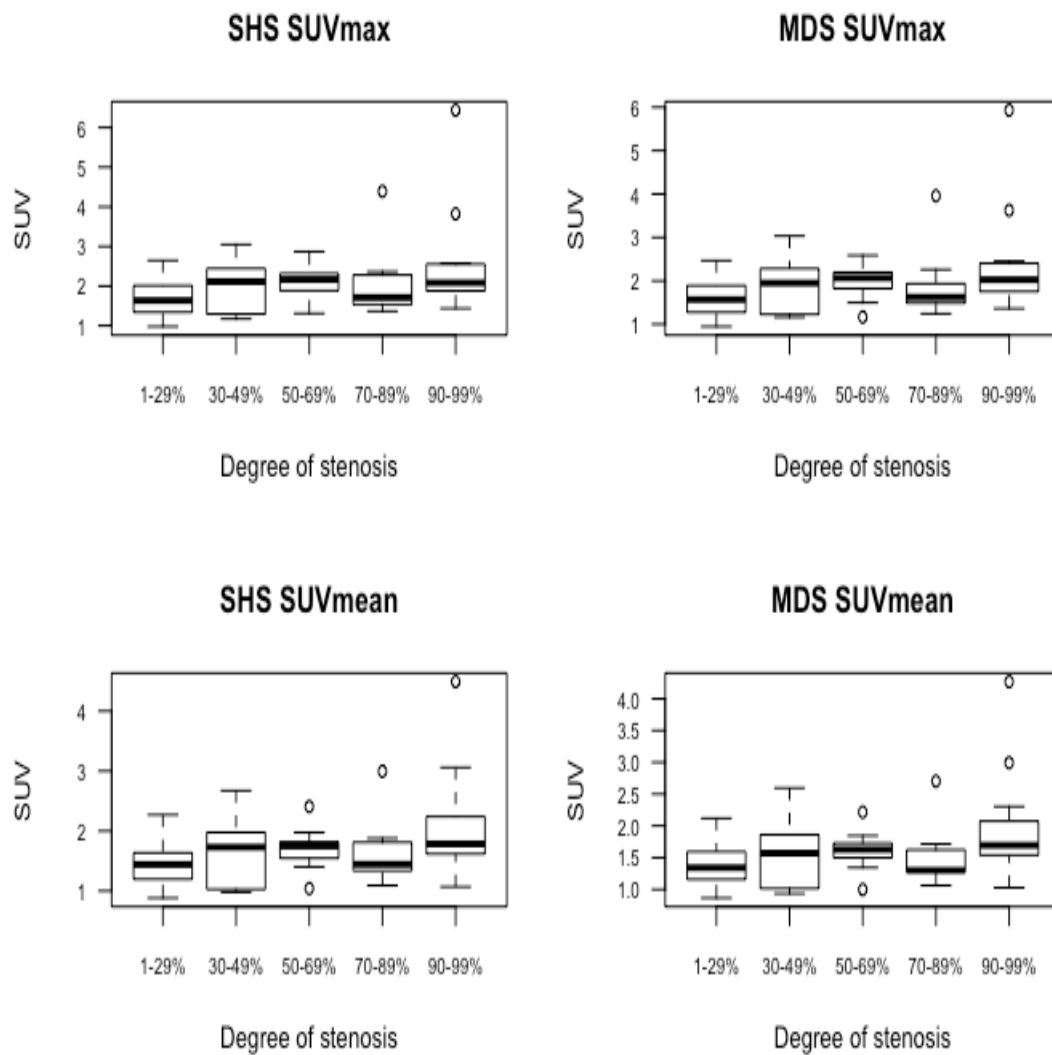


**Figure 3.8: NaF SUVs categorised by degree of luminal stenosis.**

Adjustment by venous pooling to give TBR measures also showed no significant relationship between the degree of stenosis and NaF uptake: SHS  $TBR_{max}$  ( $p=0.92$ ), MDS  $TBR_{max}$  ( $p=0.91$ ), SHS  $TBR_{mean}$  ( $p=0.84$ ), MDS  $TBR_{mean}$  ( $p=0.75$ ) (**Figure 3.9**).

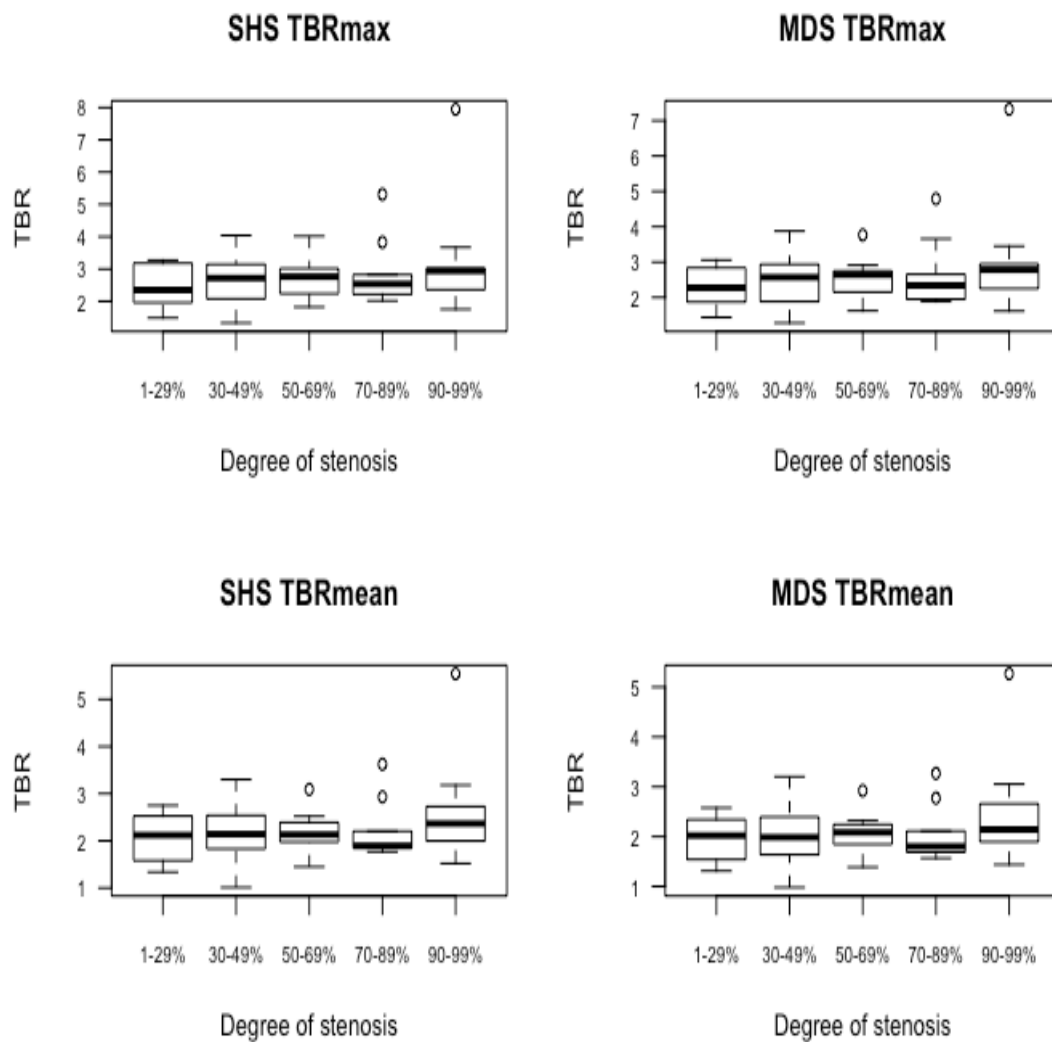


**Figure 3.9: NaF TBRs categorised by degree of luminal stenosis.**

### 3.3.5 Spatial distribution of NaF uptake

Plotting the median value of tracer uptake for each 3 mm axial slice along the length of the carotid artery demonstrates a spatial distribution of tracer uptake.

For  $SUV_{max}$ , NaF uptake shows a focal peak at the +1 slice in the symptomatic artery. In contrast, there is an attenuated pattern in the asymptomatic artery (**Figure 3.10**). Corresponding  $SUV_{mean}$  curves show a similar pattern to the corresponding  $SUV_{max}$  curves (**Figure 3.11**).

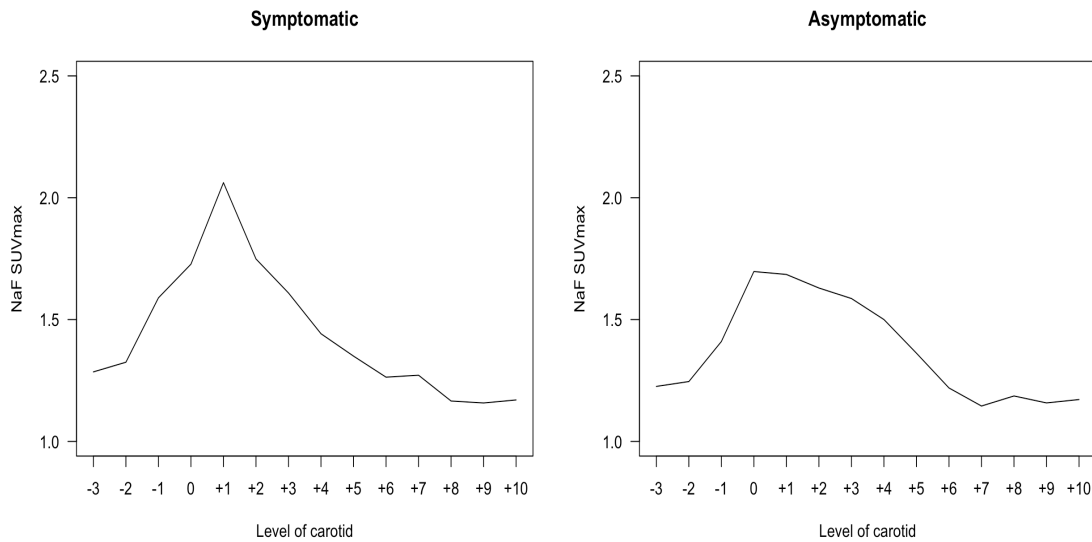


**Figure 3.10: Spatial distribution of NaF SUV<sub>max</sub>.** Median SUV<sub>max</sub> at each 3 mm slice along the artery (slice 0 being the carotid bifurcation).

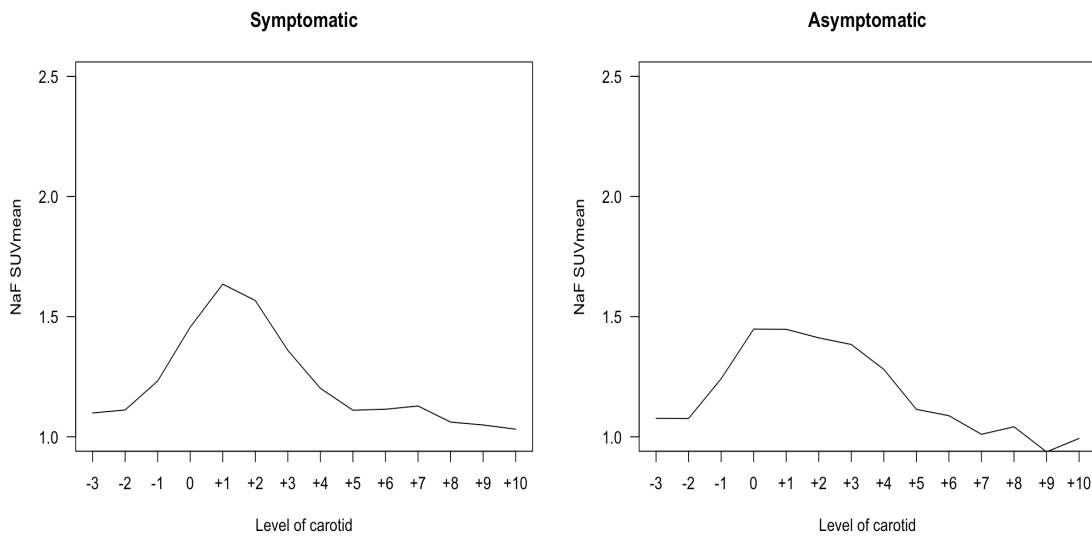


**Figure 3.11: Spatial distribution of NaF SUV<sub>mean</sub>.** Median SUV<sub>mean</sub> at each 3 mm slice along the artery (slice 0 being the carotid bifurcation).

TBR<sub>max</sub> and TBR<sub>mean</sub> in symptomatic arteries also show a peak in the slice 3 mm immediately distal to the carotid bifurcation in the internal carotid artery (**Figures 3.12 and 3.13**).

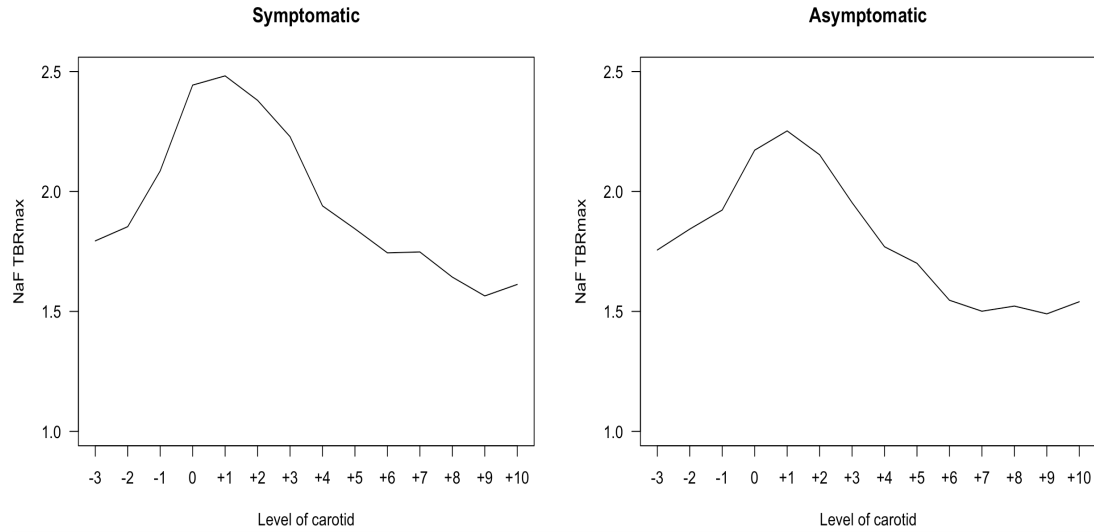


**Figure 3.12: Spatial distribution of NaF TBR<sub>max</sub>.** Median TBR<sub>max</sub> at each 3 mm slice along the artery (slice 0 being the carotid bifurcation).

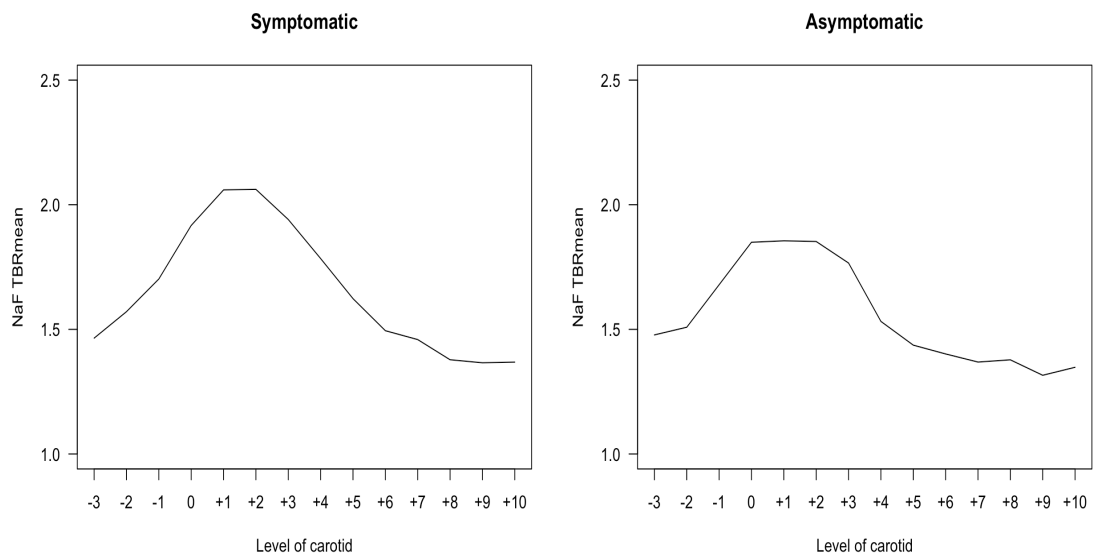


**Figure 3.13: Spatial distribution of NaF TBR<sub>mean</sub>.** Median TBR<sub>mean</sub> at each 3 mm slice along the artery (slice 0 being the carotid bifurcation).

### 3.3.6 Comparison of SUV and TBR readings

SHS SUV<sub>max</sub> and SHS TBR<sub>max</sub> had a correlation of  $r_s=0.72$  ( $p<0.001$ ), MDS SUV<sub>max</sub> and MDS TBR<sub>max</sub> had a correlation of  $r_s=0.71$  ( $p<0.001$ ), and WV SUV<sub>max</sub> and WV TBR<sub>max</sub> had a correlation of  $r_s=0.57$  ( $p<0.001$ ) across all 52 arteries (**Figure 3.14**).

SHS  $SUV_{mean}$  and SHS  $TBR_{mean}$  had a correlation of  $r_s=0.69$  ( $p<0.001$ ), MDS  $SUV_{mean}$  and MDS  $TBR_{mean}$  had a correlation of  $r_s=0.71$  ( $p<0.001$ ), and WV  $SUV_{mean}$  and WV  $TBR_{mean}$  had a correlation of  $r_s=0.61$  ( $p<0.001$ ) across all 52 arteries (**Figure 3.14**).

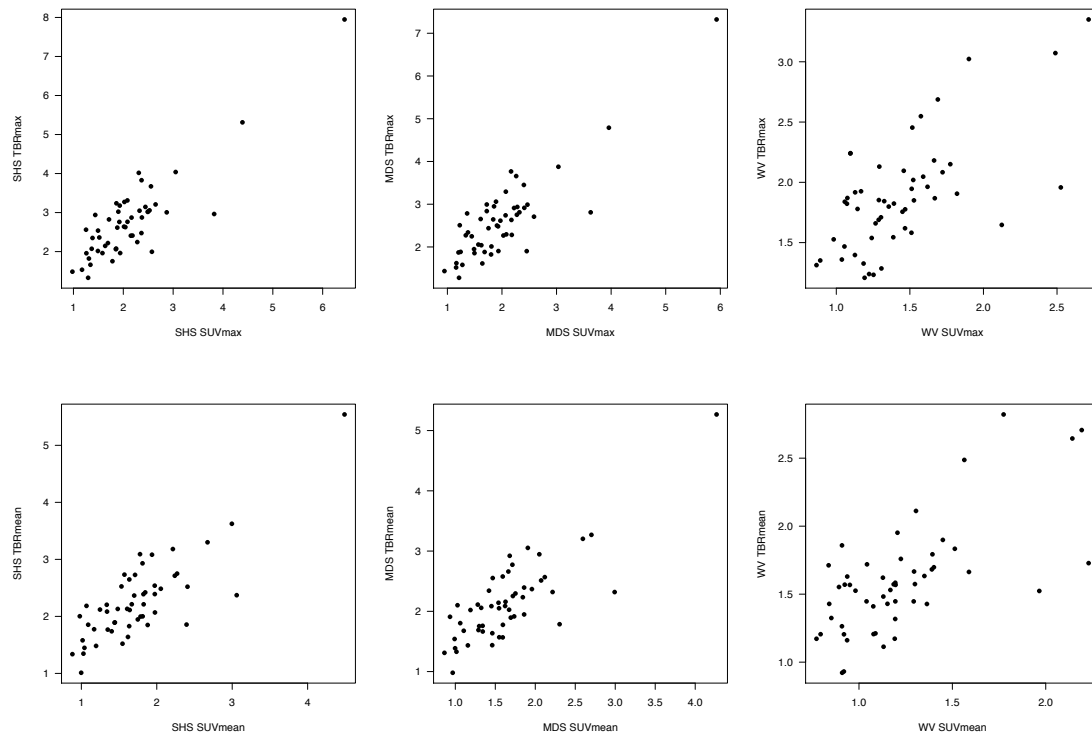


**Figure 3.14: Associations between corresponding NaF SUV and TBR measures.**

Given the above results, the blood pool activity of NaF (venous SUV) was considered. Ultimately there was no significant effect of any of the variables included above on NaF blood-pooling. There was no significant correlation between venous SUV and age ( $r=0.24$ ,  $p=0.23$ ), BMI ( $r_s=0.22$ ,  $p=0.29$ ), or stroke-to-NaF-PET/CT interval ( $r=-0.11$ ,  $p=0.58$ ). There was no difference for sex (female median 0.82 [IQR 0.25] versus male median 0.76 [IQR 0.19],  $p=0.29$ ), hypertension (hypertension mean 0.77 [SD 0.18] versus 0.79 [SD 0.15],  $p=0.67$ ), smoking (smoking mean 0.78 [SD 0.18] versus 0.78 [SD 0.15],  $p=0.97$ ), diabetes (diabetes mean 0.78 [SD 0.18] versus 0.78 [SD 0.17],  $p=0.98$ ), prior statin (prior statin mean 0.81 [SD 0.23] versus 0.76 [SD 0.13],  $p=0.50$ ), prior antiplatelet (prior antiplatelet mean 0.78 [SD 0.26] versus 0.77 [SD 0.12],  $p=0.91$ ), or cardiovascular history (cardiovascular history median 0.73 [IQR 0.31] versus 0.76 [IQR 0.12],  $p=0.26$ ).

### 3.3.7 Reproducibility

Over all 84 axial slices of the 6 participants chosen to test reproducibility, the intra-rater ICC was 0.999 for  $SUV_{max}$  and 0.995 for  $SUV_{mean}$ . Taking an artery-by-artery basis for all 12 arteries, intra-rater ICC for SHS  $SUV_{max}$  was 1.00, ICC for MDS  $SUV_{max}$  was 1.00, and MWV  $SUV_{max}$  was 0.997. The intra-rater ICCs for SHS  $SUV_{mean}$ , MDS  $SUV_{mean}$ , and MWV  $SUV_{mean}$  were 0.997, 0.995, and 0.999 respectively.

Over all 84 axial slices, the inter-rater ICC was 0.969 for  $SUV_{max}$  and 0.977 for  $SUV_{mean}$ . Inter-rater ICC for  $TBR_{max}$  was 0.955 and for  $TBR_{mean}$  was 0.93.

### 3.3.8 NaF uptake and risk factors

#### 3.3.8.1 Univariable analysis of NaF uptake according to risk factors

The effects of cardiovascular risk factors upon NaF uptake were considered on a patient-level analysis (including both symptomatic and asymptomatic arteries). Results of the univariable analyses are shown in Appendix C.

#### 3.3.8.2 Multivariable analysis of NaF uptake according to risk factors

Multivariable linear regression for each uptake measure was performed using a likelihood-ratio approach for backwards elimination as described in Chapter Two (**Tables 3.6 and 3.7**).

SHS $SUV_{max}$	AIC = 109.8	Adjusted $R^2 = 0.47$ ( $p < 0.01$ )
	Coefficient	Adjusted significance
Age	0.05	$p < 0.001$
Male sex	-0.59	$p = 0.02$
Smoker	0.57	$p = 0.01$
Current statin	1.25	$p < 0.01$
Current antiplatelet	-1.07	$p < 0.01$
Total cholesterol	-0.18	$p = 0.14$

<b>MDS SUV<sub>max</sub></b>	<b>AIC = 98.8</b>	<b>Adjusted R<sup>2</sup> = 0.49 (p&lt;0.01)</b>
	Coefficient	Adjusted significance
Age	0.04	p<0.001
Male sex	-0.53	p=0.02
Smoker	0.59	p<0.001
Current statin	1.18	p<0.001
Current antiplatelet	-1.01	p<0.001
Total cholesterol	-0.17	p=0.12
<b>WV SUV<sub>max</sub></b>	<b>AIC = 13.3</b>	<b>Adjusted R<sup>2</sup> = 0.58 (p&lt;0.01)</b>
	Coefficient	Adjusted significance
Age	0.01	p<0.01
Male sex	-0.33	p<0.01
Smoker	0.30	p<0.01
Current statin	0.61	p<0.001
Cardiovascular history	-0.49	p<0.001
Total cholesterol	-0.07	p=0.12
Thrombolysis	0.14	p=0.11
<b>SHS SUV<sub>mean</sub></b>	<b>AIC = 70.7</b>	<b>Adjusted R<sup>2</sup> = 0.51 (p&lt;0.01)</b>
	Coefficient	Adjusted significance
Age	0.03	p<0.001
Male sex	-0.47	p<0.01
Hypertension	0.35	p=0.05
Current statin	0.79	p<0.001
Cardiovascular history	-0.85	p<0.001
Thrombolysis	0.47	p=0.02
Onset-to-NaF/PET interval	0.03	p=0.08
<b>MDS SUV<sub>mean</sub></b>	<b>AIC = 63.1</b>	<b>Adjusted R<sup>2</sup> = 0.52 (p&lt;0.01)</b>
	Coefficient	Adjusted significance
Age	0.03	p<0.001
Male sex	-0.55	p<0.01
Smoking	0.34	p=0.02
Current statin	0.74	p<0.001
Cardiovascular history	-0.60	p<0.001
Thrombolysis	0.23	p=0.12
Total cholesterol	-0.12	p=0.11
<b>WV SUV<sub>mean</sub></b>	<b>AIC = 4.4</b>	<b>Adjusted R<sup>2</sup> = 0.55 (p&lt;0.01)</b>
	Coefficient	Adjusted significance
Age	0.01	p<0.01
Male sex	-0.26	p<0.01

Smoking	0.25	p<0.01
Current statin	0.46	p<0.001
Cardiovascular history	-0.39	p<0.001
Total cholesterol	-0.08	p=0.06

**Table 3.6:** Regression modeling of clinical risk factors associated with NaF SUV.

<b>SHS TBR<sub>max</sub></b>	<b>AIC = 133.9</b>	<b>Adjusted R<sup>2</sup> = 0.40 (p&lt;0.01)</b>
	Coefficient	Adjusted significance
Age	0.05	p<0.01
Male sex	-0.67	p=0.04
Smoking	0.90	p<0.01
Current statin	0.96	p=0.02
Current antiplatelet	-1.86	p<0.01
Cardiovascular history	1.08	p=0.03
Total cholesterol	-0.42	p<0.01
<b>MDS TBR<sub>max</sub></b>	<b>AIC = 123.7</b>	<b>Adjusted R<sup>2</sup> = 0.42 (p&lt;0.01)</b>
	Coefficient	Adjusted significance
Age	0.05	p<0.01
Male sex	-0.58	p=0.048
Smoking	0.92	p<0.01
Current statin	0.90	p=0.02
Current antiplatelet	-1.79	p<0.01
Cardiovascular history	1.09	p=0.02
Total cholesterol	-0.39	p<0.01
<b>WV TBR<sub>max</sub></b>	<b>AIC = 45.8</b>	<b>Adjusted R<sup>2</sup> = 0.45 (p&lt;0.01)</b>
	Coefficient	Adjusted significance
Age	0.01	p=0.045
Male sex	-0.23	p=0.09
Smoking	0.55	p<0.001
Current statin	0.45	p=0.01
Current antiplatelet	-0.87	p<0.01
Cardiovascular history	0.57	p<0.01
Total cholesterol	-0.24	p<0.001
<b>SHS TBR<sub>mean</sub></b>	<b>AIC = 91.3</b>	<b>Adjusted R<sup>2</sup> = 0.44 (p&lt;0.01)</b>
	Coefficient	Adjusted significance
Age	0.03	p<0.01
Male sex	-0.53	p=0.01
Smoking	0.66	p<0.01

Current statin	0.57	p=0.04
Current antiplatelet	-1.22	p<0.01
Cardiovascular history	0.78	p=0.02
Total cholesterol	-0.33	p<0.01
<b>MDS TBR<sub>mean</sub></b>	<b>AIC = 85.0</b>	<b>Adjusted R<sup>2</sup> = 0.44 (p&lt;0.01)</b>
	Coefficient	Adjusted significance
Age	0.03	p<0.01
Male sex	-0.48	p=0.02
Smoking	0.67	p<0.001
Current statin	0.56	p=0.03
Current antiplatelet	-1.18	p<0.01
Cardiovascular history	0.75	p=0.01
Total cholesterol	-0.31	p<0.01
<b>WV TBR<sub>mean</sub></b>	<b>AIC = 30.4</b>	<b>Adjusted R<sup>2</sup> = 0.45 (p&lt;0.01)</b>
	Coefficient	Adjusted significance
Age	0.01	p=0.046
Male sex	-0.22	p=0.07
Smoking	0.46	p<0.001
Current statin	0.32	p=0.04
Current antiplatelet	-0.65	p<0.01
Cardiovascular history	0.44	p=0.01
Total cholesterol	-0.23	p<0.001

**Table 3.7:** Regression modeling of clinical risk factors associated with NaF TBR.

### 3.3.9 Relationship with hsCRP

There was no relationship between hsCRP any measure of NaF uptake. Correlations between hsCRP and symptomatic artery SHS SUV<sub>max</sub> and WV SUV<sub>max</sub> were  $r_s=0.88$  ( $p=0.67$ ) and  $r_s=-0.05$  ( $p=0.81$ ) respectively. Between hsCRP and SHS SUV<sub>mean</sub> and WV SUV<sub>mean</sub> the Spearman's correlations were  $r_s=0.61$  ( $p=0.77$ ) and  $r_s=0.132$  ( $p=0.52$ ) respectively. There were no significant correlations between hsCRP and symptomatic artery SHS TBR<sub>max</sub> ( $r_s=-0.02$ ,  $p=0.91$ ), WV TBR<sub>max</sub> ( $r_s =0.05$ ,  $p=0.80$ ), SHS TBR<sub>mean</sub> ( $r_s=-0.01$ ,  $p=0.95$ ), and WV TBR<sub>mean</sub> ( $r_s=0.10$ ,  $p=0.61$ ).

### 3.3.10 Carotid calcification scoring

Carotid calcification scoring using the Agatston method was possible in all 26 participants. Median symptomatic artery CACS was 367 (IQR 625) versus median asymptomatic artery CACS of 324.5 (IQR 500.5) ( $p=0.36$  on Wilcoxon signed rank testing). Examining the constituent parts of calcium scoring, symptomatic carotid arteries did not differ significantly from asymptomatic arteries in terms of calcium volume (median 386 (IQR 537.5) versus 326.5 (IQR 453.5),  $p=0.35$ ) or calcium density (median 488 (IQR 940.5) versus 443 (IQR 680.25),  $p=0.36$ ).

No significant difference was observed between right or left carotid arteries for CACS (median 366.5 (IQR 595.25) versus 335.5 (IQR 502.5),  $p=0.55$ ), calcium volume (median 369 (IQR 507.5) versus 343.5 (IQR 426.75),  $p=0.51$ ), or calcium density (median 505 (IQR 883.5) versus 426 (685.75),  $p=0.59$ ).

#### 3.3.10.1 Carotid artery calcium score

On univariable analysis, the CACS had a moderate-to-strong association with age, with total CACS ( $r_s=0.75$ ), symptomatic artery CACS ( $r_s=0.64$ ), and asymptomatic artery CACS ( $r_s=0.73$ ) all being significant (all  $p<0.001$ ) (**Figure 3.15**).

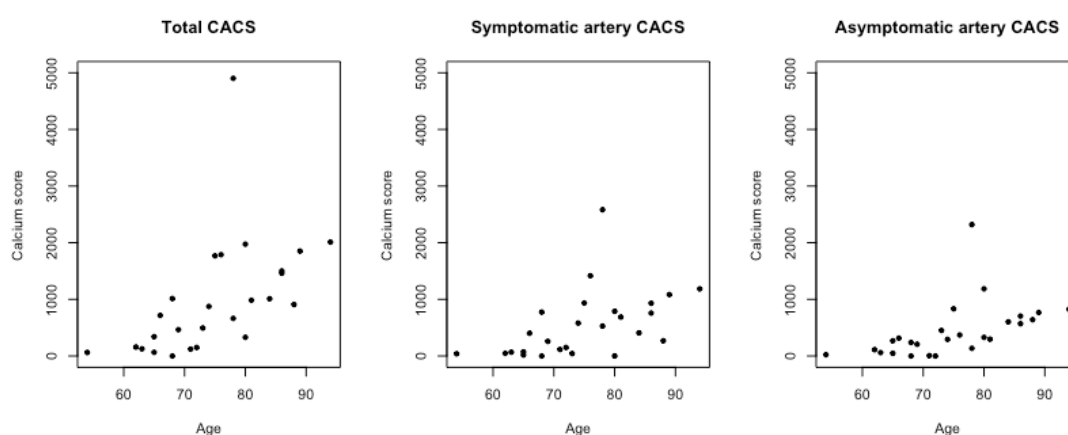


**Figure 3.15: Associations between age and carotid artery calcium score.**

Carotid calcification and its relation to risk factors (for both symptomatic and total carotid calcium score) are shown in the univariable analysis in **Table 3.8**.

	Symptomatic carotid calcium score in presence of risk factor	Symptomatic carotid calcium score in absence of risk factor	Sig.		Total carotid calcium score in presence of risk factor	Total carotid calcium score in absence of risk factor	Sig.
Male sex	233.5 (654)	535.5 (569.25)	p=0.21		660 (1337.25)	985.5 (691.75)	p=0.22
Smoking	281 (662)	657 (385)	p=0.40		545 (825)	1009 (727)	p=0.40
Diabetes mellitus	726 (IQR 245.75)	319.5 (IQR 585.75)	p=0.26		1171 (632.5)	804.5 (1287.5)	p=0.56
Hypertension	657 (894)	148 (206)	p=0.08		1009 (1179)	344 (614)	p=0.03
Prior statin	747 (454)	148 (329)	p=0.01		1682 (861)	399 (801)	p=0.004
Prior antiplatelet	876 (527)	214.5 (498)	p=0.02		1347 (832.25)	468.5 (833)	p=0.02
Cardiovascular history	702 (544.25)	214.5 (583.5)	p=0.07		1010.5 (757.5)	468.5 (1073.75)	p=0.06

**Table 3.8:** Univariable analysis for CACS and risk factors. All values median (IQR).

There was no relationship found between BMI and symptomatic carotid CACS ( $r_s=0.02$ ,  $p=0.94$ ), asymptomatic carotid CAC ( $r_s=-0.18$ ,  $p=0.38$ ), or total carotid calcium score ( $r_s=-0.06$ ,  $p=0.77$ ).

Adjustment for all variables using multiple linear regression as described in Chapter Two is shown in **Table 3.9**.

	Coefficient	Adjusted significance
<b>Symptomatic carotid CACS</b>		
Age	32.5	p=0.03
Male sex	-526.9	p=0.05
Smoking	557.0	p=0.04
Prior statin	1317.8	p<0.01
Prior antiplatelet	-808.9	p=0.04
AIC = 409.2		Adjusted R <sup>2</sup> = 0.47 (p<0.01)
<b>Total carotid artery CACS</b>		
Age	69.8	p=0.01
Male sex	-1122.15	p=0.02
Smoking	1242.2	p=0.01
Prior statin	3079.4	p<0.001
Prior antiplatelet	-2407.5	p<0.01
AIC = 439.3		Adjusted R <sup>2</sup> = 0.58 (p<0.001)

**Table 3.9:** Multiple regression analysis of risk factors associated with CACS.

### 3.3.10.2 Carotid artery calcium volume

Carotid artery calcium was strongly correlated with age in the symptomatic carotid artery ( $r_s=0.75$ ,  $p<0.001$ ) and total carotid artery volume ( $r_s=0.74$ ,  $p<0.001$ ), and moderately correlated in the asymptomatic carotid artery ( $r_s=0.63$ ,  $p<0.001$ ). Further univariable analysis is shown in **Table 3.10**.

	<b>Symptomatic carotid calcium volume in presence of risk factor</b>	<b>Symptomatic carotid calcium volume in absence of risk factor</b>	<b>Sig.</b>		<b>Total carotid calcium volume in presence of risk factor</b>	<b>Total carotid calcium volume in absence of risk factor</b>	<b>Sig.</b>
Male sex	238.5 (561.75)	505.5 (444.75)	p=0.26		668.5 (1134.5)	977 (606.75)	p=0.22
Smoking	267 (577)	609 (261)	p=0.53		514 (689)	1002 (588)	p=0.43
Diabetes mellitus	655 (226.75)	345 (524)	p=0.35		1067.5 (558.25)	853.5 (1078)	p=0.76
Hypertension	629 (779)	157 (178)	p=0.07		929 (1048)	387 (644)	p=0.04
Prior statin	679 (546)	157 (300)	p=0.01		1472 (740)	387 (773)	p<0.01
Prior antiplatelet	792 (582)	212 (464.25)	p=0.02		1200.5 (758.75)	447.5 (808)	p=0.047
Cardiovascular history	644 (448.5)	212 (522.5)	p=0.09		940.5 (598.5)	447.5 (973.5)	p=0.13

**Table 3.10:** Univariable analysis of carotid artery calcium volume and vascular risk factors. All values expressed as median (IQR).

As with CACS, carotid artery calcium volume showed no correlation with BMI for symptomatic carotid artery ( $r_s=0.03$ ,  $p=0.88$ ), asymptomatic carotid artery ( $r_s=-0.14$ ,  $p=0.50$ ), or combined carotid artery calcium volume ( $r_s=-0.06$ ,  $p=0.78$ ).

Adjustment of calcium volume for risk factors using multivariable linear regression is shown in **Table 3.11**.

	Coefficient	Adjusted significance
<b>Symptomatic carotid artery calcium volume</b>		
Age	31.2	p=0.02
Male sex	-445.9	p=0.06
Smoking	525.4	p=0.03
Prior statin	1163.0	p<0.001
Prior antiplatelet	-713.2	p=0.04
AIC = 401.3		Adjusted R <sup>2</sup> = 0.50 (p<0.01)
<b>Total carotid artery calcium volume</b>		
Age	66.2	p<0.01
Male sex	-943.5	p=0.03
Smoking	1161.8	p<0.01
Prior statin	2701.5	p<0.001
Prior antiplatelet	-2111.1	p<0.01
AIC 431.1		Adjusted R <sup>2</sup> = 0.60 (p<0.001)

**Table 3.11:** Multiple regression analysis of risk factors associated with carotid artery calcium volume.

### 3.3.10.3 Carotid artery calcium mass

As with CACS and carotid artery calcium volume, carotid artery calcium mass also showed strong correlations with age for the symptomatic carotid artery ( $r_s=0.78$ ,  $p<0.001$ ) and total carotid artery mass ( $r_s=0.74$ ,  $p<0.001$ ), and moderated correlation with age for the asymptomatic carotid artery ( $r_s=0.65$ ,  $p<0.001$ ). Further univariable analysis is shown in **Table 3.12**.

	<b>Symptomatic carotid calcium mass in presence of risk factor</b>	<b>Symptomatic carotid calcium mass in absence of risk factor</b>	<b>Sig.</b>		<b>Total carotid calcium mass in presence of risk factor</b>	<b>Total carotid calcium mass in absence of risk factor</b>	<b>Sig.</b>
Male sex	257.5 (860.25)	808 (982.75)	p=0.18		797.5 (1836.25)	1394.5 (118.5)	p=0.18
Smoking	296 (873)	951 (705)	p=0.34		792 (991)	1436 (1289)	p=0.31
Diabetes mellitus	1023.5 (437.75)	367.5 (906.75)	p=0.28		1544 (1071.25)	854.5 (1809)	p=0.61
Hypertension	951 (1460)	219 (219)	p=0.10		1353 (1817)	494 (573)	p=0.03
Prior statin	1022 (1169)	219 (507)	p<0.01		2524 (1429)	587 (1024)	p<0.01
Prior antiplatelet	1305.5 (1233)	257.5 (562.5)	p=0.02		1986.5 (1606.75)	627.5 (1172.75)	p=0.01
Cardiovascular history	991 (1047.75)	257.5 (786.25)	p=0.06		1394.5 (1424)	627.5 (1489.25)	p=0.04

**Table 3.12:** Univariable analysis of carotid artery calcium mass and vascular risk factors. All values expressed as median (IQR).

There was no association between calcium mass and BMI for symptomatic carotid arteries ( $r_s=-0.01$ ,  $p=0.95$ ), asymptomatic carotid arteries ( $r_s=-0.16$ ,  $p=0.44$ ), or total carotid artery calcium mass ( $r_s=-0.07$ ,  $p=0.72$ ).

Adjustment of calcium mass for risk factors using multivariable linear regression is shown in **Table 3.13**.

	Coefficient	Adjusted significance
<b>Symptomatic carotid artery calcium mass</b>		
Age	53.0	p=0.03
Sex	-828.0	p=0.06
Smoking	867.5	p=0.048
Prior statin	2100.7	p=0.001
Prior antiplatelet	-1237.4	p=0.05
AIC = 434.0		Adjusted R <sup>2</sup> = 0.47 (p<0.01)
<b>Total carotid artery calcium mass</b>		
Age	115.1	p=0.01
Sex	-1720.2	p=0.03
Smoking	2062.5	p=0.01
Prior statin	4937.3	p<0.001
Prior antiplatelet	-3768.6	p<0.01
AIC 464.2		Adjusted R <sup>2</sup> = 0.58 (p<0.001)

**Table 3.13:** Multiple regression analysis of risk factors associated with carotid artery calcification mass.

### 3.3.11 Spatial distribution of macrocalcification

The spatial distribution of the calcium score at each 3 mm slice along the common/internal carotid artery is shown below (**Figure 3.16**). As discussed above, there was no difference in arterial calcium scores between symptomatic and asymptomatic arteries. The slice-by-slice spatial analysis shows that the peak calcium score is similar between symptomatic and asymptomatic arteries. However, the peak calcium score is closer to the bifurcation in the symptomatic artery (corresponding to the +1 slice; 3 mm above the carotid bifurcation) in comparison to the asymptomatic artery, where the peak activity is more distal.

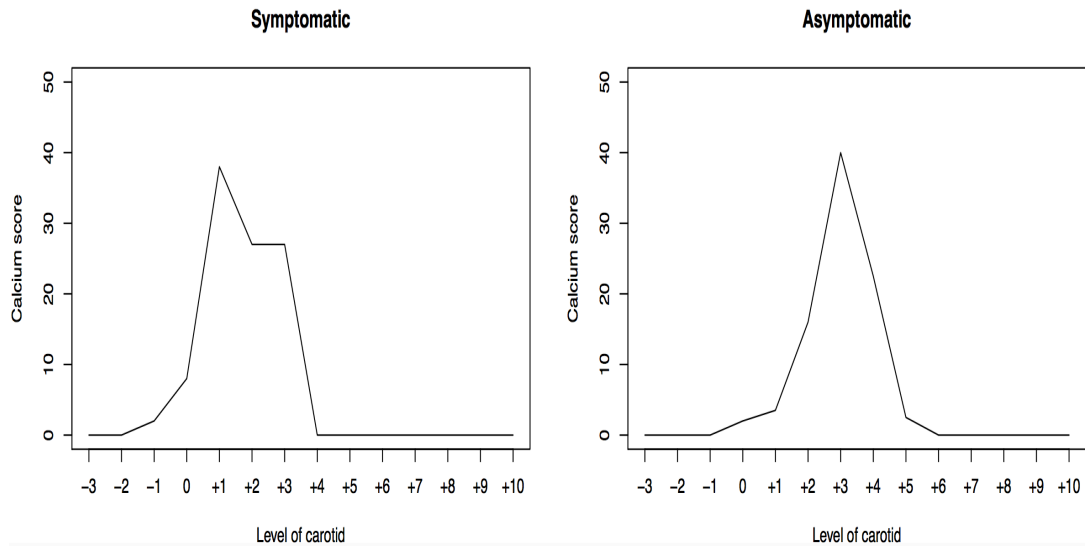


**Figure 3.16: Spatial distribution of CACS.** Median CACS at each 3 mm slice (slice 0 representing the carotid bifurcation).

### 3.3.12 Relationship between NaF uptake and macrocalcification

The relationship between microcalcification and macrocalcification may be considered on an axial slice-by-slice basis or on an artery-by-artery basis.

On a slice-by-slice basis - considering all 728 axial slices together - there were moderate correlations between Agatston score and  $SUV_{mean}$  ( $r_s=0.412$ ,  $p<0.01$ ) and  $SUV_{max}$  ( $r_s=0.427$ ,  $p<0.01$ ).

Of 364 axial slices through 26 symptomatic arteries, the overall correlation between Agatston score and  $SUV_{mean}$  was  $r_s=0.428$  ( $p<0.01$ ), and between Agatston score and  $SUV_{max}$  was  $r_s=0.430$  ( $p<0.01$ ). When considering the 173 axial slices where macrocalcification was detected, the correlation of Agatston score with  $SUV_{mean}$  and  $SUV_{max}$  weakened but remained significant ( $r_s=0.328$  and  $r_s=0.350$  respectively, both  $p<0.01$ ).

Adopting a similar approach for the 364 axial slices in the 26 asymptomatic arteries, the correlation between Agatston score and  $SUV_{mean}$  is  $r_s=0.385$  ( $p<0.01$ ), and between Agatston score and  $SUV_{max}$   $r_s=0.414$  ( $p<0.01$ ). When considering only the

159 axial slices with macrocalcification, correlation between Agatston score and  $SUV_{mean}$  and  $SUV_{max}$  was  $r_s=0.369$  and  $r_s=0.376$  respectively (both  $p<0.01$ ).

Patient-based (artery-by-artery) correlations demonstrated stronger associations. Overall the artery-by-artery (for all 52 arteries, both symptomatic and asymptomatic) Spearman correlations between CACS and SHS  $SUV_{mean}$ , MDS  $SUV_{mean}$ , and WV  $SUV_{mean}$  were  $r_s=0.630$  ( $p<0.01$ ),  $r_s=0.629$  ( $p<0.01$ ), and  $r_s=0.547$  ( $p<0.01$ ) respectively.  $SUV_{max}$  criteria demonstrated marginally stronger correlations, with correlations between CACS and SHS  $SUV_{max}$ , MDS  $SUV_{max}$ , and WV  $SUV_{max}$  being  $r_s=0.678$  ( $p<0.01$ ),  $r_s=0.667$  ( $p<0.01$ ), and  $r_s=0.571$  ( $p<0.01$ ) respectively.

These artery-by-artery correlations were then subdivided according to symptomatic/asymptomatic arteries. For the 26 symptomatic arteries, the total artery CACS had correlations with SHS  $SUV_{mean}$ , MDS  $SUV_{mean}$ , and WV  $SUV_{mean}$  of  $r_s=0.569$  ( $p<0.01$ ),  $r_s=0.581$  ( $p<0.01$ ), and  $r_s=0.483$  ( $p=0.01$ ) respectively. For corresponding  $SUV_{max}$  measures, correlations were stronger between CACS and SHS  $SUV_{max}$  and MDS  $SUV_{max}$  ( $r_s=0.649$  and  $r_s=0.633$  respectively, both  $p<0.01$ ) but comparable for WV  $SUV_{max}$  ( $r_s=0.467$ ,  $p=0.02$ ) (**Figure 3.17**).

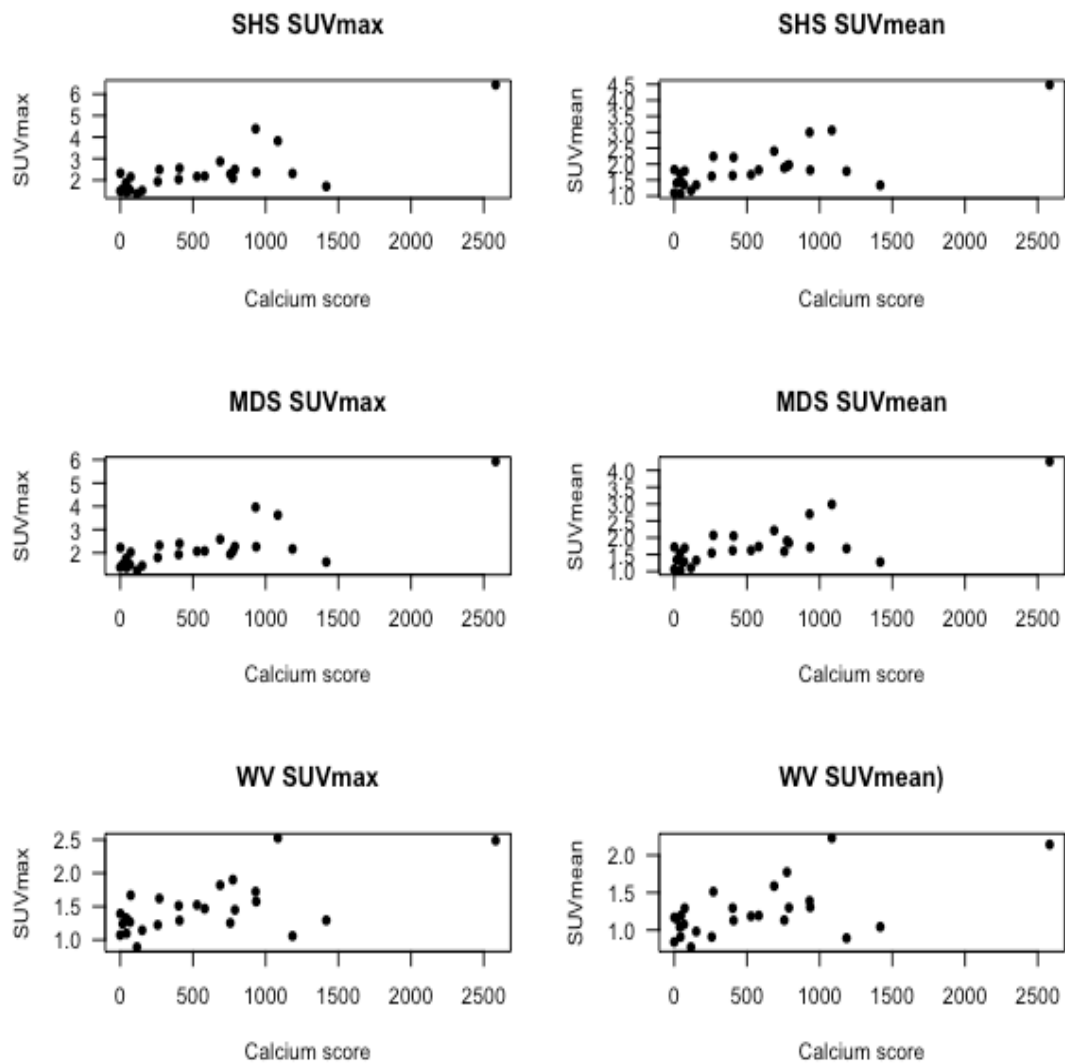


**Figure 3.17: Associations between CACS and NaF SUVs in symptomatic arteries.**

For the asymptomatic arteries, Spearman correlations were higher for all corresponding values: correlations between CACS and SHS  $SUV_{mean}$  ( $r_s=0.639$ ,  $p<0.01$ ), MDS  $SUV_{mean}$  ( $r_s=0.647$ ,  $p<0.01$ ), WV  $SUV_{mean}$  ( $r_s=0.605$ ,  $p<0.01$ ), SHS  $SUV_{max}$  ( $r_s=0.695$ ,  $p<0.01$ ), MDS  $SUV_{max}$  ( $r_s=0.690$ ,  $p<0.01$ ), and WV  $SUV_{max}$  ( $r_s=0.634$ ,  $p<0.01$ ) (**Figure 3.18**).

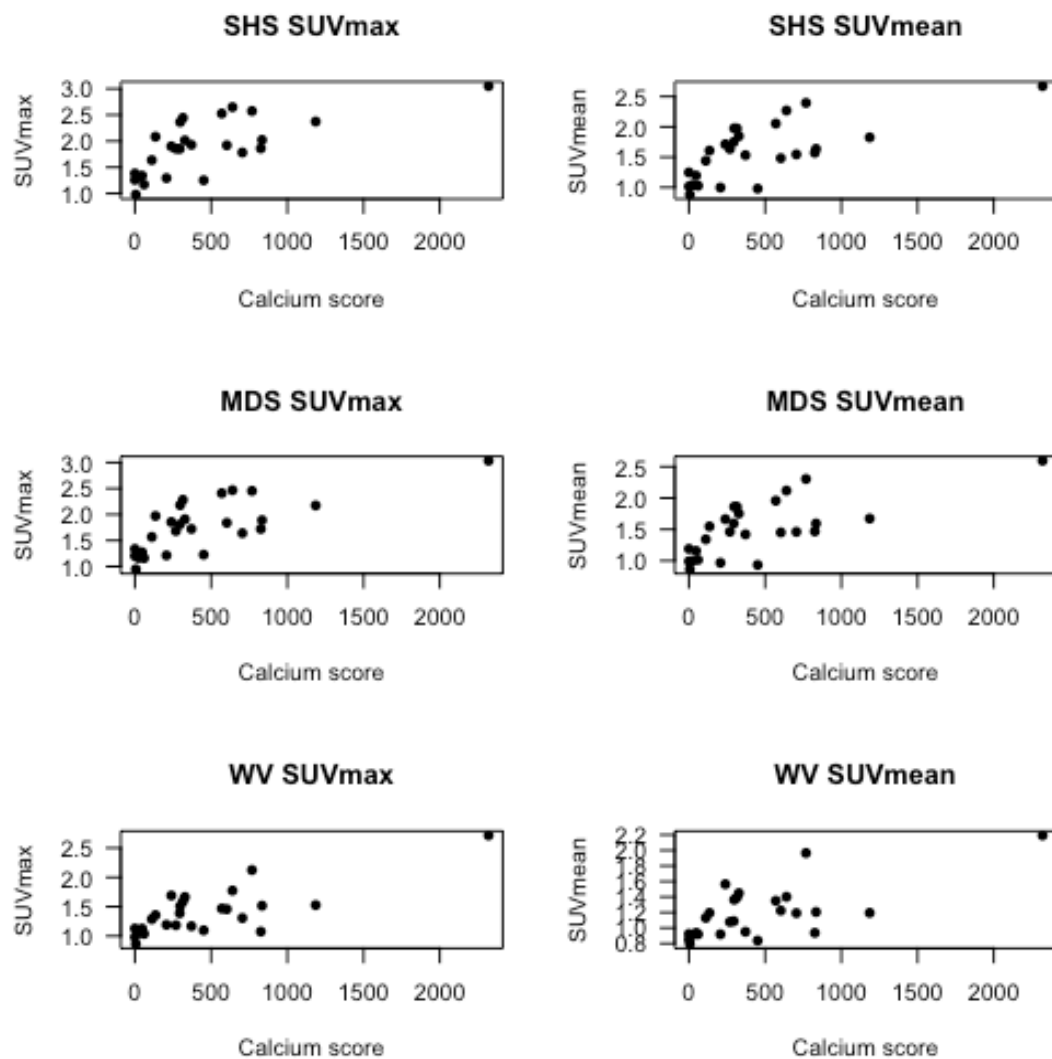


**Figure 3.18: Associations between CACS and NaF SUVs in asymptomatic arteries.**

TBR measures also showed moderate-to-strong correlations with CACS in the both symptomatic and asymptomatic arteries (**Table 3.14**).

	Symptomatic carotid arteries		Asymptomatic carotid arteries	
	Correlation	Significance	Correlation	Significance
SHS TBR <sub>max</sub>	$r_s=0.59$	$p<0.01$	$r_s=0.65$	$p<0.01$
MDS TBR <sub>max</sub>	$r_s=0.55$	$p<0.01$	$r_s=0.65$	$p<0.01$
WV TBR <sub>max</sub>	$r_s=0.45$	$p=0.02$	$r_s=0.49$	$p=0.01$
SHS TBR <sub>mean</sub>	$r_s=0.60$	$p<0.01$	$r_s=0.62$	$p<0.01$
MDS TBR <sub>mean</sub>	$r_s=0.58$	$p<0.01$	$r_s=0.62$	$p<0.01$
WV TBR <sub>mean</sub>	$r_s=0.51$	$p<0.01$	$r_s=0.49$	$p=0.01$

**Table 3.14: Correlations between CACS and NaF TBRs.**

## 3.4 Discussion

### 3.4.1 NaF-PET to identify culprit atheroma

This part of the study demonstrates that uptake of NaF in symptomatic culprit atheroma is increased compared to the non-culprit asymptomatic plaque and that uptake differentiates between symptomatic and asymptomatic arteries. It is the largest symptomatic stroke cohort investigated with NaF-PET/CT to date and is the first to have been conducted including a range of stroke severities.

The validated utility of NaF to detect microcalcification means that these radiological findings support histological studies identifying microcalcification as a key process involved in plaque destabilisation. The role of microcalcification in plaque rupture has been identified through histological and biomechanical analysis. A small study of coronary atheroma suggested that microcalcification may increase the circumferential stress in regions of a thin fibrous cap with pre-existing circumferential stress by up to a factor of two (Vengrenyuk et al., 2006). Subsequent work showed that this mechanical disruption of the fibrous cap is location specific, with microcalcification only seen to cause plaque rupture when it occurred within a region of pre-existing high background stress and in fibrous caps thinner than 80  $\mu\text{m}$ , as well as being affected by the shape of the microcalcification. Although spherical microcalcification increased circumferential stress by a factor of two as previously reported, elongated microcalcifications caused even higher stress increases (Vengrenyuk et al., 2008). In contrast to microcalcification, the same study also reported a stabilising effect of macrocalcification within the fibrous cap shoulders (Vengrenyuk et al., 2008). A larger study of 107 coronary vessels has supported these findings, indicating that that tissue stress may increase up to fivefold in the presence of concentrated microcalcification, and that stress on thin fibrous caps with no microcalcification (107 kPa) fell below the threshold believed to be necessary for rupture (300 kPa) (Maldonado et al., 2012, Cheng et al., 1993). The authors conclude that although a thin cap may reach the rupture threshold with a single microcalcification, a clustering of a sufficient number of microcalcifications may be enough to exceed the vulnerability threshold (Maldonado et al., 2012).

The inability of clinical CT, MRI, or optical coherence tomography (OCT) to detect microcalcification means that molecular imaging with NaF-PET may represent a potential method for detecting and quantifying microcalcification in clinical care. Within the coronary arteries, Joshi et al. found that NaF can identify vulnerable but non-ruptured atheroma (Joshi et al., 2014). This, along with the uptake seen in asymptomatic atheroma (Derlin et al., 2010), implies a potential role for identification of ‘at risk’ vulnerable plaques as well as detection of ruptured culprit plaques. Furthermore, it provides a potential means to quantify microcalcification and its response to treatment or as endpoints in drug discovery trials, similar to that used in the dal-plaque study measuring FDG uptake in response to therapy (Fayad et al., 2011b).

It is important to consider the nature of the ‘asymptomatic’ contralateral artery comparator. While NaF uptake was consistently higher in the symptomatic artery compared to the contralateral artery, there was consistently uptake demonstrated in this ‘asymptomatic’ artery. No study participant had a stroke in the contralateral hemisphere during the six-month study period, but it is possible that these regions in the asymptomatic artery may become symptomatic at a later date. Although this contralateral artery is ‘asymptomatic’ in that it has not ruptured and triggered a stroke event, it is likely that the contralateral arteries are substantially along the spectrum of vulnerability by nature of the individuals already proving themselves to be at high risk. These individuals typically show a moderate- to high-risk vascular risk profile, which is in turn associated with increased NaF uptake in asymptomatic individuals (Morbelli et al., 2014). The vascular risk profile and NaF uptake is explored in greater detail in subsequent sections, but the observed results raise two important considerations. Firstly, there is the uncertainty whether these contralateral arteries may become symptomatic at a later time (though intervention following this stroke event may affect their progression). Secondly, it suggests that while culprit atheroma can be reliably differentiated from high-risk plaques, the difference in uptake between symptomatic plaques and normal or low-risk plaques will be even greater. This has implications for the use of NaF-PET in individuals with low vascular risk and/or asymptomatic disease.

### 3.4.2 Spatial distribution of NaF uptake

The pattern of NaF uptake suggests that microcalcification is a focal disease, with focal measures of tracer uptake (SHS  $SUV_{max}$ , MDS  $SUV_{max}$ , SHS  $TBR_{max}$ , MDS  $TBR_{max}$ ) differing significantly between symptomatic and asymptomatic sides. However, the average  $SUV_{max}$  and  $TBR_{max}$  readings for the entire artery (WV  $SUV_{max}$  and WV  $TBR_{max}$ ) were not significantly different between symptomatic and asymptomatic sides.

The distribution of NaF uptake along the length of the symptomatic and arteries suggests a peak increase around the carotid bifurcation and proximal internal carotid artery. This peak is best visualised using  $SUV_{max}$ , which shows a focal peak in the symptomatic artery, in contrast to an attenuated and more widespread uptake in the asymptomatic artery. This peak is less distinct in the  $TBR_{max}$  curve, where both curves appear broader (Figure 3.19).

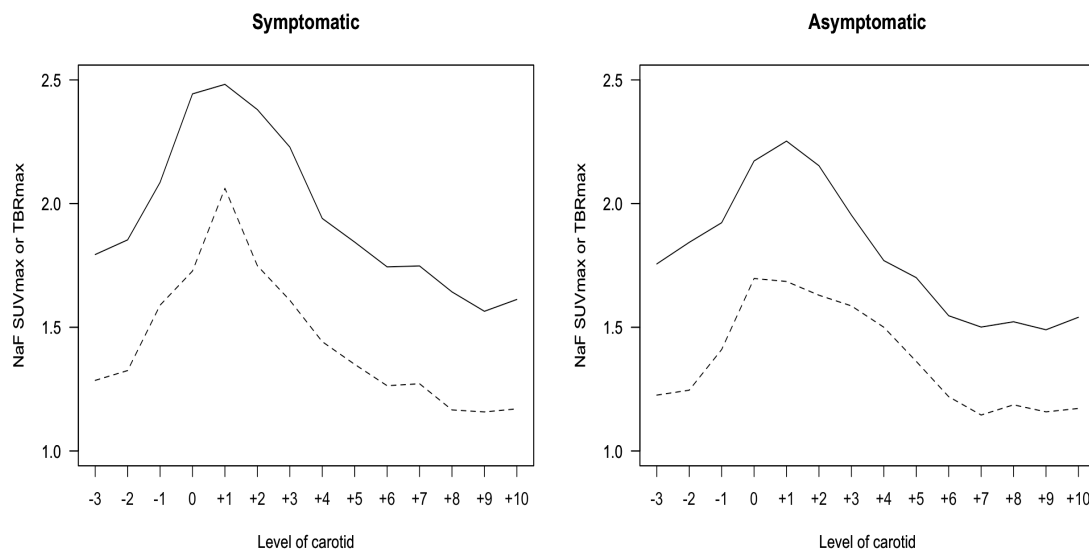


**Figure 3.19: Comparative spatial distributions of  $SUV_{max}$  and  $TBR_{max}$ .** Comparison of NaF  $TBR_{max}$  (solid line) and  $SUV_{max}$  (dotted line) along symptomatic (left) and asymptomatic (right) carotid arteries.

The pattern of disease may be further illustrated by directly comparing  $SUV_{max}$  and  $SUV_{mean}$ . As shown in Figure 3.20, the curve for symptomatic  $SUV_{max}$  is similar to the asymptomatic  $SUV_{max}$ , except at the peak corresponding to the carotid bifurcation.

Hence, this helps illustrate why SHS and MDS  $SUV_{max}$  were significantly higher for symptomatic carotid arteries, but WV  $SUV_{max}$  did not reach significance. The  $SUV_{mean}$  curves show similar patterns for the symptomatic and asymptomatic arteries along the length of the artery, again diverging primarily at the site around the carotid bifurcation but also around the distal ICA. This may illustrate why the difference between symptomatic and asymptomatic artery WV  $SUV_{mean}$  reaches significance but WV  $SUV_{max}$  does not.

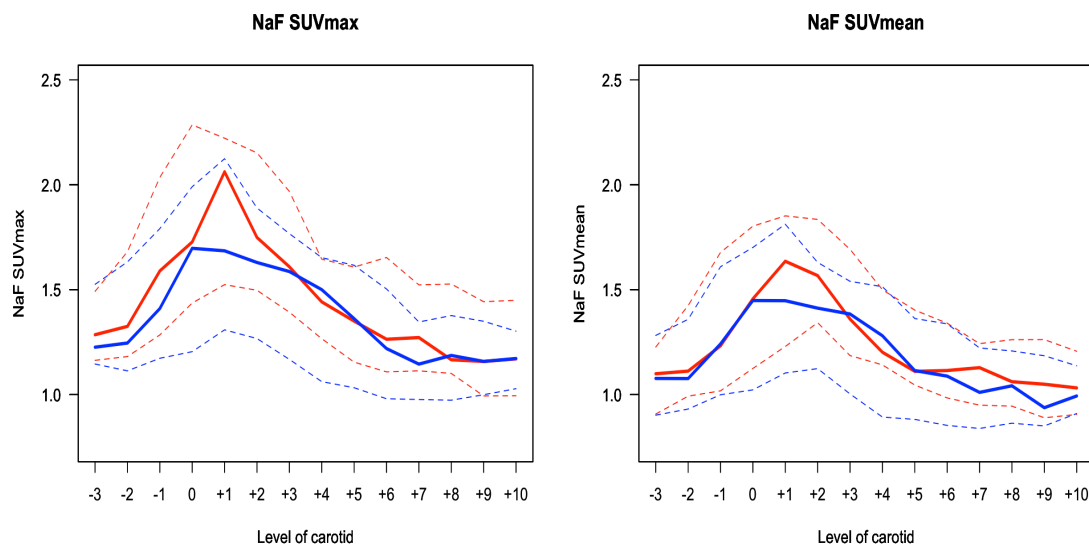


**Figure 3.20: Composite NaF SUV spatial distributions.** Comparison of NaF  $SUV_{max}$  (left) and  $SUV_{mean}$  (right) at each slice along the symptomatic (red line) and asymptomatic (blue line) artery (upper and lower interquartile limits shown by dashed lines).

A similar pattern is seen in TBR measures (**Figure 3.21**), with the symptomatic and asymptomatic artery curves diverging more than for SUV.

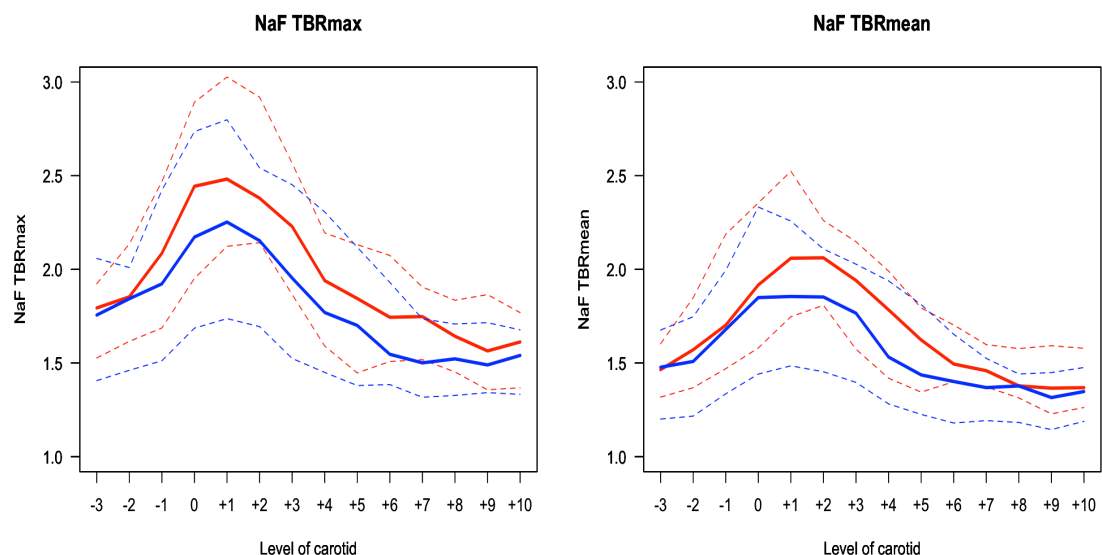


**Figure 3.21: Composite NaF TBR spatial distributions.** Comparison of NaF TBR<sub>max</sub> (left) and TBR<sub>mean</sub> (right) at each slice along the symptomatic (red line) and asymptomatic (blue line) artery (upper and lower interquartile limits shown by dashed lines).

The bifurcation as a focus of disease was investigated statistically by testing the uptake in the carotid bifurcation (defined as the median tracer uptake in the region between the -2 and +2 slices, i.e. +/- 2 slices either side of the bifurcation) and comparing it against the median ‘non-bifurcation’ arterial uptake (defined as the median uptake in the remaining nine slices that fell outside of the bifurcation). For pooled symptomatic and asymptomatic arteries, NaF tracer uptake was significantly higher in the bifurcation compared to the rest of the artery (**Table 3.15**).

	<b>Bifurcation</b>	<b>Non-bifurcation</b>	<b>Significance</b>
Median SUV <sub>max</sub> (IQR)	1.65 (0.75)	1.26 (0.42)	p<0.001
Median SUV <sub>mean</sub> (IQR)	1.35 (0.57)	1.12 (0.34)	p<0.001
Median TBR <sub>max</sub> (IQR)	2.19 (0.81)	1.71 (0.38)	p<0.001
Median TBR <sub>mean</sub> (IQR)	1.85 (0.68)	1.47 (0.29)	p<0.001

**Table 3.15:** Comparison of NaF uptake between bifurcation and non-bifurcation.

To confirm this significance was not due entirely to the symptomatic arteries, we further subdivided arteries according to whether they were symptomatic (**Table 3.16**).

	Symptomatic artery				Asymptomatic artery		
	Bifurcation	Non-bifurcation	Sig.		Bifurcation	Non-bifurcation	Sig.
Median SUV <sub>max</sub> (IQR)	1.72 (0.77)	1.28 (0.39)	p<0.001		1.52 (0.66)	1.21 (0.46)	p<0.001
Median SUV <sub>mean</sub> (IQR)	1.45 (0.53)	1.13 (0.23)	p<0.001		1.33 (0.61)	1.06 (0.37)	p<0.001
Median TBR <sub>max</sub> (IQR)	2.22 (0.72)	1.74 (0.29)	p<0.001		2.01 (0.94)	1.62 (0.37)	p<0.001
Median TBR <sub>mean</sub> (IQR)	1.92 (0.64)	1.47 (0.24)	p<0.001		1.81 (0.69)	1.44 (0.35)	p<0.001

**Table 3.16:** Comparison of NaF uptake between bifurcation and non-bifurcation according to symptomatic and non-symptomatic carotid arteries.

The significantly higher WV SUV<sub>mean</sub> and WV TBR<sub>mean</sub> (but not WV SUV<sub>max</sub> or WV TBR<sub>max</sub>) in symptomatic compared to asymptomatic arteries suggests that there may be a background level of microcalcification (potentially as a product of inflammation) along the artery but the peak accumulation is focal. This finding supports the biomechanical findings that the density of microcalcification, and the consequent stresses they produce, are a major determinant in mechanical destabilisation of the plaque.

### 3.4.3 Comparison of measures of NaF uptake

On an artery-by-artery basis there was a moderate to strong correlation between SUV and TBR for focal measures of uptake, but only moderate correlation when the whole vessel was considered.

The effect of renal impairment on NaF pharmacodynamics has received little attention, most likely due to the nature of the studies and the cohorts examined. Beheshti et al. found that renal function (dichotomised as high or low creatinine) did not affect aortic NaF uptake measured using a “global molecular calcification score (GMCS)” (Beheshti et al., 2011). This finding should be interpreted with caution as the GMCS approach (the sum of the products of each ROI volume multiplied by the SUV<sub>mean</sub> of the ROI) as this technique reduces the effect of high focal uptake (i.e. the SUV<sub>max</sub>) within the ROI. However, it is suggestive that the pharmacokinetics of NaF

uptake are not affected by renal impairment. Hence, the use of TBR to correct for blood pooling appears to be less important for NaF-PET as it does with FDG-PET, where FDG blood-pooling appears to be much more sensitive to renal function (Derlin et al., 2011a).

Blomberg et al. have reported different NaF blood pool concentrations in different vascular territories despite a prolonged circulation time (mean  $92 \pm 4$  minutes), being the highest in the internal jugular veins (Blomberg et al., 2015). The authors conclude this is likely secondary to spill-over effects from neighbouring bone structures and suggest the use of the superior vena cava for reference. This study used the proximal right internal jugular vein to measure venous uptake as the single bed position used for scanning did not include the superior vena cava. No noticeable spill-over effect was observed. To reduce any spill-over effect the average over five 3 mm slices was used in this study.

Ultimately, there appear to be fewer arguments that favour TBR over SUV for measuring NaF uptake compared to the equivalent argument in FDG-PET methodology. This is likely to relate to the consistent level of NaF blood-pool activity across subjects observed in our study. In this study both SUV and TBR were able to differentiate between symptomatic and asymptomatic atheroma. Given the overall shift towards using TBR in FDG-PET imaging studies, in the absence of a strong reason to favour one or other in NaF-PET and assuming a suitable vein is used for blood-pooling quantification, it seems sensible to adopt a similar quantification approach across different tracer studies.

The overall distribution of tracer uptake raises an important consideration about the statistical analysis of the WV artery scores. A number of papers report WV scores as the mean value, whereas we have reported WV scores as the median value. Taking  $SUV_{max}$  as an example, the slice-by-slice  $SUV_{max}$  along all 14 slices showed a non-normal distribution along 10 (38.5%) of the symptomatic arteries and along 5 (19.2%) of the asymptomatic arteries. Hence, the median value was chosen to express the average value of the WV tracer uptake to avoid the potential skew that would occur if means were used in non-normal intra-arterial distributions.

#### *3.4.4 Carotid calcification and culprit arteries*

Calcium measurements using Agatston score, volume, or mass showed no significant difference between symptomatic and asymptomatic carotid arteries. This is in-keeping with the uncertainty about the role of carotid macrocalcification discussed above. What it does suggest is that it is the microcalcification process specifically, rather than simply the presence of macrocalcification, that is key to plaque destabilisation and thromboembolism.

The difference in macrocalcification distribution seen between symptomatic and asymptomatic arteries also raises the possibility that whilst the total calcium score did not appear associated with stroke, the spatial distribution may be a contributory factor. In our study the burden of calcification in the symptomatic artery peaked in the proximal internal carotid artery, 3 mm distal to the carotid bifurcation. In contrast, the peak of macrocalcification in the asymptomatic artery was 6 mm distal to the symptomatic artery peak; approximately 1 cm distal to the origin of the internal carotid artery.

The CACS in the bifurcation region specifically was tested using the approach described in the previous section. Of the 52 carotid bifurcations, the range of CACS was 0 to 916. Bifurcations were dichotomised to 'low' (0-450) and 'high' ( $\geq 451$ ) calcification based on their Agatston score, with tracer uptake measured as the median average of these five slices. There was no significant difference between the CACS in the symptomatic bifurcation (138 [IQR 339.75]) and the asymptomatic bifurcation (98.5 [IQR 384.25]) ( $p=0.29$ ).

The association between vessel wall shear stresses and calcification is unclear, with some studies suggesting an association between high shear stresses and calcification (Samady et al., 2011) whilst others do not (Huang et al., 2001). In a comparative study of femoral and carotid plaques, an increasing proportion of calcification relative to lipid was associated with a reduced ability of atheroma to withstand stretch (Cunnane et al., 2016). However, calcium's role in vessel geometry has received less attention. Computational fluid dynamics (CFD) considers the boundary of the lumen as a rigid wall (as is likely the case with arterial calcification) and the only parameter

derived from imaging associated with wall shear stress is luminal geometry. There may be a link between calcium burden and distortion of the lumen, with higher calcium (particularly surface calcium) leading to less regular luminal geometry and impact upon wall shear stress. This work lies outside of the scope of this study but forms the basis of future work with biomechanical engineers.

#### *3.4.5 Relationship between NaF uptake and macrocalcification*

Previous NaF-PET studies have reported different correlations between NaF uptake and macrocalcification. Morbelli et al. reported no significant correlation between TBR and regional calcium load, nor were carotid TBRs significantly different between calcified versus non-calcified segments, in asymptomatic disease (Morbelli et al., 2014). Fiz et al. categorised asymptomatic plaques according to light (HU <210), medium (HU 211-510), and heavy (HU >510) attenuation values and reported a reduction in plaque average TBR with increasing calcification ( $r=-0.7$ ,  $p<0.01$ ), though it appears parametric testing was used in what is likely to be a non-normally distributed population (Fiz et al., 2015). In contrast, Derlin et al. found significant correlations between NaF uptake and calcification within the atherosclerotic lesion ( $r=0.85$ ,  $p<0.0001$ ), intensity of tracer uptake ( $SUV_{max}$ ) and calcification score ( $r=0.33$ ,  $p<0.0001$ ), and  $SUV_{max}$  and calcified lesion thickness ( $r=0.23$ ,  $p<0.01$ ) in asymptomatic disease (Derlin et al., 2011c). In a mix of symptomatic disease and asymptomatic controls, Vesey et al. reported a correlation between plaque  $SUV_{mean}$  and Agatston score of  $r=0.72$  ( $p<0.001$ ) (Vesey et al., 2017). Dweck et al. reported a significant correlation between NaF uptake and coronary Agatston scores ( $r=0.652$ ,  $p<0.001$ ) and extensive overlap between NaF uptake and macrocalcification, though there were disparate areas with notably only 59% of patients with extensive CAC scores (>1,000) showing significant NaF uptake (Dweck et al., 2012).

A strength of our study is the analysis of NaF uptake and calcification at an ROI level. For any given ROI, there was a moderate but statistically significant association between NaF uptake (using any of  $SUV_{max}$ ,  $SUV_{mean}$ ,  $TBR_{max}$ ,  $TBR_{mean}$ ) and calcium score within that ROI.

On an artery-by-artery basis, all NaF measures demonstrated a moderate but significant association with carotid Agatston score. When separating by symptomatic and asymptomatic arteries, these associations were slightly stronger in the latter. This is consistent with microcalcification and macrocalcification representing related stages in the progression of asymptomatic disease (and response to cardiovascular risk profile). The increased microcalcification, but not macrocalcification, seen in symptomatic plaque rupture then results in a reduced correlation.

When considering the bifurcation specifically, NaF uptake also showed a significant difference between the low and high CACS cohorts, with NaF uptake higher in high CACS bifurcations ( $SUV_{max}$ ,  $SUV_{mean}$ ,  $TBR_{max}$ ,  $TBR_{mean}$  all  $p < 0.05$ ) (**Figure 3.22**).

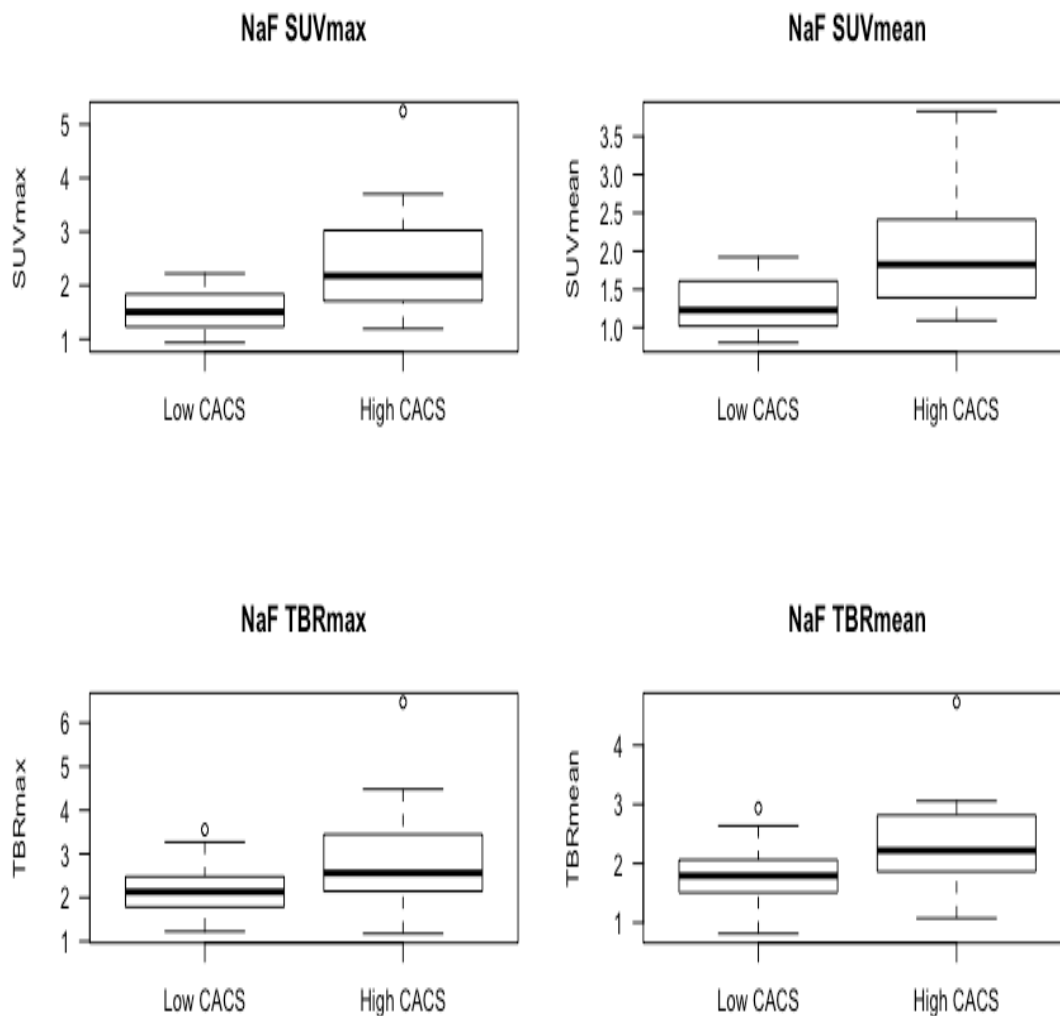


**Figure 3.22: NaF uptake in the carotid bifurcation according to the degree of macrocalcification.**

Broadly, our results appear to support the correlations reported by Derlin et al. and Vesey et al. (Derlin et al., 2011c, Vesey et al., 2017). Our study participants showed extensive calcification compared to asymptomatic populations. Only 3.8% (1/26) of participants and 5.8% (3/52) of arteries were free of calcification. In contrast, 57.2% (154/269) of asymptomatic participants were reported free of calcification in their carotids (Derlin et al., 2011c). The difference in the burden of calcification between symptomatic and asymptomatic cohorts is likely to account for some difference in the correlations.

$\mu$ PET studies have demonstrated that NaF binds only to the surface of macrocalcifications and that the fluoride ion does not permeate into the crystalline mass of large macrocalcifications (Irkle et al., 2015). The median Agatston score reported in our study was 367 (IQR 625) for symptomatic arteries and 324.5 (IQR 500.5) for asymptomatic arteries, in contrast to a median of 164 (IQR 5-494) reported by the symptomatic cohort in Vesey et al. (Vesey et al., 2017). The differences in correlations between these studies is likely to be affected by this approximate two-fold calcium burden seen in our study, with the heavy calcification likely to reduce the correlation on the artery-by-artery basis as a substantial amount of calcification lies within the calcified plaque and consequently cannot bind tracer.

The relative spatial distributions of NaF uptake and macrocalcification can be plotted and show an apparent difference in the processes relative to each other (**Figures 3.23** and **3.24**).

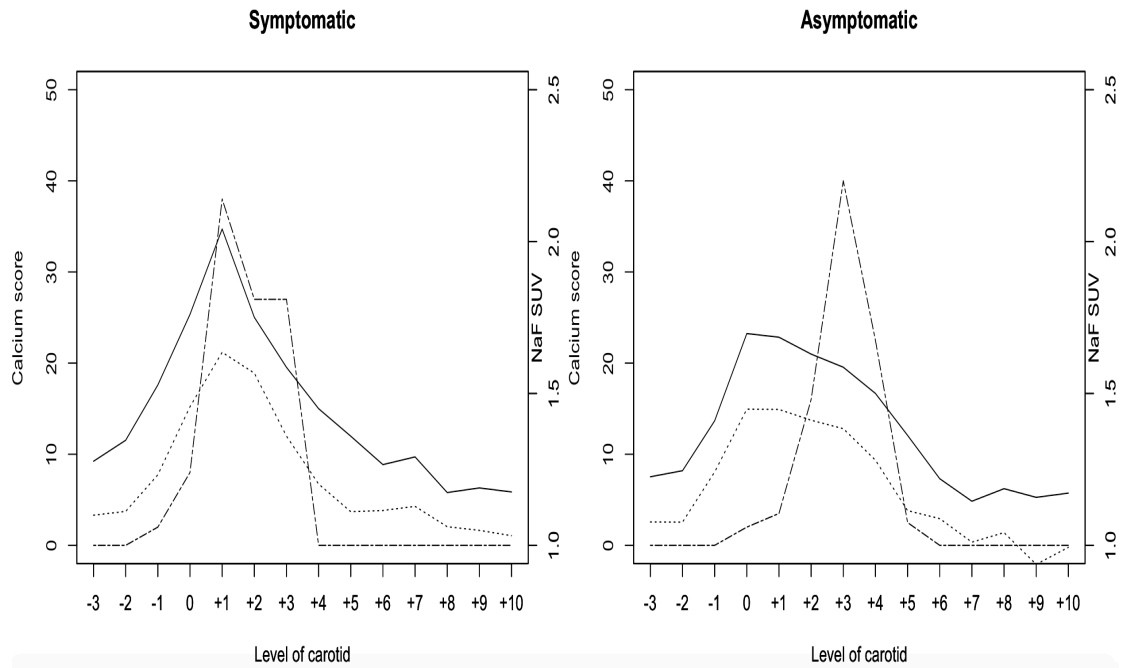


**Figure 3.23: Spatial distribution of NaF SUVs and macrocalcification.** Spatial distribution of NaF uptake and macrocalcification by symptomatic (left) and asymptomatic (right) carotid arteries.  $SUV_{max}$  = solid line,  $SUV_{mean}$  = dotted line, Agatston score = dashed line.

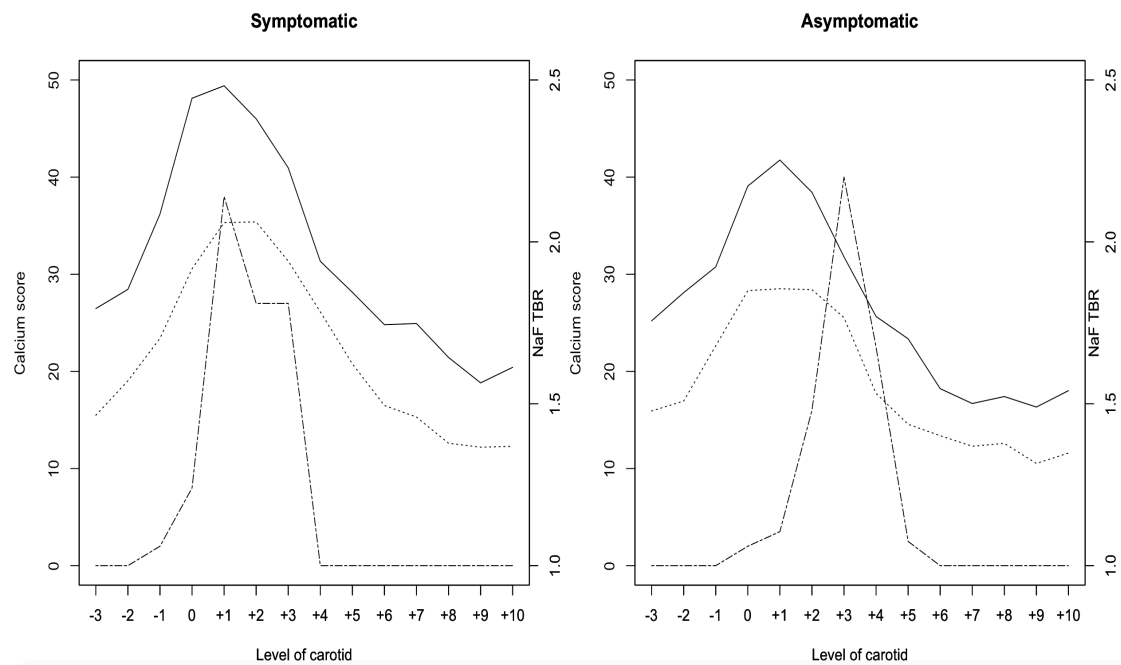


**Figure 3.24: Spatial distribution of NaF TBRs and macrocalcification.** Spatial distribution of NaF uptake and macrocalcification by symptomatic (left) and asymptomatic (right) carotid arteries.  $TBR_{max}$  = solid line,  $TBR_{mean}$  = dotted line, Agatston score = dashed line.

As previously discussed, the peak of macrocalcification appears to be shifted distally along the internal carotid artery away from the carotid bifurcation in asymptomatic relative to symptomatic carotid arteries. In symptomatic arteries the peak macrocalcification co-localises with peak NaF SUV and TBR, but in asymptomatic arteries these processes appear less related spatially. This supports the hypothesis that although the microcalcification and macrocalcification processes are related, they are distinct processes that do not necessarily co-exist.

#### *3.4.6 Relationship between NaF uptake, calcification, and vascular risk profile*

Risk factor analysis indicates that age, sex, statin therapy, antiplatelet therapy, smoking, cardiovascular history, and total cholesterol play are independently associated with increased NaF uptake. Given the moderate correlation found between NaF and macrocalcification, as well as its physiological relationship, it is unsurprising that similar risk factors (age, sex, smoking, statin therapy, and antiplatelet therapy) appear significant when considering calcium measures. Possible reasons for these associations are considered in greater detail below.

Previous NaF-PET studies have investigated the role of cardiovascular risk factors in NaF uptake in both symptomatic and asymptomatic atherosclerosis across a variety of arteries. These findings, along with the findings of this study, are summarised in **Table 3.17**.

	ICARUSS study	Derlin et al. (2011)	Dweck et al. (2012)	Janssen et al. (2013)	Morbelli et al. (2014)	Vesey et al. (2017)
Artery	Carotid	Carotid	Coronary	Superior femoral	Whole body	Carotid
Symptomatic	Symptomatic	Asymptomatic	Both	Asymptomatic	Asymptomatic	Both
Age	Yes	Yes	Yes	Yes	Yes	Yes
Sex	Yes (female)	Yes (male)	No	No	No	Not reported
Diabetes	No	No	No	Yes	Yes	Not reported
Hypertension	No	Yes	No	Yes	Yes	Not reported
Smoking	Yes	No	No	Yes	No	Not reported
Hypercholesterolaemia	Yes (for TBR)	Yes	Yes	Yes	Not reported	Not reported
BMI	No	Yes	Not reported	No	No	Not reported
Current statin	Yes	No	No	Not reported	Statin therapy excluded	Not reported
Current antiplatelet	Yes (for TBR)	Not reported	Not reported	Not reported	Not reported	Not reported
Cardiovascular history	Yes	No	Yes	Yes	Not reported	Not reported
Notes			High versus low NaF uptake. No multivariable analysis.			Correlation with overall risk score.

**Table 3.17:** Summary of vascular risk factors found to be associated with NaF uptake in literature to date.

#### 3.4.6.1 Prior statin use

Given the relatively small sample size, caution must be applied in the interpretation of significance following multivariable analysis. However, some trends emerge. All measures of NaF uptake showed an independent association with statin use. This relationship appeared to be independent of previous cardiovascular events. Interestingly, although Dweck et al. reported no difference between statin use between their control and coronary heart disease groups, there was an approximate two-fold increase in the use of atorvastatin in those showing active calcification that approached significance ( $p=0.08$ ) (Dweck et al., 2012), a result that appears to support our findings.

A similar trend was seen with macrocalcification, where higher symptomatic arteries and total carotid arterial calcification showed higher CACS, calcium volume, and calcium mass in individuals with prior statin use. This relationship was highly

statistically significant and remained independent after adjustment for other risk factors significant on univariable analysis, including prior cardiovascular events.

Lipid lowering therapies have been shown to trigger changes in the composition of the atherosclerotic plaque, favouring lesion stability (Crisby et al., 2001, Schartl et al., 2001). However, the role of calcification in these studies has often not been considered. Preclinical work has found that calcium deposition within vascular smooth muscle cells is increased by atorvastatin in a dose-dependent manner (Trion et al., 2008). A pooled analysis of plaque characteristics in 3,495 individuals undergoing IVUS found that statin therapy promoted coronary plaque calcification regardless of plaque volume progression or regression, and was independent of lipoprotein concentrations (Puri et al., 2015). Statin use was independently associated with coronary artery calcification progression in individuals with diabetes (Anand et al., 2007, Saremi et al., 2012), and observed in a cohort of individuals with end-stage renal failure (Chen et al., 2017). This latter study also found reduced *in vitro* synthesis of menaquinone-4, a form of vitamin K<sub>2</sub>, by human vascular smooth muscle cells in response to statin. This molecule has a potential role in regulating vascular calcification by inhibiting calcification via vitamin K-dependent MGP (see Chapter One) (Schurgers et al., 2013, Proudfoot and Shanahan, 2006), so a potential statin-mediated reduction may be implicated as a non-inflammatory mediated pathway promoting vascular calcification.

Some of the uncertainty surrounding the role of statins in calcification may be due to the different mechanisms underlying the calcification process. Trion et al.'s pre-clinical work considered vascular calcification through non-inflammatory-mediated mechanisms, a finding supported by the subsequent clinical findings finding the calcification changes were independent of lipoprotein changes (Trion et al., 2008, Puri et al., 2015). In contrast, pre-clinical models that have used an inflammatory-trigger for calcification have shown statins inhibit calcification, likely through their pleiotropic effects (Kizu et al., 2004).

In the carotid arteries, several studies report statin therapy increases plaque echogenicity *in vivo*, a finding consistent with increased calcification (Kadoglou et al., 2008, Yamagami et al., 2008). The formation of calcification through coalescence of

microcalcification described in Chapter One, and the correlation between NaF uptake and macrocalcification shown here, means that the finding of an association between both NaF uptake and carotid calcification with statin use is consistent a potential non-inflammatory mechanism for statin-associated vascular calcification. The role of inflammation in this mechanism will be further assessed in the next chapter.

#### *3.4.6.2 Age*

Age was consistently independently associated with NaF uptake using all measures (focal and whole vessel, as well as for both SUV and TBR). Similarly, greater vascular macrocalcification was also independently associated with increasing age. This suggests that a systemic process is taking place, independent of the cardiovascular risk factors identified here. Our results support similar findings of an association between age and NaF uptake reported by Vesey et al., Derlin et al., and Morbelli et al. (Vesey et al., 2017, Derlin et al., 2011c, Morbelli et al., 2014).

Analysis of carotid arteries in the Rotterdam study found age (OR 1.1 [1.1-1.2]) and smoking to be the strongest independent risk factors for carotid calcification measured using Agatston scoring. Although the odds ratio for age did not vary between men and women, the odds ratio for smoking differed between sex and whether current or former smoker (for men: OR 4.1 [1.5-10.8] for current smokers, OR 2.4 [1.1-5.4] for former smokers; for women: OR 2.1 [1.1-4.1] for current smokers, OR 1.1 [0.7-1.9]). Of BMI, hypertension, hypercholesterolaemia, HDL, and diabetes, none were associated with an increased odds ratio of calcification in men, but hypercholesterolaemia and hypertension were associated with carotid calcification in women (Odink et al., 2010). However, medication was not included in their multivariable models, and while previous cardiovascular history was included in the model, associations were not reported. Broadly the pattern of associations for macrocalcification is replicated in our study. The lack of an association between macrocalcification and hypertension or hypercholesterolaemia in our study may reflect the lower number of women in the study (compared to Odink et al. where they account for 52%).

Derlin et al. and Janssen et al. both report a positive association between age and NaF SUV and  $TBR_{mean}$  respectively in asymptomatic superior femoral arteries (Derlin et al., 2015). In the coronaries, a large screening study of 30,908 individuals found an increasing proportion of individuals aged over 55 years in cohorts with higher coronary artery Agatston score (Hoff et al., 2003). Allison et al. examined macrocalcification across coronary, aortic, and peripheral arteries and found that macrocalcification was typically detected earliest in the coronary arteries and the prevalence of systemic macrocalcification rose with age (Allison et al., 2004). Similar results were seen in symptomatic carotid endarterectomy specimens, where plaque calcification was again strongly associated with patient age (Redgrave et al., 2010). In a serial imaging study, age was independently predictive of development of new carotid macrocalcification (van Gils et al., 2013).

These clinical outcome studies suggest an association between age and carotid microcalcification and macrocalcification, but the mechanism remains poorly defined. The recurring theme that this age is an independent risk factor indicates it is not simply exposure to conventional cardiovascular risk factors. These findings are replicated in our results, and were consistent across all measures of NaF uptake and macrocalcification. This suggests that age propagates microcalcification and its coalescence into macrocalcification.

An emerging concept that may contribute to these observed results is “inflammaging,” the development of chronic low-grade sterile inflammation with age due to accumulated physiological insults and loss of anti-inflammatory homeostatic mechanisms (Franceschi et al., 2000). Cytokines have a clear role in plaque pathogenesis as indicated by a number of studies.  $TNF\alpha$  and IL-6 have been indicated in premature atherosclerotic disease in the carotid artery (Skoog et al., 2002, Okazaki et al., 2014). Individuals with progressive carotid stenosis have been found increasing concentrations of IL-6 and IL-10 (Puz and Lasek-Bal, 2017). Particularly relevant to our study was the observation that plaque FDG-PET  $TBR_{max}$  correlated with IL-6 ( $r=0.6$ ,  $p<0.001$ ),  $TNF\alpha$  ( $r=0.37$ ,  $p=0.02$ ), and hsCRP ( $r=0.42$ ,  $p=0.01$ ) (Poredos et al., 2016). Cytokines including IL-1 $\beta$ , IL-6, I-L8, IL-10, and  $TNF\alpha$  were associated with carotid intima-media thickness (IMT) in the left carotid artery, but curiously not in the right carotid artery, in individuals aged over 60 years (Machado-Silva et al., 2016).

Consequently, the increased levels of inflammatory cytokines, particularly IL-6 and TNF $\alpha$  (Bruunsgaard, 2002, Bruunsgaard and Pedersen, 2003), in elderly populations are likely to promote atherosclerosis and plaque inflammation. This low-grade inflammation characterised in the inflammaging process may contribute to driving microcalcification and macrocalcification. Whether there is an association between age and inflammation (measured using FDG-PET) will be explored further in the next chapter.

Inflammaging has also been implicated in vascular remodeling, particularly endothelial disruption, enhanced vascular smooth muscle cell proliferation, extracellular matrix deposition, and matrix calcification (Wang et al., 2014). Age cultured rat vascular smooth muscle cells have demonstrated co-localisation of calpain-1 and MMP-2, with the former inducing the activity of the latter (Jiang et al., 2012). Calpain-1 expression in the vascular smooth muscle cells of the human aortic intima also increases with age, particularly in atherosclerotic areas, and this is implicated in increasing alkaline phosphatase activity and decreasing the activity of calcification inhibitors osteopontin and osteonectin (Jiang et al., 2012). In so doing, this ageing process generates a cellular environment favourable for fostering the development of microcalcification and macrocalcification.

#### *3.4.6.3 Smoking*

Smoking was consistently found to be associated with increased NaF uptake and measures of arterial calcification. This supports findings of increased NaF uptake associated with smoking reported by Janssen et al. (Janssen et al., 2013). However, Morbelli et al. found that although smoking was associated with NaF TBR on univariable analysis, this association did remain significant after adjustment in multivariable analysis (Morbelli et al., 2014). Derlin et al. found no significant association between smoking and NaF uptake in their asymptomatic cohort (Derlin et al., 2011c).

Smoking has been found to be independently associated with carotid and aortic calcification (Iribarren et al., 2000, Nicoll et al., 2016). Carotid ultrasound found that smoking increased echodensity, though interestingly ex-smokers were found to have

the highest risk for high echodensity. This may be because current smokers fell into two groups: those who had calcified and were echodense versus those with soft echolucent plaques, whereas ex-smokers did not show an increased risk of echolucent plaques compared to non-smokers (Yang et al., 2015a).

Increased p-selectin expression was found to be associated with smoking in the Multi-Ethnic Study of Atherosclerosis (Bielinski et al., 2015), contributing to the development of plaques. Smoking was found to be independently associated with increased FDG-PET whole-vessel  $SUV_{max}$  and  $TBR_{max}$  in asymptomatic carotid arteries in individuals with coronary artery disease (Bucerius et al., 2011). The combination of results suggests that the effect of smoking on NaF uptake and macrocalcification is likely to be through plaque propagation and inflammation.

#### *3.4.6.4 Sex*

In NaF-PET studies in asymptomatic disease, male sex was found to be associated with increased NaF uptake by Derlin et al. (Derlin et al., 2011c) but no sex differences were reported in the other NaF-PET studies to date (see **Table 3.17**). Our results suggest that female sex was associated with higher SUV values and higher SHS and MDS TBRs, but not WV TBRs.

In contrast to our study, the carotid Agatston scores reported by Odink et al. were over two-fold greater for men than for women (median 64.1 [IQR 2-234.8] versus 25.7 [IQR 0-128.6]), though no statistical comparisons were performed comparing these (Odink et al., 2010). It should be noted that their study was performed in an asymptomatic population, while our results were taken from a symptomatic population, likely explaining why we are getting higher values.

What is not clear is why there is a reversal in the trend compared to the asymptomatic population. One possible explanation is statistical: in our small cohort only approximately one third of participants were women. This small sample may be sufficient to skew the results, particularly as a number of female participants were 'high-risk' with risk factors shown to be associated with macrocalcification in women but not in men (Odink et al., 2010). Furthermore, the female participants were older

(median 82.5 years [IQR 10.75] compared to 72.5 years [IQR 12] in men,  $p=0.03$ ) and given the strong association of age with NaF uptake and macrocalcification, this may be sufficient to remain significant even after adjustment on multivariable analysis given the small number of women.

Alternatively, our high-risk symptomatic cohort may be subject to selection bias not present in the asymptomatic population, with men with the highest calcium scores potentially having died from myocardial infarctions already.

Finally, the observed results may be capturing an important pathophysiological consideration. Although the above studies have a comparable average participant age, the distribution of men and women within these age ranges is not reported. As the women in our study were typically older, there may be a sex-specific hormonal influence contributing to female sex remaining significant after adjustment for other factors. An interaction between arterial calcification and hormonal change is indirectly suggested by the high clinical prevalence of aortic calcification in postmenopausal women with osteoporosis in contrast to the decreased incidence of coronary artery calcification seen in women with pre-menopausal levels of oestrogen independently of age (Frye et al., 1992, Hofbauer and Schoppet, 2001, Christian et al., 2002, Burke et al., 2001, Shemesh et al., 1997).  $17\beta$ -oestradiol has been shown to maintain expression of osteoprotegerin, a modulator of osteoblast differentiation, and reduce differentiation of VSMC induced by a calcifying medium (Rzewuska-Lech et al., 2005). Pedone et al. observed that a lower tibial cortical:total cross-sectional area (characteristic of osteoporosis) was associated with carotid atherosclerotic plaque development in women but not men, and that this relationship was influenced by the number of years since the menopause, but did not comment on the plaque morphology (Pedone et al., 2013). Adverse changes in cardiovascular risk profile have been observed in peri/postmenopausal change associated with increasing carotid IMT (Matthews et al., 2001, Sutton-Tyrrell et al., 1998). Both changes in vascular risk and vascular wall dysfunction may be contributing to our observed results and further work in this area, with larger sample sizes and consideration of hormonal levels, may help elucidate this.

#### 3.4.6.5 Lipid profile

Total cholesterol levels and hypercholesterolaemia have been consistently found to be associated with NaF uptake as shown in **Table 3.17**. Our results are in-keeping with this. The association of total cholesterol with microcalcification and macrocalcification is likely driven by enhanced inflammation within the atheroma secondary to adverse lipid profiles and will be considered further in the next chapter.

#### 3.4.6.6 Cardiovascular history

Carotid atherosclerosis is a common finding in individuals with coronary artery disease, with the prevalence of carotid stenosis found to rise with increasing coronary artery disease (3.6% prevalence of  $\geq 50\%$  carotid stenosis in one coronary vessel versus 12% in three-vessel disease) (Imori et al., 2014). Another large study of 1,405 individuals with coronary artery disease found a significant burden of mild carotid atherosclerosis (stenosis  $< 50\%$ ), with it found in 58% of cases. In contrast, moderate (50-70%) and severe ( $> 70\%$ ) carotid stenosis was prevalent in 12.8% and 4.6% respectively, again increasing in prevalence with increasing coronary artery disease burden (Steinvil et al., 2011).

The converse relationship of carotid disease predicting coronary artery disease is less clear. In a substudy of the large Rotterdam Study, severe asymptomatic carotid artery stenosis on ultrasound was as an independent risk factor for myocardial infarction (HR 1.83 [1.27-2.62]) but not for mild (HR 1.19 [0.75-1.88]) or moderate stenosis (HR 1.28 [0.85-1.94]) (van der Meer et al., 2004). Similar clinical outcome studies assessing the prognostic utility of carotid ultrasound on myocardial infarction have provided similar results (Salonen and Salonen, 1991, O'Leary et al., 1999). As well as these single measures of carotid stenosis, progressive carotid atherosclerosis over a six to nine month period appears to be associated with coronary events as well as with stroke events, implying a shared progression of atherosclerosis in these different arterial territories (Sabeti et al., 2007). However, different measures other than simply the degree of stenosis have provided conflicting results. No association between IMT and subsequent cardiovascular outcomes was found in one large study and one large meta-analysis (Eikendal et al., 2015, Lorenz et al., 2012). In a small

study, Adraktas et al. found significant symptomatic carotid stenosis on CTA was limited to the single artery, though non-significant atherosclerosis was observed to be systemic. However, the number of individuals with carotid stenosis in this study was in the single figures (Adraktas et al., 2010). To date, there is a paucity of studies assessing the prevalence of coronary atherosclerosis in terms of lesions in a cohort of individuals with symptomatic carotid atherosclerosis. This is likely due to limitations of requiring invasive angiography to test coronary disease, which is not indicated in intervention for symptomatic carotid atherosclerosis.

Radiological assessment of carotid arteries has shown changes in morphology in the presence of coronary artery disease. Underhill et al. found that the distal carotid bulb and proximal internal carotid artery were the most frequent sites of disease on T1-weighted MRI, and these regions showed smaller luminal area and greater mean wall thickness in individuals with coronary artery disease (defined by >50% stenosis) for men but not for women (Underhill et al., 2008). Furthermore, individuals with coronary artery disease were more likely to have carotid arterial calcification (40.2% versus 16% in controls,  $p < 0.001$ ) and lipid-rich necrotic cores (38.1% versus 18.1%,  $p = 0.002$ ). Calcification was higher in coronary artery disease than controls for both men and women, though the prevalence of lipid-rich necrotic cores in coronary artery disease versus controls was only statistically significant in men (Underhill et al., 2008). The authors propose carotid artery calcification is indicative of coronary artery disease. Our results appear to support this, though it is important to note that we did not formally assess coronary vasculature so can only conclude that it is supportive for symptomatic coronary artery disease but cannot comment on asymptomatic carotid disease. Again the differences appeared focused around the distal carotid bulb and proximal ICA, similar to the pattern of disease we have observed in this study.

Variable correlations in NaF uptake between adjacent arterial territories were reported by Dweck et al., with uptake in the ascending aorta having a moderate correlation with uptake in the coronary arteries ( $r = 0.525$ ,  $p < 0.001$ ), though there was not a reciprocal correlation between uptake in the coronary arteries and the aorta ( $r = 0.157$ ,  $p = 0.33$ ) (Dweck et al., 2012).

Ultimately, the increased NaF uptake and macrocalcification in the carotid arteries in individuals with a history of cardiovascular events seen in our study supports the view of atherosclerosis, and the pathological process within the plaques, as a systemic disease.

#### *3.4.6.7 Antiplatelet therapy*

Although statin medication has been included in the analysis of NaF uptake in previous vascular NaF-PET studies, antiplatelet medication has not. In our study, the use of antiplatelets was independently associated with higher focal NaF SUV<sub>max</sub> values (SHS SUV<sub>max</sub> and MDS SUV<sub>max</sub>), all NaF TBR measures, and total calcium measures (Agatston scores, volume, and mass). This would appear the opposite result expected from either the anti-inflammatory effects of antiplatelets or from inhibition of platelet-mediated pro-inflammatory cytokines. Aspirin has been found to improve bone mineral density in humans (Bauer et al., 1996, Carbone et al., 2003), and its use in rat models increased bone formation (independent of effect on phosphorus), increased osteocalcin and calcium binding, and reduced serum IL-6 (Lin et al., 2016). Whether aspirin has a similar effect for enhancing osteocalcin in vascular smooth muscle cells remains unknown. Although the anabolic effects of aspirin on bone architecture have been studied extensively, there is a paucity of work investigating whether it may have a role in vascular calcification. The result may also be due to the small number of individuals taking antiplatelets at the time of the stroke and requires further investigation in a larger sample or meta-analysis.

#### *3.4.6.8 Other risk factors*

The multiple linear regression models demonstrate moderate adjusted R<sup>2</sup> associations, indicating that other factors are also affecting microcalcification and macrocalcification. This is not unexpected, as the Rotterdam Study found 29% of men and 15% without conventional cardiovascular risk factors had a high coronary calcium score (Oei et al., 2004). Physical activity was associated with lower coronary, but not aortic, Agatston scores in asymptomatic individuals (Imran et al., 2016). Ethnicity has been implicated in pathophysiology (Hao et al., 2016, Gepner et al., 2015), though the large Multi-Ethnic Study of Atherosclerosis found no interaction of

ethnicity with cardiovascular risk factors for predicting cardiovascular disease and events (Polonsky et al., 2017). However, a possible role of ethnicity in this study is not applicable, as all participants were white Caucasian.

Local air pollution has been implicated in accelerating coronary artery calcification, consistent with acceleration of atherosclerosis, and its effects may be genetically-mediated (Kaufman et al., 2016, Ward-Caviness et al., 2017). Although it is difficult to include this in analysis of our data, it is an interesting to consider the role of the environment given certain geographical clusters of participants in this study (including two next-door neighbours).

#### *3.4.7 Strengths of this study*

This study has a number of strengths. It includes the largest symptomatic stroke cohort investigated with NaF-PET/CT to date and includes a spectrum of stroke clinical severity (as measured using NIHSS). Previous studies have typically included TIAs or minor strokes, whilst here we also include stroke survivors with moderate and moderate-severe severity strokes. Furthermore, all participants have acute infarcts confirmed with MRI diffusion-weighted imaging and imaging was performed in the acute phase after the infarct. Our cohort was also more reflective of the broader stroke population: we had no function-based exclusion criteria, whereas other studies have excluded individuals with a modified Rankin score above three (Vesey et al., 2017).

The use of linear regression of coronary artery scores was found to be superior to log-transformed scores (due to loss of data) for giving a true reflection of the data, as was the use of the likelihood-based model selection approach where modeling was improved by including a larger number of potential risk factors (Reilly et al., 2004). In previous studies, the distribution of calcium scores have been shown to be heavily skewed, requiring log-transformation to fit the assumptions needed for linear modeling. In contrast, in our study the majority of individuals had macrocalcification, in most cases significant, of their carotids and so the cohort effectively limited the skew of data produced by the large number of calcium-free carotids seen in asymptomatic cohorts. Furthermore, the applicability of linear regression to our results was confirmed by statistician review of the linear regression diagnostics.

### *3.4.8 Limitations of this study*

The favourable signal-to-noise ratio of NaF means that it is well-suited for imaging vascular atherosclerosis, particularly in the coronaries when compared with the limitations of FDG due to myocardial uptake. Whilst also generally favourable for carotid imaging, there are practical limitations that may pose difficulties. Carotid arteries lying close to bony structures (in particular vertebrae and the mandible) may be subject to spill-over effects from these regions. Both in this study and other NaF-PET studies this has only affected a few arteries, but it is important to consider given it may result in artefacts.

As with all prospective studies in symptomatic individuals, the numbers are relatively small. This is largely due to a combination of radiation exposure and cost. When comparing symptomatic to asymptomatic arteries there was a clear trend of increased uptake in the symptomatic side (in 23/26 participants for  $SUV_{max}$ ). However, when considering the role of cardiovascular risk factors, both univariable and multivariable modeling is potentially limited by small numbers that have the potential to skew data. The overall cohort in this study appears suitably reflective of the broader large artery atherosclerosis stroke population, with the possible exception of the sex balance. However, it is important to note that the sex ratio of stroke secondary to carotid atherosclerosis is not one-to-one, and high-risk plaque features have been associated with male sex (Ota et al., 2010a, Ota et al., 2013). Therefore, observations should be interpreted in this light and treated with a degree of caution. Further investigation of the relationships between NaF uptake and cardiovascular risk factors will require either larger studies or meta-analysis.

Although the term ‘asymptomatic’ to describe the contralateral artery, it is debatable to what extent they are truly asymptomatic. By nature of having had a stroke secondary to their carotid atherosclerosis, the participants have revealed themselves to be high-risk individuals, and it is therefore likely that contralateral arteries will demonstrate increased pathophysiology relative to either an asymptomatic or disease-free populations. In effect, this contralateral asymptomatic (by nature of not causing a stroke) artery acts as the individual’s own control, but should not be considered to be

analogous to the broader asymptomatic population. Indeed, within this cohort there are examples of NaF uptake measures being higher in one individual's asymptomatic artery than in another participant's symptomatic artery. Hence, it is hard to define an absolute NaF uptake value that denotes a vulnerable or symptomatic plaque. Such a consideration currently limits their application to clinical practice, and instead should be considered illustrative of pathological patterns or for measuring comparative change in an individual in response to intervention.

While this aspect of the study demonstrates the utility of NaF-PET/CT to discriminate between symptomatic and asymptomatic carotid atheroma, and illustrate how the tracer uptake relates to cardiovascular risks and pathophysiology, an important piece of the puzzle is missing. This missing piece is inflammation and how it relates to these processes, and is covered in the next chapter.

### **3.5 Summary of findings**

This chapter has covered:

1. NaF-PET uptake is higher in culprit atheroma and can discriminate between symptomatic and asymptomatic plaques.
2. Uptake appears to be focal and predominantly occurs around the carotid bifurcation (as shown by focal, but not whole vessel, measures of NaF uptake reaching a statistically significant difference between symptomatic and asymptomatic arteries).
3. Measures of NaF were highly reproducible, with high intra- and inter-rater ICC.
4. There is a moderate-strong association between NaF uptake and carotid artery Agatston score, though the relative spatial distributions appear to differ between symptomatic and asymptomatic arteries.
5. Microcalcification and macrocalcification appear to share common vascular risk factors.

**Chapter Four:**  
**Dual Tracer FDG and NaF PET to Investigate the Relationship between  
Inflammation and Microcalcification**

## **4.1 Introduction**

### *4.1.1 Aims of the chapter*

The previous chapter considered the use of NaF-PET to discriminate between culprit and non-culprit atheroma, as well as the spatial pattern of disease and macrocalcification. This chapter develops these findings by considering the role of inflammation in these processes, with the following specific questions:

1. Does FDG-PET also discriminate between culprit and non-culprit atheroma in our exclusively DWI-lesion positive stroke cohort?
2. Is the spatial pattern of inflammation distinct from the spatial pattern of microcalcification within the carotid artery?
3. What is the association between FDG uptake and both NaF uptake and macrocalcification in carotid atherosclerosis?

The main hypotheses in this chapter are:

- i. FDG uptake will be significantly higher in culprit atheroma versus non-culprit atheroma.
- ii. FDG uptake will be diffuse along the artery compared to the focal uptake seen with NaF.

Exploratory outcomes beyond the main hypotheses are:

1. Investigating the contribution of vascular risk factors to FDG uptake in our cohort.
2. Testing the relationship between hsCRP and FDG and NaF uptake within the atheroma.

#### *4.1.2 FDG-PET imaging of atherosclerosis*

FDG is the mainstay radioligand in PET imaging and consequently has been the most common radioligand used in imaging studies of atherosclerosis. Though primarily used for oncological imaging, incidental findings of FDG accumulation in arterial territories during whole-body scans heralded its utility for detecting and quantifying inflammation within atheroma (Yun et al., 2001). FDG, a radionucleotide analogue of glucose, accumulates intracellularly in proportion to cellular demand for glucose. It is taken up into cells via facilitated glucose transporter type (GLUT) one and three, which are upregulated during atherogenesis due to hypoxia within the atheroma core, and once inside the cytoplasm undergoes phosphorylation by hexokinase to become  $^{18}\text{F}$ -FDG-6-phosphate.  $^{18}\text{F}$ -FDG-6-phosphate lacks a 2' hydroxyl group and consequently is unable to enter the Krebs cycle and undergo glycolysis, subsequently diffusing slowly out of the cell. This resulting accumulation is readily quantifiable and can be used as a sensitive measure of metabolic activity, particularly given its very high signal-to-noise ratios in tissues without high metabolic activity (such as normal vessel wall and blood). The high concentration of proinflammatory macrophages in the vulnerable plaque provides such a tissue with a high metabolic activity.

The ability of FDG-PET to measure plaque inflammation non-invasively in a symptomatic population was demonstrated in early work by Rudd et al. where FDG uptake differentiated between symptomatic and asymptomatic carotid atheroma in human subjects (Rudd et al., 2002), a finding that was corroborated in more recent larger studies (Skagen et al., 2015). This increased uptake of FDG detected by PET/CT has been shown to correlate with histological macrophage density in animal models (Hyafil et al., 2009, Davies et al., 2010) and excised atheroma following carotid endarterectomy (Tawakol et al., 2006, Liu et al., 2015b).

FDG uptake has been shown to identify symptomatic carotid plaques that were non-stenotic on high-resolution MRI, supporting the concept that the severity of stenosis is not the sole determinant for symptomatic plaque rupture (Davies et al., 2005). However, this small study contrasted with another small pilot study that showed that

although FDG uptake was higher in symptomatic arteries, uptake also correlated with the degree of stenosis (Arauz et al., 2007). In a large FDG-PET study by Tahara et al., only 29% of asymptomatic individuals with carotid atherosclerosis found on Doppler screening had FDG uptake within the plaque, with no difference observed in the carotid intima-media thickness between inflamed and non-inflamed plaques (Tahara et al., 2007a). The observed association between increased FDG uptake with high-risk morphological plaque features measured by CT reinforces this finding and the shortcomings of solely anatomical assessments of stenosis (Figueroa et al., 2012). Multimodal imaging studies using FDG-PET and MRI have facilitated comparison of tracer uptake with more accurate assessment of plaque morphological features. Silvera et al. imaged individuals with vascular risk factors and found FDG  $TBR_{mean}$  to be higher for lipid-rich plaques, which are often vulnerable to rupture, than for collagen-rich or calcified plaques with a lower risk of rupture (Silvera et al., 2009).

In addition to its relation with the index plaque rupture, Marnane et al. demonstrated that higher FDG uptake in carotid atheroma is associated with a higher risk of recurrent cerebrovascular events, independent of the degree of luminal stenosis (Marnane et al., 2012). This is supported by an association between higher FDG uptake and microemboli detected by TCD (Moustafa et al., 2010).

FDG-PET techniques have helped elucidate the systemic nature of atherosclerosis. FDG uptake correlates closely between neighbouring arterial territories, suggesting inflammation is a global rather than localised phenomenon (Rudd et al., 2009). Joshi et al. demonstrated that FDG uptake in the aorta reflected the clinical severity of coronary syndromes, with a 20% higher TBR in the aortas of those with a recent myocardial infarction than those with stable angina. Furthermore, within the group with myocardial infarcts, the aortic FDG uptake was higher for those with an ST-elevation myocardial infarction than those with a non-ST-elevation myocardial infarction (Joshi et al., 2015). Similarly, carotid  $SUV_{mean}$  and  $TBR_{mean}$  are significantly higher for cohorts with acute coronary syndrome than for those with chronic stable angina (Kim et al., 2015).

A possible mechanism for this relationship has been demonstrated through the association between arterial inflammation and systemic metabolic syndrome. Carotid

TBR<sub>max</sub> is higher in both non-obese individuals with metabolic syndrome and obese individuals without metabolic syndrome compared to non-obese individuals without metabolic syndrome (Yoo et al., 2015). Furthermore, both low-density lipoprotein and total cholesterol has been shown to be independently associated with FDG uptake (Chróinín et al., 2014, Kaida et al., 2014). These findings go some way to explaining the association between higher Framingham risk factor scores and higher TBR.

Chróinín et al. measured symptomatic and contralateral carotid artery FDG and fasting lipid profile within seven days of the index cerebrovascular event. 47.6% and 47% of the 60 participants were already taking statin and antiplatelet medication respectively prior to the index event, which rose to 88.5% and 85% by the time of the FDG-PET/CT. On univariable analysis, LDL-C and total cholesterol were both associated with higher FDG SUVs (single hottest slice SUV<sub>max</sub>, mean of whole vessel SUV<sub>max</sub>, and mean of whole vessel SUV<sub>mean</sub>), triglycerides were associated with SUV<sub>max</sub> measures, and HDL-C was inversely associated with SUV<sub>max</sub> measures. On multivariable analysis only LDL and TC emerged as independently associated with FDG SUV<sub>max</sub>. However, no association was observed between statin therapy and plaque FDG uptake on bivariate analysis (Chróinín et al., 2014).

The accumulation of cholesterol crystals within atheroma has also been shown to promote plaque inflammation and rupture in animal models, while crystal content found in human carotid histology was found to be strongly associated with plaque disruption, thrombus, and symptoms (Abela and Aziz, 2006, Vedre et al., 2009, Abela et al., 2009). Though there is no PET radioligand for imaging cholesterol crystals, instead relying on electron microscopy, their effect on inflammation within the plaque may be measured. Patel et al. showed that ezetimibe reduced the cholesterol crystal density on electron microscopy in the aortas of atherosclerotic rabbits, with a corresponding decrease in inflammation as quantified by FDG uptake (SUV<sub>max</sub>), CRP and MMP-9 levels (Patel et al., 2011).

The interface between systemic inflammation and atheroma inflammation has been suggested by the association between periodontal inflammation and inflammatory activity within atheroma, both of which reduced in response to atorvastatin and were strongly correlated (Tonetti et al., 2007, Subramanian et al., 2013). Serum

inflammatory markers have been found to be associated with an increased risk of cardiovascular events, potentially representing either a cause or result of an upregulated inflammatory response (Danesh et al., 2004, Sarwar et al., 2012, Meuwese et al., 2007). Myeloperoxidase levels are associated with a higher FDG TBR in carotid diseased segments, independent of other conventional cardiovascular risk factors, although no independent relationship was found for hsCRP, IL-6, or MMP-9 (Duivenvoorden et al., 2013). However, other studies have provided conflicting results, with an association between higher TBR and higher levels of hsCRP (Yoo et al., 2015, Yoo et al., 2011b) and MMP-9 (Rudd et al., 2009). In comparison to blood biomarkers, FDG uptake can localise to focal sites of high inflammatory activity. The focal plaque inflammation associated with a generally upregulated inflammatory response may explain the neighboring arterial regions of FDG uptake.

Recent FDG-PET studies have continued to provide insights into the interactions and contributions of different aspects of the inflammatory process within atherosclerosis. In a prospective FDG-PET study, regions of the aorta with high SUV were more likely to develop calcification on subsequent CT imaging, independent of cardiovascular risk factors (Abdelbaky et al., 2013). Furthermore, in a substudy of the dal-PLAQUE study, Joshi et al. found that FDG TBRs reduced over six months if carotid calcification was absent, though there was no interval change in tracer uptake in carotid arteries where calcification was present (Joshi et al., 2016). Consequently, the authors concluded that calcium deposition is a propagating factor for ongoing arterial inflammation.

FDG-PET has a number of advantages compared to other imaging modalities. It is highly reproducible with high intra-observer and inter-observer agreement (Rudd et al., 2008). PET/CT using FDG has a high sensitivity for detecting inflammation in plaques, but its utility to detect inflammation may be hindered by a lack of biological specificity, especially when the ROI is in close proximity to other tissues with tracer uptake due to high resting metabolic rates (such as neurons and myocardial tissue). This may be further compounded by the low spatial resolution of PET (approximately 3 mm). Solutions for these problems are currently being developed with the advent of more cell-specific ligands and PET/MRI. Dynamic contrast-enhanced (DCE) MRI has

been shown to have superior spatial resolution than PET/CT and contrast-enhancement has been particularly effective in the assessment of fibrous cap thickness and lipid core volume, where the former enhances whilst the latter fails to enhance (Cai et al., 2005). Multicontrast-weighted MRI has been used in surveillance of asymptomatic plaques and demonstrated larger lipid cores, thicker MWT, thin/ruptured fibrous caps, and intraplaque hemorrhage to each have significantly increased hazard ratios for subsequent symptomatic events (Takaya et al., 2006). However, although MRI offers an effective method for imaging morphological features associated with plaque vulnerability, it remains dependent on accurate coil placement as well as the reproducibility of technical sequences and image generation. These considerations, along with a desire to image directly the biological activity in the plaque, has led to DCE MRI and PET/CT providing complementary imaging of the plaque, though the advent of PET/MRI may enable a fusion of these techniques and is discussed further below.

#### *4.1.3 Lessons from dual FDG and NaF PET studies*

Given the relatively recent use of NaF-PET to image vascular disease, there have been few dual tracer vascular studies. Such studies in the coronary arteries have shown a superior signal-to-noise ratio for NaF-PET. Dweck et al. found that across all four coronary territories, NaF was interpretable in 96% of ROIs but FDG was only interpretable in 51%, performing particularly poorly in the left main stem (25% of ROIs interpretable) and circumflex (33% of ROIs interpretable). This improved once into the ascending aorta (100% for both FDG and NaF) but demonstrates the potential weakness of FDG-PET interpretation when in close proximity to metabolically active structures, as is the case for the coronary and carotid arteries (Dweck et al., 2012).

A curious phenomenon has become apparent in the era of dual tracer studies. Both Dweck et al. and Vesey et al. have reported no difference in FDG uptake between those with atherosclerosis and controls, while NaF uptake has been significantly higher in culprit atherosclerosis (Dweck et al., 2012, Vesey et al., 2017). This is interesting for two reasons. Firstly, it appears to go against the general body of opinion within the literature regarding increased uptake of FDG in vulnerable plaque as discussed above. Secondly, given the aforementioned relationship between

inflammation and microcalcification (potentially triggering a vicious cycle of pathophysiology) it is curious that these studies suggest the development of the latter without the former. These findings are explored further in later discussions.

No correlation between FDG and NaF uptake on a vessel-by-vessel basis has been found in the ascending aorta, descending aorta, or coronary arteries (Dweck et al., 2012). Furthermore, although FDG uptake has been shown to correlate across neighbouring arterial regions, NaF uptake appears to show a more complex pattern. Across a whole cohort, NaF uptake in the ascending aorta and coronary arteries did correlate ( $r=0.525$ ,  $p<0.001$ ), but in those with high coronary NaF uptake this relationship did not hold ( $r=0.157$ ,  $p=0.33$ ) (Dweck et al., 2012). This suggests that in asymptomatic disease there may be low-grade widespread microcalcification but that symptomatic disease is a focal process that does not upregulate the microcalcification process in other regions (in contrast to inflammation).

## **4.2 Methods**

Methodology for this chapter is discussed in Chapter Two.

## **4.3 Results**

### *4.3.1 Study population*

Of 31 participants recruited to the ICARUSS study, 28 underwent FDG-PET/CT. Of the three that didn't undergo scanning, two clinically deteriorated and one refused the scan due to claustrophobia. Of the 28, one scan was disregarded due to an uninterpretable asymptomatic carotid artery and was excluded from analysis.

Of the remaining 27 participants, 26 also underwent NaF-PET/CT scans (as described in Chapter 3.3.1) The remaining participant underwent FDG-PET/CT but expedited CEA prevented the complementary NaF-PET/CT. Consequently, analysis of the spatial distribution of tracer uptake and its relationship with NaF uptake and microcalcification used readings from only the 26 participants who also had

accompanying NaF-PET/CT imaging. The data from the 27<sup>th</sup> participant was used solely in the analysis of the effect of vascular risk factors upon FDG uptake.

The participant characteristics of the analysed cohorts are shown in **Table 4.1** (for the 26 participant cohort) and **Table 4.2** (for the 27 participant cohort).

Mean age (years)	74.8 (SD 9.7)
Men	18 (69.2%)
Median BMI	26 (IQR 3.9)
Smoking history (current or ex-smokers)	17 (65.4%)
Diabetes mellitus	4 (15.4%)
Hypertension	17 (65.4%)
Current statin	9 (34.6%)
Current antiplatelet	8 (30.8%)
Cardiovascular history (previous ischaemic heart disease or myocardial infarction)	8 (30.8%)
Thrombolysed	6 (23.1%)
Median NIHSS	4.5 (IQR 10.75)
CEA (following imaging)	9 (34.6%)
Modal degree of symptomatic stenosis	70-89%
Mean symptom-to-scan time (days)	9.1 (SD 4.5)

**Table 4.1:** Characteristics of the 26 participant cohort.

Mean age (years)	74.3 (SD 9.8)
Men	18 (66.7%)
Median BMI	25.8 (IQR 3.7)
Smoking history (current or ex-smokers)	18 (66.7%)
Diabetes mellitus	4 (14.8%)
Hypertension	17 (63.0%)
Current statin	9 (33.3%)
Current antiplatelet	8 (29.6%)
Cardiovascular history (previous ischaemic heart disease or myocardial infarction)	8 (29.6%)
Thrombolysed	6 (22.2%)
Median NIHSS	5 (IQR 10.5)
CEA (following imaging)	10 (37%)
Modal degree of symptomatic stenosis	70-89%
Mean symptom-to-scan time (days)	9.0 (SD 4.4)

**Table 4.2:** Characteristics of the 27 participant cohort.

When comparing these two cohorts, there were no statistically significant differences in any characteristics (all  $p > 0.05$ ).

Across the 26 participants, the median injected FDG dose was 252.6 MBq (IQR 9 MBq). The median uptake time was 90 minutes (IQR 0 minutes). There were no adverse events during any scan. The mean onset to FDG-PET/CT interval was 9.1 days  $\pm$  4.5 days. FDG-PET/CT preceded NaF-PET/CT in 13 (50%) of studies. The median interval between scans was 1 day (IQR 0.75 days).

During the study, there were no new diagnoses of diabetes mellitus.

#### 4.3.2 FDG uptake in symptomatic versus asymptomatic arteries

Comparisons of FDG uptake in symptomatic and asymptomatic arteries are shown for SUV measures (**Table 4.3**) and TBR measures (**Table 4.4**) (**Figure 4.1**).

	Symptomatic carotid artery	Asymptomatic carotid artery	Significance
<b>SUV<sub>max</sub></b>			
Median SHS SUV <sub>max</sub> (IQR)	2.21 (0.65)	1.92 (0.45)	p<0.001
Median MDS SUV <sub>max</sub> (IQR)	2.15 (0.61)	1.87 (0.42)	p<0.001
Mean WV SUV <sub>max</sub> (SD)	1.94 (0.45)	1.76 (0.34)	p<0.001
<b>SUV<sub>mean</sub></b>			
Median SHS SUV <sub>mean</sub> (IQR)	1.96 (0.47)	1.75 (0.33)	p<0.001
Median MDS SUV <sub>mean</sub> (IQR)	1.91 (0.42)	1.71 (0.36)	p<0.001
Median WV SUV <sub>mean</sub> (IQR)	1.69 (0.31)	1.59 (0.28)	p<0.001

**Table 4.3:** Comparison of FDG SUV<sub>max</sub> and SUV<sub>mean</sub> measures between symptomatic and asymptomatic carotid arteries.

	Symptomatic carotid artery	Asymptomatic carotid artery	Significance
<b>TBR<sub>max</sub></b>			
Median SHS TBR <sub>max</sub> (IQR)	2.14 (0.56)	1.94 (0.43)	p<0.001
Median MDS TBR <sub>max</sub> (IQR)	2.08 (0.52)	1.89 (0.40)	p<0.001
Mean WV TBR <sub>max</sub> (SD)	1.92 (0.41)	1.71 (0.31)	p<0.001
<b>TBR<sub>mean</sub></b>			
Median SHS TBR <sub>mean</sub> (IQR)	1.88 (0.37)	1.75 (0.41)	p<0.001
Median MDS TBR <sub>mean</sub> (IQR)	1.82 (0.31)	1.68 (0.41)	p<0.001
Mean WV TBR <sub>mean</sub> (SD)	1.67 (0.32)	1.51 (0.25)	p<0.001

**Table 4.4:** Comparison of FDG TBR<sub>max</sub> and TBR<sub>mean</sub> measures between symptomatic and asymptomatic carotid arteries.

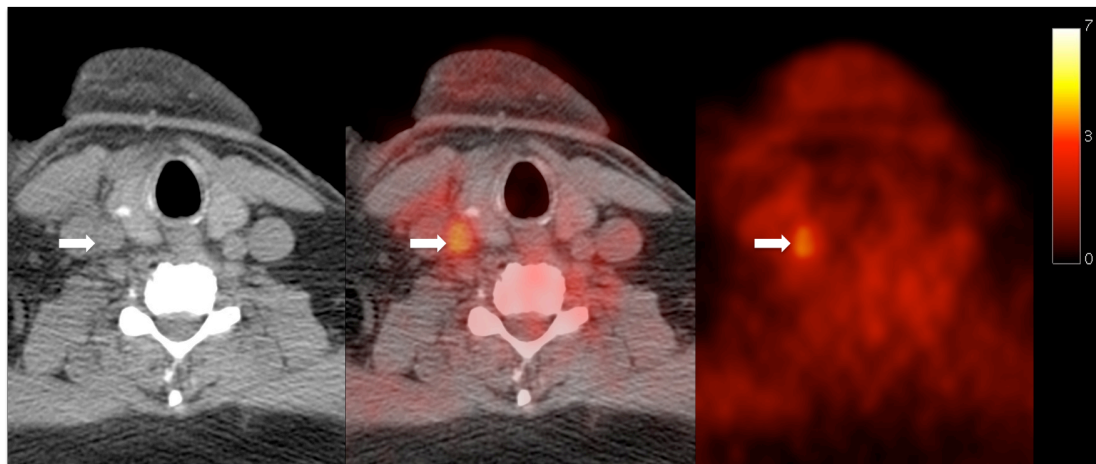


**Figure 4.1: Increased FDG uptake in symptomatic carotid atherosclerosis.** Carotid artery inflammation detected using FDG-PET. Axial CT (left), FDG-PET/CT (centre), FDG-PET (right) showing FDG uptake in a culprit atheroma in the right common carotid artery (white arrow).

There was no significant relationship between FDG SUVs and the degree of stenosis: SHS SUV<sub>max</sub> (p=0.32), MDS SUV<sub>max</sub>, (p=0.25), SHS SUV<sub>mean</sub> (p=0.25), MDS SUV<sub>mean</sub> (p=0.19) (**Figure 4.2**).

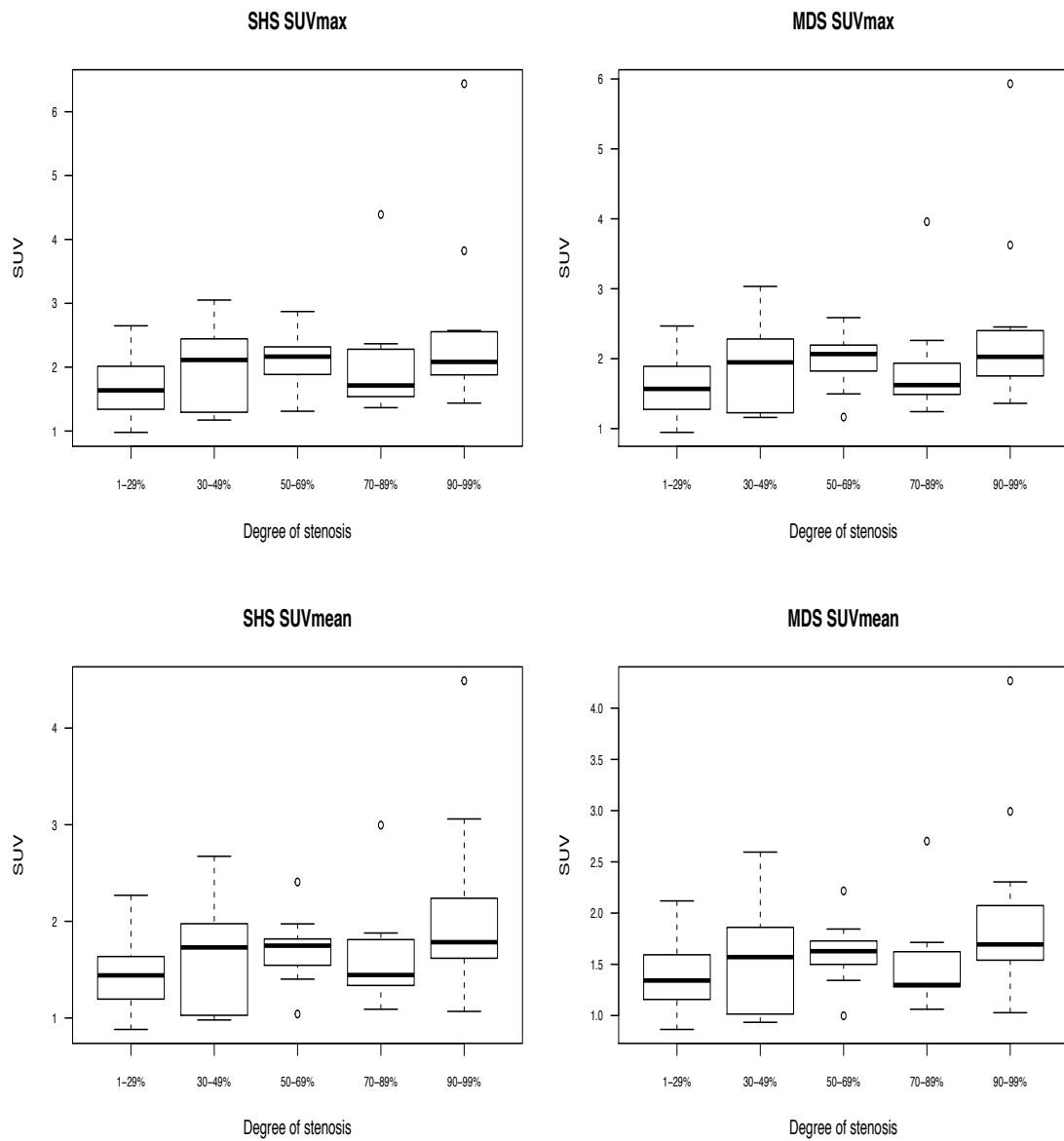


**Figure 4.2: FDG SUVs by degree of luminal stenosis. All trends  $p > 0.05$ .**

Similar results were seen between FDG TBRs and the degree of stenosis: SHS  $TBR_{max}$  ( $p=0.92$ ), MDS  $TBR_{max}$  ( $p=0.91$ ), SHS  $TBR_{mean}$  ( $p=0.84$ ), MDS  $TBR_{mean}$  ( $p=0.75$ ) (Figure 4.3).

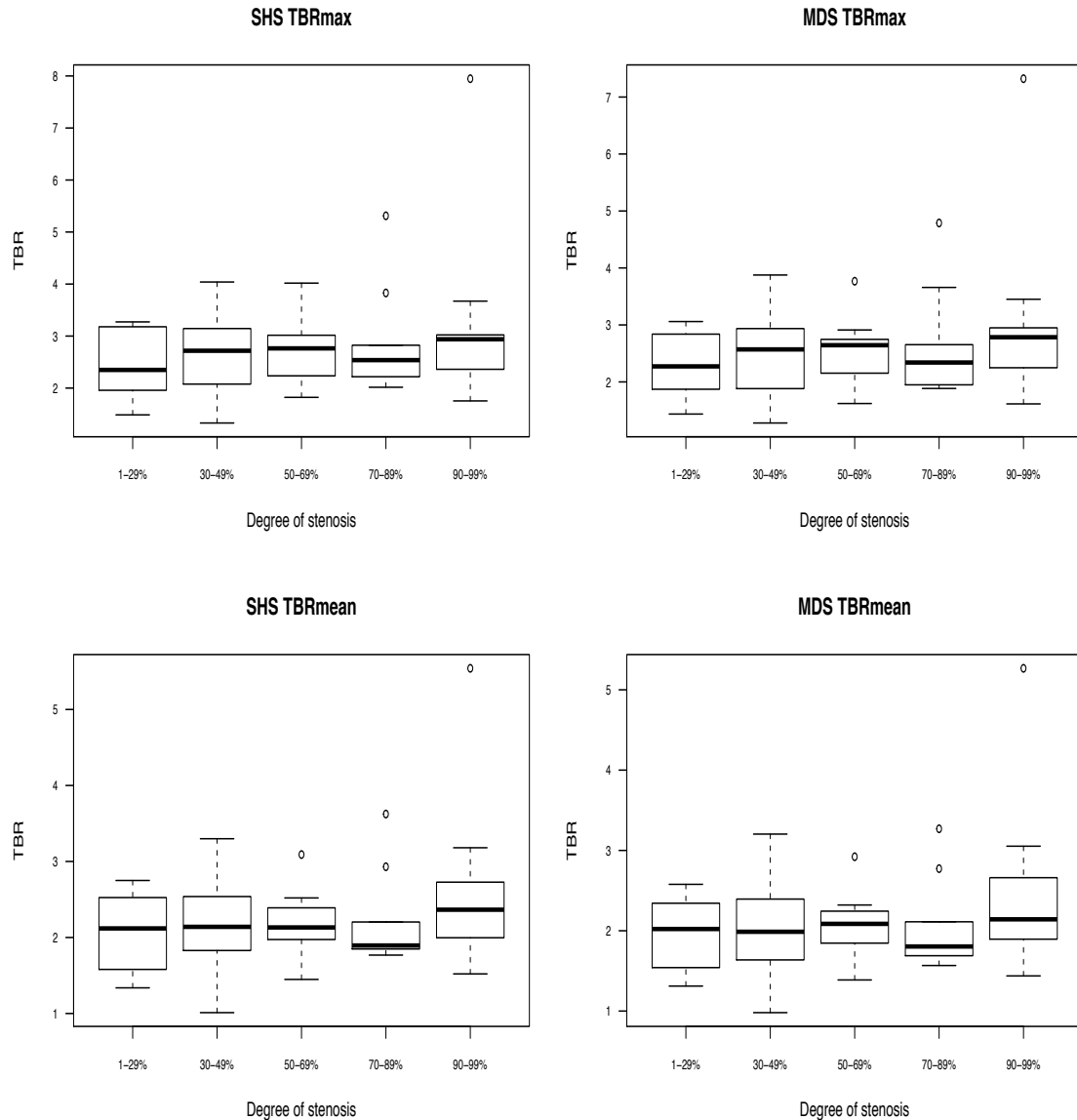


**Figure 4.3: FDG TBRs by degree of luminal stenosis.** All trends  $p > 0.05$ .

Even if only symptomatic arteries are considered, there are no significant trends between the degree of stenosis and SUV (SHS  $SUV_{max}$   $p=0.31$ , MDS  $SUV_{max}$   $p=0.23$ , SHS  $SUV_{mean}$   $p=0.24$ , MDS  $SUV_{mean}$   $p=0.12$ ) or TBR (SHS  $TBR_{max}$   $p=0.54$ , MDS  $TBR_{max}$   $p=0.53$ , SHS  $TBR_{mean}$   $p=0.35$ , MDS  $TBR_{mean}$   $p=0.29$ ).

#### 4.3.3 Spatial patterns of inflammation, microcalcification, and macrocalcification

A similar approach to the one described in Chapter Three can be adopted to investigate the spatial distribution of FDG uptake, and consequently indicate the spatial distribution of arterial inflammation. The median uptake at each 3 mm slice

along the carotid artery is shown for  $SUV_{max}$  (Figure 4.4),  $SUV_{mean}$  (Figure 4.5),  $TBR_{max}$  (Figure 4.6), and  $TBR_{mean}$  (Figure 4.7).

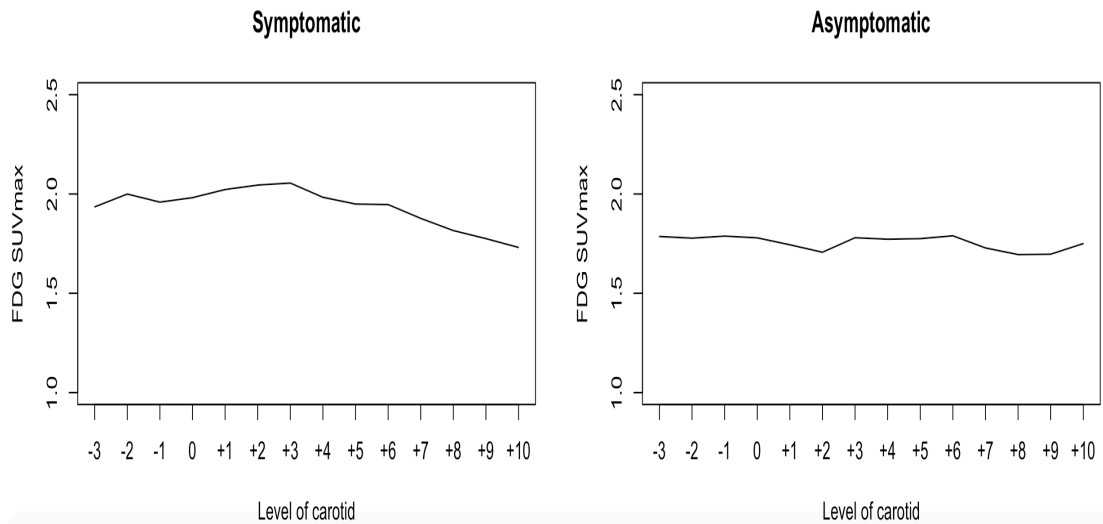


**Figure 4.4: Spatial distribution of FDG  $SUV_{max}$ .** Median  $SUV_{max}$  values at each axial slice along the artery for symptomatic and asymptomatic carotid arteries. 0 is the carotid bifurcation.

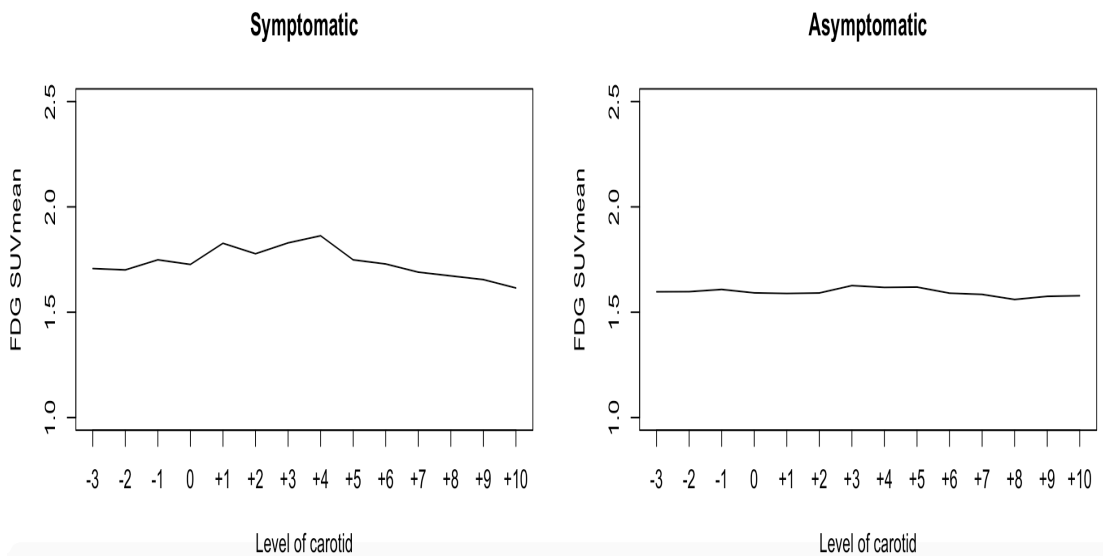


**Figure 4.5: Spatial distribution of FDG  $SUV_{mean}$ .** Median  $SUV_{mean}$  values at each axial slice along the artery for symptomatic and asymptomatic carotid arteries. 0 is the carotid bifurcation.

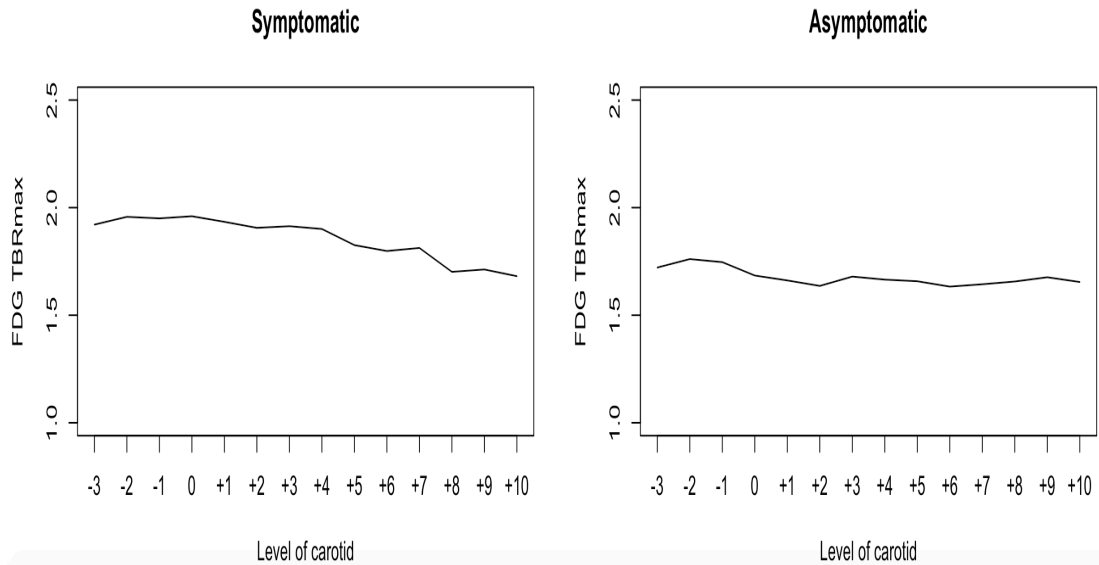


**Figure 4.6: Spatial distribution of FDG TBR<sub>max</sub>.** Median TBR<sub>max</sub> values at each axial slice along the artery for symptomatic and asymptomatic carotid arteries. 0 is the carotid bifurcation.

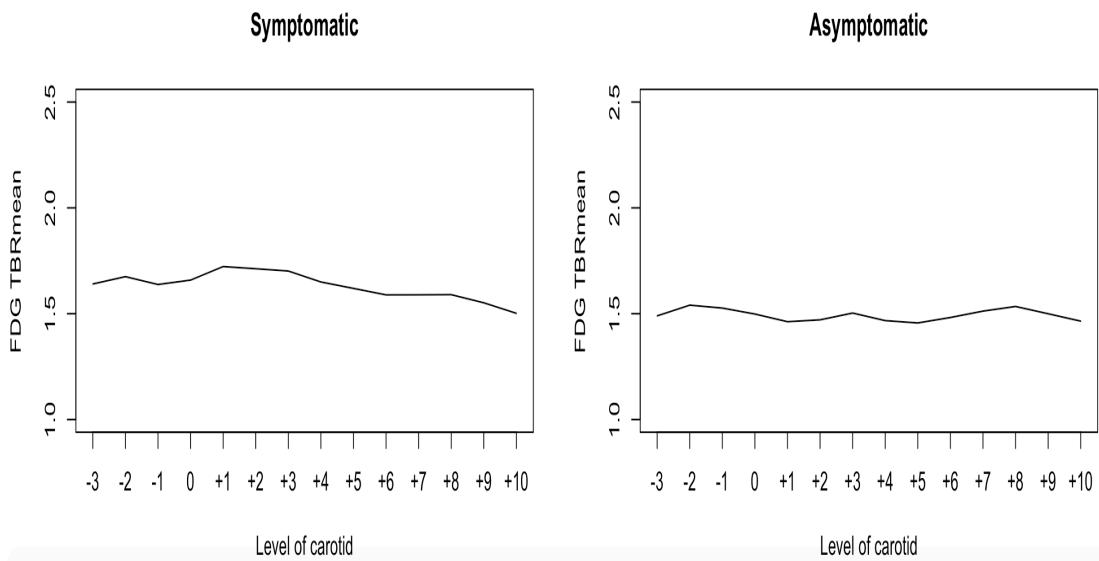


**Figure 4.7: Spatial distribution of FDG TBR<sub>mean</sub>.** Median TBR<sub>mean</sub> values at each axial slice along the artery for symptomatic and asymptomatic carotid arteries. 0 is the carotid bifurcation.

These FDG uptake distributions appear uniform across the entire artery, with the symptomatic artery consistently higher than the asymptomatic artery (**Figures 4.8 and 4.9**), supporting the finding that WV FDG uptake measures (WV SUV<sub>max</sub>, WV SUV<sub>mean</sub>, WV TBR<sub>max</sub>, and WV TBR<sub>mean</sub>) were all significantly higher in the symptomatic artery.

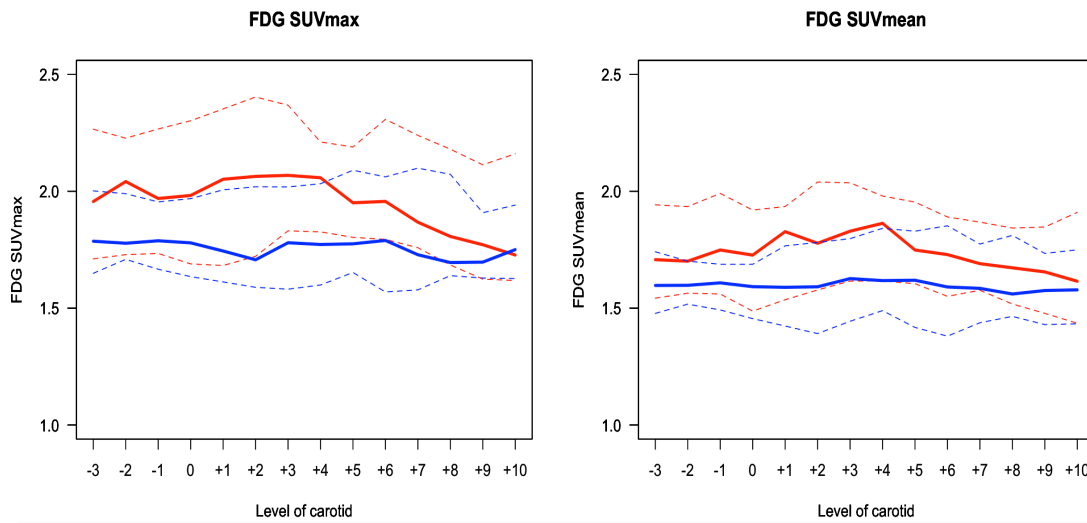


**Figure 4.8: Composite FDG SUV spatial distributions.** Median  $SUV_{max}$  (left) and  $SUV_{mean}$  (right) at each axial slice along the artery (red line = symptomatic artery, blue line = asymptomatic artery, solid line = median SUV, dashed lines = upper and lower limits of interquartile range).

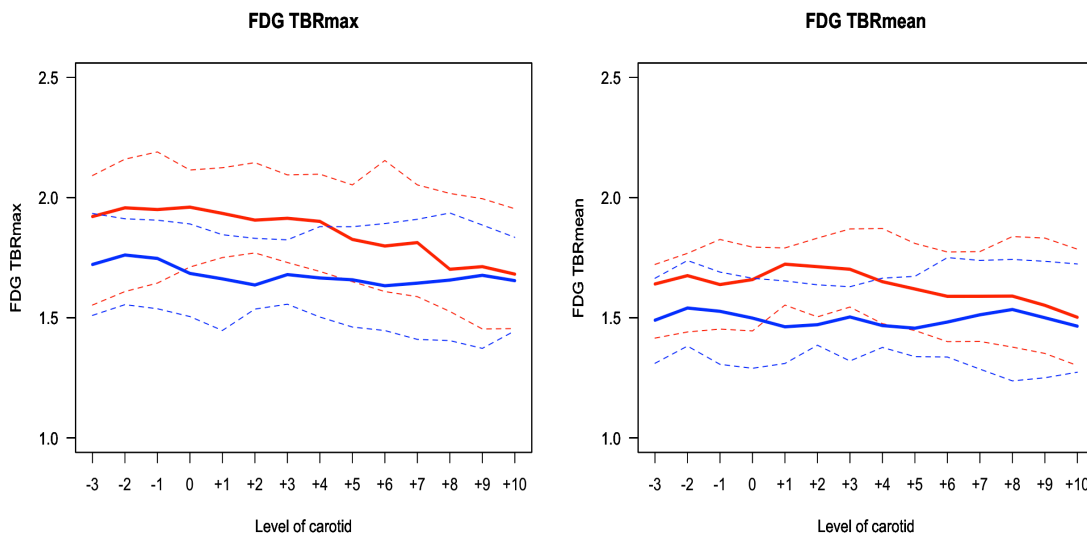


**Figure 4.9: Composite FDG TBR spatial distributions.** Median  $TBR_{max}$  (left) and  $TBR_{mean}$  (right) at each axial slice along the artery (red line = symptomatic artery, blue line = asymptomatic artery, solid line = median TBR, dashed lines = upper and lower limits of interquartile range).

Given these distributions, and those of NaF uptake in the previous chapter, we repeated the statistical comparison of bifurcation (+/- two slices either side of the bifurcation slice) versus non-bifurcation uptake as described above. NaF tracer uptake

was significantly higher in the bifurcation compared to the rest of the artery, while FDG uptake showed very little difference in uptake (**Table 4.5**).

	Bifurcation	Non-bifurcation	Significance
<b>FDG</b>			
Median SUV <sub>max</sub> (IQR)	1.87 (0.51)	1.82 (0.43)	p=0.67
Median SUV <sub>mean</sub> (IQR)	1.64 (0.39)	1.63 (0.34)	p=0.75
Median TBR <sub>max</sub> (IQR)	1.67 (0.47)	1.61 (0.41)	p=0.65
Median TBR <sub>mean</sub> (IQR)	1.62 (0.35)	1.51 (0.39)	p=0.89
<b>NaF</b>			
Median SUV <sub>max</sub> (IQR)	1.65 (0.75)	1.26 (0.42)	p<0.001
Median SUV <sub>mean</sub> (IQR)	1.35 (0.57)	1.12 (0.34)	p<0.001
Median TBR <sub>max</sub> (IQR)	2.19 (0.81)	1.71 (0.38)	p<0.001
Median TBR <sub>mean</sub> (IQR)	1.85 (0.68)	1.47 (0.29)	p<0.001

**Table 4.5:** Comparison of FDG and NaF uptake in bifurcation and non-bifurcation regions.

To confirm this significance was not due entirely to the symptomatic arteries, we further subdivided arteries according to whether they were symptomatic (**Table 4.6**).

	Symptomatic artery				Asymptomatic artery		
	Bifurcation	Non-bifurcation	Sig.		Bifurcation	Non-bifurcation	Sig.
<b>FDG</b>							
Median SUV <sub>max</sub> (IQR)	2.01 (0.62)	1.87 (0.48)	p=0.80		1.75 (0.36)	1.74 (0.46)	p=0.53
Median SUV <sub>mean</sub> (IQR)	1.77 (0.40)	1.66 (0.35)	p=0.63		1.59 (0.24)	1.59 (0.36)	p=0.73
Median TBR <sub>max</sub> (IQR)	1.83 (0.39)	1.69 (0.38)	p=0.78		1.59 (0.30)	1.54 (0.34)	p=0.55
Median TBR <sub>mean</sub> (IQR)	1.67 (0.31)	1.63 (0.42)	p=0.65		1.48 (0.37)	1.51 (0.36)	p=0.69
<b>NaF</b>							
Median SUV <sub>max</sub> (IQR)	1.72 (0.77)	1.28 (0.39)	p<0.001		1.52 (0.66)	1.21 (0.46)	p<0.001
Median SUV <sub>mean</sub> (IQR)	1.45 (0.53)	1.13 (0.23)	p<0.001		1.33 (0.61)	1.06 (0.37)	p<0.001
Median TBR <sub>max</sub> (IQR)	2.22 (0.72)	1.74 (0.29)	p<0.001		2.01 (0.94)	1.62 (0.37)	p<0.001
Median TBR <sub>mean</sub> (IQR)	1.92 (0.64)	1.47 (0.24)	p<0.001		1.81 (0.69)	1.44 (0.35)	p<0.001

**Table 4.6:** Comparison of FDG and NaF uptake between bifurcation and non-bifurcation regions according to symptomatic and non-symptomatic carotid arteries.

It is worth noting that although these tests were performed using paired testing, non-paired testing produced the same pattern of results, with no changes in what differences were statistically significant.

For completeness, we repeated the analysis comparing only the bifurcation between symptomatic and asymptomatic carotid arteries. All measures of FDG and NaF uptake were higher in the symptomatic bifurcation compared to the asymptomatic bifurcation (all  $p < 0.01$ ). In contrast, comparison of the ‘non-bifurcation’ regions found FDG uptake was significantly higher in symptomatic arteries compared to asymptomatic arteries ( $p < 0.01$  for all uptake measures) but NaF uptake did not differ significantly ( $p \geq 0.05$  for all uptake measures).

#### 4.3.4 Relationship between FDG uptake and macrocalcification

On an artery-by-artery basis, the correlations between FDG uptake measures and the whole artery CACS are shown in **Table 4.7**.

	Symptomatic artery		Asymptomatic artery	
	Correlation	Significance	Correlation	Significance
SHS SUV <sub>max</sub>	$r_s = -0.19$	$p = 0.34$	$r_s = -0.17$	$p = 0.41$
MDS SUV <sub>max</sub>	$r_s = -0.18$	$p = 0.39$	$r_s = -0.17$	$p = 0.41$
WV SUV <sub>max</sub>	$r_s = -0.21$	$p = 0.30$	$r_s = -0.10$	$p = 0.61$
SHS SUV <sub>mean</sub>	$r_s = -0.13$	$p = 0.52$	$r_s = -0.12$	$p = 0.55$
MDS SUV <sub>mean</sub>	$r_s = -0.10$	$p = 0.61$	$r_s = -0.17$	$p = 0.42$
WV SUV <sub>mean</sub>	$r_s = -0.07$	$p = 0.74$	$r_s = -0.08$	$p = 0.69$
SHS TBR <sub>max</sub>	$r_s = -0.25$	$p = 0.23$	$r_s = -0.29$	$p = 0.15$
MDS TBR <sub>max</sub>	$r_s = -0.21$	$p = 0.30$	$r_s = -0.24$	$p = 0.23$
WV TBR <sub>max</sub>	$r_s = -0.24$	$p = 0.23$	$r_s = -0.18$	$p = 0.37$
SHS TBR <sub>mean</sub>	$r_s = -0.17$	$p = 0.41$	$r_s = -0.30$	$p = 0.14$
MDS TBR <sub>mean</sub>	$r_s = -0.15$	$p = 0.47$	$r_s = -0.28$	$p = 0.16$
WV TBR <sub>mean</sub>	$r_s = -0.02$	$p = 0.93$	$r_s = -0.18$	$p = 0.37$

**Table 4.7:** Correlations between FDG uptake and whole artery CACS in symptomatic and asymptomatic arteries.

Given the relatively small size of our cohort, we also investigated whether there was a difference in FDG uptake if we dichotomised arteries based on their CACS. The range of Agatston scores in the symptomatic artery was 0-2582 and in the asymptomatic artery was 0-2320 (as discussed previously, there was no significant difference between symptomatic and asymptomatic artery CACS,  $p = 0.18$ ). Consequently, cut-offs for the dichotomisation used the median values for each: 405 and 306

respectively. There was no significant difference in any measure of FDG uptake between the low and high arterial CACS groups either when considering symptomatic or asymptomatic arteries alone, or on pooled analysis (all  $p > 0.05$ ).

We also considered whether the above approach – considering the total CACS for an artery – may be too broad a measure. As shown by the spatial distribution, the ‘most diseased segments’ of tracer uptake may not correspond spatially with macrocalcification in all arteries. Given the patterns seen in **Figures 3.21** and **3.22** in Chapter Three, this may be particularly true in asymptomatic arteries. Hence, we decided to repeat the analysis in a pre-defined area in order to consider the local interactions between FDG uptake and calcification. Therefore, we decided to test the associations between FDG uptake and macrocalcification limited to one spatial region that appears to represent the most diseased segment; the carotid bifurcation (defined spatially as above).

When comparing tracer uptake between the ‘low’ and ‘high’ CACS bifurcations described in the previous chapter, the median FDG uptake is lower in more calcified bifurcations ( $SUV_{max}$ ,  $SUV_{mean}$ ,  $TBR_{max}$  all  $p < 0.05$ ), but not  $TBR_{mean}$  ( $p = 0.14$ ) (**Figure 4.10**).

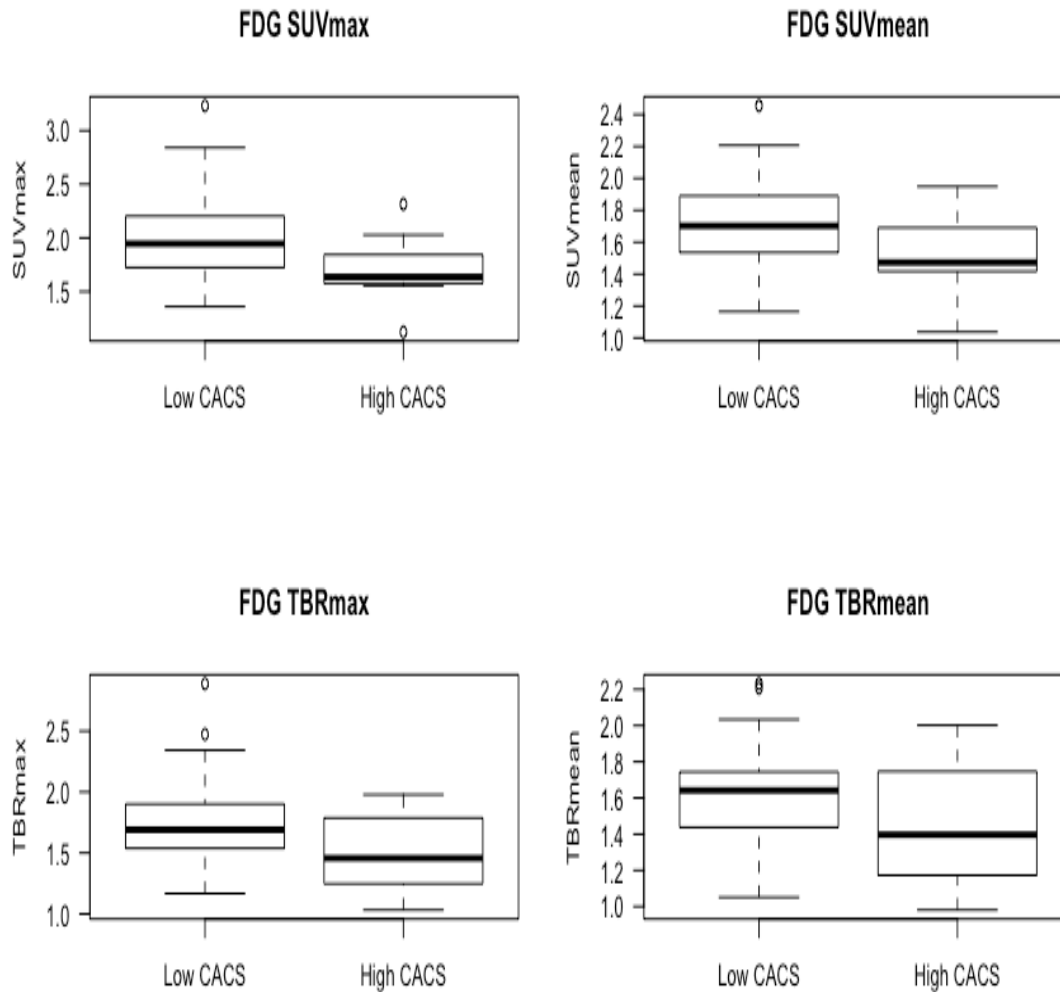


**Figure 4.10: FDG uptake in the carotid bifurcation according to degree of macrocalcification.**

#### 4.3.5 Variation in the relationship between FDG and NaF uptake according to macrocalcification

As discussed above, the suggestion of an asymmetrical distribution of calcification seen in symptomatic and asymptomatic arteries may mean that macrocalcification and the ‘most diseased’ segment of the artery may not overlap. Once again, we used the carotid bifurcation as indicative of the most diseased segment of the artery, and used the cut-offs for ‘low’ and ‘high’ calcification as discussed in the previous chapter (i.e. an Agatston score of 450).

Prior to considering macrocalcification, the correlations between are FDG and NaF within the 52 bifurcations were:  $SUV_{max}$   $r_s=0.18$  ( $p=0.20$ ),  $SUV_{mean}$   $r_s=0.23$  ( $p=0.10$ ),  $TBR_{max}$   $r_s=0.24$  ( $p=0.09$ ), and  $TBR_{mean}$   $r_s=0.30$  ( $p=0.03$ ).

The correlations between FDG and NaF uptake within the carotid bifurcations dichotomised by CACS are shown in **Table 4.8**.

	Low calcification		High calcification	
	Correlation	Sig.	Correlation	Sig.
$SUV_{max}$	$r_s=0.43$	$p<0.001$	$r_s=0.62$	$p=0.04$
$SUV_{mean}$	$r_s=0.42$	$p<0.001$	$r_s=0.66$	$p=0.02$
$TBR_{max}$	$r_s=0.21$	$p=0.18$	$r_s=0.80$	$p<0.01$
$TBR_{mean}$	$r_s=0.27$	$p=0.09$	$r_s=0.69$	$p=0.02$

**Table 4.8:** Correlations between FDG and NaF uptake in the carotid bifurcations according to the degree of macrocalcification.

#### 4.3.6 FDG uptake in TIA versus stroke

The TIA cohort from the VISION Study included 10 participants, with a mean age of  $73.3 \pm 6.40$  years. 9 (90%) were male. Readings were performed by Dr Jason Tarkin (Clinical Research Fellow, Division of Cardiovascular Medicine, University of Cambridge) as part of his PhD study.

TBR measures in the culprit plaques in our stroke cohort were compared against TBR measures of culprit plaques in a TIA cohort (**Table 4.9**).

	<b>TIA (n=10)</b>	<b>Stroke (n=26)</b>	<b>Significance</b>
<b>Symptomatic artery</b>			
Median SHS TBR <sub>max</sub> (IQR)	2.22 (0.50)	2.14 (0.56)	p=0.85
Median MDS TBR <sub>max</sub> (IQR)	2.03 (0.49)	2.08 (0.52)	p=0.75
Median WV TBR <sub>max</sub> (IQR)	1.70 (0.40)	1.89 (0.40)	p=0.34
<b>Asymptomatic artery</b>			
Median SHS TBR <sub>max</sub> (IQR)	2.10 (0.52)	1.94 (0.43)	p=0.24
Median MDS TBR <sub>max</sub> (IQR)	2.02 (0.47)	1.89 (0.40)	p=0.26
Median WV TBR <sub>max</sub> (IQR)	1.59 (0.27)	1.71 (0.36)	p=0.41

**Table 4.9:** FDG uptake in TIA and stroke. Comparison of FDG uptake in TIA (VISION Study) and ischaemic stroke (ICARUSS Study).

While there was no significant difference between TIA and stroke FDG TBR values, it is worth noting that SHS and MDS TBR<sub>max</sub> did not differ significantly between symptomatic and asymptomatic arteries in the TIA cohort (p=0.43 and p=0.49 respectively), though WV TBR<sub>max</sub> did differ significantly between symptomatic and asymptomatic arteries (p=0.02), as per published results for the VISION Study (Tarkin et al., 2017).

#### *4.3.7 Effect of cardiovascular risk factors on FDG uptake*

Univariable analysis of the effects of cardiovascular risk factors on FDG uptake is included in Appendix D.

#### *4.3.8 Multivariable analysis of FDG uptake according to risk factors*

Reviewing the results of the univariable analysis indicates that there is an interaction between diabetes mellitus and blood sugar in our cohort. Individuals with diabetes

had a higher blood sugar after the overnight fast than those without diabetes (median 6.7 [IQR 0.8] and 5.3 [IQR 1.3] mmol/L respectively,  $p=0.02$ ).

Given this, we included an interaction term between diabetes mellitus and blood sugar in our regression model. The fit of the model (using SHS  $SUV_{max}$  as an example) was assessed using the AIC for models with no interaction term (AIC 120.95), both interaction and variables separately (AIC 121.37), and interaction only (118.34). This makes logical sense, as diabetes mellitus and blood sugar are unlikely to be sufficiently independent in our study to be included as independent factors, particularly given the small numbers and the aforementioned difference in blood sugar levels. Therefore, regression analysis with backwards elimination was performed with the interaction of diabetes and blood sugar replacing diabetes and blood sugar in the model (**Table 4.10**).

<b>SHS <math>TBR_{max}</math></b>	AIC = 86.98	Adjusted $R^2 = 0.24$ ( $p<0.001$ )
	<b>Coefficient</b>	<b>Significance</b>
Smoking	0.51	$p<0.01$
Diabetes: blood sugar	-0.06	$p=0.04$
<b>MDS <math>TBR_{max}</math></b>	AIC = 82.729	Adjusted $R^2 = 0.24$ ( $p<0.001$ )
	<b>Coefficient</b>	<b>Significance</b>
Smoking	0.49	$p<0.01$
Diabetes: blood sugar	-0.06	$p=0.04$
<b>WV <math>TBR_{max}</math></b>	AIC = 37.732	Adjusted $R^2 = 0.26$ ( $p<0.001$ )
	<b>Coefficient</b>	<b>Significance</b>
Smoking	0.31	$p<0.01$
Diabetes: blood sugar	-0.04	$p=0.07$
Current antiplatelet	-0.17	$p=0.09$
<b>SHS <math>TBR_{mean}</math></b>	AIC = 44.259	Adjusted $R^2 = 0.29$ ( $p<0.001$ )
	<b>Coefficient</b>	<b>Significance</b>
Smoking	0.37	$p<0.001$
Diabetes: blood sugar	-0.04	$p=0.06$
Current antiplatelet	-0.17	$p=0.11$
<b>MDS <math>TBR_{mean}</math></b>	AIC = 41.86	Adjusted $R^2 = 0.27$ ( $p<0.001$ )
	<b>Coefficient</b>	<b>Significance</b>
Smoking	0.35	$p<0.001$
Diabetes: blood sugar	-0.04	$p=0.07$
Current antiplatelet	-0.17	$p=0.10$
<b>WV <math>TBR_{mean}</math></b>	AIC = 9.67	Adjusted $R^2 = 0.27$ ( $p<0.001$ )
	<b>Coefficient</b>	<b>Significance</b>
Smoking	0.24	$p<0.01$
Cardiovascular history: current statin	-0.22	$p=0.01$

**Table 4.10:** Multiple linear regression for vascular risk factors and FDG TBRs.

It is worth noting several points in the above modeling. Firstly, inclusion of diabetes and blood sugar as well as the interaction between them produced the same outcomes,

as diabetes and blood sugar were eliminated in the backwards regression. Similarly, inclusion of interactions between statins and total cholesterol, statins and antiplatelets, antiplatelets and cardiovascular history, statin and cardiovascular history made no differences to the modeling with the exception of WV TBR<sub>mean</sub> (where an interaction between cardiovascular history and statin use was found to be significant).

#### *4.3.9 hsCRP and the inflammation/microcalcification/macrocification complex*

For FDG, in symptomatic arteries the following correlations were observed between hsCRP and SHS SUV<sub>max</sub> ( $r_s=0.49$ ,  $p=0.02$ ), MDS SUV<sub>max</sub> ( $r_s=0.49$ ,  $p=0.02$ ), WV SUV<sub>max</sub> ( $r_s=0.39$ ,  $p=0.07$ ), SHS SUV<sub>mean</sub> ( $r_s=0.42$ ,  $p=0.06$ ), MDS SUV<sub>mean</sub> ( $r_s=0.39$ ,  $p=0.08$ ), WV SUV<sub>mean</sub> ( $r_s=0.14$ ,  $p=0.53$ ), SHS TBR<sub>max</sub> ( $r_s=0.57$ ,  $p<0.01$ ), MDS TBR<sub>max</sub> ( $r_s=0.53$ ,  $p=0.01$ ), WV TBR<sub>max</sub> ( $r_s=0.50$ ,  $p=0.02$ ), SHS TBR<sub>mean</sub> ( $r_s=0.52$ ,  $p=0.02$ ), MDS TBR<sub>mean</sub> ( $r_s=0.47$ ,  $p=0.03$ ), WV TBR<sub>mean</sub> ( $r_s=0.28$ ,  $p=0.20$ ). For FDG uptake in asymptomatic arteries, the following correlations were observed between hsCRP and SHS SUV<sub>max</sub> ( $r_s=0.13$ ,  $p=0.57$ ), MDS SUV<sub>max</sub> ( $r_s=0.12$ ,  $p=0.60$ ), WV SUV<sub>max</sub> ( $r_s=-0.02$ ,  $p=0.93$ ), SHS SUV<sub>mean</sub> ( $r_s=-0.12$ ,  $p=0.59$ ), MDS SUV<sub>mean</sub> ( $r_s=-0.13$ ,  $p=0.58$ ), WV SUV<sub>mean</sub> ( $r_s=-0.09$ ,  $p=0.69$ ), SHS TBR<sub>max</sub> ( $r_s=0.28$ ,  $p=0.21$ ), MDS TBR<sub>max</sub> ( $r_s=0.29$ ,  $p=0.20$ ), WV TBR<sub>max</sub> ( $r_s=0.24$ ,  $p=0.28$ ), SHS TBR<sub>mean</sub> ( $r_s=0.15$ ,  $p=0.50$ ), MDS TBR<sub>mean</sub> ( $r_s=0.12$ ,  $p=0.59$ ), WV TBR<sub>mean</sub> ( $r_s=0.19$ ,  $p=0.39$ ). The association between hsCRP and NaF uptake has already been discussed in the previous chapter.

Given the previous findings, correlations between hsCRP with both FDG and NaF uptake were adjusted by the degree of macrocalcification, and are shown in **Tables 4.11** and **4.12** respectively.

	Low artery CACS (CACS 0-499)		High artery CACS (CACS $\geq$ 500)	
	Correlation	Sig.	Correlation	Sig.
<b>Symptomatic artery</b>				
SHS SUV <sub>max</sub>	$r_s=0.89$	$p<0.001$	$r_s=-0.21$	$p=0.51$
MDS SUV <sub>max</sub>	$r_s=0.90$	$p<0.001$	$r_s=-0.18$	$p=0.57$
WV SUV <sub>max</sub>	$r_s=0.93$	$p<0.001$	$r_s=-0.32$	$p=0.31$
SHS SUV <sub>mean</sub>	$r_s=0.87$	$p<0.001$	$r_s=-0.29$	$p=0.37$
MDS SUV <sub>mean</sub>	$r_s=0.83$	$p<0.001$	$r_s=-0.22$	$p=0.48$
WV SUV <sub>mean</sub>	$r_s=0.60$	$p=0.02$	$r_s=-0.27$	$p=0.40$
SHS TBR <sub>max</sub>	$r_s=0.69$	$p<0.01$	$r_s=0.15$	$p=0.64$
MDS TBR <sub>max</sub>	$r_s=0.68$	$p<0.01$	$r_s=0.12$	$p=0.72$
WV TBR <sub>max</sub>	$r_s=0.62$	$p=0.02$	$r_s=0.13$	$p=0.70$
SHS TBR <sub>mean</sub>	$r_s=0.45$	$p=0.11$	$r_s=0.13$	$p=0.68$
MDS TBR <sub>mean</sub>	$r_s=0.46$	$p=0.10$	$r_s=0.13$	$p=0.68$
WV TBR <sub>mean</sub>	$r_s=0.26$	$p=0.37$	$r_s=0.13$	$p=0.68$
<b>Asymptomatic artery</b>				
SHS SUV <sub>max</sub>	$r_s=0.43$	$p=0.09$	$r_s=0.07$	$p=0.88$
MDS SUV <sub>max</sub>	$r_s=0.40$	$p=0.11$	$r_s=0.02$	$p=0.98$
WV SUV <sub>max</sub>	$r_s=0.30$	$p=0.24$	$r_s=0.00$	$p=1.00$
SHS SUV <sub>mean</sub>	$r_s=0.13$	$p=0.61$	$r_s=0.03$	$p=0.95$
MDS SUV <sub>mean</sub>	$r_s=0.10$	$p=0.69$	$r_s=0.07$	$p=0.88$
WV SUV <sub>mean</sub>	$r_s=0.18$	$p=0.48$	$r_s=0.07$	$p=0.88$
SHS TBR <sub>max</sub>	$r_s=0.44$	$p=0.08$	$r_s=-0.20$	$p=0.61$
MDS TBR <sub>max</sub>	$r_s=0.38$	$p=0.13$	$r_s=-0.15$	$p=0.71$
WV TBR <sub>max</sub>	$r_s=0.31$	$p=0.22$	$r_s=0.02$	$p=0.98$
SHS TBR <sub>mean</sub>	$r_s=0.27$	$p=0.29$	$r_s=-0.03$	$p=0.95$
MDS TBR <sub>mean</sub>	$r_s=0.21$	$p=0.41$	$r_s=-0.15$	$p=0.71$
WV TBR <sub>mean</sub>	$r_s=0.29$	$p=0.25$	$r_s=-0.10$	$p=0.81$

**Table 4.11:** Correlations between FDG uptake measures and hsCRP by extent of arterial calcification.

	Low artery CACS (CACS 0-499)		High artery CACS (CACS ≥500)	
	Correlation	Sig.	Correlation	Sig.
<b>Symptomatic artery</b>				
SHS SUV <sub>max</sub>	r <sub>s</sub> =0.43	p=0.12	r <sub>s</sub> =0.00	p=1.00
MDS SUV <sub>max</sub>	r <sub>s</sub> =0.43	p=0.12	r <sub>s</sub> =-0.13	p=0.68
WV SUV <sub>max</sub>	r <sub>s</sub> =0.32	p=0.27	r <sub>s</sub> =-0.22	p=0.50
SHS SUV <sub>mean</sub>	r <sub>s</sub> =0.31	p=0.29	r <sub>s</sub> =-0.08	p=0.80
MDS SUV <sub>mean</sub>	r <sub>s</sub> =0.37	p=0.19	r <sub>s</sub> =-0.22	p=0.48
WV SUV <sub>mean</sub>	r <sub>s</sub> =0.53	p=0.05	r <sub>s</sub> =-0.13	p=0.68
SHS TBR <sub>max</sub>	r <sub>s</sub> =0.43	p=0.12	r <sub>s</sub> =0.01	p=0.97
MDS TBR <sub>max</sub>	r <sub>s</sub> =0.47	p=0.09	r <sub>s</sub> =0.02	p=0.96
WV TBR <sub>max</sub>	r <sub>s</sub> =0.49	p=0.08	r <sub>s</sub> =-0.09	p=0.78
SHS TBR <sub>mean</sub>	r <sub>s</sub> =0.39	p=0.17	r <sub>s</sub> =-0.06	p=0.85
MDS TBR <sub>mean</sub>	r <sub>s</sub> =0.40	p=0.16	r <sub>s</sub> =-0.10	p=0.75
WV TBR <sub>mean</sub>	r <sub>s</sub> =0.72	p<0.01	r <sub>s</sub> =-0.13	p=0.70
<b>Asymptomatic artery</b>				
SHS SUV <sub>max</sub>	r <sub>s</sub> =0.05	p=0.85	r <sub>s</sub> =-0.13	p=0.74
MDS SUV <sub>max</sub>	r <sub>s</sub> =0.18	p=0.49	r <sub>s</sub> =-0.13	p=0.74
WV SUV <sub>max</sub>	r <sub>s</sub> =0.24	p=0.35	r <sub>s</sub> =-0.02	p=0.98
SHS SUV <sub>mean</sub>	r <sub>s</sub> =0.02	p=0.93	r <sub>s</sub> =-0.27	p=0.49
MDS SUV <sub>mean</sub>	r <sub>s</sub> =0.06	p=0.82	r <sub>s</sub> =-0.27	p=0.49
WV SUV <sub>mean</sub>	r <sub>s</sub> =0.20	p=0.45	r <sub>s</sub> =-0.10	p=0.81
SHS TBR <sub>max</sub>	r <sub>s</sub> =0.13	p=0.62	r <sub>s</sub> =0.03	p=0.95
MDS TBR <sub>max</sub>	r <sub>s</sub> =0.16	p=0.53	r <sub>s</sub> =0.07	p=0.88
WV TBR <sub>max</sub>	r <sub>s</sub> =0.31	p=0.23	r <sub>s</sub> =0.35	p=0.36
SHS TBR <sub>mean</sub>	r <sub>s</sub> =0.14	p=0.59	r <sub>s</sub> =0.10	p=0.81
MDS TBR <sub>mean</sub>	r <sub>s</sub> =0.14	p=0.59	r <sub>s</sub> =0.17	p=0.68
WV TBR <sub>mean</sub>	r <sub>s</sub> =0.22	p=0.39	r <sub>s</sub> =0.18	p=0.64

**Table 4.12:** Correlations between NaF uptake measures and hsCRP by extent of arterial calcification.

## 4.4 Discussion

### 4.4.1 FDG-PET can differentiate between symptomatic versus asymptomatic atheroma in individuals with stroke

This study supports previous studies demonstrating the ability of FDG-PET to differentiate between culprit atheroma and asymptomatic plaques. The increased FDG uptake we see in the culprit plaque, as well as increased uptake in the contralateral arteries in this symptomatic cohort, likely reflects the inflammatory burden (Tawakol et al., 2005, Tawakol et al., 2006) and high-risk morphological features (Davies et al., 2005, Figueroa et al., 2012, Silvera et al., 2009, Lei-xing et al., 2014) as demonstrated by previous studies discussed in greater detail above. Here we demonstrate increased FDG uptake in culprit plaques in an exclusively MRI-confirmed stroke cohort.

Two recent dual tracer PET studies have recently reported significantly higher NaF uptake, but interestingly not FDG uptake, in symptomatic atheroma (Vesey et al., 2017, Quirce et al., 2016). Vesey et al. found no significant difference in any FDG SUV or TBR measures between the culprit vessel and either the contralateral artery (p values between 0.35 and 0.76) or controls who had recently experienced a stroke due to a cause not attributed to carotid disease (p values 0.27 to 0.93) (Vesey et al., 2017).

In contrast, our study reports significantly higher NaF *and* FDG uptake in the SHS and MDS focal regions, and higher WV FDG uptake, in the symptomatic carotid artery compared to the asymptomatic carotid artery. There are a number of possible explanations for why this may be the case.

Given the difference in our cohorts we also compared FDG uptake in culprit plaques in individuals with strokes against those in individuals with TIAs. A parallel is the difference in uptake with different severities of coronary syndromes. Increased FDG uptake in the aorta was seen for myocardial infarction compared to stable angina, while uptake with ST-elevation myocardial infarction was higher than uptake in non-ST-elevation myocardial infarctions (Joshi et al., 2015). Higher carotid FDG uptake was observed in individuals with acute coronary syndrome than those with chronic stable angina (Kim et al., 2015).

Comparing the TBR measures of our exclusively stroke cohort against the TBR measures in a TIA cohort (performed using a comparable protocol in another study within our group) did not reveal any statistically significant differences. However, the effect of cardiovascular risk profile and other intangible factors upon FDG uptake means that these readings may not be readily comparable. As discussed previously, our study, like a number of previous studies, uses the individual's contralateral artery to control for variations in cardiovascular risk profiles between individuals. Here it is not possible to do that. In future studies, matching individuals between cohorts based on vascular risk profile may be one way of overcoming this limitation, but in practice the wide variation is likely to make this extremely difficult. The alternative method to detect an absolute difference in FDG uptake in culprit plaques between TIA and stroke cohorts would be to recruit large cohorts, thereby diluting this variation (an

approach seen in the retrospective PET studies of asymptomatic oncological cohorts). For example, based on these results, 184 participants (92 in each cohort) would need to be recruited to detect a 10% reduction in FDG MDS TBR<sub>max</sub> with 80% power at an alpha of 0.05. Hence, our relatively small numbers may limit the ability to detect a statistically significant difference given the very similar readings.

That said, it is curious that in the three studies with TIA with or without minor strokes, there was no significant difference observed in FDG uptake at the most diseased segment between symptomatic and asymptomatic arteries (Vesey et al., 2017, Quirce et al., 2016, Tarkin et al., 2017). This is illustrated in the results from the VISION study shown here. Although the absolute FDG TBR values did not differ between TIA and stroke cohorts in our results, more severe neurological events appeared associated with a statistically significant increase in FDG uptake in the most diseased segment of the artery relative to the asymptomatic artery, while in the TIA cohorts the FDG uptake in most diseased segment of the symptomatic artery showed no statistical difference relative to the asymptomatic artery (i.e. the ‘culprit’ plaque was not significantly higher than the basal state of vascular inflammation seen in systemic atherosclerosis). Admittedly the participants in the TIA cohort did not have MRI imaging to assess for infarction, but given the clinical improvement to baseline neurological function, any infarct found on MRI is likely to be small. Nevertheless, even if some of these TIAs were in fact ‘minor’ strokes, our stroke participants presented with more severe clinical presentations as illustrated by their infarct volumes and clinical severity. Ultimately, this observation is more hypothesis-generating than it is definitive, and future work will need larger numbers (or pool data in meta-analysis) in order to investigate further.

Further potential causes for a failure to differentiate between symptomatic and asymptomatic plaques in these studies involve the non-specific nature of FDG. Although this may be a contributing factor, to find these results reproduced across these studies, especially given the body of previous studies demonstrating the utility of FDG-PET to detect culprit plaques, suggests a physiological cause rather than a methodological one. Finally, the lack of a significant difference between individuals with carotid atherosclerosis and controls seen by Vesey et al. may be due to the use of controls who had recently had a stroke, albeit of non-carotid aetiology, as recent

myocardial ischaemic injury may increase FDG uptake in non-culprit plaques, though it is not known if the same occurs in cerebrovascular ischaemia (Tawakol et al., 2017, Dutta et al., 2012, Emami et al., 2015a).

Our study found no relationship between the degree of stenosis and tracer uptake. This supports reports from earlier studies (Chróinín et al., 2014, Lei-xing et al., 2014). Indeed, culprit atheroma have been identified using FDG-PET in atheroma that would be considered sub-clinical using a solely anatomical (>50% stenosis) clinical criterion (Davies et al., 2005). Interestingly, in a longitudinal FDG-PET study of an asymptomatic oncological cohort, a significant decrease in mean luminal area within the carotid arteries was observed despite a significant reduction in carotid TBR, again suggesting a lack of direct associations between the degree of stenosis and tracer uptake (Hetterich et al., 2015).

Arauz et al. did report a significant correlation between the degree of carotid stenosis and FDG uptake, but it should be noted that this was a small study using a dichotomised SUV measure (SUV  $\geq 2.7$  and  $< 2.3$ ) with only 2 of 13 symptomatic participants demonstrating weak uptake (Arauz et al., 2007). Muller et al. also found a weak but statistically significant correlation between the degree of stenosis and FDG uptake, though this study only considered stenoses  $\geq 50\%$  and in symptomatic arteries the difference between the moderate and severely stenosed arteries did not reach statistical significance (Muller et al., 2014). This study also reinforced the importance of factors other than the degree of stenosis, as no correlation was observed between the degree of stenosis and the presence of symptoms or MES (Muller et al., 2014).

Increased FDG uptake has been observed even at the earliest stages of atherosclerosis. FDG TBR is correlated with the degree of endothelial dysfunction – an early change in atherogenesis (Ross, 1993) – independently of conventional cardiovascular risk factors (Honda et al., 2016). This, along with increased FDG uptake with cardiovascular risk factors and atheroma core development, partly explains increased uptake in asymptomatic arteries, and why this ‘background’ level of tracer uptake will vary between individuals. This variability, along with heterogeneous populations, methodologies, and outcome measures, has limited the capacity to define tracer uptake thresholds to risk-stratify vulnerable plaques. This is further compounded by

the typically small sample sizes of the studies. van der Valk et al. propose a FDG maximum TBR of 1.84 as the upper limit of physiological uptake in the carotid, corresponding to the 90<sup>th</sup> centile of controls (van der Valk et al., 2016). However, it is important to note that in this study the average BMI was 25, which may increase tracer uptake as part of a metabolic syndrome as described above. This threshold is supported by Tawakol et al., who found an incremental increase in the macrophage area of carotid plaques with increasing TBR: plaques below 1.8 had a macrophage area of 0-5%, between 1.8-2.8 had 5-15%, and above 2.8 had a macrophage areas above 15% (Tawakol et al., 2006). Marnane et al. found a one unit increase in symptomatic artery FDG mean SUV resulted in an adjusted (for age and degree of stenosis) hazard ratio of recurrent stroke at 90 days of 6.1 (95% CI 1.3-28.8, p=0.02), with a mean SUV threshold of 1.85 providing an optimal balance of sensitivity (61.5%) and specificity (78.7%) to discriminate between individuals at low and high risk of recurrence (Marnane et al., 2012). For PET to be utilised clinically for risk stratification, risk thresholds need to be established for tracer uptake and future work should look towards harmonising study protocols to facilitate meta-analysis.

In this study we compared the symptomatic carotid artery to the contralateral artery, as per well-established methodology (Rudd et al., 2002). Typically the participants in this study had bilateral carotid atherosclerosis, though the degree of stenosis was not necessarily symmetrical (Appendix B). However, as seen above, the degree of stenosis did not appear to have a relationship between tracer uptake. What it does mean is that each contralateral carotid serves as a control having been exposed to the same patient-specific vascular risk factors as the symptomatic artery. Consequently, the finding that FDG uptake was higher in the symptomatic artery in 23/26 (88.5%) participants (for SHS SUV<sub>max</sub> and SHS TBR<sub>max</sub>) in risk factor-matched conditions suggests that the additional uptake represents the key inflammatory process leading to plaque rupture.

Finally, a degree of caution should be applied when considering the different metrics of tracer uptake. Although a similar pattern of results is seen for SUV and TBR measures, it is important to note that most of these metrics are related. Consequently, it is important to consider the potential for type one errors from multiple comparison

testing, and hence further replication and validation in larger samples (with pre-specified endpoints and subgroup analyses) would be advantageous.

#### 4.4.2 Spatial distribution of inflammation relative to microcalcification

Our findings demonstrate that FDG and NaF uptake showed two distinct spatial patterns of uptake, suggesting different patterns of inflammation and microcalcification within atherosclerosis. This can be best visualised by combining the previous spatial distribution plots (**Figures 4.11-4.14**):

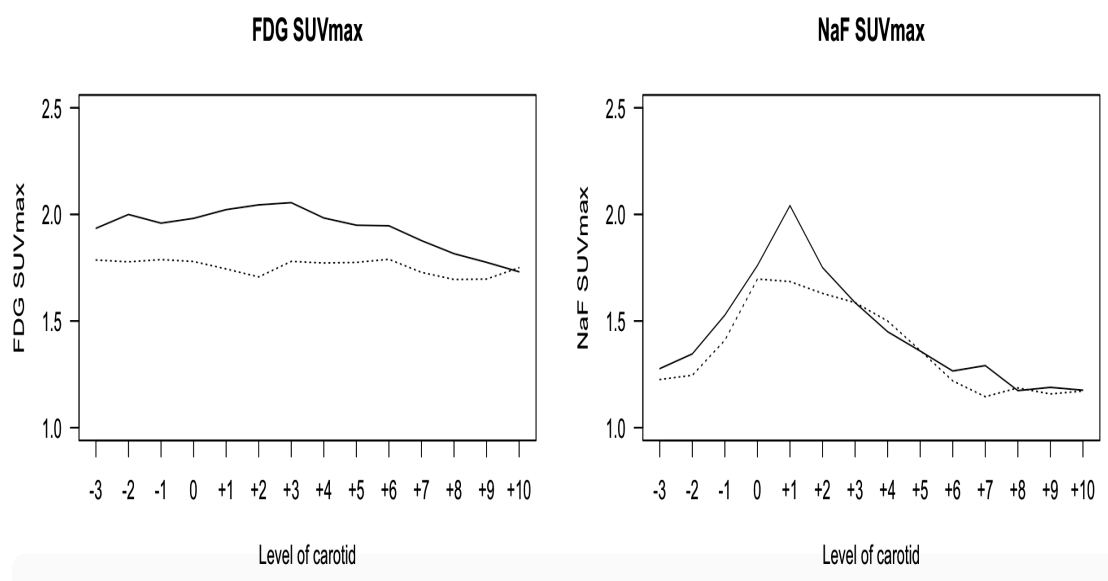


**Figure 4.11: Comparative spatial distributions of FDG and NaF SUV<sub>max</sub>.** Left = FDG, right = NaF; solid lines = symptomatic arteries, dashed lines = asymptomatic arteries.

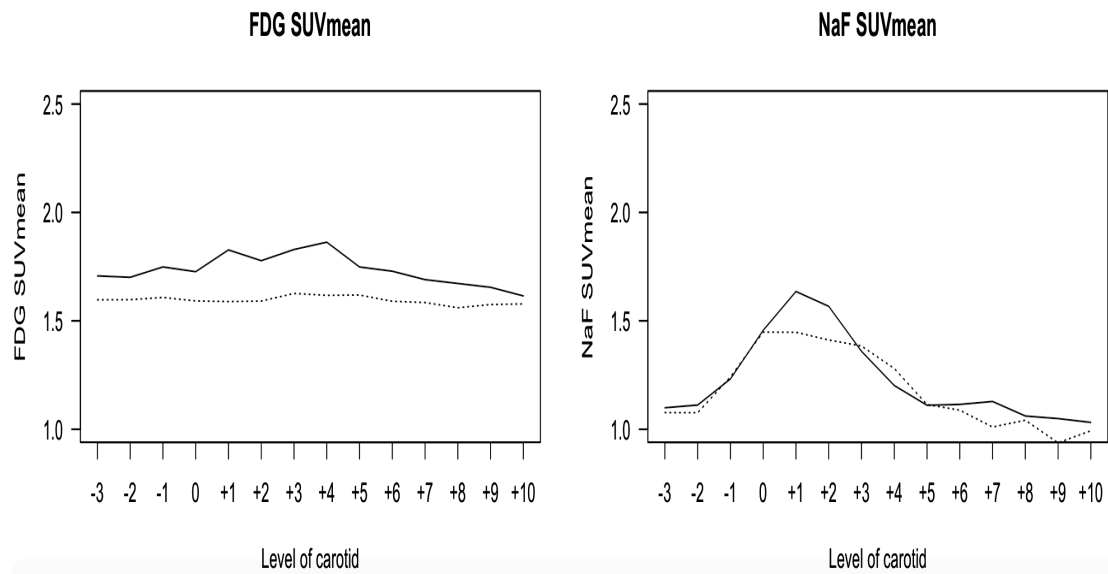


**Figure 4.12: Comparative spatial distributions of FDG and NaF  $SUV_{mean}$ .** Left = FDG, right = NaF; solid lines = symptomatic arteries, dashed lines = asymptomatic arteries.

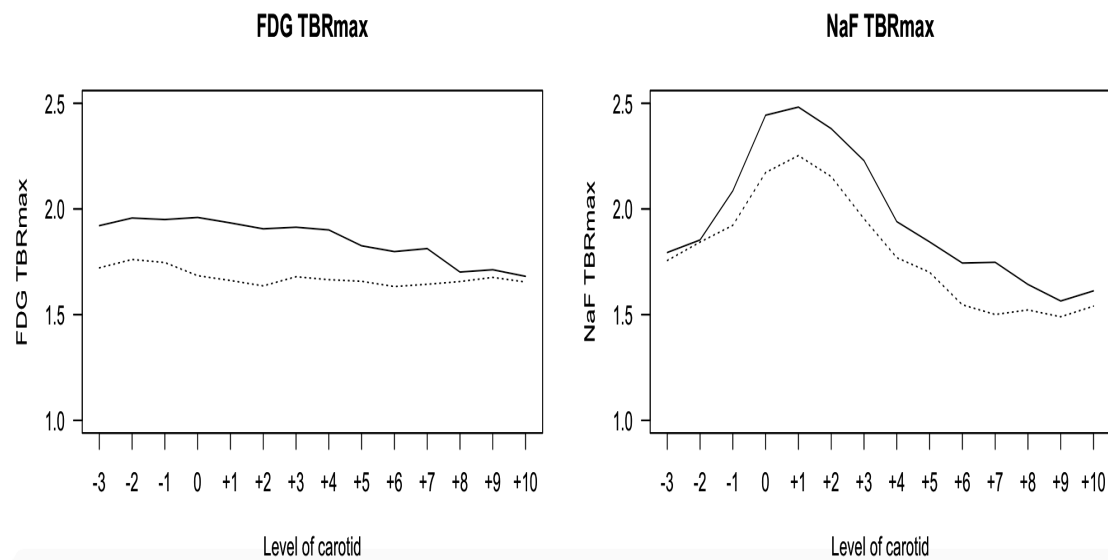


**Figure 4.13: Comparative spatial distributions of FDG and NaF  $TBR_{max}$ .** Left = FDG, right = NaF; solid lines = symptomatic arteries, dashed lines = asymptomatic arteries.

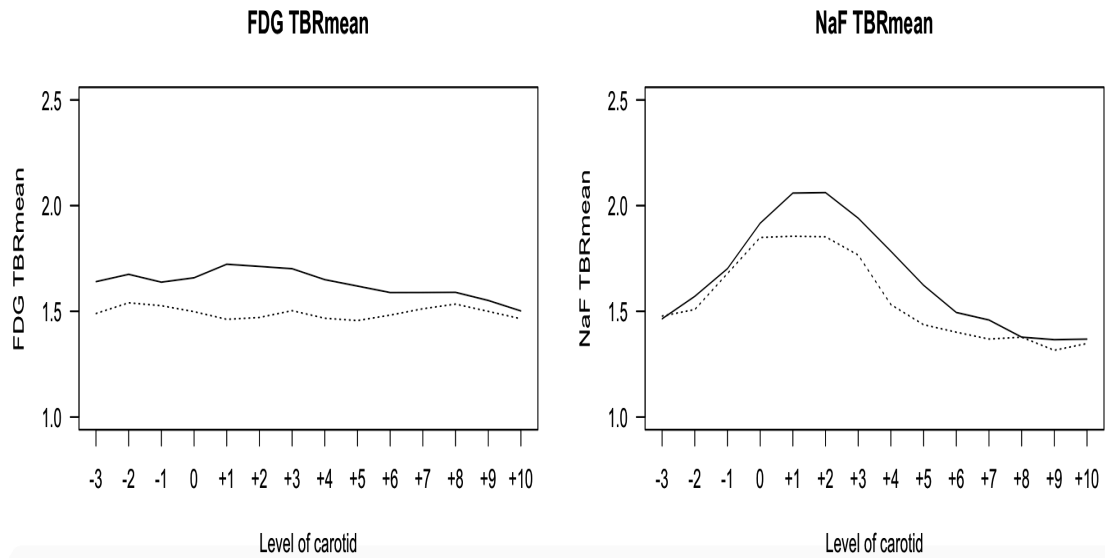


**Figure 4.14: Comparative spatial distributions of FDG and NaF  $TBR_{mean}$ .** Left = FDG, right = NaF; solid lines = symptomatic arteries, dashed lines = asymptomatic arteries.

This pattern suggests that microcalcification is not simply an automatic consequence of inflammation. If that were the case, then one would expect the NaF uptake curves to mirror the FDG uptake curves (i.e. NaF curves would appear relatively flat). Instead we see two distinct patterns. The FDG uptake curves appear flat with the symptomatic curve with higher uptake typically running parallel to the curve the asymptomatic artery, suggesting that inflammation is upregulated and diffuse along the artery with no obvious nidus. This pattern of FDG uptake is consistent with previous FDG studies that indicate that atherosclerosis is a diffuse inflammatory disease (Rudd et al., 2009, Joshi et al., 2015). Our findings that generalised (WV) uptake is significantly higher in symptomatic arteries than asymptomatic arteries supports this.

In contrast, the NaF curve shows peak uptake around the distal bifurcation/proximal internal carotid artery. As shown by the spatial distribution curves, and discussed in the previous chapter, the curves for the symptomatic and asymptomatic arteries overlap for large portions of the artery, with divergence focused around the peak uptake in the bifurcation. This illustrates the finding of higher focal measures (SHS and MDS) of NaF uptake in symptomatic arteries to be strongly statistically significant.

The results of comparing the bifurcation with non-bifurcation support the bifurcation being a focal point of NaF uptake – statistically higher than in the rest of the artery – and that the most diseased segments are typically found in this region, while FDG uptake is diffuse with no higher uptake seen at the bifurcation than along the rest of the artery. Furthermore, the focal pattern of NaF uptake and diffuse pattern of FDG uptake is significantly higher in symptomatic arteries compared to asymptomatic arteries.

The presence of a peak around the bifurcation/proximal internal carotid artery suggests a biomechanical element. A similar phenomenon has been observed in apolipoprotein E<sup>-/-</sup> mouse models, where there was a strong association between the presence of macrophages and osteogenic activity but osteogenic signal peaked at the carotid bifurcation (Aikawa et al., 2007).

The interaction between the haemodynamics and the endothelium within arteries is complex. Shear stress, the force per unit area created when a tangential force (such as blood flow) acts on a surface (Davies, 2009), prompts a mechanically-triggered release of endothelial-derived factors (Corson et al., 1996, Griffith, 2002). Chronic changes in shear stress may also prompt structural remodeling of the arterial wall (Langille and O'Donnell, 1986), including conditions seen in atherosclerosis with signaling such as heparin-binding epidermal growth factor-like growth factor (Zhang et al., 2008, Reynolds et al., 2002).

Disturbed flow was found to be associated with up-regulation of inflammatory gene expression (including IL-1 $\alpha$ , IL-6, MCP-1), some molecules related to cellular adhesion (e.g. von Willebrand factor and CD44, but not VCAM-1, ICAM-1, e-selectin, or p-selectin), and antioxidative enzymes in regions of disturbed flow in pig aortas (Passerini et al., 2004). Other studies support this, finding that laminar flow was associated with an atheroprotective gene expression profile while disturbed flow prompted upregulation of atherogenic gene expression, though have found upregulation of NF-kB and VCAM-1 associated with non-laminar flow (Brooks et al., 2002, Mohan et al., 1997).

It has been recognised for some time that the carotid bifurcation represents a focal point for atherogenesis, with the majority of atherosclerotic plaques occurring within this region (Wolf and Werthessen, 1979, Glagov et al., 1988). Early stress modeling reported that the carotid bifurcation represented a point of maximal circumferential stress, with the point of bifurcation (corresponding to our ‘slice 0’) experiencing approximately 9-14 times the circumferential stress of the distal common carotid artery focused over a small area, while the carotid sinus bulb experienced increased but lower (3-4 times) the stresses compared to the common carotid artery (Salzar et al., 1995). The same study also considered the angle between the internal and external carotid arteries at the point of bifurcation, finding the angle to be between 27-50° in their samples, and this variation fits with earlier findings that plaques occurred at sites demonstrating most transformation (Macfarlane et al., 1983, Salzar et al., 1995).

Shear stress behaves in a different manner, with disordered flow and low shear stresses found to be associated with intimal thickening (Zarins et al., 1983, Ku et al., 1985). Arterial branch points are particularly prone to disordered flow due to the phenomenon of ‘flow separation;’ in effect a pocket of turbulent flow downstream of the bifurcation demonstrating oscillatory and multidirectional flow with fluctuating gradients of shear stress (**Figure 4.15**) (Davies, 2009). Development of the plaque also distorts the geometry of the bifurcation, potentially expanding the area experiencing flow separation seen at both the bifurcation and distal to the plaque.

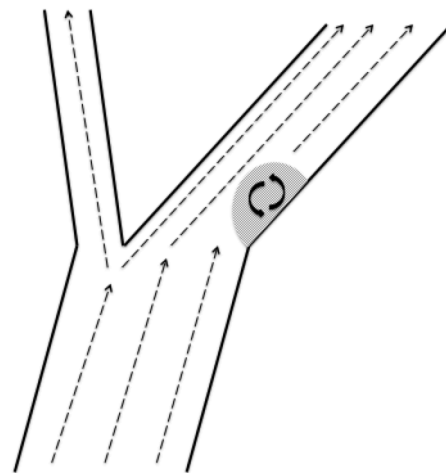


**Figure 4.15: Blood flow at an arterial branch point.** Shaded area represents an area of flow separation due to the angle of the branch (adapted with permission from Davies et al., 2009).

This in turn may become a vicious cycle as the development of the plaque further reduces shear stress. However, it is important to note that there are two regions of shear stress change neighbouring the plaque that experience opposite effects. Although Poiseuille flow rarely exists in large arteries due to their curve and branches, the Navier-Stokes equation is frequently utilised to estimate haemodynamic values (Davies, 2009):

$$\tau = 4\mu Q/R^3$$

Where:

$\tau$  = shear stress

$\mu$  = fluid viscosity

Q = flow rate

R = arterial radius

This equation demonstrates clearly how shear stresses across the plaque will be *increased* by the narrowing of an artery during stenosis. However, the flow distal to the plaque also experiences flow separation with disrupted flow downstream of the lesion (**Figure 4.16**) (Davies, 2009). Both endothelial cell density and gene expression varies spatially across the plaque, with impaired cellular regulation noted in the regions of disrupted flow (DePaola et al., 1992, DePaola et al., 1999, Davies et al., 1999, Passerini et al., 2004).

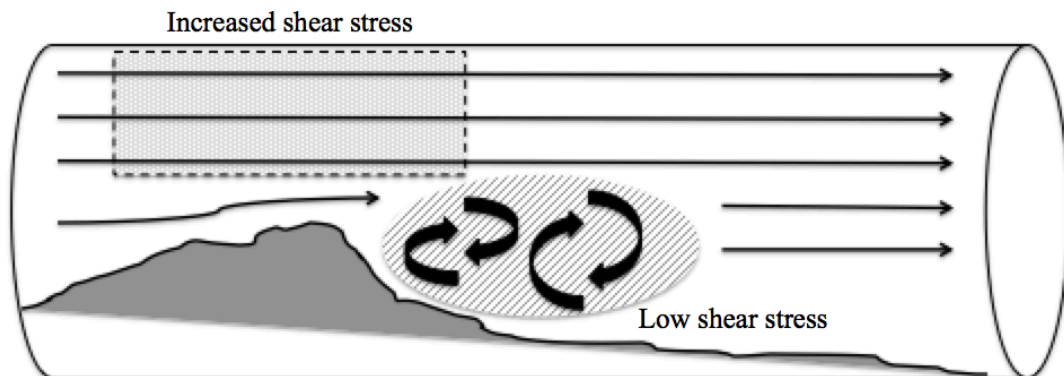


**Figure 4.16: Blood flow across an atherosclerotic plaque** (adapted with permission from Davies et al., 2009).

The mechanically-induced cellular response within endothelial cells in response to shear stresses involves both the cell cytoskeleton and nuclear transcription (Ni et al., 2010, Wu et al., 2015). However, overall this process remains poorly understood. The above discussion may explain the initiation and propagation of inflammation in a plaque that in turn provokes the systemic inflammatory response within atherosclerosis described above, but does not explain the focal peak of NaF uptake suggesting a focal microcalcific process.

The majority of research investigating haemodynamic effects on vascular biology has focused on the endothelium. This largely reflects their position as the cell type most exposed to haemodynamic forces. However, in the context of microcalcification it is likely that the osteoblast-like cell derived from vascular smooth muscle cells is the key cell type. In healthy vessel walls the VSMCs are less affected by shear stresses due to their location in the media, and hence protected by the endothelial cells and intima. However, vascular injury (including inflammatory injury) and remodeling may affect VSMCs, including their differentiation into different phenotypes, either through three possible mechanisms: (1) cytokine signaling from endothelial cells, (2) exposure of VSMCs to transmural interstitial flow shear stresses, (3) direct exposure of the superficial layer of VSMCs to blood flow shear stress (Shi and Tarbell, 2011). Wang et al. report that VSMCs can be subjected to shear stress through normal transmural interstitial flow at a level approximately one tenth the level of experienced by endothelial cells, though this level is sufficient to affect VSMC biology (Wang and Tarbell, 1995, Alshihabi et al., 1996, Tada and Tarbell, 2000).

Non-laminar shear stress has been implicated in the promotion of VSMC differentiation into the synthetic phenotype (Asada et al., 2005, Klein et al., 2017, Wang et al., 2006). Transmission of mechanical signals (including tensile, compressive, or shear forces) may be transmitted through the extracellular matrix and trigger change from contractile to synthetic phenotypes (Stegemann et al., 2005). Cellular bioengineering models have found that cyclic tensile stress increased alkaline phosphatase expression and mineralisation activity in aortic VSMCs through a mechanism independent of the recognised mitogen-activated protein kinase (MAPK) signaling pathway (Simmons et al., 2004). The effect of concomitant cyclic strain and low shear stress in triggering a phenotypic change away from a contractile type was further exacerbated by chronic hyperglycaemia (Chawla et al., 2016), a finding that may important in the context of restenosis after intervention.

The constellation of these results raises several possibilities, while also requiring an appreciation of the limitations of the study. The diffuse FDG uptake may represent a diffuse inflammatory response to a focal mechanical shear stress-induced injury. However, the diffuse infiltration by inflammatory cells is more likely to account for

the higher FDG uptake, as well as explaining why the symptomatic artery had higher uptake than the contralateral artery. It is also important to consider the non-specific nature of FDG uptake and whether this may limit the ability to observe a focal peak. However, the fact that FDG uptake was consistently higher in the symptomatic artery would make this less likely. One way to determine between these different considerations would be to use a radiotracer with improved specificity for inflammatory cells. Consequently, we intend to perform a similar spatial analysis of recent work using  $^{68}\text{Ga}$ -DOTATATE-PET in carotid atherosclerosis. DOTATATE demonstrates high specific binding activity to SST<sub>2</sub>, which is upregulated on the cell surface of macrophages (Dalm et al., 2003, Armani et al., 2007) and its use as a novel PET radiotracer will be discussed further in Chapter Eight.

As discussed in the previous chapter, NaF has a much higher specificity for microcalcification than FDG has for inflammation. The peak observed in NaF, but not for FDG, suggests that either this difference is due to the difference in specificities (i.e. both inflammation and microcalcification have a similar histological distribution that was not reflected here) or that microcalcification is a more focal process and more affected by mechanical shear forces. Given the above discussions, the latter appears more likely given previous histological findings that microcalcification is a focal process. Whether this focal disease relates to the local effects of shear stress, either through an endothelium-mediated process or directly upon VSMCs, requires further work to elucidate the mechanism.

Ultimately these results support the concept of inflammation as a diffuse process and microcalcification as a focal process, with biomechanical factors contributing more to the development of the latter than the former. With this in mind, work in collaboration with the bioengineers (Dr Zhongzhao Teng, Senior Research Associate, Biomedical Engineering, University of Cambridge) is currently being undertaken to perform stress analysis specific to the carotid arteries in our cohort, with the aim of relating this to the spatial pattern of FDG and NaF uptake.

#### *4.4.3 Physiological relationship between inflammation and macrocalcification*

While the above section considered the spatial distribution of tracer uptake – and their molecular targets – relative to the anatomy and mechanical forces of the carotid artery, it is also possible to measure the physiological processes (inflammation, microcalcification, and macrocalcification) relative to each other. The previous chapter has already considered the relationship between microcalcification and macrocalcification, so in this chapter we will consider how inflammation fits within this trinity.

In our study, bifurcations with higher CACSs had statistically lower median FDG  $SUV_{max}$ ,  $SUV_{mean}$ , and  $TBR_{max}$ . This supports the suggestion of negative associations between FDG uptake and macrocalcification in the artery-based analysis. Given our relatively small sample size, dichotomising calcification rather than assessing correlations using continuous scores may provide sufficient statistical power to detect differences. Furthermore, it also indicates that the relationship between FDG and macrocalcification is local; considering inflammation in the same region as macrocalcification (as per the bifurcation-based analysis) as opposed to the artery-based analysis that considers how inflammatory activity affects the overall CACS of the artery (as dichotomising the artery-based CACS did not reveal any difference in FDG uptake). Arguably the co-localised disease processes of the bifurcation-based analysis are more likely to illustrate localised interactions in the pathophysiology, while the artery-based analysis considers how the inflammatory activity anywhere in the artery may drive calcification wherever the peak macrocalcification falls spatially within the artery.

Studies comparing FDG uptake and macrocalcification in larger samples have been performed retrospectively in neurovascularly asymptomatic cohorts, and appear to support the negative association observed in our study. FDG TBR was found to be reduced, but present, in calcified versus non-calcified carotid plaques and this matched histological measures of inflammation with reduced inflammation in calcified plaques (Figueroa et al., 2012). In an early retrospective study of 122 individuals with cancer, Ben-Haim et al. found atherosclerotic lesions at 349 sites in 100 individuals. Of these, 7% demonstrated co-localised FDG uptake and

calcification, 8% FDG uptake without overt macrocalcification, and 85% had macrocalcification without FDG uptake. Hence, of all lesions demonstrating FDG uptake, 55.8% did not demonstrate calcification. It is important to note that in this study, only 11 lesions (3.2%) were found in the carotid artery. Of these, 1 (9.1%) had co-localised FDG uptake and macrocalcification, and the remainder (10, 90.9%) demonstrated macrocalcification without FDG uptake. Those without any lesions detectable either using PET or CT were typically younger and were less likely to have smoked (24% versus 55%) (Ben-Haim et al., 2004).

Different arterial regions have been found to display different rates of progression for inflammation and macrocalcification. The interval increase of both FDG SUV<sub>max</sub> and Agatston score in the abdominal aorta was greater than that seen in the thoracic aorta. Furthermore, for the whole aorta the rate of FDG SUV<sub>max</sub> increase was independently associated with visceral fat while the rate of Agatston score increase was associated with age and smoking habit (Ryu et al., 2013). Similarly, a longitudinal FDG-PET/CT study in an oncology cohort (mean follow-up 14.6 ± 3.6 months) found that TBR decreased significantly over this period only in the carotid artery (thoracic aorta, abdominal aorta, and iliac arteries remained unchanged) – though disease activity was low throughout (TBR of 1.26 ± 0.20 reducing to 1.19 ± 0.20) – but Agatston score in all arterial territories increased significantly. This increase was independently associated with hypertension in the thoracic aorta and iliac arteries, but not in the carotid arteries (Hetterich et al., 2015).

Our ability to draw conclusions for the associations between FDG uptake and macrocalcification is in part limited by the large variation in macrocalcification, with no significant difference observed between symptomatic and asymptomatic cohorts (as discussed in the previous chapter). The greater sensitivity of NaF may provide a more sensitive means to detect the interaction between inflammation and active calcification.

#### *4.4.4 Physiological relationship inflammation and microcalcification, and modulation by macrocalcification*

In a retrospective analysis of a cohort of individuals undergoing dual FDG-PET/CT and NaF-PET/CT, 221 asymptomatic atheroma (26 non-calcified, 195 calcified) across all arterial territories were divided into groups based upon macrocalcification (“non-calcified” calcium density <130 HU, “mildly calcified” calcium density 130-399 HU, and “severely calcified” calcium density  $\geq$ 400 HU). The TBR<sub>max</sub> of both tracers was observed to correlate across all lesions ( $r_s=0.5$ ,  $p<0.01$ ). The highest TBR<sub>max</sub> for each tracer was observed in the non-calcified lesions, but no correlation between them was found in these lesions ( $r=0.06$ ,  $p=0.76$ ). However, in mildly calcified and severely calcified plaques FDG and NaF TBR<sub>max</sub> were correlated ( $r=0.7$  and  $r=0.4$  respectively, both  $p<0.01$ ), although tracer uptake was lower. Finally, of interest in future longitudinal studies, NaF TBR<sub>max</sub> increased significantly (and macrocalcification increased, but narrowly missed statistical significance) while FDG TBR<sub>max</sub> decreased by repeat imaging at  $15\pm 4$  months, though it is important to note that individuals taking statins, ezetimibe, or PCSK9 inhibitors were excluded, as were any individuals who developed symptomatic disease between baseline and follow-up scans (Li et al., 2017).

In our study, the bifurcation approach showed FDG uptake falls and NaF rises in regions with higher macrocalcification. When considering the correlation between FDG and NaF uptake, these correlations are statistically significant for SUV in both calcification cohorts, and approaching significance for TBR. As shown by the SUV values, the strength of the association between FDG and NaF uptake at the bifurcation increases between low and high calcification ( $r_s=0.43$  and  $r_s=0.62$  respectively, both  $p<0.05$ ).

Given our relatively small sample it was felt appropriate simply to dichotomise macrocalcification within the bifurcation in order to maximise statistical power to detect a difference and correlations. Larger studies or meta-analyses of FDG and NaF correlations in symptomatic disease would help elucidate this further, but this study demonstrates that macrocalcification influences the strength of these associations and that it is an important factor to include in future studies.

Our observation that the degree of calcification strengthens the association between FDG and NaF uptake in symptomatic cohorts, alongside similar findings by Li et al. in an asymptomatic cohort (Li et al., 2017), raises the question of what pathophysiological interactions are occurring in the plaque. Li et al. hypothesise that their results indicate the progression of plaque from macrophage-induced osteogenic differentiation of smooth muscle cells to cause mineralisation, which is further promoted by ongoing macrophage infiltration, with late changes associated with ongoing inflammation complemented by apoptosis of lipid-laden macrophages inducing calcium deposition in smooth muscle cells (Li et al., 2017, New et al., 2013, Proudfoot et al., 2000). IL-1 $\beta$ , IL-6, IL-8, TNF- $\alpha$ , and TGF- $\beta$  production by macrophages has been implicated in promoting mineralisation of vascular cells (Watson et al., 1994, Parhami et al., 2002, Tintut et al., 2000). Supporting this, inflammation appears to precede mineralisation in *in vivo* animal models (Aikawa et al., 2007).

In apolipoprotein E<sup>-/-</sup> mouse models a strong correlation between macrophage burden and osteogenic activity, as well as spatial co-localisation, was observed. Both increased concomitantly with age and decreased concomitantly with statin treatment. There was also an increase in the concomitant uptake with time ( $r=0.12$  at 20 weeks versus  $r=0.46$  at 30 weeks) (Aikawa et al., 2007). Interestingly, this study also showed an increase in osteogenic activity with age, supporting our findings of age being independently associated with both NaF uptake and macrocalcification.

Like most symptomatic vascular PET/CT studies, our study is limited by relatively small numbers. This is accentuated when diving into sub-groups based upon calcification. The relatively small sample may result in correlations being influenced by outliers, arguably more for symptomatic arteries than for asymptomatic arteries when observing the spread. It would be advantageous to validate this trend in a larger sample.

The above discussion has assumed that the observed FDG uptake entirely reflects inflammation. However, there is a more complex process potentially at play. In more advanced atherosclerotic plaques, increasing necrotic core size, plaque thickness,

distance from the luminal wall, and increased oxygen demand from foam cells, all contribute to hypoxia within the plaque (Leppanen et al., 2006). This hypoxia has recently been imaged using PET using  $^{18}\text{F}$ -fluoromisonidazole (FMISO), a 2-nitroimidazole that undergoes selective bioreduction and accumulates within hypoxic cells (Takasawa et al., 2008). Importantly, higher FMISO uptake has been observed in symptomatic than asymptomatic atheroma and correlated with FDG uptake, consistent with hypoxia as either a contributing factor to inflammation or playing a direct role in FDG uptake (Joshi et al., 2017). Consequently, the FDG uptake in the older, more calcified plaques in our study may be influenced by increasing levels of hypoxia. Hypoxia, and consequent apoptosis, may in turn lead to increased calcification in these more advanced plaques. In this current study it is not possible to measure the relative effects on FDG uptake of inflammation and hypoxia, but future dual FMISO and NaF-PET studies may help elucidate this relationship.

#### *4.4.5 Risk factors affecting FDG uptake*

In contrast to the emerging relationships between vascular risk factors and NaF uptake discussed in the previous chapter, the relationships between the vascular risk factors affecting FDG uptake are well defined. Arguably our cohort, given their high-risk and symptomatic nature, is not the most appropriate cohort in which to evaluate the effect of cardiovascular risk factors on FDG uptake. Instead, larger studies in asymptomatic oncological cohorts are likely to be more reflective of the physiological influences on arterial FDG uptake. However, the results in our cohort do suggest that smoking and the interaction between diabetes and blood sugar were significantly associated with FDG uptake, consistent with previous findings. These findings fall outside the scope of this chapter, and indeed the overall study, but for completeness are considered in further detail in Appendix E.

#### *4.4.6 hsCRP as a biomarker in specific plaque types*

The exploratory endpoint of hsCRP as a biomarker is discussed further in Appendix F.

## 4.5 Summary of findings

Returning to the aims of this chapter, the following areas have been addressed:

1. FDG-PET was found to discriminate between culprit and non-culprit atheroma in our exclusively DWI-lesion positive cohort.
2. FDG uptake was spatially diffuse in contrast to the largely focal uptake of NaF, indicative of two related but distinct pathophysiological processes.
3. It is important to consider the pathophysiological interactions between inflammation, microcalcification, and macrocalcification within a co-localised area rather than on an artery-basis. Consideration of these processes at the carotid bifurcation revealed:
  - a. FDG uptake is significantly lower and NaF uptake significantly higher in bifurcations with higher macrocalcification.
  - b. FDG and NaF uptake correlated with increasing strength of association with increasing macrocalcification.
4. Smoking proved to be risk factor consistently independently associated with FDG uptake. The interaction between diabetes and blood sugar also appeared to have a very mild negative association with FDG uptake.
5. A positive correlation between hsCRP and FDG uptake was observed in arteries with a lower burden of macrocalcification, but not in arteries with more extensive macrocalcification.

The previous two chapters have considered the localised pathophysiology within the carotid plaque. The next step is to consider how these processes relate to both acute and chronic cerebrovascular pathology.

## **Chapter Five: Carotid Atherosclerosis and Small Vessel Disease**

### **5.1 Introduction**

#### *5.1.1 Aims of this chapter*

So far in this thesis we have considered the local implications of tracer uptake for the plaque and its stability. In this next section of the thesis we will now investigate how vascular pathophysiology may have downstream consequences affecting the brain, first considering chronic cerebrovascular disease before addressing acute cerebrovascular pathology in the next chapter. The specific question for this chapter is:

1. Is inflammation within carotid atheroma is associated with the extent of chronic cerebral small vessel disease?

The main hypothesis is:

- i. Increased FDG TBR within the carotid arteries will be associated with more severe chronic small vessel disease (measured using the Fazekas scale).

#### *5.1.2 Introduction to small vessel disease*

Small vessel disease (SVD) represents a spectrum in both its pathophysiology and its clinical consequences. SVD may be defined as “a sporadic intrinsic process affecting small cerebral arterioles, capillaries and sometimes venules” (Wardlaw et al., 2013), though the term has largely become synonymous with ischaemic change resulting from disease of the small arteries and arterioles. Such ischaemic change is typically a late consequence of arteriosclerosis and characterised by changes including fibrinoid necrosis, lipohyalinosis, and microatheroma (Pantoni, 2010).

SVD may include focal lacunar infarcts, accounting for up to 25% of ischaemic strokes, or subcortical vascular disease resulting in diffuse white matter change characterised by neuronal loss, demyelination, and gliosis (Markus et al., 2000).

Imaging of the small vessels themselves has historically proven difficult, though the emergence of 7-T MRI is likely to improve this. Until this technique becomes more widespread, the mainstay of imaging has been with 1.5T or 3T MRI that is able to detect ‘leukoaraiosis,’ the effects on cerebral tissue from diffuse white matter disease. Leukoaraiosis, also known as white matter hyperintensities (WMHs), appear hyperintense on T2-weighted fluid-attenuated inversion recovery (FLAIR) sequences without prominent hypointensity on T1-weighted images (DeBette and Markus, 2010) or periventricular lucency on CT. Leukoaraiosis typically occurs in regions of the brain at the terminal end of penetrating arterioles, primarily the periventricular regions and the centrum semiovale, which will be most vulnerable to hypoperfusion (Pantoni and Garcia, 1997).

The NASCET study provided an estimate of the prevalence and natural history of white matter disease in individuals with symptomatic carotid artery disease. Of 596 (40.6%) participants without evidence of leukoaraiosis at baseline, 21% (18% restricted leukoaraiosis, 3% widespread leukoaraiosis) developed leukoaraiosis over an average follow-up of 6.4 years. These individuals were significantly older than those who did not develop leukoaraiosis. Over a similar time period, 28 (31.5%) of the 89 patients with pre-existing leukoaraiosis at baseline showed radiological progression. The individuals who developed leukoaraiosis were 1.5Times more likely to have a stroke during this follow-up period compared to those who did not develop leukoaraiosis (after adjustment for age and severity of carotid stenosis), with approximately two thirds having large artery aetiology and one third having lacunar strokes (Streifler et al., 2003).

WMHs are common and become increasingly prevalent with age. In a substudy of the Framingham Heart Study, 313 (14%) individuals were found to have extensive WMHs and were older than the cohort without extensive WMHs (DeBette et al., 2010). The link between increasing age and incidental finding of WMHs is well recognised (Habes et al., 2016).

The clinical consequences of ischaemic SVD are numerous. It is a major risk factor for future stroke and dementia, with one large meta-analysis finding hazard ratios of 3.3 [95% CI 2.6 – 4.4] and 1.9 [95% CI 1.3 – 2.8] respectively with WMHs (DeBette

and Markus, 2010). Severity of SVD has also been implicated in cognitive impairment in independently-living elderly individuals (van der Flier et al., 2005), depression (Herrmann et al., 2008, Khalaf et al., 2015, Taylor et al., 2003), gait disturbance and falls (de Laat et al., 2011, Baezner et al., 2008, Blahak et al., 2009), urinary continence (Poggesi et al., 2008), and general functional decline (Inzitari et al., 2009).

Small vessel disease may influence stroke recurrence. In individuals with TIA or minor stroke, white matter disease was independently associated with an increased risk of stroke recurrence after adjustment for cardiovascular risk factors (van Swieten et al., 1992).

Leukoaraiosis has important implications for prognosis after stroke. In individuals who experienced mild strokes, the presence of severe leukoaraiosis was associated with a poorer recovery (both NIHSS and mRS) at 90 days, independent of age (Onteddu et al., 2015). Similar results have been seen in stroke recovery up to six months after adjustment for cardiovascular risk factors, NIHSS, and acute infarct volume (Henninger et al., 2012, Arsava et al., 2009). Individuals with severe leukoaraiosis were 11-times more likely to have final infarct volumes greater than 27 mL (a threshold with sensitivity 0.86 and specificity 0.69 to predict favourable mRS outcomes) with both infarct volume above this threshold and leukoaraiosis being independently associated with poor 90-day mRS outcomes (mRS 3-6) (Henninger et al., 2014), and this effect may be more pronounced in men than women (Henninger et al., 2013). Associated with this, leukoaraiosis was found to correlate with the amount of penumbra that progressed to infarction (Ay et al., 2008). Final infarct volume thresholds associated with 90 day mRS outcomes were significantly larger for individuals with absent/mild versus more extensive leukoaraiosis (Patti et al., 2016). It is also an important consideration affecting the correlation between infarct volume and NIHSS, as well as being influenced by the hemisphere (Helenius and Henninger, 2015, Helenius et al., 2016). Finally, the poor outcomes seen with increasing leukoaraiosis appear to vary between stroke subtypes, with poorer mRS outcomes found across WMH quintiles for large artery atherosclerosis subtypes but not in small vessel and cardioembolic subtypes (Ryu et al., 2017).

### *5.1.3 Relationship between carotid disease and small vessel disease*

A number of studies have considered the relationship between carotid pathology and the development of WMHs, with varying results. In part, these differing findings may be explained by different cohorts and methods, in particular the pattern of WMHs assessed (ipsilateral hemisphere or globally) and what measure of carotid disease is used (such as IMT, presence of plaque, degree of luminal stenosis).

In the 1980s, Fazekas et al. investigated the relationship between carotid disease and white matter disease; finding that the presence of global WMHs were associated with an increased prevalence of asymptomatic subclinical carotid artery disease (<50% stenosis) and lower cerebral blood flow, as well as a history of diabetes, hypertension, and cardiovascular disease. However, no participants were found with carotid artery stenosis of  $\geq 50\%$  (Fazekas et al., 1988). More recently, Romero et al. performed semi-automated volumetric measurement of global WMH burden in a cohort from the Framingham Study and found that ICA IMT, but not CCA IMT, was significantly independently associated with a higher prevalence of large WMHs (OR 1.19, 95% CI 1.03–1.38). Furthermore, asymptomatic ICA stenoses of  $\geq 25\%$  and  $\geq 50\%$  were independently associated with large WMHs (OR 1.76 [95% CI 1.27–2.45] and OR 2.35 [95% CI 1.08–5.13] respectively) after adjustment for cardiovascular risk factors (Romero et al., 2009). Of relevance for later chapters, this study also found stenosis  $>50\%$  to be associated with poorer executive function (but not verbal memory or nonverbal memory) after adjustment for cardiovascular risk factors (Romero et al., 2009).

Manolio et al. found that the extent of global white matter disease (measured using a visual score) was independently associated with ICA IMT, but not degree of stenosis, after adjustment for age, sex, and cardiovascular risk factors. However, the degree of stenosis was associated with WMH burden when adjusted only for age and sex. Interestingly, of those with measurable plaque, the effect of lesion density on white matter burden narrowly missed a significant trend when adjusting for age, sex, and cardiovascular risk profile ( $p=0.07$ ), with calcified lesions associated with the highest burden of white matter disease, but further adjustment for IMT or carotid stenosis reduced this trend further ( $p=0.15$ ) (Manolio et al., 1999). This finding was supported

by later work that found that Agatston score at the carotid bifurcation in neurovascularly asymptomatic trauma patients was not independently associated with white matter change after adjustment for age ( $r=0.07$ ,  $p=0.14$ ) (Fanning et al., 2006). This study also found carotid calcification and white matter score were independently associated with age, a finding replicated in our study.

In the Rotterdam study, Bots et al. considered the right carotid artery only and found an independent association between white matter change and CCA IMT (with an increase of 0.1 mm associated with a 50% increase in the probability of white matter lesions) and the presence of plaque at the carotid bifurcation, but not the degree of luminal stenosis (Bots et al., 1993).

Other studies have not found an association between carotid stenosis and global WMH burden after adjustment for other cardiovascular risk factors in both asymptomatic and stroke cohorts (Lindgren et al., 1994, Schmidt et al., 1992, Adachi et al., 1997). Indeed, in one early study of 31 individuals who had experienced a stroke, significant carotid disease ( $\geq 50\%$  stenosis) was actually less common than in age-matched controls who had stroke but no leukoaraiosis (Bogousslavsky et al., 1987).

In contrast to the global assessment of WMHs, other studies have considered the presence of white matter lesions in the ipsilateral hemisphere to carotid stenosis. In a large substudy of the NASCET study, there was no association found between the degree of leukoaraiosis on CT and the degree of ipsilateral symptomatic carotid stenosis (Streifler et al., 1995). In a more recent study, Potter et al. found no association between carotid stenosis and white matter lesion measured using the Fazekas scale, both before and after adjustment for conventional cardiovascular risk factors (Potter et al., 2012).

The possible roles of plaque morphology and biomechanics in WMH development have been investigated in recent years, with conflicting results. Altaf et al. reported that histologically complicated type VI carotid plaques, in contrast to uncomplicated AHA type V plaques, were associated with an approximate doubling in the number of WMHs in the ipsilateral hemisphere, but the age-adjusted increased WMH volume

narrowly missed statistical significance. Furthermore, the degree of carotid stenosis did not appear to have an effect (Altaf et al., 2006). Later work found that the presence of intraplaque haemorrhage detected on fat-suppressed black-blood T1-weighted MRA was associated with larger WMH volumes in both the ipsilateral and contralateral hemispheres. Again, they found no relationship between WMH volumes and the degree of stenosis (Altaf et al., 2008). In contrast, Patterson et al. performed high-resolution MRI quantification of the carotid plaque morphology and tested the associations with a modified Scheltens score (a semi-quantitative score of lesions incorporating scoring of peri-ventricular disease, white matter lesions in each of the lobes, basal ganglia lesions, and infra-tentorial foci of hyperintensities (Scheltens et al., 1993)), and found no associations between WMH severity and the proportion of lipid core, intraplaque haemorrhage, fibrous cap status, or modified AHA score for the plaque (Patterson et al., 2009).

Recently Rundek et al. have reported that a larger carotid diameter in diastole, suggestive of outward remodeling, was independently associated with global log-transformed WMH volume in a large cohort of stroke-free individuals in the Northern Manhattan Study (Rundek et al., 2017). A large meta-analysis has also shown that carotid artery stiffness was associated with an increased risk of SVD (van Sloten et al., 2015). Once again this association may not be entirely due to haemodynamics, as an association between inflammation and carotid stiffening has been reported and may be contributory (van Bussel et al., 2011, van Bussel et al., 2012).

Berman et al. also considered the vulnerability of the plaque, rather than just the degree of stenosis, and any association with WMHs. Increased carotid plaque strain, detected by ultrasound-based strain imaging and indicative of decreasing plaque stability, was associated with both increased microembolic signals on TCD and increased WMH burden, with the presence of microembolic signals itself being positively associated with WMH volume after adjustment for other cardiovascular factors (Berman et al., 2015).

The apparent differences between IMT, presence and number of plaques, and degree of carotid stenosis was illustrated in a systematic review of 32 studies including 17,721 patients: 7 of 23 studies reported a significant association between carotid

stenosis and leukoaraiosis, 11 of 14 studies reported a significant association between carotid plaque and leukoaraiosis, and 9 out of 9 studies found a significant association between carotid IMT and leukoaraiosis (Liao et al., 2015). Meta-analysis of these subgroup results report positive associations with leukoaraiosis for the presence of plaque (OR 3.53, 95% CI 1.83–6.79) and IMT (mean difference 0.11, 95% CI 0.01–0.22), but curiously produced a negative association with the degree of stenosis (OR 0.53, 95% CI 0.32–0.87) (Liao et al., 2015). The reason, and possible mechanism, for this is not clear. The heterogeneity of the pooled cohort with symptomatic and asymptomatic carotids is one possibility, with the consequent secondary prevention medication (particularly blood pressure control) likely to reduce the development of white matter disease. It may also be indicative of inflammation, rather than stenosis, as a possible mechanism.

#### *5.1.4 Pathophysiology of small vessel disease*

There are several contributing pathophysiological processes proposed in the aetiology of small vessel disease, including (1) hypoperfusion, (2) arteriolosclerosis, and (3) blood-brain barrier permeability. White matter lesions as a straightforward product of cerebral hypoperfusion is a controversial hypothesis, given the lack of a strong positive association between carotid stenosis and leukoaraiosis. In one study carotid stenosis  $\geq 70\%$  was found to be significantly associated with both reduced cerebral blood flow (CBF) and increased leukoaraiosis compared to controls, but the reduction in CBF was not associated with the severity of leukoaraiosis (Patankar et al., 2006). It is likely that the reduced CBF associated with small vessel disease is more local, with MR perfusion imaging having shown reduced white matter but normal grey matter CBF in individuals with ischaemic leukoaraiosis (Markus et al., 2000).

Arteriolosclerosis involves a constellation of pathological changes in small vessels – loss of smooth muscle cells from the tunica media, deposition of fibro-hyaline material, thickening of the vessel wall, and narrowing of the lumen – typically in response to age and hypertension (Pantoni, 2010). Microatheroma may contribute to local hypoperfusion; resulting in chronic, diffuse, subclinical ischaemia that causes incomplete infarction (typified by demyelination, loss of oligodendrocytes, and axonal damage) that produces leukoaraiosis, or acute localised ischaemia resulting in

focal complete infarction and pan-necrosis to produce a lacunar infarct (Pantoni, 2010). The pathophysiology underlying leukoaraiosis, and associated cognitive decline, has been investigated extensively using a range of animal models and injury mechanisms (Hainsworth et al., 2012, Jiwa et al., 2010).

The pathological mechanisms between periventricular white matter lesions and subcortical white matter lesions may differ, with periventricular white matter lesions found to be associated with both the number of carotid plaques and IMT, while neither were associated with subcortical white matter, in a large population study (de Leeuw et al., 2000). This may be due to the greater vulnerability of the periventricular regions in relation to reduced blood flow (Pantoni and Garcia, 1997). However, others have questioned whether different mechanisms are involved or whether differences in distribution represent different stages of disease (Wardlaw et al., 2013).

The final pathology of interest is one that is increasingly recognised and is likely to play a mechanistic role in our cohort; endothelial failure and blood-brain barrier dysfunction.

#### *5.1.5 Endothelial failure, inflammation, and blood-brain barrier dysfunction*

Endothelial dysfunction has been observed both locally and systemically in individuals with SVD. In CADASIL (cerebral autosomal dominant arteriopathy with subcortical infarcts and leukoencephalopathy) - a hereditary arteriopathy – there is evidence of impaired endothelium-dependent vasodilatation in peripheral arteries (Stenborg et al., 2007). Similar findings have been suggested in pilot work in individuals with sporadic SVD, and that systemic endothelial dysfunction correlates with the extent of leukoaraiosis (Zupan et al., 2015). Interestingly, both the cerebrovascular endothelial and systemic endothelial dysfunction found in individuals with lacunar infarcts and matched vascular risk factors were improved with atorvastatin treatment (Pretnar-Oblak et al., 2006). This suggests further pleiotropic effects of statins, such as their anti-inflammatory effect or activation of eNOS (Balakumar et al., 2012).

The potential systemic nature of endothelial dysfunction has implications for the blood-brain barrier (BBB); a network that regulates the transport of metabolites and nutrients into the brain, controls transport of metabolic waste products into the blood, and limits the entry of potentially neurotoxic plasma components and pathogens from the systemic circulation (Zhao et al., 2015). Endothelial cells form the main anatomical element of the BBB, though it is important to note that these endothelial cells are specialised compared to endothelial cells found elsewhere, with continuous intercellular tight junctions, a lack of fenestrations, and low rates of transcytosis (Abbott et al., 2006, Obermeier et al., 2013). Maintenance of the BBB is provided by interaction with astrocytes, pericytes, and extracellular matrix components (Obermeier et al., 2013).

Loss of BBB integrity is observed across a range of CNS pathologies, as well as in normal ageing (Farrall and Wardlaw, 2009), though it remains a subject of debate over whether it is a cause or effect and to what extent it involves a vicious cycle between the two. Oxidative stress may affect BBB integrity either through direct damage to the cells themselves, their interaction through tight junctions, or through promotion of inflammatory cytokines and MMPs (Pun et al., 2009).

MMPs, particularly MMP-9, have been implicated in BBB dysfunction in both acute stroke and in small vessel disease. MMP-9 may be directly involved in disruption of the BBB. At the basal lamina of the BBB unit, type IV collagen and laminin are MMP-9 substrates, and MMP-9 has been implicated in the disruption of the integrity of the BBB (Gidday et al., 2005, Kumari et al., 2011, Guo et al., 2008). The tight junctions between the endothelial cells of the BBB are normally maintained by a variety of specialised proteins, including ZO-1, which has been found to be a MMP-9 substrate (Harkness et al., 2000). Degradation of these tight junctions was reduced in MMP-9 knock-out rats, as was 24-hour infarct volumes (Asahi et al., 2001).

There is evidence of increased BBB permeability in individuals with WMHs, with the highest permeability seen within the centre of WMHs and in those with the most extensive white matter disease (Hanyu et al., 2002, Taheri et al., 2011a, Starr et al., 2003). BBB permeability was also increased in the normal-appearing white matter in

individuals with leukoaraiosis, suggesting that BBB disruption is causative in the development of WMHs (Topakian et al., 2010).

Given the aforementioned role of MMPs, particularly MMP-9, in atheroma destabilisation, we sought to establish the relationship between carotid plaque inflammation measured using FDG-PET/CT and the presence of leukoaraiosis.

## **5.2 Methods**

Methodology for this chapter is discussed in Chapter Two.

## **5.3 Results**

### *5.3.1 Study cohort*

Twenty-six participants were included in this substudy, corresponding to the 26 participant cohort who underwent complete baseline investigations (FDG-PET/CT, NaF-PET/CT, and baseline brain MRI). As a cohort, their overall clinical details were described in previous chapters. For this substudy, the cohort was dichotomised according to the global Fazekas scale: no/mild leukoaraiosis: 15 participants, moderate/severe: 11 participants. The pattern of disease was predominantly periventricular. The clinical characteristics are shown in **Table 5.1**.

	No/mild leukoaraiosis n=15	Moderate/severe leukoaraiosis n=11	Significance
Mean age (SD) (years)	71.5 (±8.5)	79.4 (±9.7)	p=0.04
Number of males (%)	11 (73.3%)	7 (63.3%)	p=0.60
Mean BMI (SD)	26.0 (±4.2)	28.3 (±5.3)	p=0.26
Current/former smoker (%)	10 (66.7%)	7 (63.3%)	p=0.87
Diabetes mellitus (%)	1 (6.7%)	3 (27.3%)	p=0.15
Hypertension (%)	11 (73.3%)	6 (54.5%)	p=0.32
Current statin (%)	7 (46.7%)	2 (18.2%)	p=0.13
Current antiplatelet (%)	5 (33.3%)	3 (27.3%)	p=0.74
History of cardiovascular disease (%)	5 (33.3%)	3 (27.3%)	p=0.74
Total cholesterol	4.55 (±1.3)	4.5 (±0.88)	p=0.91
Median NIHSS (IQR)	5 (12)	4 (8)	p=0.70
Thrombolysed	2 (13.3%)	4 (36.4%)	p=0.17
Modal degree of symptomatic artery stenosis	70-89%	70-89%	
Maximum stenosis in symptomatic artery: CCA ICA	1 (6.7%) 14 (93.3%)	1 (9.1%) 10 (90.9%)	p=0.82
Modal degree of asymptomatic artery stenosis	30-49%	30-49%	
Maximum stenosis in asymptomatic artery: CCA ICA	3 (20%) 12 (80%)	2 (18.2%) 9 (81.8%)	p=0.90
CEA	5 (33.3%)	4 (36.4%)	p=0.87
Mean onset-to-FDG- PET/CT (SD) (days)	9.2 (±4.8)	8.9 (±4.7)	P=0.88

**Table 5.1:** Clinical characteristics according to dichotomised severity of leukoaraiosis.

### 5.3.2 FDG uptake according to leukoaraiosis severity

FDG uptake according the severity of leukoaraiosis is illustrated in **Figure 5.1** and full results shown in **Table 5.2**.

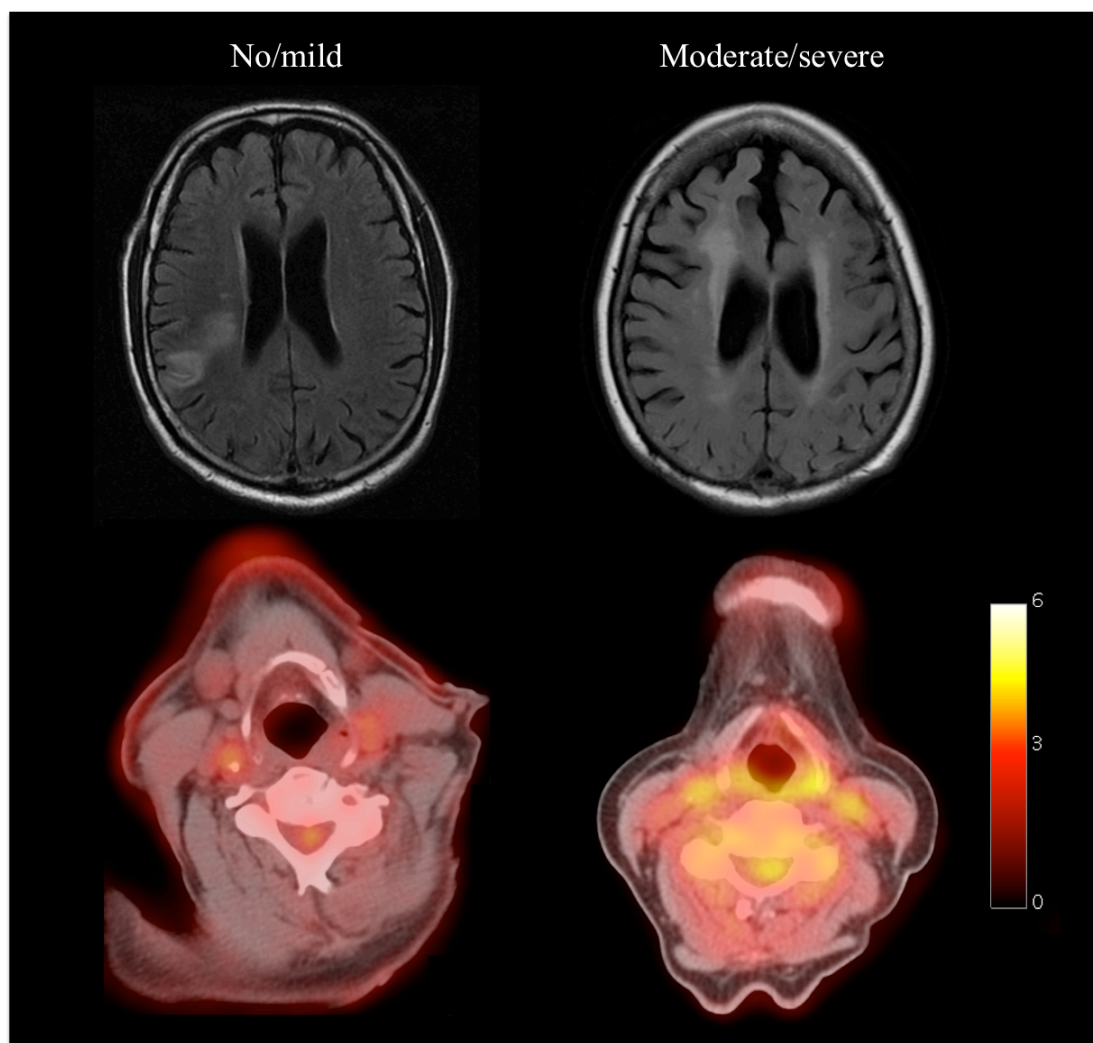


**Figure 5.1: Carotid FDG uptake according to leukoaraiosis severity.** Left: no/mild leukoaraiosis (hyperintensity represents acute infarction) with associated low carotid FDG uptake; Right: moderate/severe leukoaraiosis with higher associated carotid FDG uptake. Both FDG-PET/CT images are set at the same scale, with the scale bar showing FDG SUV.

	Culprit artery				Non-culprit artery		
	No/mild leukoaraiosis	Moderate/severe leukoaraiosis	Sig.		No/mild leukoaraiosis	Moderate/severe leukoaraiosis	Sig.
SHS SUV <sub>max</sub>	2.21 (0.53)	2.63 (0.60)	p=0.38		1.86 (0.24)	2.28 (0.53)	p=0.04
MDS SUV <sub>max</sub>	2.15 (0.52)	2.56 (0.55)	p=0.36		1.82 (0.26)	2.22 (0.53)	p=0.02
WV SUV <sub>max</sub>	1.90 (0.45)	2.04 (0.47)	p=0.41		1.68 (0.23)*	1.99 (0.30)*	p<0.01
SHS SUV <sub>mean</sub>	1.94 (0.31)	2.19 (0.51)	p=0.26		1.66 (0.24)	2.28 (0.53)	p=0.04
MDS SUV <sub>mean</sub>	1.87 (0.31)	2.11 (0.48)	p=0.26		1.82 (0.26)	2.22 (0.53)	p=0.02
WV SUV <sub>mean</sub>	1.67 (0.24)*	1.92 (0.42)*	p=0.09		1.68 (0.23)*	1.99 (0.30)*	p<0.01
SHS TBR <sub>max</sub>	2.07 (0.38)	2.23 (0.57)	p=0.20		1.79 (0.32)*	2.09 (0.53)*	p=0.11
MDS TBR <sub>max</sub>	2.03 (0.30)	2.19 (0.56)	p=0.15		1.74 (0.31)*	2.03 (0.48)*	p=0.10
WV TBR <sub>max</sub>	1.85 (0.36)*	2.01 (0.49)*	p=0.35		1.60 (0.27)*	1.82 (0.30)*	p=0.06
SHS TBR <sub>mean</sub>	1.74 (0.37)	1.91 (0.24)	p=0.15		1.58 (0.25)*	1.88 (0.38)*	p=0.04
MDS TBR <sub>mean</sub>	1.72 (0.31)	1.84 (0.24)	p=0.12		1.54 (0.24)*	1.82 (0.36)*	p=0.04
WV TBR <sub>mean</sub>	1.59 (0.28)*	1.75 (0.37)*	p=0.22		1.42 (0.23)*	1.61 (0.24)*	p=0.047

**Table 5.2:** Comparison of FDG uptake between Fazekas score dichotomisation for culprit and non-culprit carotid arteries. All values expressed as median (IQR), except where denoted with an asterisk, where values are mean (SD).

There was no significant difference in blood sugar at the time of scan between cohorts (no/mild leukoaraiosis: median 5.7 mmol/L [IQR 1.9], moderate/severe leukoaraiosis: 5.4 mmol/L [IQR 1.05],  $p=0.96$ ).

### *5.3.3 Logistic regression of vascular features in relation to leukoaraiosis severity*

It is important to consider the terms included within the logistic regression, most of which have already been discussed in Chapter Four. We included an interaction term between FDG uptake and the interaction of diabetes mellitus and blood sugar, as this was observed in our cohort. We also included the following interaction terms for variables that were found on the revised multivariable analysis in Chapter Four: (1) FDG and smoking, (2) statin use and total cholesterol. No association between FDG uptake and age was observed with our cohort, and repeat univariable correlation showed no correlation between these variables (all  $p>0.05$ ). Hence, they were treated as independent variables within our logistic regression model. All other variables in the univariable analysis (with total cholesterol used for lipid profile) were included in the model prior to backwards elimination.

Results for the regression analysis for non-culprit ('asymptomatic') arteries are shown in **Table 5.3**.

<b>SHS TBR<sub>max</sub></b>	AIC = 20.1		Adjusted R <sup>2</sup> = 0.63 (p<0.001)
	<b>Coefficient</b>	<b>OR (95% CI)</b>	<b>Significance</b>
FDG uptake	1.40	4.06 [1.91 – 8.63]	p<0.01
Smoking	1.82	6.21 [1.42 – 27.1]	p=0.03
Age	0.03	1.03 [1.02 – 1.05]	p<0.001
Current statin	-0.34	0.71 [0.54 – 0.93]	p=0.02
FDG:Smoking interaction	-1.06	-	p=0.02
FDG:diabetes:blood sugar interaction	0.07	-	p<0.001
<b>MDS TBR<sub>max</sub></b>	AIC = 20.6		Adjusted R <sup>2</sup> = 0.62 (p<0.001)
	<b>Coefficient</b>	<b>OR (95% CI)</b>	<b>Significance</b>
FDG uptake	1.38	3.98 [1.84 – 8.59]	p<0.01
Smoking	1.71	5.55 [1.23 – 25.0]	p=0.04
Age	0.03	1.03 [1.02 – 1.05]	p<0.001
Current statin	-0.35	0.71 [0.54 – 0.93]	p=0.02
FDG:Smoking interaction	-1.00	-	p=0.03
FDG:diabetes:blood sugar interaction	0.07	-	p<0.001
<b>WV TBR<sub>max</sub></b>	AIC = 23.9		Adjusted R <sup>2</sup> = 0.57 (p<0.001)
	<b>Coefficient</b>	<b>OR (95% CI)</b>	<b>Significance</b>
FDG uptake	1.82	6.18 [2.10 – 18.2]	p<0.01
Age	0.03	1.03 [1.01 – 1.05]	p<0.01
Current statin	-0.33	0.72 [0.53 – 0.97]	p=0.04
Diabetes	0.76	2.15 [1.41 – 3.28]	p<0.01
Smoking	2.12	8.34 [1.14 – 61.0]	p=0.05
FDG:smoking interaction	-1.30	-	p=0.05
<b>SHS TBR<sub>mean</sub></b>	AIC = 19.0		Adjusted R <sup>2</sup> = 0.65 (p<0.001)
	<b>Coefficient</b>	<b>OR (95% CI)</b>	<b>Significance</b>
FDG uptake	1.76	5.84 [2.47 – 13.79]	p<0.001
Smoking	1.97	7.19 [1.41 – 36.63]	p=0.03
Age	0.03	1.03 [1.02 – 1.05]	p<0.001
Diabetes	0.76	2.15 [1.48 – 3.12]	p<0.001
Current statin	-0.29	0.75 [0.57 – 0.98]	p=0.05
FDG:diabetes:blood sugar	-1.23	-	p=0.02

interaction			
<b>MDS TBR<sub>mean</sub></b>	AIC = 19.1		Adjusted R <sup>2</sup> = 0.64 (p<0.001)
	<b>Coefficient</b>	<b>OR (95% CI)</b>	<b>Significance</b>
FDG uptake	1.74	5.70 [2.40 – 13.54]	p<0.001
Smoking	1.86	6.40 [1.25 – 32.79]	p=0.04
Age	0.03	1.03 [1.02 – 1.05]	p<0.001
Current statin	-0.31	0.74 [0.56 – 0.97]	p=0.04
Diabetes	0.76	2.13 [1.46 – 3.12]	p<0.001
FDG:diabetes:blood sugar interaction	-1.18	-	p=0.03
<b>WV TBR<sub>mean</sub></b>	AIC = 24.6		Adjusted R <sup>2</sup> = 0.56 (p<0.001)
	<b>Coefficient</b>	<b>OR (95% CI)</b>	<b>Significance</b>
FDG uptake	2.14	8.48 [2.28 – 31.57]	p<0.01
Age	0.03	1.03 [1.02 – 1.05]	p<0.001
Current statin	-0.33	0.72 [0.53 – 0.97]	p=0.04
Diabetes	0.75	2.11 [1.36 – 3.28]	p<0.01
Smoking	2.34	10.37 [1.09 – 98.21]	p=0.06
FDG:diabetes:blood sugar interaction	-1.60	-	p=0.05

**Table 5.3:** Multiple logistic regression for factors associated with severity of leukoaraiosis for the non-culprit artery.

Repeating the analyses with interaction terms between (1) FDG uptake and age, and (2) FDG uptake and current statin use did not affect the results.

We also performed the same regression analysis on the culprit ('symptomatic') arteries (**Table 5.4**).

<b>SHS TBR<sub>max</sub></b>	AIC = 29.2		Adjusted R <sup>2</sup> = 0.48 (p<0.01)
	<b>Coefficient</b>	<b>OR (95% CI)</b>	<b>Significance</b>
FDG uptake	0.74	2.09 [1.07 – 4.10]	p=0.04
Age	0.03	1.03 [1.01 – 1.05]	p<0.01
Current statin	-0.43	0.65 [0.47 – 0.90]	p=0.02
Smoking	1.12	3.08 [0.69 – 13.71]	p=0.16
FDG:Smoking interaction	-0.60	-	p=0.13
FDG:diabetes:blood sugar interaction	0.06	-	p<0.01
<b>MDS TBR<sub>max</sub></b>	AIC = 28.9		Adjusted R <sup>2</sup> = 0.48 (p<0.01)
	<b>Coefficient</b>	<b>OR (95% CI)</b>	<b>Significance</b>
FDG uptake	0.76	2.14 [1.07 – 4.28]	p=0.04
Age	0.03	1.03 [1.01 – 1.05]	p<0.01
Current statin	-0.44	0.64 [0.46 – 0.89]	p=0.02
Smoking	1.09	2.96 [0.66 – 13.32]	p=0.17
FDG:Smoking interaction	-0.60	-	p=0.14
FDG:diabetes:blood sugar interaction	0.06	-	p<0.01
<b>WV TBR<sub>max</sub></b>	AIC = 27.2		Adjusted R <sup>2</sup> = 0.49 (p<0.001)
	<b>Coefficient</b>	<b>OR (95% CI)</b>	<b>Significance</b>
FDG uptake	0.42	1.52 [1.06 – 2.17]	p=0.03
Age	0.03	1.03 [1.01 – 1.05]	p<0.01
Current statin	-0.46	0.63 [0.46 – 0.86]	p<0.01
FDG:diabetes:blood sugar interaction	0.05	-	p<0.01
<b>SHS TBR<sub>mean</sub></b>	AIC = 23.9		Adjusted R <sup>2</sup> = 0.57 (p<0.001)
	<b>Coefficient</b>	<b>OR (95% CI)</b>	<b>Significance</b>
FDG uptake	1.46	4.30 [1.67 – 11.06]	p<0.01
Smoking	1.94	6.98 [1.19 – 41.03]	p=0.04
Age	0.03	1.03 [1.02 – 1.05]	p<0.01
Current statin	-0.41	0.67 [0.50 – 0.89]	p=0.01
FDG:Smoking interaction	-1.20	-	p=0.03
FDG:diabetes:blood sugar interaction	0.07	-	p<0.01

<b>MDS TBR<sub>mean</sub></b>	AIC = 24.7		Adjusted R <sup>2</sup> = 0.56 (p<0.001)
	<b>Coefficient</b>	<b>OR (95% CI)</b>	<b>Significance</b>
FDG uptake	1.52	4.59 [1.65 – 12.78]	p<0.01
Smoking	2.04	7.71 [1.21 – 49.29]	p=0.04
Age	0.03	1.03 [1.01 – 1.05]	p<0.01
Current statin	-0.41	0.66 [0.50 – 0.89]	p=0.01
FDG:Smoking interaction	-1.28	-	p=0.03
FDG:diabetes:blood sugar interaction	0.07	-	p<0.01
<b>WV TBR<sub>mean</sub></b>	AIC = 22.6		Adjusted R <sup>2</sup> = 0.59 (p<0.001)
	<b>Coefficient</b>	<b>OR (95% CI)</b>	<b>Significance</b>
FDG uptake	1.91	6.72 [2.05 – 22.00]	p<0.01
Smoking	2.17	8.79 [1.20 – 64.37]	p=0.046
Age	0.03	1.03 [1.02 – 1.05]	p<0.001
Current statin	-0.41	0.66 [0.50 – 0.87]	p<0.01
FDG:Smoking interaction	-1.49	-	p=0.04
FDG:diabetes:blood sugar interaction	0.08	-	p<0.01

**Table 5.4:** Multiple logistic regression for factors associated with severity of leukoaraiosis for the culprit artery.

Again, there was no interaction seen between FDG uptake and age or between FDG uptake and current statin use in our regression model.

#### 5.3.4 NaF uptake according to leukoaraiosis severity

Given the association found between FDG uptake and WMHs, we also looked at whether there was any accompanying association between NaF uptake and WMHs (**Table 5.5**).

	Culprit artery				Non-culprit artery		
	No/mild leukoaraiosis	Moderate/severe leukoaraiosis	Sig.		No/mild leukoaraiosis	Moderate/severe leukoaraiosis	Sig.
SHS SUV <sub>max</sub>	1.94 (0.80)	2.28 (0.35)	p=0.54		1.51 (0.59)*	1.99 (0.44)*	p=0.36
MDS SUV <sub>max</sub>	1.80 (0.71)	2.07 (0.34)	p=0.54		1.70 (0.57)*	1.88 (0.41)*	p=0.35
WV SUV <sub>max</sub>	1.46 (0.38)*	1.48 (0.43)*	p=0.88		1.19 (0.38)	1.46 (0.46)	p=0.22
SHS SUV <sub>mean</sub>	1.70 (0.52)	1.82 (0.42)	p=0.47		1.80 (0.50)*	1.70 (0.41)*	p=0.31
MDS SUV <sub>mean</sub>	1.55 (0.50)	1.68 (0.37)	p=0.44		1.43 (0.47)*	1.62 (0.38)*	p=0.27
WV SUV <sub>mean</sub>	1.19 (0.26)	1.17 (0.35)	p=1.00		1.08 (0.28)	1.22 (0.36)	p=0.10
SHS TBR <sub>max</sub>	2.61 (0.87)	2.96 (0.60)	p=0.28		2.37 (0.78)*	2.62 (0.53)*	p=0.35
MDS TBR <sub>max</sub>	2.44 (0.77)	2.81 (0.69)	p=0.24		2.23 (0.73)*	2.48 (0.50)*	p=0.32
WV TBR <sub>max</sub>	1.84 (0.47)	1.85 (0.14)	p=0.72		1.58 (0.51)	1.92 (0.40)	p=0.18
SHS TBR <sub>mean</sub>	2.18 (0.62)	2.37 (0.80)	p=0.33		1.97 (0.60)*	2.23 (0.45)*	p=0.22
MDS TBR <sub>mean</sub>	2.10 (0.56)	2.25 (0.64)	p=0.33		1.87 (0.58)*	2.13 (0.41)*	p=0.19
WV TBR <sub>mean</sub>	1.57 (0.28)	1.57 (0.17)	p=0.65		1.43 (0.39)	1.63 (0.23)	p=0.08

**Table 5.5:** Comparison of NaF uptake between dichotomised leukoaraiosis severity cohorts for culprit and non-culprit carotid arteries. All values expressed as median (IQR), except where denoted with an asterisk, where values are mean (SD).

### *5.3.5 Macrocalcification and leukoaraiosis severity*

There was no significant difference between the no/mild and moderate/severe leukoaraiosis cohorts for total carotid artery calcification score (494 [IQR 1492.5] versus 909 [IQR 742],  $p=0.68$ ), culprit carotid artery calcification score (258 [IQR 803] versus 408 [IQR 556],  $p=0.92$ ), or non-culprit carotid artery calcification score (294 [IQR 425] versus 328 [IQR 485.5],  $p=0.76$ ).

### *5.3.6 hsCRP and leukoaraiosis severity*

There was no significant difference between hsCRP levels between the no/mild and moderate/severe leukoaraiosis cohorts (median 5.6 [IQR 8.27] versus 5.89 [IQR 28.46] mg/L,  $p=0.16$ ).

### *5.3.7 Fazekas score reproducibility*

Inter-rater reproducibility of Fazekas scoring had an ICC of 0.91.

## **5.4 Discussion**

### *5.4.1 Association between carotid plaque physiology and white matter disease*

Our study is novel in relating the presence of leukoaraiosis to the physiological activity within atherosclerosis measured using PET, rather than simply the degree of anatomical luminal stenosis, and we demonstrate an independent association between FDG TBR and the severity of leukoaraiosis.

This relationship, and the regression models themselves, were stronger when considering the contralateral non-culprit (“asymptomatic”) artery rather than the culprit artery. This is likely to be because the non-culprit artery in effect acts as a ‘barometer’ for the systemic inflammation within atherosclerosis, as suggested by the correlation between neighbouring arterial regions demonstrated by Rudd et al. (Rudd et al., 2009). In contrast, the symptomatic artery represents a region with potentially

disproportionate uptake. The median absolute difference between MDS  $TBR_{max}$  in culprit and non-culprit arteries was 0.24 (IQR 0.37) and median relative ratio was 1.13 (IQR 0.18). This represents a peak focus of disease that may not be reflective of the general burden of atherosclerotic inflammation either spatially or temporally. This is reflected in the superior applicability of the models in the non-culprit artery. Furthermore, the above results indicate that as one moves towards more diffuse measures of FDG uptake in the culprit artery (i.e.  $TBR_{mean}$  rather than  $TBR_{max}$ , and the median WV), the results start to approximate those of the non-culprit artery. Given that WMH represent chronic disease developing over a longer time course than acute stroke, it is therefore likely that the non-culprit artery gives a better representation of the long-term pathophysiology to which the brain has been exposed.

Previous studies have demonstrated an association between FDG uptake and serum MMP-9 concentrations. The mean of whole carotid artery FDG  $TBR_{max}$  was found to have a moderate correlation with serum MMP-9 concentrations ( $r=0.50$ ,  $p=0.01$ ) and an inverse correlation with serum plasminogen activator inhibitor-1 ( $r=-0.39$ ,  $p=0.03$ ) (Rudd et al., 2009). Other studies have also reported an association between FDG uptake and serum MMP-9 concentrations (Saito et al., 2013, Wu et al., 2012). Supporting these findings is the observation that a 12-week course of atorvastatin 40 mg/day resulted in a significant reduction in both atheroma TBR and MMP-9 over the study period, and that there was a moderate correlation between the reduction in plaque TBR and reduction in MMP-9 concentration ( $r=0.56$ ,  $p=0.05$ ) (Wu et al., 2012).

Given the aforementioned relationships between MMP-9 levels and BBB dysfunction, and between BBB permeability and the development of leukoaraiosis, there is a clear line of potential causality between the chronic inflammation within carotid plaques and the development of leukoaraiosis.

These findings are consistent with the global impression that leukoaraiosis is associated with carotid IMT and the presence of plaques, but not stenosis (which may be physiological heterogeneous, with some a spectrum of plaque vulnerability). The contradictory findings with stenosis may be due to different plaque activity within different cohorts, as we have shown that FDG uptake does not appear to relate to the

degree of luminal stenosis (Chapter Four). It may also agree with studies demonstrating an association between plaque morphology and the development of leukoaraiosis, as FDG (Silvera et al., 2009, Figueroa et al., 2012).

Furthermore, in the studies investigating the association between carotid disease and leukoaraiosis discussed above, it is not always considered what medication an individual is taking (or may have started taking during a follow-up period). This may have implications for the physiological status of the carotid plaque and may contribute to conflicting results between studies only assessing the degree of luminal stenosis. For example, in Schmidt et al. (Schmidt et al., 1992), the stroke cohort are likely to have received secondary prevention and this may contribute to carotid stenosis being found to be significant on univariable but not multivariable analysis. Similarly, Adachi et al. recruited participants who had evidence of unilateral or bilateral carotid stenosis but there is no comment on medication or inclusion of these in the regression analyses (Adachi et al., 1997).

#### *5.4.2 Risk factors associated with leukoaraiosis*

Previous reviews have highlighted the inconsistent associations found between leukoaraiosis and a range of vascular risk factors (Grueter and Schulz, 2012). A notable exception is age, which most studies have found to be independently associated with the development of WMHs (Padovani et al., 1997, Lindgren et al., 1994, van Swieten et al., 1992). Our results agree with this, finding a small but significant increase in the odds of moderate/severe leukoaraiosis for each year increase in age. This risk did not appear to interact with FDG uptake in the carotid in this cohort, supporting our earlier regression analysis of vascular risk factors.

Hypertension has previously been reported to be strongly associated with WMHs (Padovani et al., 1997, Streifler et al., 1995, Adachi et al., 1997). We did not find this association in our study. The most likely reason is the combination of a small sample in individuals where there is a high prevalence of hypertension (by nature of our cohort compared to the general population).

### 5.4.3 Limitations

We observed a high prevalence of extensive white matter disease in this study (42%). This is likely due to the overall age of the cohort (mean age  $74.8 \pm 9.7$ ) and age of the moderate/severe leukoaraiosis cohort (mean age  $79.4 \pm 9.70$ ). Furthermore, our cohort is not reflective of the general population. Our cohort demonstrates both a higher burden of cardiovascular risk factors and all have had a stroke. However, we feel that this study provides important mechanistic insights with potential implications in this high-risk vascular group.

Our study was performed in individuals with symptomatic carotid stenosis rather than in an asymptomatic cohort. Increased FDG uptake has been reported following myocardial infarction (Dutta et al., 2012), though whether FDG uptake increases in plaques following stroke is unclear. However, we observed no difference between TIA and stroke patients in terms of carotid FDG uptake, suggesting that cerebral infarction is not associated with higher uptake than those with ischaemia but no infarction. Hence, due to this and the consistent lower uptake in the non-culprit artery that we observed in this cohort, we feel that the non-culprit artery is likely to remain a reasonable barometer for atherosclerotic inflammation for an individual rather than be dramatically upregulated following an ischaemic event.

Our study measured carotid FDG uptake at a single time point, and that time point was after the stroke event. Consequently, it is not possible to consider the length of exposure between the inflamed carotid plaque and any BBB disruption and development of leukoaraiosis. The radiation exposure involved in PET scanning precludes repeated imaging, and this is further compounded by uncertainty over when to image. This is likely to preclude future longitudinal PET studies investigating this association. Whether structural imaging and serum MMP-9 concentrations are sufficiently predictive would be an important area to consider in future work.

We did not measure MMP-9 levels in our study, so cannot assess its role as a potential mechanistic link between FDG uptake and leukoaraiosis. Previous work demonstrating an association between FDG uptake and MMP-9 would suggest this as

a plausible mechanism, but future work should include this biomarker to support this hypothesis.

#### *5.4.4 Implications and future work*

Although white matter disease may be a ubiquitous incidental finding and appear asymptomatic, it is not a benign pathology. A number of studies have found increased severity of WMH is associated with poorer cognitive performance, particularly executive tasks (Brickman et al., 2011). Cognitive performance for our cohort is discussed in Chapter Seven.

In this part of the study we have not measured white matter volumes, nor have we investigated the three-month repeat imaging for changes in leukoaraiosis burden. Semi-quantitative scale changes have been shown to be less reliable for measuring progression of white matter disease (Gouw et al., 2008), so future work assessing this will require use of either progression scales (such as the Rotterdam Progression Scale) or volumetric measurement. Furthermore, our study is limited by a small sample size. To corroborate these findings, replication in a larger sample is required.

A possible association between inflamed plaques and leukoaraiosis and cognitive decline would strengthen an argument for screening for disease and early intervention. This intervention would likely require systemic treatment with anti-inflammatory medication rather than surgical intervention given the diffuse nature of the disease. For example, the presence of ‘asymptomatic’ carotid disease on ultrasound, potentially risk stratified by MMP-9 concentrations, may facilitate targeted therapy with systemic treatment to reduce the metabolic activity of the plaque and its downstream consequences.

## 5.5 Summary of findings

This chapter has discussed:

1. The severity of leukoaraiosis is associated with FDG within carotid plaques, with the non-culprit atheroma providing a better model of the association.
2. This association remains independent of other cerebrovascular risk factors.
3. Age is also independently associated with leukoaraiosis severity, while statins appear to be negatively associated (independent of their effect upon FDG uptake within the carotid plaque).

While leukoaraiosis represents a chronic cerebrovascular pathology, similar mechanisms may also influence acute cerebrovascular pathology. We will explore this in the next chapter.

**Chapter Six:**  
**Inflammation within Carotid Atheroma and the Evolution of Cerebral  
Infarction**

**6.1 Introduction**

*6.1.1 Aims of this chapter*

The previous chapter considered how inflammation within the carotid plaque was associated with chronic cerebrovascular disease. Many of the mechanisms are also implicated in acute infarction. This chapter will consider how inflammation influences the evolution of the acute ischaemic lesion, and has the following specific questions:

1. Is inflammation within the carotid plaque associated with the size of the initial infarct?
2. How does inflammation within the carotid plaque affect the evolution of the infarct during the early post-stroke period?

The main hypothesis is:

- i. Higher FDG uptake within the carotid plaque will be associated with larger infarct volumes.

The secondary hypothesis is:

- ii. Higher FDG uptake within the carotid plaque will be associated with greater expansion of the infarct in the early (three month) post-stroke period.

*6.1.2 Inflammatory pathways contributing to infarct volumes*

The inflammatory response to stroke has been acknowledged for some time. In contrast, the contribution of inflammation to stroke pathogenesis is now increasingly recognised. There are a number of proposed pathways through which inflammation

may affect the volume of the acute infarct and its development. These pathways may occur in isolation or may interact. The main pathways we will consider in this chapter are:

1. The microglial response around the infarct.
2. Disruption of the BBB in acute stroke.
3. Infiltration of circulating inflammatory cells into the CNS.
4. Thromboinflammation.

Each of these will be considered in greater detail below, along with how imaging has informed our understanding of the evolution of the infarct.

### *6.1.3 The microglial response in ischaemic stroke*

Ischaemic injury to the brain provokes a reactive gliosis involving activation of astrocytes and microglia, the resident macrophages of the central nervous system. Although neuroinflammation is generally seen as contributing to pathophysiology in most neurodegenerative conditions, it is believed to play a complex dual role following ischaemia.

Microglia express toll-like receptors (TLRs) and nucleotide-binding oligomerisation domain-like receptors (NOD-like receptors, NLRs) that detect pathogenic material or cellular injury, such as ischaemic injury (Taylor and Sansing, 2013). The post-infarct microglial response involves two arms: pro-inflammatory M1 and anti-inflammatory M2 microglial subtypes, with an early polarisation from M2 to M1 subtypes in peri-infarct regions (Wang and Feuerstein, 2004). M1 microglia exert neurotoxic effects through production of reactive oxygen species and pro-inflammatory proteins, which may themselves perform a dual role. MMP-9 produced by M1 microglia exacerbates ischaemic damage by promoting blood-brain barrier disruption and neuronal death in the early stages post-infarct, but may promote brain regeneration and neurovascular remodeling in latter phases (Amantea et al., 2009, Kriz, 2006). The M2 microglial subtype is predominantly protective, with associated neuronal survival (Xia et al., 2015).

Arterial occlusion from a thromboembolus results in ischaemia, cell death, generation of ROS, and release of cellular contents from necrotic cells (Iadecola and Anrather, 2011, Bours et al., 2006). ATP released from necrotic cells has been found to trigger cytokine release (particularly IL-6) from microglia via stimulation of the P2X7 receptor (Shieh et al., 2014). Further activation of microglia comes from cellular release of danger-associated molecular pattern molecules (DAMPs) that bind to TLRs (Marsh et al., 2009).

A dynamic spatiotemporal relationship has been observed in microglial activation and phenotype following ischaemic injury in mouse models. M2 microglia were found early after ischaemia but ischaemic neurons promoted polarisation to the M1 phenotype over time with accumulation of these cells around the peri-infarct boundary (Hu et al., 2012). Furthermore, induction of microglia to the M2 phenotype was associated with improved neuronal survival compared to those induced to the M1 phenotype, and that a mix of M1 and M2 microglia also promoted neuronal survival (Hu et al., 2012).

Hu et al. further demonstrated a polarisation of microglia/macrophages towards the destructive M1 phenotype from the neuroprotective M2 phenotype after transient cerebral ischaemia in mouse models (Hu et al., 2012). A pro-inflammatory environment, such as that found with arterial atheroma, also modulated the activation of bone marrow-derived macrophages, with pro-inflammatory cytokines and increasing age associated with macrophage infiltration across the blood-brain barrier in rat models (Barrett et al., 2015).

Minocycline, a tetracycline derivative with anti-inflammatory and anti-microglial activity, reduced MMP-9, TNF- $\alpha$ , and IL-1 $\beta$  levels in hypertensive rats following MCAO compared to the contralateral cortex and was associated with enhanced expression of tight junction proteins at the BBB, lower BBB permeability, activation of neuroprotective microglia/macrophage phenotypes, and smaller infarct sizes (Yang et al., 2015b). Whilst the results of this study demonstrate the detrimental role of inflammation in stroke, the wide-ranging effects of minocycline means that it is difficult to know whether its observed beneficial effects are driven primarily through

effects on blood brain barrier permeability or the modulation of microglia/macrophage subtypes.

However, the purpose of this section is not to consider simply how microglia are activated following ischaemic injury, but rather to explore how inflammation may affect this interaction. As alluded to above, it has been found possible to trigger microglial polarisation *in vitro* using either pro-inflammatory cytokines (e.g. IFN- $\gamma$  and LPS) or anti-inflammatory cytokines (IL-4 and IL-10) (Ding et al., 1988, Durafourt et al., 2012).

Animal studies have suggested that cerebrovascular risk factors and co-morbidities may in some way 'prime' the brain for larger strokes. Drake et al. found that corpulent (obese, atherosclerotic-prone, and insulin-resistant) rats had increased intracerebral  $^{18}\text{F}$ -DPA-714 uptake on PET and immunohistochemical evidence of microglial activation (Drake et al., 2011). DPA-714 ( $^8\text{F}$ -*N,N*-diethyl-2-(2-(4-(2-fluoroethoxy)phenyl)-5,7-dimethylpyrazolo[1,5- $\alpha$ ]pyrimidin-3-yl)acetamide) is a radiotracer specific to the translocator protein 18kDa (TSPO) expressed on microglia (and upregulated upon their activation) but not astrocytes following ischaemic damage (Stephenson et al., 1995), and hence this finding suggests increased activity is present before any acute infarction.

Furthermore, the same study reported a pilot study of eight humans (four with vascular risk factors but no evidence of brain damage and four age-matched controls) who underwent PK11195 intracerebral PET. The risk-factor group had higher CRP at baseline (mean 9.15 [range 12.99-13.26] versus 0.76 [range 0.55-1.00]) and three of the four had increased PK11195 signal across neocortical areas but not periventricular or white matter regions (compared to none of the four controls) (Drake et al., 2011).

#### *6.1.4 Disruption of the blood-brain barrier in acute stroke*

As well as its presence in the carotid plaque, MMP-9 is produced by activated microglia (Liuzzi et al., 1999, Gottschall and Deb, 1996). The previous chapter has discussed the association observed between MMP-9 concentrations and FDG uptake

in a carotid plaque, as well as the proposed direct effects of MMP-9 upon the BBB. Here we consider its role, and the integrity of the BBB, following acute infarction.

Animal models indicate that BBB dysfunction after stroke is biphasic: an initial increased permeability within hours of infarct and then a second period 24-72 hours following infarct (Kuroiwa et al., 1985, Belayev et al., 1996). This biphasic response may reflect the different mechanisms at work: reperfusion-driven oxidative stress at the BBB is associated with increased transcytosis in endothelial cells through an increase in the number of vesicles facilitating this process (Engelhardt and Sorokin, 2009). In rat models, this has been shown to occur as early as 6-hours after stroke while tight junction disruption, typically mediated by MMP-9 and MMP-3, occurred two days later (Knowland et al., 2014, Rosenberg and Yang, 2007). In a hypertensive rat model, MMP-2 was found in peri-vascular astrocytes and was increased within three hours of reperfusion. In contrast, MMP-3 and MMP-9 (localising to activated microglia and ischaemic neurons, with MMP-9 also detected at endothelial cells and neutrophils) were observed at 24 hours (Rosenberg et al., 2001). Similar results were seen by Yang et al., and that BBB degradation was reversed by inhibition of MMPs (Yang et al., 2007).

In humans, Brouns et al. found that MMP-9 levels rose in the acute phase and then dropped over the first 24-hours in those individuals with no stroke progression and a 3-month mRS 0-2. In contrast, those with stroke progression and poor mRS outcomes had a different temporal pattern, with MMP-9 levels increasing over the first 72-hours (for individuals with stroke progression) or steady over the first 72-hours (for individuals with 3-month mRS  $\geq 3$ ) (Brouns et al., 2011). Post-mortem human brains have shown a spatial distribution of MMP-9, with MMP-9 concentrations found highest in the infarct core, though peri-infarct tissue also showed elevated levels compared to the contralateral hemisphere (Rosell et al., 2006).

In acute cardioembolic stroke, MMP-9 concentrations independently predicted final NIHSS ( $r=0.486$ ,  $p=0.002$ ), correlated with infarct volume ( $r=0.385$ ,  $p=0.02$ ), and were significantly reduced by reperfusion (Montaner et al., 2001a). MMP-9 levels are implicated in an increased risk of late haemorrhagic transformation in cardioembolic strokes (Montaner et al., 2001b), and large parenchymal haemorrhage after

thrombolysis (Montaner et al., 2003). The addition of tissue plasminogen activator was found to upregulate MMP-9 concentrations *in vivo* in rats, and in human cerebral microvascular endothelial cells *in vitro* (Tsuji et al., 2005, Wang et al., 2003). Further work has suggested that a potential disruption of BBB permeability by tPA is not limited to the MMP-9 pathway (Copin et al., 2011). Finally, a small study has found a positive correlation between post-stroke MMP-9 concentration and serum tau protein concentration, itself likely representing the extent of neuronal injury and stroke volume (Kurzepa et al., 2010, Bitsch et al., 2002).

Pre-ischaemic exercise was shown to have a beneficial effect in rats, with associated increased expression of TIMP-1, reduced BBB permeability, and smaller infarct volumes (Guo et al., 2008). In similar models, pre-ischaemic exercise was associated with reduced cerebral oedema after transient MCAO via down-regulation of aquaporin-4 (Shamsaei et al., 2017, He et al., 2014, Han et al., 2015). Pharmacological reduction of MMP-9 in rat models was also associated with a reduction in post-ischaemic oedema and improved neurological recovery (Zhou et al., 2011, Liu et al., 2014).

#### *6.1.5 Infiltration of circulating inflammatory cells into the central nervous system*

The infiltration of systemic activated cytotoxic monocyte/macrophages into the brain remains controversial but several studies have suggested movement across a disrupted blood brain barrier directly contributing to hypoxic neuronal cell damage in animal models of stroke (Tanaka et al., 2003, Girard et al., 2013).

The migration of neutrophils post-stroke remains subject to debate. Enzmann et al. found polymorphonuclear granulocytes were limited to the luminal surfaces and perivascular surfaces with no evidence of parenchymal infiltration in human specimens (Enzmann et al., 2013). However, the post-mortem study by Rosell et al. found neutrophils present in the core of the infarct, and localised with MMP-9 (Rosell et al., 2006). Furthermore, the role of neutrophils is also unclear. When administered acutely, neutrophil inhibition reduced infarct volumes after transient MCAO in rats, but not with permanent occlusion (Jiang et al., 1998). However, a similar approach in human stroke patients did not improve clinical recovery. No measurement of infarct

volumes was conducted, but given the lack of clinical efficacy in this large sample it is unlikely an effect was present (Krams et al., 2003). Hence, this implies a limited contribution from neutrophils.

Diet-induced atherosclerosis was found to be associated with leucocyte infiltration in ApoE<sup>-/-</sup> mice, and the presence of atherosclerotic plaques was associated with microglial and leucocyte recruitment within the brain (Drake et al., 2011).

#### *6.1.6 Inflammatory cytokines and their effect on infarct development*

Non-cellular aspects of immunity may also contribute to injury. Chemokine-binding protein (binding a broad spectrum of CC, CXC, XC, MCP-1 and CXCL2/MIP-2 chemokines) have been found to reduce infiltration of leukocytes transiently and reduce infarct volumes, with improved neurological recovery observed (Lee et al., 2015b). Such chemokines have also been found to be upregulated in atherosclerosis and indicated in its pathophysiology (Lin et al., 2014).

#### *6.1.7 Thromboinflammation*

In addition to inflammatory cell infiltration, another mechanism affecting the size of the infarct and severity of the stroke is thrombus burden. The contribution of inflammation within the plaque through thromboinflammation has been discussed previously (Chapter 1.1.8). Essentially, the thrombogenic environment appears to be influenced by both the level of inflammation (either locally to the plaque or systemically) and morphology of the atheroma. Hence, higher macrophage-driven atheroma inflammation may be associated with increased thrombus formation and/or size, and in consequently associated with larger infarcts.

#### *6.1.8 Understanding the evolution of acute ischaemic stroke using PET*

Just as PET imaging of carotid atherosclerosis has informed our understanding of the physiological processes taking place *in vivo*, so too has intracerebral PET informed our understanding of the pathophysiology of acute ischaemic injury, the salvageable

penumbra, and subsequent neuroinflammation. All are relevant in this context and discussed below.

#### *6.1.8.1 PET imaging of the developing acute infarct*

Early  $^{15}\text{O}$ -PET measuring tissue perfusion (using CBF) and cerebral metabolic rate of oxygen consumption ( $\text{CMRO}_2$ ) identified three distinct groups within a cohort of ischaemic stroke patients: extensive areas of greatly reduced CBF and  $\text{CMRO}_2$ , extensive moderate CBF reduction but only focal areas of marked  $\text{CMRO}_2$  reduction, and increased CBF with only focal areas showing reduced  $\text{CMRO}_2$ . Although small studies, these patterns showed proof of principle and matched clinical outcomes, with poor, variable, and good outcomes respectively, independent of initial neurological status (Marchal et al., 1993, Marchal et al., 1995). Acute  $^{15}\text{O}$ -PET has found salvageable penumbra of 10-52% of the infarct volume up to 17 hours post-infarct (Marchal et al., 1996). The presence of penumbra beyond conventional clinical thrombolysis windows has led some to call for prospective studies assessing the selection for thrombolysis on a case-by-case physiological basis (most likely assessed by CT-perfusion) rather than absolute time cut-offs (Agarwal et al., 2015, Bivard et al., 2015).

Findings of co-registered  $^{15}\text{O}$ -PET and DWI indicated that the DWI lesion includes not only an infarct core but also penumbra (Guadagno et al., 2004). This was supported by further work mapping CBF,  $\text{CMRO}_2$ , and oxygen extraction fraction (OEF) onto DWI lesions, which showed a heterogeneous pattern of oxygen metabolism within the DWI lesion, as well as variation between individuals, and supported the patterns of oxygen metabolism seen in the earlier  $^{15}\text{O}$ -PET work (Guadagno et al., 2005, Marchal et al., 1993), indicating that some of DWI lesion may be reversible and represent salvageable tissue. Furthermore, “misery perfusion” – regions exhibiting low CBF, high OEF, but only moderately reduced  $\text{CMRO}_2$  – was the predominant pattern in the DWI lesion and was also seen outside of the DWI ROI, suggesting that there is regional variation determining different perfusion thresholds (Guadagno et al., 2005, Guadagno et al., 2006). The use of voxel-based mapping in  $^{15}\text{O}$ -PET has allowed thresholds for irreversible tissue damage to be estimated: 8.43 mL/100 mL/min for CBF and 0.87 mL/100 mL/min for  $\text{CMRO}_2$ . Infarcts with higher

proportions of voxels below these thresholds were associated with larger final infarct volumes and poorer neurological outcomes at two months (Marchal et al., 1999). The reversibility of DWI lesions, and the salvageable tissue it may contain, has important implications for both research methodology, including our study, that measure infarct volume as an endpoint, as well as clinical practice.

Penumbra mapping has advanced with the introduction of newer PET radiotracers. FMISO, accumulating within hypoxic but viable cells, was seen in the peripheries of the infarct in 9 of 13 of individuals scanned within 48-hours of infarction but none of those scanned at 6-11 days (Read et al., 1998). Studies using MRI data to strictly define the infarct core found FMISO uptake in both the penumbra and core (Alawneh et al., 2014). FMISO studies have demonstrated temporospatial evolution of infarction, with tracer uptake moving from the centre to the periphery with increasing time post-infarct (Markus et al., 2003, Markus et al., 2004a). This suggests that there is a region of the core that, while unsalvageable and destined to infarct, still demonstrates sufficient activity for FMISO uptake. Conversely, FMISO uptake is also seen in tissue beyond the symptomatic tissue on co-registered MRI, suggesting oligoemic tissue also experiences hypoxia (Alawneh et al., 2014, Spratt et al., 2009).

FMISO uptake in the acute stage may also be able to predict outcomes, with 80% of those with uptake showing an increase in infarct volume compared to no infarct growth in those without FMISO uptake (Lee et al., 2015a). This is unsurprising given the nature of the tissue represented by FMISO uptake, but given the limited ability of MRI to differentiate between penumbra and benign oligoemia, this method for quantifying vulnerable tissue may have important implications for prognostication. A higher proportion of surviving tissue measured by FMISO-PET at 12 hours and between 12-48 hours post-stroke was associated with better neurological recovery at 3 months (Markus et al., 2004b). Supporting the findings of  $^{15}\text{O}$ -PET, FMISO uptake has also been seen up to 131 hours after the stroke (Lee et al., 2015a). These findings suggest potentially salvageable tissue beyond current clinical intervention windows.

Impaired functional recovery despite successful reperfusion of penumbra is an important clinical issue.  $^{11}\text{C}$ -flumazenil (FMZ) offers insights into this phenomenon by allowing *in vivo* imaging of selective neuronal loss (SNL) following ischaemic

stroke. SNL differs from “pannecrosis” – the widespread necrosis of cells including glial cells, neurons, and white matter – in that there is selective death of neurons but other cells and the extracellular matrix are preserved (Baron et al., 2014). This selective loss of neurons is associated with poorer functional recovery as these activated neurons, found predominantly in the peri-infarct cortical areas, determine neuroplasticity after stroke (Cramer, 2008).

FMZ is an antagonist to the benzodiazepine binding site of gamma aminobutyric acid-type A (GABA-A) receptors, mainly found on neurons. Consequently, SNL results in decreased FMZ uptake. FMZ-PET shows potential in differentiating unsalvageable tissue from viable penumbra, with the region of decreased FMZ uptake corresponding with final infarct volume (Heiss et al., 1998). The ability to differentiate between viable and non-viable tissue has implications for reperfusion therapy. In 11 patients undergoing thrombolysis with decreased CBF, only the 4 individuals with decreased FMZ uptake showed evolution to an infarct (Heiss et al., 2000).

FMZ-PET has suggested significant SNL in salvaged penumbra, with the reduction in FMZ binding proportional to acute-stage hypoperfusion and resulting in reduced neuronal activation on MRI (Guadagno et al., 2008, Carrera et al., 2013). Such findings have clear ramifications for the functional recovery in such salvaged penumbra, as well as a potential mechanism to explain mismatch of functional deficit and radiological findings in the sub-acute to chronic setting.

Similar findings associated with carotid stenosis have been seen with decreased FMZ binding borderzone territories with reduced CBF but without evidence of infarction, suggesting that haemodynamic compromise from large artery disease may be associated with SNL (Kuroda et al., 2004).

FMZ-PET has informed our understanding of oedema formation after middle cerebral artery infarction. The use of infarct volume as the conventional predictor for malignant oedema has a low positive predictive value. In contrast, FMZ-PET within 24-hours of infarct found that volume of severe ischaemia, rather than total perfusion deficit, predicted development of malignant oedema with a high positive predictive value (Dohmen et al., 2012).

#### 6.1.8.2 PET imaging of post-infarct neuroinflammation

Imaging neuroinflammation *in vivo* is possible through the use of PK11195 targeting translocator protein (TSPO) expressed on microglia (and upregulated upon their activation) but not astrocytes following ischaemic damage (Stephenson et al., 1995). The temporal pattern of microglial activity in humans post-infarct with PK11195-PET shows minimal binding within 72-hours, increasing within a week before falling by 25-30 days (Price et al., 2006). The spatial distribution of tracer uptake mirrored that described in hypoxia, with uptake initially seen in the core at 7-14 days before the peri-infarct zone showed a higher degree of uptake in the sub-acute phase. Importantly, there was also increased tracer uptake in the contralateral hemisphere at latter time points, suggesting that neuroinflammation extends beyond the infarct (Price et al., 2006, Thiel and Heiss, 2011). Similar temporal patterns were seen by Gerhard et al., though spatial evolution of PK11195 uptake showed movement from the peri-ischaemic region to increasing overlap with the MRI-defined infarct region (Gerhard et al., 2005). This study, along with others, suggests longterm microglial activation remote from the infarct up to 150 days post-infarct (Gerhard et al., 2005, Pappata et al., 2000).

It is important to note that differences in spatial patterns may be due to a combination of small samples and slightly different time intervals, potentially catching different stages of systemic infiltration. More recent animal studies demonstrated a lack of PK11195 in the infarct core, instead localising to normoperfused peri-infarct regions and co-localising with increased FDG uptake suggesting increased energy demand in these regions (Schroeter et al., 2009). However, caution should again be exercised when comparing binding behavior between species.

Remote microglial activation likely indicates Wallerian degeneration along anatomically-connected neural networks (Katchanov et al., 2003, Weishaupt et al., 2016). Co-registering PK11195 with diffusion tensor imaging (DTI), which images the direction of water diffusion in order to identify neural tracts, after subcortical infarction showed uptake occurred only in an antegrade direction and only if the pyramidal tracts were affected, suggesting the spread of activated microglia is specific

to affected tracts rather than a non-specific disseminated response (Radlinska et al., 2009, Thiel et al., 2010). The extent of remote microglial activation appears independent of infarct size or clinical severity. One clinical study has shown differing clinical patterns depending upon the location of activated microglial activity; initial PK11195 uptake in the tracts was associated with improved clinical outcomes while persistent tracer uptake in the infarct was associated with poorer clinical outcomes (Thiel et al., 2010).

Quantification of these temporospatial patterns of PK11195 uptake is challenging due to non-specific binding, resulting in sub-optimal signal-to-noise ratios, and difficulty in defining a reference region for comparison, hence study results should be interpreted with this caveat. Newer second-generation TSPO radioligands have increased specificity (resulting in improved signal-to-noise) and advantageous pharmacokinetics. However, an emergent physiological factor has limited their wider adoption. <sup>11</sup>C-PBR28 was shown to have improved specificity by a dual PK11195 and PBR28 rat study (Imaizumi et al., 2007), but subsequent work comparing receptor binding between animal models and humans found receptor binding to be markedly lower in humans compared to monkeys, and that there was variation in the human binding with some showing no specific binding (Fujita et al., 2008). Subsequent studies have revealed polymorphism in the gene Ala147Th that results in high-affinity and low-affinity binders, with heterozygous individuals displaying intermediate affinity binding (Owen et al., 2011, Kreisl et al., 2013). In contrast, PK11195 does not appear to have variable affinity as it binds to a different site on the TSPO (Owen et al., 2010). These findings show it is important to exercise caution when comparing tracer pharmacokinetics between different animal species and humans, as well as human subject comparisons.

The short half-life of <sup>11</sup>C-labeled radiotracers has important implications for research and clinical use. The half-life of 20.38 minutes for PK11195 means that an on-site cyclotron is essential (Chauveau et al., 2008). In contrast, the 110-minute half-life of <sup>18</sup>F-labeled radiotracers makes imaging possible without a cyclotron onsite. One example is <sup>18</sup>F-*N,N*-diethyl-2-(2-(4-(2-fluoroethoxy)phenyl)-5,7-dimethylpyrazolo[1,5- $\alpha$ ]pyrimidin-3-yl)acetamide (DPA-714). DPA-714 rapidly accumulates within the infarct, with detectable uptake reaching a peak 5 minutes after

tracer injection, and supports earlier findings that the extent of microglial activation does not correlate with the size of the infarct (Ribeiro et al., 2014). No direct comparison between PK11195 and DPA-714 has been performed in humans, though direct comparison in rat models shows DPA-714 to have a superior signal-to-noise ratio (Boutin et al., 2013, Chauveau et al., 2009).  $^{11}\text{C}$ -vinpocetine demonstrated higher uptake in infarct core, peri-infarct region, and contralateral hemisphere than PK11195 in human subjects post-infarct, though the difference did not reach statistical significance (Gulyas et al., 2012b, Gulyas et al., 2012a). Newer TSPO ligands, such as  $^{18}\text{F}$ -GE-180, have shown superiority to PK11195 in animal models but their application within humans is yet to be seen. Furthermore, it remains to be seen if DPA-714, vinpocetine, and GE-180 are also affected by variable TSPO affinity.

#### *6.1.9 Pathophysiology of MRI lesions*

It is believed that the different pathophysiologies of post-infarct oedema may have different patterns of lesions on MRI. Cytotoxic oedema, and the consequent reduction in extracellular water content, reduces the diffusivity of water molecules and increases the signal on DWI without a change in T2 signal. In contrast, vasogenic oedema and the associated increased tissue water content increases T2 and FLAIR signals (Ayata and Ropper, 2002). FLAIR lesions have been found to have a high sensitivity for detecting cerebral ischaemia (Noguchi et al., 1997), but typically occur at a later time point. DWI hyperintensities are believed to occur within minutes of insult, while in rat models undergoing permanent MCAO, it took 3.5 hours for T2 hyperintensities to develop (Loubinoux et al., 1997).

## **6.2 Methods**

Methodology for this chapter is discussed in Chapter Two.

## 6.3 Results

### 6.3.1 Study cohort

This aspect of the study considers three cohorts: (1) the cohort of 26 participants who underwent complete baseline investigations, (2) the cohort of 24 participants who underwent complete baseline and follow-up imaging, and (3) the cohort of 19 participants who had baseline FLAIR volumes  $>1\text{mL}$  (**Figure 6.1**). No infarct appeared consistent with a lacunar subtype in terms of size and location.

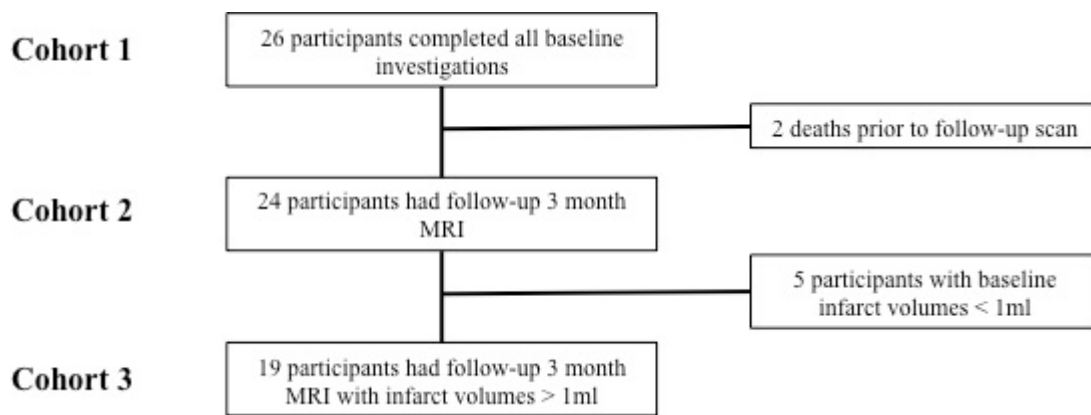


**Figure 6.1:** Derivation of cohorts in the ischaemic lesion volume part of the study.

Cohort one was used for investigating baseline DWI and FLAIR lesion volumes in relation to FDG uptake, cohort two was used for investigating follow-up FLAIR lesion volumes in relation to FDG uptake, and cohort 3 was used for comparing the change in FLAIR lesion volumes.

Clinical characteristics of each cohort are shown below (**Table 6.1**). Although groups are not directly compared, statistical analysis for significant trends across the groups are included for completeness (these cohorts did not differ significantly in relation to their clinical characteristics).

	<b>Cohort 1 (n=26)</b>	<b>Cohort 2 (n=24)</b>	<b>Cohort 3 (n=19)</b>	<b>Sig.</b>
Mean age (SD)	74.8 (9.7)	73.5 (8.9)	73.6 (9.4)	p=0.90
Male sex	18 (69.2%)	18 (75%)	14 (73.7%)	p=0.94
Median BMI (IQR)	26 (3.9)	26 (3.4)	25.8 (3.2)	p=0.98
Smoking history	17 (65.4%)	16 (66.7%)	12 (63.2%)	p=0.71
Diabetes mellitus	4 (15.4%)	3 (12.5%)	2 (10.5%)	p=1.00
Hypertension	17 (65.4%)	16 (66.7%)	11 (57.9%)	p=0.77
Current statin	9 (34.6%)	9 (37.5%)	6 (31.6%)	p=0.80
Current antiplatelet	8 (30.8%)	7 (29.2%)	4 (21.1%)	p=0.79
Cardiovascular history	8 (30.8%)	7 (29.2%)	4 (21.1%)	p=0.79
Mean symptom-scan time (SD) (days)	7.2 (3.8)	7 (3.6)	6.9 (2.7)	p=0.99
CEA	9 (34.6%)	9 (37.5%)	8 (42%)	p=0.75
Thrombolysis	6 (23.1%)	6 (25%)	5 (26.3%)	p=1.00

**Table 6.1:** Clinical characteristics of each cohort.

Follow-up imaging was performed at a median of 98 (IQR 12.5) days following stroke onset.

### 6.3.2 Baseline infarct volumes

In our cohort the median baseline DWI total volume was 3.38 mL (IQR 17.14 mL). The median baseline FLAIR total volume was significantly larger at 5.96 mL (IQR 16.80 mL) ( $p=0.04$ ), with a median difference of 0.30 mL (IQR 2.26 mL). The median FLAIR:DWI ratio was 1.32 (IQR 0.79).

If considering only the baseline primary lesion, the range of DWI volumes was slightly lower, predominantly in the range of DWI volumes. The median DWI lesion volume was 3.34 mL (IQR 5.96 mL) and median FLAIR lesion volume was 5.96 mL

(IQR 17.08 mL) ( $p=0.003$ ). The median absolute difference between FLAIR and DWI lesion was 0.30 mL (IQR 1.89 mL) and median FLAIR:DWI ratio 1.32 (IQR 0.78).

### 6.3.3 Follow-up infarct volumes and evolution

Comparing median total FLAIR volumes at baseline and at three months showed a significant decrease in lesion volume (5.96 mL [IQR 16.80 mL] versus 2.38 mL [IQR 19.23 mL] respectively,  $p=0.04$ ). Similar results were seen when comparing median primary lesion FLAIR volumes at baseline and three-month follow-up (5.96 mL [IQR 17.08 mL] versus 2.05 mL [IQR 19.23 mL] respectively,  $p=0.04$ ).

In contrast, there was no significant difference seen between baseline total DWI volumes and follow-up total FLAIR volumes ( $p=0.62$ ) or between baseline primary lesion DWI volumes and follow-up primary lesion FLAIR volume ( $p=0.99$ ). In fact, baseline and follow-up DWI volumes were strongly correlated: baseline DWI total lesion volume and follow-up FLAIR total lesion volume ( $r_s=0.76$ ,  $p<0.001$ ), and DWI primary lesion volume and follow-up FLAIR primary lesion volume ( $r_s=0.77$ ,  $p<0.001$ ).

### 6.3.4 Relationship between FDG uptake and baseline DWI volume

The relationships between FDG TBR measures and baseline DWI total lesion volume and baseline DWI primary lesion volume are shown below (**Tables 6.2** and **6.3**).

	Symptomatic carotid			Asymptomatic carotid	
	$r_s$	Sig.		$r_s$	Sig.
SHS TBR <sub>max</sub>	0.17	$p=0.45$		0.30	$p=0.17$
MDS TBR <sub>max</sub>	0.13	$p=0.55$		0.28	$p=0.20$
WV TBR <sub>max</sub>	0.25	$p=0.24$		0.14	$p=0.53$
SHS TBR <sub>mean</sub>	0.23	$p=0.29$		0.22	$p=0.32$
MDS TBR <sub>mean</sub>	0.23	$p=0.30$		0.22	$p=0.30$
WV TBR <sub>mean</sub>	0.20	$p=0.37$		0.16	$p=0.48$

**Table 6.2:** Correlations between FDG TBR measures and baseline DWI total lesion volume.

	Symptomatic carotid			Asymptomatic carotid	
	r <sub>s</sub>	Sig.		r <sub>s</sub>	Sig.
SHS TBR <sub>max</sub>	0.14	p=0.52		0.27	p=0.21
MDS TBR <sub>max</sub>	0.10	p=0.64		0.26	p=0.22
WV TBR <sub>max</sub>	0.24	p=0.26		0.12	p=0.57
SHS TBR <sub>mean</sub>	0.20	p=0.36		0.20	p=0.36
MDS TBR <sub>mean</sub>	0.19	p=0.38		0.20	p=0.36
WV TBR <sub>mean</sub>	0.17	p=0.45		0.14	p=0.52

**Table 6.3:** Correlations between FDG TBR measures and baseline DWI primary lesion volume.

### 6.3.5 Relationship between FDG uptake and baseline FLAIR volume

The relationships between FDG TBR measures and baseline FLAIR total lesion volume and baseline FLAIR primary lesion volume are shown below (**Tables 6.4 and 6.5**).

	Symptomatic carotid			Asymptomatic carotid	
	r <sub>s</sub>	Sig.		r <sub>s</sub>	Sig.
SHS TBR <sub>max</sub>	0.24	p=0.25		0.39	p=0.06
MDS TBR <sub>max</sub>	0.22	p=0.30		0.38	p=0.07
WV TBR <sub>max</sub>	0.38	p=0.07		0.27	p=0.19
SHS TBR <sub>mean</sub>	0.30	p=0.15		0.32	p=0.13
MDS TBR <sub>mean</sub>	0.30	p=0.16		0.31	p=0.14
WV TBR <sub>mean</sub>	0.28	p=0.19		0.25	p=0.25

**Table 6.4:** Correlations between FDG TBR measures and baseline FLAIR total lesion size.

	Symptomatic carotid			Asymptomatic carotid	
	$r_s$	Sig.		$r_s$	Sig.
SHS TBR <sub>max</sub>	0.22	p=0.31		0.38	p=0.07
MDS TBR <sub>max</sub>	0.19	p=0.38		0.36	p=0.08
WV TBR <sub>max</sub>	0.36	p=0.08		0.26	p=0.22
SHS TBR <sub>mean</sub>	0.27	p=0.20		0.30	p=0.15
MDS TBR <sub>mean</sub>	0.26	p=0.21		0.29	p=0.17
WV TBR <sub>mean</sub>	0.25	p=0.24		0.24	p=0.27

**Table 6.5:** Correlations between FDG TBR measures and baseline FLAIR primary lesion size.

### 6.3.6 Relationship between FDG uptake and baseline DWI and FLAIR mismatch

Associations between FDG TBR and the difference between DWI and FLAIR volumes at baseline were calculated for total lesion volumes (**Table 6.6**) and primary lesion volumes (**Table 6.7**).

	Symptomatic carotid			Asymptomatic carotid	
	$r_s$	Sig.		$r_s$	Sig.
SHS TBR <sub>max</sub>	0.18	p=0.47		0.09	p=0.72
MDS TBR <sub>max</sub>	0.19	p=0.44		0.04	p=0.87
WV TBR <sub>max</sub>	0.22	p=0.38		0.13	p=0.60
SHS TBR <sub>mean</sub>	0.05	p=0.86		0.09	p=0.74
MDS TBR <sub>mean</sub>	0.08	p=0.75		0.05	p=0.83
WV TBR <sub>mean</sub>	-0.02	p=0.93		-0.07	p=0.77

**Table 6.6:** Correlations between FDG TBR measures and difference in volume between FLAIR and DWI total lesion volumes.

	Symptomatic carotid			Asymptomatic carotid	
	$r_s$	Sig.		$r_s$	Sig.
SHS TBR <sub>max</sub>	0.25	p=0.32		0.10	p=0.69
MDS TBR <sub>max</sub>	0.25	p=0.32		0.04	p=0.87
WV TBR <sub>max</sub>	0.20	p=0.43		0.15	p=0.55
SHS TBR <sub>mean</sub>	0.12	p=0.64		0.07	p=0.79
MDS TBR <sub>mean</sub>	0.16	p=0.53		0.05	p=0.84
WV TBR <sub>mean</sub>	0.01	p=0.98		-0.03	p=0.90

**Table 6.7:** Correlations between FDG TBR measures and difference in volume between FLAIR and DWI primary lesion volumes.

### 6.3.7 Relationship between FDG uptake and follow-up FLAIR volume

The relationships between FDG TBR measures and follow-up FLAIR total lesion volume and follow-up FLAIR primary lesion volume are shown below (**Tables 6.8** and **6.9**).

	Symptomatic carotid			Asymptomatic carotid	
	$r_s$	Sig.		$r_s$	Sig.
SHS TBR <sub>max</sub>	0.31	p=0.14		0.48	p=0.02
MDS TBR <sub>max</sub>	0.29	p=0.17		0.47	p=0.02
WV TBR <sub>max</sub>	0.49	p=0.02		0.36	p=0.08
SHS TBR <sub>mean</sub>	0.39	p=0.06		0.38	p=0.07
MDS TBR <sub>mean</sub>	0.39	p=0.07		0.38	p=0.07
WV TBR <sub>mean</sub>	0.36	p=0.09		0.35	p=0.10

**Table 6.8:** Correlations between FDG TBR measures and follow-up FLAIR total lesion size.

	Symptomatic carotid			Asymptomatic carotid	
	r <sub>s</sub>	Sig.		r <sub>s</sub>	Sig.
SHS TBR <sub>max</sub>	0.29	p=0.17		0.47	p=0.02
MDS TBR <sub>max</sub>	0.27	p=0.21		0.46	p=0.03
WV TBR <sub>max</sub>	0.48	p=0.02		0.35	p=0.09
SHS TBR <sub>mean</sub>	0.37	p=0.08		0.37	p=0.07
MDS TBR <sub>mean</sub>	0.36	p=0.08		0.37	p=0.08
WV TBR <sub>mean</sub>	0.33	p=0.12		0.33	p=0.11

**Table 6.9:** Correlations between FDG TBR measures and follow-up FLAIR primary lesion size.

### 6.3.8 Relationship between FDG uptake and FLAIR lesion evolution

Of the 24 participants with baseline and follow-up FLAIR volumes, 5 (20.8%) had initial FLAIR volumes below 1 mL and were excluded from primary analysis. Of the remaining 19 participants, 12 (63.2%) demonstrated a decrease in FLAIR volume at repeat imaging, with the remainder seen to have an increase in FLAIR volume between the two time points. In the group with a FLAIR volume increase, the median percentage increase was 19.5% (IQR 124%). For those with a decrease in FLAIR volume, the median volume decrease was 61.8% (IQR 64.7%).

Alternatively, if those with a volume change of  $\pm 10\%$  from baseline are considered as a separate “no change” cohort, 10 (52.6%) participants showed a FLAIR volume decrease, 5 (26.3%) showed no change in volume, and 4 (21.1%) showed an increase in FLAIR volume between baseline and repeat imaging.

The relationships between FDG TBRs are shown for volume change (mL) in the total lesion volume (**Table 6.10**) and primary lesion volume (**Figure 6.2, Table 6.11**).

	Symptomatic carotid			Asymptomatic carotid	
	$r_s$	Sig.		$r_s$	Sig.
SHS TBR <sub>max</sub>	0.31	p=0.19		0.47	p=0.04
MDS TBR <sub>max</sub>	0.31	p=0.19		0.52	p=0.02
WV TBR <sub>max</sub>	0.45	p=0.05		0.57	p=0.01
SHS TBR <sub>mean</sub>	0.44	p=0.06		0.47	p=0.04
MDS TBR <sub>mean</sub>	0.42	p=0.08		0.49	p=0.04
WV TBR <sub>mean</sub>	0.51	p=0.03		0.71	p=8.9x10 <sup>-4</sup>

**Table 6.10:** Correlations between FDG TBR and FLAIR total volume change (mL).

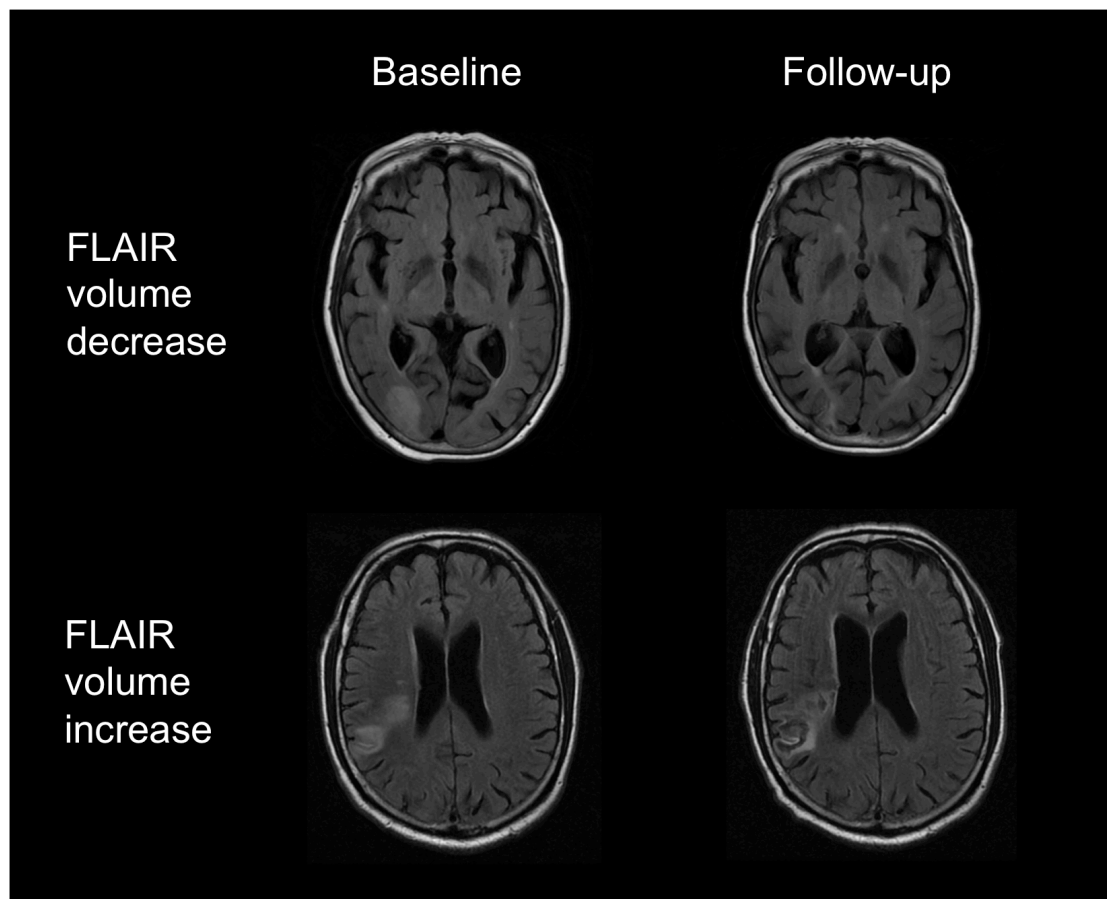


**Figure 6.2: FLAIR lesion evolution.** Axial FLAIR images at baseline (left column) and follow-up (right column) illustrating FLAIR primary lesion volume decrease (top row) or increase (bottom row).

	Symptomatic carotid			Asymptomatic carotid	
	$r_s$	Sig.		$r_s$	Sig.
SHS TBR <sub>max</sub>	0.38	p=0.11		0.51	p=0.03
MDS TBR <sub>max</sub>	0.38	p=0.11		0.57	p=0.01
WV TBR <sub>max</sub>	0.49	p=0.04		0.61	p=0.007
SHS TBR <sub>mean</sub>	0.51	p=0.03		0.50	p=0.03
MDS TBR <sub>mean</sub>	0.48	p=0.04		0.52	p=0.02
WV TBR <sub>mean</sub>	0.56	p=0.01		0.72	p=6.8x10 <sup>-4</sup>

**Table 6.11:** Correlations between FDG TBR and FLAIR primary lesion volume change.

Using the asymptomatic WV TBR<sub>mean</sub> as an example, the relationship can be visualised as per **Figure 6.3**.

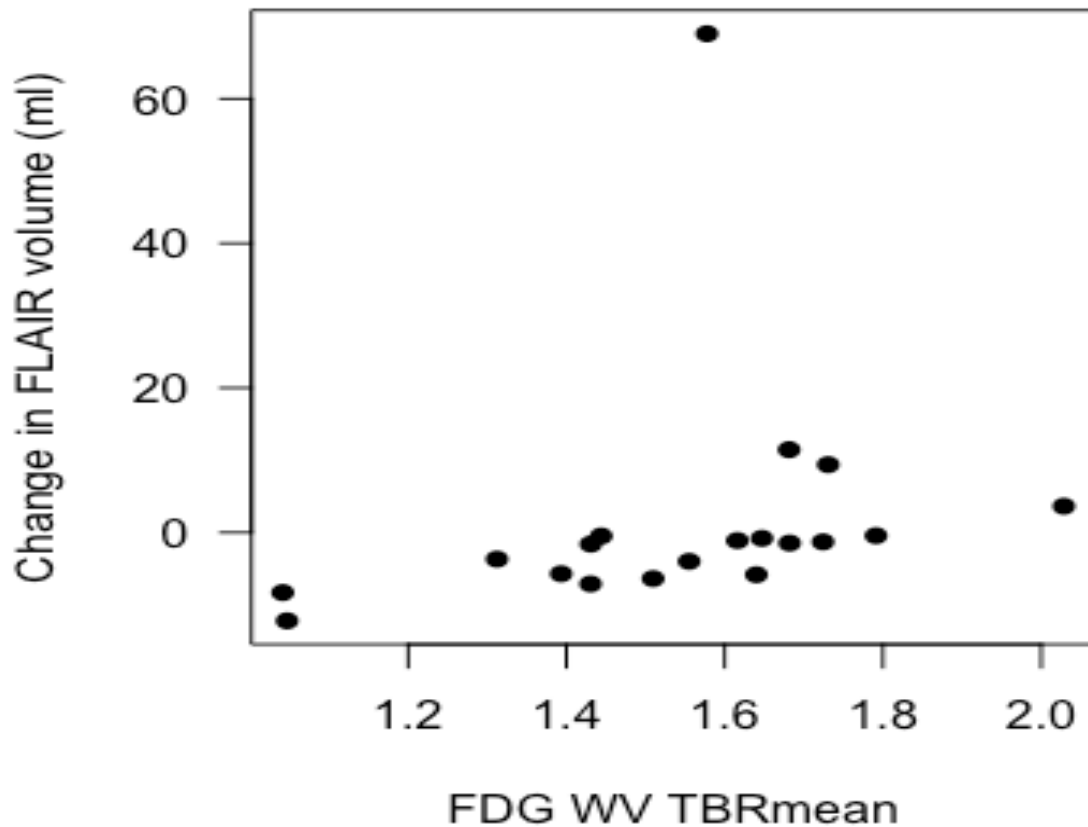


**Figure 6.3:** Association between FDG uptake and change in FLAIR volume. Scatterplot showing change in FLAIR primary lesion volume according to asymptomatic FDG WV TBR<sub>mean</sub>.

Similarly, visualisation of WV TBR<sub>max</sub> of the asymptomatic carotid artery and change in FLAIR volume lesion (with the above outlier removed for illustrative purposes) shows a positive association (**Figure 6.4**).

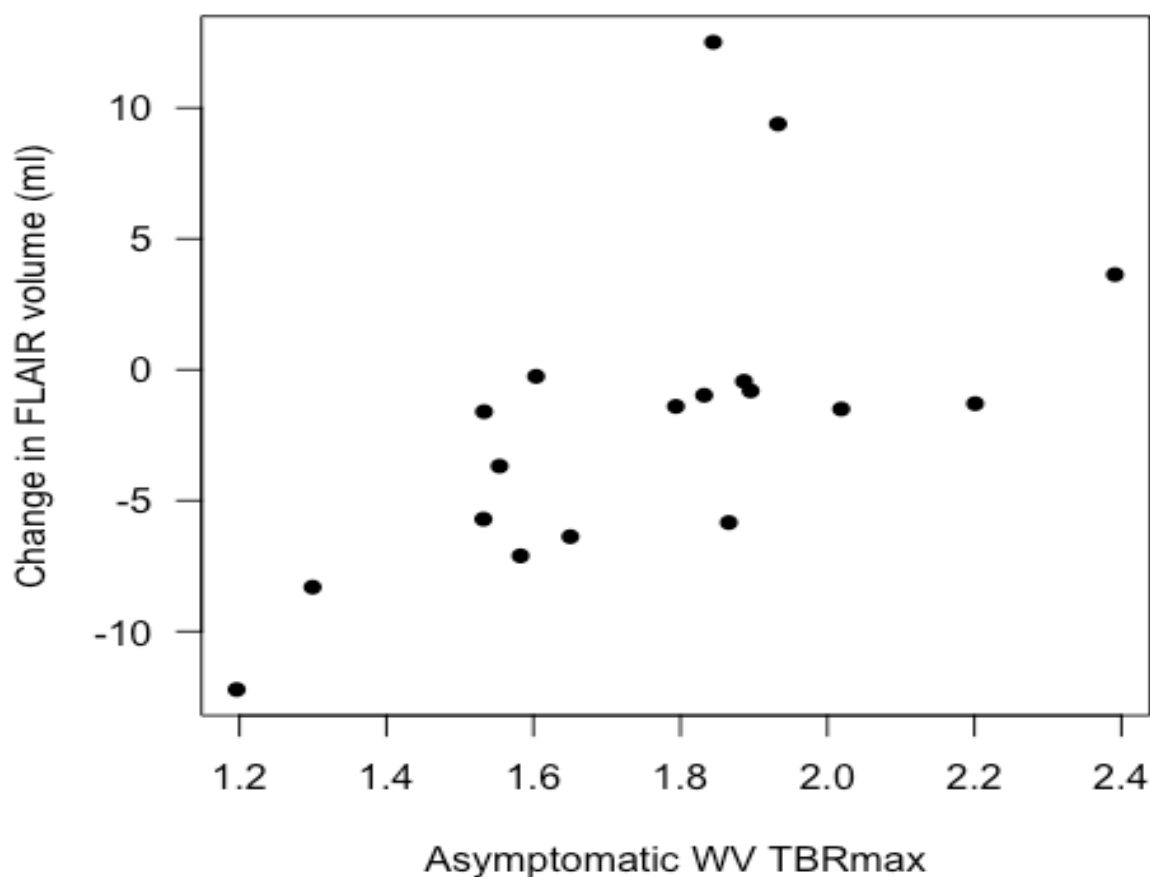


**Figure 6.4: Association between FDG uptake and change in FLAIR volume (adjusted).** Scatterplot of asymptomatic artery WV TBR<sub>max</sub> and change in FLAIR lesion volume (mL) (with outlier removed for illustrative purposes).

### 6.3.9 Role of thrombolysis in lesion evolution

Of the 19 participants with sufficient volumes for reliable comparisons, 5 (26.3%) were thrombolysed. There was no difference between the change in FLAIR volumes for total lesion volumes (-0.49 [IQR 5.27] and -1.53 [IQR 4.89] mL for thrombolysed and non-thrombolysed participants respectively,  $p=0.62$ ). Similar results were seen in FLAIR volume change in the primary lesion (-0.44 [IQR 5.45] versus -1.45 [IQR 4.85] mL,  $p=0.62$ ).

### *6.3.10 Carotid endarterectomy in lesion evolution*

Of the 19 participants with sufficient volumes for reliable comparisons, 8 (42.1%) had a CEA performed between baseline and follow-up MRI assessment. Between the CEA and non-CEA cohort, there was no difference in FLAIR lesion change for total lesion volumes (-1.04 [IQR 6.72] and -1.46 [IQR 5.78] mL,  $p=1.00$ ) or primary lesion volumes (-1.02 [IQR 7.13] and -1.4 [IQR 5.85] mL,  $p=1.00$ ).

### *6.3.11 Stroke event to baseline MRI interval and lesion characteristics*

There was a non-significant, but approaching significance, negative association between the time between the onset-to-MRI interval and both change in FLAIR total lesion volume change ( $r_s=-0.37$ ,  $p=0.12$ ) and FLAIR primary lesion volume change ( $r_s=-0.41$ ,  $p=0.08$ ).

There was a significant positive correlation between the onset-to-MRI interval and the difference between DWI and FLAIR volumes for both total lesion volumes ( $r_s=0.69$ ,  $p=0.002$ ) and primary lesion volumes ( $r_s=0.62$ ,  $p=0.006$ ).

### *6.3.12 Regression analysis of carotid FDG uptake and FLAIR lesion evolution*

Regression analysis was performed for power- and log-transformed FLAIR primary lesion volume change (transformed to meet assumptions for regression), and modeling included interaction terms for FDG uptake and smoking, and the interaction between FDG uptake, diabetes, and blood sugar (as per chapter 4). Results for this regression analysis are shown in **Table 6.12**.

Culprit artery			Non-culprit artery		
<b>SHS TBR<sub>max</sub></b>		Adjusted R <sup>2</sup> =0.95 (p<0.001)	<b>SHS TBR<sub>max</sub></b>		Adjusted R <sup>2</sup> =0.95 (p<0.001)
	Coefficient	Adjusted significance		Coefficient	Adjusted significance
FDG uptake	0.08	p=0.38	FDG uptake	0.34	p=0.047
Diabetes	-9.30	p<0.001	Diabetes	-10.34	p<0.001
Current antiplatelet	-0.56	p=0.02	CEA	0.33	p=0.03
Onset to scan interval	-0.08	p<0.01	Thrombolysis	-0.39	p=0.02
Current statin	0.44	p=0.06	Onset to scan interval	-0.06	p=0.02
Hypertension	-0.29	p=0.06	Hypertension	-0.27	p=0.08
Thrombolysis	-0.31	p=0.05	Male sex	-0.18	p=0.16
			Current statin	0.16	p=0.33
<b>MDS TBR<sub>max</sub></b>		Adjusted R <sup>2</sup> =0.95 (p<0.001)	<b>MDS TBR<sub>max</sub></b>		Adjusted R <sup>2</sup> =0.96 (p<0.001)
	Coefficient	Adjusted significance		Coefficient	Adjusted significance
FDG uptake	0.08	p=0.37	FDG uptake	0.40	p=0.03
Diabetes	-9.41	p<0.001	Diabetes	-10.25	p<0.001
Current antiplatelet	-0.56	p=0.02	CEA	0.34	p=0.02
Onset to scan interval	-0.08	p<0.01	Thrombolysis	-0.40	p=0.02
Current statin	0.44	p=0.06	Onset to scan interval	-0.06	p=0.02
Hypertension	-0.29	p=0.06	Hypertension	-0.25	p=0.08
Thrombolysis	-0.31	p=0.05	Male sex	-0.18	p=0.14
			Current statin	0.16	p=0.31
<b>WV TBR<sub>max</sub></b>		Adjusted R <sup>2</sup> =0.96 (p<0.001)	<b>WV TBR<sub>max</sub></b>		Adjusted R <sup>2</sup> =0.98 (p<0.001)
	Coefficient	Adjusted significance		Coefficient	Adjusted significance
FDG uptake	0.32	p=0.04	FDG uptake	0.81	p<0.01
Diabetes	-10.96	p<0.001	Diabetes	-10.05	p<0.001
CEA	0.36	p=0.01	CEA	0.49	p<0.01
Thrombolysis	-0.43	p<0.01	Thrombolysis	-0.52	p<0.001
Onset to scan interval	-0.07	p<0.01	Onset to scan interval	-0.06	p<0.01
Hypertension	-0.18	p=0.12	Hypertension	-0.13	p=0.17
			Male sex	-0.11	p=0.24
			Current antiplatelet	0.15	p=0.28

**Table 6.12:** Regression analysis of factors associated with FLAIR primary lesion volume evolution.

### *6.3.13 hsCRP and infarct evolution*

There was no association between hsCRP and baseline DWI total volume ( $r_s=0.10$ ,  $p=0.65$ ), baseline FLAIR total lesion volume ( $r_s=0.25$ ,  $p=0.23$ ), the difference between baseline FLAIR and DWI total volumes ( $r_s=-0.13$ ,  $p=0.61$ ), or the difference in FLAIR lesion total volumes between baseline and follow-up ( $r_s=0.34$ ,  $p=0.15$ ).

There was a non-significant, but nearing significance, positive association between hsCRP and follow-up FLAIR total lesion volume ( $r_s=0.39$ ,  $p=0.06$ ), follow-up FLAIR primary lesion volume ( $r_s=0.40$ ,  $p=0.05$ ).

## **6.4 Discussion**

Our results in this aspect of the study indicate that although carotid atheroma inflammation does not appear to play a role in determining baseline lesion size, it is associated with the evolution of the FLAIR lesion and there is suggestion that it may also be related to final FLAIR lesion volume. This discussion will consider the development of the infarct in chronological order.

### *6.4.1 Carotid inflammation and baseline infarct volume*

We found no association between carotid FDG uptake and either baseline DWI or FLAIR lesion volumes. Some associations between baseline FLAIR volumes and FDG uptake (SHS and MDS  $TBR_{max}$  in the asymptomatic artery, and WV  $TBR_{max}$  in the symptomatic artery) approached but did not reach statistical significance. Considering only those who did not receive thrombolysis did not move any relationships to statistical significance.

These results are not entirely unexpected. The development of ischaemic lesions will be affected by the extent of a participant's collateral arteries, as well as the extent of any clot fragmentation. We also do not know the extent and duration of ischaemia (including the timing of any reperfusion) in these individuals, all of which may affect baseline lesion development. In rat models, the severity of ischaemia has been

implicated in the time taken for infarcts to develop and their reversibility (Du et al., 1996, Neumann-Haefelin et al., 2000, Schwamm et al., 1998).

Another possibility is methodological. Our participants showed a variation in the interval between the onset of symptoms and MRI scanning. This variation was due to a number of reasons: waiting for carotid imaging and availability of MRI scanning were the two main contributing factors, but other factors including clinical status and rehabilitation, and fitting imaging around other study investigations, affected the time taken to perform baseline imaging. DWI lesions have been found to increase in the subacute period (appearing to peak at approximately 70 hours) before reducing in size after the first week (Beaulieu et al., 1999, Lansberg et al., 2001). Hence, this variability in the interval between symptom onset and MRI may affect our observed relationship between FDG uptake and DWI volume, and the difference in volumes between FLAIR and DWI lesions.

Time from onset was not found to correlate with DWI lesion volume in humans with stroke, supporting the argument that other factors are more influential in the development of the infarct and that growth is not simply a linear, with a wide variation in growth rates from  $<1$  mL/h to  $>70$  mL/h (Hakimelahi et al., 2014). This lack of a clear relationship persisted even if sub-categorised the site of occlusion. It is interesting to note that the quoted figure of the loss of 1.9 million neurons per minute after infarct corresponds to an infarct growth rate of 5.4 mL/h, approximately half the rate in the study by Hakimelahi et al. (Saver, 2006, Hakimelahi et al., 2014). Hence, simply considering the infarct volume as a function of time fails to account for the variable effects of collateral supply.

#### *6.4.2 Carotid inflammation, final lesion size, and lesion evolution*

While the previous section has considered lesion evolution in the acute and sub-acute period, evolution of the lesion in the early recovery period has received less attention. However, lesion evolution has also been dynamic over the first month after stroke. In our study we found that of the 19 individuals analysed for FLAIR primary lesion volume change between baseline and follow-up, 12 (63.2%) showed a decrease in FLAIR volume to below 90% of the baseline volume, 4 (21.1%) showed a stable

appearance (within  $\pm 10\%$  of the baseline FLAIR volume), and 3 (15.8%) showed an increase ( $>10\%$  increase above the baseline FLAIR volume). We have shown that the absolute primary lesion volume difference is correlated with asymptomatic artery and generalised (i.e. whole vessel) symptomatic artery FDG uptake, and atheromatous inflammation by inference.

As discussed above, the increase in lesion volume, and difference between FLAIR and DWI lesion volumes, in the subacute setting likely reflects the development of vasogenic oedema. Ritzl et al. found that although day eight FLAIR lesions were larger than corresponding DWI lesion volumes, day 124 FLAIR lesions were all smaller than day eight FLAIR lesions and baseline DWI lesions, with a correlation coefficient of 0.8 ( $p=0.02$ ) between acute DWI lesion and final FLAIR volume (Ritzl et al., 2004). Importantly to note, 7 (58.3%) of the cohort had been thrombolysed (compared to 5, 26.3%, in our comparison cohort). Our results broadly support this, with the majority reducing in volume, suggesting resolving vasogenic oedema.

However, the FLAIR hyperintensity may represent more than simply vasogenic oedema. Other potential factors include reactive gliosis or leukocyte infiltration, both of which will contribute to the FLAIR lesion. Increased atherosclerotic inflammation, may exacerbate each of these three processes and mean that the FLAIR lesion fails to resolve; remaining either static or even increasing in volume. Indeed, when comparing those who had FLAIR lesion decrease (at least a 10% reduction from baseline volume) to a pooled cohort of those with static ( $\pm 10\%$  of baseline volume) and increased ( $>10\%$  of baseline) volumes, we find the latter have increased asymptomatic artery values consistent with the above results (median asymptomatic MDS  $TBR_{max}$  1.80 [IQR 0.30] versus 2.03 [IQR 0.26] respectively,  $p=0.04$ ).

Although the stronger relationship was seen for FDG uptake and FLAIR primary lesion volume change, there was also suggestion of a relationship between focal asymptomatic FDG uptake (SHS and MDS  $TBR_{max}$ ) or symptomatic WV  $TBR_{max}$  and follow-up FLAIR primary lesion volume (with other measures approaching significance, as shown above). These similar patterns of associations between generalised atheromatous inflammation and infarct development appear consistent:

the inflammation appears to be associated with both greater interval change and greater final volumes.

The pattern that we see of asymptomatic artery rather than symptomatic artery having an association with the pattern of disease is consistent with the results seen with small vessel disease in the previous chapter. Once again, the non-culprit artery is likely to serve as a 'barometer' of atheroma inflammation; giving an overall impression of the extent of inflammation in contrast to the disproportionately elevated activity seen in the culprit plaque.

The potential pathophysiological mechanisms behind these observed results were described above and reflect similar pathologies to those already discussed in the development of small vessel disease in the previous chapter. The lack of an association between FDG measures and baseline infarct volume suggests that inflammation within the culprit plaque did not lead to bigger clot formation. However, the consistent association between FDG measures and FLAIR lesion evolution and an indication of an association with final infarct volume suggests that the atheromatous inflammation plays more of a role in infarct development, most likely through a MMP-9-mediated disruption of the BBB. From our results it is difficult to say how much of the lesion evolution may be due to pre-existing BBB disruption and 'priming' of the brain for injury (Drake et al., 2011) or whether it enhances the extent and duration BBB permeability in the acute and early recovery period remains unclear, though the pattern of results is perhaps more consistent with the latter.

This change in lesion volumes in the weeks following stroke raises the methodological concern of when to image the 'final infarct' volume. The typical final volume of a large vessel, supratentorial ischaemic stroke is 54 mL (Saver, 2006), but there is wide variation. Beaulieu et al. performed serial lesion imaging with MRI, finding that the DWI lesion volume increased and reached a peak at five to seven days post-infarct, but that DWI lesion at 30 days was on average 180% of the volume of the lesion in the early (< 7 hours after onset) phase, with 7 (47%) showing DWI lesion enlargement, 3 (20%) remaining unchanged, and 5 (33%) decreasing in volume over this time (Beaulieu et al., 1999). Our results are consistent with the findings that MRI

hyperintensities continue to evolve in between the subacute and early chronic phase post-infarct.

Our results found no significant difference between baseline DWI volumes and follow-up FLAIR lesion volumes, in contrast to the significant difference between baseline and follow-up FLAIR lesion volumes, and that baseline DWI volumes and follow-up FLAIR lesion volumes were highly correlated. Similar associations have been reported previously (Beaulieu et al., 1999, Schwamm et al., 1998).

The finding of hsCRP having a near-significant association with final FLAIR primary lesion volume is consistent with some earlier studies showing a relationship between infarct volume and CRP (Youn et al., 2012, Ormstad et al., 2011, Smith et al., 2004). However, in our study we cannot show causation in this association; whether raised hsCRP levels are a reflection of the more extensive cerebral tissue involvement or relate to the increased inflammation within the carotid plaque remains unclear.

Finally, it is appropriate to consider the other cardiovascular variables in our regression models. The high adjusted  $R^2$  values indicate that the model explains a large extent of our data, but it is important to recognise that the size of the cohort is relatively small. It is likely that the large effect of diabetes, and its *negative* association with FLAIR lesion growth, is due to the small proportion of participants with diabetes in a small sample having a disproportionate effect. The negative association between FLAIR lesion evolution and thrombolysis appears to have a more plausible mechanism, perhaps reflecting a favourable effect on the penumbra. The positive association between FLAIR lesion growth and CEA is a curious result, and it is possible that it may be a consequence of the small sample size or may represent a physiological phenomenon, such as vasogenic oedema or inflammatory change, following reperfusion. For example, new BBB disruption, revealed by delayed gadolinium enhancement of cerebrospinal fluid space on FLAIR imaging, associated with carotid intervention was found in 17.8% of cases 24-hours following CEA or carotid stenting, and development of symptoms was associated with age, leukoaraiosis, and higher post-procedural systolic blood pressure (Cho et al., 2014). There is little work exploring how carotid intervention influences the development of FLAIR lesions between the subacute and early chronic phases, and may be an avenue

for further work. However, the move towards early carotid intervention after stroke alongside the evolution of MRI hyperintensities in the subacute setting may cause significant confounding.

#### *6.4.3 Limitations*

As mentioned above, the variation in the onset-to-MRI interval has a confounding effect when investigating the association between FDG uptake and baseline lesion volume. Hence, it is difficult to make conclusions based upon these results. Future work will require a fixed onset-to-MRI interval, which will necessitate expedited investigations and scanning. However, the results for the evolution of the lesion and final infarct volume are less likely to be affected by this initial interval, and adjustment for this interval on multiple regression analysis did not alter the significant associations seen between FDG uptake and FLAIR lesion evolution on univariable analysis.

Ischaemic lesion dynamics in humans remain hard to investigate, and typically rely on extrapolation from animal models. Hence, it is particularly important to consider this point when applying the results from animal studies of infarct evolution (typically showing a logarithmic expansion) to human evolution, where the human cerebrum and vasculature is more complex (Markus et al., 2003, Zhang et al., 2015, Bardutzky et al., 2005a). Indeed, there is also variation within species (Bardutzky et al., 2005b). Furthermore, the experimental model of ischaemia may also affect lesion evolution, with embolic MCAO found to develop larger infarcts and to have more extensive diffusion/perfusion mismatch of longer duration than mechanical MCAO in rat models (Henninger et al., 2006).

As with previous chapters, another consideration is the small cohort studied here, as occurs frequently for symptomatic PET studies. This may limit the ability to detect significance in some instances, particularly those approaching statistical significance (such as with the baseline FLAIR and follow-up FLAIR volumes, and the association between final FLAIR volume and serum hsCRP). Larger sample sizes would be advantageous to test further these associations. Future multicentre studies would help

address this issue, though it would be essential that common protocols and harmonised measuring techniques are used across centres as discussed previously.

#### *6.4.4 Future work*

The most significant advance would be to delineate the mechanism underlying the persistence or increase in FLAIR hyperintensity volume. One potential approach to differentiate between cellular effects versus vasogenic oedema would be through considering the degree of local anatomical distortion on neighbouring cerebral structures that occurs with oedema. Co-registration of T1 and T2 maps using rigid body and non-linear registration methods currently under development and described by Harston et al. can then identify an ‘oedema metric’ (Harston et al., 2017). Work to analyse the ICARUSS study dataset using these techniques in collaboration with Dr George Harston (Clinical Lecturer, Acute Vascular Imaging Centre, Radcliffe Department of Medicine, University of Oxford) is in the initial stages.

### **6.5 Summary of findings**

This chapter has discussed:

1. There was no association between carotid FDG uptake and baseline lesion volumes on DWI or FLAIR.
2. There was an association between carotid FDG uptake in the asymptomatic artery, and the diffuse measures of uptake in the symptomatic artery, and FLAIR volume change between baseline and follow-up.
3. There is a suggestion that some measures of FDG uptake were associated with final lesion volume.

## Chapter Seven: Clinical Outcomes

### 7.1 Introduction

#### *7.1.1 Aims of this chapter*

Previous chapters have demonstrated how inflammation detected by FDG-PET is associated with the presence of chronic small vessel disease and the evolution of the acute infarct. In this chapter we aim to investigate the clinical impact upon the individual, with the following questions:

1. Is inflammation within the carotid plaque associated with poorer functional (mRS) and disability (BI) outcomes?
2. Is inflammation within the carotid plaque associated with poorer cognitive performance?

The main hypotheses are:

- i. Inflammation will be associated with poorer functional outcomes and greater disability following stroke.
- ii. Inflammation will be associated with poorer performance on cognitive testing.

#### *7.1.2 Functional outcomes*

Inflammation may be implicated in functional recovery following stroke through a number of mechanisms. As discussed in the previous chapter, atheromatous inflammation measured by FDG uptake appears to be associated with increased FLAIR lesion volume expansion in the early post-stroke period.

Baseline volume measured using CT at 6-11 days post-infarct showed a moderate correlation with three-month clinical outcomes (NIHSS:  $r=0.56$ , Barthel Index:  $r=0.46$ , mortality:  $r=0.32$ ) (Saver et al., 1999). However, others have reported that

infarct volume does not provide any additional predictive value to a seven-day NIHSS for predicting clinical outcomes at three months (Johnston et al., 2002).

Alternatively, inflammation has been implicated to affect clinical outcomes through mechanisms other than infarct size. For example, CRP has also been implicated in neurological recovery from stroke. In a large study of 3,653 patients with first-ever ischaemic stroke, higher hsCRP levels were significantly associated with modified Rankin scores  $\geq 3$  at 3 months, after adjustment for age, sex, baseline NIHSS, stroke subtype, conventional cardiovascular risk factors and thrombolysis (Matsuo et al., 2016).

There are potential shortcomings with the use of inflammatory biomarkers after stroke. IL-6 exhibits a temporal pattern of expression after stroke; increasing in the first 10 hours after a stroke prior to reaching a plateau until 72 hours after the event. By seven days, levels had returned to baseline (Fassbender et al., 1994). Furthermore, IL-6 concentrations had moderate correlations with the volume of infarct (4-hour IL-6  $r=0.78$ , day 1  $r=0.62$ , day 5  $r=0.68$ , all  $p<0.05$ ), and inverse correlations with neurological outcomes ( $r=-0.70$  with Barthel Index at 14-21 days (Fassbender et al., 1994). This raises two important considerations. Firstly, the timing of testing is important. Secondly, the correlation between inflammatory biomarkers and lesion volume does not help differentiate between two possible causative pathways, i.e. whether inflammation exacerbates infarct volume or larger infarct volumes increase IL-6 levels. Given the temporal evolution of IL-6 expression, the latter is more likely.

CRP was elevated in 21% of individuals with acute ischaemic stroke compared to 4% of a TIA control group, with CRP concentrations  $>7$  mg/L having an increased risk of severe stroke and larger volumes of infarction (Luo et al., 2012). Another small study found a positive association between CRP and prognosis after acute ischaemic stroke, but no relationship between cytokine levels and infarct volume (Sahan et al., 2013).

Serum CRP was also found to rise over the 48-hours after acute ischaemic stroke, and this appeared to be driven primarily by an increase in CRP in the large artery atheroma subtype between day one and two: no significant difference in CRP was seen between small vessel occlusion and large artery atheroma cohorts on day one,

and while there was no change in CRP levels for the small vessel occlusion group between day one and two, CRP rose significantly in the large artery atherosclerosis group by day two and was also significantly higher than for small vessel occlusion cohort at this time point (Park et al., 2012). Furthermore, day two CRP, but not day one CRP, was significantly correlated with infarct volume ( $r=0.38$ ), NIHSS ( $r=0.46$ ), and 3 month mRS ( $r=0.36$ ) (Park et al., 2012).

Further associations between inflammatory marker peak concentrations and CT-measured cerebral infarct volume at 5 days (IL-6:  $r=0.62$ ,  $p=0.006$ ; CRP:  $r=0.66$ ,  $p<0.01$ ), NIHSS at 5-7 days (IL-6:  $r=0.66$ ,  $p<0.001$ ; CRP:  $r=0.54$ ,  $p<0.001$ ), 3-month mRS (IL-6:  $r=0.72$ ,  $p<0.001$ ; CRP:  $r=0.63$ ,  $p<0.001$ ), 3-month Barthel Index (IL-6:  $r=-0.74$ ,  $p<0.001$ ; CRP:  $r=-0.58$ ,  $p<0.001$ ), and 12 month mRS (IL-6:  $r=0.77$ ,  $p<0.001$ ; CRP:  $r=0.65$ ,  $p<0.001$ ) were reported by Smith et al., and the authors report exclusion of individuals with overt infection did not materially alter these findings, but did not report the exact figures for CRP (Smith et al., 2004). It is important to note that it was not possible in this study to assess the relationship of clinical outcomes with inflammatory markers after adjustment for infarct volume due to the small sample.

### *7.1.3 Post-stroke cognition*

Both carotid disease and inflammation have been implicated in cognitive dysfunction following stroke. In a middle-aged (mean 45.3, SD 3.6, years at baseline) cohort, increased CCA IMT was independently negatively associated with processing speed, narrowly missed significance for a negative association with executive function ( $p=0.07$ ), but showed no association with verbal memory (Zeki Al Hazzouri et al., 2015).

More developed atherosclerosis has also been implicated with effects on cognition, with the presence of plaque, number of plaques, and total plaque area found to be associated with poorer outcomes on verbal memory testing after adjustment for cardiovascular risk factors and education in the large Tromsø study (Arntzen et al., 2012). However, this study did not find an effect of CCA IMT after adjustment with this more extensive regression analysis.

Given earlier findings that only ICA IMT, and not CCA IMT, was associated with WMHs (Romero et al., 2009), it is important to consider in these cognition studies whether the location of testing may affect outcomes.

In a follow-up study of the Northern Manhattan Study, no association was found between plaque burden and cognition. As the authors acknowledge, their participants with carotid plaques may have received primary prevention that may have attenuated the disease. However, carotid IMT (average of CCA, bifurcation, and ICA IMT bilaterally in this study) was associated with poorer baseline episode memory, semantic memory, and processing speed but only in individuals who were *APOE*  $\epsilon 4$  carriers (Gardener et al., 2017).

Interestingly, Brickman et al. suggest that cognitive reserve (psychosocial factors including exposure to cognitively-stimulating activity throughout life) has a modifying effect on the relationship between WMHs and cognitive function, but only in women. When adjusting for the degree of cognitive function, there was a positive association between the degree of cognitive reserve and WMH volume, suggesting that a larger extent of WMH can be accommodated to produce the same level of executive function in individuals with higher cognitive reserve. The same phenomenon was not observed in men (Brickman et al., 2011).

Inflammatory cytokines have been implicated in cognitive dysfunction in individuals without focal brain injury. IL-6 was independently negatively associated with minimal state examination (MMSE) scores after adjustment for sociodemographic and vascular risk factors in a cohort of stroke-free individuals enrolled in the Northern Manhattan Study (Wright et al., 2006). An association between IL-6 and cognitive function have been reported elsewhere in a prospective analysis (Mooijaart et al., 2013). CRP has also been found to be negatively associated with a range of cognitive features using a range of cognitive tests (Kuo et al., 2005, Komulainen et al., 2007), though other studies have found no association (Dik et al., 2005). CRP has been found to be positively associated with cognitive performance after adjustment for vascular risk factors and disease (Mooijaart et al., 2011). Finally, there is evidence that there

may be a dose-response relationship to inflammatory molecules, and that particular allelic variants may enhance the effect (Schram et al., 2007).

## 7.2 Methods

Methodology for this chapter is discussed in Chapter Two.

## 7.3 Results

### 7.3.1 Modified Rankin scale outcomes

The distribution of mRS for the study participants at baseline and at three-month follow-up is shown in **Figure 7.1**.

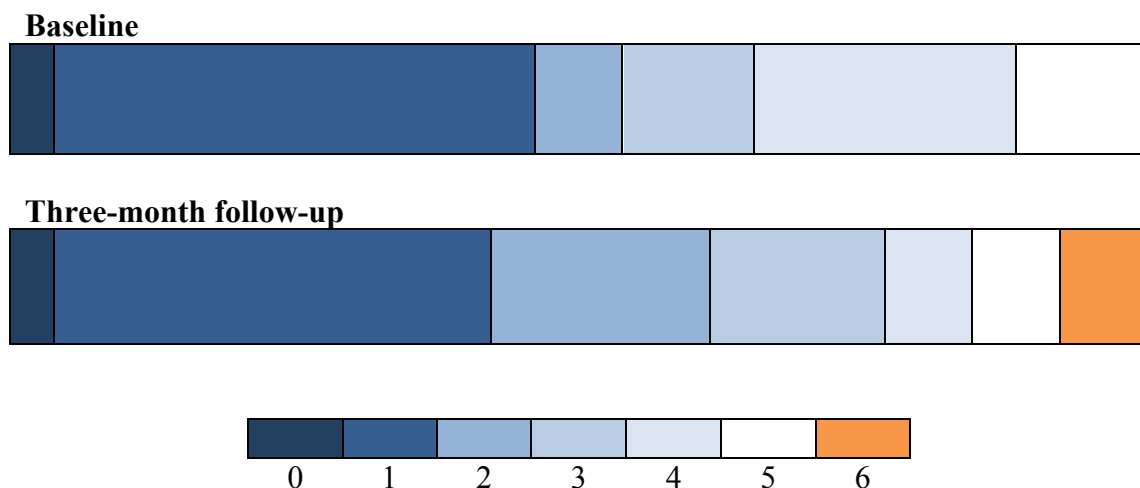


**Figure 7.1: Modified Rankin scale for study participants at baseline and three months.**

#### 7.3.1.1 Baseline modified Rankin scale

At baseline, there was no significant difference in FDG TBRs between the mRS 0-1 group and the mRS 2-6 groups in symptomatic arteries (SHS  $TBR_{max}$   $p=0.52$ , MDS  $TBR_{max}$   $p=0.57$ , WV  $TBR_{max}$   $p=0.38$ , SHS  $TBR_{mean}$   $p=0.47$ , MDS  $TBR_{mean}$   $p=0.43$ , WV  $TBR_{mean}$   $p=0.34$ ) or asymptomatic arteries (SHS  $TBR_{max}$   $p=0.62$ , MDS  $TBR_{max}$

p=0.73, WV TBR<sub>max</sub> p=0.91, SHS TBR<sub>mean</sub> p=0.70, MDS TBR<sub>mean</sub> p=0.68, WV TBR<sub>mean</sub> p=0.52).

Furthermore, relaxing the criteria for a ‘good’ outcome to mRS 0-2 did not affect the results. There was no statistically significant difference in FDG TBRs between ‘good’ and ‘bad’ outcome groups for either the symptomatic artery (SHS TBR<sub>max</sub> p=0.52, MDS TBR<sub>max</sub> p=0.57, WV TBR<sub>max</sub> p=0.38, SHS TBR<sub>mean</sub> p=0.47, MDS TBR<sub>mean</sub> p=0.43, WV TBR<sub>mean</sub> p=0.34) or asymptomatic artery (SHS TBR<sub>max</sub> p=0.62, MDS TBR<sub>max</sub> p=0.73, WV TBR<sub>max</sub> p=0.91, SHS TBR<sub>mean</sub> p=0.79, MDS TBR<sub>mean</sub> p=0.68, WV TBR<sub>mean</sub> p=0.52).

### *7.3.1.2 Three-month modified Rankin scale*

At three-month follow-up, there was no significant difference in FDG TBRs between the mRS 0-1 group and the mRS 2-6 groups in symptomatic arteries (SHS TBR<sub>max</sub> p=0.47, MDS TBR<sub>max</sub> p=0.61, WV TBR<sub>max</sub> p=0.44, SHS TBR<sub>mean</sub> p=0.68, MDS TBR<sub>mean</sub> p=0.68, WV TBR<sub>mean</sub> p=0.88) or asymptomatic arteries (SHS TBR<sub>max</sub> p=0.54, MDS TBR<sub>max</sub> p=0.57, WV TBR<sub>max</sub> p=0.57, SHS TBR<sub>mean</sub> p=0.68, MDS TBR<sub>mean</sub> p=0.68, WV TBR<sub>mean</sub> p=0.33).

Similarly, considering mRS 0-2 to be a ‘good’ outcome did not reveal statistically different FDG TBRs between ‘good’ and ‘bad’ outcome groups for either the symptomatic artery (SHS TBR<sub>max</sub> p=0.42, MDS TBR<sub>max</sub> p=0.39, WV TBR<sub>max</sub> p=0.26, SHS TBR<sub>mean</sub> p=0.59, MDS TBR<sub>mean</sub> p=0.55, WV TBR<sub>mean</sub> p=0.52) or asymptomatic artery (SHS TBR<sub>max</sub> p=0.82, MDS TBR<sub>max</sub> p=0.74, WV TBR<sub>max</sub> p=0.59, SHS TBR<sub>mean</sub> p=0.86, MDS TBR<sub>mean</sub> p=0.78, WV TBR<sub>mean</sub> p=0.42).

### *7.3.2 Barthel index*

#### *7.3.2.1 Baseline Barthel index*

The median BI at baseline was 90 (IQR 50). No significant associations were found between BI and TBR measures in either the symptomatic or asymptomatic arteries (**Table 7.1**).

	Symptomatic artery			Asymptomatic artery	
	Correlation	Sig.		Correlation	Sig.
SHS TBR <sub>max</sub>	r <sub>s</sub> =-0.31	p=0.12		r <sub>s</sub> =-0.26	p=0.20
MDS TBR <sub>max</sub>	r <sub>s</sub> =-0.30	p=0.13		r <sub>s</sub> =-0.27	p=0.19
WV TBR <sub>max</sub>	r <sub>s</sub> =-0.37	p=0.06		r <sub>s</sub> =-0.22	p=0.28
SHS TBR <sub>mean</sub>	r <sub>s</sub> =-0.33	p=0.10		r <sub>s</sub> =-0.19	p=0.37
MDS TBR <sub>mean</sub>	r <sub>s</sub> =-0.33	p=0.10		r <sub>s</sub> =-0.18	p=0.37
WV TBR <sub>mean</sub>	r <sub>s</sub> =-0.29	p=0.15		r <sub>s</sub> =-0.26	p=0.19

**Table 7.1:** Associations between FDG TBRs and baseline BI.

### 7.3.2.2 Three-month Barthel index

The median BI at three months post-event was 95 (IQR 16.25). Excluding the two individuals who died between baseline and three-month follow-up, there was a significant improvement in BI between baseline and three-month follow-up (median 90 [IQR 42.5] versus 95 [IQR 16.25] respectively,  $p < 0.01$  on paired testing).

Associations between FDG uptake and BI at three months are shown in **Table 7.2**.

	Symptomatic artery			Asymptomatic artery	
	Correlation	Sig.		Correlation	Sig.
SHS TBR <sub>max</sub>	r <sub>s</sub> =-0.36	p=0.09		r <sub>s</sub> =-0.26	p=0.22
MDS TBR <sub>max</sub>	r <sub>s</sub> =-0.32	p=0.13		r <sub>s</sub> =-0.25	p=0.23
WV TBR <sub>max</sub>	r <sub>s</sub> =-0.48	p=0.02		r <sub>s</sub> =-0.23	p=0.28
SHS TBR <sub>mean</sub>	r <sub>s</sub> =-0.31	p=0.14		r <sub>s</sub> =-0.17	p=0.43
MDS TBR <sub>mean</sub>	r <sub>s</sub> =-0.34	p=0.11		r <sub>s</sub> =-0.17	p=0.42
WV TBR <sub>mean</sub>	r <sub>s</sub> =-0.33	p=0.12		r <sub>s</sub> =-0.27	p=0.20

**Table 7.2:** Associations between FDG TBRs and three-month BI.

### 7.3.3 Cognitive function

#### 7.3.3.1 Baseline MoCA

Of the 26 individuals analysed in the primary cohort, 20 (76.9%) were able to undergo cognitive testing. Six participants were excluded due to either aphasia (five participants) or limited English (one participant).

Correlations between FDG uptake and baseline MoCA scores are shown in **Table 7.3**.

	Symptomatic artery			Asymptomatic artery	
	Correlation	Sig.		Correlation	Sig.
SHS TBR <sub>max</sub>	r <sub>s</sub> =-0.40	p=0.08		r <sub>s</sub> =-0.10	p=0.69
MDS TBR <sub>max</sub>	r <sub>s</sub> =-0.37	p=0.12		r <sub>s</sub> =-0.07	p=0.77
WV TBR <sub>max</sub>	r <sub>s</sub> =-0.33	p=0.15		r <sub>s</sub> =-0.12	p=0.62
SHS TBR <sub>mean</sub>	r <sub>s</sub> =-0.29	p=0.22		r <sub>s</sub> =-0.02	p=0.95
MDS TBR <sub>mean</sub>	r <sub>s</sub> =-0.32	p=0.17		r <sub>s</sub> =-0.05	p=0.82
WV TBR <sub>mean</sub>	r <sub>s</sub> =-0.25	p=0.28		r <sub>s</sub> =-0.09	p=0.69

**Table 7.3:** Associations between FDG uptake and baseline MoCA score.

Of 20 individuals with interpretable MoCA scores, 9 (45%) had evidence of cognitive impairment (MoCA <26) at baseline testing. Comparative FDG uptake in those with and without cognitive impairment at baseline is shown in **Table 7.4**.

	Cognitive impairment n=9	Normal cognition n=11	Significance
<b>Symptomatic artery</b>			
Mean SHS TBR <sub>max</sub> (SD)	2.63 (0.88)	2.21 (0.57)	p=0.24
Mean MDS TBR <sub>max</sub> (SD)	2.55 (0.86)	2.16 (0.56)	p=0.27
Mean WV TBR <sub>max</sub> (SD)	2.07 (0.55)	1.88 (0.36)	p=0.41
Median SHS TBR <sub>mean</sub> (IQR)	1.97 (0.41)	1.86 (0.30)	p=0.37
Median MDS TBR <sub>mean</sub> (IQR)	1.91 (0.37)	1.81 (0.27)	p=0.33
Mean WV TBR <sub>mean</sub> (SD)	1.73 (0.42)	1.65 (0.29)	p=0.66
<b>Asymptomatic artery</b>			
Mean SHS TBR <sub>max</sub> (SD)	2.04 (0.61)	1.89 (0.32)	p=0.54
Mean MDS TBR <sub>max</sub> (SD)	1.96 (0.56)	1.86 (0.30)	p=0.65
Mean WV TBR <sub>max</sub> (SD)	1.72 (0.38)	1.71 (0.25)	p=0.91
Mean SHS TBR <sub>mean</sub> (SD)	1.77 (0.46)	1.69 (0.23)	p=0.66
Mean MDS TBR <sub>mean</sub> (SD)	1.71 (0.44)	1.66 (0.22)	p=0.73
Mean WV TBR <sub>mean</sub> (SD)	1.50 (0.31)	1.53 (0.19)	p=0.81

**Table 7.4:** FDG uptake measures in individuals with cognitive impairment and normal cognition at baseline.

### 7.3.3.2 Follow-up MoCA

There was a moderate correlation between baseline MoCA and three-month MoCA scores (r<sub>s</sub>=0.46, p=0.046).

Correlations between FDG uptake at baseline and three-month MoCA scores are shown in **Table 7.5**.

	Symptomatic artery			Asymptomatic artery	
	Correlation	Sig.		Correlation	Sig.
SHS TBR <sub>max</sub>	r <sub>s</sub> =-0.51	p=0.02		r <sub>s</sub> =-0.08	p=0.74
MDS TBR <sub>max</sub>	r <sub>s</sub> =-0.49	p=0.03		r <sub>s</sub> =-0.09	p=0.71
WV TBR <sub>max</sub>	r <sub>s</sub> =-0.34	p=0.15		r <sub>s</sub> =-0.04	p=0.87
<b>Symptomatic artery</b>					
SHS TBR <sub>mean</sub>	r <sub>s</sub> =-0.32	p=0.18		r <sub>s</sub> =0.03	p=0.90
MDS TBR <sub>mean</sub>	r <sub>s</sub> =-0.35	p=0.14		r <sub>s</sub> =-0.02	p=0.93
WV TBR <sub>mean</sub>	r <sub>s</sub> =-0.24	p=0.33		r <sub>s</sub> =0.00	p=0.99

**Table 7.5:** Associations between FDG uptake and three-month MoCA score.

At repeat assessment, 3 (27.3%) of 11 participants without cognitive impairment at baseline showed evidence of cognitive impairment on repeat testing. In contrast, of the nine participants with cognitive impairment at baseline, three (33%) were above the cognitive impairment threshold on repeat testing, and one (11.1%) had died. FDG uptake in these groups at three-month repeat testing is shown in **Table 7.6**.

	Cognitive impairment n=8	Normal cognition n=11	Significance
<b>Symptomatic artery</b>			
Mean SHS TBR <sub>max</sub> (SD)	2.93 (0.76)	2.12 (0.44)	p=0.02
Mean MDS TBR <sub>max</sub> (SD)	2.84 (0.74)	2.07 (0.42)	p=0.02
Median WV TBR <sub>max</sub> (IQR)	2.17 (0.44)	1.73 (0.36)	p=0.06
Median SHS TBR <sub>mean</sub> (IQR)	2.05 (0.53)	1.86 (0.30)	p=0.06
Median MDS TBR <sub>mean</sub> (IQR)	1.98 (0.54)	1.81 (0.27)	p=0.06
Median WV TBR <sub>mean</sub> (IQR)	1.76 (0.38)	1.47 (0.34)	p=0.13
<b>Asymptomatic artery</b>			
Median SHS TBR <sub>max</sub> (IQR)	1.99 (0.11)	1.88 (0.46)	p=0.31
Median MDS TBR <sub>max</sub> (IQR)	1.96 (0.12)	1.83 (0.42)	p=0.24
Mean WV TBR <sub>max</sub> (SD)	1.76 (0.22)	1.73 (0.32)	p=0.83
Mean SHS TBR <sub>mean</sub> (SD)	1.82 (0.38)	1.72 (0.29)	p=0.54
Mean MDS TBR <sub>mean</sub> (SD)	1.77 (0.34)	1.67 (0.29)	p=0.49
Mean WV TBR <sub>mean</sub> (SD)	1.55 (0.23)	1.52 (0.24)	p=0.80

**Table 7.6:** FDG uptake measures in individuals with cognitive impairment and normal cognition at three months.

Individuals with cognitive impairment had a higher median hsCRP concentration than those with normal cognition, though the result narrowly missed statistical significance (9.37 [IQR 18.38] versus 3.9 [IQR 6.09] mg/L,  $p=0.09$ ).

### 7.3.3.3 Multiple logistic regression analysis of cognitive results

Logistic regression for cognitive impairment on three-month follow-up MoCA is shown in **Table 7.7**. Prior to backwards elimination, the regression model was optimised by testing inclusion of interaction terms. Subsequently, interaction terms were included for FDG uptake:smoking; FDG uptake:leukoaraiosis severity; and FDG uptake:follow-up FLAIR lesion volume. Including age:leukoaraiosis severity or age:sex did not affect the models.

Culprit artery			Non-culprit artery		
SHS TBR <sub>max</sub>		Adjusted R <sup>2</sup> =0.91 ( $p=0.01$ )	SHS TBR <sub>max</sub>		Adjusted R <sup>2</sup> =0.73 ( $p<0.01$ )
	OR [95% CI]	Adjusted significance		OR [95% CI]	Adjusted significance
FDG uptake	7.34 [4.00-13.50]	$p<0.01$	Follow-up FLAIR volume	1.00 [1.00-1.00]	$p<0.001$
Smoking	136.87 [28.28-662.37]	$p<0.01$	Age	1.03 [1.01-1.05]	$p=0.01$
Mod/severe leukoaraiosis	0.07 [0.02-0.22]	$p=0.01$	Male sex	0.66 [0.48-0.89]	$p=0.02$
Follow-up FLAIR volume	1.00 [1.00-1.00]	$p=0.02$	Hypertension	0.77 [0.55-1.08]	$p=0.17$
Diabetes	139.35 [11.41-1702.61]	$p=0.02$			
Male sex	0.86 [0.69-1.06]	$p=0.23$			
Hypertension	1.93 [1.42-2.63]	$p=0.1$			
Current statin	0.77 [0.55-1.07]	$p=0.19$			
Current antiplatelet	3.85 [2.54-5.84]	$p<0.01$			
CEA	2.45 [1.82-3.29]	$p<0.01$			
MDS TBR <sub>max</sub>		Adjusted R <sup>2</sup> =0.91 ( $p=0.01$ )	MDS TBR <sub>max</sub>		Adjusted R <sup>2</sup> =0.71 ( $p<0.01$ )
	OR [95% CI]	Adjusted significance		OR [95% CI]	Adjusted significance

FDG uptake	8.73 [4.67-16.34]	p<0.01	Follow-up FLAIR volume	1.00 [1.00-1.00]	p<0.001
Smoking	172.26 [33.02-898.64]	p<0.01	Age	1.03 [1.01-1.05]	p=0.01
Mod/severe leukoaraiosis	0.08 [0.03-0.24]	p=0.01	Male sex	0.65 [0.47-0.89]	p=0.02
Follow-up FLAIR volume	1.00 [1.00-1.00]	p=0.02	Hypertension	0.76 [0.54-1.07]	p=0.15
Diabetes	112.28 [12.82-983.11]	p=0.01			
Male sex	0.82 [0.66-1.01]	p=0.14			
Hypertension	2.06 [1.49-2.84]	p=0.01			
Current statin	0.75 [0.54-1.05]	p=0.17			
Current antiplatelet	3.96 [2.60-6.04]	p<0.01			
CEA	2.48 [1.83-3.38]	p<0.01			
<b>WV TBR<sub>max</sub></b>		Adjusted R <sup>2</sup> =0.74 (p<0.01)	<b>WV TBR<sub>max</sub></b>		Adjusted R <sup>2</sup> =0.70 (p=0.04)
	OR [95% CI]	Adjusted significance		OR [95% CI]	Adjusted significance
FDG uptake	1.36 [0.76-2.44]	p=0.33	Smoking	0.00 [0.00-0.05]	p=0.01
Follow-up FLAIR volume	1.00 [1.00-1.00]	p<0.001	Mod/severe leukoaraiosis	16,219 [102.05-2,578.092]	p<0.01
Age	1.03 [1.01-1.05]	p<0.01	Follow-up FLAIR volume	1.00 [1.00-1.00]	p<0.01
Male sex	0.76 [0.56-1.03]	p=0.11	Diabetes	9.25 [0.22-390.19]	p=0.29
			Hypertension	0.22 [0.09-0.51]	p=0.01
			Current statin	7.51 [2.99-18.89]	p<0.01
			Current antiplatelet	0.08 [0.02-0.27]	p<0.01
			CEA	0.22 [0.10-0.48]	p<0.01

**Table 7.7:** Multiple logistic regression for factors associated with cognitive impairment on three-month MoCA.

#### 7.3.4 Contribution of cerebrovascular disease

On univariable analysis, there was no significant difference in baseline MoCA scores for individuals with no/mild leukoaraiosis versus moderate/severe leukoaraiosis (mean 25.8±3.29 versus 22.9±5.32 respectively, p=0.16). There was no association between the dichotomised severity of leukoaraiosis and the presence of cognitive impairment (MoCA <26) at baseline (p=0.37).

On univariable analysis, there was also no significant difference in three-month MoCA scores for individuals with no/mild leukoaraiosis and moderate/severe leukoaraiosis (mean  $27.5 \pm 3.5$  and  $25 \pm 5$  respectively,  $p=0.25$ ). There was no association between the dichotomised severity of leukoaraiosis and the presence of cognitive impairment (MoCA  $<26$ ) at three months ( $p=0.37$ ).

There was no association between the three-month FLAIR primary lesion volume and three-month MoCA on univariable analysis ( $r_s=-0.16$ ,  $p=0.53$ ).

## 7.4 Discussion

### 7.4.1 Cognitive outcomes

In this substudy we found a positive relationship between FDG uptake – and by implication inflammation – within the symptomatic plaque and cognitive impairment (defined as a MoCA score  $<26$ ) at three months following stroke. This relationship appears to remain significant after adjustment for other vascular risk factors, leukoaraiosis, and final infarct volume. Correspondingly, there was also a moderate negative correlation between FDG uptake in the symptomatic plaque and three-month MoCA score.

Components of the inflammatory response may be directly neurotoxic. In an *in vitro* model, CRP was shown to undergo cellular uptake into human-derived neuronal cells, and potentially neurotoxic (Duong et al., 1998). It has been postulated that the role of CRP as an opsonin in an innate immune response may contribute to this, as well as having a microvascular effect (Kuo et al., 2005).

The results of the logistic regression are interesting, though the size of the cohort limits the ability to form definitive conclusions. In particular, previously FDG uptake in the *asymptomatic* artery appeared to have the strongest association with the severity of leukoaraiosis and stroke lesion evolution. However, here it appears that it is uptake in the *symptomatic* plaque that has a significant association with cognitive dysfunction. Indeed, we found that FDG uptake was eliminated in the regression

model for whole vessel and all asymptomatic  $TBR_{max}$  measures. The overall pattern suggests that while the background level vascular inflammation may ‘prime’ the brain for injury and promote BBB permeability, the increased inflammation associated with the symptomatic plaque may exacerbate cognitive impairment through neurotoxicity, potentially via a CRP-mediated mechanism given the near-significant result difference in hsCRP concentration. However, there is also the possibility that this may be secondary to the relatively small size of the cohort.

The small size of the cohort may also be responsible for a few curious findings on the regression analysis, despite the high adjusted  $R^2$  values for the models. Some vascular risk factors followed expected results (e.g. diabetes and hypertension associated with worse cognitive function) but others appeared counter-factual. For example, leukoaraiosis appearing to be protective for cognitive impairment in the symptomatic artery models (though dramatically increased the risk in the asymptomatic artery models). However, on univariable analysis, MoCA scores did not appear to differ significantly between those with no/mild leukoaraiosis and moderate/severe leukoaraiosis at either baseline or at three-month follow-up. This may be consistent with not all white matter disease being symptomatic, as well as our analysis being limited by a small sample. Consequently, it is likely that this association is a product of both these considerations, rather than reflecting a physiological mechanism.

Similarly, CEA appeared to increase the risk of cognitive impairment in symptomatic artery models, but was protective in asymptomatic artery models. The association between revascularisation therapy and cognition is incompletely understood, though it has been suggested that both carotid artery stenting (CAS) and CEA may improve cognitive dysfunction (Antonopoulos et al., 2015, Germano da Paz et al., 2014, Lal et al., 2011). Again, it is likely that the small proportion of individuals undergoing CEA in our sample may contribute to this finding. However, this observation is consistent with the findings in the previous chapter that CEA appeared positively associated with FLAIR lesion evolution, and hence may reflect the clinical outcomes in our limited CEA cohort.

#### *7.4.2 Modified Rankin scale outcomes*

There was no statistically significant association between any measure of FDG uptake in either symptomatic or asymptomatic artery and ‘good’ versus ‘poor’ mRS outcomes (using either mRS 0-1 or mRS 0-2 to represent a ‘good’ outcome). There are several likely reasons for this. Firstly, although our study found an association between carotid inflammation and FLAIR lesion evolution and some association with final infarct volume, we did not consider the location of the infarct. Consequently, small infarcts in strategic areas will have a much larger effect upon functional status than moderately-sized infarcts in less strategic areas.

Given the size of our study, the limited spread of FDG TBRs, and potential shortcomings of the mRS (broad ordinal categories and subjectivity), it is unsurprising that no statistically significant trend was detected. Further work in this area would require larger sample sizes and consideration of infarct location.

#### *7.4.3 Barthel index outcomes*

The BI, with a larger spread of scores, may offer increased sensitivity to detect changes in disability. In our study we found only WV  $TBR_{max}$  to have a significant negative correlation with BI at three months. Given the lack of a clear trend in these results, this isolated finding should be treated with caution and may be hypothesis-generating for future work.

## **7.5 Summary of findings**

This chapter has discussed:

1. An independent negative relationship was observed between FDG uptake within the symptomatic carotid plaque and poorer cognitive performance at three months after stroke.
2. There was a suggestion that increased diffuse FDG uptake within the symptomatic artery is associated with greater disability on the BI.
3. No relationship was found between arterial FDG uptake and outcome measured using the mRS.

**Chapter Eight:**  
**From the Vulnerable Plaque to the Vulnerable Brain:**  
**General Discussion and Future Work**

**8.1 Summary of work**

This thesis considers the pathophysiological processes occurring within the carotid atherosclerotic plaque, and systemic atherosclerosis more broadly, and how their contribution to plaque vulnerability may be imaged non-invasively *in vivo*. It also investigates how atherosclerosis may influence the development of chronic cerebrovascular disease, the evolution of the lesion in the early post-stroke period, and the clinical outcome for the stroke survivor. In other words, we expand our focus beyond the vulnerable plaque to include the vascular contribution to the “vulnerable brain.”

*8.1.1 Inflammation, microcalcification, and the vulnerable plaque*

As shown in Chapters Three and Four, inflammation and microcalcification represent key processes in plaque rupture; contributing to biochemical and mechanical plaque destabilisation respectively. PET imaging using FDG to quantify inflammation and NaF to quantify microcalcification has shown that both these radiotracers may discriminate between symptomatic and asymptomatic plaques non-invasively *in vivo*. Furthermore, the tracer uptake – and by implication the pathophysiological processes they represent – shows distinct patterns between the radiotracers. Microcalcification appears to occur in a focal manner, with SHS and MDS, but not WV,  $SUV_{max}$  and  $TBR_{max}$  significantly higher in symptomatic plaques than asymptomatic plaques. This is visualised by the spatial distribution curves in Chapter Three, and further reinforced by the finding of increased NaF uptake in the bifurcation versus ‘non-bifurcation’ regions in Chapter Four. In contrast, FDG uptake appears a more diffuse phenomenon.

The ability to quantify microcalcification *in vivo* has potential use within drug discovery trials, in the same way that FDG uptake has been used in recent studies (Fayad et al., 2011b, Fayad et al., 2011a, Mani et al., 2014). The ‘vicious cycle’ of

inflammation and microcalcification discussed in Chapter One, and demonstrated by the positive association between FDG and NaF uptake in advanced, more heavily-calcified bifurcations, offers the potential to target both components of this relationship. Given the inter-related nature of inflammation and microcalcification, yet distinct spatial distributions, it appears likely that microcalcification is driven by a combination of generalised inflammation and local mechanical forces. The interaction between cellular processes responsible for inflammation and microcalcification have been discussed in Chapters One, Three, and Four. Chapters One and Three have also discussed the molecular pathways contributing to vascular calcification, as well as a potential role for statins promoting micro- and macrocalcification. Targeting of these processes to either reduce microcalcification, or to encourage macrocalcification that may confer stability, may potentially be monitored using NaF-PET. Furthermore, the use of PET may facilitate our understanding of the mechanisms of emerging vascular therapies: for example, proprotein convertase subtilisin-kexin type 9 (PCSK9) inhibitors have been shown to reduce atherosclerotic plaque volume (Nicholls et al., 2016) but it is currently unknown how they influence plaque inflammation and microcalcification.

Our results highlight that smoking has a consistent and powerful association with vascular inflammation and microcalcification. As a modifiable risk factor, smoking cessation may have clear implications for not only the stability of the plaque, but also the downstream consequences of the plaque pathophysiology on the brain. Other factors, including age and medication use, also appear to influence the development of micro- and macrocalcification.

### *8.1.2 Beyond the vulnerable plaque – the “vulnerable brain”*

Although a key triggering event in stroke, plaque rupture is only part of the complex pathophysiology of cerebrovascular disease. It has been known for some time that inflammation within atherosclerosis represents a systemic process (Rudd et al., 2009), and our results support the diffuse nature of this inflammation. The findings discussed in Chapters Five and Six indicate that the general burden of systemic atherosclerosis, in particular its constituent inflammatory activity, appears associated with the

development of chronic small vessel disease and with evolution of the post-infarct lesion.

Our results support those seen in pro-atherogenic mouse models and early human pilot studies with cardiovascular risk factors who were found to demonstrate increased microglial activation in the absence of an acute event; demonstrating brains “primed” with inflammation (Drake et al., 2011). In our study cohort, we hypothesise that prolonged exposure to inflammatory-mediators, in particular MMP-9, is associated with BBB disruption that predisposes to the development of leukoaraiosis. Given that these findings are unlikely to develop acutely, it suggests that chronic atheromatous inflammation is associated with the development of chronic cerebrovascular disease. As discussed in Chapter Five, the strongest association is with the non-culprit artery and this likely represents the general inflammatory atherogenic environment, rather than the symptomatic plaque that represents a disproportionately increased diseased segment. Hence, it is not simply the vulnerable plaque that must be considered but rather the entire arterial system, and consequently the overall exposure to vascular risk factors.

General atheromatous inflammation in the asymptomatic artery also appears to have important implications for the evolution of the acute lesion. As shown in Chapter Six, generalised atheromatous inflammation appears associated with greater interval change in FLAIR hyperintensity volume and there is suggestion that it is also associated with final FLAIR hyperintensity volume. The apparent lack of a relationship with baseline DWI or FLAIR hyperintensity volumes suggests that this is not mediated through the size of the thrombus, and the fact that the association appears strongest with the asymptomatic artery again suggests that it is the generalised burden of vascular disease that is influencing the lesion evolution. Hence, we postulate that this may also reflect BBB dysfunction and a “primed” brain for injury.

Such priming of the brain is likely to involve stimulation of microglia in response to peripheral inflammatory changes, triggering neuroinflammatory changes and affecting endogenous repair mechanisms within the brain in the absence of acute injury. Furthermore, increased BBB permeability mediated by MMP-9 may exacerbate this

through increased cellular infiltration. For example, increased T-lymphocyte infiltration of the choroid plexus has been observed in ApoE<sup>-/-</sup> mice on an atherogenic diet (Drake et al., 2011). These constellation of neuroinflammatory changes and BBB permeability may also have repercussions for cerebral autoregulation, meaning that the brain becomes more vulnerable to pressure changes in the systemic circulation. Consequently, these pathophysiological processes may be contributing to chronic brain changes even in the absence of acute ischaemia, and may provide mechanisms for the findings we report in Chapter Five. Furthermore, the altered neuroinflammatory status and reduced protective homeostatic mechanisms may mean that the brain has less reserve to withstand injury at the time of acute ischaemia, contributing to the pattern of infarct development we have described in Chapter Six.

### *8.1.3 Beyond the biology – the “vulnerable patient”*

Unsurprisingly there was no clear association between functional outcomes and FDG uptake within the carotid arteries, as discussed in Chapter Seven. What was interesting was the finding of higher FDG uptake in the symptomatic plaque in those individuals who had cognitive impairment, even after adjustment for leukoaraiosis, final infarct volume, and other cardiovascular risk factors. As previously discussed, it is curious that in this regard the symptomatic plaque appears to be the region associated with the outcome, rather than the non-culprit artery as seen in leukoaraiosis and acute lesion evolution. The finding that CEA did not seem to reduce this risk may imply that the mechanism for this occurs early after symptomatic plaque rupture. Further work is required to consider whether it is the location of the infarct or whether more generalised inflammatory-mediated network disruption is contributing to these findings.

## **8.2 Alternative approaches and future directions in PET imaging of atherosclerosis.**

Although FDG-PET has become a mainstay of metabolic imaging in atherosclerosis in a relatively short time, its lack of specificity means that proximity of the artery of interest to other highly metabolically active structures, such as the myocardium, limits its utility. Alternative radiotracers targeting macrophage-driven inflammation via their

expression of TSPO have been investigated with the goal of providing higher specificity than that offered by FDG.  $^{11}\text{C}$ -PK11195 targets TSPO expressed on macrophages and microglia and has been shown to detect these inflammatory cells in atheroma and around the stroke penumbra respectively. Specific to atherosclerosis, PK11195 uptake was found to be higher in inflamed than non-inflamed plaques in a mouse model, though its utility as a tracer was limited due to a non-significant difference between plaque and healthy vessel wall (Laitinen et al., 2009). This likely reflects the ubiquitous nature of TSPO expression by a range of cells and organs, despite the upregulation in activated plaque macrophages, but may also reflect the limitations of using mouse models of plaque, especially vulnerable plaques, compared to humans. Subsequent studies in human subjects have shown more promise, with PK11195 TBR found to be higher in symptomatic versus asymptomatic carotid arteries (TBR 1.06 +/- 0.2 and 0.86 +/- 0.11 respectively,  $p=0.001$ ) despite a lower grade of stenosis in asymptomatic arteries (Gaemperli et al., 2012). PK11195 uptake has been found to co-localise with activated macrophages using autoradiography and CD68 staining of *ex vivo* carotid histology (Fujimura et al., 2008, Bird et al., 2010). However, the ubiquitous uptake in healthy vessel wall may limit the utility of PK11195-PET in clinical atherosclerosis imaging.

$^{11}\text{C}$ -PBR28 was shown to have improved specificity in a dual tracer PK11195 and PBR28 rat study (Imaizumi et al., 2007), but subsequent work comparing receptor binding between animal models and humans found receptor binding to be markedly lower in humans compared to monkeys, and that there was variation in the human binding with some showing no specific binding (Fujita et al., 2008). Subsequent studies have revealed polymorphism in the gene Ala147Th that results in high-affinity and low-affinity binders, with heterozygous individuals displaying intermediate affinity binding (Owen et al., 2011, Kreisl et al., 2013). In contrast, PK11195 does not appear to have variable affinity as it binds to a different site on the TSPO (Owen et al., 2010). These findings show it is important to exercise caution when comparing tracer pharmacokinetics between different animal species and humans, as well as human subject comparisons.

Newer TSPO ligands are in development, labeled with  $^{18}\text{F}$  rather than  $^{11}\text{C}$ . There has been increasing interest in  $^{18}\text{F}$ -GE-180 to replace PK-11195 as the TSPO ligand of

choice to image neuro- and potentially atherosclerotic plaque inflammation. Animal models have shown  $^{18}\text{F}$ -GE-180 to have a significantly higher binding potential than that of PK-11195, improved signal-to-noise ratio, and lower non-specific binding in and around infarcted cerebral tissue (Dickens et al., 2014, Boutin et al., 2015). The use of  $^{18}\text{F}$  in contrast to  $^{11}\text{C}$  has other benefits including a longer half-life. However, the utility of such second-generation TSPO radioligands in PET imaging may be limited owing to variable receptor binding affinity due to genetic polymorphisms (Kreisl et al., 2013, Guo et al., 2013, Lavisse et al., 2015). Further work is required to assess the utility of  $^{18}\text{F}$ -GE-180 and other second-generation TSPO ligands for imaging both plaque inflammation and neuroinflammation.

A promising new radiotracer is  $^{68}\text{Ga}$ -DOTATATE. Somatostatin receptor subtype-2 (SST<sub>2</sub>) is upregulated on the cell surface of macrophages, to which DOTATATE demonstrates high specific binding activity (Dalm et al., 2003, Armani et al., 2007). The low physiological expression of SST<sub>2</sub> by the myocardium suggests this tracer may be advantageous for targeting disease in the coronary arteries.

Vascular  $^{68}\text{Ga}$ -DOTATATE uptake has been imaged in asymptomatic individuals with cardiovascular risk factors and coronary calcification (Mojtahedi et al., 2015, Li et al., 2012, Rominger et al., 2010) and in aortic atherosclerotic plaques in a mouse model (Rinne et al., 2015). In a retrospective series of DOTATATE-PET imaging performed in oncological practice, Rominger et al. found  $^{68}\text{Ga}$ -DOTATATE-PET to have an excellent intra-reader and inter-reader reproducibility for TBR readings in the left anterior descending coronary artery (intra-class correlation coefficients of 0.97 and 0.94 respectively) (Rominger et al., 2010).

$^{64}\text{Cu}$ -DOTATATE has also been investigated for use in carotid imaging. The longer half-life of  $^{64}\text{Cu}$  compared to  $^{68}\text{Ga}$  (12.7 hours versus 68 minutes) and shorter maximum positron range provide several theoretical advantages, although this must be balanced against the wider availability of the generator-produced  $^{68}\text{Ga}$  compared to the cyclotron-produced  $^{64}\text{Cu}$ . In a proof of principle study using PET/MRI, Pedersen et al. demonstrated carotid  $^{64}\text{Cu}$ -DOTATATE uptake correlated with gene expression of macrophage markers CD68 and CD163 using univariable analysis, though only correlation with CD163 expression remained significant on multivariable analysis

(Pedersen et al., 2015). The propensity of DOTATATE towards CD163+ macrophages, as well as findings of atheromatous regions with DOTATATE but no FDG uptake, suggests that DOTATATE is able to identify a different component of the inflammatory process compared to conventional FDG-PET (Rominger et al., 2010, Pedersen et al., 2015). Increased  $^{64}\text{Cu}$ -DOTATATE signal has also been reported in individuals with cardiovascular risk factors in a retrospective study (Malmberg et al., 2015).

$^{68}\text{Ga}$ -DOTATATE has recently been demonstrated to differentiate between symptomatic and asymptomatic carotid plaques, with uptake correlating strongly with histological macrophage burden and Framingham risk scores (Tarkin et al., 2017). A DOTATATE  $\text{TBR}_{\text{max}}$  of greater than 2.66 had 87.5% sensitivity and 78.4% specificity to detect culprit coronary segments (Tarkin et al., 2017). The superior specificity of DOTATATE relative to FDG results in improved signal-to-noise ratio, particularly in the coronary arteries. Tracer production does not require a cyclotron meaning imaging is much cheaper than using FDG and does not require pre-scan fasting.

### **8.3 Planned papers from this thesis**

Three main papers are planned based upon the work described in this thesis:

- The dual tracer FDG and NaF study demonstrating the different spatial patterns of tracer uptake (Chapters Three and Four).
- The association between carotid FDG uptake and the extent of leukoaraiosis (Chapter Five).
- The association between carotid FDG uptake and stroke lesion evolution (Chapter Six).

## 8.4 Ongoing and future work

### 8.4.1 *Vascular imaging*

The work presented in this thesis is limited in its single timepoint assessment of FDG and NaF uptake. Although a number of studies have shown that FDG uptake decreases with therapy (Tahara et al., 2006, Mizoguchi et al., 2011), there have been no equivalent studies for NaF. Serial imaging post-stroke would help elucidate whether the microcalcification process changes following rupture and/or in response to secondary prevention therapies.

As discussed previously, FDG is limited in its specificity. We are currently analysing the results of the TIA cohort of the VISION study to investigate whether the spatial distribution of DOTATATE uptake mirrors that seen with FDG (Tarkin et al., 2017). Furthermore, it would be advantageous to validate our findings of the association between vascular inflammation and both small vessel disease and lesion evolution using DOTATATE-PET.

A subgroup of our participants underwent direct thrombus imaging, a T1-based sequence described in Chapter Two (**Figure 8.1**). Future work will include an analysis of the relationship between the presence of thrombus and both FDG and NaF uptake, potentially elucidating the thromboinflammatory process. However, conclusions will be limited in our cohort given the small number of individuals imaged and the heterogeneity in both the stroke-to-scan interval and whether the individual was thrombolysed. Future work would benefit from expedited imaging of symptomatic plaques in individuals who had not been thrombolysed.

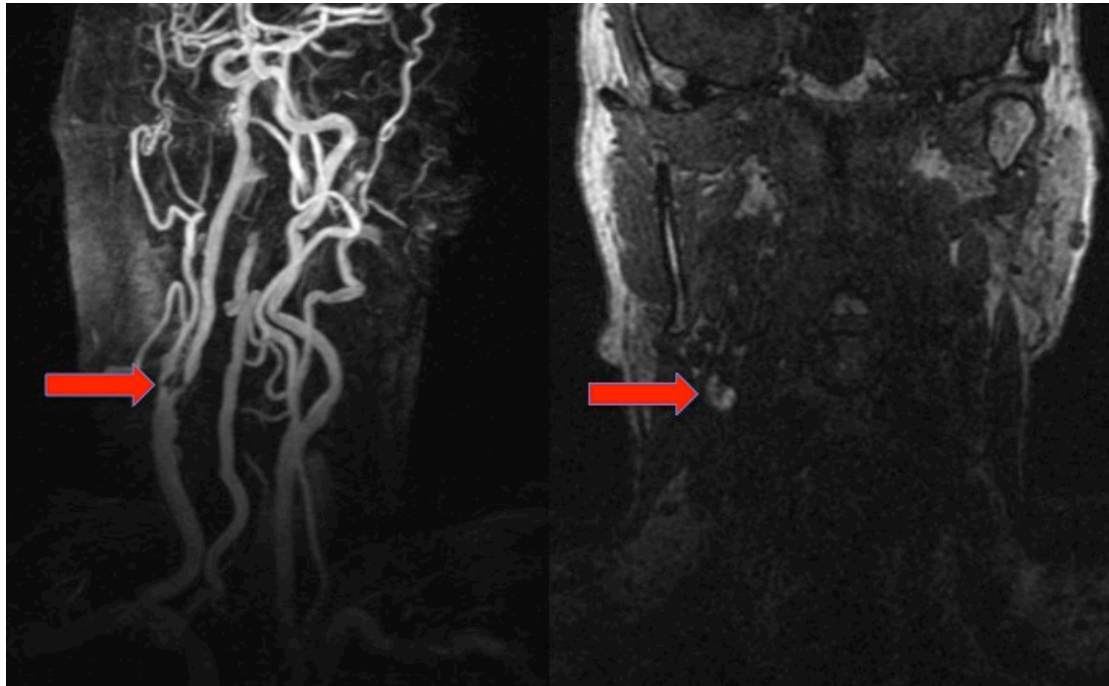


**Figure 8.1: Direct thrombus imaging.** Positive direct thrombus imaging sequence showing thrombus in the presence of a symptomatic right internal carotid artery stenosis (red arrow).

The increasing availability of PET/MRI enables concurrent high-resolution assessment of tracer uptake and plaque morphology. A promising avenue of investigation may involve DOTATATE imaging of plaque inflammation and how it relates to high-risk morphological features (such as intra-plaque haemorrhage and thin fibrous cap), potentially in a longitudinal study. Similarly, NaF uptake could also be compared with plaque morphology, though the limited ability of MRI to image calcification means that currently PET/CT is likely to remain the imaging modality of choice.

#### *8.4.2 Imaging the vulnerable brain*

The finding that inflammation within the systemic vasculature appears associated with deleterious effects in the setting of both chronic and acute cerebrovascular disease provokes questions about the mechanisms behind these results. There are several potential imaging studies that may help elucidate this relationship. Firstly, concurrent dual tracer PET imaging assessing carotid inflammation and microglial activation would help establish the correlation between inflammation on either side of the BBB.

PK11195 would appear the radiotracer most suited to this role, having demonstrated both carotid and microglial uptake as discussed above, though it remains a suboptimal tracer to use due to ubiquitous uptake. Whether newer radiotracers targeting the TSPO may overcome these limitations remains to be seen.

As discussed, our postulated mechanism underlying this association is MMP-9-mediated disruption of BBB. In recent years, dynamic contrast-enhanced T1-based sequences, such as the T1 mapping with partial inversion recovery (TAPIR) sequence (Taheri et al., 2011b, Taheri et al., 2011a), have been used to measure BBB permeability. The use of MRI to measure BBB permeability alongside PET imaging of the vasculature may help support or refute our hypothesis.

Finally, our finding that increased FDG within the symptomatic plaque appeared associated with poorer cognition at three months post-stroke is an interesting one with potential significant quality of life implications for the stroke survivor. A limitation of our study is that our cohort all had a stroke, and hence it is impossible to measure cognition prior to the event. It would be interesting to investigate if FDG uptake in asymptomatic atherosclerosis affects network integrity using diffusion tensor imaging in such individuals.

#### *8.4.3 Considerations for future work*

Although the findings discussed in this thesis suggest interesting and plausible pathophysiological processes, it is also necessary to exercise a degree of caution in their interpretation. The limitations of our study described in the previous chapters need to be considered when planning future work. In particular, this thesis includes several subgroups and subgroup analyses, raising the risk of type one error. Furthermore, although a generally consistent pattern of results was seen across different SUV or TBR measures, it is important to recognise that these metrics are related. Hence, future work should aim to adopt a single standard measure. Finally, the study is limited in its size. Ultimately, these findings need to be replicated and verified in larger samples with clear pre-specified primary and sub-group analyses.

## 8.5 Conclusion

Stroke is one of the leading causes of adult disability in the Western World. It is a cruel disease; striking quickly and frequently leaving life-changing repercussions. It affects not only the individual, but also their families, carers, health services, and the wider economy, with an estimated cost to the United Kingdom economy of £8.9 billion per annum (Saka et al., 2009). As a major cause of ischaemic stroke, carotid atherosclerosis represents an important pathology, but one that still we do not fully understand. Why the disease becomes symptomatic in some individuals, while others live with quiescent disease for years, remains an important clinical question. Despite this, our conventional clinical management remains anatomically-focused, rather than physiological-based, with the degree of luminal stenosis being the driving factor for determining therapy decisions.

The findings of this thesis have potential implications for future clinical and research exploitation. From a vascular perspective, the ability to detect pathophysiology associated with the vulnerable plaque may yield novel therapeutic targets, facilitate the use of molecular endpoints in drug discovery trials, or allow evaluation of response to treatment, particularly those in high-risk or treatment-resistant groups. Given the cost, availability of PET scanning, and radiation exposure, it is unlikely that PET imaging will feature as a second-line risk-stratification tool after other modes of screening for carotid disease. However, the suggestion that current or emerging biomarkers may be able to act as surrogate markers is an enticing one.

Our findings that molecular processes within atherosclerosis not only influence plaque vulnerability, but may also prime the vulnerable brain for injury, have the potential for development to provide useful information for prognostication in the acute clinical setting. It may also have implications for reducing the burden of small vessel disease, vascular cognitive impairment, and disability after stroke through targeting these processes using novel anti-atherosclerotic or anti-inflammatory therapies.

Atherosclerosis is a systemic disease and affects the individual in more ways than simply plaque rupture. However, its complexity may also provide the means and

opportunity to reduce the effects of cerebrovascular disease or, better yet, to prevent them occurring in the first place.

**Appendix A:**  
**Prizes, Papers, and Presentations during PhD**

**Prizes**

- 2017      **Mansell Memorial Prize for Neuroscience**, Medical Society of London.
- 2017      **BHF Centre for Research Excellence Annual Symposium Poster Prize**.
- 2016      Shortlisted for the Warlow Prize, British Association of Stroke Physicians.
- 2016      **Binks Young Investigator Award**, British Atherosclerosis Society.
- 2016      **President's Prize**, Lipids, Metabolism and Cardiovascular Section, Royal Society of Medicine.
- 2016      **Harvey Prize for Vascular Medicine**, Royal Society of Medicine.
- 2016      **Trainee Presentation 1<sup>st</sup> Prize**, British Geriatrics Society Cardiovascular Section.
- 2016      **Master's Essay Prize**, Gonville and Caius College, University of Cambridge.
- 2016      Shortlisted for the Gordon Holmes Prize for Neuroscience, Royal Society of Medicine.
- 2016      Shortlisted for the Vice-Chancellor's Award for Public Engagement, University of Cambridge.
- 2016      **Wellcome Trust Image Award** for image demonstrating PhD research.
- 2015      Selected for the **Rising Star Programme** at the University of Cambridge.
- 2015      **Public Engagement Image Prize**, Cambridge Science Festival, University of Cambridge.
- 2014      **Public Engagement Presentation Prize** by School of Life Sciences, University of Cambridge.
- 2014      Selected for the **European Stroke Organisation Summer School** (Glasgow 2014).

## Publications

1. **Evans NR**, Tarkin JM, Buscombe JR, Markus HS, Rudd JHF, Warburton EA. PET Imaging of the Neurovascular Interface in Cerebrovascular Disease. *Nat Rev Neurol* 2017 [In press].
2. Tarkin JM, Joshi FR, **Evans NR**, ..., Warburton EA, Davenport AP, Rudd JHF. Atherosclerotic Inflammation Imaging Using  $^{68}\text{Ga}$ -DOTATATE PET Outperforms  $^{18}\text{F}$ -FDG PET: Validation from Gene-to-Patient. The Vision Study. *J Am Coll Cardiol* 2017;69(14):1774-91.
3. Induruwa I, **Evans NR**, Aziz A, Reddy S, Khadjooi K, Romero-Ortuno R. Clinical frailty is independently associated with non-prescription of anticoagulation in older patients with atrial fibrillation. *Geriatr Gerontol Int* 2017 [In press].
4. Hammad B, **Evans NR**, Rudd JHF, Tawakol A. Molecular Imaging of Atherosclerosis with Integrated PET Imaging. *J Nucl Cardiol* 2017;24(3):938-943.
5. Stoker TB, **Evans NR**, Warburton EA. Internal Carotid Artery Dissection. *Br J Hosp Med* 2016;77(12):708-711.
6. Sriranjana RS, Tarkin JM, **Evans NR**, Chowdhury MM, Rudd JR. Imaging unstable plaque. *Q J Nucl Med Mol Imaging* 2016;60(3):205-18.
7. Stoker TB, **Evans NR**. Managing Risk After Intracerebral Hemorrhage in Concomitant Atrial Fibrillation and Cerebral Amyloid Angiopathy. *Stroke* 2016;47(7):e190-192.
8. **Evans NR**, Tarkin JM, Chowdhury MM, Warburton EA, Rudd JH. PET Imaging of Atherosclerotic Disease: Advancing Plaque Assessment from Anatomy to Pathophysiology. *Curr Atheroscler Rep* 2016;18(6):30-42.
9. **Evans NR**, Warne B, Wood DF. Developing a Pragmatic Medical Curriculum for the 21<sup>st</sup> Century. *Med Educ* 2016;50(12):1192-1194.
10. Tarkin JM, Dweck MR, **Evans NR**, Takx R, Brown AJ, Tawakol A, Fayad ZA, Rudd JHF. Imaging Atherosclerosis. *Circ Res* 2016;118(4):750-69.
11. **Evans NR**, Besser MW, Khadjooi K. Activated prothrombin complex in the management of direct thrombin inhibitor-associated intracerebral haemorrhage. *QJM* 2016;109(6):415-6.

12. **Evans NR**, Harper V, Scoffings DJ, Warburton EA. Running, ischaemic stroke and carotid artery dissection. *QJM* 2015;108(12):973-4.

### **Conference oral presentations**

1. Age is an Independent Predictor of Paroxysmal Atrial Fibrillation in Embolic Strokes of Undetermined Source. UK Stroke Forum 2016. Liverpool, UK.
2. Non-invasive Identification of Culprit Carotid Atheroma using Sodium Fluoride Positron Emission Tomography. British Atherosclerosis Society Conference 2016. Cambridge, UK.
3. Non-invasive detection of vulnerable carotid atheroma in stroke: imaging inflammation at the neurovascular interface. The Inflamed Brain 2016. Cambridge, UK.
4. Non-invasive Identification of Vulnerable Carotid Atheroma in Cerebrovascular Disease using Sodium Fluoride Positron Emission Tomography. Gordon Holmes Prize 2016, Royal Society of Medicine. London, UK.
5. Managing Risk After Intracerebral Hemorrhage in Concomitant Atrial Fibrillation and Cerebral Amyloid Angiopathy. European Stroke Organisation Conference 2016. Barcelona, Spain.
6. Sodium fluoride-positron emission tomography provides a non-invasive method for identifying symptomatic plaques in carotid artery stenosis. BHF-Cambridge Cardiovascular Early Careers Event 2015. Cambridge, UK.
7. Activated Prothrombin Complex in the Management of Direct Thrombin Inhibitor-associated Intracerebral Haemorrhage. European Stroke Conference 2015. Vienna, Austria.

**Appendix B:**  
**Degrees of Carotid Stenosis**

Participant ID	Symptomatic side	Degree of stenosis: symptomatic artery	Degree of stenosis: Asymptomatic artery
3455	Right	50-69%	1-29%
2547	Right	>90%	50-69%
1483	Right	50-69%	30-49%
3914	Right	>90%	>90%
5505	Right	70-89%	1-29%
7346	Right	70-89%	1-29%
4549	Left	>90%	>90%
9508	Right	>90%	50-69%
5341	Right	70-89%	1-29%
3612	Right	70-89%	>90%
6995	Left	70-89%	1-29%
3399	Left	70-89%	30-49%
2812	Right	50-69%	50-69%
7119	Right	50-69%	1-29%
9681	Right	50-69%	30-49%
6996	Right	70-89%	30-49%
9391	Right	>90%	30-49%
3488	Right	>90%	1-29%
3356	Left	>90%	30-49%
5936	Right	70-89%	1-29%
1133	Right	>90%	30-49%
7622	Left	>90%	30-49%
8904	Left	50-69%	30-49%
5377	Right	70-89%	30-49%
4187	Left	>90%	1-29%
5048	Left	50-69%	50-69%

**Table B.1:** Symptomatic side and degree of stenosis in each carotid artery for each participant (in the 26 participant cohort).

**Appendix C:**  
**NaF Univariable Analysis**

	Correlation	Significance		Correlation	Significance
SHS SUV <sub>max</sub>	r <sub>s</sub> =0.64	p<0.01	SHS TBR <sub>max</sub>	r <sub>s</sub> =0.50	p<0.01
MDS SUV <sub>max</sub>	r <sub>s</sub> =0.63	p<0.01	MDS TBR <sub>max</sub>	r <sub>s</sub> =0.49	p<0.01
WV SUV <sub>max</sub>	r <sub>s</sub> =0.36	p<0.01	WV TBR <sub>max</sub>	r <sub>s</sub> =0.23	p=0.09
SHS SUV <sub>mean</sub>	r <sub>s</sub> =0.59	p<0.01	SHS TBR <sub>mean</sub>	r <sub>s</sub> =0.50	p<0.01
MDS SUV <sub>mean</sub>	r <sub>s</sub> =0.58	p<0.01	MDS TBR <sub>mean</sub>	r <sub>s</sub> =0.48	p<0.01
WV SUV <sub>mean</sub>	r <sub>s</sub> =0.38	p<0.01	WV TBR <sub>mean</sub>	r <sub>s</sub> =0.31	p=0.03

**Table C.1:** Correlations between age and NaF uptake.

	Female	Male	Significance		Female	Male	Significance
SHS SUV <sub>max</sub>	2.30 (0.70)	1.91 (0.71)	p=0.08	SHS TBR <sub>max</sub>	2.88 (1.17)	2.59 (0.95)	p=0.38
MDS SUV <sub>max</sub>	2.05 (0.67)	1.83 (0.67)	p=0.12	MDS TBR <sub>max</sub>	2.68 (1.22)	2.49 (0.82)	p=0.47
WV SUV <sub>max</sub>	1.32 (0.44)	1.37 (0.40)	p=0.69	WV TBR <sub>max</sub>	1.85 (0.57)	1.82 (0.42)	p=0.69
SHS SUV <sub>mean</sub>	1.83 (0.68)	1.64 (0.51)	p=0.08	SHS TBR <sub>mean</sub>	2.44 (1.04)	2.12 (0.54)	p=0.27
MDS SUV <sub>mean</sub>	1.64 (0.62)	1.60 (0.47)	p=0.14	MDS TBR <sub>mean</sub>	2.23 (1.09)	2.04 (0.54)	p=0.39
WV SUV <sub>mean</sub>	1.16 (0.50)	1.18 (0.35)	p=0.66	WV TBR <sub>mean</sub>	1.59 (0.47)	1.57 (0.29)	p=0.75

**Table C.2:** NaF uptake by sex. All values are median (IQR).

	Correlation	Significance		Correlation	Significance
SHS SUV <sub>max</sub>	r <sub>s</sub> =0.04	p=0.80	SHS TBR <sub>max</sub>	r <sub>s</sub> =-0.14	p=0.31
MDS SUV <sub>max</sub>	r <sub>s</sub> =0.03	p=0.83	MDS TBR <sub>max</sub>	r <sub>s</sub> =-0.16	p=0.27
WV SUV <sub>max</sub>	r <sub>s</sub> =0.15	p=0.28	WV TBR <sub>max</sub>	r <sub>s</sub> =-0.16	p=0.26
SHS SUV <sub>mean</sub>	r <sub>s</sub> =0.09	p=0.51	SHS TBR <sub>mean</sub>	r <sub>s</sub> =-0.11	p=0.42
MDS SUV <sub>mean</sub>	r <sub>s</sub> =0.07	p=0.63	MDS TBR <sub>mean</sub>	r <sub>s</sub> =-0.12	p=0.41
WV SUV <sub>mean</sub>	r <sub>s</sub> =0.15	p=0.30	WV TBR <sub>mean</sub>	r <sub>s</sub> =-0.16	p=0.26

**Table C.3:** Correlations between BMI and NaF uptake.

	Current /former smoker	Non- smoker	Significance		Current /former smoker	Non- smoker	Significance
SHS SUV <sub>max</sub>	1.92 (0.63)	2.32 (0.79)	p=0.19	SHS TBR <sub>max</sub>	2.59 (1.01)	2.85 (0.67)	p=0.40
MDS SUV <sub>max</sub>	1.83 (0.59)	2.05 (0.76)	p=0.30	MDS TBR <sub>max</sub>	2.46 (1.02)	2.65 (0.56)	p=0.57
WV SUV <sub>max</sub>	1.34 (0.43)	1.38 (0.33)	p=0.90	WV TBR <sub>max</sub>	1.83 (0.58)	1.85 (0.33)	p=0.70
SHS SUV <sub>mean</sub>	1.64 (0.45)	1.85 (0.80)	p=0.31	SHS TBR <sub>mean</sub>	2.10 (0.67)	2.21 (0.62)	p=0.49
MDS SUV <sub>mean</sub>	1.57 (0.41)	1.63 (0.71)	p=0.52	MDS TBR <sub>mean</sub>	2.05 (0.67)	2.10 (0.52)	p=0.64
WV SUV <sub>mean</sub>	1.16 (0.37)	1.19 (0.39)	p=0.92	WV TBR <sub>mean</sub>	1.54 (0.43)	1.57 (0.25)	p=0.74

**Table C.4:** NaF uptake by smoking status. All values are median (IQR).

	Diabetes	No diabetes	Significance		Diabetes	No diabetes	Significance
SHS SUV <sub>max</sub>	1.99 (0.63)	1.98 (0.80)	p=0.91	SHS TBR <sub>max</sub>	2.69 (0.95)	2.63 (0.96)	p=0.81
MDS SUV <sub>max</sub>	1.89 (0.56)	1.87 (0.74)	p=0.85	MDS TBR <sub>max</sub>	2.58 (1.14)	2.50 (0.82)	p=0.77
WV SUV <sub>max</sub>	1.39 (0.47)	1.34 (0.38)	p=0.66	WV TBR <sub>max</sub>	1.78 (0.77)	1.85 (0.42)	p=0.76
SHS SUV <sub>mean</sub>	1.80 (0.47)	1.64 (0.53)	p=0.56	SHS TBR <sub>mean</sub>	2.28 (1.03)	2.13 (0.67)	p=0.72
MDS SUV <sub>mean</sub>	1.63 (0.49)	1.57 (0.49)	p=0.65	MDS TBR <sub>mean</sub>	2.21 (1.20)	2.07 (0.57)	p=0.65
WV SUV <sub>mean</sub>	1.27 (0.34)	1.16 (0.37)	p=0.39	WV TBR <sub>mean</sub>	1.58 (0.60)	1.57 (0.29)	p=0.91

**Table C.5:** NaF uptake by diabetes status. All values are median (IQR).

	Hypertension	No hypertension	Significance		Hypertension	No hypertension	Significance
SHS SUV <sub>max</sub>	2.08 (0.61)	1.74 (0.71)	p=0.04	SHS TBR <sub>max</sub>	2.91 (0.73)	2.23 (0.51)	p<0.01
MDS SUV <sub>max</sub>	2.02 (0.55)	1.63 (0.59)	p=0.03	MDS TBR <sub>max</sub>	2.72 (0.65)	2.05 (0.45)	p<0.01
WV SUV <sub>max</sub>	1.45 (0.39)	1.24 (0.33)	p=0.06	WV TBR <sub>max</sub>	1.86 (0.48)	1.70 (0.59)	p<0.01
SHS SUV <sub>mean</sub>	1.76 (0.48)	1.50 (0.56)	p=0.05	SHS TBR <sub>mean</sub>	2.37 (0.69)	1.87 (0.43)	p<0.01
MDS SUV <sub>mean</sub>	1.67 (0.47)	1.40 (0.49)	p=0.03	MDS TBR <sub>mean</sub>	2.20 (0.65)	1.76 (0.48)	p<0.01
WV SUV <sub>mean</sub>	1.19 (0.34)	1.10 (0.36)	p=0.09	WV TBR <sub>mean</sub>	1.60 (0.30)	1.44 (0.39)	p<0.01

**Table C.6:** NaF uptake by hypertension status. All values are median (IQR).

	Current statin	No statin	Significance		Current statin	No statin	Significance
SHS SUV <sub>max</sub>	2.37 (0.89)	1.87 (0.66)	p<0.01	SHS TBR <sub>max</sub>	2.98 (0.52)	2.38 (1.00)	p=0.01
MDS SUV <sub>max</sub>	2.18 (0.73)	1.74 (0.62)	p<0.01	MDS TBR <sub>max</sub>	2.77 (0.40)	2.27 (0.92)	p<0.01
WV SUV <sub>max</sub>	1.52 (0.48)	1.28 (0.37)	p<0.01	WV TBR <sub>max</sub>	1.94 (0.48)	1.81 (0.52)	p=0.01
SHS SUV <sub>mean</sub>	2.11 (0.83)*	1.54 (0.37)*	p=0.01	SHS TBR <sub>mean</sub>	2.38 (0.58)	2.04 (0.67)	p=0.01
MDS SUV <sub>mean</sub>	2.00 (0.79)*	1.46 (0.33)*	p=0.01	MDS TBR <sub>mean</sub>	2.28 (0.62)	1.96 (0.70)	p=0.01
WV SUV <sub>mean</sub>	1.45 (0.45)*	1.10 (0.20)*	p<0.01	WV TBR <sub>mean</sub>	1.67 (0.29)	1.50 (0.41)	p=0.01

**Table C.7:** NaF uptake by statin therapy. All values are median (IQR) except for those marked with an asterisk, where values are mean (SD).

	TC		Triglycerides		HDL		LDL		TC:HDL ratio	
	r <sub>s</sub>	Sig.	r <sub>s</sub>	Sig.						
SHS SUV <sub>max</sub>	-0.18	p=0.20	0.20	p=0.16	0.26	p=0.08	-0.28	p=0.05	-0.34	p=0.02
MDS SUV <sub>max</sub>	-0.20	p=0.16	0.20	p=0.17	0.23	p=0.12	-0.31	p=0.03	-0.35	p=0.01
WV SUV <sub>max</sub>	-0.28	p=0.04	0.14	p=0.32	0.06	p=0.68	-0.38	p<0.01	-0.31	p=0.03
SHS SUV <sub>mean</sub>	-0.19	p=0.18	0.25	p=0.08	0.28	p=0.05	-0.33	p=0.02	-0.37	p<0.01
MDS SUV <sub>mean</sub>	-0.19	p=0.19	0.24	p=0.09	0.25	p=0.09	-0.32	p=0.03	-0.35	p=0.01
WV SUV <sub>mean</sub>	-0.30	p=0.03	0.17	p=0.25	0.03	p=0.82	-0.44	p<0.01	-0.33	p=0.02
SHS TBR <sub>max</sub>	-0.33	p=0.02	-0.17	p=0.23	-0.07	p=0.63	-0.29	p=0.046	-0.29	p=0.045
MDS TBR <sub>max</sub>	-0.35	p=0.01	-0.19	p=0.18	-0.11	p=0.44	-0.31	p=0.03	-0.29	p=0.048
WV TBR <sub>max</sub>	-0.41	p<0.01	-0.33	p=0.02	-0.31	p=0.03	-0.35	p=0.02	-0.23	p=0.11
SHS TBR <sub>mean</sub>	-0.33	p=0.02	-0.15	p=0.30	-0.08	p=0.58	-0.31	p=0.03	-0.28	p=0.05
MDS TBR <sub>mean</sub>	-0.34	p=0.01	-0.16	p=0.26	-0.10	p=0.52	-0.33	p=0.02	-0.30	p=0.04
WV TBR <sub>mean</sub>	-0.45	p<0.01	-0.30	p=0.04	-0.32	p=0.03	-0.40	p<0.01	-0.26	p=0.08

**Table C.8:** Correlations between NaF uptake and lipid profile. TC = total cholesterol, HDL = high-density lipoprotein, LDL = low-density lipoprotein.

	Current antiplatelet	No antiplatelet	Significance		Current antiplatelet	No antiplatelet	Significance
SHS SUV <sub>max</sub>	2.13 (0.68)	1.93 (0.82)	p=0.16	SHS TBR <sub>max</sub>	2.98 (0.65)	2.47 (1.02)	p=0.04
MDS SUV <sub>max</sub>	2.08 (0.70)	1.82 (0.76)	p=0.11	MDS TBR <sub>max</sub>	2.80 (0.51)	2.31 (0.89)	p=0.02
WV SUV <sub>max</sub>	1.47 (0.60)	1.31 (0.35)	p=0.27	WV TBR <sub>max</sub>	1.92 (0.41)	1.81 (0.53)	p=0.09
SHS SUV <sub>mean</sub>	1.80 (0.58)	1.63 (0.51)	p=0.11	SHS TBR <sub>mean</sub>	2.43 (0.68)	2.10 (0.64)	p=0.03
MDS SUV <sub>mean</sub>	1.71 (0.57)	1.54 (0.45)	p=0.08	MDS TBR <sub>mean</sub>	2.32 (0.64)	2.02 (0.64)	p=0.02
WV SUV <sub>mean</sub>	1.27 (0.62)	1.16 (0.36)	p=0.31	WV TBR <sub>mean</sub>	1.65 (0.18)	1.50 (0.42)	p=0.07

**Table C.9:** NaF uptake by antiplatelet therapy. All values are median (IQR).

	Cardiovascular history	No cardiovascular history	Significance		Cardiovascular history	No cardiovascular history	Significance
SHS SUV <sub>max</sub>	2.00 (0.55)	1.98 (0.86)	p=0.39	SHS TBR <sub>max</sub>	3.01 (0.55)	2.38 (0.99)	p<0.01
MDS SUV <sub>max</sub>	1.96 (0.51)	1.85 (0.80)	p=0.28	MDS TBR <sub>max</sub>	2.81 (0.46)	2.27 (0.89)	p<0.01
WV SUV <sub>max</sub>	1.42 (0.41)	1.32 (0.40)	p=0.85	WV TBR <sub>max</sub>	1.92 (0.33)	1.79 (0.51)	p=0.04
SHS SUV <sub>mean</sub>	1.76 (0.48)	1.64 (0.54)	p=0.38	SHS TBR <sub>mean</sub>	2.50 (0.70)	2.04 (0.63)	p<0.01
MDS SUV <sub>mean</sub>	1.67 (0.48)	1.55 (0.46)	p=0.31	MDS TBR <sub>mean</sub>	2.33 (0.67)	1.96 (0.64)	p<0.01
WV SUV <sub>mean</sub>	1.16 (0.42)	1.18 (0.37)	p=0.90	WV TBR <sub>mean</sub>	1.65 (0.17)	1.50 (0.42)	p=0.04

**Table C.10:** NaF uptake by cardiovascular history. All values are median (IQR).

	Left	Right	Significance		Left	Right	Significance
SHS SUV <sub>max</sub>	1.98 (0.92)	1.95 (0.85)	p=0.78	SHS TBR <sub>max</sub>	2.60 (1.01)	2.73 (0.94)	p=0.60
MDS SUV <sub>max</sub>	1.88 (0.78)	1.85 (0.74)	p=0.78	MDS TBR <sub>max</sub>	2.50 (0.91)	2.57 (0.95)	p=0.70
WV SUV <sub>max</sub>	1.41 (0.49)	1.31 (0.31)	p=0.99	WV TBR <sub>max</sub>	1.86 (0.53)	1.82 (0.35)	p=0.81
SHS SUV <sub>mean</sub>	1.67 (0.55)	1.65 (0.60)	p=0.68	SHS TBR <sub>mean</sub>	2.12 (0.83)	2.19 (0.66)	p=0.72
MDS SUV <sub>mean</sub>	1.61 (0.52)	1.59 (0.59)	p=0.84	MDS TBR <sub>mean</sub>	2.02 (0.76)	2.11 (0.60)	p=0.62
WV SUV <sub>mean</sub>	1.19 (0.46)	1.14 (0.26)	p=0.96	WV TBR <sub>mean</sub>	1.56 (0.43)	1.57 (0.24)	p=0.96

**Table C.11:** NaF uptake by arterial side. All values are median (IQR).

	Correlation	Significance		Correlation	Significance
SHS SUV <sub>max</sub>	$r_s=-0.10$	p=0.50	SHS TBR <sub>max</sub>	$r_s=0.01$	p=0.94
MDS SUV <sub>max</sub>	$r_s=-0.07$	p=0.65	MDS TBR <sub>max</sub>	$r_s=0.03$	p=0.86
WV SUV <sub>max</sub>	$r_s=-0.01$	p=0.96	WV TBR <sub>max</sub>	$r_s=-0.01$	p=0.96
SHS SUV <sub>mean</sub>	$r_s=-0.03$	p=0.83	SHS TBR <sub>mean</sub>	$r_s=0.03$	p=0.83
MDS SUV <sub>mean</sub>	$r_s=-0.01$	p=0.93	MDS TBR <sub>mean</sub>	$r_s=0.02$	p=0.90
WV SUV <sub>mean</sub>	$r_s=0.03$	p=0.82	WV TBR <sub>mean</sub>	$r_s=0.00$	p=0.99

**Table C.12:** Correlations between stroke onset-to-scan interval and NaF uptake.

	Thrombolysed	Not thrombolysed	Significance		Thrombolysed	Not thrombolysed	Significance
SHS SUV <sub>max</sub>	1.89 (0.65)	2.02 (0.78)	p=0.42	SHS TBR <sub>max</sub>	2.41 (0.38)	2.85 (1.03)	p=0.37
MDS SUV <sub>max</sub>	1.82 (0.61)	1.90 (0.71)	p=0.50	MDS TBR <sub>max</sub>	2.28 (0.33)	2.64 (1.02)	p=0.41
WV SUV <sub>max</sub>	1.34 (0.34)	1.34 (0.44)	p=0.43	WV TBR <sub>max</sub>	1.84 (0.32)	1.84 (0.56)	p=0.68
SHS SUV <sub>mean</sub>	1.64 (0.47)	1.68 (0.59)	p=0.47	SHS TBR <sub>mean</sub>	2.04 (0.20)	2.21 (0.83)	p=0.38
MDS SUV <sub>mean</sub>	1.53 (0.41)	1.59 (0.58)	p=0.56	MDS TBR <sub>mean</sub>	1.97 (0.29)	2.13 (0.84)	p=0.46
WV SUV <sub>mean</sub>	1.11 (0.27)	1.19 (0.46)	p=0.37	WV TBR <sub>mean</sub>	1.49 (0.31)	1.57 (0.30)	p=0.45

**Table C.13:** NaF uptake by thrombolysis status. All values are median (IQR).

**Appendix D:**  
**FDG Univariable Analysis**

	Correlation	Significance		Correlation	Significance
SHS SUV <sub>max</sub>	r <sub>s</sub> =0.00	p=0.95	SHS TBR <sub>max</sub>	r <sub>s</sub> =-0.23	p=0.09
MDS SUV <sub>max</sub>	r <sub>s</sub> =0.00	p=0.99	MDS TBR <sub>max</sub>	r <sub>s</sub> =-0.22	p=0.11
WV SUV <sub>max</sub>	r <sub>s</sub> =0.04	p=0.76	WV TBR <sub>max</sub>	r=-0.22	p=0.11
SHS SUV <sub>mean</sub>	r <sub>s</sub> =0.06	p=0.66	SHS TBR <sub>mean</sub>	r <sub>s</sub> =-0.26	p=0.05
MDS SUV <sub>mean</sub>	r <sub>s</sub> =0.06	p=0.66	MDS TBR <sub>mean</sub>	r <sub>s</sub> =-0.26	p=0.06
WV SUV <sub>mean</sub>	r <sub>s</sub> =0.11	p=0.43	WV TBR <sub>mean</sub>	r=-0.23	p=0.09

**Table D.1:** Association between age and FDG uptake.

	Female	Male	Significance		Female	Male	Significance
SHS SUV <sub>max</sub>	2.01 (0.40)	2.18 (0.49)	p=0.17	SHS TBR <sub>max</sub>	2.10 (0.40)	2.00 (0.48)	p=0.89
MDS SUV <sub>max</sub>	1.93 (0.39)	2.13 (0.50)	p=0.13	MDS TBR <sub>max</sub>	2.04 (0.36)	1.97 (0.47)	p=0.96
WV SUV <sub>max</sub>	1.76 (0.34)	1.89 (0.43)	p=0.34	WV TBR <sub>max</sub>	1.89 (0.35)	1.75 (0.36)	p=0.51
SHS SUV <sub>mean</sub>	1.81 (0.26)	1.92 (0.38)	p=0.60	SHS TBR <sub>mean</sub>	1.89 (0.37)	1.77 (0.33)	p=0.55
MDS SUV <sub>mean</sub>	1.78 (0.33)	1.89 (0.38)	p=0.51	MDS TBR <sub>mean</sub>	1.82 (0.31)	1.73 (0.34)	p=0.52
WV SUV <sub>mean</sub>	1.61 (0.26)	1.65 (0.27)	p=0.72	WV TBR <sub>mean</sub>	1.61 (0.28)*	1.58 (0.31)*	p=0.65

**Table D.2:** FDG uptake by sex. All values expressed as median (IQR), except those denoted with an asterisk, where values are mean (SD).

	Correlation	Significance		Correlation	Significance
SHS SUV <sub>max</sub>	r <sub>s</sub> =0.19	p=0.18	SHS TBR <sub>max</sub>	r <sub>s</sub> =-0.04	p=0.76
MDS SUV <sub>max</sub>	r <sub>s</sub> =0.19	p=0.16	MDS TBR <sub>max</sub>	r <sub>s</sub> =-0.04	p=0.78
WV SUV <sub>max</sub>	r <sub>s</sub> =0.20	p=0.14	WV TBR <sub>max</sub>	r <sub>s</sub> =-0.06	p=0.68
SHS SUV <sub>mean</sub>	r <sub>s</sub> =0.19	p=0.16	SHS TBR <sub>mean</sub>	r <sub>s</sub> =0.00	p=0.98
MDS SUV <sub>mean</sub>	r <sub>s</sub> =0.20	p=0.16	MDS TBR <sub>mean</sub>	r <sub>s</sub> =0.00	p=0.98
WV SUV <sub>mean</sub>	r <sub>s</sub> =0.24	p=0.08	WV TBR <sub>mean</sub>	r <sub>s</sub> =0.03	p=0.84

**Table D.3:** Association between BMI and FDG uptake.

	Current /former smoker	Non- smoker	Significance		Current /former smoker	Non- smoker	Significance
SHS SUV <sub>max</sub>	2.14 (0.59)	2.01 (0.45)	p=0.32	SHS TBR <sub>max</sub>	2.10 (0.47)	1.75 (0.49)	p<0.001
MDS SUV <sub>max</sub>	2.08 (0.63)	1.98 (0.46)	p=0.33	MDS TBR <sub>max</sub>	2.06 (0.44)	1.70 (0.48)	p<0.001
WV SUV <sub>max</sub>	1.89 (0.48)	1.76 (0.33)	p=0.72	WV TBR <sub>max</sub>	1.93 (0.36)*	1.58 (0.30)*	p<0.001
SHS SUV <sub>mean</sub>	1.90 (0.42)	1.82 (0.33)	p=0.60	SHS TBR <sub>mean</sub>	1.89 (0.39)	1.53 (0.36)	p<0.001
MDS SUV <sub>mean</sub>	1.87 (0.43)	1.79 (0.39)	p=0.74	MDS TBR <sub>mean</sub>	1.84 (0.35)	1.51 (0.35)	p<0.001
WV SUV <sub>mean</sub>	1.64 (0.29)	1.61 (0.24)	p=0.89	WV TBR <sub>mean</sub>	1.68 (0.29)*	1.40 (0.21)*	p<0.001

**Table D.4:** FDG uptake by smoking status. All values expressed as median (IQR), except those denoted with an asterisk, where values are mean (SD).

	Diabetes	No diabetes	Significance		Diabetes	No diabetes	Significance
SHS SUV <sub>max</sub>	1.99 (0.30)	2.18 (0.66)	p=0.30	SHS TBR <sub>max</sub>	1.64 (0.76)	2.08 (0.52)	p=0.02
MDS SUV <sub>max</sub>	1.95 (0.30)	2.11 (0.68)	p=0.41	MDS TBR <sub>max</sub>	1.60 (0.76)	2.03 (0.50)	p=0.03
WV SUV <sub>max</sub>	1.77 (0.22)	1.90 (0.50)	p=0.59	WV TBR <sub>max</sub>	1.50 (0.68)	1.84 (0.38)	p=0.05
SHS SUV <sub>mean</sub>	1.75 (0.21)	1.91 (0.51)	p=0.39	SHS TBR <sub>mean</sub>	1.47 (0.74)	1.82 (0.41)	p=0.06
MDS SUV <sub>mean</sub>	1.70 (0.20)	1.87 (0.52)	p=0.41	MDS TBR <sub>mean</sub>	1.44 (0.74)	1.77 (0.31)	p=0.09
WV SUV <sub>mean</sub>	1.62 (0.20)	1.65 (0.37)	p=0.99	WV TBR <sub>mean</sub>	1.34 (0.68)	1.59 (0.28)	p=0.24

**Table D.5:** FDG uptake by diabetes status. All values are expressed as median (IQR).

	Hypertension	No hypertension	Significance		Hypertension	No hypertension	Significance
SHS SUV <sub>max</sub>	2.04 (0.76)	2.14 (0.32)	p=0.55	SHS TBR <sub>max</sub>	1.99 (0.44)	2.09 (0.46)	p=0.53
MDS SUV <sub>max</sub>	2.02 (0.74)	2.07 (0.29)	p=0.45	MDS TBR <sub>max</sub>	1.94 (0.39)	2.04 (0.43)	p=0.49
WV SUV <sub>max</sub>	1.80 (0.49)	1.90 (0.31)	p=0.24	WV TBR <sub>max</sub>	1.75 (0.33)	1.91 (0.40)	p=0.17
SHS SUV <sub>mean</sub>	1.77 (0.46)	1.93 (0.29)	p=0.33	SHS TBR <sub>mean</sub>	1.77 (0.42)	1.86 (0.31)	p=0.36
MDS SUV <sub>mean</sub>	1.74 (0.48)	1.88 (0.29)	p=0.30	MDS TBR <sub>mean</sub>	1.73 (0.38)	1.81 (0.27)	p=0.28
WV SUV <sub>mean</sub>	1.60 (0.40)	1.69 (0.16)	p=0.12	WV TBR <sub>mean</sub>	1.56 (0.30)*	1.65 (0.29)*	p=0.29

**Table D.6:** FDG uptake by smoking status. All values expressed as median (IQR), except those denoted with an asterisk, where values are mean (SD).

	Current statin	No statin	Significance		Current statin	No statin	Significance
SHS SUV <sub>max</sub>	1.97 (0.57)	2.15 (0.51)	p=0.59	SHS TBR <sub>max</sub>	1.85 (0.50)	2.10 (0.46)	p=0.04
MDS SUV <sub>max</sub>	1.95 (0.56)	2.09 (0.49)	p=0.60	MDS TBR <sub>max</sub>	1.82 (0.53)	2.04 (0.45)	p=0.04
WV SUV <sub>max</sub>	1.76 (0.51)	1.90 (0.38)	p=0.66	WV TBR <sub>max</sub>	1.68 (0.33)*	1.89 (0.38)*	p=0.047
SHS SUV <sub>mean</sub>	1.77 (0.44)	1.90 (0.37)	p=0.59	SHS TBR <sub>mean</sub>	1.65 (0.40)	1.88 (0.31)	p=0.02
MDS SUV <sub>mean</sub>	1.74 (0.45)	1.87 (0.36)	p=0.70	MDS TBR <sub>mean</sub>	1.63 (0.41)	1.81 (0.25)	p=0.03
WV SUV <sub>mean</sub>	1.59 (0.37)	1.66 (0.23)	p=0.57	WV TBR <sub>mean</sub>	1.48 (0.28)*	1.65 (0.29)*	p=0.049

**Table D.7:** FDG uptake by statin medication. All values expressed as median (IQR), except those denoted with an asterisk, where values are mean (SD).

	TC		Triglycerides		HDL		LDL		TC:HDL ratio	
	r <sub>s</sub>	Sig.								
SHS SUV <sub>max</sub>	-0.05	p=0.70	0.23	p=0.12	-0.28	p=0.05	-0.13	p=0.36	0.14	p=0.34
MDS SUV <sub>max</sub>	-0.06	p=0.65	0.23	p=0.11	-0.27	p=0.06	-0.16	p=0.29	0.12	p=0.43
WV SUV <sub>max</sub>	-0.08	p=0.58	0.28	p=0.05	-0.20	p=0.18	-0.18	p=0.22	0.06	p=0.70
SHS SUV <sub>mean</sub>	-0.03	p=0.83	0.18	p=0.22	-0.17	p=0.25	-0.15	p=0.32	0.07	p=0.62
MDS SUV <sub>mean</sub>	-0.05	p=0.73	0.17	p=0.25	-0.17	p=0.25	-0.17	p=0.26	0.05	p=0.74
WV SUV <sub>mean</sub>	-0.06	p=0.67	0.26	p=0.07	-0.08	p=0.57	-0.21	p=0.15	-0.03	p=0.86
SHS TBR <sub>max</sub>	0.06	p=0.67	0.05	p=0.74	-0.22	p=0.14	0.02	p=0.91	0.22	p=0.13
MDS TBR <sub>max</sub>	0.05	p=0.71	0.04	p=0.76	-0.21	p=0.16	0.00	p=0.99	0.20	p=0.16
WV TBR <sub>max</sub>	0.04	p=0.80	0.08	p=0.59	-0.20	p=0.17	-0.02	p=0.92	0.20	p=0.16
SHS TBR <sub>mean</sub>	0.08	p=0.56	-0.01	p=0.94	-0.15	p=0.31	0.02	p=0.88	0.19	p=0.20
MDS TBR <sub>mean</sub>	0.07	p=0.61	-0.04	p=0.80	-0.14	p=0.36	0.01	p=0.94	0.16	p=0.28
WV TBR <sub>mean</sub>	0.04	p=0.79	0.06	p=0.66	-0.07	p=0.65	-0.06	p=0.67	0.08*	p=0.57

**Table D.8:** Correlations between FDG uptake and lipid profile. TC = total cholesterol, HDL = high-density lipoprotein, LDL = low-density lipoprotein.

\* Pearson correlation.

	Current antiplatelet	No antiplatelet	Significance		Current antiplatelet	No antiplatelet	Significance
SHS SUV <sub>max</sub>	1.97 (0.50)	2.15 (0.58)	p=0.52	SHS TBR <sub>max</sub>	1.87 (0.60)	2.08 (0.56)	p=0.10
MDS SUV <sub>max</sub>	1.95 (0.55)	2.09 (0.57)	p=0.49	MDS TBR <sub>max</sub>	1.84 (0.63)	2.03 (0.53)	p=0.11
WV SUV <sub>max</sub>	1.76 (0.49)	1.90 (0.39)	p=0.55	WV TBR <sub>max</sub>	1.66 (0.30)*	1.88 (0.39)*	p=0.03
SHS SUV <sub>mean</sub>	1.77 (0.35)	1.90 (0.43)	p=0.65	SHS TBR <sub>mean</sub>	1.70 (0.53)	1.85 (0.36)	p=0.07
MDS SUV <sub>mean</sub>	1.74 (0.43)	1.87 (0.43)	p=0.63	MDS TBR <sub>mean</sub>	1.66 (0.49)	1.80 (0.31)	p=0.08
WV SUV <sub>mean</sub>	1.59 (0.28)	1.66 (0.24)	p=0.53	WV TBR <sub>mean</sub>	1.47 (0.25)*	1.64 (0.30)*	p=0.04

**Table D.9:** FDG uptake by antiplatelet medication. All values expressed as median (IQR), except those denoted with an asterisk, where values are mean (SD).

	Cardiovascular history	No cardiovascular history	Significance		Cardiovascular history	No cardiovascular history	Significance
SHS SUV <sub>max</sub>	1.97 (0.41)	2.15 (0.58)	p=0.39	SHS TBR <sub>max</sub>	1.85 (0.60)	2.08 (0.52)	p=0.03
MDS SUV <sub>max</sub>	1.95 (0.45)	2.09 (0.57)	p=0.34	MDS TBR <sub>max</sub>	1.82 (0.60)	2.03 (0.50)	p=0.04
WV SUV <sub>max</sub>	1.76 (0.40)	1.90 (0.44)	p=0.45	WV TBR <sub>max</sub>	1.63 (0.29)*	1.89 (0.39)*	p<0.01
SHS SUV <sub>mean</sub>	1.77 (0.27)	1.90 (0.44)	p=0.54	SHS TBR <sub>mean</sub>	1.65 (0.53)	1.85 (0.35)	p=0.03
MDS SUV <sub>mean</sub>	1.74 (0.35)	1.87 (0.44)	p=0.54	MDS TBR <sub>mean</sub>	1.63 (0.49)	1.80 (0.33)	p=0.02
WV SUV <sub>mean</sub>	1.59 (0.24)	1.66 (0.28)	p=0.37	WV TBR <sub>mean</sub>	1.43 (0.23)*	1.66 (0.30)*	p<0.01

**Table D.10:** FDG uptake by cardiovascular history. All values expressed as median (IQR), except those denoted with an asterisk, where values are mean (SD).

	Left	Right	Significance		Left	Right	Significance
SHS SUV <sub>max</sub>	2.09 (0.50)	2.13 (0.59)	p=0.33	SHS TBR <sub>max</sub>	2.00 (0.42)	2.09 (0.49)	p=0.57
MDS SUV <sub>max</sub>	2.03 (0.51)	2.07 (0.59)	p=0.32	MDS TBR <sub>max</sub>	1.98 (0.48)	2.04 (0.47)	p=0.57
WV SUV <sub>max</sub>	1.89 (0.40)	1.89 (0.40)	p=0.29	WV TBR <sub>max</sub>	1.77 (0.32)*	1.87 (0.43)*	p=0.35
SHS SUV <sub>mean</sub>	1.79 (0.43)	1.90 (0.39)	p=0.24	SHS TBR <sub>mean</sub>	1.79 (0.38)	1.86 (0.40)	p=0.43
MDS SUV <sub>mean</sub>	1.75 (0.41)	1.89 (0.38)	p=0.27	MDS TBR <sub>mean</sub>	1.74 (0.35)	1.81 (0.33)	p=0.41
WV SUV <sub>mean</sub>	1.61 (0.35)	1.65 (0.22)	p=0.29	WV TBR <sub>mean</sub>	1.55 (0.25)*	1.63 (0.34)*	p=0.29

**Table D.11:** FDG uptake by artery side. All values expressed as median (IQR), except those denoted with an asterisk, where values are mean (SD).

	Correlation	Significance		Correlation	Significance
SHS SUV <sub>max</sub>	$r_s=-0.02$	p=0.88	SHS TBR <sub>max</sub>	$r_s=-0.02$	p=0.88
MDS SUV <sub>max</sub>	$r_s=0.01$	p=0.97	MDS TBR <sub>max</sub>	$r_s=0.01$	p=0.96
WV SUV <sub>max</sub>	$r_s=-0.05$	p=0.73	WV TBR <sub>max</sub>	$r_s=0.03$	p=0.83
SHS SUV <sub>mean</sub>	$r_s=-0.08$	p=0.59	SHS TBR <sub>mean</sub>	$r_s=-0.05$	p=0.72
MDS SUV <sub>mean</sub>	$r_s=-0.07$	p=0.63	MDS TBR <sub>mean</sub>	$r_s=-0.05$	p=0.74
WV SUV <sub>mean</sub>	$r_s=-0.10$	p=0.45	WV TBR <sub>mean</sub>	$r_s=-0.03$	p=0.82

**Table D.12:** Association between stroke onset-to-scan interval and FDG uptake.

	Thrombolysed	Not thrombolysed	Significance		Thrombolysed	Not thrombolysed	Significance
SHS SUV <sub>max</sub>	2.23 (0.41)	2.05 (0.52)	p=0.20	SHS TBR <sub>max</sub>	2.12 (0.31)	2.01 (0.46)	p=0.54
MDS SUV <sub>max</sub>	2.19 (0.45)	2.01 (0.51)	p=0.16	MDS TBR <sub>max</sub>	2.04 (0.30)	2.196 (0.46)	p=0.52
WV SUV <sub>max</sub>	1.98 (0.34)	1.80 (0.46)	p=0.12	WV TBR <sub>max</sub>	1.88 (0.35)*	1.80 (0.39)*	p=0.52
SHS SUV <sub>mean</sub>	1.96 (0.41)	1.86 (0.39)	p=0.12	SHS TBR <sub>mean</sub>	1.89 (0.32)	1.80 (0.43)	p=0.44
MDS SUV <sub>mean</sub>	1.93 (0.41)	1.84 (0.39)	p=0.10	MDS TBR <sub>mean</sub>	1.83 (0.29)	1.77 (0.40)	p=0.39
WV SUV <sub>mean</sub>	1.76 (0.28)	1.61 (0.28)	p=0.06	WV TBR <sub>mean</sub>	1.66 (0.28)*	1.57 (0.30)*	p=0.31

**Table D.13:** FDG uptake according to thrombolysis. All values expressed as median (IQR), except those denoted with an asterisk, where values are mean (SD).

	Correlation	Significance		Correlation	Significance
SHS SUV <sub>max</sub>	$r_s=-0.05$	p=0.70	SHS TBR <sub>max</sub>	$r_s=0.12$	p=0.38
MDS SUV <sub>max</sub>	$r_s=-0.06$	p=0.64	MDS TBR <sub>max</sub>	$r_s=0.10$	p=0.45
WV SUV <sub>max</sub>	$r_s=-0.06$	p=0.68	WV TBR <sub>max</sub>	$r_s=0.12$	p=0.38
SHS SUV <sub>mean</sub>	$r_s=-0.07$	p=0.63	SHS TBR <sub>mean</sub>	$r_s=0.10$	p=0.48
MDS SUV <sub>mean</sub>	$r_s=-0.08$	p=0.59	MDS TBR <sub>mean</sub>	$r_s=0.10$	p=0.48
WV SUV <sub>mean</sub>	$r_s=-0.10$	p=0.48	WV TBR <sub>mean</sub>	$r_s=0.11$	p=0.41

**Table D.14:** Association between FDG uptake and NIHSS.

## **Appendix E:**

### **Vascular Risk Factors Influencing FDG Uptake**

In contrast to the relationships between risk factors and NaF uptake discussed in Chapter Three, the models exploring the relationships between risk factors and FDG uptake found in Chapter Four were less robust. This is perhaps best illustrated by the overall adjusted  $R^2$  for each model: models for SUV measures showed that the model had a negligible contribution and failed to reach significance. TBR models fared better, but adjusted  $R^2$  of the models were weak, though statistically significant. This illustrates how correction for tracer blood-pooling improves the strength of the model for FDG uptake, in contrast to NaF models that showed moderate and statistically significant adjusted  $R^2$  values regardless of whether SUV or TBR was used (though SUV models had marginally superior adjusted  $R^2$  values).

The reasonably poor risk factor models of FDG uptake may reflect the non-specific nature of FDG uptake, particularly when compared to the higher specificity of NaF uptake. This, combined with the relatively small sample size of this study, limits the ability to measure associations between tracer uptake and risk factors. A larger sample would be required for robust trends to be established. The above models suggest that a large contribution towards FDG uptake is coming from other considerations beyond conventional cardiovascular risk factors, and larger samples may allow more variables to be included in the model. With that caveat, some interesting results were observed and are discussed below.

#### *E.1 Smoking and FDG uptake*

The strongest independent association after adjustment for other risk factors was seen between smoking and FDG uptake. This association was consistent across both SUV and TBR measures, with the exception of WV SUV measures, and was stronger for focal (SHS and MDS) measures of uptake. In-keeping with the above discussion, adjustment for blood-pooling activity resulted in a stronger association, with coefficients for SHS TBR<sub>max</sub> and MDS TBR<sub>max</sub> of 0.64 and 0.61 respectively. The fact that WV TBR<sub>max</sub> and WV TBR<sub>mean</sub> ( $\beta=0.46$  and  $\beta=0.32$  respectively) were

weaker but remained statistically independently significant suggests that the effects of smoking are systemic but particularly exacerbate the focal plaque.

In existing studies, smoking was independently associated with higher  $\text{wholevesselTBR}_{\max}$ , but not  $\text{wholevesselSUV}_{\max}$ , and single hottest segment uptake in the carotid arteries of individuals with coronary artery disease (Bucerius et al., 2011). Bucerius et al. investigated the effect of diabetes on FDG uptake in individuals with cardiovascular disease using a similar multiple regression analysis with backward elimination. They found smoking and BMI to be independently associated with glucose-corrected  $\text{FDG}_{\text{meanTBR}}$  in individuals with diabetes but only BMI was independently associated with glucose-corrected  $\text{FDG}_{\text{meanSUV}}$  in these individuals. In participants without diabetes, hypertension was consistently independently associated with both  $\text{FDG}_{\text{meanSUV}}$  and  $\text{meanTBR}$  (Bucerius et al., 2012). In a cohort with cardiovascular history or cardiovascular risk factors, Rudd et al. found that mean TBR in the iliac arteries was higher for smokers than non-smokers, but did not find the same finding for the carotids or aorta (Rudd et al., 2009).

There was a minimal ( $\beta=0.09$ ,  $p=0.006$ ) correlation between smoking and increase in an individual's mean TBR across all vascular territories in a retrospective longitudinal study of an oncology cohort, though this did not remain significant for separate vascular territories (Hetterich et al., 2015).

Other studies have found no relationship between smoking and FDG uptake when considering lesions pooled from all arterial regions in non-cardiovascular cohorts (Tahara et al., 2007b, Yoo et al., 2011a, Strobl et al., 2013), though it should be noted that Tahara et al. considered only current smokers not ever smokers. In Strobl et al., the rate of smoking was low (32 participants, 10.2%). Furthermore, age ( $\geq 65$  years), male sex, and BMI proved independently associated with FDG TBR (Strobl et al., 2013).

Curiously, Chróinín et al. found current smoking to be associated with lower FDG SUV measures. In this study current smokers tended to be younger and were less likely to have hypertension, with the authors concluding that smoking may have been

associated with other unmeasured factors that reduced plaque inflammation in these individuals (Chr  n  n et al., 2014).

In this study, smoking was the only risk factor that was found to be consistently independently associated with both FDG and NaF uptake. Cigarette smoke contains more than 4,800 compounds and each puff of a cigarette contains approximately  $10^{15}$  free radicals (Siasos et al., 2014, Pryor and Stone, 1993). It is one of the most potent modifiable cardiovascular risk factors and affects atherogenesis and thromboinflammation through a variety of complex mechanisms and interactions (**Figure E.1**) (Siasos et al., 2014, Ambrose and Barua, 2004).

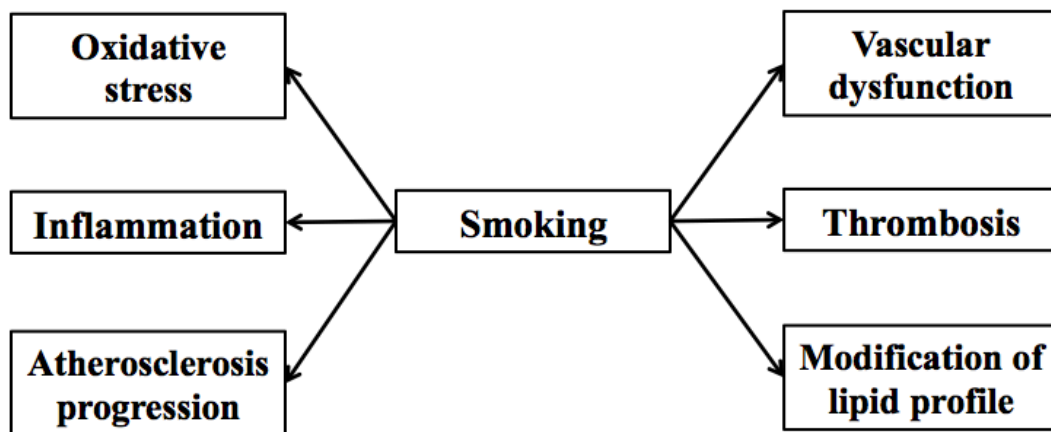


**Figure E.1: Pathophysiological mechanisms of smoking in vascular disease.**

The production of free radicals and ROS in response to smoking has been implicated in the disruption of eNOS activity and consequent NO production (Barua et al., 2003). This results in impaired vasoreactivity in response to cigarette smoking (Mayhan and Patel, 1997, Rubenstein et al., 1991) and a phenotypic change in VSMC from a contractile to a synthetic type (Yoshiyama et al., 2014). The ubiquitous effects of NO also have implications for atherogenesis via effects on the regulation of inflammation, leukocyte adhesion, platelet activation, and thrombosis (Napoli and Ignarro, 2001).

Cigarette smoking has been implicated in promoting inflammation directly, causing an estimated 20-25% increase in the peripheral blood leukocyte count (Smith and Fischer, 2001) while also upregulating VCAM-1 and ICAM-1 (Mazzone et al., 2001,

Thorand et al., 2006) and monocyte integrins (Weber et al., 1996) to increase recruitment at the early stages of atherogenesis (Adams et al., 1997).

An individual's lipid profile also appears to be associated with cigarette smoking, though how much this is a covariate with other features of the metabolic syndrome is difficult to establish. Higher LDL levels have been observed in smokers and non-smokers in a dose-dependent manner (Craig et al., 1989), and smoking appears to promote the oxidation of LDL (Heitzer et al., 1996, Yokode et al., 1988, Frei et al., 1991, Pech-Amsellem et al., 1996).

While these above mechanisms linked with smoking are likely to promote atherogenesis and enhance plaque development in a fashion likely to cause increased FDG and NaF uptake, in the context of the wider study it is also advantageous to consider how cigarette smoking may affect thrombosis directly. Smoking appears to increase platelet aggregation (Fusegawa et al., 1999, Blache, 1995), and this effect seems to become more marked in older individuals (Rival et al., 1987). Suggested mechanisms for this include increased peroxidised free fatty acids (Blache, 1995), reduced platelet-derived NO (Ichiki et al., 1996, Takajo et al., 2001), and increased prothrombotic factors (Kannel et al., 1987, Smith et al., 1997). Interestingly, platelet-derived NO showed a significant increase within seven days of smoking cessation, but quickly returned to baseline upon resuming smoking (Morita et al., 2005). Dysregulation of fibrinolysis has also been indicated to be a consequence of smoking, with release of tissue plasminogen activator (t-PA) from endothelial cells in smokers found to be approximately half of that for non-smokers in response to substance P (Newby et al., 1999), as well as being inversely correlated with atheroma volume (Newby et al., 2001). Protease-activated receptor-1 (PAR-1) activating peptide has also been implicated in both vasodilation and induction of t-PA release, with a significant reduction of both demonstrated in smokers compared to non-smokers (Lang et al., 2008).

### *E.2 Diabetes and hyperglycaemia*

Impaired glycaemic control and diabetes mellitus has been found to be independently associated with both the presence and extent of carotid atherosclerosis (Mostaza et al.,

2015). Tahara et al. observed that individuals with inflammatory carotid atheroma (defined as an equivalent of WV SUV<sub>max</sub>  $\geq 1.6$ ) had greater BMI, waist circumference, and a higher prevalence of antihypertensive use than those with non-inflammatory carotid atheroma (Tahara et al., 2007a). This supported earlier findings in asymptomatic atheroma in a large oncological population that FDG SUV was independently associated with components of metabolic syndrome (waist circumference, hypertensive medication, carotid IMT, and increased with the accumulation of metabolic syndrome features) and independently inversely associated with HDL (Tahara et al., 2007b). In their study, HbA<sub>1c</sub> showed an increase with quartiles of SUV, but narrowly missed statistical significance, while fasting plasma glucose did not show a significant trend across SUV quartiles (Tahara et al., 2007b). Furthermore, after adjustment for blood glucose levels, the presence of diabetes was associated with higher FDG uptake (Bucierius et al., 2012). In the same study, increased FDG uptake was seen with higher fasting blood glucose, a result that the authors attribute to increased oxidative stress and endothelial dysfunction (Bucierius et al., 2012).

In contrast, other human studies have not found an independent association of diabetes with FDG uptake (Rudd et al., 2009, Tahara et al., 2007a, Chróinín et al., 2014). Similarly, a mouse model over-expressing insulin-like growth factor II (IGF-II) to simulate diabetes mellitus found no significant difference in FDG uptake between this diabetic model and the non-diabetic comparator (Silvola et al., 2011).

Two possible reasons may account for our finding of an inverse relationship between diabetes mellitus and FDG uptake on univariable analysis. Firstly, the number of participants with diabetes was relatively small in our study (4 participants, all type 2 diabetes mellitus), and hence may introduce statistical bias. The more likely second cause is a physiological consideration: in our study, individuals with diabetes had a significantly higher blood sugar than those without diabetes, though all participants had blood sugars within the specified range for FDG-PET scanning. Again, the fact that this difference reaches significance may be a result of the small numbers of participants with diabetes, though the fact that the blood sugar was higher in individuals with type two diabetes than those without is unsurprising. Indeed, once the interaction between diabetes and blood sugar was included in the multiple regression

model, the interaction remained significant but neither diabetes or blood sugar proved to be independently significant.

As already discussed, FDG is a glucose analogue. Hence, high blood glucose concentrations have the potential to competitively inhibit FDG uptake (Zhao et al., 2001). In clinical oncology usage, hyperglycaemia, but not diabetes mellitus itself, was implicated in reducing the sensitivity of FDG-PET to detect malignancy (Rabkin et al., 2010, Lee et al., 2006). Tumour uptake of FDG (as well as uptake in the brain, small bowel, and ovaries) is significantly reduced during hyperglycaemia (Wahl et al., 1992, Torizuka et al., 1997), but appeared to have little effect in inflammatory cells (Zhuang et al., 2001).

The effect of diabetes and/or hyperglycaemia in FDG uptake in atherosclerosis is less clear. This contrast may be due to the complex nature of atherosclerosis, where plaques will exhibit not only inflammation but also hypoxia, which is also implicated to increase FDG uptake (Joshi et al., 2017). Hence, it is potentially hard to tease out the differing and opposing effects of diabetes-accelerated plaque pathophysiology and hyperglycaemia.

Macrophages express insulin receptors, but not the GLUT-4 glucose transporter that are insulin-responsive (Fu et al., 2004). *Ex vivo* studies have found FDG uptake in human monocytes and macrophages decreases with increasing glucose concentration of the medium (Deichen et al., 2003). As well as the impact of hyperglycaemia in competition with FDG during uptake, Zhao et al. found that hyperglycaemia reduced GLUT-1 in rat models of inflammatory lesions of non-infectious origin (Zhao et al., 2002).

In humans, a negative association was found between pre-scan blood sugar and FDG  $\text{meanTBR}_{\text{max}}$  and  $\text{meanSUV}_{\text{max}}$  (analogous to our WV  $\text{TBR}_{\text{max}}$  and WV  $\text{SUV}_{\text{max}}$ ) in the carotid arteries, as well as increased venous FDG uptake in the superior vena cava (Bucerius et al., 2014). Blood glucose levels higher than 7 mmol/L were associated with lower TBR values, but blood sugars below this level did not appear to affect TBR (Bucerius et al., 2014).

For this reason, 7 mmol/L was adopted as the cut-off for the pre-scan blood glucose for participants without diabetes in our study. Evidence for a suitable threshold for individuals with diabetes is lacking. Methods for correcting for hyperglycaemia have been proposed by the European Association of Nuclear Medicine for use in oncological PET imaging (Boellaard et al., 2015), and has been tested in one vascular PET study where blood sugar was corrected post hoc to 5 mmol/L ( $SUV_{gluc} = SUV \times \text{blood glucose in mg/dL} / 90$ ) (Bucerius et al., 2012), but further work is required to validate this approach within the complex atherosclerotic plaque.

Diabetes and blood sugar on their own were not associated with increased FDG uptake in our regression analysis, but the interaction of diabetes and blood sugar was found to have a very minor negative association with FDG TBR. Overall this suggests that our initial impression that diabetes being associated with decreased FDG uptake is actually due to the effect of increased blood sugar in individuals with diabetes.

### *E.3 Other risk factors*

Two further points emerged in the linear regression models. There was a trend towards current antiplatelet having a negative association with some TBR measures, though narrowly missed significance. This was a mild negative association but appears consistent with the mild anti-inflammatory effects of antiplatelets. Relatively little attention has been paid to individuals taking antiplatelets in the large retrospective studies in oncological cohorts, and this may warrant further attention in future studies.

The second point to emerge is the negative association between WV  $TBR_{mean}$  and the interaction between current statin use in individuals with previous cardiovascular events. In our study, statin medication was associated with lower TBR measures on univariable analysis, though this significance was lost on multivariable modeling (with the exception of the interaction with cardiovascular history in the WV  $TBR_{mean}$  regression). Caution should be applied to avoid over-interpreting the isolated result, but it may partially explain why we observed significantly lower FDG TBRs in individuals with previous cardiovascular events, rather than the expect higher uptake.

Statin medications have been associated with a reduction in plaque FDG uptake, typically independently of the effects on lipid profile and in a dose-dependent manner (Wu et al., 2012, Tawakol et al., 2013, Tahara et al., 2006). Non-pleiotropic effects of statins have been supported by the observation that high dose atorvastatin reduced periodontal inflammation more than low dose atorvastatin, and that this reduction in periodontal inflammation correlated with the reduction in carotid TBR ( $r=0.61$ ,  $p<0.001$ ) (Subramanian et al., 2013).

In contrast, Tawakol et al. also found no association between  $TBR_{mean}$  and statins, as well as no association with diabetes, age, lipid profile, sex, smoking, BMI or blood pressure (Tawakol et al., 2006). Tahara et al. found no significant difference in the proportion of individuals on statin medications between each quartile of FDG SUV in their large asymptomatic cohort, but did find statins attenuated FDG SUVs in an LDL-C-independent manner in a prior smaller study (Tahara et al., 2007b, Tahara et al., 2006). In this latter study, and others, decrease in FDG uptake appears inversely correlated with HDL-C (Tahara et al., 2006, Lee et al., 2008).

These differences may be partly explained by the nature of the studies; static single studies versus dynamic follow-up studies. Typically the effect sizes from statins are relatively small in absolute terms, and may struggle to reach statistical significance when using unpaired testing, but may reach strong statistical significance on paired testing.

## **Appendix F:**

### **hsCRP as a Biomarker in Specific Plaque Types**

In our study hsCRP was found to have a moderate-strong correlation with all FDG  $SUV_{max}$ ,  $SUV_{mean}$ , and  $TBR_{max}$  measures, but not  $TBR_{mean}$ , in symptomatic arteries with low macrocalcification. There were no significant correlations between hsCRP and FDG uptake in symptomatic arteries with high macrocalcification or asymptomatic arteries regardless of the level of calcification.

CRP has been found to be present in the arterial wall in early atherosclerotic lesions in a diffuse pattern, frequently co-localising with the terminal complement complex, and in foam cells (Torzewski et al., 1998). Further work showed that enzymatically-degraded LDL within early atherosclerotic plaques binds CRP and provoke complement activation that may contribute to plaque progression, though this may only occur at higher enzymatically-degraded LDL concentrations (Bhakdi et al., 1999, Bhakdi et al., 2004).

A number of studies have indicated that components of the atherosclerotic plaque may produce CRP themselves, with CRP mRNA found in smooth muscle-like cells and macrophages in the thickened intima of plaques (Yasojima et al., 2001). Incubation of human coronary artery smooth muscle cells with a combination of pro-inflammatory IL-1 $\beta$  and IL-6 was found to induce the cells to produce CRP (Calabro et al., 2003).

CRP itself acts as a mediator within the plaque to promote atherogenesis; upregulating MCP-1 (an upregulation that was attenuated by addition of simvastatin and fenofibrate) (Pasceri et al., 2001, Han et al., 2004), and inhibiting NO release from endothelial cells and promoting endothelial cell dysfunction (Verma et al., 2002, Verma et al., 2004, Fujii et al., 2006). CRP may also directly influence plaque rupture, such as through promoting release of MMP-1, MMP-3, MMP-9, MMP-11, MMP-14 release from monocyte-derived macrophages (Williams et al., 2004, Montero et al., 2006, Nakai et al., 2017, Singh et al., 2008).

These studies indicate the increase of CRP in burgeoning plaques. Arguably the greater relevance for our study is how CRP behaves in more advanced plaques.

Histological analysis of 38 CEA specimens found CRP mRNA levels were higher in ulcerated but non-complicated plaques compared to ulcerated plaques with intra-plaque haemorrhage, which represented more advanced plaques with low cellular content and a high necrotic component (Krupinski et al., 2006). Also of note in this study was that plaque CRP expression was independent of both vascular risk factors and serum CRP. Other studies have also reported CRP production by smooth muscle cells in active atherosclerotic disease but not in end-stage plaques with heavy calcification (Jabs et al., 2003).

Our results appear to support this pattern. In symptomatic arteries, the median hsCRP in the low CACS cohort was nearly double that in the higher high CACS cohort, though did not reach significance likely due to the small sample size (7.625 versus 4.39,  $p=0.30$ ). Similarly, FDG uptake was higher in the lower calcification cohort, but again did not reach statistical significance (e.g. median SHS  $TBR_{max}$  2.20 [IQR 0.46] versus 2.06 [IQR 0.66] in low versus high calcification respectively,  $p=0.14$ ).

These differences may explain the different patterns of correlation seen in our results. Although both FDG and hsCRP showed lower but non-significant concentrations with plaques with lower calcification, the absolute difference in hsCRP between the two groups is comparatively large relative to the modest changes in FDG uptake (**Figure F.1**). Consequently, any correlation is weaker (and in this case, non-significant).

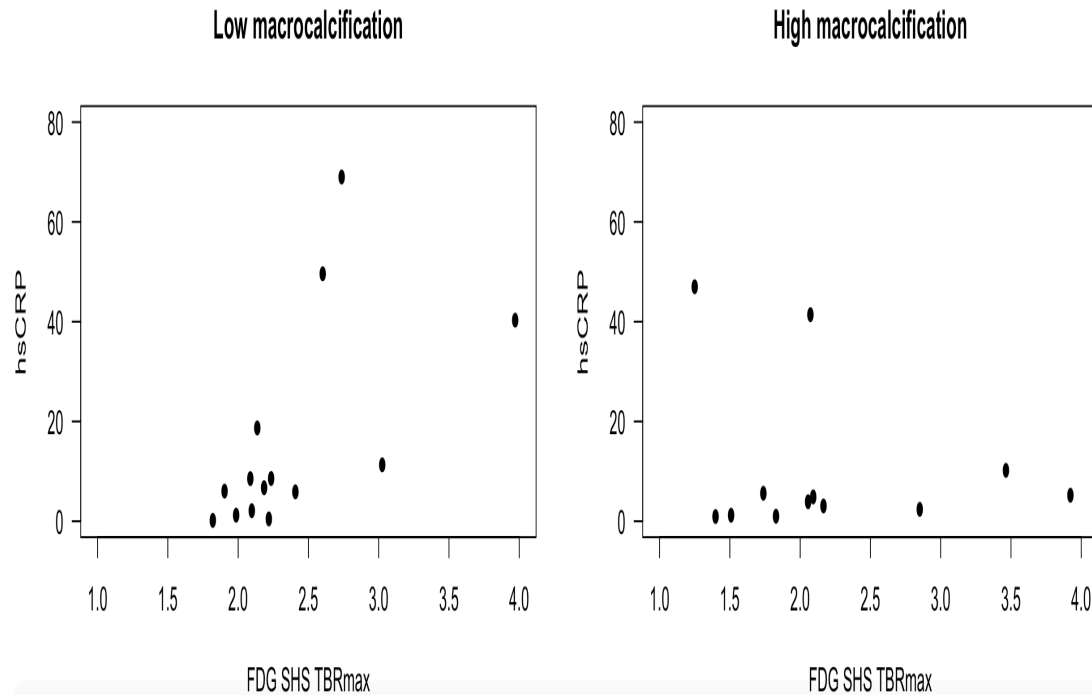


**Figure F.1: hsCRP, FDG uptake, and macrocalcification.** Scatterplot of FDG SHS TBRmax against hsCRP for low macrocalcification plaques (left) and high macrocalcification plaques (right).

The finding of low hsCRP when plaques have extensive macrocalcification fits with the aforementioned *ex vivo* findings of lower CRP in advanced plaques. The presence of two outliers makes the correlation non-significant. Although none of the participants were overtly septic, it is possible that these outliers may be due to subclinical infection that is not uncommon after stroke. Interestingly, if one removes these two outliers in the above example, there is a moderate correlation that matches that

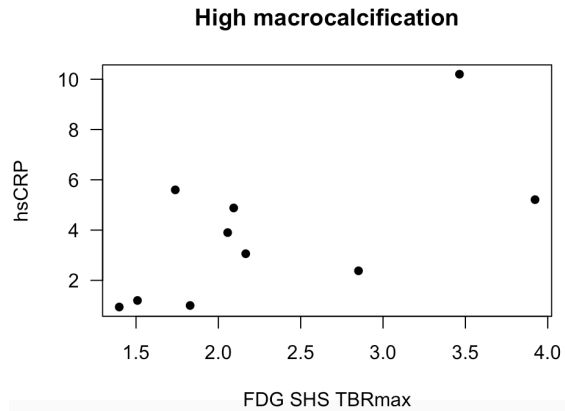


**Figure F.2: hsCRP, FDG uptake, and macrocalcification (adjusted).** Revised scatterplot showing association between FDG SHS TBRmax and hsCRP (with two potential outliers removed).

seen in the low macrocalcification group that is statistically significant ( $r=0.64$ ,  $p=0.047$ ) (Figure F.2). If one re-tests the correlations across all FDG uptake measures without the two outliers then the correlations are found to be modest and statistically

significant for all TBR measures (**Table F.1**). Therefore, caution should be applied when interpreting these results.

	High artery CACS (CACS $\geq 500$ )	
	Correlation	Sig.
SHS SUV <sub>max</sub>	r=0.30	p=0.40
MDS SUV <sub>max</sub>	r <sub>s</sub> =0.20	p=0.58
WV SUV <sub>max</sub>	r <sub>s</sub> =-0.04	p=0.92
SHS SUV <sub>mean</sub>	r=0.33	p=0.35
MDS SUV <sub>mean</sub>	r=0.33	p=0.35
WV SUV <sub>mean</sub>	r=0.13	p=0.71
SHS TBR <sub>max</sub>	r=0.64	p=0.047
MDS TBR <sub>max</sub>	r <sub>s</sub> =0.64	p=0.047
WV TBR <sub>max</sub>	r=0.64	p=0.046
SHS TBR <sub>mean</sub>	r=0.70	p=0.03
MDS TBR <sub>mean</sub>	r=0.70	p=0.03
WV TBR <sub>mean</sub>	r=0.66	p=0.04

**Table F.1:** Revised correlations between FDG uptake and hsCRP in symptomatic arteries with high CACS.

There have been a number of studies that have examined the association between FDG uptake and various biomarkers. A large retrospective review of 130 participants in the dal-PLAQUE study found a positive correlation between baseline carotid TBR and myeloperoxidase and aortic TBR and lipoprotein-associated phospholipase A<sub>2</sub>. In contrast, no association was found between TBR and hsCRP, IL-6, or MMP-9 (Duivenvoorden et al., 2013).

Rudd et al. report a non-significant trend between CRP and FDG whole vessel mean TBR<sub>max</sub> of the descending aorta (r=0.43, p=0.06) but no association was reported for readings from the carotid artery (Rudd et al., 2009). In contrast, in 216 asymptomatic individuals undergoing oncology scans, hsCRP concentrations showed a weak ( $\beta=0.119$ ) but positive association with carotid artery mean WV SUV<sub>max</sub> (Tahara et al., 2007b).

As discussed in the previous chapter, it is important to note that the asymptomatic plaques are non-culprit plaques but in a symptomatic individual with a contralateral symptomatic plaque. This is important when considering the hsCRP as a systemic marker, as hsCRP concentrations are more likely to be influenced by the higher level

of activity in the symptomatic side. This is likely why there is a statistically significant correlation between hsCRP and FDG uptake in symptomatic arteries but not with FDG uptake in asymptomatic arteries. Therefore, within this study it is arguably only appropriate to consider the relationship of hsCRP with FDG uptake in the symptomatic artery.

No clear trends in correlation were observed between hsCRP and any measure of NaF uptake for either symptomatic or asymptomatic arteries, though we observed a moderate but statistically significant correlation between WV TBR<sub>mean</sub> and hsCRP in symptomatic arteries with low calcification. A few other measures (WV SUV<sub>mean</sub>, SHS/MDS/WV TBR<sub>max</sub>) had moderate correlations in symptomatic arteries with low calcification that approached statistical significance. However, given the lack of a clear trend in these results (especially when compared with the pattern of association between FDG uptake and hsCRP), these findings should be treated with caution. The suggestion that the relationship between hsCRP and NaF uptake differed based on the amount of macrocalcification would appear to be in-keeping with the earlier discussion, but it would be advantageous to investigate further using a larger sample.

The overall role of hsCRP in vascular disease remains controversial. An association between CRP and cardiovascular risk has been reported in a number of studies (Danesh et al., 2004, Ridker et al., 1998, Ridker et al., 2000). However, this relationship remains controversial. In the JUPITER substudy of the Multi-Ethnic Study of Atherosclerosis, there was no significant difference in the event rate of cardiovascular disease between the low hsCRP ( $\leq 2$  mg/L) and high hsCRP ( $\geq 2$  mg/L) cohorts after adjustment for age, sex, and race (Blaha et al., 2011).

CRP has been evaluated in regards to stroke-specific events. In a large study, Ford et al. report that CRP was significantly higher in those with a self-reported history of stroke, and the highest concentration cohort had an adjusted odds ratio of stroke (compared to lowest concentration) of 1.71 (95% CI 1.11-2.64) (Ford and Giles, 2000). In the Framingham Study, increased CRP was associated with first stroke or TIA, with men and women in the highest quartile of CRP having a two-fold and three-fold relative risk compared to the lowest quartiles respectively, and remained

statistically significant after adjustment for conventional cardiovascular risk factors (Rost et al., 2001).

Further studies have suggested a role for CRP for risk-stratification of ischaemic events after TIA (Purroy et al., 2007). In individuals with intracranial large artery occlusive disease, a hsCRP cut-off of 1.41 mg/dL was an independent predictor of new ischaemic events (Arenillas et al., 2003).

Elkind et al. considered the association of hsCRP with stroke recurrence, finding those with the highest quartile of hsCRP ( $>4.86$  mg/L) had an adjusted hazard ratio of 2.32 (95% CI 1.15-4.68) of recurrent stroke after lacunar stroke, with no interaction with statin use found at baseline, while intermediate quartiles had an increased but non-statistically significant recurrent stroke risk (Elkind et al., 2014). Consequently, the authors conclude that there may be a threshold effect at  $\sim 1$  mg/L above which the recurrent risk is increased, but no significant effect when considered as a continuous measure (Elkind et al., 2014).

The association between CRP and cerebral infarction has also been reported by other groups. Youn et al. found a statistically significant Spearman correlation of 0.24 between hsCRP and DWI lesion volume in a cohort of acute ischaemic strokes where approximately half the patients had large artery atherosclerosis (Youn et al., 2012). It is interesting to note that this study found a difference in the levels of hsCRP according to TOAST subtype, with cardioembolic stroke demonstrating the highest levels, and cardioembolic strokes representing a higher proportion of strokes at the higher two quartiles of DWI lesion volume. In contrast, large artery atherosclerosis had a much wider range of hsCRP values reported and constituted a more uniform trend across quartiles of DWI volumes. A similar variation in immunoinflammatory activation according to the subtype of ischaemic stroke has also been noted when comparing lacunar and non-lacunar stroke, and across all TOAST subtypes (Licata et al., 2006, Licata et al., 2009).

Ormstad et al. performed a battery of CRP and cytokines in individuals with recent ( $<72$ h) ischaemic stroke with neuroimaging (either CT or MRI) at 1-7 days after onset of symptoms. CRP levels correlated with infarct volume ( $r=0.47$ ,  $p=0.005$ ) but had no

relationship with lateralisation (Ormstad et al., 2011). Individuals with CRP above 2.5g/L had a median infarct volume of 11cm<sup>3</sup> compared to a median infarct volume of 1cm<sup>3</sup> in those below this value.

Pedersen et al. report CRP was elevated from 24 hours to 1 week after an infarct, and was correlated with terminal SC5b-9 complement complex levels, with CRP increase correlated with the size of the infarct (Pedersen et al., 2004).

However, not all studies have found a relationship between CRP and infarct volumes. Waje-Andreassen et al. found no correlation between CRP and infarct volume using CT or MRI between 5-7 days after ischaemic stroke (Waje-Andreassen et al., 2005). However, this was a small study with a heterogeneous population (including one thrombolysed individual) and no consideration was given of stroke aetiology or location. This study used peak CRP readings and it is worth noting that the peak CRP concentrations were recorded anywhere from 12 hours to 3 months after the infarct.

Marquardt et al. report that hsCRP levels were not raised after stroke – although levels were higher in individuals with stroke than in healthy controls, they did not differ from levels in from risk factor-matched controls – but CRP correlated with NIHSS. hsCRP was elevated only in those with the largest infarcts (larger than 1/3 of the MCA territory) but not in less extensive non-lacunar infarcts or lacunar strokes. Furthermore, the presence of two or more cardiovascular risk factors was associated with higher hsCRP levels at day 1 and day 14 after stroke, while treatment with aspirin was found to reduce hsCRP levels in the subacute phase (at days 14 and 90) (Marquardt et al., 2005).

As well as potentially reflecting the volume of infarct damage, CRP has also been directly implicated in exacerbating ischaemic injury at the time of the event. In animal models of myocardial ischaemia, addition of human CRP increased infarct size after coronary ligation (Griselli et al., 1999). Similar results were observed in animal models of cerebral infarction, where the addition of human CRP in adult rats undergoing MCAO resulted in significantly larger cerebral infarct volumes (Gill et al., 2004).

Inflammation may influence thrombosis. In individuals with acute ischaemic stroke, there was a weak but significant correlation between CRP and mean platelet volume, and both these criteria were found to be significantly higher in patients who died (Arikanoglu et al., 2013). CRP has also been observed in mouse models to promote the formation of monocyte-platelet aggregates via P-selecting glycoprotein ligand-1 binding, as well promoting thrombotic occlusion following arterial injury (Danenberg et al., 2007, Danenberg et al., 2003).

One mechanism by which CRP contributes to thromboinflammation is via prostaglandin pathways: human recombinant CRP was found to disrupt the oxygenase-prostanoid pathway in mouse models, resulting in increased prothrombotic thromboxane receptor levels, that could be ameliorated by aspirin (Grad et al., 2009). Further thromboxane receptor knock-out mice studies have supported this pathway in modulating CRP-induced platelet-endothelial adhesion and intravascular thrombosis (Grad et al., 2012).

Thromboxane pathways have been shown to be vital for the progression of plaque pathophysiology, and selective thromboxane receptor inhibition was observed to cause plaque regression and phenotypic change favouring stability in a rabbit model (Capone et al., 2004, Cheng et al., 2002, Viles-Gonzalez et al., 2005).

Interestingly, the role of thromboxane may not be limited to thrombosis. Thromboxane B2 concentrations were found to be elevated in a small cohort of individuals with depression (Lieb et al., 1983) whilst a number of small studies have reported an association between platelet activation and depression (Berk and Plein, 2000, Canan et al., 2012, Morel-Kopp et al., 2009, Moreno et al., 2013, Musselman et al., 1996, Neubauer et al., 2013). Thromboxane receptors are expressed on neurons within the central nervous system and use of thromboxane receptor antagonists were observed to activate nuclei within the limbic system, though did not appear to change behaviour, in mouse models (Mitsumori et al., 2011, Rebel et al., 2015). Animal studies have also suggested that inhibition of the thromboxane receptor results in reduced myocardial infarct volumes (Singh et al., 1997, Grover and Schumacher, 1988).

Overall these results suggest that CRP is more than a mere surrogate marker of inflammatory activity, but instead has direct proinflammatory and prothrombotic effects.

## References

- Abbott, N. J., Ronnback, L. & Hansson, E. 2006. Astrocyte-endothelial interactions at the blood-brain barrier. *Nat Rev Neurosci*, 7, 41-53.
- Abdelbaky, A., Corsini, E., Figueroa, A. L., Fontanez, S., Subramanian, S., Ferencik, M., . . . Tawakol, A. 2013. Focal arterial inflammation precedes subsequent calcification in the same location: a longitudinal FDG-PET/CT study. *Circ Cardiovasc Imaging*, 6, 747-54.
- Abela, G. S. & Aziz, K. 2006. Cholesterol crystals rupture biological membranes and human plaques during acute cardiovascular events--a novel insight into plaque rupture by scanning electron microscopy. *Scanning*, 28, 1-10.
- Abela, G. S., Aziz, K., Vedre, A., Pathak, D. R., Talbott, J. D. & Dejong, J. 2009. Effect of cholesterol crystals on plaques and intima in arteries of patients with acute coronary and cerebrovascular syndromes. *Am J Cardiol*, 103, 959-68.
- Abela, G. S., Vedre, A., Janoudi, A., Huang, R., Durga, S. & Tamhane, U. 2011. Effect of statins on cholesterol crystallization and atherosclerotic plaque stabilization. *Am J Cardiol*, 107, 1710-7.
- Achenbach, S., Moselewski, F., Ropers, D., Ferencik, M., Hoffmann, U., Macneill, B., . . . Brady, T. J. 2004. Detection of calcified and noncalcified coronary atherosclerotic plaque by contrast-enhanced, submillimeter multidetector spiral computed tomography: a segment-based comparison with intravascular ultrasound. *Circulation*, 109, 14-7.
- Adachi, T., Takagi, M., Hoshino, H. & Inafuku, T. 1997. Effect of extracranial carotid artery stenosis and other risk factors for stroke on periventricular hyperintensity. *Stroke*, 28, 2174-9.
- Adams, M. R., Jessup, W. & Celermajer, D. S. 1997. Cigarette smoking is associated with increased human monocyte adhesion to endothelial cells: reversibility with oral L-arginine but not vitamin C. *J Am Coll Cardiol*, 29, 491-7.
- Adraktas, D. D., Brasic, N., Furtado, A. D., Cheng, S. C., Ordovas, K., Chun, K., . . . Wintermark, M. 2010. Carotid atherosclerosis does not predict coronary, vertebral, or aortic atherosclerosis in patients with acute stroke symptoms. *Stroke*, 41, 1604-9.

- Agarwal, S., Warburton, E. A. & Baron, J. C. 2015. From Time is brain to Physiology is brain: a case for reflection in acute stroke treatment decisions. *Brain*, 138, 1768-70.
- Agatston, A. S., Janowitz, W. R., Hildner, F. J., Zusmer, N. R., Viamonte, M., Jr. & Detrano, R. 1990. Quantification of coronary artery calcium using ultrafast computed tomography. *J Am Coll Cardiol*, 15, 827-32.
- Aikawa, E., Nahrendorf, M., Figueiredo, J. L., Swirski, F. K., Shtatland, T., Kohler, R. H., . . . Weissleder, R. 2007. Osteogenesis associates with inflammation in early-stage atherosclerosis evaluated by molecular imaging in vivo. *Circulation*, 116, 2841-50.
- Al-Mutairy, A., Soliman, A., Melhem, E. R., Hurst, R., Krejza, J. & Al-Okaili, R. 2009. Carotid calcium scoring may correlate in males with the traditional Framingham epidemiologic risk variables for stroke. *Surg Neurol*, 71, 197-200.
- Alawneh, J. A., Moustafa, R. R., Marrapu, S. T., Jensen-Kondering, U., Morris, R. S., Jones, P. S., . . . Baron, J. C. 2014. Diffusion and perfusion correlates of the 18F-MISO PET lesion in acute stroke: pilot study. *Eur J Nucl Med Mol Imaging*, 41, 736-44.
- Albuquerque, L. C., Narvaes, L. B., Maciel, A. A., Staub, H., Friedrich, M., Filho, J. R., . . . Rohde, L. E. 2007. Intraplaque hemorrhage assessed by high-resolution magnetic resonance imaging and C-reactive protein in carotid atherosclerosis. *J Vasc Surg*, 46, 1130-7.
- Alheid, U., Frolich, J. C. & Forstermann, U. 1987. Endothelium-derived relaxing factor from cultured human endothelial cells inhibits aggregation of human platelets. *Thromb Res*, 47, 561-71.
- Allan, L. M., Rowan, E. N., Thomas, A. J., Polvikoski, T. M., O'brien, J. T. & Kalaria, R. N. 2013. Long-term incidence of depression and predictors of depressive symptoms in older stroke survivors. *Br J Psychiatry*, 203, 453-60.
- Allison, M. A., Criqui, M. H. & Wright, C. M. 2004. Patterns and risk factors for systemic calcified atherosclerosis. *Arterioscler Thromb Vasc Biol*, 24, 331-6.
- Alshihabi, S. N., Chang, Y. S., Frangos, J. A. & Tarbell, J. M. 1996. Shear stress-induced release of PGE2 and PGI2 by vascular smooth muscle cells. *Biochem Biophys Res Commun*, 224, 808-14.

- Altaf, N., Daniels, L., Morgan, P. S., Lowe, J., Gladman, J., Macsweeney, S. T., . . . Auer, D. P. 2006. Cerebral white matter hyperintense lesions are associated with unstable carotid plaques. *Eur J Vasc Endovasc Surg*, 31, 8-13.
- Altaf, N., Morgan, P. S., Moody, A., Macsweeney, S. T., Gladman, J. R. & Auer, D. P. 2008. Brain white matter hyperintensities are associated with carotid intraplaque hemorrhage. *Radiology*, 248, 202-9.
- Amantea, D., Nappi, G., Bernardi, G., Bagetta, G. & Corasaniti, M. T. 2009. Post-ischemic brain damage: pathophysiology and role of inflammatory mediators. *Febs j*, 276, 13-26.
- Ambrose, J. A. & Barua, R. S. 2004. The pathophysiology of cigarette smoking and cardiovascular disease: an update. *J Am Coll Cardiol*, 43, 1731-7.
- Anand, D. V., Lim, E., Darko, D., Bassett, P., Hopkins, D., Lipkin, D., . . . Lahiri, A. 2007. Determinants of progression of coronary artery calcification in type 2 diabetes role of glycemic control and inflammatory/vascular calcification markers. *J Am Coll Cardiol*, 50, 2218-25.
- Anderson, H. C. & Reynolds, J. J. 1973. Pyrophosphate stimulation of calcium uptake into cultured embryonic bones. Fine structure of matrix vesicles and their role in calcification. *Dev Biol*, 34, 211-27.
- Antonopoulos, C. N., Kakisis, J. D., Sfyroeras, G. S., Moulakakis, K. G., Kallinis, A., Giannakopoulos, T. & Liapis, C. D. 2015. The impact of carotid artery stenting on cognitive function in patients with extracranial carotid artery stenosis. *Ann Vasc Surg*, 29, 457-69.
- Arauz, A., Hoyos, L., Zenteno, M., Mendoza, R. & Alexanderson, E. 2007. Carotid plaque inflammation detected by 18F-fluorodeoxyglucose-positron emission tomography. Pilot study. *Clin Neurol Neurosurg*, 109, 409-12.
- Arboix, A. 2015. Cardiovascular risk factors for acute stroke: Risk profiles in the different subtypes of ischemic stroke. *World J Clin Cases*, 3, 418-29.
- Arenillas, J. F., Alvarez-Sabin, J., Molina, C. A., Chacon, P., Montaner, J., Rovira, A., . . . Quintana, M. 2003. C-reactive protein predicts further ischemic events in first-ever transient ischemic attack or stroke patients with intracranial large-artery occlusive disease. *Stroke*, 34, 2463-8.
- Arikanoglu, A., Yucel, Y., Acar, A., Cevik, M. U., Akil, E. & Varol, S. 2013. The relationship of the mean platelet volume and C-reactive protein levels with mortality in ischemic stroke patients. *Eur Rev Med Pharmacol Sci*, 17, 1774-7.

- Armani, C., Catalani, E., Balbarini, A., Bagnoli, P. & Cervia, D. 2007. Expression, pharmacology, and functional role of somatostatin receptor subtypes 1 and 2 in human macrophages. *J Leukoc Biol*, 81, 845-55.
- Arndt, H., Smith, C. W. & Granger, D. N. 1993. Leukocyte-endothelial cell adhesion in spontaneously hypertensive and normotensive rats. *Hypertension*, 21, 667-73.
- Arntzen, K. A., Schirmer, H., Johnsen, S. H., Wilsgaard, T. & Mathiesen, E. B. 2012. Carotid atherosclerosis predicts lower cognitive test results: a 7-year follow-up study of 4,371 stroke-free subjects - the Tromso study. *Cerebrovasc Dis*, 33, 159-65.
- Arsava, E. M., Rahman, R., Rosand, J., Lu, J., Smith, E. E., Rost, N. S., . . . Ay, H. 2009. Severity of leukoaraiosis correlates with clinical outcome after ischemic stroke. *Neurology*, 72, 1403-10.
- Asada, H., Paszkowiak, J., Teso, D., Alvi, K., Thorisson, A., Frattini, J. C., . . . Dardik, A. 2005. Sustained orbital shear stress stimulates smooth muscle cell proliferation via the extracellular signal-regulated protein kinase 1/2 pathway. *J Vasc Surg*, 42, 772-80.
- Asahi, M., Wang, X., Mori, T., Sumii, T., Jung, J. C., Moskowitz, M. A., . . . Lo, E. H. 2001. Effects of matrix metalloproteinase-9 gene knock-out on the proteolysis of blood-brain barrier and white matter components after cerebral ischemia. *J Neurosci*, 21, 7724-32.
- Ay, H., Arsava, E. M., Rosand, J., Furie, K. L., Singhal, A. B., Schaefer, P. W., . . . Sorensen, A. G. 2008. Severity of leukoaraiosis and susceptibility to infarct growth in acute stroke. *Stroke*, 39, 1409-13.
- Ayata, C. & Ropper, A. H. 2002. Ischaemic brain oedema. *J Clin Neurosci*, 9, 113-24.
- Baber, U., Mehran, R., Sartori, S., Schoos, M. M., Sillesen, H., Muntendam, P., . . . Fuster, V. 2015. Prevalence, impact, and predictive value of detecting subclinical coronary and carotid atherosclerosis in asymptomatic adults: the BioImage study. *J Am Coll Cardiol*, 65, 1065-74.
- Baezner, H., Blahak, C., Poggesi, A., Pantoni, L., Inzitari, D., Chabriat, H., . . . Hennerici, M. G. 2008. Association of gait and balance disorders with age-related white matter changes: the LADIS study. *Neurology*, 70, 935-42.

- Balakumar, P., Kathuria, S., Taneja, G., Kalra, S. & Mahadevan, N. 2012. Is targeting eNOS a key mechanistic insight of cardiovascular defensive potentials of statins? *J Mol Cell Cardiol*, 52, 83-92.
- Bardutzky, J., Shen, Q., Bouley, J., Sotak, C. H., Duong, T. Q. & Fisher, M. 2005a. Perfusion and diffusion imaging in acute focal cerebral ischemia: temporal vs. spatial resolution. *Brain Res*, 1043, 155-62.
- Bardutzky, J., Shen, Q., Henninger, N., Bouley, J., Duong, T. Q. & Fisher, M. 2005b. Differences in ischemic lesion evolution in different rat strains using diffusion and perfusion imaging. *Stroke*, 36, 2000-5.
- Barnett, H. J., Taylor, D. W., Eliasziw, M., Fox, A. J., Ferguson, G. G., Haynes, R. B., . . . Spence, J. D. 1998. Benefit of carotid endarterectomy in patients with symptomatic moderate or severe stenosis. North American Symptomatic Carotid Endarterectomy Trial Collaborators. *N Engl J Med*, 339, 1415-25.
- Baron, J. C., Yamauchi, H., Fujioka, M. & Endres, M. 2014. Selective neuronal loss in ischemic stroke and cerebrovascular disease. *J Cereb Blood Flow Metab*, 34, 2-18.
- Barrett, J. P., Costello, D. A., O'sullivan, J., Cowley, T. R. & Lynch, M. A. 2015. Bone marrow-derived macrophages from aged rats are more responsive to inflammatory stimuli. *J Neuroinflammation*, 12, 67.
- Barua, R. S., Ambrose, J. A., Srivastava, S., Devoe, M. C. & Eales-Reynolds, L. J. 2003. Reactive oxygen species are involved in smoking-induced dysfunction of nitric oxide biosynthesis and upregulation of endothelial nitric oxide synthase: an in vitro demonstration in human coronary artery endothelial cells. *Circulation*, 107, 2342-7.
- Basavaraj, M. G., Sovershaev, M. A., Egorina, E. M., Gruber, F. X., Bogdanov, V. Y., Fallon, J. T., . . . Hansen, J. B. 2012. Circulating monocytes mirror the imbalance in TF and TFPI expression in carotid atherosclerotic plaques with lipid-rich and calcified morphology. *Thromb Res*, 129, e134-41.
- Bauer, D. C., Orwoll, E. S., Fox, K. M., Vogt, T. M., Lane, N. E., Hochberg, M. C., . . . Nevitt, M. C. 1996. Aspirin and NSAID use in older women: effect on bone mineral density and fracture risk. Study of Osteoporotic Fractures Research Group. *J Bone Miner Res*, 11, 29-35.

- Baumer, Y., Mccurdy, S., Weatherby, T. M., Mehta, N. N., Halbherr, S., Halbherr, P., . . . Boisvert, W. A. 2017. Hyperlipidemia-induced cholesterol crystal production by endothelial cells promotes atherogenesis. *Nat Commun*, 8, 1129.
- Beaulieu, C., De Crespigny, A., Tong, D. C., Moseley, M. E., Albers, G. W. & Marks, M. P. 1999. Longitudinal magnetic resonance imaging study of perfusion and diffusion in stroke: evolution of lesion volume and correlation with clinical outcome. *Ann Neurol*, 46, 568-78.
- Beheshti, M., Saboury, B., Mehta, N. N., Torigian, D. A., Werner, T., Mohler, E., . . . Alavi, A. 2011. Detection and global quantification of cardiovascular molecular calcification by fluoro18-fluoride positron emission tomography/computed tomography--a novel concept. *Hell J Nucl Med*, 14, 114-20.
- Belayev, L., Busto, R., Zhao, W. & Ginsberg, M. D. 1996. Quantitative evaluation of blood-brain barrier permeability following middle cerebral artery occlusion in rats. *Brain Res*, 739, 88-96.
- Ben-Haim, S., Kupzov, E., Tamir, A. & Israel, O. 2004. Evaluation of 18F-FDG uptake and arterial wall calcifications using 18F-FDG PET/CT. *J Nucl Med*, 45, 1816-21.
- Berk, M. & Plein, H. 2000. Platelet supersensitivity to thrombin stimulation in depression: a possible mechanism for the association with cardiovascular mortality. *Clin Neuropharmacol*, 23, 182-5.
- Berman, S. E., Wang, X., Mitchell, C. C., Kundu, B., Jackson, D. C., Wilbrand, S. M., . . . Dempsey, R. J. 2015. The relationship between carotid artery plaque stability and white matter ischemic injury. *Neuroimage Clin*, 9, 216-22.
- Bhakdi, S., Torzewski, M., Klouche, M. & Hemmes, M. 1999. Complement and atherogenesis: binding of CRP to degraded, nonoxidized LDL enhances complement activation. *Arterioscler Thromb Vasc Biol*, 19, 2348-54.
- Bhakdi, S., Torzewski, M., Paprotka, K., Schmitt, S., Barsoom, H., Suriyaphol, P., . . . Husmann, M. 2004. Possible protective role for C-reactive protein in atherogenesis: complement activation by modified lipoproteins halts before detrimental terminal sequence. *Circulation*, 109, 1870-6.
- Bielinski, S. J., Berardi, C., Decker, P. A., Kirsch, P. S., Larson, N. B., Pankow, J. S., . . . Tsai, M. Y. 2015. P-selectin and subclinical and clinical atherosclerosis: the Multi-Ethnic Study of Atherosclerosis (MESA). *Atherosclerosis*, 240, 3-9.

- Bird, J. L., Izquierdo-Garcia, D., Davies, J. R., Rudd, J. H., Probst, K. C., Figg, N., . . . Warburton, E. A. 2010. Evaluation of translocator protein quantification as a tool for characterising macrophage burden in human carotid atherosclerosis. *Atherosclerosis*, 210, 388-91.
- Bitar, R., Moody, A. R., Leung, G., Symons, S., Crisp, S., Butany, J., . . . Maggisano, R. 2008. In vivo 3D high-spatial-resolution MR imaging of intraplaque hemorrhage. *Radiology*, 249, 259-67.
- Bitsch, A., Horn, C., Kemmling, Y., Seipelt, M., Hellenbrand, U., Stiefel, M., . . . Otto, M. 2002. Serum tau protein level as a marker of axonal damage in acute ischemic stroke. *Eur Neurol*, 47, 45-51.
- Bivard, A., Levi, C., Krishnamurthy, V., Mcelduff, P., Miteff, F., Spratt, N. J., . . . Parsons, M. 2015. Perfusion computed tomography to assist decision making for stroke thrombolysis. *Brain*, 138, 1919-31.
- Bjerrum, I. S., Sand, N. P., Poulsen, M. K., Norgaard, B. L., Sidelmann, J. J., Johansen, A., . . . Diederichsen, A. C. 2013. Non-invasive assessments reveal that more than half of randomly selected middle-aged individuals have evidence of subclinical atherosclerosis: a DanRisk substudy. *Int J Cardiovasc Imaging*, 29, 301-8.
- Blache, D. 1995. Involvement of hydrogen and lipid peroxides in acute tobacco smoking-induced platelet hyperactivity. *Am J Physiol*, 268, H679-85.
- Blaha, M. J., Budoff, M. J., Defilippis, A. P., Blankstein, R., Rivera, J. J., Agatston, A., . . . Nasir, K. 2011. Associations between C-reactive protein, coronary artery calcium, and cardiovascular events: implications for the JUPITER population from MESA, a population-based cohort study. *The Lancet*, 378, 684-692.
- Blahak, C., Baezner, H., Pantoni, L., Poggesi, A., Chabriat, H., Erkinjuntti, T., . . . Hennerici, M. G. 2009. Deep frontal and periventricular age related white matter changes but not basal ganglia and infratentorial hyperintensities are associated with falls: cross sectional results from the LADIS study. *J Neurol Neurosurg Psychiatry*, 80, 608-13.
- Blau, M., Nagler, W. & Bender, M. A. 1962. Fluorine-18: a new isotope for bone scanning. *J Nucl Med*, 3, 332-4.
- Blomberg, B. A., Thomassen, A., De Jong, P. A., Simonsen, J. A., Lam, M. G., Nielsen, A. L., . . . Hoiland-Carlsen, P. F. 2015. Impact of Personal

- Characteristics and Technical Factors on Quantification of Sodium 18F-Fluoride Uptake in Human Arteries: Prospective Evaluation of Healthy Subjects. *J Nucl Med*, 56, 1534-40.
- Boellaard, R., Delgado-Bolton, R., Oyen, W. J., Giammarile, F., Tatsch, K., Eschner, W., . . . Krause, B. J. 2015. FDG PET/CT: EANM procedure guidelines for tumour imaging: version 2.0. *Eur J Nucl Med Mol Imaging*, 42, 328-54.
- Bogousslavsky, J., Regli, F. & Uske, A. 1987. Leukoencephalopathy in patients with ischemic stroke. *Stroke*, 18, 896-9.
- Boring, L., Gosling, J., Cleary, M. & Charo, I. F. 1998. Decreased lesion formation in CCR2<sup>-/-</sup> mice reveals a role for chemokines in the initiation of atherosclerosis. *Nature*, 394, 894-7.
- Bots, M. L., Looman, S. J., Koudstaal, P. J., Hofman, A., Hoes, A. W. & Grobbee, D. E. 1996. Prevalence of stroke in the general population. The Rotterdam Study. *Stroke*, 27, 1499-501.
- Bots, M. L., Van Swieten, J. C., Breteler, M. M., De Jong, P. T., Van Gijn, J., Hofman, A. & Grobbee, D. E. 1993. Cerebral white matter lesions and atherosclerosis in the Rotterdam Study. *Lancet*, 341, 1232-7.
- Bours, M. J., Swennen, E. L., Di Virgilio, F., Cronstein, B. N. & Dagnelie, P. C. 2006. Adenosine 5'-triphosphate and adenosine as endogenous signaling molecules in immunity and inflammation. *Pharmacol Ther*, 112, 358-404.
- Boutet, C., Rouffange-Leclair, L., Schneider, F., Camdessanche, J. P., Antoine, J. C. & Barral, F. G. 2016. Visual Assessment of Age-Related White Matter Hyperintensities Using FLAIR Images at 3 T: Inter- and Intra-Rater Agreement. *Neurodegener Dis*, 16, 279-83.
- Boutin, H., Murray, K., Pradillo, J., Maroy, R., Smigova, A., Gerhard, A., . . . Trigg, W. 2015. 18F-GE-180: a novel TSPO radiotracer compared to 11C-R-PK11195 in a preclinical model of stroke. *Eur J Nucl Med Mol Imaging*, 42, 503-11.
- Boutin, H., Prenant, C., Maroy, R., Galea, J., Greenhalgh, A. D., Smigova, A., . . . Rothwell, N. J. 2013. [18F]DPA-714: direct comparison with [11C]PK11195 in a model of cerebral ischemia in rats. *PLoS One*, 8, e56441.
- Brand, K., Page, S., Rogler, G., Bartsch, A., Brandl, R., Knuechel, R., . . . Neumeier, D. 1996. Activated transcription factor nuclear factor-kappa B is present in the atherosclerotic lesion. *J Clin Invest*, 97, 1715-22.

- Brickman, A. M., Siedlecki, K. L., Muraskin, J., Manly, J. J., Luchsinger, J. A., Yeung, L. K., . . . Stern, Y. 2011. White matter hyperintensities and cognition: testing the reserve hypothesis. *Neurobiol Aging*, 32, 1588-98.
- Brooks, A. R., Lelkes, P. I. & Rubanyi, G. M. 2002. Gene expression profiling of human aortic endothelial cells exposed to disturbed flow and steady laminar flow. *Physiol Genomics*, 9, 27-41.
- Brouns, R., Wauters, A., De Surgeloose, D., Marien, P. & De Deyn, P. P. 2011. Biochemical markers for blood-brain barrier dysfunction in acute ischemic stroke correlate with evolution and outcome. *Eur Neurol*, 65, 23-31.
- Bruunsgaard, H. 2002. Effects of tumor necrosis factor-alpha and interleukin-6 in elderly populations. *Eur Cytokine Netw*, 13, 389-91.
- Bruunsgaard, H. & Pedersen, B. K. 2003. Age-related inflammatory cytokines and disease. *Immunol Allergy Clin North Am*, 23, 15-39.
- Bucerius, J., Duivenvoorden, R., Mani, V., Moncrieff, C., Rudd, J. H., Calcagno, C., . . . Fayad, Z. A. 2011. Prevalence and risk factors of carotid vessel wall inflammation in coronary artery disease patients: FDG-PET and CT imaging study. *JACC Cardiovasc Imaging*, 4, 1195-205.
- Bucerius, J., Hyafil, F., Verberne, H. J., Slart, R. H., Lindner, O., Sciagra, R., . . . Hacker, M. 2015. Position paper of the Cardiovascular Committee of the European Association of Nuclear Medicine (EANM) on PET imaging of atherosclerosis. *Eur J Nucl Med Mol Imaging*.
- Bucerius, J., Mani, V., Moncrieff, C., Machac, J., Fuster, V., Farkouh, M. E., . . . Fayad, Z. A. 2014. Optimizing 18F-FDG PET/CT imaging of vessel wall inflammation: the impact of 18F-FDG circulation time, injected dose, uptake parameters, and fasting blood glucose levels. *Eur J Nucl Med Mol Imaging*, 41, 369-83.
- Bucerius, J., Mani, V., Moncrieff, C., Rudd, J. H., Machac, J., Fuster, V., . . . Fayad, Z. A. 2012. Impact of noninsulin-dependent type 2 diabetes on carotid wall 18F-fluorodeoxyglucose positron emission tomography uptake. *J Am Coll Cardiol*, 59, 2080-8.
- Burke, A. P., Farb, A., Malcom, G. & Virmani, R. 2001. Effect of menopause on plaque morphologic characteristics in coronary atherosclerosis. *Am Heart J*, 141, S58-62.

- Busse, R., Luckhoff, A. & Bassenge, E. 1987. Endothelium-derived relaxant factor inhibits platelet activation. *Naunyn Schmiedebergs Arch Pharmacol*, 336, 566-71.
- Cai, J., Hatsukami, T. S., Ferguson, M. S., Kerwin, W. S., Saam, T., Chu, B., . . . Yuan, C. 2005. In Vivo Quantitative Measurement of Intact Fibrous Cap and Lipid-Rich Necrotic Core Size in Atherosclerotic Carotid Plaque: Comparison of High-Resolution, Contrast-Enhanced Magnetic Resonance Imaging and Histology. *Circulation*, 112, 3437-3444.
- Calabro, P., Willerson, J. T. & Yeh, E. T. 2003. Inflammatory cytokines stimulated C-reactive protein production by human coronary artery smooth muscle cells. *Circulation*, 108, 1930-2.
- Callegari, A., Coons, M. L., Ricks, J. L., Rosenfeld, M. E. & Scatena, M. 2014. Increased calcification in osteoprotegerin-deficient smooth muscle cells: Dependence on receptor activator of NF-kappaB ligand and interleukin 6. *J Vasc Res*, 51, 118-31.
- Canan, F., Dikici, S., Kutlucan, A., Celbek, G., Coskun, H., Gungor, A., . . . Kocaman, G. 2012. Association of mean platelet volume with DSM-IV major depression in a large community-based population: the MELEN study. *J Psychiatr Res*, 46, 298-302.
- Capone, M. L., Tacconelli, S., Sciulli, M. G., Grana, M., Ricciotti, E., Minuz, P., . . . Patrignani, P. 2004. Clinical pharmacology of platelet, monocyte, and vascular cyclooxygenase inhibition by naproxen and low-dose aspirin in healthy subjects. *Circulation*, 109, 1468-71.
- Carbone, L. D., Tylavsky, F. A., Cauley, J. A., Harris, T. B., Lang, T. F., Bauer, D. C., . . . Kritchevsky, S. B. 2003. Association between bone mineral density and the use of nonsteroidal anti-inflammatory drugs and aspirin: impact of cyclooxygenase selectivity. *J Bone Miner Res*, 18, 1795-802.
- Carr, S., Farb, A., Pearce, W. H., Virmani, R. & Yao, J. S. 1996. Atherosclerotic plaque rupture in symptomatic carotid artery stenosis. *J Vasc Surg*, 23, 755-65; discussion 765-6.
- Carrera, E., Jones, P. S., Morris, R. S., Alawneh, J., Hong, Y. T., Aigbirhio, F. I., . . . Baron, J. C. 2013. Is neural activation within the rescued penumbra impeded by selective neuronal loss? *Brain*, 136, 1816-29.

- Cayatte, A. J., Palacino, J. J., Horten, K. & Cohen, R. A. 1994. Chronic inhibition of nitric oxide production accelerates neointima formation and impairs endothelial function in hypercholesterolemic rabbits. *Arterioscler Thromb*, 14, 753-9.
- Chauveau, F., Boutin, H., Van Camp, N., Dolle, F. & Tavitian, B. 2008. Nuclear imaging of neuroinflammation: a comprehensive review of [<sup>11</sup>C]PK11195 challengers. *Eur J Nucl Med Mol Imaging*, 35, 2304-19.
- Chauveau, F., Van Camp, N., Dolle, F., Kuhnast, B., Hinnen, F., Damont, A., . . . Tavitian, B. 2009. Comparative evaluation of the translocator protein radioligands <sup>11</sup>C-DPA-713, <sup>18</sup>F-DPA-714, and <sup>11</sup>C-PK11195 in a rat model of acute neuroinflammation. *J Nucl Med*, 50, 468-76.
- Chawla, V., Simionescu, A., Langan, E. M., 3rd & Laberge, M. 2016. Influence of Clinically Relevant Mechanical Forces on Vascular Smooth Muscle Cells Under Chronic High Glucose: An In Vitro Dynamic Disease Model. *Ann Vasc Surg*, 34, 212-26.
- Chen, N. X., O'Neill, K. D., Chen, X. & Moe, S. M. 2008. Annexin-mediated matrix vesicle calcification in vascular smooth muscle cells. *J Bone Miner Res*, 23, 1798-805.
- Chen, W. & Dilsizian, V. 2013. Targeted PET/CT imaging of vulnerable atherosclerotic plaques: microcalcification with sodium fluoride and inflammation with fluorodeoxyglucose. *Curr Cardiol Rep*, 15, 364.
- Chen, W. & Dilsizian, V. 2015. PET Assessment of Vascular Inflammation and Atherosclerotic Plaques: SUV or TBR? *J Nucl Med*.
- Chen, Z., Qureshi, A. R., Parini, P., Hurt-Camejo, E., Ripsweden, J., Brismar, T. B., . . . Stenvinkel, P. 2017. Does statins promote vascular calcification in chronic kidney disease? *Eur J Clin Invest*, 47, 137-148.
- Cheng, G. C., Loree, H. M., Kamm, R. D., Fishbein, M. C. & Lee, R. T. 1993. Distribution of circumferential stress in ruptured and stable atherosclerotic lesions. A structural analysis with histopathological correlation. *Circulation*, 87, 1179-87.
- Cheng, Y., Austin, S. C., Rocca, B., Koller, B. H., Coffman, T. M., Grosser, T., . . . Fitzgerald, G. A. 2002. Role of prostacyclin in the cardiovascular response to thromboxane A<sub>2</sub>. *Science*, 296, 539-41.

- Cho, A. H., Cho, Y. P., Lee, D. H., Kwon, T. W., Kwon, S. U., Suh, D. C., . . . Kang, D. W. 2014. Reperfusion injury on magnetic resonance imaging after carotid revascularization. *Stroke*, 45, 602-4.
- Christian, R. C., Harrington, S., Edwards, W. D., Oberg, A. L. & Fitzpatrick, L. A. 2002. Estrogen status correlates with the calcium content of coronary atherosclerotic plaques in women. *J Clin Endocrinol Metab*, 87, 1062-7.
- Chróinín, D. N., Marnane, M., Akijian, L., Merwick, Á., Fallon, E., Horgan, G., . . . Kelly, P. J. 2014. Serum lipids associated with inflammation-related PET-FDG uptake in symptomatic carotid plaque. *Neurology*, 82, 1693-1699.
- Chung, J. W., Park, S. H., Kim, N., Kim, W. J., Park, J. H., Ko, Y., . . . Bae, H. J. 2014. Trial of ORG 10172 in Acute Stroke Treatment (TOAST) classification and vascular territory of ischemic stroke lesions diagnosed by diffusion-weighted imaging. *J Am Heart Assoc*, 3, e001119.
- Cocker, M. S., Spence, J. D., Hammond, R., Wells, G., Dekemp, R. A., Lum, C., . . . Beanlands, R. S. 2016. [18F]-NaF PET/CT Identifies Active Calcification in Carotid Plaque. *JACC Cardiovasc Imaging*.
- Copin, J. C., Bengualid, D. J., Da Silva, R. F., Kargiotis, O., Schaller, K. & Gasche, Y. 2011. Recombinant tissue plasminogen activator induces blood-brain barrier breakdown by a matrix metalloproteinase-9-independent pathway after transient focal cerebral ischemia in mouse. *Eur J Neurosci*, 34, 1085-92.
- Corson, M. A., James, N. L., Latta, S. E., Nerem, R. M., Berk, B. C. & Harrison, D. G. 1996. Phosphorylation of endothelial nitric oxide synthase in response to fluid shear stress. *Circ Res*, 79, 984-91.
- Craig, W. Y., Palomaki, G. E. & Haddow, J. E. 1989. Cigarette smoking and serum lipid and lipoprotein concentrations: an analysis of published data. *Bmj*, 298, 784-8.
- Cramer, S. C. 2008. Repairing the human brain after stroke: I. Mechanisms of spontaneous recovery. *Ann Neurol*, 63, 272-87.
- Crisby, M., Nordin-Fredriksson, G., Shah, P. K., Yano, J., Zhu, J. & Nilsson, J. 2001. Pravastatin treatment increases collagen content and decreases lipid content, inflammation, metalloproteinases, and cell death in human carotid plaques: implications for plaque stabilization. *Circulation*, 103, 926-33.
- Culebras, A., Otero, C., Toledo, J. R. & Rubin, B. S. 1989. Computed tomographic study of cervical carotid calcification. *Stroke*, 20, 1472-6.

- Cunnane, E. M., Mulvihill, J. J., Barrett, H. E., Hennessy, M. M., Kavanagh, E. G. & Walsh, M. T. 2016. Mechanical properties and composition of carotid and femoral atherosclerotic plaques: A comparative study. *J Biomech*, 49, 3697-3704.
- Cybulsky, M. I. & Gimbrone, M. A., Jr. 1991. Endothelial expression of a mononuclear leukocyte adhesion molecule during atherogenesis. *Science*, 251, 788-91.
- Cybulsky, M. I., Iiyama, K., Li, H., Zhu, S., Chen, M., Iiyama, M., . . . Milstone, D. S. 2001. A major role for VCAM-1, but not ICAM-1, in early atherosclerosis. *J Clin Invest*, 107, 1255-62.
- Dalm, V. A., Van Hagen, P. M., Van Koetsveld, P. M., Achilefu, S., Houtsmuller, A. B., Pols, D. H., . . . Hofland, L. J. 2003. Expression of somatostatin, cortistatin, and somatostatin receptors in human monocytes, macrophages, and dendritic cells. *Am J Physiol Endocrinol Metab*, 285, E344-53.
- Danenberg, H. D., Kantak, N., Grad, E., Swaminathan, R. V., Lotan, C. & Edelman, E. R. 2007. C-reactive protein promotes monocyte-platelet aggregation: an additional link to the inflammatory-thrombotic intricacy. *Eur J Haematol*, 78, 246-52.
- Danenberg, H. D., Szalai, A. J., Swaminathan, R. V., Peng, L., Chen, Z., Seifert, P., . . . Edelman, E. R. 2003. Increased thrombosis after arterial injury in human C-reactive protein-transgenic mice. *Circulation*, 108, 512-5.
- Danesh, J., Wheeler, J. G., Hirschfield, G. M., Eda, S., Eiriksdottir, G., Rumley, A., . . . Gudnason, V. 2004. C-reactive protein and other circulating markers of inflammation in the prediction of coronary heart disease. *N Engl J Med*, 350, 1387-97.
- Davenpeck, K. L., Gauthier, T. W. & Lefler, A. M. 1994. Inhibition of endothelial-derived nitric oxide promotes P-selectin expression and actions in the rat microcirculation. *Gastroenterology*, 107, 1050-8.
- Davies, J. R., Izquierdo-Garcia, D., Rudd, J. H., Figg, N., Richards, H. K., Bird, J. L., . . . Warburton, E. A. 2010. FDG-PET can distinguish inflamed from non-inflamed plaque in an animal model of atherosclerosis. *Int J Cardiovasc Imaging*, 26, 41-8.
- Davies, J. R., Rudd, J. H., Fryer, T. D., Graves, M. J., Clark, J. C., Kirkpatrick, P. J., . . . Weissberg, P. L. 2005. Identification of culprit lesions after transient

- ischemic attack by combined 18F fluorodeoxyglucose positron-emission tomography and high-resolution magnetic resonance imaging. *Stroke*, 36, 2642-7.
- Davies, P. F. 2009. Hemodynamic shear stress and the endothelium in cardiovascular pathophysiology. *Nat Clin Pract Cardiovasc Med*, 6, 16-26.
- Davies, P. F., Polacek, D. C., Handen, J. S., Helmke, B. P. & Depaola, N. 1999. A spatial approach to transcriptional profiling: mechanotransduction and the focal origin of atherosclerosis. *Trends Biotechnol*, 17, 347-51.
- De Caterina, R., Libby, P., Peng, H. B., Thannickal, V. J., Rajavashisth, T. B., Gimbrone, M. A., Jr., . . . Liao, J. K. 1995. Nitric oxide decreases cytokine-induced endothelial activation. Nitric oxide selectively reduces endothelial expression of adhesion molecules and proinflammatory cytokines. *J Clin Invest*, 96, 60-8.
- De Laat, K. F., Tuladhar, A. M., Van Norden, A. G., Norris, D. G., Zwiers, M. P. & De Leeuw, F. E. 2011. Loss of white matter integrity is associated with gait disorders in cerebral small vessel disease. *Brain*, 134, 73-83.
- De Leeuw, F. E., De Groot, J. C., Bots, M. L., Wittman, J. C., Oudkerk, M., Hofman, A., . . . Breteler, M. M. 2000. Carotid atherosclerosis and cerebral white matter lesions in a population based magnetic resonance imaging study. *J Neurol*, 247, 291-6.
- De Weerd, M., Greving, J. P., Hedblad, B., Lorenz, M. W., Mathiesen, E. B., O'leary, D. H., . . . Bots, M. L. 2010. Prevalence of asymptomatic carotid artery stenosis in the general population: an individual participant data meta-analysis. *Stroke*, 41, 1294-7.
- DeBette, S., Beiser, A., Decarli, C., Au, R., Himali, J. J., Kelly-Hayes, M., . . . Seshadri, S. 2010. Association of MRI markers of vascular brain injury with incident stroke, mild cognitive impairment, dementia, and mortality: the Framingham Offspring Study. *Stroke*, 41, 600-6.
- DeBette, S. & Markus, H. S. 2010. The clinical importance of white matter hyperintensities on brain magnetic resonance imaging: systematic review and meta-analysis. *Bmj*, 341, c3666.
- Deichen, J., Prante, O., Gack, M., Schmiedehausen, K. & Kuwert, T. 2003. Uptake of [18F]fluorodeoxyglucose in human monocyte-macrophages in vitro. *European Journal of Nuclear Medicine and Molecular Imaging*, 30, 267-273.

- Del Zoppo, G. J., Schmid-Schonbein, G. W., Mori, E., Copeland, B. R. & Chang, C. M. 1991. Polymorphonuclear leukocytes occlude capillaries following middle cerebral artery occlusion and reperfusion in baboons. *Stroke*, 22, 1276-83.
- Depaola, N., Davies, P. F., Pritchard, W. F., Jr., Florez, L., Harbeck, N. & Polacek, D. C. 1999. Spatial and temporal regulation of gap junction connexin43 in vascular endothelial cells exposed to controlled disturbed flows in vitro. *Proc Natl Acad Sci U S A*, 96, 3154-9.
- Depaola, N., Gimbrone, M. A., Jr., Davies, P. F. & Dewey, C. F., Jr. 1992. Vascular endothelium responds to fluid shear stress gradients. *Arterioscler Thromb*, 12, 1254-7.
- Derlin, T., Habermann, C. R., Hahne, J. D., Apostolova, I., Klutmann, S., Mester, J. & Buchert, R. 2011a. Quantification of [18F]-FDG uptake in atherosclerotic plaque: impact of renal function. *Ann Nucl Med*, 25, 586-91.
- Derlin, T., Janssen, T., Salamon, J., Veldhoen, S., Busch, J. D., Schon, G., . . . Adam, G. 2015. Age-related differences in the activity of arterial mineral deposition and regional bone metabolism: a 18F-sodium fluoride positron emission tomography study. *Osteoporos Int*, 26, 199-207.
- Derlin, T., Richter, U., Bannas, P., Begemann, P., Buchert, R., Mester, J. & Klutmann, S. 2010. Feasibility of 18F-sodium fluoride PET/CT for imaging of atherosclerotic plaque. *J Nucl Med*, 51, 862-5.
- Derlin, T., Toth, Z., Papp, L., Wisotzki, C., Apostolova, I., Habermann, C. R., . . . Klutmann, S. 2011b. Correlation of inflammation assessed by 18F-FDG PET, active mineral deposition assessed by 18F-fluoride PET, and vascular calcification in atherosclerotic plaque: a dual-tracer PET/CT study. *J Nucl Med*, 52, 1020-7.
- Derlin, T., Wisotzki, C., Richter, U., Apostolova, I., Bannas, P., Weber, C., . . . Klutmann, S. 2011c. In vivo imaging of mineral deposition in carotid plaque using 18F-sodium fluoride PET/CT: correlation with atherogenic risk factors. *J Nucl Med*, 52, 362-8.
- Devuyst, G., Karapanayiotides, T., Ruchat, P., Pusztaszeri, M., Lobrinus, J. A., Jonasson, L., . . . Bogousslavsky, J. 2005. Ultrasound measurement of the fibrous cap in symptomatic and asymptomatic atheromatous carotid plaques. *Circulation*, 111, 2776-82.

- Dhore, C. R., Cleutjens, J. P., Lutgens, E., Cleutjens, K. B., Geusens, P. P., Kitslaar, P. J., . . . Daemen, M. J. 2001. Differential expression of bone matrix regulatory proteins in human atherosclerotic plaques. *Arterioscler Thromb Vasc Biol*, 21, 1998-2003.
- Dickens, A. M., Vainio, S., Marjamaki, P., Johansson, J., Lehtiniemi, P., Rokka, J., . . . Airas, L. 2014. Detection of microglial activation in an acute model of neuroinflammation using PET and radiotracers 11C-(R)-PK11195 and 18F-GE-180. *J Nucl Med*, 55, 466-72.
- Dik, M. G., Jonker, C., Hack, C. E., Smit, J. H., Comijs, H. C. & Eikelenboom, P. 2005. Serum inflammatory proteins and cognitive decline in older persons. *Neurology*, 64, 1371-7.
- Ding, A. H., Nathan, C. F. & Stuehr, D. J. 1988. Release of reactive nitrogen intermediates and reactive oxygen intermediates from mouse peritoneal macrophages. Comparison of activating cytokines and evidence for independent production. *J Immunol*, 141, 2407-12.
- Doherty, T. M., Asotra, K., Fitzpatrick, L. A., Qiao, J. H., Wilkin, D. J., Detrano, R. C., . . . Rajavashisth, T. B. 2003. Calcification in atherosclerosis: bone biology and chronic inflammation at the arterial crossroads. *Proc Natl Acad Sci U S A*, 100, 11201-6.
- Dohmen, C., Galldik, N., Bosche, B., Kracht, L. & Graf, R. 2012. The severity of ischemia determines and predicts malignant brain edema in patients with large middle cerebral artery infarction. *Cerebrovasc Dis*, 33, 1-7.
- Drake, C., Boutin, H., Jones, M. S., Denes, A., Mccoll, B. W., Selvarajah, J. R., . . . Allan, S. M. 2011. Brain inflammation is induced by co-morbidities and risk factors for stroke. *Brain Behav Immun*, 25, 1113-22.
- Du, C., Hu, R., Csernansky, C. A., Hsu, C. Y. & Choi, D. W. 1996. Very delayed infarction after mild focal cerebral ischemia: a role for apoptosis? *J Cereb Blood Flow Metab*, 16, 195-201.
- Duivenvoorden, R., Mani, V., Woodward, M., Kallend, D., Suchankova, G., Fuster, V., . . . Fayad, Z. A. 2013. Relationship of serum inflammatory biomarkers with plaque inflammation assessed by FDG PET/CT: the dal-PLAQUE study. *JACC Cardiovasc Imaging*, 6, 1087-94.

- Duncan, P. W., Bode, R. K., Min Lai, S. & Perera, S. 2003. Rasch analysis of a new stroke-specific outcome scale: the Stroke Impact Scale. *Arch Phys Med Rehabil*, 84, 950-63.
- Duong, T., Acton, P. J. & Johnson, R. A. 1998. The in vitro neuronal toxicity of pentraxins associated with Alzheimer's disease brain lesions. *Brain Res*, 813, 303-12.
- Durafourt, B. A., Moore, C. S., Zammit, D. A., Johnson, T. A., Zaguia, F., Guiot, M. C., . . . Antel, J. P. 2012. Comparison of polarization properties of human adult microglia and blood-derived macrophages. *Glia*, 60, 717-27.
- Dutta, P., Courties, G., Wei, Y., Leuschner, F., Gorbатов, R., Robbins, C. S., . . . Nahrendorf, M. 2012. Myocardial infarction accelerates atherosclerosis. *Nature*, 487, 325-9.
- Dweck, M. R., Chow, M. W., Joshi, N. V., Williams, M. C., Jones, C., Fletcher, A. M., . . . Newby, D. E. 2012. Coronary arterial <sup>18</sup>F-sodium fluoride uptake: a novel marker of plaque biology. *J Am Coll Cardiol*, 59, 1539-48.
- Eesa, M., Hill, M. D., Al-Khathaami, A., Al-Zawahmah, M., Sharma, P., Menon, B. K., . . . Goyal, M. 2010. Role of CT angiographic plaque morphologic characteristics in addition to stenosis in predicting the symptomatic side in carotid artery disease. *AJNR Am J Neuroradiol*, 31, 1254-60.
- Egorina, E. M., Sovershaev, M. A., Bogdanov, V. Y., Sovershaev, T. A., Fallon, J. T., Seredkina, N., . . . Hansen, J. B. 2011. Low thrombogenicity of calcified atherosclerotic plaques is associated with bone morphogenetic protein-2-dependent inhibition of tissue factor expression. *Blood Coagul Fibrinolysis*, 22, 642-50.
- Ehara, S., Kobayashi, Y., Yoshiyama, M., Shimada, K., Shimada, Y., Fukuda, D., . . . Ueda, M. 2004. Spotty calcification typifies the culprit plaque in patients with acute myocardial infarction: an intravascular ultrasound study. *Circulation*, 110, 3424-9.
- Eikendal, A. L., Groenewegen, K. A., Anderson, T. J., Britton, A. R., Engstrom, G., Evans, G. W., . . . Den Ruijter, H. M. 2015. Common carotid intima-media thickness relates to cardiovascular events in adults aged <45 years. *Hypertension*, 65, 707-13.
- Elias-Smale, S. E., Odink, A. E., Wieberdink, R. G., Hofman, A., Hunink, M. G., Krestin, G. P., . . . Wittteman, J. C. 2010. Carotid, aortic arch and coronary

- calcification are related to history of stroke: the Rotterdam Study. *Atherosclerosis*, 212, 656-60.
- Elias-Smale, S. E., Wieberdink, R. G., Odink, A. E., Hofman, A., Hunink, M. G., Koudstaal, P. J., . . . Witteman, J. C. 2011. Burden of atherosclerosis improves the prediction of coronary heart disease but not cerebrovascular events: the Rotterdam Study. *Eur Heart J*, 32, 2050-8.
- Elkeles, R. S., Godsland, I. F., Feher, M. D., Rubens, M. B., Roughton, M., Nugara, F., . . . Flather, M. D. 2008. Coronary calcium measurement improves prediction of cardiovascular events in asymptomatic patients with type 2 diabetes: the PREDICT study. *Eur Heart J*, 29, 2244-51.
- Elkind, M. S., Luna, J. M., McClure, L. A., Zhang, Y., Coffey, C. S., Roldan, A., . . . Benavente, O. R. 2014. C-reactive protein as a prognostic marker after lacunar stroke: levels of inflammatory markers in the treatment of stroke study. *Stroke*, 45, 707-16.
- Ellingsen, T. S., Lappegard, J., Skjelbakken, T., Braekkan, S. K. & Hansen, J. B. 2015. Red cell distribution width is associated with incident venous thromboembolism (VTE) and case-fatality after VTE in a general population. *Thromb Haemost*, 113, 193-200.
- Emami, H., Singh, P., Macnabb, M., Vucic, E., Lavender, Z., Rudd, J. H., . . . Tawakol, A. 2015a. Splenic metabolic activity predicts risk of future cardiovascular events: demonstration of a cardiosplenic axis in humans. *JACC Cardiovasc Imaging*, 8, 121-30.
- Emami, H., Vucic, E., Subramanian, S., Abdelbaky, A., Fayad, Z. A., Du, S., . . . Tawakol, A. 2015b. The effect of BMS-582949, a P38 mitogen-activated protein kinase (P38 MAPK) inhibitor on arterial inflammation: a multicenter FDG-PET trial. *Atherosclerosis*, 240, 490-6.
- Engelhardt, B. & Sorokin, L. 2009. The blood-brain and the blood-cerebrospinal fluid barriers: function and dysfunction. *Semin Immunopathol*, 31, 497-511.
- Engelse, M. A., Neele, J. M., Bronckers, A. L., Pannekoek, H. & De Vries, C. J. 2001. Vascular calcification: expression patterns of the osteoblast-specific gene core binding factor alpha-1 and the protective factor matrix gla protein in human atherogenesis. *Cardiovasc Res*, 52, 281-9.
- Enzmann, G., Mysiorek, C., Gorina, R., Cheng, Y. J., Ghavampour, S., Hannocks, M. J., . . . Sorokin, L. 2013. The neurovascular unit as a selective barrier to

- polymorphonuclear granulocyte (PMN) infiltration into the brain after ischemic injury. *Acta Neuropathol*, 125, 395-412.
- Erl, W., Weber, C., Wardemann, C. & Weber, P. C. 1997. alpha-Tocopheryl succinate inhibits monocytic cell adhesion to endothelial cells by suppressing NF-kappa B mobilization. *Am J Physiol*, 273, H634-40.
- Ershler, W. B. & Keller, E. T. 2000. Age-associated increased interleukin-6 gene expression, late-life diseases, and frailty. *Annu Rev Med*, 51, 245-70.
- European Carotid Surgery Trialists' Collaborative Group 1998. Randomised trial of endarterectomy for recently symptomatic carotid stenosis: final results of the MRC European Carotid Surgery Trial (ECST). *Lancet*, 351, 1379-87.
- Evans, N. R., Tarkin, J. M., Buscombe, J. R., Markus, H. S., Rudd, J. H. F. & Warburton, E. A. 2017. PET Imaging of the Neurovascular Interface in Cerebrovascular Disease. *Nat Rev Neurol*, [In Press].
- Everett, B. M., Pradhan, A. D., Solomon, D. H., Paynter, N., Macfadyen, J., Zaharris, E., . . . Ridker, P. M. 2013. Rationale and design of the Cardiovascular Inflammation Reduction Trial: a test of the inflammatory hypothesis of atherothrombosis. *Am Heart J*, 166, 199-207.e15.
- Executive Committee for the Asymptomatic Carotid Atherosclerosis Study 1995. Endarterectomy for asymptomatic carotid artery stenosis. *Jama*, 273, 1421-8.
- Fanning, N. F., Walters, T. D., Fox, A. J. & Symons, S. P. 2006. Association between calcification of the cervical carotid artery bifurcation and white matter ischemia. *AJNR Am J Neuroradiol*, 27, 378-83.
- Farrall, A. J. & Wardlaw, J. M. 2009. Blood-brain barrier: ageing and microvascular disease--systematic review and meta-analysis. *Neurobiol Aging*, 30, 337-52.
- Fassbender, K., Rossol, S., Kammer, T., Daffertshofer, M., Wirth, S., Dollman, M. & Hennerici, M. 1994. Proinflammatory cytokines in serum of patients with acute cerebral ischemia: kinetics of secretion and relation to the extent of brain damage and outcome of disease. *J Neurol Sci*, 122, 135-9.
- Fayad, Z. A., Mani, V., Woodward, M., Kallend, D., Abt, M., Burgess, T., . . . Tawakol, A. 2011a. Safety and efficacy of dalcetrapib on atherosclerotic disease using novel non-invasive multimodality imaging (dal-PLAQUE): a randomised clinical trial. *Lancet*, 378, 1547-59.
- Fayad, Z. A., Mani, V., Woodward, M., Kallend, D., Bansilal, S., Pozza, J., . . . Farkouh, M. E. 2011b. Rationale and design of dal-PLAQUE: a study

- assessing efficacy and safety of dalcetrapib on progression or regression of atherosclerosis using magnetic resonance imaging and 18F-fluorodeoxyglucose positron emission tomography/computed tomography. *Am Heart J*, 162, 214-221.e2.
- Fazekas, F., Chawluk, J. B., Alavi, A., Hurtig, H. I. & Zimmerman, R. A. 1987. MR signal abnormalities at 1.5 T in Alzheimer's dementia and normal aging. *AJR Am J Roentgenol*, 149, 351-6.
- Fazekas, F., Niederkorn, K., Schmidt, R., Offenbacher, H., Horner, S., Bertha, G. & Lechner, H. 1988. White matter signal abnormalities in normal individuals: correlation with carotid ultrasonography, cerebral blood flow measurements, and cerebrovascular risk factors. *Stroke*, 19, 1285-8.
- Fifer, K. M., Qadir, S., Subramanian, S., Vijayakumar, J., Figueroa, A. L., Truong, Q. A., . . . Tawakol, A. 2011. Positron emission tomography measurement of periodontal 18F-fluorodeoxyglucose uptake is associated with histologically determined carotid plaque inflammation. *J Am Coll Cardiol*, 57, 971-6.
- Figueroa, A. L., Subramanian, S. S., Cury, R. C., Truong, Q. A., Gardecki, J. A., Tearney, G. J., . . . Tawakol, A. 2012. Distribution of inflammation within carotid atherosclerotic plaques with high-risk morphological features: a comparison between positron emission tomography activity, plaque morphology, and histopathology. *Circ Cardiovasc Imaging*, 5, 69-77.
- Fiz, F., Morbelli, S., Piccardo, A., Bauckneht, M., Ferrarazzo, G., Pesarino, E., . . . Sambucetti, G. 2015. 18F-NaF uptake by the atherosclerotic plaque at PET/CT imaging: inverse correlation between calcification density and mineral metabolic activity. *J Nucl Med*.
- Folco, E. J., Sheikine, Y., Rocha, V. Z., Christen, T., Shvartz, E., Sukhova, G. K., . . . Libby, P. 2011. Hypoxia but not inflammation augments glucose uptake in human macrophages: Implications for imaging atherosclerosis with 18fluorine-labeled 2-deoxy-D-glucose positron emission tomography. *J Am Coll Cardiol*, 58, 603-14.
- Ford, E. S. & Giles, W. H. 2000. Serum C-reactive protein and self-reported stroke: findings from the Third National Health and Nutrition Examination Survey. *Arterioscler Thromb Vasc Biol*, 20, 1052-6.

- Forstermann, U. 2008. Oxidative stress in vascular disease: causes, defense mechanisms and potential therapies. *Nat Clin Pract Cardiovasc Med*, 5, 338-49.
- Franceschi, C., Bonafe, M., Valensin, S., Olivieri, F., De Luca, M., Ottaviani, E. & De Benedictis, G. 2000. Inflamm-aging. An evolutionary perspective on immunosenescence. *Ann N Y Acad Sci*, 908, 244-54.
- Frei, B., Forte, T. M., Ames, B. N. & Cross, C. E. 1991. Gas phase oxidants of cigarette smoke induce lipid peroxidation and changes in lipoprotein properties in human blood plasma. Protective effects of ascorbic acid. *Biochem J*, 277 ( Pt 1), 133-8.
- Frodl, T. & Amico, F. 2014. Is there an association between peripheral immune markers and structural/functional neuroimaging findings? *Prog Neuropsychopharmacol Biol Psychiatry*, 48, 295-303.
- Frye, M. A., Melton, L. J., 3rd, Bryant, S. C., Fitzpatrick, L. A., Wahner, H. W., Schwartz, R. S. & Riggs, B. L. 1992. Osteoporosis and calcification of the aorta. *Bone Miner*, 19, 185-94.
- Fu, Y., Maianu, L., Melbert, B. R. & Garvey, W. T. 2004. Facilitative glucose transporter gene expression in human lymphocytes, monocytes, and macrophages: a role for GLUT isoforms 1, 3, and 5 in the immune response and foam cell formation. *Blood Cells Mol Dis*, 32, 182-90.
- Fujii, H., Li, S. H., Szmitko, P. E., Fedak, P. W. & Verma, S. 2006. C-reactive protein alters antioxidant defenses and promotes apoptosis in endothelial progenitor cells. *Arterioscler Thromb Vasc Biol*, 26, 2476-82.
- Fujimura, Y., Hwang, P. M., Trout Iii, H., Kozloff, L., Imaizumi, M., Innis, R. B. & Fujita, M. 2008. Increased peripheral benzodiazepine receptors in arterial plaque of patients with atherosclerosis: an autoradiographic study with [(3)H]PK 11195. *Atherosclerosis*, 201, 108-11.
- Fujita, M., Imaizumi, M., Zoghbi, S. S., Fujimura, Y., Farris, A. G., Suhara, T., . . . Innis, R. B. 2008. Kinetic analysis in healthy humans of a novel positron emission tomography radioligand to image the peripheral benzodiazepine receptor, a potential biomarker for inflammation. *Neuroimage*, 40, 43-52.
- Fusegawa, Y., Goto, S., Handa, S., Kawada, T. & Ando, Y. 1999. Platelet spontaneous aggregation in platelet-rich plasma is increased in habitual smokers. *Thromb Res*, 93, 271-8.

- Gaemperli, O., Shalhoub, J., Owen, D. R., Lamare, F., Johansson, S., Fouladi, N., . . . Camici, P. G. 2012. Imaging intraplaque inflammation in carotid atherosclerosis with <sup>11</sup>C-PK11195 positron emission tomography/computed tomography. *Eur Heart J*, 33, 1902-10.
- Galis, Z. S., Muszynski, M., Sukhova, G. K., Simon-Morrissey, E., Unemori, E. N., Lark, M. W., . . . Libby, P. 1994. Cytokine-stimulated human vascular smooth muscle cells synthesize a complement of enzymes required for extracellular matrix digestion. *Circ Res*, 75, 181-9.
- Gardener, H., Caunca, M. R., Dong, C., Cheung, Y. K., Elkind, M. S. V., Sacco, R. L., . . . Wright, C. B. 2017. Ultrasound Markers of Carotid Atherosclerosis and Cognition: The Northern Manhattan Study. *Stroke*, 48, 1855-1861.
- Garg, U. C. & Hassid, A. 1989. Nitric oxide-generating vasodilators and 8-bromocyclic guanosine monophosphate inhibit mitogenesis and proliferation of cultured rat vascular smooth muscle cells. *J Clin Invest*, 83, 1774-7.
- Gauthier, T. W., Scalia, R., Murohara, T., Guo, J. P. & Lefer, A. M. 1995. Nitric oxide protects against leukocyte-endothelium interactions in the early stages of hypercholesterolemia. *Arterioscler Thromb Vasc Biol*, 15, 1652-9.
- Gepner, A. D., Colangelo, L. A., Reilly, N., Korcarz, C. E., Kaufman, J. D. & Stein, J. H. 2015. Carotid Artery Longitudinal Displacement, Cardiovascular Disease and Risk Factors: The Multi-Ethnic Study of Atherosclerosis. *PLoS One*, 10, e0142138.
- Gerhard, A., Schwarz, J., Myers, R., Wise, R. & Banati, R. B. 2005. Evolution of microglial activation in patients after ischemic stroke: a [<sup>11</sup>C](R)-PK11195 PET study. *Neuroimage*, 24, 591-5.
- Germano Da Paz, O., Guillaumon, A. T., Lopes, T. M., Weiler, M., Cendes, F. & Balthazar, M. L. 2014. Carotid stenting versus endarterectomy cognitive outcomes. *Ann Vasc Surg*, 28, 893-900.
- Giannotti, N., O'connell, M. J., Foley, S. J., Kelly, P. J. & McNulty, J. P. 2017. Carotid atherosclerotic plaques standardised uptake values: software challenges and reproducibility. *EJNMMI Res*, 7, 39.
- Gidday, J. M., Gasche, Y. G., Copin, J. C., Shah, A. R., Perez, R. S., Shapiro, S. D., . . . Park, T. S. 2005. Leukocyte-derived matrix metalloproteinase-9 mediates blood-brain barrier breakdown and is proinflammatory after transient focal cerebral ischemia. *Am J Physiol Heart Circ Physiol*, 289, H558-68.

- Gill, R., Kemp, J. A., Sabin, C. & Pepys, M. B. 2004. Human C-reactive protein increases cerebral infarct size after middle cerebral artery occlusion in adult rats. *J Cereb Blood Flow Metab*, 24, 1214-8.
- Gimbrone, M. A., Jr., Topper, J. N., Nagel, T., Anderson, K. R. & Garcia-Cardena, G. 2000. Endothelial dysfunction, hemodynamic forces, and atherogenesis. *Ann N Y Acad Sci*, 902, 230-9; discussion 239-40.
- Girard, S., Brough, D., Lopez-Castejon, G., Giles, J., Rothwell, N. J. & Allan, S. M. 2013. Microglia and macrophages differentially modulate cell death after brain injury caused by oxygen-glucose deprivation in organotypic brain slices. *Glia*, 61, 813-24.
- Glagov, S., Zarins, C., Giddens, D. P. & Ku, D. N. 1988. Hemodynamics and atherosclerosis. Insights and perspectives gained from studies of human arteries. *Arch Pathol Lab Med*, 112, 1018-31.
- Gottschall, P. E. & Deb, S. 1996. Regulation of matrix metalloproteinase expressions in astrocytes, microglia and neurons. *Neuroimmunomodulation*, 3, 69-75.
- Gouw, A. A., Van Der Flier, W. M., Van Straaten, E. C., Pantoni, L., Bastos-Leite, A. J., Inzitari, D., . . . Barkhof, F. 2008. Reliability and sensitivity of visual scales versus volumetry for evaluating white matter hyperintensity progression. *Cerebrovasc Dis*, 25, 247-53.
- Grad, E., Golomb, M., Koroukhov, N., Lawson, J. A., Lotan, C., Fitzgerald, G. A. & Danenberg, H. D. 2009. Aspirin reduces the prothrombotic activity of C-reactive protein. *J Thromb Haemost*, 7, 1393-400.
- Grad, E., Pachino, R. M., Fitzgerald, G. A. & Danenberg, H. D. 2012. Role of Thromboxane Receptor in C-Reactive Protein-Induced Thrombosis. *Arteriosclerosis, Thrombosis, and Vascular Biology*, 32, 2468-2474.
- Griffith, T. M. 2002. Endothelial control of vascular tone by nitric oxide and gap junctions: a haemodynamic perspective. *Biorheology*, 39, 307-18.
- Griselli, M., Herbert, J., Hutchinson, W. L., Taylor, K. M., Sohail, M., Krausz, T. & Pepys, M. B. 1999. C-reactive protein and complement are important mediators of tissue damage in acute myocardial infarction. *J Exp Med*, 190, 1733-40.
- Grover, G. J. & Schumacher, W. A. 1988. Effect of the thromboxane receptor antagonist SQ 29,548 on myocardial infarct size in dogs. *J Cardiovasc Pharmacol*, 11, 29-35.

- Grueter, B. E. & Schulz, U. G. 2012. Age-related cerebral white matter disease (leukoaraiosis): a review. *Postgrad Med J*, 88, 79-87.
- Guadagno, J. V., Jones, P. S., Aigbirhio, F. I., Wang, D., Fryer, T. D., Day, D. J., . . . Baron, J. C. 2008. Selective neuronal loss in rescued penumbra relates to initial hypoperfusion. *Brain*, 131, 2666-78.
- Guadagno, J. V., Warburton, E. A., Aigbirhio, F. I., Smielewski, P., Fryer, T. D., Harding, S., . . . Baron, J. C. 2004. Does the acute diffusion-weighted imaging lesion represent penumbra as well as core? A combined quantitative PET/MRI voxel-based study. *J Cereb Blood Flow Metab*, 24, 1249-54.
- Guadagno, J. V., Warburton, E. A., Jones, P. S., Day, D. J., Aigbirhio, F. I., Fryer, T. D., . . . Baron, J. C. 2006. How affected is oxygen metabolism in DWI lesions?: A combined acute stroke PET-MR study. *Neurology*, 67, 824-9.
- Guadagno, J. V., Warburton, E. A., Jones, P. S., Fryer, T. D., Day, D. J., Gillard, J. H., . . . Baron, J. C. 2005. The diffusion-weighted lesion in acute stroke: heterogeneous patterns of flow/metabolism uncoupling as assessed by quantitative positron emission tomography. *Cerebrovasc Dis*, 19, 239-46.
- Gulyas, B., Toth, M., Schain, M., Airaksinen, A., Vas, A., Kostulas, K., . . . Halldin, C. 2012a. Evolution of microglial activation in ischaemic core and peri-infarct regions after stroke: a PET study with the TSPO molecular imaging biomarker [ $^{11}\text{C}$ ]vinpocetine. *J Neurol Sci*, 320, 110-7.
- Gulyas, B., Toth, M., Vas, A., Shchukin, E., Kostulas, K., Hillert, J. & Halldin, C. 2012b. Visualising neuroinflammation in post-stroke patients: a comparative PET study with the TSPO molecular imaging biomarkers [ $^{11}\text{C}$ ]PK11195 and [ $^{11}\text{C}$ ]vinpocetine. *Curr Radiopharm*, 5, 19-28.
- Guo, M., Cox, B., Mahale, S., Davis, W., Carranza, A., Hayes, K., . . . Ding, Y. 2008. Pre-ischemic exercise reduces matrix metalloproteinase-9 expression and ameliorates blood-brain barrier dysfunction in stroke. *Neuroscience*, 151, 340-51.
- Guo, Q., Colasanti, A., Owen, D. R., Onega, M., Kamalakaran, A., Bennacef, I., . . . Gunn, R. N. 2013. Quantification of the specific translocator protein signal of  $^{18}\text{F}$ -PBR111 in healthy humans: a genetic polymorphism effect on in vivo binding. *J Nucl Med*, 54, 1915-23.

- Habes, M., Erus, G., Toledo, J. B., Zhang, T., Bryan, N., Launer, L. J., . . . Davatzikos, C. 2016. White matter hyperintensities and imaging patterns of brain ageing in the general population. *Brain*, 139, 1164-79.
- Hainsworth, A. H., Brittain, J. F. & Khatun, H. 2012. Pre-clinical models of human cerebral small vessel disease: utility for clinical application. *J Neurol Sci*, 322, 237-40.
- Hakimelahi, R., Vachha, B. A., Copen, W. A., Papini, G. D., He, J., Higazi, M. M., . . . Gonzalez, R. G. 2014. Time and diffusion lesion size in major anterior circulation ischemic strokes. *Stroke*, 45, 2936-41.
- Han, D., Sun, M., He, P. P., Wen, L. L., Zhang, H. & Feng, J. 2015. Ischemic Postconditioning Alleviates Brain Edema After Focal Cerebral Ischemia Reperfusion in Rats Through Down-Regulation of Aquaporin-4. *J Mol Neurosci*, 56, 722-9.
- Han, K. H., Hong, K. H., Park, J. H., Ko, J., Kang, D. H., Choi, K. J., . . . Park, S. J. 2004. C-reactive protein promotes monocyte chemoattractant protein-1--mediated chemotaxis through upregulating CC chemokine receptor 2 expression in human monocytes. *Circulation*, 109, 2566-71.
- Hanyu, H., Asano, T., Tanaka, Y., Iwamoto, T., Takasaki, M. & Abe, K. 2002. Increased blood-brain barrier permeability in white matter lesions of Binswanger's disease evaluated by contrast-enhanced MRI. *Dement Geriatr Cogn Disord*, 14, 1-6.
- Hao, G., Wang, X., Treiber, F. A., Davis, H., Leverett, S., Su, S. & Kapuku, G. 2016. Growth of Carotid Intima-Media Thickness in Black and White Young Adults. *J Am Heart Assoc*, 5.
- Hardie, A. D., Kramer, C. M., Raghavan, P., Baskurt, E. & Nandalur, K. R. 2007. The impact of expansive arterial remodeling on clinical presentation in carotid artery disease: a multidetector CT angiography study. *AJNR Am J Neuroradiol*, 28, 1067-70.
- Harkness, K. A., Adamson, P., Sussman, J. D., Davies-Jones, G. A., Greenwood, J. & Woodroffe, M. N. 2000. Dexamethasone regulation of matrix metalloproteinase expression in CNS vascular endothelium. *Brain*, 123 ( Pt 4), 698-709.

- Harston, G. W., Minks, D., Sheerin, F., Payne, S. J., Chappell, M., Jezzard, P., . . . Kennedy, J. 2017. Optimizing image registration and infarct definition in stroke research. *Ann Clin Transl Neurol*, 4, 166-174.
- Hausmann, D., Johnson, J. A., Sudhir, K., Mullen, W. L., Friedrich, G., Fitzgerald, P. J., . . . Yock, P. G. 1996. Angiographically silent atherosclerosis detected by intravascular ultrasound in patients with familial hypercholesterolemia and familial combined hyperlipidemia: correlation with high density lipoproteins. *J Am Coll Cardiol*, 27, 1562-70.
- Hawkins, R. A., Choi, Y., Huang, S. C., Hoh, C. K., Dahlbom, M., Schiepers, C., . . . Phelps, M. E. 1992. Evaluation of the skeletal kinetics of fluorine-18-fluoride ion with PET. *J Nucl Med*, 33, 633-42.
- Hayashi, K., Nakamura, S., Nishida, W. & Sobue, K. 2006. Bone morphogenetic protein-induced MSX1 and MSX2 inhibit myocardin-dependent smooth muscle gene transcription. *Mol Cell Biol*, 26, 9456-70.
- He, Z., Wang, X., Wu, Y., Jia, J., Hu, Y., Yang, X., . . . Leung, M. C. 2014. Treadmill pre-training ameliorates brain edema in ischemic stroke via down-regulation of aquaporin-4: an MRI study in rats. *PLoS One*, 9, e84602.
- Heiss, W. D., Grond, M., Thiel, A., Ghaemi, M., Sobesky, J., Rudolf, J., . . . Wienhard, K. 1998. Permanent cortical damage detected by flumazenil positron emission tomography in acute stroke. *Stroke*, 29, 454-61.
- Heiss, W. D., Kracht, L., Grond, M., Rudolf, J., Bauer, B., Wienhard, K. & Pawlik, G. 2000. Early [(11)C]Flumazenil/H(2)O positron emission tomography predicts irreversible ischemic cortical damage in stroke patients receiving acute thrombolytic therapy. *Stroke*, 31, 366-9.
- Heitzer, T., Yla-Herttuala, S., Luoma, J., Kurz, S., Munzel, T., Just, H., . . . Drexler, H. 1996. Cigarette smoking potentiates endothelial dysfunction of forearm resistance vessels in patients with hypercholesterolemia. Role of oxidized LDL. *Circulation*, 93, 1346-53.
- Helenius, J., Goddeau, R. P., Jr., Moonis, M. & Henninger, N. 2016. Impact of Leukoaraiosis Burden on Hemispheric Lateralization of the National Institutes of Health Stroke Scale Deficit in Acute Ischemic Stroke. *Stroke*, 47, 24-30.
- Helenius, J. & Henninger, N. 2015. Leukoaraiosis Burden Significantly Modulates the Association Between Infarct Volume and National Institutes of Health Stroke Scale in Ischemic Stroke. *Stroke*, 46, 1857-63.

- Henninger, N., Khan, M. A., Zhang, J., Moonis, M. & Goddeau, R. P., Jr. 2014. Leukoaraiosis predicts cortical infarct volume after distal middle cerebral artery occlusion. *Stroke*, 45, 689-95.
- Henninger, N., Lin, E., Baker, S. P., Wakhloo, A. K., Takhtani, D. & Moonis, M. 2012. Leukoaraiosis predicts poor 90-day outcome after acute large cerebral artery occlusion. *Cerebrovasc Dis*, 33, 525-31.
- Henninger, N., Lin, E., Haussen, D. C., Lehman, L. L., Takhtani, D., Selim, M. & Moonis, M. 2013. Leukoaraiosis and sex predict the hyperacute ischemic core volume. *Stroke*, 44, 61-7.
- Henninger, N., Sicard, K. M., Schmidt, K. F., Bardutzky, J. & Fisher, M. 2006. Comparison of ischemic lesion evolution in embolic versus mechanical middle cerebral artery occlusion in Sprague Dawley rats using diffusion and perfusion imaging. *Stroke*, 37, 1283-7.
- Herman, M. P., Sukhova, G. K., Libby, P., Gerdes, N., Tang, N., Horton, D. B., . . . Schonbeck, U. 2001. Expression of neutrophil collagenase (matrix metalloproteinase-8) in human atheroma: a novel collagenolytic pathway suggested by transcriptional profiling. *Circulation*, 104, 1899-904.
- Herrmann, L. L., Le Masurier, M. & Ebmeier, K. P. 2008. White matter hyperintensities in late life depression: a systematic review. *J Neurol Neurosurg Psychiatry*, 79, 619-24.
- Hetterich, H., Rominger, A., Walter, L., Habs, M., Volpers, S., Hacker, M., . . . Saam, T. 2015. Natural history of atherosclerotic disease progression as assessed by F-FDG PET/CT. *Int J Cardiovasc Imaging*.
- Ho, J. S., Cannaday, J. J., Barlow, C. E., Reinhardt, D. B. & Wade, W. A. 2012. Computed tomography detection of carotid calcium and subclinical carotid atherosclerosis. *Int J Cardiovasc Imaging*, 28, 1601-7.
- Hofbauer, L. C. & Schoppet, M. 2001. Osteoprotegerin: a link between osteoporosis and arterial calcification? *Lancet*, 358, 257-9.
- Hoff, J. A., Daviglius, M. L., Chomka, E. V., Krainik, A. J., Sevrukov, A. & Kondos, G. T. 2003. Conventional coronary artery disease risk factors and coronary artery calcium detected by electron beam tomography in 30,908 healthy individuals. *Ann Epidemiol*, 13, 163-9.

- Hoffman, E. J., Huang, S. C. & Phelps, M. E. 1979. Quantitation in positron emission computed tomography: 1. Effect of object size. *J Comput Assist Tomogr*, 3, 299-308.
- Holschermann, H., Hilgendorff, A., Kemkes-Matthes, B., Schonburg, M., Bauer, E. P., Tillmanns, H. & Haberbosch, W. 2000. Simvastatin attenuates vascular hypercoagulability in cardiac transplant recipients. *Transplantation*, 69, 1830-6.
- Honda, A., Tahara, N., Nitta, Y., Tahara, A., Igata, S., Bekki, M., . . . Fukumoto, Y. 2016. Vascular Inflammation Evaluated by [18F]-Fluorodeoxyglucose-Positron Emission Tomography/Computed Tomography Is Associated With Endothelial Dysfunction. *Arteriosclerosis, Thrombosis, and Vascular Biology*, 36, 1980-1988.
- Horti, A. G., Wang, Y., Minn, I., Lan, X., Wang, J., Koehler, R. C., . . . Pomper, M. G. 2016. 18F-FNDP for PET Imaging of Soluble Epoxide Hydrolase. *J Nucl Med*, 57, 1817-1822.
- Howard, D. P., Van Lammeren, G. W., Rothwell, P. M., Redgrave, J. N., Moll, F. L., De Vries, J. P., . . . Pasterkamp, G. 2015. Symptomatic carotid atherosclerotic disease: correlations between plaque composition and ipsilateral stroke risk. *Stroke*, 46, 182-9.
- Howren, M. B., Lamkin, D. M. & Suls, J. 2009. Associations of depression with C-reactive protein, IL-1, and IL-6: a meta-analysis. *Psychosom Med*, 71, 171-86.
- Hruska, K. A., Mathew, S. & Saab, G. 2005. Bone morphogenetic proteins in vascular calcification. *Circ Res*, 97, 105-14.
- Hu, X., Li, P., Guo, Y., Wang, H., Leak, R. K., Chen, S., . . . Chen, J. 2012. Microglia/macrophage polarization dynamics reveal novel mechanism of injury expansion after focal cerebral ischemia. *Stroke*, 43, 3063-70.
- Huang, H., Virmani, R., Younis, H., Burke, A. P., Kamm, R. D. & Lee, R. T. 2001. The impact of calcification on the biomechanical stability of atherosclerotic plaques. *Circulation*, 103, 1051-6.
- Huet, P., Burg, S., Le Guludec, D., Hyafil, F. & Buvat, I. 2015. Variability and uncertainty of FDG PET imaging protocols for assessing inflammation in atherosclerosis: suggestions for improvement. *J Nucl Med*, 56, 552-9.
- Hyafil, F., Cornily, J. C., Rudd, J. H., Machac, J., Feldman, L. J. & Fayad, Z. A. 2009. Quantification of inflammation within rabbit atherosclerotic plaques using the

- macrophage-specific CT contrast agent N1177: a comparison with 18F-FDG PET/CT and histology. *J Nucl Med*, 50, 959-65.
- Hyman, M. C., Petrovic-Djergovic, D., Visovatti, S. H., Liao, H., Yanamadala, S., Bouis, D., . . . Pinsky, D. J. 2009. Self-regulation of inflammatory cell trafficking in mice by the leukocyte surface apyrase CD39. *J Clin Invest*, 119, 1136-49.
- Iadecola, C. & Anrather, J. 2011. The immunology of stroke: from mechanisms to translation. *Nat Med*, 17, 796-808.
- Ichiki, K., Ikeda, H., Haramaki, N., Ueno, T. & Imaizumi, T. 1996. Long-term smoking impairs platelet-derived nitric oxide release. *Circulation*, 94, 3109-14.
- Iiyama, K., Hajra, L., Iiyama, M., Li, H., Dichiaro, M., Medoff, B. D. & Cybulsky, M. I. 1999. Patterns of vascular cell adhesion molecule-1 and intercellular adhesion molecule-1 expression in rabbit and mouse atherosclerotic lesions and at sites predisposed to lesion formation. *Circ Res*, 85, 199-207.
- Imaizumi, M., Kim, H. J., Zoghbi, S. S., Briard, E., Hong, J., Musachio, J. L., . . . Fujita, M. 2007. PET imaging with [11C]PBR28 can localize and quantify upregulated peripheral benzodiazepine receptors associated with cerebral ischemia in rat. *Neurosci Lett*, 411, 200-5.
- Imori, Y., Akasaka, T., Ochiai, T., Oyama, K., Tobita, K., Shishido, K., . . . Saito, S. 2014. Co-existence of carotid artery disease, renal artery stenosis, and lower extremity peripheral arterial disease in patients with coronary artery disease. *Am J Cardiol*, 113, 30-5.
- Imran, T. F., Patel, Y., Ellison, R. C., Carr, J. J., Arnett, D. K., Pankow, J. S., . . . Djousse, L. 2016. Walking and Calcified Atherosclerotic Plaque in the Coronary Arteries: The National Heart, Lung, and Blood Institute Family Heart Study. *Arterioscler Thromb Vasc Biol*, 36, 1272-7.
- Inzitari, D., Pracucci, G., Poggesi, A., Carlucci, G., Barkhof, F., Chabriat, H., . . . Pantoni, L. 2009. Changes in white matter as determinant of global functional decline in older independent outpatients: three year follow-up of LADIS (leukoaraiosis and disability) study cohort. *Bmj*, 339, b2477.
- Iribarren, C., Sidney, S., Sternfeld, B. & Browner, W. S. 2000. Calcification of the aortic arch: risk factors and association with coronary heart disease, stroke, and peripheral vascular disease. *Jama*, 283, 2810-5.

- Irkle, A., Vesey, A. T., Lewis, D. Y., Skepper, J. N., Bird, J. L., Dweck, M. R., . . . Davenport, A. P. 2015. Identifying active vascular microcalcification by (18)F-sodium fluoride positron emission tomography. *Nat Commun*, 6, 7495.
- Izquierdo-Garcia, D., Davies, J. R., Graves, M. J., Rudd, J. H., Gillard, J. H., Weissberg, P. L., . . . Warburton, E. A. 2009. Comparison of methods for magnetic resonance-guided [18-F]fluorodeoxyglucose positron emission tomography in human carotid arteries: reproducibility, partial volume correction, and correlation between methods. *Stroke*, 40, 86-93.
- Jabs, W. J., Theissing, E., Nitschke, M., Bechtel, J. F., Duchrow, M., Mohamed, S., . . . Bartels, C. 2003. Local generation of C-reactive protein in diseased coronary artery venous bypass grafts and normal vascular tissue. *Circulation*, 108, 1428-31.
- Janoudi, A., Shamoun, F. E., Kalavakunta, J. K. & Abela, G. S. 2016. Cholesterol crystal induced arterial inflammation and destabilization of atherosclerotic plaque. *Eur Heart J*, 37, 1959-67.
- Janssen, T., Bannas, P., Herrmann, J., Veldhoen, S., Busch, J. D., Treszl, A., . . . Derlin, T. 2013. Association of linear (1)(8)F-sodium fluoride accumulation in femoral arteries as a measure of diffuse calcification with cardiovascular risk factors: a PET/CT study. *J Nucl Cardiol*, 20, 569-77.
- Jha, R., Battey, T. W., Pham, L., Lorenzano, S., Furie, K. L., Sheth, K. N. & Kimberly, W. T. 2014. Fluid-attenuated inversion recovery hyperintensity correlates with matrix metalloproteinase-9 level and hemorrhagic transformation in acute ischemic stroke. *Stroke*, 45, 1040-5.
- Jiang, L., Zhang, J., Monticone, R. E., Telljohann, R., Wu, J., Wang, M. & Lakatta, E. G. 2012. Calpain-1 regulation of matrix metalloproteinase 2 activity in vascular smooth muscle cells facilitates age-associated aortic wall calcification and fibrosis. *Hypertension*, 60, 1192-9.
- Jiang, N., Chopp, M. & Chahwala, S. 1998. Neutrophil inhibitory factor treatment of focal cerebral ischemia in the rat. *Brain Res*, 788, 25-34.
- Jiwa, N. S., Garrard, P. & Hainsworth, A. H. 2010. Experimental models of vascular dementia and vascular cognitive impairment: a systematic review. *J Neurochem*, 115, 814-28.

- Johansson, E., Cuadrado-Godia, E., Hayden, D., Bjellerup, J., Ois, A., Roquer, J., . . . Kelly, P. J. 2016. Recurrent stroke in symptomatic carotid stenosis awaiting revascularization: A pooled analysis. *Neurology*, 86, 498-504.
- Johnson, R. C., Leopold, J. A. & Loscalzo, J. 2006. Vascular calcification: pathobiological mechanisms and clinical implications. *Circ Res*, 99, 1044-59.
- Johnston, K. C., Wagner, D. P., Haley, E. C., Jr. & Connors, A. F., Jr. 2002. Combined clinical and imaging information as an early stroke outcome measure. *Stroke*, 33, 466-72.
- Jono, S., Mckee, M. D., Murry, C. E., Shioi, A., Nishizawa, Y., Mori, K., . . . Giachelli, C. M. 2000. Phosphate regulation of vascular smooth muscle cell calcification. *Circ Res*, 87, E10-7.
- Joshi, F. R., Manavaki, R., Fryer, T. D., Figg, N. L., Sluimer, J. C., Aigbirhio, F. I., . . . Rudd, J. H. 2017. Vascular Imaging With 18F-Fluorodeoxyglucose Positron Emission Tomography Is Influenced by Hypoxia. *J Am Coll Cardiol*, 69, 1873-1874.
- Joshi, F. R., Rajani, N. K., Abt, M., Woodward, M., Bucarius, J., Mani, V., . . . Rudd, J. H. 2016. Does Vascular Calcification Accelerate Inflammation?: A Substudy of the dal-PLAQUE Trial. *J Am Coll Cardiol*, 67, 69-78.
- Joshi, N. V., Toor, I., Shah, A. S., Carruthers, K., Vesey, A. T., Alam, S. R., . . . Newby, D. E. 2015. Systemic Atherosclerotic Inflammation Following Acute Myocardial Infarction: Myocardial Infarction Begets Myocardial Infarction. *J Am Heart Assoc*, 4, e001956.
- Joshi, N. V., Vesey, A. T., Williams, M. C., Shah, A. S., Calvert, P. A., Craighead, F. H., . . . Newby, D. E. 2014. 18F-fluoride positron emission tomography for identification of ruptured and high-risk coronary atherosclerotic plaques: a prospective clinical trial. *Lancet*, 383, 705-13.
- Kadoglou, N. P., Gerasimidis, T., Moumtzouoglou, A., Kapelouzou, A., Sailer, N., Fotiadis, G., . . . Liapis, C. D. 2008. Intensive lipid-lowering therapy ameliorates novel calcification markers and GSM score in patients with carotid stenosis. *Eur J Vasc Endovasc Surg*, 35, 661-8.
- Kaida, H., Tahara, N., Tahara, A., Honda, A., Nitta, Y., Igata, S., . . . Fukumoto, Y. 2014. Positive correlation between malondialdehyde-modified low-density lipoprotein cholesterol and vascular inflammation evaluated by 18F-FDG PET/CT. *Atherosclerosis*, 237, 404-9.

- Kannel, W. B., D'agostino, R. B. & Belanger, A. J. 1987. Fibrinogen, cigarette smoking, and risk of cardiovascular disease: insights from the Framingham Study. *Am Heart J*, 113, 1006-10.
- Kapeller, P., Barber, R., Vermeulen, R. J., Ader, H., Scheltens, P., Freidl, W., . . . Fazekas, F. 2003. Visual rating of age-related white matter changes on magnetic resonance imaging: scale comparison, interrater agreement, and correlations with quantitative measurements. *Stroke*, 34, 441-5.
- Kapustin, A. N., Davies, J. D., Reynolds, J. L., McNair, R., Jones, G. T., Sidibe, A., . . . Shanahan, C. M. 2011. Calcium regulates key components of vascular smooth muscle cell-derived matrix vesicles to enhance mineralization. *Circ Res*, 109, e1-12.
- Karunakaran, D., Geoffrion, M., Wei, L., Gan, W., Richards, L., Shangari, P., . . . Rayner, K. J. 2016. Targeting macrophage necroptosis for therapeutic and diagnostic interventions in atherosclerosis. *Sci Adv*, 2, e1600224.
- Katano, H., Mase, M., Nishikawa, Y. & Yamada, K. 2015. Calcified carotid plaques show double symptomatic peaks according to agatston calcium score. *J Stroke Cerebrovasc Dis*, 24, 1341-50.
- Katano, H. & Yamada, K. 2007. Analysis of calcium in carotid plaques with Agatston scores for appropriate selection of surgical intervention. *Stroke*, 38, 3040-4.
- Katchanov, J., Waeber, C., Gertz, K., Gietz, A., Winter, B., Bruck, W., . . . Endres, M. 2003. Selective neuronal vulnerability following mild focal brain ischemia in the mouse. *Brain Pathol*, 13, 452-64.
- Kaufman, J. D., Adar, S. D., Barr, R. G., Budoff, M., Burke, G. L., Curl, C. L., . . . Watson, K. E. 2016. Association between air pollution and coronary artery calcification within six metropolitan areas in the USA (the Multi-Ethnic Study of Atherosclerosis and Air Pollution): a longitudinal cohort study. *Lancet*, 388, 696-704.
- Kellner-Weibel, G., Yancey, P. G., Jerome, W. G., Walser, T., Mason, R. P., Phillips, M. C. & Rothblat, G. H. 1999. Crystallization of free cholesterol in model macrophage foam cells. *Arterioscler Thromb Vasc Biol*, 19, 1891-8.
- Kelly-Arnold, A., Maldonado, N., Laudier, D., Aikawa, E., Cardoso, L. & Weinbaum, S. 2013. Revised microcalcification hypothesis for fibrous cap rupture in human coronary arteries. *Proc Natl Acad Sci U S A*, 110, 10741-6.

- Kessinger, C. W., Kim, J. W., Henke, P. K., Thompson, B., McCarthy, J. R., Hara, T., . . . Jaffer, F. A. 2015. Statins improve the resolution of established murine venous thrombosis: reductions in thrombus burden and vein wall scarring. *PLoS One*, 10, e0116621.
- Khalaf, A., Edelman, K., Tudorascu, D., Andreescu, C., Reynolds, C. F. & Aizenstein, H. 2015. White Matter Hyperintensity Accumulation During Treatment of Late-Life Depression. *Neuropsychopharmacology*, 40, 3027-35.
- Khan, B. V., Parthasarathy, S. S., Alexander, R. W. & Medford, R. M. 1995. Modified low density lipoprotein and its constituents augment cytokine-activated vascular cell adhesion molecule-1 gene expression in human vascular endothelial cells. *J Clin Invest*, 95, 1262-70.
- Kim, S., Lee, S., Kim, J. B., Na, J. O., Choi, C. U., Lim, H. E., . . . Kim, J. W. 2015. Concurrent Carotid Inflammation in Acute Coronary Syndrome as Assessed by (18)F-FDG PET/CT: A Possible Mechanistic Link for Ischemic Stroke. *J Stroke Cerebrovasc Dis*, 24, 2547-54.
- Kirsch, T. & Wuthier, R. E. 1994. Stimulation of calcification of growth plate cartilage matrix vesicles by binding to type II and X collagens. *J Biol Chem*, 269, 11462-9.
- Kitagawa, T., Yamamoto, H., Toshimitsu, S., Sasaki, K., Senoo, A., Kubo, Y., . . . Kihara, Y. 2017. 18F-sodium fluoride positron emission tomography for molecular imaging of coronary atherosclerosis based on computed tomography analysis. *Atherosclerosis*.
- Kizu, A., Shioi, A., Jono, S., Koyama, H., Okuno, Y. & Nishizawa, Y. 2004. Statins inhibit in vitro calcification of human vascular smooth muscle cells induced by inflammatory mediators. *J Cell Biochem*, 93, 1011-9.
- Klein, B., Destephens, A., Dumeny, L., Hu, Q., He, Y., O'malley, K., . . . Berceci, S. 2017. Hemodynamic Influence on Smooth Muscle Cell Kinetics and Phenotype During Early Vein Graft Adaptation. *Ann Biomed Eng*, 45, 644-655.
- Knowland, D., Arac, A., Sekiguchi, K. J., Hsu, M., Lutz, S. E., Perrino, J., . . . Agalliu, D. 2014. Stepwise recruitment of transcellular and paracellular pathways underlies blood-brain barrier breakdown in stroke. *Neuron*, 82, 603-17.

- Kolodgie, F. D., Gold, H. K., Burke, A. P., Fowler, D. R., Kruth, H. S., Weber, D. K., . . . Virmani, R. 2003. Intraplaque Hemorrhage and Progression of Coronary Atheroma. *New England Journal of Medicine*, 349, 2316-2325.
- Komulainen, P., Lakka, T. A., Kivipelto, M., Hassinen, M., Penttila, I. M., Helkala, E. L., . . . Rauramaa, R. 2007. Serum high sensitivity C-reactive protein and cognitive function in elderly women. *Age Ageing*, 36, 443-8.
- Kraft, P., Gob, E., Schuhmann, M. K., Gobel, K., Deppermann, C., Thielmann, I., . . . Kleinschnitz, C. 2013. FTY720 ameliorates acute ischemic stroke in mice by reducing thrombo-inflammation but not by direct neuroprotection. *Stroke*, 44, 3202-10.
- Krams, M., Lees, K. R., Hacke, W., Grieve, A. P., Orgogozo, J.-M. & Ford, G. A. 2003. Acute Stroke Therapy by Inhibition of Neutrophils (ASTIN). *An Adaptive Dose-Response Study of UK-279,276 in Acute Ischemic Stroke*, 34, 2543-2548.
- Kreisl, W. C., Jenko, K. J., Hines, C. S., Lyoo, C. H., Corona, W., Morse, C. L., . . . Innis, R. B. 2013. A genetic polymorphism for translocator protein 18 kDa affects both in vitro and in vivo radioligand binding in human brain to this putative biomarker of neuroinflammation. *J Cereb Blood Flow Metab*, 33, 53-8.
- Kriz, J. 2006. Inflammation in ischemic brain injury: timing is important. *Crit Rev Neurobiol*, 18, 145-57.
- Krupinski, J., Turu, M. M., Font, M. A., Catena, E., Slevin, M., Morchon, S., . . . Martinez-Gonzalez, J. 2008. Blood-borne tissue factor activity predicts major cerebrovascular events in patients undergoing carotid endarterectomy: results from a 1-year follow-up study. *Cerebrovasc Dis*, 25, 32-9.
- Krupinski, J., Turu, M. M., Martinez-Gonzalez, J., Carvajal, A., Juan-Babot, J. O., Iborra, E., . . . Badimon, L. 2006. Endogenous expression of C-reactive protein is increased in active (ulcerated noncomplicated) human carotid artery plaques. *Stroke*, 37, 1200-4.
- Ku, D. N., Giddens, D. P., Zarins, C. K. & Glagov, S. 1985. Pulsatile flow and atherosclerosis in the human carotid bifurcation. Positive correlation between plaque location and low oscillating shear stress. *Arteriosclerosis*, 5, 293-302.
- Kubes, P., Suzuki, M. & Granger, D. N. 1991. Nitric oxide: an endogenous modulator of leukocyte adhesion. *Proc Natl Acad Sci U S A*, 88, 4651-5.

- Kumari, R., Willing, L. B., Patel, S. D., Baskerville, K. A. & Simpson, I. A. 2011. Increased cerebral matrix metalloproteinase-9 activity is associated with compromised recovery in the diabetic db/db mouse following a stroke. *J Neurochem*, 119, 1029-40.
- Kuo, H. K., Yen, C. J., Chang, C. H., Kuo, C. K., Chen, J. H. & Sorond, F. 2005. Relation of C-reactive protein to stroke, cognitive disorders, and depression in the general population: systematic review and meta-analysis. *Lancet Neurol*, 4, 371-80.
- Kuroda, S., Shiga, T., Ishikawa, T., Houkin, K., Narita, T., Katoh, C., . . . Iwasaki, Y. 2004. Reduced blood flow and preserved vasoreactivity characterize oxygen hypometabolism due to incomplete infarction in occlusive carotid artery diseases. *J Nucl Med*, 45, 943-9.
- Kuroiwa, T., Ting, P., Martinez, H. & Klatzo, I. 1985. The biphasic opening of the blood-brain barrier to proteins following temporary middle cerebral artery occlusion. *Acta Neuropathol*, 68, 122-9.
- Kurzepa, J., Bielewicz, J., Grabarska, A., Stelmasiak, Z., Stryjecka-Zimmer, M. & Bartosik-Psujek, H. 2010. Matrix metalloproteinase-9 contributes to the increase of tau protein in serum during acute ischemic stroke. *J Clin Neurosci*, 17, 997-9.
- Kwee, R. M. 2010. Systematic review on the association between calcification in carotid plaques and clinical ischemic symptoms. *J Vasc Surg*, 51, 1015-25.
- Lacey, D. L., Timms, E., Tan, H. L., Kelley, M. J., Dunstan, C. R., Burgess, T., . . . Boyle, W. J. 1998. Osteoprotegerin ligand is a cytokine that regulates osteoclast differentiation and activation. *Cell*, 93, 165-76.
- Laitinen, I., Marjamaki, P., Nagren, K., Laine, V. J., Wilson, I., Leppanen, P., . . . Knuuti, J. 2009. Uptake of inflammatory cell marker [11C]PK11195 into mouse atherosclerotic plaques. *Eur J Nucl Med Mol Imaging*, 36, 73-80.
- Lal, B. K., Younes, M., Cruz, G., Kapadia, I., Jamil, Z. & Pappas, P. J. 2011. Cognitive changes after surgery vs stenting for carotid artery stenosis. *J Vasc Surg*, 54, 691-8.
- Lanfranconi, S. & Markus, H. S. 2013. Stroke subtyping for genetic association studies? A comparison of the CCS and TOAST classifications. *Int J Stroke*, 8, 626-31.

- Lang, N. N., Gudmundsdottir, I. J., Boon, N. A., Ludlam, C. A., Fox, K. A. & Newby, D. E. 2008. Marked impairment of protease-activated receptor type 1-mediated vasodilation and fibrinolysis in cigarette smokers: smoking, thrombin, and vascular responses in vivo. *J Am Coll Cardiol*, 52, 33-9.
- Langille, B. L. & O'donnell, F. 1986. Reductions in arterial diameter produced by chronic decreases in blood flow are endothelium-dependent. *Science*, 231, 405-7.
- Lansberg, M. G., O'brien, M. W., Tong, D. C., Moseley, M. E. & Albers, G. W. 2001. Evolution of cerebral infarct volume assessed by diffusion-weighted magnetic resonance imaging. *Arch Neurol*, 58, 613-7.
- Lappégard, J., Ellingsen, T. S., Skjelbakken, T., Mathiesen, E. B., Njolstad, I., Wilsgaard, T., . . . Hansen, J. B. 2016. Red cell distribution width is associated with future risk of incident stroke. The Tromso Study. *Thromb Haemost*, 115, 126-34.
- Lappégard, J., Ellingsen, T. S., Vik, A., Skjelbakken, T., Brox, J., Mathiesen, E. B., . . . Hansen, J. B. 2015. Red cell distribution width and carotid atherosclerosis progression. The Tromso Study. *Thromb Haemost*, 113, 649-54.
- Lavisse, S., Garcia-Lorenzo, D., Peyronneau, M. A., Bodini, B., Thiriez, C., Kuhnast, B., . . . Bottlaender, M. 2015. Optimized Quantification of Translocator Protein Radioligand (1)(8)F-DPA-714 Uptake in the Brain of Genotyped Healthy Volunteers. *J Nucl Med*, 56, 1048-54.
- Leatham, E. W., Bath, P. M., Tooze, J. A. & Camm, A. J. 1995. Increased monocyte tissue factor expression in coronary disease. *Br Heart J*, 73, 10-3.
- Lederman, R. J., Raylman, R. R., Fisher, S. J., Kison, P. V., San, H., Nabel, E. G. & Wahl, R. L. 2001. Detection of atherosclerosis using a novel positron-sensitive probe and 18-fluorodeoxyglucose (FDG). *Nucl Med Commun*, 22, 747-53.
- Lee, E., Grodzinsky, A. J., Libby, P., Clinton, S. K., Lark, M. W. & Lee, R. T. 1995. Human vascular smooth muscle cell-monocyte interactions and metalloproteinase secretion in culture. *Arterioscler Thromb Vasc Biol*, 15, 2284-9.
- Lee, G. H., Kim, J. S., Oh, S. J., Kang, D. W., Kim, J. S. & Kwon, S. U. 2015a. (18)F-fluoromisonidazole (FMISO) Positron Emission Tomography (PET) Predicts Early Infarct Growth in Patients with Acute Ischemic Stroke. *J Neuroimaging*, 25, 652-5.

- Lee, S., Chu, H. X., Kim, H. A., Real, N. C., Sharif, S., Fleming, S. B., . . . Sobey, C. G. 2015b. Effect of a broad-specificity chemokine-binding protein on brain leukocyte infiltration and infarct development. *Stroke*, 46, 537-44.
- Lee, S. J., On, Y. K., Lee, E. J., Choi, J. Y., Kim, B. T. & Lee, K. H. 2008. Reversal of vascular 18F-FDG uptake with plasma high-density lipoprotein elevation by atherogenic risk reduction. *J Nucl Med*, 49, 1277-82.
- Lee, W. W., Chung, J. H., Jang, S. J., Eo, J. S., Park, S. Y., Sung, S. W., . . . Kim, S. E. 2006. Consideration of serum glucose levels during malignant mediastinal lymph node detection in non-small-cell lung cancer by FDG-PET. *J Surg Oncol*, 94, 607-13.
- Lei-Xing, X., Jing-Jing, G., Jing-Xue, N., Juan, W., Juan, L., Chang-Zai, L., . . . Hong-Bin, L. 2014. Combined application of 18F-fluorodeoxyglucose positron emission tomography/computed tomography and magnetic resonance imaging in early diagnosis of vulnerable carotid atherosclerotic plaques. *J Int Med Res*, 42, 213-23.
- Lenglet, S., Quercioli, A., Fabre, M., Galan, K., Pelli, G., Nencioni, A., . . . Montecucco, F. 2014. Statin treatment is associated with reduction in serum levels of receptor activator of NF-kappaB ligand and neutrophil activation in patients with severe carotid stenosis. *Mediators Inflamm*, 2014, 720987.
- Leppanen, O., Bjornheden, T., Evaldsson, M., Boren, J., Wiklund, O. & Levin, M. 2006. ATP depletion in macrophages in the core of advanced rabbit atherosclerotic plaques in vivo. *Atherosclerosis*, 188, 323-30.
- Li, H., Cybulsky, M. I., Gimbrone, M. A., Jr. & Libby, P. 1993. An atherogenic diet rapidly induces VCAM-1, a cytokine-regulatable mononuclear leukocyte adhesion molecule, in rabbit aortic endothelium. *Arterioscler Thromb*, 13, 197-204.
- Li, H., Horke, S. & Forstermann, U. 2014. Vascular oxidative stress, nitric oxide and atherosclerosis. *Atherosclerosis*, 237, 208-19.
- Li, X., Heber, D., Cal Gonzales, J., Karanikas, G., Mayerhoefer, M. E., Rasul, S., . . . Hacker, M. 2017. Association between osteogenesis and inflammation during the progression of calcified plaque as evaluated by combined 18F-NaF and 18F-FDG PET/CT. *J Nucl Med*.
- Li, X., Samnick, S., Lapa, C., Israel, I., Buck, A. K., Kreissl, M. C. & Bauer, W. 2012. 68Ga-DOTATATE PET/CT for the detection of inflammation of large

- arteries: correlation with  $^{18}\text{F}$ -FDG, calcium burden and risk factors. *EJNMMI Res*, 2, 52.
- Liao, S. Q., Li, J. C., Zhang, M., Wang, Y. J., Li, B. H., Yin, Y. W., . . . Zhang, L. L. 2015. The association between leukoaraiosis and carotid atherosclerosis: a systematic review and meta-analysis. *Int J Neurosci*, 125, 493-500.
- Libby, P. 2002. Inflammation in atherosclerosis. *Nature*, 420, 868-74.
- Libby, P. 2008. The molecular mechanisms of the thrombotic complications of atherosclerosis. *J Intern Med*, 263, 517-27.
- Libby, P., Tabas, I., Fredman, G. & Fisher, E. A. 2014. Inflammation and its resolution as determinants of acute coronary syndromes. *Circ Res*, 114, 1867-79.
- Licata, G., Tuttolomondo, A., Corrao, S., Di Raimondo, D., Fernandez, P., Caruso, C., . . . Pinto, A. 2006. Immunoinflammatory activation during the acute phase of lacunar and non-lacunar ischemic stroke: association with time of onset and diabetic state. *Int J Immunopathol Pharmacol*, 19, 639-46.
- Licata, G., Tuttolomondo, A., Di Raimondo, D., Corrao, S., Di Sciacca, R. & Pinto, A. 2009. Immuno-inflammatory activation in acute cardio-embolic strokes in comparison with other subtypes of ischaemic stroke. *Thromb Haemost*, 101, 929-37.
- Lieb, J., Karmali, R. & Horrobin, D. 1983. Elevated levels of prostaglandin E2 and thromboxane B2 in depression. *Prostaglandins Leukot Med*, 10, 361-7.
- Lin, J., Kakkar, V. & Lu, X. 2014. Impact of MCP-1 in atherosclerosis. *Curr Pharm Des*, 20, 4580-8.
- Lin, S., Lee, W. Y., Huang, M., Fu, Z., Liang, Y., Wu, H., . . . Li, G. 2016. Aspirin prevents bone loss with little mechanical improvement in high-fat-fed ovariectomized rats. *Eur J Pharmacol*, 791, 331-338.
- Lindgren, A., Roijer, A., Rudling, O., Norrving, B., Larsson, E. M., Eskilsson, J., . . . Johansson, B. B. 1994. Cerebral lesions on magnetic resonance imaging, heart disease, and vascular risk factors in subjects without stroke. A population-based study. *Stroke*, 25, 929-34.
- Liu, A., Ming, J. Y., Fiskesund, R., Ninio, E., Karabina, S. A., Bergmark, C., . . . Frostegard, J. 2015a. Induction of dendritic cell-mediated T-cell activation by modified but not native low-density lipoprotein in humans and inhibition by

- annexin a5: involvement of heat shock proteins. *Arterioscler Thromb Vasc Biol*, 35, 197-205.
- Liu, J., Kerwin, W. S., Caldwell, J. H., Ferguson, M. S., Hippe, D. S., Alessio, A. M., . . . Yuan, C. 2015b. High resolution FDG-microPET of carotid atherosclerosis: plaque components underlying enhanced FDG uptake. *Int J Cardiovasc Imaging*.
- Liu, L., Gardecki, J. A., Nadkarni, S. K., Toussaint, J. D., Yagi, Y., Bouma, B. E. & Tearney, G. J. 2011. Imaging the subcellular structure of human coronary atherosclerosis using micro-optical coherence tomography. *Nat Med*, 17, 1010-4.
- Liu, Y., Wang, D., Wang, H., Qu, Y., Xiao, X. & Zhu, Y. 2014. The protective effect of HET0016 on brain edema and blood-brain barrier dysfunction after cerebral ischemia/reperfusion. *Brain Res*, 1544, 45-53.
- Liuzzi, G. M., Santacrose, M. P., Peumans, W. J., Van Damme, E. J., Dubois, B., Opdenakker, G. & Riccio, P. 1999. Regulation of gelatinases in microglia and astrocyte cell cultures by plant lectins. *Glia*, 27, 53-61.
- Lo, S. K., Cheung, A., Zheng, Q. & Silverstein, R. L. 1995. Induction of tissue factor on monocytes by adhesion to endothelial cells. *J Immunol*, 154, 4768-77.
- Lorenz, M. W., Polak, J. F., Kavousi, M., Mathiesen, E. B., Volzke, H., Tuomainen, T. P., . . . Thompson, S. G. 2012. Carotid intima-media thickness progression to predict cardiovascular events in the general population (the PROG-IMT collaborative project): a meta-analysis of individual participant data. *Lancet*, 379, 2053-62.
- Loubinoux, I., Volk, A., Borredon, J., Guirimand, S., Tiffon, B., Seylaz, J. & Meric, P. 1997. Spreading of vasogenic edema and cytotoxic edema assessed by quantitative diffusion and T2 magnetic resonance imaging. *Stroke*, 28, 419-26; discussion 426-7.
- Luby, M., Bykowski, J. L., Schellinger, P. D., Merino, J. G. & Warach, S. 2006. Intra- and interrater reliability of ischemic lesion volume measurements on diffusion-weighted, mean transit time and fluid-attenuated inversion recovery MRI. *Stroke*, 37, 2951-6.
- Luo, G., Ducey, P., Mckee, M. D., Pinero, G. J., Loyer, E., Behringer, R. R. & Karsenty, G. 1997. Spontaneous calcification of arteries and cartilage in mice lacking matrix GLA protein. *Nature*, 386, 78-81.

- Luo, Y., Wang, Z., Li, J. & Xu, Y. 2012. Serum CRP concentrations and severity of ischemic stroke subtypes. *Can J Neurol Sci*, 39, 69-73.
- Macfarlane, T. W., Canham, P. B. & Roach, M. R. 1983. Shape changes at the apex of isolated human cerebral bifurcations with changes in transmural pressure. *Stroke*, 14, 70-6.
- Machado-Silva, W., Henriques, A. D., Souza, G. D., Gomes, L., Ferreira, A. P., Brito, C. J., . . . Nobrega, O. T. 2016. Serum Immune Mediators Independently Associate with Atherosclerosis in the Left (But Not Right) Carotid Territory of Older Individuals. *J Stroke Cerebrovasc Dis*, 25, 2851-2858.
- Maganto-Garcia, E., Tarrío, M. L., Grabie, N., Bu, D. X. & Lichtman, A. H. 2011. Dynamic changes in regulatory T cells are linked to levels of diet-induced hypercholesterolemia. *Circulation*, 124, 185-95.
- Maldonado, N., Kelly-Arnold, A., Vengrenyuk, Y., Laudier, D., Fallon, J. T., Virmani, R., . . . Weinbaum, S. 2012. A mechanistic analysis of the role of microcalcifications in atherosclerotic plaque stability: potential implications for plaque rupture. *Am J Physiol Heart Circ Physiol*, 303, H619-28.
- Mallat, Z. & Tedgui, A. 2000. Apoptosis in the vasculature: mechanisms and functional importance. *Br J Pharmacol*, 130, 947-62.
- Malmberg, C., Ripa, R. S., Johnbeck, C. B., Knigge, U., Langer, S. W., Mortensen, J., . . . Kjaer, A. 2015. <sup>64</sup>Cu-DOTATATE for Noninvasive Assessment of Atherosclerosis in Large Arteries and Its Correlation with Risk Factors: Head-to-Head Comparison with <sup>68</sup>Ga-DOTATOC in 60 Patients. *J Nucl Med*, 56, 1895-900.
- Mani, V., Woodward, M., Samber, D., Bucarius, J., Tawakol, A., Kallend, D., . . . Fayad, Z. A. 2014. Predictors of change in carotid atherosclerotic plaque inflammation and burden as measured by <sup>18</sup>F-FDG-PET and MRI, respectively, in the dal-PLAQUE study. *Int J Cardiovasc Imaging*, 30, 571-82.
- Mann, J. M. & Davies, M. J. 1996. Vulnerable plaque. Relation of characteristics to degree of stenosis in human coronary arteries. *Circulation*, 94, 928-31.
- Manolio, T. A., Burke, G. L., O'leary, D. H., Evans, G., Beauchamp, N., Knepper, L. & Ward, B. 1999. Relationships of cerebral MRI findings to ultrasonographic carotid atherosclerosis in older adults : the Cardiovascular Health Study. CHS Collaborative Research Group. *Arterioscler Thromb Vasc Biol*, 19, 356-65.

- Marchal, G., Beaudouin, V., Rioux, P., De La Sayette, V., Le Doze, F., Viader, F., . . . Baron, J. C. 1996. Prolonged persistence of substantial volumes of potentially viable brain tissue after stroke: a correlative PET-CT study with voxel-based data analysis. *Stroke*, 27, 599-606.
- Marchal, G., Benali, K., Iglesias, S., Viader, F., Derlon, J. M. & Baron, J. C. 1999. Voxel-based mapping of irreversible ischaemic damage with PET in acute stroke. *Brain*, 122 ( Pt 12), 2387-400.
- Marchal, G., Rioux, P., Serrati, C., Furlan, M., Derlon, J. M., Viader, F. & Baron, J. C. 1995. Value of acute-stage positron emission tomography in predicting neurological outcome after ischemic stroke: further assessment. *Stroke*, 26, 524-5.
- Marchal, G., Serrati, C., Rioux, P., Petit-Taboue, M. C., Viader, F., De La Sayette, V., . . . Et Al. 1993. PET imaging of cerebral perfusion and oxygen consumption in acute ischaemic stroke: relation to outcome. *Lancet*, 341, 925-7.
- Markus, H. S., Lythgoe, D. J., Ostegaard, L., O'sullivan, M. & Williams, S. C. 2000. Reduced cerebral blood flow in white matter in ischaemic leukoaraiosis demonstrated using quantitative exogenous contrast based perfusion MRI. *J Neurol Neurosurg Psychiatry*, 69, 48-53.
- Markus, R., Donnan, G., Kazui, S., Read, S. & Reutens, D. 2004a. Penumbra topography in human stroke: methodology and validation of the 'Penumbrogram'. *Neuroimage*, 21, 1252-9.
- Markus, R., Reutens, D. C., Kazui, S., Read, S., Wright, P., Chambers, B. R., . . . Donnan, G. A. 2003. Topography and temporal evolution of hypoxic viable tissue identified by 18F-fluoromisonidazole positron emission tomography in humans after ischemic stroke. *Stroke*, 34, 2646-52.
- Markus, R., Reutens, D. C., Kazui, S., Read, S., Wright, P., Pearce, D. C., . . . Donnan, G. A. 2004b. Hypoxic tissue in ischaemic stroke: persistence and clinical consequences of spontaneous survival. *Brain*, 127, 1427-36.
- Marnane, M., Merwick, A., Sheehan, O. C., Hannon, N., Foran, P., Grant, T., . . . Kelly, P. J. 2012. Carotid plaque inflammation on 18F-fluorodeoxyglucose positron emission tomography predicts early stroke recurrence. *Ann Neurol*, 71, 709-18.

- Marquardt, L., Ruf, A., Mansmann, U., Winter, R., Bugge, F., Kallenberg, K. & Grau, A. J. 2005. Inflammatory response after acute ischemic stroke. *J Neurol Sci*, 236, 65-71.
- Marsh, B. J., Williams-Karnesky, R. L. & Stenzel-Poore, M. P. 2009. Toll-like receptor signaling in endogenous neuroprotection and stroke. *Neuroscience*, 158, 1007-20.
- Matsuo, R., Ago, T., Hata, J., Wakisaka, Y., Kuroda, J., Kuwashiro, T., . . . Kamouchi, M. 2016. Plasma C-Reactive Protein and Clinical Outcomes after Acute Ischemic Stroke: A Prospective Observational Study. *PLoS One*, 11, e0156790.
- Matthews, K. A., Kuller, L. H., Sutton-Tyrrell, K. & Chang, Y. F. 2001. Changes in cardiovascular risk factors during the perimenopause and postmenopause and carotid artery atherosclerosis in healthy women. *Stroke*, 32, 1104-11.
- Mayhan, W. G. & Patel, K. P. 1997. Effect of nicotine on endothelium-dependent arteriolar dilatation in vivo. *American Journal of Physiology - Heart and Circulatory Physiology*, 272, H2337-H2342.
- Mayr, M., Sidibe, A. & Zampetaki, A. 2008. The paradox of hypoxic and oxidative stress in atherosclerosis. *J Am Coll Cardiol*, 51, 1266-7.
- Mazzone, A., Cusa, C., Mazzucchelli, I., Vezzoli, M., Ottini, E., Ghio, S., . . . Zuccaro, P. 2001. Cigarette smoking and hypertension influence nitric oxide release and plasma levels of adhesion molecules. *Clin Chem Lab Med*, 39, 822-6.
- Mckinney, A. M., Casey, S. O., Teksam, M., Lucato, L. T., Smith, M., Truwit, C. L. & Kieffer, S. 2005. Carotid bifurcation calcium and correlation with percent stenosis of the internal carotid artery on CT angiography. *Neuroradiology*, 47, 1-9.
- Medoc, M., Dhilly, M., Matesic, L., Toutain, J., Krause-Heuer, A. M., Delamare, J., . . . Sobrio, F. 2016. In Vivo Evaluation of Radiofluorinated Caspase-3/7 Inhibitors as Radiotracers for Apoptosis Imaging and Comparison with [(18)F]ML-10 in a Stroke Model in the Rat. *Mol Imaging Biol*, 18, 117-26.
- Meuwese, M. C., Stroes, E. S., Hazen, S. L., Van Miert, J. N., Kuivenhoven, J. A., Schaub, R. G., . . . Boekholdt, S. M. 2007. Serum myeloperoxidase levels are associated with the future risk of coronary artery disease in apparently healthy

- individuals: the EPIC-Norfolk Prospective Population Study. *J Am Coll Cardiol*, 50, 159-65.
- Michel, J. B., Virmani, R., Arbustini, E. & Pasterkamp, G. 2011. Intraplaque haemorrhages as the trigger of plaque vulnerability. *Eur Heart J*, 32, 1977-85, 1985a, 1985b, 1985c.
- Migdalski, A., Kotschy, M. & Jawien, A. 2005. Tissue factor, tissue factor pathway inhibitor and vascular endothelial growth factor-A in carotid atherosclerotic plaques. *Eur J Vasc Endovasc Surg*, 30, 41-7.
- Mikhaylova, L., Malmquist, J. & Nurminskaya, M. 2007. Regulation of in vitro vascular calcification by BMP4, VEGF and Wnt3a. *Calcif Tissue Int*, 81, 372-81.
- Mintz, G. S., Painter, J. A., Pichard, A. D., Kent, K. M., Satler, L. F., Popma, J. J., . . . Leon, M. B. 1995. Atherosclerosis in angiographically "normal" coronary artery reference segments: an intravascular ultrasound study with clinical correlations. *J Am Coll Cardiol*, 25, 1479-85.
- Mitsumori, T., Furuyashiki, T., Momiyama, T., Nishi, A., Shuto, T., Hayakawa, T., . . . Narumiya, S. 2011. Thromboxane receptor activation enhances striatal dopamine release, leading to suppression of GABAergic transmission and enhanced sugar intake. *Eur J Neurosci*, 34, 594-604.
- Miura, T., Matsukawa, N., Sakurai, K., Katano, H., Ueki, Y., Okita, K., . . . Ojika, K. 2011. Plaque vulnerability in internal carotid arteries with positive remodeling. *Cerebrovasc Dis Extra*, 1, 54-65.
- Mizoguchi, M., Tahara, N., Tahara, A., Nitta, Y., Kodama, N., Oba, T., . . . Imaizumi, T. 2011. Pioglitazone attenuates atherosclerotic plaque inflammation in patients with impaired glucose tolerance or diabetes a prospective, randomized, comparator-controlled study using serial FDG PET/CT imaging study of carotid artery and ascending aorta. *JACC Cardiovasc Imaging*, 4, 1110-8.
- Mohan, S., Mohan, N. & Sprague, E. A. 1997. Differential activation of NF-kappa B in human aortic endothelial cells conditioned to specific flow environments. *Am J Physiol*, 273, C572-8.
- Mojtahedi, A., Alavi, A., Thamake, S., Amerinia, R., Ranganathan, D., Tworowska, I. & Delpassand, E. S. 2015. Assessment of vulnerable atherosclerotic and

- fibrotic plaques in coronary arteries using (68)Ga-DOTATATE PET/CT. *Am J Nucl Med Mol Imaging*, 5, 65-71.
- Montaner, J., Alvarez-Sabin, J., Molina, C., Angles, A., Abilleira, S., Arenillas, J., . . . Monasterio, J. 2001a. Matrix metalloproteinase expression after human cardioembolic stroke: temporal profile and relation to neurological impairment. *Stroke*, 32, 1759-66.
- Montaner, J., Alvarez-Sabin, J., Molina, C. A., Angles, A., Abilleira, S., Arenillas, J. & Monasterio, J. 2001b. Matrix metalloproteinase expression is related to hemorrhagic transformation after cardioembolic stroke. *Stroke*, 32, 2762-7.
- Montaner, J., Molina, C. A., Monasterio, J., Abilleira, S., Arenillas, J. F., Ribo, M., . . . Alvarez-Sabin, J. 2003. Matrix metalloproteinase-9 pretreatment level predicts intracranial hemorrhagic complications after thrombolysis in human stroke. *Circulation*, 107, 598-603.
- Montero, I., Orbe, J., Varo, N., Beloqui, O., Monreal, J. I., Rodriguez, J. A., . . . Paramo, J. A. 2006. C-reactive protein induces matrix metalloproteinase-1 and -10 in human endothelial cells: implications for clinical and subclinical atherosclerosis. *J Am Coll Cardiol*, 47, 1369-78.
- Mooijart, S. P., Sattar, N., Trompet, S., Lucke, J., Stott, D. J., Ford, I., . . . De Craen, A. J. 2013. Circulating interleukin-6 concentration and cognitive decline in old age: the PROSPER study. *J Intern Med*, 274, 77-85.
- Mooijart, S. P., Sattar, N., Trompet, S., Polisecki, E., De Craen, A. J., Schaefer, E. J., . . . Westendorp, R. G. 2011. C-reactive protein and genetic variants and cognitive decline in old age: the PROSPER study. *PLoS One*, 6, e23890.
- Moore, K. J., Sheedy, F. J. & Fisher, E. A. 2013. Macrophages in atherosclerosis: a dynamic balance. *Nat Rev Immunol*, 13, 709-21.
- Morbelli, S., Fiz, F., Piccardo, A., Picori, L., Massollo, M., Pestarino, E., . . . Sambuceti, G. 2014. Divergent determinants of 18F-NaF uptake and visible calcium deposition in large arteries: relationship with Framingham risk score. *Int J Cardiovasc Imaging*, 30, 439-47.
- Moreira, D. M., Lueneberg, M. E., Da Silva, R. L., Fattah, T. & Mascia Gottschall, C. A. 2013. Rationale and design of the TETHYS trial: the effects of methotrexate therapy on myocardial infarction with ST-segment elevation. *Cardiology*, 126, 167-70.

- Morel-Kopp, M. C., Mclean, L., Chen, Q., Tofler, G. H., Tennant, C., Maddison, V. & Ward, C. M. 2009. The association of depression with platelet activation: evidence for a treatment effect. *J Thromb Haemost*, 7, 573-81.
- Moreno, J., Gaspar, E., Lopez-Bello, G., Juarez, E., Alcazar-Leyva, S., Gonzalez-Trujano, E., . . . Alvarado-Vasquez, N. 2013. Increase in nitric oxide levels and mitochondrial membrane potential in platelets of untreated patients with major depression. *Psychiatry Res*, 209, 447-52.
- Moreno, P. R., Bernardi, V. H., Lopez-Cuellar, J., Murcia, A. M., Palacios, I. F., Gold, H. K., . . . Fallon, J. T. 1996. Macrophages, smooth muscle cells, and tissue factor in unstable angina. Implications for cell-mediated thrombogenicity in acute coronary syndromes. *Circulation*, 94, 3090-7.
- Moreno, P. R., Purushothaman, K. R., Fuster, V., Echeverri, D., Trusczyńska, H., Sharma, S. K., . . . O'connor, W. N. 2004. Plaque neovascularization is increased in ruptured atherosclerotic lesions of human aorta: implications for plaque vulnerability. *Circulation*, 110, 2032-8.
- Morita, H., Ikeda, H., Haramaki, N., Eguchi, H. & Imaizumi, T. 2005. Only two-week smoking cessation improves platelet aggregability and intraplatelet redox imbalance of long-term smokers. *J Am Coll Cardiol*, 45, 589-94.
- Mostaza, J. M., Lahoz, C., Salinero-Fort, M. A., De Burgos-Lunar, C., Laguna, F., Estirado, E., . . . Lopez, S. 2015. Carotid atherosclerosis severity in relation to glycemic status: a cross-sectional population study. *Atherosclerosis*, 242, 377-82.
- Moustafa, R. R., Izquierdo-Garcia, D., Fryer, T. D., Graves, M. J., Rudd, J. H., Gillard, J. H., . . . Warburton, E. A. 2010. Carotid plaque inflammation is associated with cerebral microembolism in patients with recent transient ischemic attack or stroke: a pilot study. *Circ Cardiovasc Imaging*, 3, 536-41.
- Muir, K. W., Weir, C. J., Murray, G. D., Povey, C. & Lees, K. R. 1996. Comparison of neurological scales and scoring systems for acute stroke prognosis. *Stroke*, 27, 1817-20.
- Muller, H. F., Viaccoz, A., Fisch, L., Bonvin, C., Lovblad, K. O., Ratib, O., . . . Sztajzel, R. 2014. 18FDG-PET-CT: an imaging biomarker of high-risk carotid plaques. Correlation to symptoms and microembolic signals. *Stroke*, 45, 3561-6.

- Musselman, D. L., Tomer, A., Manatunga, A. K., Knight, B. T., Porter, M. R., Kasey, S., . . . Nemeroff, C. B. 1996. Exaggerated platelet reactivity in major depression. *Am J Psychiatry*, 153, 1313-7.
- Nagel, T., Resnick, N., Dewey, C. F., Jr. & Gimbrone, M. A., Jr. 1999. Vascular endothelial cells respond to spatial gradients in fluid shear stress by enhanced activation of transcription factors. *Arterioscler Thromb Vasc Biol*, 19, 1825-34.
- Nakahara, T., Dweck, M. R., Narula, N., Pisapia, D., Narula, J. & Strauss, H. W. 2017. Coronary Artery Calcification: From Mechanism to Molecular Imaging. *JACC Cardiovasc Imaging*, 10, 582-593.
- Nakai, K., Tanaka, H., Yamanaka, K., Takahashi, Y., Murakami, F., Matsuike, R., . . . Maeno, M. 2017. Effects of C-reactive protein on the expression of matrix metalloproteinases and their inhibitors via Fcγ receptors on 3T3-L1 adipocytes. *Int J Med Sci*, 14, 484-493.
- Nakai, Y., Iwabuchi, K., Fujii, S., Ishimori, N., Dashtsoodol, N., Watano, K., . . . Onoe, K. 2004. Natural killer T cells accelerate atherogenesis in mice. *Blood*, 104, 2051-9.
- Nakaki, T., Nakayama, M. & Kato, R. 1990. Inhibition by nitric oxide and nitric oxide-producing vasodilators of DNA synthesis in vascular smooth muscle cells. *Eur J Pharmacol*, 189, 347-53.
- Nakamura, Y., Takemori, H., Shiraishi, K., Inoki, I., Sakagami, M., Shimakura, A., . . . Kobayashi, K. 1996. Compensatory enlargement of angiographically normal coronary segments in patients with coronary artery disease. In vivo documentation using intravascular ultrasound. *Angiology*, 47, 775-81.
- Nandalur, K. R., Baskurt, E., Hagspiel, K. D., Finch, M., Phillips, C. D., Bollampally, S. R. & Kramer, C. M. 2006. Carotid artery calcification on CT may independently predict stroke risk. *AJR*, 186, 547-52.
- Napoli, C. & Ignarro, L. J. 2001. Nitric oxide and atherosclerosis. *Nitric Oxide*, 5, 88-97.
- Narumi, S., Sasaki, M., Ohba, H., Ogasawara, K., Kobayashi, M., Natori, T., . . . Terayama, Y. 2014. Predicting carotid plaque characteristics using quantitative color-coded T1-weighted MR plaque imaging: correlation with carotid endarterectomy specimens. *AJNR Am J Neuroradiol*, 35, 766-71.

- National Institute for Health and Care Excellence 2010. *Chest pain of recent onset: assessment and diagnosis*, London, NICE.
- Nelson, J. W., Young, J. M., Borkar, R. N., Woltjer, R. L., Quinn, J. F., Silbert, L. C., . . . Alkayed, N. J. 2014. Role of soluble epoxide hydrolase in age-related vascular cognitive decline. *Prostaglandins Other Lipid Mediat*, 113-115, 30-7.
- Neubauer, H., Petrak, F., Zahn, D., Pepinghege, F., Hagele, A. K., Pirkl, P. A., . . . Herpertz, S. 2013. Newly diagnosed depression is associated with increased beta-thromboglobulin levels and increased expression of platelet activation markers and platelet derived CD40-CD40L. *J Psychiatr Res*, 47, 865-71.
- Neumann, A. B., Jonsdottir, K. Y., Mouridsen, K., Hjort, N., Gyldensted, C., Bizzi, A., . . . Ostergaard, L. 2009. Interrater agreement for final infarct MRI lesion delineation. *Stroke*, 40, 3768-71.
- Neumann-Haefelin, T., Kastrup, A., De Crespigny, A., Yenari, M. A., Ringer, T., Sun, G. H. & Moseley, M. E. 2000. Serial MRI after transient focal cerebral ischemia in rats: dynamics of tissue injury, blood-brain barrier damage, and edema formation. *Stroke*, 31, 1965-72; discussion 1972-3.
- New, S. E., Goettsch, C., Aikawa, M., Marchini, J. F., Shibasaki, M., Yabusaki, K., . . . Aikawa, E. 2013. Macrophage-derived matrix vesicles: an alternative novel mechanism for microcalcification in atherosclerotic plaques. *Circ Res*, 113, 72-7.
- New, S. E. P. & Aikawa, E. 2013. Role of Extracellular Vesicles in De Novo Mineralization. *An Additional Novel Mechanism of Cardiovascular Calcification*, 33, 1753-1758.
- Newby, D. E., Mcleod, A. L., Uren, N. G., Flint, L., Ludlam, C. A., Webb, D. J., . . . Boon, N. A. 2001. Impaired coronary tissue plasminogen activator release is associated with coronary atherosclerosis and cigarette smoking: direct link between endothelial dysfunction and atherothrombosis. *Circulation*, 103, 1936-41.
- Newby, D. E., Wright, R. A., Labinjoh, C., Ludlam, C. A., Fox, K. A., Boon, N. A. & Webb, D. J. 1999. Endothelial dysfunction, impaired endogenous fibrinolysis, and cigarette smoking: a mechanism for arterial thrombosis and myocardial infarction. *Circulation*, 99, 1411-5.

- Ni, C. W., Qiu, H., Rezvan, A., Kwon, K., Nam, D., Son, D. J., . . . Jo, H. 2010. Discovery of novel mechanosensitive genes in vivo using mouse carotid artery endothelium exposed to disturbed flow. *Blood*, 116, e66-73.
- Niccoli Asabella, A., Ciccone, M. M., Cortese, F., Scicchitano, P., Gesualdo, M., Zito, A., . . . Rubini, G. 2014. Higher reliability of 18F-FDG target background ratio compared to standardized uptake value in vulnerable carotid plaque detection: a pilot study. *Ann Nucl Med*, 28, 571-9.
- Nicholls, S. J., Puri, R., Anderson, T., Ballantyne, C. M., Cho, L., Kastelein, J. J., . . . Nissen, S. E. 2016. Effect of Evolocumab on Progression of Coronary Disease in Statin-Treated Patients: The GLAGOV Randomized Clinical Trial. *Jama*, 316, 2373-2384.
- Nicholls, S. J., Tuzcu, E. M., Wolski, K., Sipahi, I., Schoenhagen, P., Crowe, T., . . . Nissen, S. E. 2007. Coronary artery calcification and changes in atheroma burden in response to established medical therapies. *J Am Coll Cardiol*, 49, 263-70.
- Nicoll, R., Wiklund, U., Zhao, Y., Diederichsen, A., Mickley, H., Ovrehus, K., . . . Henein, M. 2016. Gender and age effects on risk factor-based prediction of coronary artery calcium in symptomatic patients: A Euro-CCAD study. *Atherosclerosis*, 252, 32-9.
- Noguchi, K., Ogawa, T., Inugami, A., Fujita, H., Hatazawa, J., Shimosegawa, E., . . . Seto, H. 1997. MRI of acute cerebral infarction: a comparison of FLAIR and T2-weighted fast spin-echo imaging. *Neuroradiology*, 39, 406-10.
- North American Symptomatic Carotid Endarterectomy Trial Collaborators 1991. Beneficial effect of carotid endarterectomy in symptomatic patients with high-grade carotid stenosis. *N Engl J Med*, 325, 445-53.
- O'leary, D. H., Polak, J. F., Kronmal, R. A., Manolio, T. A., Burke, G. L. & Wolfson, S. K., Jr. 1999. Carotid-artery intima and media thickness as a risk factor for myocardial infarction and stroke in older adults. Cardiovascular Health Study Collaborative Research Group. *N Engl J Med*, 340, 14-22.
- Obermeier, B., Daneman, R. & Ransohoff, R. M. 2013. Development, maintenance and disruption of the blood-brain barrier. *Nat Med*, 19, 1584-96.
- Odink, A. E., Van Der Lugt, A., Hofman, A., Hunink, M. G., Breteler, M. M., Krestin, G. P. & Wittman, J. C. 2007. Association between calcification in

- the coronary arteries, aortic arch and carotid arteries: the Rotterdam study. *Atherosclerosis*, 193, 408-13.
- Odink, A. E., Van Der Lugt, A., Hofman, A., Hunink, M. G., Breteler, M. M., Krestin, G. P. & Witteman, J. C. 2010. Risk factors for coronary, aortic arch and carotid calcification; The Rotterdam Study. *J Hum Hypertens*, 24, 86-92.
- Oei, H. H., Vliegenthart, R., Hofman, A., Oudkerk, M. & Witteman, J. C. 2004. Risk factors for coronary calcification in older subjects. The Rotterdam Coronary Calcification Study. *Eur Heart J*, 25, 48-55.
- Oh, M., Kim, J. Y., Shin, K. H., Park, S. H., Ryu, J. S., Kim, J. S., . . . Moon, D. H. 2010. Imaging Atherosclerosis in the Carotid Arteries with F-18-Fluoro-2-deoxy-D-glucose Positron Emission Tomography: Effect of Imaging Time after Injection on Quantitative Measurement. *Nucl Med Mol Imaging*, 44, 261-6.
- Okazaki, S., Sakaguchi, M., Miwa, K., Furukado, S., Yamagami, H., Yagita, Y., . . . Kitagawa, K. 2014. Association of interleukin-6 with the progression of carotid atherosclerosis: a 9-year follow-up study. *Stroke*, 45, 2924-9.
- Onteddu, S. R., Goddeau, R. P., Jr., Minaeian, A. & Henninger, N. 2015. Clinical impact of leukoaraiosis burden and chronological age on neurological deficit recovery and 90-day outcome after minor ischemic stroke. *J Neurol Sci*, 359, 418-23.
- Ormstad, H., Aass, H. C., Lund-Sorensen, N., Amthor, K. F. & Sandvik, L. 2011. Serum levels of cytokines and C-reactive protein in acute ischemic stroke patients, and their relationship to stroke lateralization, type, and infarct volume. *J Neurol*, 258, 677-85.
- Ota, H., Reeves, M. J., Zhu, D. C., Majid, A., Collar, A., Yuan, C. & Demarco, J. K. 2010a. Sex differences in patients with asymptomatic carotid atherosclerotic plaque: in vivo 3.0-T magnetic resonance study. *Stroke*, 41, 1630-5.
- Ota, H., Reeves, M. J., Zhu, D. C., Majid, A., Collar, A., Yuan, C. & Demarco, J. K. 2013. Sex differences of high-risk carotid atherosclerotic plaque with less than 50% stenosis in asymptomatic patients: an in vivo 3T MRI study. *AJNR Am J Neuroradiol*, 34, 1049-55, s1.
- Ota, H., Yarnykh, V. L., Ferguson, M. S., Underhill, H. R., Demarco, J. K., Zhu, D. C., . . . Yuan, C. 2010b. Carotid intraplaque hemorrhage imaging at 3.0-T MR

- imaging: comparison of the diagnostic performance of three T1-weighted sequences. *Radiology*, 254, 551-63.
- Otsuka, F., Sakakura, K., Yahagi, K., Joner, M. & Virmani, R. 2014. Has our understanding of calcification in human coronary atherosclerosis progressed? *Arterioscler Thromb Vasc Biol*, 34, 724-36.
- Ott, I., Andrassy, M., Ziegler-Schallberger, D., Geith, S., Schomig, A. & Neumann, F. J. 2001. Regulation of monocyte procoagulant activity in acute myocardial infarction: role of tissue factor and tissue factor pathway inhibitor-1. *Blood*, 97, 3721-6.
- Owen, D. R., Gunn, R. N., Rabiner, E. A., Bennacef, I., Fujita, M., Kreisl, W. C., . . . Parker, C. A. 2011. Mixed-affinity binding in humans with 18-kDa translocator protein ligands. *J Nucl Med*, 52, 24-32.
- Owen, D. R., Howell, O. W., Tang, S. P., Wells, L. A., Bennacef, I., Bergstrom, M., . . . Parker, C. A. 2010. Two binding sites for [3H]PBR28 in human brain: implications for TSPO PET imaging of neuroinflammation. *J Cereb Blood Flow Metab*, 30, 1608-18.
- Owens, A. P., 3rd & Mackman, N. 2012. Sources of tissue factor that contribute to thrombosis after rupture of an atherosclerotic plaque. *Thromb Res*, 129 Suppl 2, S30-3.
- Padovani, A., Di Piero, V., Bragoni, M., Di Biase, C., Trasimeni, G., Lannili, M., . . . Lenzi, G. L. 1997. Correlates of leukoaraiosis and ventricular enlargement on magnetic resonance imaging: a study in normal elderly and cerebrovascular patients. *Eur J Neurol*, 4, 15-23.
- Panizo, S., Cardus, A., Encinas, M., Parisi, E., Valcheva, P., Lopez-Ongil, S., . . . Valdivielso, J. M. 2009. RANKL increases vascular smooth muscle cell calcification through a RANK-BMP4-dependent pathway. *Circ Res*, 104, 1041-8.
- Pantoni, L. 2010. Cerebral small vessel disease: from pathogenesis and clinical characteristics to therapeutic challenges. *Lancet Neurol*, 9, 689-701.
- Pantoni, L., Basile, A. M., Pracucci, G., Asplund, K., Bogousslavsky, J., Chabriat, H., . . . Inzitari, D. 2005. Impact of age-related cerebral white matter changes on the transition to disability -- the LADIS study: rationale, design and methodology. *Neuroepidemiology*, 24, 51-62.

- Pantoni, L. & Garcia, J. H. 1997. Pathogenesis of leukoaraiosis: a review. *Stroke*, 28, 652-9.
- Pappata, S., Levasseur, M., Gunn, R. N., Myers, R., Crouzel, C., Syrota, A., . . . Banati, R. B. 2000. Thalamic microglial activation in ischemic stroke detected in vivo by PET and [11C]PK1195. *Neurology*, 55, 1052-4.
- Parhami, F., Basseri, B., Hwang, J., Tintut, Y. & Demer, L. L. 2002. High-density lipoprotein regulates calcification of vascular cells. *Circ Res*, 91, 570-6.
- Park, H. Y., Jun, C. D., Jeon, S. J., Choi, S. S., Kim, H. R., Choi, D. B., . . . Park, D. S. 2012. Serum YKL-40 levels correlate with infarct volume, stroke severity, and functional outcome in acute ischemic stroke patients. *PLoS One*, 7, e51722.
- Pasceri, V., Cheng, J. S., Willerson, J. T. & Yeh, E. T. 2001. Modulation of C-reactive protein-mediated monocyte chemoattractant protein-1 induction in human endothelial cells by anti-atherosclerosis drugs. *Circulation*, 103, 2531-4.
- Passerini, A. G., Polacek, D. C., Shi, C., Francesco, N. M., Manduchi, E., Grant, G. R., . . . Davies, P. F. 2004. Coexisting proinflammatory and antioxidative endothelial transcription profiles in a disturbed flow region of the adult porcine aorta. *Proc Natl Acad Sci U S A*, 101, 2482-7.
- Patankar, T., Widjaja, E., Chant, H., Mccollum, C., Baldwin, R., Jeffries, S., . . . Jackson, A. 2006. Relationship of deep white matter hyperintensities and cerebral blood flow in severe carotid artery stenosis. *Eur J Neurol*, 13, 10-6.
- Patel, R., Janoudi, A., Vedre, A., Aziz, K., Tamhane, U., Rubinstein, J., . . . Abela, G. S. 2011. Plaque Rupture and Thrombosis Are Reduced by Lowering Cholesterol Levels and Crystallization With Ezetimibe and Are Correlated With Fluorodeoxyglucose Positron Emission Tomography. *Arteriosclerosis, Thrombosis, and Vascular Biology*, 31, 2007-2014.
- Patterson, A. J., Jm, U. K.-I., Tang, T. Y., Scoffings, D. J., Howarth, S. P., Graves, M. J. & Gillard, J. H. 2009. Association between white matter ischaemia and carotid plaque morphology as defined by high-resolution in vivo MRI. *Eur J Vasc Endovasc Surg*, 38, 149-54.
- Patti, J., Helenius, J., Puri, A. S. & Henninger, N. 2016. White Matter Hyperintensity-Adjusted Critical Infarct Thresholds to Predict a Favorable 90-Day Outcome. *Stroke*, 47, 2526-33.

- Pech-Amsellem, M. A., Myara, I., Storogenko, M., Demuth, K., Proust, A. & Moatti, N. 1996. Enhanced modifications of low-density lipoproteins (LDL) by endothelial cells from smokers: a possible mechanism of smoking-related atherosclerosis. *Cardiovasc Res*, 31, 975-83.
- Pedersen, E. D., Waje-Andreassen, U., Vedeler, C. A., Aamodt, G. & Mollnes, T. E. 2004. Systemic complement activation following human acute ischaemic stroke. *Clin Exp Immunol*, 137, 117-22.
- Pedersen, S. F., Sandholt, B. V., Keller, S. H., Hansen, A. E., Clemmensen, A. E., Sillesen, H., . . . Kjaer, A. 2015. <sup>64</sup>Cu-DOTATATE PET/MRI for Detection of Activated Macrophages in Carotid Atherosclerotic Plaques: Studies in Patients Undergoing Endarterectomy. *Arterioscler Thromb Vasc Biol*, 35, 1696-703.
- Pedone, C., Scarlata, S., Napoli, N., Lauretani, F., Bandinelli, S., Ferrucci, L. & Incalzi, R. A. 2013. Relationship between bone cross-sectional area and indices of peripheral artery disease. *Calcif Tissue Int*, 93, 508-16.
- Peerschke, E. I., Yin, W. & Ghebrehiwet, B. 2010. Complement activation on platelets: implications for vascular inflammation and thrombosis. *Mol Immunol*, 47, 2170-5.
- Peeters, W., Hellings, W. E., De Kleijn, D. P., De Vries, J. P., Moll, F. L., Vink, A. & Pasterkamp, G. 2009. Carotid atherosclerotic plaques stabilize after stroke: insights into the natural process of atherosclerotic plaque stabilization. *Arterioscler Thromb Vasc Biol*, 29, 128-33.
- Pendlebury, S. T., Cuthbertson, F. C., Welch, S. J., Mehta, Z. & Rothwell, P. M. 2010. Underestimation of cognitive impairment by Mini-Mental State Examination versus the Montreal Cognitive Assessment in patients with transient ischemic attack and stroke: a population-based study. *Stroke*, 41, 1290-3.
- Platzek, I., Sieron, D., Wiggermann, P. & Laniado, M. 2014. Carotid Artery Stenosis: Comparison of 3D Time-of-Flight MR Angiography and Contrast-Enhanced MR Angiography at 3T. *Radiol Res Pract*, 2014, 508715.
- Poggesi, A., Pracucci, G., Chabriat, H., Erkinjuntti, T., Fazekas, F., Verdelho, A., . . . Pantoni, L. 2008. Urinary complaints in nondisabled elderly people with age-related white matter changes: the Leukoaraiosis And DISability (LADIS) Study. *J Am Geriatr Soc*, 56, 1638-43.

- Polonsky, T. S., Ning, H., Daviglius, M. L., Liu, K., Burke, G. L., Cushman, M., . . . Lloyd-Jones, D. M. 2017. Association of Cardiovascular Health With Subclinical Disease and Incident Events: The Multi-Ethnic Study of Atherosclerosis. *J Am Heart Assoc*, 6.
- Poredos, P., Spirkoska, A., Lezaic, L., Mijovski, M. B. & Jezovnik, M. K. 2016. Patients with an Inflamed Atherosclerotic Plaque have Increased Levels of Circulating Inflammatory Markers. *J Atheroscler Thromb*.
- Potter, G. M., Doubal, F. N., Jackson, C. A., Sudlow, C. L., Dennis, M. S. & Wardlaw, J. M. 2012. Lack of association of white matter lesions with ipsilateral carotid artery stenosis. *Cerebrovasc Dis*, 33, 378-84.
- Pretnar-Oblak, J., Sabovic, M., Sebestjen, M., Pogacnik, T. & Zaletel, M. 2006. Influence of atorvastatin treatment on L-arginine cerebrovascular reactivity and flow-mediated dilatation in patients with lacunar infarctions. *Stroke*, 37, 2540-5.
- Price, C. J., Wang, D., Menon, D. K., Guadagno, J. V., Cleij, M., Fryer, T., . . . Warburton, E. A. 2006. Intrinsic activated microglia map to the peri-infarct zone in the subacute phase of ischemic stroke. *Stroke*, 37, 1749-53.
- Proudfoot, D. & Shanahan, C. M. 2006. Molecular mechanisms mediating vascular calcification: role of matrix Gla protein. *Nephrology (Carlton)*, 11, 455-61.
- Proudfoot, D., Skepper, J. N., Hegyi, L., Bennett, M. R., Shanahan, C. M. & Weissberg, P. L. 2000. Apoptosis regulates human vascular calcification in vitro: evidence for initiation of vascular calcification by apoptotic bodies. *Circ Res*, 87, 1055-62.
- Pryor, W. A. & Stone, K. 1993. Oxidants in cigarette smoke. Radicals, hydrogen peroxide, peroxyxynitrate, and peroxyxynitrite. *Ann N Y Acad Sci*, 686, 12-27; discussion 27-8.
- Pun, P. B., Lu, J. & Mochhala, S. 2009. Involvement of ROS in BBB dysfunction. *Free Radic Res*, 43, 348-64.
- Puri, R., Nicholls, S. J., Shao, M., Kataoka, Y., Uno, K., Kapadia, S. R., . . . Nissen, S. E. 2015. Impact of Statins on Serial Coronary Calcification During Atheroma Progression and Regression. *Journal of the American College of Cardiology*, 65, 1273-1282.

- Purroy, F., Montaner, J., Molina, C. A., Delgado, P., Arenillas, J. F., Chacon, P., . . . Alvarez-Sabin, J. 2007. C-reactive protein predicts further ischemic events in transient ischemic attack patients. *Acta Neurol Scand*, 115, 60-6.
- Puz, P. & Lasek-Bal, A. 2017. Repeated measurements of serum concentrations of TNF-alpha, interleukin-6 and interleukin-10 in the evaluation of internal carotid artery stenosis progression. *Atherosclerosis*, 263, 97-103.
- Qian, Z., Anderson, H., Marvasti, I., Akram, K., Vazquez, G., Rinehart, S. & Voros, S. 2010. Lesion- and vessel-specific coronary artery calcium scores are superior to whole-heart Agatston and volume scores in the diagnosis of obstructive coronary artery disease. *J Cardiovasc Comput Tomogr*, 4, 391-9.
- Quirce, R., Martinez-Rodriguez, I., Banzo, I., Jimenez-Bonilla, J., Martinez-Amador, N., Ibanez-Bravo, S., . . . Carril, J. M. 2016. New insight of functional molecular imaging into the atheroma biology: 18F-NaF and 18F-FDG in symptomatic and asymptomatic carotid plaques after recent CVA. Preliminary results. *Clin Physiol Funct Imaging*, 36, 499-503.
- Quirce, R., Martinez-Rodriguez, I., De Arcocha Torres, M., Jimenez-Bonilla, J. F., Banzo, I., Rebollo, M., . . . Carril, J. M. 2013. Contribution of 18F-sodium fluoride PET/CT to the study of the carotid atheroma calcification. *Rev Esp Med Nucl Imagen Mol*, 32, 22-5.
- Rabkin, Z., Israel, O. & Keidar, Z. 2010. Do hyperglycemia and diabetes affect the incidence of false-negative 18F-FDG PET/CT studies in patients evaluated for infection or inflammation and cancer? A Comparative analysis. *J Nucl Med*, 51, 1015-20.
- Radlinska, B. A., Ghinani, S. A., Lyon, P., Jolly, D., Soucy, J. P., Minuk, J., . . . Thiel, A. 2009. Multimodal microglia imaging of fiber tracts in acute subcortical stroke. *Ann Neurol*, 66, 825-32.
- Radomski, M. W., Palmer, R. M. & Moncada, S. 1987. The role of nitric oxide and cGMP in platelet adhesion to vascular endothelium. *Biochem Biophys Res Commun*, 148, 1482-9.
- Read, S. J., Hirano, T., Abbott, D. F., Sachinidis, J. I., Tochon-Danguy, H. J., Chan, J. G., . . . Donnan, G. A. 1998. Identifying hypoxic tissue after acute ischemic stroke using PET and 18F-fluoromisonidazole. *Neurology*, 51, 1617-21.
- Rebel, A. A., Urquhart, S. A., Puig, K. L., Ghatak, A., Brose, S. A., Golovko, M. Y. & Combs, C. K. 2015. Brain changes associated with thromboxane receptor

- antagonist SQ 29,548 treatment in a mouse model. *J Neurosci Res*, 93, 1279-92.
- Redgrave, J. N., Gallagher, P., Lovett, J. K. & Rothwell, P. M. 2008. Critical cap thickness and rupture in symptomatic carotid plaques: the oxford plaque study. *Stroke*, 39, 1722-9.
- Redgrave, J. N., Lovett, J. K. & Rothwell, P. M. 2010. Histological features of symptomatic carotid plaques in relation to age and smoking: the oxford plaque study. *Stroke*, 41, 2288-94.
- Reilly, M. P., Wolfe, M. L., Localio, A. R. & Rader, D. J. 2004. Coronary artery calcification and cardiovascular risk factors: impact of the analytic approach. *Atherosclerosis*, 173, 69-78.
- Rekhter, M. D., Zhang, K., Narayanan, A. S., Phan, S., Schork, M. A. & Gordon, D. 1993. Type I collagen gene expression in human atherosclerosis. Localization to specific plaque regions. *Am J Pathol*, 143, 1634-48.
- Reynolds, C. M., Eguchi, S., Frank, G. D. & Motley, E. D. 2002. Signaling mechanisms of heparin-binding epidermal growth factor-like growth factor in vascular smooth muscle cells. *Hypertension*, 39, 525-9.
- Ribeiro, M. J., Vercouillie, J., Debiais, S., Cottier, J. P., Bonnaud, I., Camus, V., . . . Guilloteau, D. 2014. Could (18) F-DPA-714 PET imaging be interesting to use in the early post-stroke period? *EJNMMI Res*, 4, 28.
- Ridker, P. M., Buring, J. E., Shih, J., Matias, M. & Hennekens, C. H. 1998. Prospective study of C-reactive protein and the risk of future cardiovascular events among apparently healthy women. *Circulation*, 98, 731-3.
- Ridker, P. M., Everett, B. M., Thuren, T., Macfadyen, J. G., Chang, W. H., Ballantyne, C., . . . Glynn, R. J. 2017. Antiinflammatory Therapy with Canakinumab for Atherosclerotic Disease. *N Engl J Med*, 377, 1119-1131.
- Ridker, P. M., Hennekens, C. H., Buring, J. E. & Rifai, N. 2000. C-reactive protein and other markers of inflammation in the prediction of cardiovascular disease in women. *N Engl J Med*, 342, 836-43.
- Rinne, P., Hellberg, S., Kiugel, M., Virta, J., Li, X. G., Kakela, M., . . . Roivainen, A. 2015. Comparison of Somatostatin Receptor 2-Targeting PET Tracers in the Detection of Mouse Atherosclerotic Plaques. *Mol Imaging Biol*.
- Ritzl, A., Meisel, S., Wittsack, H. J., Fink, G. R., Siebler, M., Modder, U. & Seitz, R. J. 2004. Development of brain infarct volume as assessed by magnetic

- resonance imaging (MRI): follow-up of diffusion-weighted MRI lesions. *J Magn Reson Imaging*, 20, 201-7.
- Rival, J., Riddle, J. M. & Stein, P. D. 1987. Effects of chronic smoking on platelet function. *Thromb Res*, 45, 75-85.
- Romero, J. R., Beiser, A., Seshadri, S., Benjamin, E. J., Polak, J. F., Vasan, R. S., . . . Wolf, P. A. 2009. Carotid artery atherosclerosis, MRI indices of brain ischemia, aging, and cognitive impairment: the Framingham study. *Stroke*, 40, 1590-6.
- Rominger, A., Saam, T., Vogl, E., Ubleis, C., La Fougere, C., Forster, S., . . . Hacker, M. 2010. In vivo imaging of macrophage activity in the coronary arteries using 68Ga-DOTATATE PET/CT: correlation with coronary calcium burden and risk factors. *J Nucl Med*, 51, 193-7.
- Rosell, A., Ortega-Aznar, A., Alvarez-Sabin, J., Fernandez-Cadenas, I., Ribo, M., Molina, C. A., . . . Montaner, J. 2006. Increased brain expression of matrix metalloproteinase-9 after ischemic and hemorrhagic human stroke. *Stroke*, 37, 1399-406.
- Rosenberg, G. A., Cunningham, L. A., Wallace, J., Alexander, S., Estrada, E. Y., Grossetete, M., . . . Gearing, A. 2001. Immunohistochemistry of matrix metalloproteinases in reperfusion injury to rat brain: activation of MMP-9 linked to stromelysin-1 and microglia in cell cultures. *Brain Res*, 893, 104-12.
- Rosenberg, G. A. & Yang, Y. 2007. Vasogenic edema due to tight junction disruption by matrix metalloproteinases in cerebral ischemia. *Neurosurg Focus*, 22, E4.
- Rosner, D., Stoneman, V., Littlewood, T., Mccarthy, N., Figg, N., Wang, Y., . . . Bennett, M. 2006. Interferon-gamma induces Fas trafficking and sensitization to apoptosis in vascular smooth muscle cells via a PI3K- and Akt-dependent mechanism. *Am J Pathol*, 168, 2054-63.
- Ross, R. 1993. The pathogenesis of atherosclerosis: a perspective for the 1990s. *Nature*, 362, 801-9.
- Ross, R. 1999. Atherosclerosis--an inflammatory disease. *N Engl J Med*, 340, 115-26.
- Rost, N. S., Wolf, P. A., Kase, C. S., Kelly-Hayes, M., Silbershatz, H., Massaro, J. M., . . . Wilson, P. W. 2001. Plasma concentration of C-reactive protein and risk of ischemic stroke and transient ischemic attack: the Framingham study. *Stroke*, 32, 2575-9.

- Rotering, S., Deuther-Conrad, W., Cumming, P., Donat, C. K., Scheunemann, M., Fischer, S., . . . Brust, P. 2014. Imaging of alpha7 nicotinic acetylcholine receptors in brain and cerebral vasculature of juvenile pigs with [(18)F]NS14490. *EJNMMI Res*, 4, 43.
- Rothwell, P. M. & Warlow, C. P. 1999. Prediction of benefit from carotid endarterectomy in individual patients: a risk-modelling study. European Carotid Surgery Trialists' Collaborative Group. *Lancet*, 353, 2105-10.
- Rothwell, P. M. & Warlow, C. P. 2005. Timing of TIAs preceding stroke: time window for prevention is very short. *Neurology*, 64, 817-20.
- Rousset, O. G., Ma, Y. & Evans, A. C. 1998. Correction for partial volume effects in PET: principle and validation. *J Nucl Med*, 39, 904-11.
- Rozie, S., De Weert, T. T., De Monye, C., Homburg, P. J., Tanghe, H. L., Dippel, D. W. & Van Der Lugt, A. 2009. Atherosclerotic plaque volume and composition in symptomatic carotid arteries assessed with multidetector CT angiography; relationship with severity of stenosis and cardiovascular risk factors. *Eur Radiol*, 19, 2294-301.
- Rubenstein, I., Yong, T., Rennard, S. I. & Mayhan, W. G. 1991. Cigarette smoke extract attenuates endothelium-dependent arteriolar dilatation in vivo. *Am J Physiol*, 261, H1913-8.
- Rudd, J. H., Myers, K. S., Bansilal, S., Machac, J., Pinto, C. A., Tong, C., . . . Fayad, Z. A. 2008. Atherosclerosis inflammation imaging with 18F-FDG PET: carotid, iliac, and femoral uptake reproducibility, quantification methods, and recommendations. *J Nucl Med*, 49, 871-8.
- Rudd, J. H., Myers, K. S., Bansilal, S., Machac, J., Rafique, A., Farkouh, M., . . . Fayad, Z. A. 2007. (18)Fluorodeoxyglucose positron emission tomography imaging of atherosclerotic plaque inflammation is highly reproducible: implications for atherosclerosis therapy trials. *J Am Coll Cardiol*, 50, 892-6.
- Rudd, J. H., Myers, K. S., Bansilal, S., Machac, J., Woodward, M., Fuster, V., . . . Fayad, Z. A. 2009. Relationships among regional arterial inflammation, calcification, risk factors, and biomarkers: a prospective fluorodeoxyglucose positron-emission tomography/computed tomography imaging study. *Circ Cardiovasc Imaging*, 2, 107-15.
- Rudd, J. H. F., Warburton, E. A., Fryer, T. D., Jones, H. A., Clark, J. C., Antoun, N., . . . Weissberg, P. L. 2002. Imaging Atherosclerotic Plaque Inflammation With

- [18F]-Fluorodeoxyglucose Positron Emission Tomography. *Circulation*, 105, 2708-2711.
- Rundek, T., Della-Morte, D., Gardener, H., Dong, C., Markert, M. S., Gutierrez, J., . . . Wright, C. B. 2017. Relationship between carotid arterial properties and cerebral white matter hyperintensities. *Neurology*, 88, 2036-2042.
- Rutten, B., Tersteeg, C., Vrijenhoek, J. E., Van Holten, T. C., Elsenberg, E. H., Mak-Nienhuis, E. M., . . . Roest, M. 2014. Increased platelet reactivity is associated with circulating platelet-monocyte complexes and macrophages in human atherosclerotic plaques. *PLoS One*, 9, e105019.
- Ryu, W. S., Woo, S. H., Schellingerhout, D., Jang, M. U., Park, K. J., Hong, K. S., . . . Kim, D. E. 2017. Stroke outcomes are worse with larger leukoaraiosis volumes. *Brain*, 140, 158-170.
- Ryu, Y., Yoshida, K., Suzuki, Y., Nakadate, M., Umehara, I., Tomita, M. & Shibuya, H. 2013. Long-term changes of aortic 18F-FDG uptake and calcification in health-screening subjects. *Ann Nucl Med*, 27, 239-46.
- Rzewuska-Lech, E., Jayachandran, M., Fitzpatrick, L. A. & Miller, V. M. 2005. Differential effects of 17beta-estradiol and raloxifene on VSMC phenotype and expression of osteoblast-associated proteins. *Am J Physiol Endocrinol Metab*, 289, E105-12.
- Sabeti, S., Schlager, O., Exner, M., Mlekusch, W., Amighi, J., Dick, P., . . . Schillinger, M. 2007. Progression of carotid stenosis detected by duplex ultrasonography predicts adverse outcomes in cardiovascular high-risk patients. *Stroke*, 38, 2887-94.
- Sadat, U., Teng, Z., Young, V. E., Walsh, S. R., Li, Z. Y., Graves, M. J., . . . Gillard, J. H. 2010. Association between Biomechanical Structural Stresses of Atherosclerotic Carotid Plaques and Subsequent Ischaemic Cerebrovascular Events – A Longitudinal in Vivo Magnetic Resonance Imaging-based Finite element Study. *European Journal of Vascular and Endovascular Surgery*, 40, 485-491.
- Sahan, M., Sebe, A., Acikalin, A., Akpınar, O., Koc, F., Ay, M. O., . . . Satar, S. 2013. Acute-phase reactants and cytokines in ischemic stroke: do they have any relationship with short-term mortality? *Eur Rev Med Pharmacol Sci*, 17, 2773-7.

- Saito, H., Kuroda, S., Hirata, K., Magota, K., Shiga, T., Tamaki, N., . . . Houkin, K. 2013. Validity of dual MRI and F-FDG PET imaging in predicting vulnerable and inflamed carotid plaque. *Cerebrovasc Dis*, 35, 370-7.
- Saka, O., Mcguire, A. & Wolfe, C. 2009. Cost of stroke in the United Kingdom. *Age Ageing*, 38, 27-32.
- Salonen, J. T. & Salonen, R. 1991. Ultrasonographically assessed carotid morphology and the risk of coronary heart disease. *Arterioscler Thromb*, 11, 1245-9.
- Salzar, R. S., Thubrikar, M. J. & Eppink, R. T. 1995. Pressure-induced mechanical stress in the carotid artery bifurcation: a possible correlation to atherosclerosis. *J Biomech*, 28, 1333-40.
- Samady, H., Eshtehardi, P., Mcdaniel, M. C., Suo, J., Dhawan, S. S., Maynard, C., . . . Giddens, D. P. 2011. Coronary artery wall shear stress is associated with progression and transformation of atherosclerotic plaque and arterial remodeling in patients with coronary artery disease. *Circulation*, 124, 779-88.
- Saremi, A., Bahn, G. & Reaven, P. D. 2012. Progression of vascular calcification is increased with statin use in the Veterans Affairs Diabetes Trial (VADT). *Diabetes Care*, 35, 2390-2.
- Sarwar, N., Butterworth, A. S., Freitag, D. F., Gregson, J., Willeit, P., Gorman, D. N., . . . Danesh, J. 2012. Interleukin-6 receptor pathways in coronary heart disease: a collaborative meta-analysis of 82 studies. *Lancet*, 379, 1205-13.
- Saver, J. L. 2006. Time Is Brain—Quantified. *Stroke*, 37, 263-266.
- Saver, J. L., Johnston, K. C., Homer, D., Wityk, R., Koroshetz, W., Truskowski, L. L. & Haley, E. C. 1999. Infarct volume as a surrogate or auxiliary outcome measure in ischemic stroke clinical trials. The RANTTAS Investigators. *Stroke*, 30, 293-8.
- Schartl, M., Bocksch, W., Koschyk, D. H., Voelker, W., Karsch, K. R., Kreuzer, J., . . . Gross, M. 2001. Use of intravascular ultrasound to compare effects of different strategies of lipid-lowering therapy on plaque volume and composition in patients with coronary artery disease. *Circulation*, 104, 387-92.
- Scheltens, P., Barkhof, F., Leys, D., Pruvo, J. P., Nauta, J. J., Vermersch, P., . . . Valk, J. 1993. A semiquantitative rating scale for the assessment of signal hyperintensities on magnetic resonance imaging. *J Neurol Sci*, 114, 7-12.
- Schmidt, R., Fazekas, F., Kleinert, G., Offenbacher, H., Gindl, K., Payer, F., . . . Lechner, H. 1992. Magnetic resonance imaging signal hyperintensities in the

- deep and subcortical white matter. A comparative study between stroke patients and normal volunteers. *Arch Neurol*, 49, 825-7.
- Schonbeck, U., Mach, F., Sukhova, G. K., Murphy, C., Bonnefoy, J. Y., Fabunmi, R. P. & Libby, P. 1997. Regulation of matrix metalloproteinase expression in human vascular smooth muscle cells by T lymphocytes: a role for CD40 signaling in plaque rupture? *Circ Res*, 81, 448-54.
- Schram, M. T., Euser, S. M., De Craen, A. J., Witteman, J. C., Frolich, M., Hofman, A., . . . Westendorp, R. G. 2007. Systemic markers of inflammation and cognitive decline in old age. *J Am Geriatr Soc*, 55, 708-16.
- Schroeter, M., Dennin, M. A., Walberer, M., Backes, H., Neumaier, B., Fink, G. R. & Graf, R. 2009. Neuroinflammation extends brain tissue at risk to vital peri-infarct tissue: a double tracer [11C]PK11195- and [18F]FDG-PET study. *J Cereb Blood Flow Metab*, 29, 1216-25.
- Schurgers, L. J., Uitto, J. & Reutelingsperger, C. P. 2013. Vitamin K-dependent carboxylation of matrix Gla-protein: a crucial switch to control ectopic mineralization. *Trends Mol Med*, 19, 217-26.
- Schwamm, L. H., Koroshetz, W. J., Sorensen, A. G., Wang, B., Copen, W. A., Budzik, R., . . . Gonzalez, R. G. 1998. Time course of lesion development in patients with acute stroke: serial diffusion- and hemodynamic-weighted magnetic resonance imaging. *Stroke*, 29, 2268-76.
- Schwartz, G. G., Olsson, A. G., Abt, M., Ballantyne, C. M., Barter, P. J., Brumm, J., . . . Wright, R. S. 2012. Effects of dalcetrapib in patients with a recent acute coronary syndrome. *N Engl J Med*, 367, 2089-99.
- Selathurai, A., Deswaerte, V., Kanellakis, P., Tipping, P., Toh, B. H., Bobik, A. & Kyaw, T. 2014. Natural killer (NK) cells augment atherosclerosis by cytotoxic-dependent mechanisms. *Cardiovasc Res*, 102, 128-37.
- Sexton, T. R., Wallace, E. L., Macaulay, T. E., Charnigo, R. J., Evangelista, V., Campbell, C. L., . . . Smyth, S. S. 2015. The effect of rosuvastatin on thromboinflammation in the setting of acute coronary syndrome. *J Thromb Thrombolysis*, 39, 186-95.
- Shamsaei, N., Erfani, S., Fereidoni, M. & Shahbazi, A. 2017. Neuroprotective Effects of Exercise on Brain Edema and Neurological Movement Disorders Following the Cerebral Ischemia and Reperfusion in Rats. *Basic Clin Neurosci*, 8, 77-84.

- Shemesh, J., Frenkel, Y., Leibovitch, L., Grossman, E., Pines, A. & Motro, M. 1997. Does hormone replacement therapy inhibit coronary artery calcification? *Obstet Gynecol*, 89, 989-92.
- Shi, Z. D. & Tarbell, J. M. 2011. Fluid flow mechanotransduction in vascular smooth muscle cells and fibroblasts. *Ann Biomed Eng*, 39, 1608-19.
- Shieh, C. H., Heinrich, A., Serchov, T., Van Calker, D. & Biber, K. 2014. P2X7-dependent, but differentially regulated release of IL-6, CCL2, and TNF-alpha in cultured mouse microglia. *Glia*, 62, 592-607.
- Siasos, G., Tsigkou, V., Kokkou, E., Oikonomou, E., Vavuranakis, M., Vlachopoulos, C., . . . Tousoulis, D. 2014. Smoking and atherosclerosis: mechanisms of disease and new therapeutic approaches. *Curr Med Chem*, 21, 3936-48.
- Sillescu, H., Muntendam, P., Adourian, A., Entekin, R., Garcia, M., Falk, E. & Fuster, V. 2012. Carotid plaque burden as a measure of subclinical atherosclerosis: comparison with other tests for subclinical arterial disease in the High Risk Plaque BioImage study. *JACC Cardiovasc Imaging*, 5, 681-9.
- Silvera, S. S., Aidi, H. E., Rudd, J. H., Mani, V., Yang, L., Farkouh, M., . . . Fayad, Z. A. 2009. Multimodality imaging of atherosclerotic plaque activity and composition using FDG-PET/CT and MRI in carotid and femoral arteries. *Atherosclerosis*, 207, 139-43.
- Silvola, J. M., Saraste, A., Laitinen, I., Savisto, N., Laine, V. J., Heinonen, S. E., . . . Knuuti, J. 2011. Effects of age, diet, and type 2 diabetes on the development and FDG uptake of atherosclerotic plaques. *JACC Cardiovasc Imaging*, 4, 1294-301.
- Simmons, C. A., Nikolovski, J., Thornton, A. J., Matlis, S. & Mooney, D. J. 2004. Mechanical stimulation and mitogen-activated protein kinase signaling independently regulate osteogenic differentiation and mineralization by calcifying vascular cells. *J Biomech*, 37, 1531-41.
- Singh, B. & Chaudhuri, T. K. 2014. Role of C-reactive protein in schizophrenia: an overview. *Psychiatry Res*, 216, 277-85.
- Singh, J., Seth, S. D., Manchanda, S. C. & Seth, S. 1997. Protective actions of a thromboxane receptor antagonist, SQ 29548 on the ischemic myocardium: morphologic and hemodynamic effects. *Prostaglandins Leukot Essent Fatty Acids*, 56, 105-10.

- Singh, N., Moody, A. R., Roifman, I., Bluemke, D. A. & Zavodni, A. E. 2015. Advanced MRI for carotid plaque imaging. *Int J Cardiovasc Imaging*.
- Singh, U., Dasu, M. R., Yancey, P. G., Afify, A., Devaraj, S. & Jialal, I. 2008. Human C-reactive protein promotes oxidized low density lipoprotein uptake and matrix metalloproteinase-9 release in Wistar rats. *J Lipid Res*, 49, 1015-23.
- Skagen, K., Johnsrud, K., Evensen, K., Scott, H., Krohg-Sorensen, K., Reier-Nilsen, F., . . . Russell, D. 2015. Carotid plaque inflammation assessed with (18)F-FDG PET/CT is higher in symptomatic compared with asymptomatic patients. *Int J Stroke*, 10, 730-6.
- Skjelbakken, T., Lappegard, J., Ellingsen, T. S., Barrett-Connor, E., Brox, J., Lochen, M. L., . . . Hansen, J. B. 2014. Red cell distribution width is associated with incident myocardial infarction in a general population: the Tromso Study. *J Am Heart Assoc*, 3.
- Skoog, T., Dichtl, W., Boquist, S., Skoglund-Andersson, C., Karpe, F., Tang, R., . . . Hamsten, A. 2002. Plasma tumour necrosis factor-alpha and early carotid atherosclerosis in healthy middle-aged men. *Eur Heart J*, 23, 376-83.
- Sluimer, J. C., Gasc, J. M., Van Wanroij, J. L., Kisters, N., Groeneweg, M., Sollewijn Gelpke, M. D., . . . Bijmens, A. P. 2008. Hypoxia, hypoxia-inducible transcription factor, and macrophages in human atherosclerotic plaques are correlated with intraplaque angiogenesis. *J Am Coll Cardiol*, 51, 1258-65.
- Smith, C. J., Emsley, H. C., Gavin, C. M., Georgiou, R. F., Vail, A., Barberan, E. M., . . . Tyrrell, P. J. 2004. Peak plasma interleukin-6 and other peripheral markers of inflammation in the first week of ischaemic stroke correlate with brain infarct volume, stroke severity and long-term outcome. *BMC Neurol*, 4, 2.
- Smith, C. J. & Fischer, T. H. 2001. Particulate and vapor phase constituents of cigarette mainstream smoke and risk of myocardial infarction. *Atherosclerosis*, 158, 257-67.
- Smith, F. B., Lee, A. J., Fowkes, F. G., Price, J. F., Rumley, A. & Lowe, G. D. 1997. Hemostatic factors as predictors of ischemic heart disease and stroke in the Edinburgh Artery Study. *Arterioscler Thromb Vasc Biol*, 17, 3321-5.
- Smith, J. D., Trogan, E., Ginsberg, M., Grigaux, C., Tian, J. & Miyata, M. 1995. Decreased atherosclerosis in mice deficient in both macrophage colony-stimulating factor (op) and apolipoprotein E. *Proc Natl Acad Sci U S A*, 92, 8264-8.

- Sovershaev, M. A., Egorina, E. M., Bogdanov, V. Y., Seredkina, N., Fallon, J. T., Valkov, A. Y., . . . Hansen, J. B. 2010. Bone morphogenetic protein -7 increases thrombogenicity of lipid-rich atherosclerotic plaques via activation of tissue factor. *Thromb Res*, 126, 306-10.
- Spratt, N. J., Donnan, G. A. & Howells, D. W. 2009. Characterisation of the timing of binding of the hypoxia tracer FMISO after stroke. *Brain Res*, 1288, 135-42.
- Springer, T. A. 1994. Traffic signals for lymphocyte recirculation and leukocyte emigration: the multistep paradigm. *Cell*, 76, 301-14.
- Starr, J. M., Wardlaw, J., Ferguson, K., MacLulich, A., Deary, I. J. & Marshall, I. 2003. Increased blood-brain barrier permeability in type II diabetes demonstrated by gadolinium magnetic resonance imaging. *J Neurol Neurosurg Psychiatry*, 74, 70-6.
- Stegemann, J. P., Hong, H. & Nerem, R. M. 2005. Mechanical, biochemical, and extracellular matrix effects on vascular smooth muscle cell phenotype. *J Appl Physiol (1985)*, 98, 2321-7.
- Steinvil, A., Sadeh, B., Arbel, Y., Justo, D., Belei, A., Borenstein, N., . . . Halkin, A. 2011. Prevalence and predictors of concomitant carotid and coronary artery atherosclerotic disease. *J Am Coll Cardiol*, 57, 779-83.
- Steitz, S. A., Speer, M. Y., Curinga, G., Yang, H. Y., Haynes, P., Aebbersold, R., . . . Giachelli, C. M. 2001. Smooth muscle cell phenotypic transition associated with calcification: upregulation of Cbfa1 and downregulation of smooth muscle lineage markers. *Circ Res*, 89, 1147-54.
- Stenborg, A., Kalimo, H., Viitanen, M., Terent, A. & Lind, L. 2007. Impaired endothelial function of forearm resistance arteries in CADASIL patients. *Stroke*, 38, 2692-7.
- Stephenson, D. T., Schober, D. A., Smalstig, E. B., Mincy, R. E., Gehlert, D. R. & Clemens, J. A. 1995. Peripheral benzodiazepine receptors are colocalized with activated microglia following transient global forebrain ischemia in the rat. *J Neurosci*, 15, 5263-74.
- Streifler, J. Y., Eliasziw, M., Benavente, O. R., Alamowitch, S., Fox, A. J., Hachinski, V. & Barnett, H. J. 2003. Development and progression of leukoaraiosis in patients with brain ischemia and carotid artery disease. *Stroke*, 34, 1913-6.
- Streifler, J. Y., Eliasziw, M., Benavente, O. R., Hachinski, V. C., Fox, A. J. & Barnett, H. J. 1995. Lack of relationship between leukoaraiosis and carotid

- artery disease. The North American Symptomatic Carotid Endarterectomy Trial. *Arch Neurol*, 52, 21-4.
- Strobl, F. F., Rominger, A., Wolpers, S., Rist, C., Bamberg, F., Thierfelder, K. M., . . . Saam, T. 2013. Impact of cardiovascular risk factors on vessel wall inflammation and calcified plaque burden differs across vascular beds: a PET-CT study. *Int J Cardiovasc Imaging*, 29, 1899-908.
- Subramanian, S., Emami, H., Vucic, E., Singh, P., Vijayakumar, J., Fifer, K. M., . . . Tawakol, A. 2013. High-dose atorvastatin reduces periodontal inflammation: a novel pleiotropic effect of statins. *J Am Coll Cardiol*, 62, 2382-91.
- Sukhova, G. K., Schonbeck, U., Rabkin, E., Schoen, F. J., Poole, A. R., Billingham, R. C. & Libby, P. 1999. Evidence for increased collagenolysis by interstitial collagenases-1 and -3 in vulnerable human atheromatous plaques. *Circulation*, 99, 2503-9.
- Sulter, G., Steen, C. & De Keyser, J. 1999. Use of the Barthel index and modified Rankin scale in acute stroke trials. *Stroke*, 30, 1538-41.
- Sutton-Tyrrell, K., Lassila, H. C., Meilahn, E., Bunker, C., Matthews, K. A. & Kuller, L. H. 1998. Carotid atherosclerosis in premenopausal and postmenopausal women and its association with risk factors measured after menopause. *Stroke*, 29, 1116-21.
- Tada, S. & Tarbell, J. M. 2000. Interstitial flow through the internal elastic lamina affects shear stress on arterial smooth muscle cells. *Am J Physiol Heart Circ Physiol*, 278, H1589-97.
- Tahara, N., Kai, H., Ishibashi, M., Nakaura, H., Kaida, H., Baba, K., . . . Imaizumi, T. 2006. Simvastatin attenuates plaque inflammation: evaluation by fluorodeoxyglucose positron emission tomography. *J Am Coll Cardiol*, 48, 1825-31.
- Tahara, N., Kai, H., Nakaura, H., Mizoguchi, M., Ishibashi, M., Kaida, H., . . . Imaizumi, T. 2007a. The prevalence of inflammation in carotid atherosclerosis: analysis with fluorodeoxyglucose-positron emission tomography. *Eur Heart J*, 28, 2243-8.
- Tahara, N., Kai, H., Yamagishi, S.-I., Mizoguchi, M., Nakaura, H., Ishibashi, M., . . . Imaizumi, T. 2007b. Vascular Inflammation Evaluated by [18F]-Fluorodeoxyglucose Positron Emission Tomography Is Associated With the

- Metabolic Syndrome. *Journal of the American College of Cardiology*, 49, 1533-1539.
- Taheri, S., Gasparovic, C., Huisa, B. N., Adair, J. C., Edmonds, E., Prestopnik, J., . . . Rosenberg, G. A. 2011a. Blood-brain barrier permeability abnormalities in vascular cognitive impairment. *Stroke*, 42, 2158-63.
- Taheri, S., Gasparovic, C., Shah, N. J. & Rosenberg, G. A. 2011b. Quantitative measurement of blood-brain barrier permeability in human using dynamic contrast-enhanced MRI with fast T1 mapping. *Magn Reson Med*, 65, 1036-42.
- Takajo, Y., Ikeda, H., Haramaki, N., Murohara, T. & Imaizumi, T. 2001. Augmented oxidative stress of platelets in chronic smokers. Mechanisms of impaired platelet-derived nitric oxide bioactivity and augmented platelet aggregability. *J Am Coll Cardiol*, 38, 1320-7.
- Takami, T., Yamano, S., Okada, S., Sakuma, M., Morimoto, T., Hashimoto, H., . . . Saito, Y. 2012. Major risk factors for the appearance of white-matter lesions on MRI in hypertensive patients with controlled blood pressure. *Vasc Health Risk Manag*, 8, 169-76.
- Takasawa, M., Moustafa, R. R. & Baron, J. C. 2008. Applications of nitroimidazole in vivo hypoxia imaging in ischemic stroke. *Stroke*, 39, 1629-37.
- Takaya, N., Yuan, C., Chu, B., Saam, T., Underhill, H., Cai, J., . . . Hatsukami, T. S. 2006. Association Between Carotid Plaque Characteristics and Subsequent Ischemic Cerebrovascular Events: A Prospective Assessment With MRI—Initial Results. *Stroke*, 37, 818-823.
- Tanaka, R., Komine-Kobayashi, M., Mochizuki, H., Yamada, M., Furuya, T., Migita, M., . . . Urabe, T. 2003. Migration of enhanced green fluorescent protein expressing bone marrow-derived microglia/macrophage into the mouse brain following permanent focal ischemia. *Neuroscience*, 117, 531-9.
- Tarkin, J. M., Joshi, F. R., Evans, N. R., Chowdhury, M. M., Figg, N. L., Shah, A. V., . . . Rudd, J. H. 2017. Detection of Atherosclerotic Inflammation by <sup>68</sup>Ga-DOTATATE PET Compared to [<sup>18</sup>F]FDG PET Imaging. *J Am Coll Cardiol*, 69, 1774-1791.
- Tawakol, A., Fayad, Z. A., Mogg, R., Alon, A., Klimas, M. T., Dansky, H., . . . Shankar, S. S. 2013. Intensification of statin therapy results in a rapid reduction in atherosclerotic inflammation: results of a multicenter

- fluorodeoxyglucose-positron emission tomography/computed tomography feasibility study. *J Am Coll Cardiol*, 62, 909-17.
- Tawakol, A., Migrino, R. Q., Bashian, G. G., Bedri, S., Vermylen, D., Cury, R. C., . . . Fischman, A. J. 2006. In vivo 18F-fluorodeoxyglucose positron emission tomography imaging provides a noninvasive measure of carotid plaque inflammation in patients. *J Am Coll Cardiol*, 48, 1818-24.
- Tawakol, A., Migrino, R. Q., Hoffmann, U., Abbara, S., Houser, S., Gewirtz, H., . . . Fischman, A. J. 2005. Noninvasive in vivo measurement of vascular inflammation with F-18 fluorodeoxyglucose positron emission tomography. *J Nucl Cardiol*, 12, 294-301.
- Tawakol, A., Osborne, M. T. & Fayad, Z. A. 2017. Molecular Imaging of Atheroma: Deciphering How and When to Use 18F-Sodium Fluoride and 18F-Fluorodeoxyglucose. *Circ Cardiovasc Imaging*, 10.
- Taylor, R. A. & Sansing, L. H. 2013. Microglial responses after ischemic stroke and intracerebral hemorrhage. *Clin Dev Immunol*, 2013, 746068.
- Taylor, W. D., Steffens, D. C., Macfall, J. R., Mcquoid, D. R., Payne, M. E., Provenzale, J. M. & Krishnan, K. R. 2003. White matter hyperintensity progression and late-life depression outcomes. *Arch Gen Psychiatry*, 60, 1090-6.
- Thiel, A. & Heiss, W. D. 2011. Imaging of microglia activation in stroke. *Stroke*, 42, 507-12.
- Thiel, A., Radlinska, B. A., Paquette, C., Sidel, M., Soucy, J. P., Schirmacher, R. & Minuk, J. 2010. The temporal dynamics of poststroke neuroinflammation: a longitudinal diffusion tensor imaging-guided PET study with 11C-PK11195 in acute subcortical stroke. *J Nucl Med*, 51, 1404-12.
- Thorand, B., Baumert, J., Doring, A., Schneider, A., Chambless, L., Lowel, H., . . . Koenig, W. 2006. Association of cardiovascular risk factors with markers of endothelial dysfunction in middle-aged men and women. Results from the MONICA/KORA Augsburg Study. *Thromb Haemost*, 95, 134-41.
- Tintut, Y., Patel, J., Parhami, F. & Demer, L. L. 2000. Tumor necrosis factor-alpha promotes in vitro calcification of vascular cells via the cAMP pathway. *Circulation*, 102, 2636-42.

- Tonetti, M. S., D'aiuto, F., Nibali, L., Donald, A., Storry, C., Parkar, M., . . . Deanfield, J. 2007. Treatment of periodontitis and endothelial function. *N Engl J Med*, 356, 911-20.
- Topakian, R., Barrick, T. R., Howe, F. A. & Markus, H. S. 2010. Blood-brain barrier permeability is increased in normal-appearing white matter in patients with lacunar stroke and leucoaraiosis. *J Neurol Neurosurg Psychiatry*, 81, 192-7.
- Torizuka, T., Clavo, A. C. & Wahl, R. L. 1997. Effect of hyperglycemia on in vitro tumor uptake of tritiated FDG, thymidine, L-methionine and L-leucine. *J Nucl Med*, 38, 382-6.
- Torzewski, J., Torzewski, M., Bowyer, D. E., Frohlich, M., Koenig, W., Waltenberger, J., . . . Hombach, V. 1998. C-reactive protein frequently colocalizes with the terminal complement complex in the intima of early atherosclerotic lesions of human coronary arteries. *Arterioscler Thromb Vasc Biol*, 18, 1386-92.
- Trion, A., Schutte-Bart, C., Bax, W. H., Jukema, J. W. & Van Der Laarse, A. 2008. Modulation of calcification of vascular smooth muscle cells in culture by calcium antagonists, statins, and their combination. *Mol Cell Biochem*, 308, 25-33.
- Tsao, P. S., Buitrago, R., Chan, J. R. & Cooke, J. P. 1996. Fluid flow inhibits endothelial adhesiveness. Nitric oxide and transcriptional regulation of VCAM-1. *Circulation*, 94, 1682-9.
- Tsao, P. S., Wang, B., Buitrago, R., Shyy, J. Y. & Cooke, J. P. 1997. Nitric oxide regulates monocyte chemotactic protein-1. *Circulation*, 96, 934-40.
- Tsuji, K., Aoki, T., Tejima, E., Arai, K., Lee, S. R., Atochin, D. N., . . . Lo, E. H. 2005. Tissue plasminogen activator promotes matrix metalloproteinase-9 upregulation after focal cerebral ischemia. *Stroke*, 36, 1954-9.
- Tyson, K. L., Reynolds, J. L., McNair, R., Zhang, Q., Weissberg, P. L. & Shanahan, C. M. 2003. Osteo/chondrocytic transcription factors and their target genes exhibit distinct patterns of expression in human arterial calcification. *Arterioscler Thromb Vasc Biol*, 23, 489-94.
- Ulusoy, F. R., Yolcu, M., Ipek, E., Korkmaz, A. F., Gurler, M. Y. & Gulbaran, M. 2015. Coronary Artery Disease Risk Factors, Coronary Artery Calcification and Coronary Bypass Surgery. *J Clin Diagn Res*, 9, Oc06-10.

- Underhill, H. R., Yuan, C., Terry, J. G., Chen, H., Espeland, M. A., Hatsukami, T. S., . . . Crouse, J. R., 3rd 2008. Differences in carotid arterial morphology and composition between individuals with and without obstructive coronary artery disease: a cardiovascular magnetic resonance study. *J Cardiovasc Magn Reson*, 10, 31.
- Usman, A., Sadat, U., Graves, M. J. & Gillard, J. H. 2015. Magnetic resonance imaging of atherothrombotic plaques. *J Clin Neurosci*.
- Valkanova, V., Ebmeier, K. P. & Allan, C. L. 2013. CRP, IL-6 and depression: a systematic review and meta-analysis of longitudinal studies. *J Affect Disord*, 150, 736-44.
- Van Bussel, B. C., Henry, R. M., Schalkwijk, C. G., Dekker, J. M., Nijpels, G. & Stehouwer, C. D. 2012. Low-grade inflammation, but not endothelial dysfunction, is associated with greater carotid stiffness in the elderly: the Hoorn Study. *J Hypertens*, 30, 744-52.
- Van Bussel, B. C., Schouten, F., Henry, R. M., Schalkwijk, C. G., De Boer, M. R., Ferreira, I., . . . Stehouwer, C. D. 2011. Endothelial dysfunction and low-grade inflammation are associated with greater arterial stiffness over a 6-year period. *Hypertension*, 58, 588-95.
- Van Der Flier, W. M., Van Straaten, E. C., Barkhof, F., Verdelho, A., Madureira, S., Pantoni, L., . . . Scheltens, P. 2005. Small vessel disease and general cognitive function in nondisabled elderly: the LADIS study. *Stroke*, 36, 2116-20.
- Van Der Meer, I. M., Bots, M. L., Hofman, A., Del Sol, A. I., Van Der Kuip, D. A. & Witteman, J. C. 2004. Predictive value of noninvasive measures of atherosclerosis for incident myocardial infarction: the Rotterdam Study. *Circulation*, 109, 1089-94.
- Van Der Valk, F. M., Verweij, S. L., Zwinderman, K. A., Strang, A. C., Kaiser, Y., Marquering, H. A., . . . Rudd, J. H. 2016. Thresholds for Arterial Wall Inflammation Quantified by 18F-FDG PET Imaging: Implications for Vascular Interventional Studies. *JACC Cardiovasc Imaging*, 9, 1198-1207.
- Van Dijk, A. C., Fonville, S., Zadi, T., Van Hattem, A. M., Saiedie, G., Koudstaal, P. J. & Van Der Lugt, A. 2014. Association between arterial calcifications and nonlacunar and lacunar ischemic strokes. *Stroke*, 45, 728-33.
- Van Dijk, A. C., Truijman, M. T., Hussain, B., Zadi, T., Saiedie, G., De Rotte, A. A., . . . Van Der Lugt, A. 2015. Intraplaque Hemorrhage and the Plaque Surface in

- Carotid Atherosclerosis: The Plaque At RISK Study (PARISK). *AJNR Am J Neuroradiol*.
- Van Gils, M. J., Bodde, M. C., Cremers, L. G., Dippel, D. W. & Van Der Lugt, A. 2013. Determinants of calcification growth in atherosclerotic carotid arteries; a serial multi-detector CT angiography study. *Atherosclerosis*, 227, 95-9.
- Van Sloten, T. T., Protogerou, A. D., Henry, R. M., Schram, M. T., Launer, L. J. & Stehouwer, C. D. 2015. Association between arterial stiffness, cerebral small vessel disease and cognitive impairment: A systematic review and meta-analysis. *Neurosci Biobehav Rev*, 53, 121-30.
- Van Swieten, J. C., Kappelle, L. J., Algra, A., Van Latum, J. C., Koudstaal, P. J. & Van Gijn, J. 1992. Hypodensity of the cerebral white matter in patients with transient ischemic attack or minor stroke: influence on the rate of subsequent stroke. Dutch TIA Trial Study Group. *Ann Neurol*, 32, 177-83.
- Vandenabeele, P., Galluzzi, L., Vanden Berghe, T. & Kroemer, G. 2010. Molecular mechanisms of necroptosis: an ordered cellular explosion. *Nat Rev Mol Cell Biol*, 11, 700-14.
- Vattikuti, R. & Towler, D. A. 2004. Osteogenic regulation of vascular calcification: an early perspective. *Am J Physiol Endocrinol Metab*, 286, E686-96.
- Vedre, A., Pathak, D. R., Crimp, M., Lum, C., Koochesfahani, M. & Abela, G. S. 2009. Physical factors that trigger cholesterol crystallization leading to plaque rupture. *Atherosclerosis*, 203, 89-96.
- Vengrenyuk, Y., Cardoso, L. & Weinbaum, S. 2008. Micro-CT based analysis of a new paradigm for vulnerable plaque rupture: cellular microcalcifications in fibrous caps. *Mol Cell Biomech*, 5, 37-47.
- Vengrenyuk, Y., Carlier, S., Xanthos, S., Cardoso, L., Ganatos, P., Virmani, R., . . . Weinbaum, S. 2006. A hypothesis for vulnerable plaque rupture due to stress-induced debonding around cellular microcalcifications in thin fibrous caps. *Proc Natl Acad Sci U S A*, 103, 14678-83.
- Verma, S., Kuliszewski, M. A., Li, S. H., Szmítko, P. E., Zucco, L., Wang, C. H., . . . Kutryk, M. J. 2004. C-reactive protein attenuates endothelial progenitor cell survival, differentiation, and function: further evidence of a mechanistic link between C-reactive protein and cardiovascular disease. *Circulation*, 109, 2058-67.

- Verma, S., Wang, C. H., Li, S. H., Dumont, A. S., Fedak, P. W., Badiwala, M. V., . . . Stewart, D. J. 2002. A self-fulfilling prophecy: C-reactive protein attenuates nitric oxide production and inhibits angiogenesis. *Circulation*, 106, 913-9.
- Vesey, A. T., Jenkins, W. S., Irkle, A., Moss, A., Sng, G., Forsythe, R. O., . . . Newby, D. E. 2017. 18F-Fluoride and 18F-Fluorodeoxyglucose Positron Emission Tomography After Transient Ischemic Attack or Minor Ischemic Stroke: Case-Control Study. *Circ Cardiovasc Imaging*, 10.
- Viles-Gonzalez, J. F., Fuster, V., Corti, R., Valdiviezo, C., Hutter, R., Corda, S., . . . Badimon, J. J. 2005. Atherosclerosis regression and TP receptor inhibition: effect of S18886 on plaque size and composition--a magnetic resonance imaging study. *Eur Heart J*, 26, 1557-61.
- Virmani, R., Kolodgie, F. D., Burke, A. P., Finn, A. V., Gold, H. K., Tulenko, T. N., . . . Narula, J. 2005. Atherosclerotic plaque progression and vulnerability to rupture: angiogenesis as a source of intraplaque hemorrhage. *Arterioscler Thromb Vasc Biol*, 25, 2054-61.
- Wahl, R. L., Henry, C. A. & Ethier, S. P. 1992. Serum glucose: effects on tumor and normal tissue accumulation of 2-[F-18]-fluoro-2-deoxy-D-glucose in rodents with mammary carcinoma. *Radiology*, 183, 643-7.
- Waje-Andreassen, U., Krakenes, J., Ulvestad, E., Thomassen, L., Myhr, K. M., Aarseth, J. & Vedeler, C. A. 2005. IL-6: an early marker for outcome in acute ischemic stroke. *Acta Neurol Scand*, 111, 360-5.
- Wang, C. Y., Mayo, M. W., Korneluk, R. G., Goeddel, D. V. & Baldwin, A. S., Jr. 1998. NF-kappaB antiapoptosis: induction of TRAF1 and TRAF2 and c-IAP1 and c-IAP2 to suppress caspase-8 activation. *Science*, 281, 1680-3.
- Wang, D. M. & Tarbell, J. M. 1995. Modeling interstitial flow in an artery wall allows estimation of wall shear stress on smooth muscle cells. *J Biomech Eng*, 117, 358-63.
- Wang, H., Yan, S., Chai, H., Riha, G. M., Li, M., Yao, Q. & Chen, C. 2006. Shear stress induces endothelial transdifferentiation from mouse smooth muscle cells. *Biochem Biophys Res Commun*, 346, 860-5.
- Wang, M., Jiang, L., Monticone, R. E. & Lakatta, E. G. 2014. Proinflammation: the key to arterial aging. *Trends Endocrinol Metab*, 25, 72-9.
- Wang, X. & Feuerstein, G. Z. 2004. The Janus face of inflammation in ischemic brain injury. *Acta Neurochir Suppl*, 89, 49-54.

- Wang, X., Lee, S. R., Arai, K., Lee, S. R., Tsuji, K., Rebeck, G. W. & Lo, E. H. 2003. Lipoprotein receptor-mediated induction of matrix metalloproteinase by tissue plasminogen activator. *Nat Med*, 9, 1313-7.
- Ward-Caviness, C. K., Neas, L. M., Blach, C., Haynes, C. S., Larocque-Abramson, K., Grass, E., . . . Hauser, E. R. 2017. A genome-wide trans-ethnic interaction study links the PIGR-FCAMR locus to coronary atherosclerosis via interactions between genetic variants and residential exposure to traffic. *PLoS One*, 12, e0173880.
- Wardlaw, J. M., Smith, C. & Dichgans, M. 2013. Mechanisms of sporadic cerebral small vessel disease: insights from neuroimaging. *Lancet Neurol*, 12, 483-97.
- Watson, K. E., Bostrom, K., Ravindranath, R., Lam, T., Norton, B. & Demer, L. L. 1994. TGF-beta 1 and 25-hydroxycholesterol stimulate osteoblast-like vascular cells to calcify. *J Clin Invest*, 93, 2106-13.
- Weber, C., Erl, W., Weber, K. & Weber, P. C. 1996. Increased adhesiveness of isolated monocytes to endothelium is prevented by vitamin C intake in smokers. *Circulation*, 93, 1488-92.
- Weishaupt, N., Zhang, A., Deziel, R. A., Tasker, R. A. & Whitehead, S. N. 2016. Prefrontal Ischemia in the Rat Leads to Secondary Damage and Inflammation in Remote Gray and White Matter Regions. *Front Neurosci*, 10, 81.
- Wilhelm, A. J., Zabalawi, M., Grayson, J. M., Weant, A. E., Major, A. S., Owen, J., . . . Sorci-Thomas, M. G. 2009. Apolipoprotein A-I and its role in lymphocyte cholesterol homeostasis and autoimmunity. *Arterioscler Thromb Vasc Biol*, 29, 843-9.
- Williams, T. N., Zhang, C. X., Game, B. A., He, L. & Huang, Y. 2004. C-reactive protein stimulates MMP-1 expression in U937 histiocytes through Fc[gamma]RII and extracellular signal-regulated kinase pathway:: an implication of CRP involvement in plaque destabilization. *Arterioscler Thromb Vasc Biol*, 24, 61-6.
- Wintermark, M., Arora, S., Tong, E., Vittinghoff, E., Lau, B. C., Chien, J. D., . . . Saloner, D. 2008. Carotid plaque computed tomography imaging in stroke and nonstroke patients. *Ann Neurol*, 64, 149-57.
- Wolf, S. & Werthessen, N. T. 1979. Dynamics of arterial flow. *Adv Exp Med Biol*, 115, 1-472.

- Wright, C. B., Sacco, R. L., Rundek, T., Delman, J., Rabbani, L. & Elkind, M. 2006. Interleukin-6 is associated with cognitive function: the Northern Manhattan Study. *J Stroke Cerebrovasc Dis*, 15, 34-8.
- Wu, C., Huang, R. T., Kuo, C. H., Kumar, S., Kim, C. W., Lin, Y. C., . . . Fang, Y. 2015. Mechanosensitive PPAP2B Regulates Endothelial Responses to Atherorelevant Hemodynamic Forces. *Circ Res*, 117, e41-e53.
- Wu, L. N., Genge, B. R., Lloyd, G. C. & Wuthier, R. E. 1991. Collagen-binding proteins in collagenase-released matrix vesicles from cartilage. Interaction between matrix vesicle proteins and different types of collagen. *J Biol Chem*, 266, 1195-203.
- Wu, Y. W., Kao, H. L., Huang, C. L., Chen, M. F., Lin, L. Y., Wang, Y. C., . . . Yang, W. S. 2012. The effects of 3-month atorvastatin therapy on arterial inflammation, calcification, abdominal adipose tissue and circulating biomarkers. *Eur J Nucl Med Mol Imaging*, 39, 399-407.
- Xia, C. Y., Zhang, S., Gao, Y., Wang, Z. Z. & Chen, N. H. 2015. Selective modulation of microglia polarization to M2 phenotype for stroke treatment. *Int Immunopharmacol*, 25, 377-82.
- Yamagami, H., Sakaguchi, M., Furukado, S., Hoshi, T., Abe, Y., Hougaku, H., . . . Kitagawa, K. 2008. Statin therapy increases carotid plaque echogenicity in hypercholesterolemic patients. *Ultrasound Med Biol*, 34, 1353-9.
- Yang, D., Iyer, S., Gardener, H., Della-Morte, D., Crisby, M., Dong, C., . . . Rundek, T. 2015a. Cigarette Smoking and Carotid Plaque Echodensity in the Northern Manhattan Study. *Cerebrovasc Dis*, 40, 136-43.
- Yang, Y., Estrada, E. Y., Thompson, J. F., Liu, W. & Rosenberg, G. A. 2007. Matrix metalloproteinase-mediated disruption of tight junction proteins in cerebral vessels is reversed by synthetic matrix metalloproteinase inhibitor in focal ischemia in rat. *J Cereb Blood Flow Metab*, 27, 697-709.
- Yang, Y., Salayandia, V. M., Thompson, J. F., Yang, L. Y., Estrada, E. Y. & Yang, Y. 2015b. Attenuation of acute stroke injury in rat brain by minocycline promotes blood-brain barrier remodeling and alternative microglia/macrophage activation during recovery. *J Neuroinflammation*, 12, 26.
- Yarnykh, V. L., Terashima, M., Hayes, C. E., Shimakawa, A., Takaya, N., Nguyen, P. K., . . . Yuan, C. 2006. Multicontrast black-blood MRI of carotid arteries:

- Comparison between 1.5 and 3 tesla magnetic field strengths. *Journal of Magnetic Resonance Imaging*, 23, 691-698.
- Yasojima, K., Schwab, C., McGeer, E. G. & McGeer, P. L. 2001. Generation of C-reactive protein and complement components in atherosclerotic plaques. *Am J Pathol*, 158, 1039-51.
- Yilmaz, G. & Granger, D. N. 2010. Leukocyte recruitment and ischemic brain injury. *Neuromolecular Med*, 12, 193-204.
- Yokode, M., Kita, T., Arai, H., Kawai, C., Narumiya, S. & Fujiwara, M. 1988. Cholesteryl ester accumulation in macrophages incubated with low density lipoprotein pretreated with cigarette smoke extract. *Proc Natl Acad Sci U S A*, 85, 2344-8.
- Yoo, H. J., Kim, S., Hwang, S. Y., Hong, H. C., Choi, H. Y., Seo, J. A., . . . Choi, K. M. 2015. Vascular inflammation in metabolically abnormal but normal-weight and metabolically healthy obese individuals analyzed with (1)(8)F-fluorodeoxyglucose positron emission tomography. *Am J Cardiol*, 115, 523-8.
- Yoo, H. J., Kim, S., Park, M. S., Choi, H. Y., Yang, S. J., Seo, J. A., . . . Choi, K. M. 2011a. Serum adipocyte fatty acid-binding protein is associated independently with vascular inflammation: analysis with (18)F-fluorodeoxyglucose positron emission tomography. *J Clin Endocrinol Metab*, 96, E488-92.
- Yoo, H. J., Kim, S., Park, M. S., Yang, S. J., Kim, T. N., Seo, J. A., . . . Choi, K. M. 2011b. Vascular inflammation stratified by C-reactive protein and low-density lipoprotein cholesterol levels: analysis with 18F-FDG PET. *J Nucl Med*, 52, 10-7.
- Yoshida, K., Fukumitsu, R., Kurosaki, Y., Funaki, T., Kikuchi, T., Takahashi, J. C., . . . Miyamoto, S. 2015. The association between expansive arterial remodeling detected by high-resolution MRI in carotid artery stenosis and clinical presentation. *J Neurosurg*, 1-7.
- Yoshiyama, S., Chen, Z., Okagaki, T., Kohama, K., Nasu-Kawaharada, R., Izumi, T., . . . Nakamura, A. 2014. Nicotine exposure alters human vascular smooth muscle cell phenotype from a contractile to a synthetic type. *Atherosclerosis*, 237, 464-70.
- Youn, C. S., Choi, S. P., Kim, S. H., Oh, S. H., Jeong, W. J., Kim, H. J. & Park, K. N. 2012. Serum highly selective C-reactive protein concentration is associated

- with the volume of ischemic tissue in acute ischemic stroke. *Am J Emerg Med*, 30, 124-8.
- Young, V. E., Patterson, A. J., Tunnicliffe, E. M., Sadat, U., Graves, M. J., Tang, T. Y., . . . Gillard, J. H. 2012. Signal-to-noise ratio increase in carotid atheroma MRI: a comparison of 1.5 and 3 T. *Br J Radiol*, 85, 937-44.
- Yuan, C., Beach, K. W., Smith, L. H., Jr. & Hatsukami, T. S. 1998. Measurement of atherosclerotic carotid plaque size in vivo using high resolution magnetic resonance imaging. *Circulation*, 98, 2666-71.
- Yuan, C., Zhang, S.-X., Polissar, N. L., Echelard, D., Ortiz, G., Davis, J. W., . . . Hatsukami, T. S. 2002. Identification of Fibrous Cap Rupture With Magnetic Resonance Imaging Is Highly Associated With Recent Transient Ischemic Attack or Stroke. *Circulation*, 105, 181-185.
- Yun, M., Yeh, D., Araujo, L. I., Jang, S., Newberg, A. & Alavi, A. 2001. F-18 FDG uptake in the large arteries: a new observation. *Clin Nucl Med*, 26, 314-9.
- Zarins, C. K., Giddens, D. P., Bharadvaj, B. K., Sottiurai, V. S., Mabon, R. F. & Glagov, S. 1983. Carotid bifurcation atherosclerosis. Quantitative correlation of plaque localization with flow velocity profiles and wall shear stress. *Circ Res*, 53, 502-14.
- Zeicher, A. M., Fisslthaler, B., Schray-Utz, B. & Busse, R. 1995. Nitric oxide modulates the expression of monocyte chemoattractant protein 1 in cultured human endothelial cells. *Circ Res*, 76, 980-6.
- Zeki Al Hazzouri, A., Vittinghoff, E., Sidney, S., Reis, J. P., Jacobs, D. R., Jr. & Yaffe, K. 2015. Intima-Media Thickness and Cognitive Function in Stroke-Free Middle-Aged Adults: Findings From the Coronary Artery Risk Development in Young Adults Study. *Stroke*, 46, 2190-6.
- Zhang, H., Sunnarborg, S. W., Mcnaughton, K. K., Johns, T. G., Lee, D. C. & Faber, J. E. 2008. Heparin-Binding Epidermal Growth Factor-Like Growth Factor Signaling in Flow-Induced Arterial Remodeling. *Circulation Research*, 102, 1275-1285.
- Zhang, X., Tong, F., Li, C. X., Yan, Y., Kempf, D., Nair, G., . . . Howell, L. 2015. Temporal evolution of ischemic lesions in nonhuman primates: a diffusion and perfusion MRI study. *PLoS One*, 10, e0117290.
- Zhao, S., Kuge, Y., Tsukamoto, E., Mochizuki, T., Kato, T., Hikosaka, K., . . . Tamaki, N. 2001. Effects of insulin and glucose loading on FDG uptake in

- experimental malignant tumours and inflammatory lesions. *Eur J Nucl Med*, 28, 730-5.
- Zhao, S., Kuge, Y., Tsukamoto, E., Mochizuki, T., Kato, T., Hikosaka, K., . . . Tamaki, N. 2002. Fluorodeoxyglucose uptake and glucose transporter expression in experimental inflammatory lesions and malignant tumours: effects of insulin and glucose loading. *Nucl Med Commun*, 23, 545-50.
- Zhao, Z., Nelson, A. R., Betsholtz, C. & Zlokovic, B. V. 2015. Establishment and Dysfunction of the Blood-Brain Barrier. *Cell*, 163, 1064-78.
- Zhou, J., Li, J., Rosenbaum, D. M. & Barone, F. C. 2011. Thrombopoietin protects the brain and improves sensorimotor functions: reduction of stroke-induced MMP-9 upregulation and blood-brain barrier injury. *J Cereb Blood Flow Metab*, 31, 924-33.
- Zhuang, H. M., Cortes-Blanco, A., Pourdehnad, M., Adam, L. E., Yamamoto, A. J., Martinez-Lazaro, R., . . . Alavi, A. 2001. Do high glucose levels have differential effect on FDG uptake in inflammatory and malignant disorders? *Nucl Med Commun*, 22, 1123-8.
- Zoller, B., Melander, O., Svensson, P. & Engstrom, G. 2014. Red cell distribution width and risk for venous thromboembolism: a population-based cohort study. *Thromb Res*, 133, 334-9.
- Zupan, M., Sabovic, M., Zaletel, M., Popovic, K. S. & Zvan, B. 2015. The presence of cerebral and/or systemic endothelial dysfunction in patients with leukoaraiosis--a case control pilot study. *BMC Neurol*, 15, 158.